Advanced Energy Efficient Roof System

DE-FC26-04NT42114
Final Report
Volume I: Main Report

to
Parrish Galusky
Marc LaFrance
Department of Energy
National Energy Technology Laboratory
Energy Efficient Buildings Technologies
3610 Collins Ferry Road, P.O. Box 880
Morgantown, WV 26507-0880

Submitted by
University of Minnesota
Technical Contact: Professor Jane H. Davidson
Department of Mechanical Engineering
111 Church St., S. E.
Minneapolis, MN 55455
TEL: 612-626-9850
FAX: 612-625-6069
EMAIL: JHD@me.umn.edu

December 17, 2008

Advanced Energy Efficient Roof system

This report provides the final results of a collaboration of the University of Minnesota and industry partners to develop an innovative residential roof with the primary objective of creating a more energy efficient building envelope. The research and development focused on a panelized roof system. The design approach and examples of panel design and implementation in residential buildings are presented in Volume I. Economic and energy analyses compare the projected cost and savings in energy used for space heating. Volume II includes appendices with additional information on approach as well as supplemental results.

Major contributors to the effort are:

Jane H. Davidson, Susan C. Mantell
G.L. Di Muoio, G. Mittelman, C. Briscoe, B. Schoenbauer, and D. Huang
Department of Mechanical Engineering
University of Minnesota

T. Okazaki, C.K. Shield, B.J. Siljenberg
Department of Civil Engineering
University of Minnesota

John C. Carmody, and G.E. Mosiman
Center for Sustainable Building Research
University of Minnesota

David H. MacDonald
Mattson MacDonald Young
Minneapolis, Minnesota

Peter Kalish
GE Global Research
Niskayuna, NY 12309

Additional contributors include Jim Petersen, Pulte Home Sciences, Larry Wrass, formerly with Pulte Homes, and Ducker Worldwide. Mike Krupa, BASF, provided valuable expertise on foam properties and manufactured components for the prototypes with foam. Kennotech of Finland provided valuable expertise on laser welding and fabricated the truss core panel prototypes.

This report was prepared with the support of the U.S. Department of Energy, under Award No. DE-FC26-04NT42114. However, any opinions, findings, conclusions, or recommendations expressed herein are those of the author(s) and do not necessarily reflect the views of the DOE.

EXECUTIVE SUMMARY

Motivation and Objective

Energy consumption in buildings represents 40 percent of primary U.S. energy consumption, split almost equally between residential (22%) and commercial (18%) buildings.[1] Space heating (31%) and cooling (12%) account for approximately 9 quadrillion Btu. Improvements in the building envelope can have a significant impact on reducing energy consumption. Thermal losses (or gains) from the roof make up 14 percent of the building component energy load. Infiltration through the building envelope, including the roof, accounts for an additional 28 percent of the heating loads and 16 percent of the cooling loads. These figures provide a strong incentive to develop and implement more energy efficient roof systems.

The roof is perhaps the most challenging component of the building envelope to change for many reasons.

- The engineered roof truss, which has been around since 1956, is relatively low cost and is the industry standard.
- The roof has multiple functions.
- A typical wood frame home lasts a long time.
- Building codes vary across the country.
- Customer and trade acceptance of new building products and materials may impede market penetration.
- The energy savings of a new roof system must be balanced with other requirements such as first and life-cycle costs, durability, appearance, and ease of construction.

Conventional residential roof construction utilizes closely spaced roof trusses supporting a layer of sheathing and roofing materials. Gypsum board is typically attached to the lower chord of the trusses forming the finished ceiling for the occupied space. Often in warmer climates, the HVAC system and ducts are placed in the unconditioned and otherwise unusable attic. High temperature differentials and leaky ducts result in thermal losses. Penetrations through the ceilings are notoriously difficult to seal and lead to moisture and air infiltration. These issues all contribute to greater energy use and have led builders to consider construction of a conditioned attic. The options considered to-date are not ideal. One approach is to insulate between the trusses at the roof plane. The construction process is time consuming and costs more than conventional attic construction. Moreover, the problems of air infiltration and thermal bridges across the insulation remain. Another approach is to use structurally insulated panels (SIPs), but conventional SIPs are unlikely to be the ultimate solution because an additional

[1] The energy consumption data in this paper are abstracted from the DOE 2007 Building Energy Data Book and represent EIA data from 2004. Primary energy consumption accounts for the generation, transmission and distribution losses.

underlying support structure is required except for short spans. In addition, wood spline and metal locking joints can result in thermal bridges and gaps in the foam.

This study undertook a more innovative approach to roof construction. The goal was to design and evaluate a modular energy efficient panelized roof system with the following attributes:

- a conditioned and clear attic space for HVAC equipment and additional finished area in the attic,
- manufactured panels that provide structure, insulation, and accommodate a variety of roofing materials,
- panels that require support only at the ends,
- optimal energy performance by minimizing thermal bridging and air infiltration,
- minimal risk of moisture problems,
- minimum 50-year life,
- applicable to a range of house styles, climates and conditions,
- easy erection in the field,
- the option to incorporate factory-installed solar systems into the panel, and
- lowest possible cost.

A nationwide market study shows there is a defined market opportunity for such a panelized roof system with production and semi-custom builders in the United States. Senior personnel at top builders expressed interest in the performance attributes and indicate long-term opportunity exists if the system can deliver a clear value proposition. Specifically, builders are interested in 1) reducing construction cycle time (cost) and 2) offering increased energy efficiency to the homebuyer. Additional living space under the roof panels is another low-cost asset identified as part of the study. The market potential is enhanced through construction activity levels in target markets. Southern markets, from Florida to Texas account for 50 percent of the total new construction angled-roof volume. California contributes an additional 13 percent share of market volume. These states account for 28 to 30 million squares (2.8 to 3 billion square feet) of new construction angled roof opportunity. The major risk to implementation is the uncertainty of incorporating new design and construction elements into the construction process. By coordinating efforts to enhance the drivers for adoption and minimize the barriers, the panelized roof system stands to capitalize on a growing market demand for energy efficient building alternatives and create a compelling case for market adoption.

Design Approach

The panelized roof system was developed in a collaborative effort of the University of Minnesota Institute of Technology and College of Design and industry partners including Pulte Home Sciences, GE Global Research, Kennotech (Finland), BASF and Mattson Macdonald Young Structural Engineers. Initially a number of design options were considered. Two panel concepts were selected for further development based on acceptance by the builder partner, ability to meet applicable standards and codes

on structure and hygrothermal performance, manufacturability, constructability, architectural integration, and cost. Industry collaborators were selected in two competitive Requests for Proposal.

The structural and hygrothermal performance of the two designs were evaluated for application across the U.S. A specialized computational program based on engineering principles was developed to design panels to meet the structural requirements of U.S. homes. The results were validated through testing of large scale prototypes fabricated by the industry collaborators. Testing was performed at the University of Minnesota's Department of Civil Engineering Structures Laboratory. Additional material characterization tests were performed by BASF. The hygrothermal performance (thermal and moisture) was simulated for eight representative U.S. sites. In this report, specification of panel geometry and manufacture of the two panel types are provided for a range of expected applications. Connections and architectural details at panel to panel, ridge, soffit and gable end joints that satisfy structural, hygrothermal performance requirements are described. GE Global Research and the University of Minnesota developed concepts to integrate solar photovoltaics (PV) into the roof panel.

A typical production home (1155 square foot living area plus garage) for the southwest region of the U.S. was selected to evaluate application of the panelized roof system. Architectural details and a life cycle cost analysis for production quantities are presented for this representative home for five roof/ceiling options: A) the conventional single-story home with trusses and an unconditioned attic; B) a modified version of option A with loose fill insulation at the roof plane, C) an energy efficient home with a panelized roof and an occupied attic; D) an energy efficient home with a panelized roof and cathedral ceilings in most of the living space, and E) a solar home identical to option D with solar photovoltaic panels and a solar water heater. The cost estimation includes production costs from material through factory investment and expense, construction costs, and energy costs and available financial incentives for energy efficiency. The economic analysis is provided in an Excel spreadsheet, which permits the user to modify many of the assumed inputs including the cost of energy.

Panel Options

The two panels designs are referred to as the truss core panel[2] (Figures 2.1-1 through 2.1-4) and the stiffened plate panel (Figures 2.2-1 and 2.2-2). These panels share several common features, most notably separate structural and foam insulating components that are manufactured as an assembly, and similar connectors at panel-to-panel, soffit, ridge and gable end wall joints. The structural component is fabricated from cold rolled steel sheet stock. It is cut, galvanized to prevent corrosion and laser welded. The insulation is polyurethane that is foamed-in-place during manufacture either

[2] U.S. patent pending

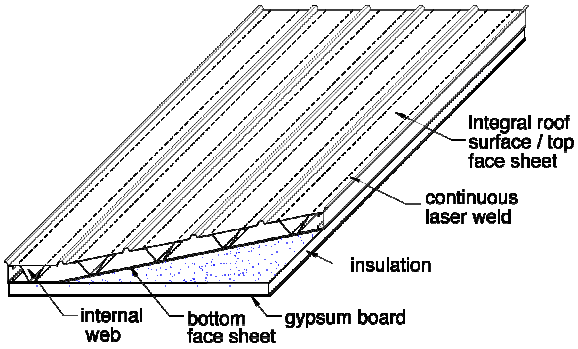

Figure 1: Truss core roof panel with interior foam and an integral metal roof (not to scale).

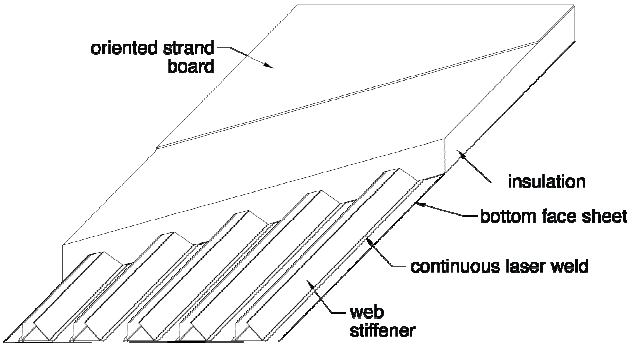

Figure 2: Stiffened plate roof panel with nailbase top sheet (not to scale).

on the interior or exterior of the structural member as appropriate for the climate and panel configuration.

The structural component of the truss core panel (Figure 1) is comprised of two steel face sheets and internal steel V-channels (referred to as the web) laser welded continuously to the face sheets. The edges of the structural component parallel to the V-channels are finished with a laser welded C-channel. All steel components are galvanized. Panels would be installed such that the webs are oriented longitudinally, with webs spanning the longest unsupported length. For the panel option shown in Figure 1, the face sheet is the exterior finish and the steel structure serves as an exterior vapor barrier. The standing metal ridges provide a flexible design platform on which to integrate solar photovoltaics and to take advantage of the natural air flow beneath the PV to increase solar-to-electric efficiency. Other versions of the truss core panel are suitable for application of conventional roof finishes including asphalt shingles or tile. The PUR can be placed on either the interior (as shown) or exterior of the steel structure. This versatility allows use of the truss core panel in virtually any climate. The best option will depend on geographic location and builder and homeowner preference.

The structural component of the stiffened plate panel (Figure 2) is comprised of V-shaped stiffeners welded to a single steel sheet. The orientation of the webs shown in Figure 2, with the face sheet on the interior surface, is required to sustain the structural loads, particularly the live and dead loads. As with the truss core panel, stiffened plate panels would be installed such that the web stiffeners are oriented longitudinally, with webs spanning the longest unsupported length. The steel structure serves as an interior vapor barrier; PUR is attached on the exterior of the structure. The exterior OSB finish sheet permits a nail base final roof cover. An integral metal roof finish is a second option. The potential advantage of the stiffened plate in comparison to the truss core is a reduction in number of welds and cost of galvanization. The drawbacks are the panel weighs more than the truss core panel for most regions of the country, the structure is restricted to wind speeds of 90 mph, the option to invert the panel placing the insulation

on the inside is not available due to the difficulty in adequately sealing the panels against air and vapor movement at the soffit end, and more foam is required to meet target R-values and prevent moisture problems.

Recommended Truss Core Panel

The truss core panel is the most flexible and versatile system and is recommended over the stiffened plate panel for further development. Panels can satisfy thermal and structural loading requirements throughout the United States for a range of roof spans and roof slopes. Panel configuration can be tailored for warm and cold climates with different finish options. In all cases, the basic criteria of the building envelope are met including providing adequate insulation without thermal bridging, managing vapor and moisture for a given climate, and providing an attractive appearance. In addition, the steel structural component can be used for flooring in the attic or other sections of the living space.

Representative panels designs are included in the report. Designs include specification of materials, dimensions, manufacture, connectors, and production and construction costs. The weight and depth of the panel depend on the horizontal span length, roof slope and climate. The standard width is 8 ft. An example truss core panel is one designed for a southern home with a 20 ft horizontal span and a 6/12 roof pitch. The total depth of the panel is 10.7 in. including a 5.5 in. deep structural component (compatible with 2x6 wood frame construction) and 5.2 in. layer of PUR to achieve R-30 (h-ft^2-°F/Btu). The panel weighs 5.53 lb/ft^2. For regions with higher snow loads and heating loads the panel is slightly deeper and heavier. The panel is finished in the factory with either an integral metal roof or with an OSB surface compatible with standard roofing materials. The integral metal roof has a PVDF coating to provide a durable and architecturally acceptable finish. The interior surface is finished with gypsum board during manufacture.

Architectural details including field assembly procedures are provided. These details ensure drainage of rainwater, a continuous moisture barrier, minimize infiltration and thermal bridging, and ease of field assembly. Panel to panel connectors join adjacent panels very simply at the steel structure and thus avoid conductive paths across the foam. Ridge, soffit and gable end connectors are comprised of sheet metal assemblies that conform to the angles at the ridge, soffit and gable ends. A ridge beam (or equivalent) is needed to avoid an overly complex connection at the soffit.

Figure 3 shows an example of a panelized roof applied to the plan of a home currently constructed in Las Vegas. Panelized construction increases the finished space from 1155 to 1878 ft^2. The availability of structure along the centerline of the house allows the span of this system to be half of the overall width of the house, or about 15 feet. Columns are located in walls that align vertically on both floors. The second story contains two large bedrooms and a large bathroom plus three closets. The added space in the second story is possible because the use of roof panels, as opposed to a truss system, provides clear space under an insulated roof.

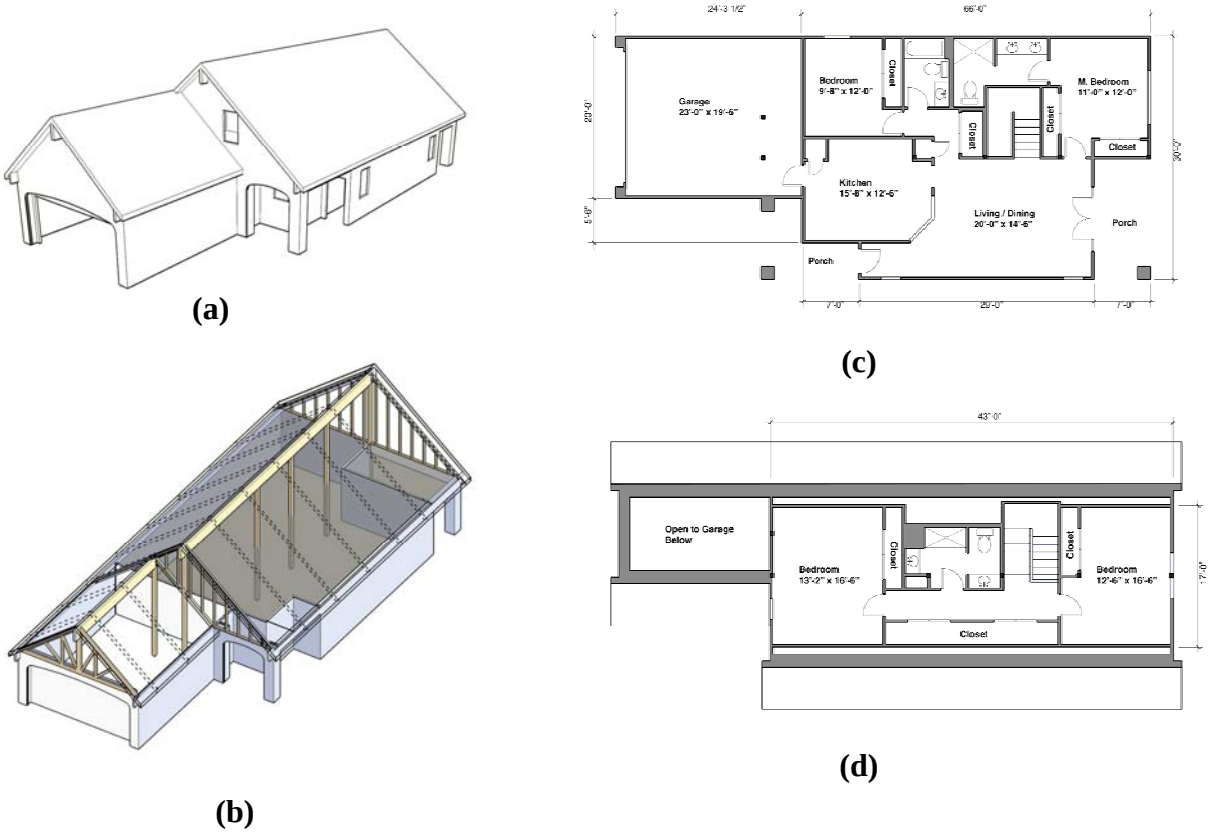

Figure 3: Panelized roof home with occupied attic: (a) two-story 1878 ft^2 home with 10/12 roof pitch; (b) panelized structure with ridge beam and columns ; (c) first floor plan; (d) second floor plan.

Economic Assessment

The panelized roof system has a number of performance advantages over conventional roof construction. These include factory quality production that yields superior thermal and moisture performance, the ease of placing HVAC equipment in a conditioned attic, the possibility of converting the attic to occupied space at reduced cost compared to a home with trusses, and the option for factory installed solar PV and solar thermal modules, and reduced construction cycle time particularly in solar homes. Cost and material savings result if the panel also serves as the outer roof surface.

At 50,000 parts per year, production cost for an 8 by 17.5 ft rafter panel is $9.41 per square foot prior to sales markup. Panel cost is not very sensitive to increases in production volume above 50,000. Seventy percent of the production cost is due to materials with the remainder split roughly equally between labor and overhead. As a result, panel costs would expect to fluctuate as material costs change in the commodities market. Production cost of the ceiling panel is $4.76 per square foot. Again, material

costs represent the largest cost at 66% of this value. With a sales markup of 25%, the rafter and ceiling panels would sell for $11.89/ft^2 and $6.01/ft^2, respectively.

The benefits to the homeowner of the panelized roof are the savings in energy costs over the lifetime of the home and the added space if the attic is converted to living area. An economic analysis was performed to assess the life cycle cost and benefits of panelized roof construction compared to conventional truss construction. The economic analysis was applied to a $350,000, 1155 square foot home with a 5/12 simple gable roof (option A). Panelized construction will cost an additional $20,692 for a shallow slope roof with cathedral ceilings (option D). The cost difference is primarily due to material costs. Our initial estimate is that field erection time is similar to conventional roof construction. The primary benefit of the panelized home is a 29% reduction in energy used for space heating and cooling. Per finished area, the annual HVAC energy use is 3.52 kWh/ft^2. The energy savings are attributed primarily to reduced air infiltration and to a lesser extent to the higher effective R-value. One important result of the analysis is the significant projected reduction in PV cost when PV modules are integrated with the roof panel during production. With the factory installation of a 2.5KW PV system on three roof panels, the panelized house would cost $17,367 more than the same house without PV, but at $6.95/W the cost for PV compares favorably to typical residential installed systems that cost $9/W or more. The PV system meets the net annual heating and cooling load.

Panelized roofs have greater economic benefit when conditioned attic space is converted to living space. This conversion is most appropriate for a steep roof. Increasing the roof pitch of panelized roof to 10/12 and converting the 723 ft^2 attic to a second floor living space (Figure 3), costs $50,007 more than the conventional house. The cost per square foot of living space is reduced 25 percent to $148/ft^2 compared to $197/ft^2. Per finished area, the annual HVAC energy use is reduced 45 percent to 2.72 kWh/ft^2. The added living space in this house is valuable space for the homeowner.

Final Assessment and Recommendation

The truss core panelized roof system offers a promising technology for achieving a more energy efficient home. The results of the study reveal that the panel meets the structural, moisture, and thermal requirements of an energy efficient home and provides a substantial energy savings compared to conventional roofs. The panelized roof system is designed to be placed on any conventionally-built house and is adaptable to a wide range of house types and styles. Manufacturing processes and on-site erection procedures appear feasible and there are interested manufacturers.

The proposed system is projected to cost more than today's conventional roofing. The cost difference is offset the ability to convert the attic space to living space at reduced cost, a substantial increase in energy efficiency, and for solar integrated panels, lower installed cost.

As a follow up to the present study, a key question is how to have the benefits of the system at a reduced cost. One design assumption may be at least partially responsible

for the resulting higher costs – the desire of the building partner at the onset of the project that the panel system have no intermediate support structure. The reason for this criterion was to minimize the number of elements on site and provide a completely clear, conditioned attic. It might be preferable to use a portion of the attic space for structural components. We recommend future study to develop potentially more efficient structural options that take advantage of geometry such as panels spanning shorter distances between beams, trusses or other intermediate supports.

Another option to improve panelized construction is to consider a redesign of the entire house. The truss core panel was developed independently of the rest of the house. While this approach makes sense in terms of the broadest possible application and market, it does not permit the synergies that would occur with a whole house panelized system where connection systems and construction methods can be completely optimized. For example, the entire house shell could be erected at once if its structure, wall, and roof panels were part of the same system. Such a system could lead to further performance enhancements and cost reductions. House designs could be developed that use the system more efficiently while still providing a variety of styles and options.

Although the current conditions of the construction industry present challenges in commercializing an innovative roof system, a definite need and market fit has been identified for changes in construction that reduce energy consumption and benefit the homeowner.

Table of Contents

Volume I

1.0 Introduction

The University of Minnesota and its industry partners collaborated over the course of this project to develop a panelized residential roof system with the major objective of creating a more energy efficient building envelope than is possible with conventional roof construction.

Conventional residential roof construction in the United States utilizes closely spaced roof trusses supporting a layer of sheathing and roofing materials. Gypsum board is typically attached to the lower chord of the trusses forming the finished ceiling for the occupied space. With insulation placed above the ceiling plane, the attic is unconditioned and is typically vented at the soffit and the ridge. Often in warmer climates, the HVAC system and ducts are placed in the otherwise unusable attic. While this roof system has benefited from efficiency improvements and costs have become optimized over time, it still has disadvantages the industry would like to overcome. High temperature differentials and leaky ducts result in thermal losses. Penetrations through the ceilings for ducts, plumbing and electrical are notoriously difficult to seal and lead to moisture and air infiltration problems. Often there is insufficient space for adequate insulation at the roof/wall interface.

Recently techniques have been employed to move the insulation from the ceiling plane to the space between the trusses at the roof plane thus creating a conditioned attic. The energy benefits of placing mechanical equipment and ducts inside the conditioned attic have been documented (e.g., Desjarlais et al., 2004; Hendron et al., 2004; Rudd 2005). Desjarlais et al. (2004) modeled the energy savings of a conditioned attic in diverse climates (Atlanta, Boulder, Dallas, Miami, Minneapolis, and Phoenix) and found that for ducts of typical length and leakage rates, energy savings of 5 to 40% could be realized, depending on climate and insulation level. Energy savings will also depend on the roof surface area and air infiltration through the roof.

One approach to achieve a conditioned attic is to insulate between the trusses at the roof plane. However, with closely-spaced trusses and insulation applied from below, the construction process is time consuming, involves several trades, and costs more than conventional attic construction. Moreover, this approach does not solve air and infiltration problems at the roof. Another approach is to use structurally insulated panels (SIPs) made of OSB and polystyrene (either XPS or EPS) or polyurethane (PUR) placed on supporting beams and/or trusses. Conventional SIP construction is unlikely to be the ultimate solution because of the limited span without an additional underlying support structure. In addition, wood spline and metal locking joints utilized in traditional SIP construction can result in thermal bridges and gaps in the foam. For cathedral ceilings, custom-designed rafter systems can be used; however a custom designed option requires high-level workmanship.

The objective of this project was to develop a self-supporting panelized roof that eliminates the disadvantages of current approaches to achieving a conditioned attic space.

The goal of the project that emerged from this objective was to create the next generation roof system with the following characteristics:

- manufactured production quality panels that incorporate structure, insulation, and possibly the interior and exterior finish materials,
- panels that only require support at the ends with no intermediate supporting structure,
- optimal energy performance by minimizing thermal bridging and creating airtight seals of all joints,
- minimal risk of moisture problems,
- durable with at least a 50-year life,
- applicable to a range of design styles, climates and conditions,
- fast, easy erection in the field,
- potential for incorporation of factory-installed solar systems into the panel, and
- lowest possible costs.

Two examples with the best cost-benefit picture are 1) a steep sloping roof with occupied space in the attic (Figure 1.0-1), and 2) a shallow sloping roof with no attic (Figure 1.0-2).

There is a defined market opportunity for the panelized roof system with production and semi-custom builders in the South and West regions of the United States. (A market study is provided in Appendix A.) Furthermore, the potential of reduced on-site labor provides a compelling case for adoption with builders and contractors in Central and Northern regions of the country where labor rates account for an average of 43 percent more in construction cost. Senior personnel at top builders expressed interest in the performance attributes and indicate long-term opportunity exists if the system can deliver a clear value proposition.

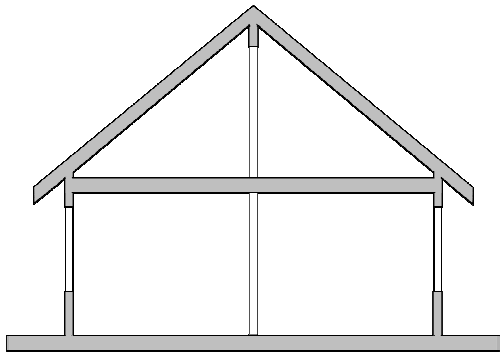

Figure 1.0-1: Panelized roof system with steep slope roof (10/12 pitch).

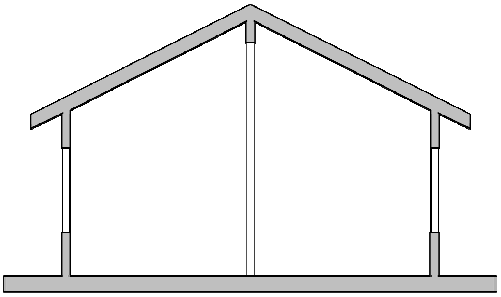

Figure 1.0-2: Panelized roof system with shallow slope roof (6/12 pitch).

2.0 Panel Designs

In developing panel designs we considered various performance attributes including: structural, hygrothermal (thermal and moisture performance), architectural, manufacturability and cost. During Budget Period 1, a number of panel designs and potential materials were evaluated based on these features (Davidson et al., 2006). Two design concepts were selected in concert with our building partner. Models of these concepts were developed and used to assess feasibility. During Budget Periods 2 (Davidson et al., 2007a,b), and 3, we established contacts with potential commercial and manufacturing partners (BASF, Comau-Pico, DOW, GE, Precision Light Systems, Kenno Tech, Kysor, Pulte, Rosette Systems, Strongwell) and solicited their input through an RFP process to help refine the panel designs and assess manufacturability. GE Global Research initiated a project to consider integration of the photovoltaics and solar thermal systems with the panel.

Two designs were down selected during Budget Period 3. The truss core panel (Figures 2.1-1 through 2.1-4) and the stiffened plate panel (Figures 2.2-1 and 2.2-2). These designs share several common features, specifically separate structural and insulating components easily manufactured as an assembly, and connectors. The advantages of this approach are the structural capability does not depend on the foam properties, which can degrade with time, the panel is not subject to thermal bowing, and the insulating value of the foam is not compromised by thermal bridges.

The structural component is fabricated from steel sheet stock. Cold rolled steel with a galvanized coating is recommended to prevent corrosion. This material is well suited for production manufacturing and is compatible with laser welding.

A PUR insulation layer is foamed-in-place during manufacture either on the interior or exterior of the structural member as appropriate for the climate and desired appearance. A variety of foams were evaluated in our consideration of hygrothermal performance and manufacturability. Polyurethane (PUR) is recommended for a number of reasons. It can be foamed *in-situ* and is thus suitable for a continuous manufacturing process, adheres to steel and OSB, has a service temperature of 194 to 248°F, is not susceptible to mold, and is recommended over thermoplastic foams (such as polystyrene) in the event of fire (Davies, 1994). Details of materials selection and material properties are included in Appendix B.

Simple connectors were designed to connect the panels to each other and at the soffit and ridge of the home. A ridge beam is recommended to reduce the complexity of the connection at the soffit. Full details of the connectors are provided in section 4.3.

2.1 Truss Core Panel

Four versions of the truss core roof panel are shown in Figures 2.1-1 through 2.1-4. The drawings illustrate the basic layers in the various designs. Details of the geometry and edge finish are provided in section 4. In each panel, the steel structural component is comprised of two face sheets and an internal metal web (core). The internal web consists

of V-channels continuously laser welded to the face sheets. Panels are installed such that the webs are oriented longitudinally, with webs spanning the longest unsupported length. The edges of the structural component parallel to the V-channels are finished with a laser welded C-channel. The edge that meets the ridge has a metal end cap. The edge that meets the soffit has either a metal end cap or blocking. The choice of edge finish is based on the house plan and is described in the architectural details in section 4.3. PUR foam and finish layers are attached to the steel structure in the factory as the panels are welded and assembled. The required depth of insulation depends on the desired R-value. The soffit and ridge edges are cut to match the roof slope. The length, weight and depth of the panel depend on the horizontal span length, roof slope and climate. The standard width is 8 ft. Examples of panels for U.S. climate zones and representative homes are provided in section 4.1. For southern climates, panels are 10 to 12 in. deep. Simple connectors are used to join the panels to each other and at the soffit and ridge of the home. Full details of the connectors are provided in section 4.2.

The panel shown in Figure 2.1-1 is intended for warmer climates. The conventional rule of thumb is building assemblies need to be protected from moisture transport from the exterior in warm moist climates (Lstiburek, 2002, Künzel, 2005). In this panel, the steel structural component is the exterior vapor barrier. The top structural sheet of the structural component serves as an integral, finished roof surface. The corrugated metal surface is galvanized and painted in the factory. This corrugated surface connects to adjacent panels to form a weather-tight roof. The integral metal roof option will reduce landfill waste compared to conventional roof finishes and eliminates the need for additional roof covering. PUR is attached during manufacture to the interior of the steel structural component. The interior gypsum board finish sheet is attached to the foam during the same manufacturing step. For R-30 h-ft^2-°F/Btu[3], the depth of the PUR is 5.2 in. For R-40, the depth is 6.9 in.

The panel shown in Figure 2.1-2 is also intended for warmer regions of the U.S. Again the steel structural component provides an exterior vapor barrier and PUR is attached to the interior side of the steel structure. The major difference in this panel and the panel depicted in Figure 2.1-1 is the roof finish. The exterior of the panel is a sheet of OSB. The OSB provides the nailing surface for application of traditional roof finish layers. In this case, EPS or PUR foam is adhered to the steel and OSB, providing space for properly driven fasteners.

The panels shown in Figure 2.1-3 and 2.1-4 are intended for cooler climates. The conventional rule of thumb in severe cold climates is building assemblies need to be protected from moisture transport from the interior. The panel shown in Figure 2.1-3 has an integral metal roof. The insulation is located on the exterior of the structural component. The corrugated sheet that serves as the final roof finish is attached to the PUR during manufacture. The disadvantage of this arrangement is that the steel sheets

[3] All R-values are reported in units of h-ft^2-°F/Btu. The units on R-value are not repeated in the remainder of the text.

create a vapor barrier on both sides of the PUR. The foam must be protected from moisture transport at the ridge, the soffit and gable end walls as shown in section 4.3. An interior finish such as gypsum board may be attached to the steel structure during construction.

The panel shown in Figure 2.1-4 has an OSB finish layer on the exterior of the panel. The OSB is attached as part of the foaming process. In this arrangement, water vapor transport is from the exterior of the panel and the steel structure serves as a vapor barrier on the conditioned side of the panel. The OSB sheet facilitates attachment of conventional exterior roofing materials. This panel has excellent hygrothermal performance in warm, dry climates as well as cool climates.

Without insulation, the truss core design is well suited for relatively thin ceiling panels. Gypsum board can be attached to the steel structure during manufacture. Construction of a panelized attic does not require use of a panelized attic floor. The attic floor can be constructed using conventional framing.

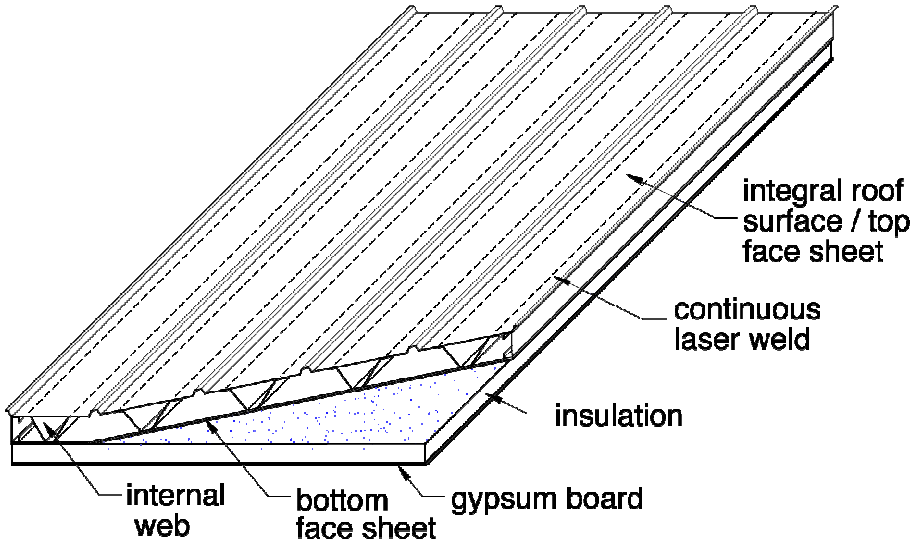

Figure 2.1-1: Truss core roof panel with interior foam and an integral metal roof.

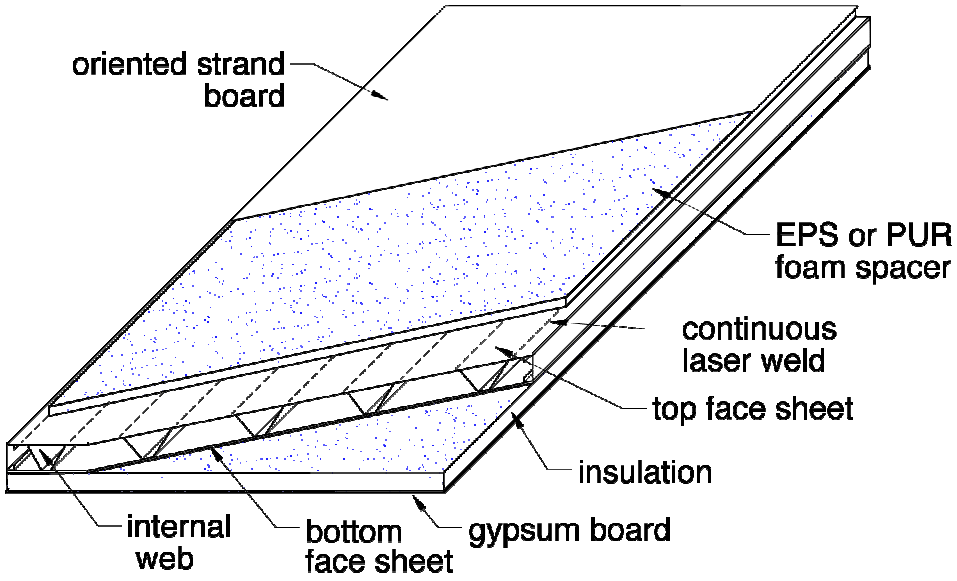

Figure 2.1-2: Truss core roof panel with interior foam and nailbase top sheet.

-

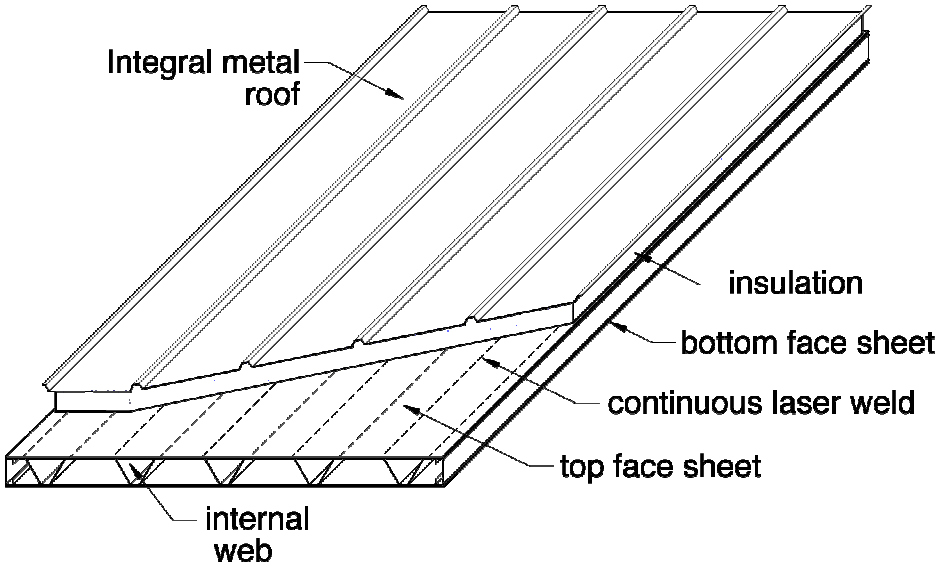

Figure 2.1-3: Truss core roof panel with exterior foam and integral metal roof.

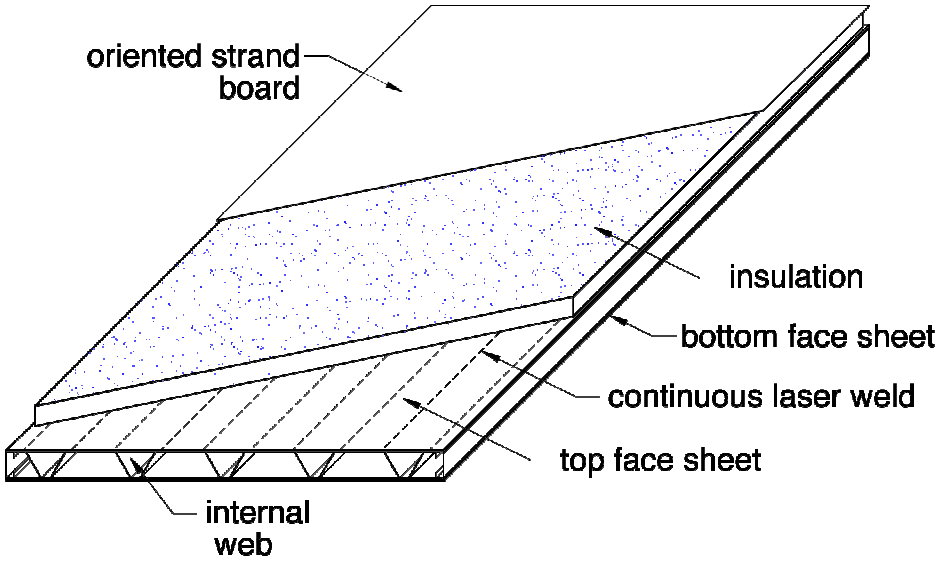

Figure 2.1-4: Truss core roof panel with exterior foam and nailbase top sheet.

2.2 Stiffened Plate Panel

The stiffened plate panel differs from the truss core panel in the structural component. Figures 2.2-1 and 2.2-2 illustrate the basic layers in two feasible designs. Details of the geometry and edge finish are provided in section 5. The steel structural component is comprised of V-shaped stiffeners welded to a *single* steel sheet. The panel is named the stiffened plate because the webs stiffen the flat metal sheet. As with the truss core panel, stiffened plate panels are installed such that the web stiffeners are oriented longitudinally, with webs spanning the longest unsupported length.

The PUR foam is attached to the steel structure so that it adheres to the corrugated surface. The option of attaching the foam to the flat metal surface was discarded because of the appearance. The deep contours of the V-stiffeners are visually unacceptable as a finished roof surface. The panel is always oriented so that the steel sheet is on the interior. The option to invert the panel, placing the structure on the exterior, was considered, but abandoned due to the difficulty in adequately sealing the panels against air and vapor movement at the soffit end. PUR foam and finish layers are attached to the steel structure in the factory as the panels are welded and assembled.

The edges of the panel that run from soffit to ridge do not have a cap to avoid thermal bridges across the foam. The edge that meets the ridge also has no cap. The edge that meets the soffit and gable end wall has blocking. The soffit and ridge edges are cut to match the roof slope.

With the limitations in orientation discussed above, the stiffened plate panel presents two options. Figure 2.2-1 shows the panel with an integral metal roof finish. Together the structural steel component and the exterior steel finish sheet create a vapor barrier on both sides of the PUR. The integral metal roof is fastened to adjacent panels to

create a weather-tight roof. The foam is protected from moisture transport at the ridge and the soffit as described in the architectural details provided in section 5.3. The depth of the PUR foam is that required to achieve either R-30 or R-40, as required by the geographic location. More foam is required than in the truss core panel because the V-webs extend into the foam.

Figure 2.2-2 shows the panel with an OSB exterior finish sheet, which facilitates attachment of conventional exterior roofing materials. In this option, the steel structure is the interior vapor barrier. Hygrothermal analysis suggests that R-40 is required in warm, humid climates to prevent condensation at the PUR/steel interface. In hot dry climates, condensation is not a problem and R-30 is sufficient to prevent moisture related problems. .

The length, weight and depth of the panel depend on the horizontal span length, roof slope and climate. The standard width is 8 ft. Examples of panels for U.S. climate zones and representative homes are provided in section 5.1. For southern climates, panels are 12 in. deep. The connectors that join the panels to each other and at the soffit and ridge of the home are similar to the connectors for the truss core panel. Full details of the connectors are provided in section 5.2.

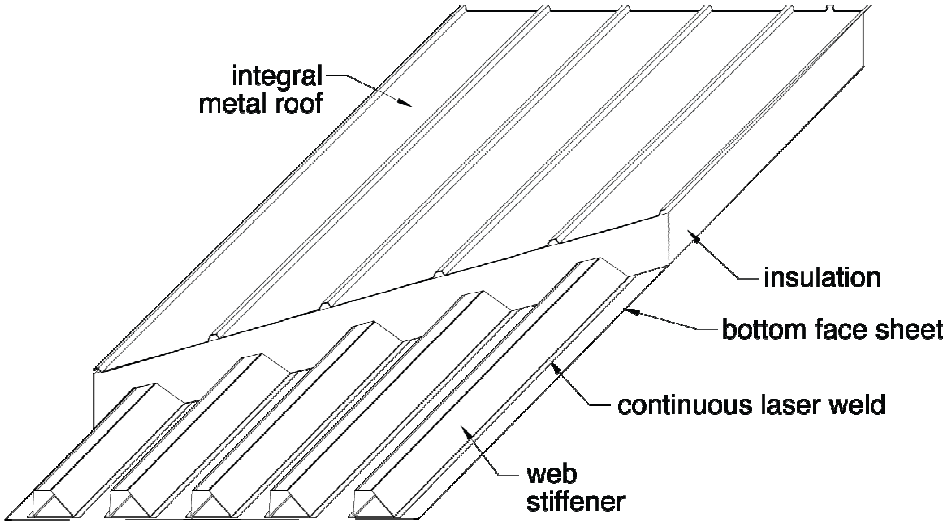

Figure 2.2-1: Stiffened plate roof panel with integral metal roof.

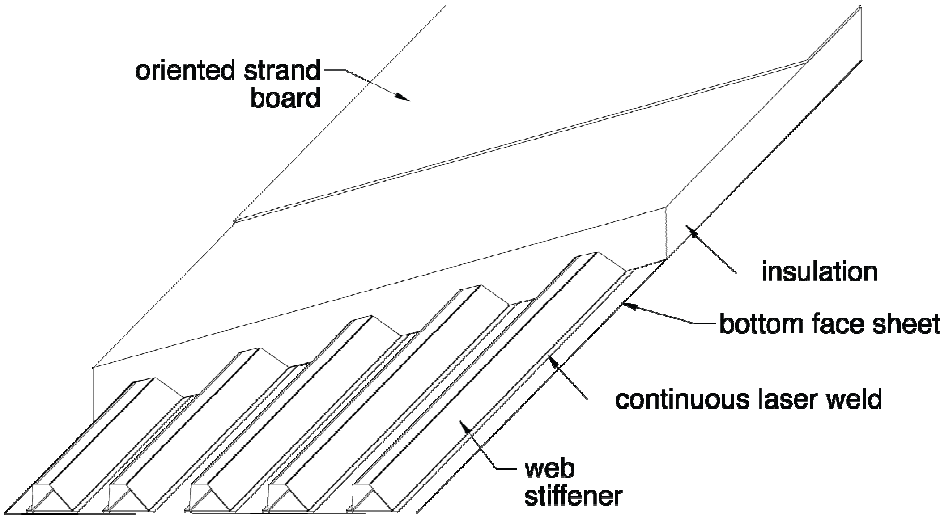

Figure 2.2-2: Stiffened plate roof panel with nailbase top sheet.

3.0 Design Approach and Assessment

In designing the panels and in assessing their relative performance, a number of attributes including manufacturability, field installation, and cost, were considered. All panels must meet the structural and hygrothermal requirements for U.S. homes. Structural loads and thermal requirements (R-value) for three U.S. climate zones (I, II, and III), corresponding to the southern, middle and northern regions of the U.S. (Figure 3.0-1), were considered. Models were developed based on engineering principles to ensure that panel designs satisfied the structural requirements. Truss core and stiffened plate prototypes were designed and fabricated to validate the structural performance models and to evaluate panel manufacturing techniques. Hygrothermal performance of the panels was modeled using WUFI and ANSYS commercial software for a number of U.S. cities selected to represent the expected range of humidity and temperature conditions.

Architectural details were developed for representative houses with gable end roofs: a steep sloped roof, and a shallow sloped roof (Figures 1.0-1 and 1.0-2). Horizontal spans from 12 ft to 20 ft were considered. Connections and architectural details at panel to panel, ridge, soffit and gable end joints were designed to satisfy structural, hygrothermal performance requirements. Constructability and aesthetics were considered and reviewed by our building partner.

Working with our building partner, a typical production home (1155 square feet living area) for the southwest region of the U.S. was identified. Architectural details and a life cycle cost analysis for production quantities were developed for this representative home for five roof/ceiling options: A) the baseline single story with trusses and insulation at the ceiling plane; B) a more energy efficient version of A with insulation at the roof plane; C) a panelized steep sloped roof with an occupied attic; D) a panelized shallow sloped roof with cathedral ceilings; and E) a panelized shallow sloped roof with solar PV and solar hot water systems. (The options are described in section 8.)

Manufacture and economic analyses were performed in partnership with our industrial partners.

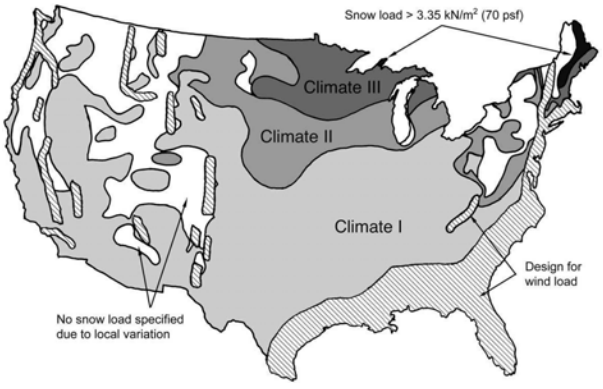

Figure 3.0-1: Map of US with climates zones (ICC, 2003a).

3.1 Structural Design Approach

Panel and joint designs were evaluated for distributed live, dead and wind loads defined by the International Residential Building code (ICC, 2003a). The live component accounts for snow loads and is defined for each of the three U.S. climate zones shown in Figure 3.0-1. The dead component consists of the weight of the panel plus shingles and other materials added to the roof. Wind loads were calculated following the components and cladding section of the International Residential Building code. We evaluated panel and joint designs for 90 and 130 mph wind loads. A complete description of panel and joint structural loads can be found in Appendix C.

Structural performance of the truss core and stiffened plate panel was evaluated by considering performance criteria for stiffness (deflection), the onset of face sheet buckling, web shear buckling, postbuckling flexural capacity and web crippling. The panel deflection limit, horizontal span length/240, is set by the International Residential Building code (ICC, 2003a). Limiting loads for buckling, flexural capacity and web crippling were found following the approaches described in the American Iron and Steel Institute's specification for light gage steel structures (AISI, 2001) and by Timoshenko (Timoshenko and Gere, 1961). In the case of web crippling, which is local buckling failure of the webs at the supports, a new set of empirical constants was derived to account for the unique truss core and stiffened plate geometries. Several large scale prototypes of the truss core and stiffened plate panel were fabricated and tested. These tests were designed specifically to evaluate models of panel flexure, buckling, postbuckling behavior and web crippling. There was excellent agreement between model prediction of prototype panel performance and the experimental results.

Subsequently, a MATLAB program that incorporates these models of panel structural performance was developed. This custom program allows for design and evaluation of either a truss core panel or a stiffened plate panel. The program has several options including: 1) given a specific panel geometry and applied loads, the safety factors for each structural performance criteria can be evaluated; and 2) given the desired safety factors and loads, the lightest weight panel which satisfies the structural performance criteria is identified. Utilizing this program, roof panels for the steep sloped and shallow sloped roofs in the three U.S. climate zones were designed. A detailed description of the structural analysis and test results for the prototype panels can be found in Appendix D and Appendix E, respectively.

3.2 Hygrothermal Design

Panel hygrothermal performance for roof assemblies was evaluated to select the depth of insulation required to achieve the R-value specified by the International Energy Conservation Code (ICC, 2003b) and to avoid moisture related problems. The approach and results are summarized in this section. A more detailed description is provided in Appendix F.

In the case of the *truss core panel*, the metal components are separated from the foam and thus the depth of the foam is specified by the product of required R-value and

the bulk thermal conductivity of 2.25 lb/ft^3 PUR as reported by the manufacturer (0.0144 Btu/h-ft-°F). The ICC recommends R-30 for any site with less than 4500 heating degree days (HDD) and R-40 for sites with more than 6000 HDD. We assigned R-40 for all sites with HDD greater than 4500. The hygrothermal performance was modeled with WUFI 2D-3.0 (Künzel and Kiessl, 1997; Künzel et al., 2005) for a number of U.S. cities representing a range of typical climates. Selected cities are Atlanta, Boston, Houston, Los Angeles, International Falls, Miami, Phoenix, and Seattle. Table 3.2-1 lists the heating and cooling degree days and required R-value of these cities. The moisture performance of the panel was modeled with using the cold year, WUFI-ORNL/IBP database. Simulations were performed for all panel options which permit moisture transport through the panel (Figures 2.1-1, 2.1-2, and 2.1-4). The WUFI simulations were carried out for 3 years to ensure independency of the results on the initial conditions and to observe the seasonal as variations in moisture transport. Data from year 3 are used to assess the potential for failure due to i) condensation, ii) mold or mildew, iii) wood decay, and iv) metal corrosion. Gypsum and OSB are susceptible to mold at RH greater than 80%. Brief periods of high RH are acceptable as long as the monthly average is less than 80%. The maximum allowable moisture content in the OSB layer is 20% (ASHRAE, 2005). A number of criteria have been suggested to assess the risk and rate of corrosion of carbon steel and other metals. Corrosion of carbon steel can begin at 60% RH, but the rate of corrosion is very low for RH less than 80%. ISO standards (9223 and 9224) specify that corrosion is likely if relative humidity at the metal surface is greater than 80% and the temperature is above freezing. The number of hours for which a metal surface is exposed to these conditions is termed the Time of Wetness (TOW). We report the TOW at the interface of the truss core metal face sheet and the PUR.

For the interior foam truss core panel (Figures 2.1-1 and 2.1-2), the steel structure provides a vapor barrier at the exterior of the panel. Moisture transport is from the interior conditioned space. The WUFI data show that these panels have excellent hygrothermal performance in Los Angeles, Miami, and Phoenix. In Atlanta, Houston, and Seattle, the only potential problem is corrosion of unprotected metal at the PUR/steel interface. We recommend galvanization of the steel structure to lessen the risk of corrosion in all climates.

For the exterior foam truss core panel with a conventional roof finish (Figure 2.1-4), the steel structure provides a vapor barrier at the interior of the panel. Moisture transport is from the exterior and thus outdoor conditions control hygrothermal performance. This panel performs well in cold climates and in warm, dry climates. It has excellent hygrothermal performance in Boston, International Falls, Los Angeles, Phoenix and Seattle. On the other hand, in Atlanta, Houston, and Miami, there is risk of corrosion of the steel at the PUR/metal interface unless the steel is adequately protected by galvanization. The risk of mold and mildew in the OSB finish sheet can be alleviated by use of a borate or copper treated OSB.

In the case of the *stiffened plate panel*, the steel webs provide a conductive path through the foam and consequently the portion of the foam between the webs is less

effective per unit depth as an insulating layer than the foam above the V-webs. A two-dimensional finite element model of conduction in the metal/foam assembly was used to determine the depth of foam required to achieve the target R-value. As discussed in section 4, the stiffened plate panel is most suitable for warmer climates. It is heavier than the truss core panel is cooler climates with higher loads. Consequently, hygrothermal performance was simulated in Phoenix and Houston. These cities were selected to represent moist and dry warm climates, respectively. The stiffened plate panel shown in Figure 2.2-2 with R-30 has no anticipated moisture risks in Phoenix. However, the WUFI simulations indicate that in Houston, R-42 is required to prevent condensation at the PUR/steel interface at the top of the V-webs.

Table 3.2-1: Sites simulated with WUFI.

Site	Heating degree days (HDD)[1]	Cooling degree days (CDD)[2]	R-value
Atlanta	2827	1810	30
Boston	5630	777	40
Houston	1525	2893	30
International Falls	10,264	233	40
Los Angeles	1274	679	30
Miami	149	4361	30
Phoenix	1027	1226	30
Seattle	4797	173	40

[1] http://www.ncdc.noaa.gov/oa/climate/online/ccd/nrmhdd.txt

[2] http://www.ncdc.noaa.gov/oa/climate/online/ccd/nrmcdd.txt

3.3 Architectural Approach

Architectural details incorporate the structural, thermal, and hygrothermal design specifications for the panel and address the aesthetics and constructability of the system applied to a house. The architectural details focus on the joints that occur between panels and where the panels rest on the structure and building envelope below. This report shows the most common details that occur in all houses—the panel to panel, soffit, ridge and gable end joints. In houses with more complex roof shapes, additional details must be addressed as roof hips and valleys as well as any roof penetration or dormer conditions.

The basic principles used in developing the architectural details are as follows:

- create overlapping layers to ensure drainage of rainwater,
- design panels and joints to be easy to assemble in the field with a minimum number of parts,
- provide a continuous moisture barrier on the interior of the assembly in the exterior foam panel and on the exterior of the assembly in the interior foam panel, and
- minimize thermal bridging.

3.4 Manufacture Approach

The approach to manufacture the panels was developed with input from industry through the request for proposal (RFP) and prototyping process. In the RFP process, the University of Minnesota developed panel details while Pulte Home Sciences provided market/builder requirements. We identified vendors from within the U.S. and internationally with the capability of manufacturing roof panels. This information provided the basis for two RFP cycles: one for a truss core panel (March 2006) and one for a foam integrated panel (December 2006). RFP responses described panel manufacturing processes, production equipment requirements and estimates of panel production costs. Feasible and cost effective manufacturing processes were identified through this process. In particular, the laser welding process for fabricating structural components and the foam in place process for applying PUR insulation in the factory were identified as key manufacturing processes.

The prototyping process also served to evaluate the suitability of laser welding and foam in place PUR for roof panel applications. Prototypes were fabricated with similar sheet metal materials and thicknesses and similar foam depth to simulate potential manufacturing challenges. The findings from the process of fabricating the prototypes are incorporated in the manufacturing plans presented in sections 4.4 and 5.4.

Details of the RFP process including vendor responses can be found in the topical year report for Year 1 (Davidson et al., 2006) and the addendum for Extended Budget Period 2 (Davidson et al., 2007b).

3.5 Economic Approach

For the panelized roof system to be commercially viable, it must compete economically with existing roof products. Roofing has seen a gradual reduction in installed cost to the point where a new roofing product, like the panelized roof, may struggle to compete in today's market on the basis of first cost. Because the panelized roof has the advantage of decreased energy costs and easier installation of solar options, it is necessary to look at the cost in relation to value provided to the homeowner as well as production and sales costs.

When costing new products, like the roof panel, it is necessary to consider all contributors to product cost, from material through factory investment and expense. GE's Global Research Center performs cost analyses of many new products and has developed a methodology for capturing costs – particularly when there are sparse data to support the cost estimate. Figure 3.5-1 describes the steps in creating a new product cost model. The diagram indicates a flow of activity from product through completed model. This succession of actions is necessary as data collected on earlier steps drive costs estimated in later steps.

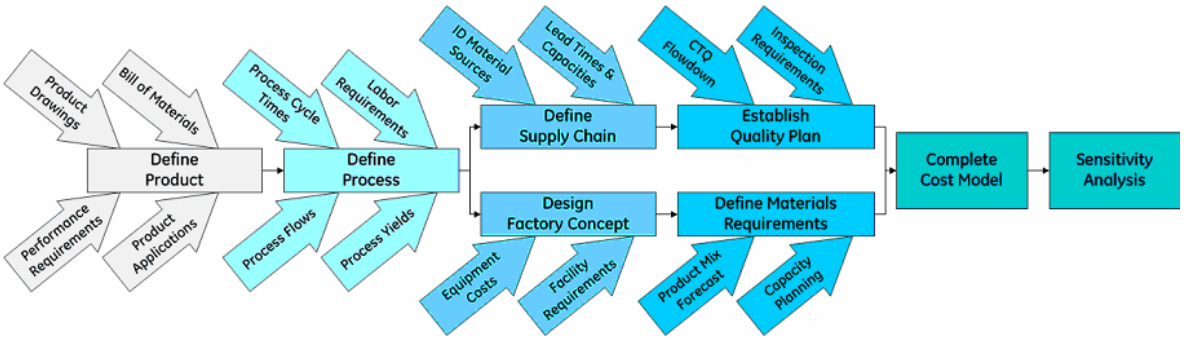

Figure 3.5-1: Steps to create a new product cost model.

All product costing begins with a clear understanding of the product to be produced. The product definition drives decisions about how the manufacturing process would be set up, including sequence of manufacturing steps, which parts would be sourced and how automated each step might be. From this process description, a factory concept and supply chain can be envisioned, driving raw material costs, shipping costs and capital expenditure. Any additional costs, such as those related to quality controls or inefficiencies related to product mix can be added.

The UMN and GE team constructed a cost and value spreadsheet model for the panelized system and the optional system with integrated solar photovoltaics and solar hot water (see section 9). The model provides a comparable view of several roofing options with an eye toward overall economic value to the homeowner and energy savings. The economic analysis of a solar-integrated roof panel was intended to assess whether costs associated with factory installation of PV modules would be less than costs experienced during site installation and if the energy benefits of solar technology might be improved by the modified mounting design. Because the economic model was developed from the homeowner's perspective, it reports benefits in monthly energy and cash flow impact. A flow chart of the spreadsheet is shown in Figure 3.5-2. Costs captured in the model include the following.

- Material costs – A bill of material (BOM) was created for the panel and costs for each raw material and sourced component were estimated based upon vendor discussions.
- Labor – A detailed process flow was developed that captures each step of the manufacturing process. For each process step, an estimate was made of workstation capacity and labor content.
- Capital equipment – The process flow also provided a means of assessing the amount of capital equipment required. Specific machines were identified and listed in the costing spreadsheet along with an estimated cost to install. This total plant and equipment cost estimate drove depreciation, which rolled into the overall cost calculation.
- Manufacturing overhead – The process complexity drove an estimate of engineering and management labor cost along with energy consumption cost.

The capital equipment list captures the footprint for each workstation, giving a total floor space requirement that drove building lease cost.

- Sales markup – The user can specify a sales margin for the panels as a percent of production plus material costs. Twenty five percent is assumed in the current model.
- Construction labor – A comparison was made of the process steps to construct a house with different roof options. Only those costs that differed between house options were included as part of the cost analysis. All construction steps that were common between the house options were assumed to cost the same (hence, left out of the cost analysis). For each construction step, labor costs were estimated from a construction cost database. Where historical data were unavailable, benchmark data were used (i.e., costs for similar activities were used as an input to the estimate).
- Construction material – As in the labor calculation, material costs were only captured in the analysis if they were used in construction steps that differed between house options. The roof panel was considered a "construction material" for house designs that used the panelized roof.
- Construction tooling/equipment – The rental of equipment to support construction of the roof was captured for relevant steps in the process. As with labor, the equipment rental cost was estimated from historical data.
- Energy cost – The electricity rate is a user input value. A rate of $0.10 is assumed in the current model.
- Home financing – The mortgage term and interest rate are user input values.

Several contributors to homeowner benefit are captured in the economic model. These include:

- Energy savings – Energy consumption for home heating, cooling and hot water are input by the user and must be determined external to the spreadsheet. Electricity use is calculated on a per square foot basis and as a monthly average. Cost is compared to a base case home.
- Government incentives – Several active incentive programs, for energy efficient roofing, high efficiency insulation, and solar are included. These incentives have a defined time limit. The model was set up to allow changes to the values in case of incentive expiration or introduction of new incentives.
- Living space – The model provides home cost per square foot because one of the house designs provides increase living space in the attic. The economic model does not take any credit for the value to the homeowner of increased living space. However, the panelized roofing system allows for an increase in space at a minimal additional cost so it was judged to be a benefit worth capturing.
- Monthly cost – Cost to the homeowner includes mortgage and energy costs for space conditioning and hot water.

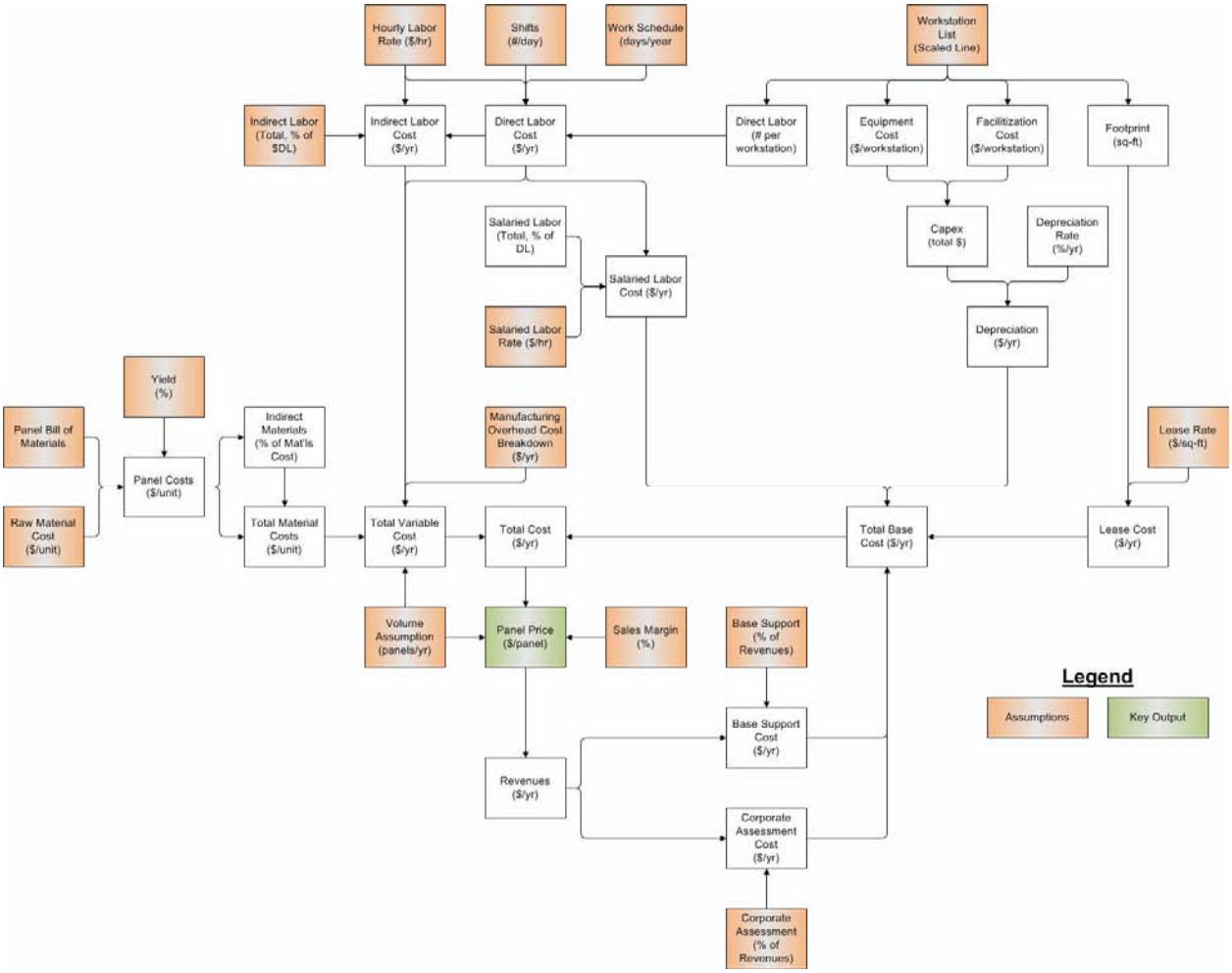

Figure 3.5-2: Flow chart of the spreadsheet cost model for roof panel production.

4.0 Truss Core Panel

In this section, truss core panel geometries, connections and architectural details are presented for two houses with gable style roofs. The roof slope is either steep or shallow. The details provided in this section are a result of extensive structural and hygrothermal analysis, and careful consideration of architectural constraints.

4.1 Panel Geometries

Figures 4.1-1 through 4.1-4 depict example truss core panels as delivered to the job site. The structural and insulation component details in these figures are specific for climates I and III. The figures include the details regarding interior and exterior finish; the details regarding truss core geometry and foam depth for any climate can be substituted. The truss core panel can be designed to satisfy thermal and structural loading requirements throughout the United States for a range of roof spans and roof slopes.

Figures 4.1-1 and 4.1-2 show the panel with interior insulation and either an integral metal roof (Figure 4.1-1) or an OSB exterior for finish with traditional shingle roof (Figure 4.1-2). Figures 4.1-3 and 4.1-4 show the panel with either an integral metal roof exterior insulation and or an OSB nailbase exterior finish sheet. Steel C channels, 18 ga, are laser welded to the longitudinal edges of the structural component to add structural stiffness and to prevent damage during shipping. The edges at the ridge and soffit are cut at an angle (to accommodate the roof slope) and blocked/capped as required for moisture management. Both temperature and humidity will play a role in determining the appropriate location for the foam. In general, a panel configuration, with interior insulation, is recommended for warm climates, while the panel configuration with exterior insulation is recommended for cold climates. These figures also include specific details such as foam depth and structural panel geometry. Depth of the foam layer is determined by the desired R-value. The panel structural component is designed to achieve a minimum weight panel for a particular set of wind, live and dead loads.

The panel structural geometry (depth, sheet thickness, web thickness and number of webs) defined in Figures 4.1-1 and 4.1-2 is specific for a roof subjected to 90 mph wind loads, live loads and dead loads as prescribed for climate I. The roof has a shallow 6/12 pitch and a ridge to soffit *horizontal* span of 20 ft. The insulation thickness is that required to achieve R-30. For this loading configuration the wind uplift loads are of a similar magnitude to the live and dead loads. Thus the panel sheet thicknesses for each component are similar, ranging from 0.34 inches for the interior face sheets and webs to 0.042 inches for the exterior face sheet. The six webs are laser welded at equally spaced intervals, 16 inch on center, over the panel width. Steel C channels, 18 ga, are laser welded to the panel longitudinal edges to add structural stiffness and to prevent damage during shipping. The structural depth is 5.5 inches, corresponding to a depth that is compatible with 2x6 wood frame construction. The foam is 5.2 inches deep to provide R-30. The interior finish is 0.5 in. thick gypsum board for the panels with interior insulation.

For the panel with the integral metal roof (Figure 4.1-1), the exterior face sheet of the truss core panel serves as both the face sheet and the roof finish. The metal corrugations are located at even intervals between webs to ensure that the web/exterior face sheet welds do not occur at a corrugation. The corrugated exterior surface has one longitudinal edge with a corrugation designed to interlock and seal with an adjacent panel (see section 4.3). In this way, the attachment appears as a corrugation. The integral metal roof has a PVDF coating, to provide a durable and architecturally acceptable finish. The panel that is compatible with standard roofing materials (Figure 4.1-2) is finished with a 0.4375 (7/16) inch thick OSB sheet. This sheet is adhesively bonded to a 1 inch thick foam backing layer. The intention of the foam backing layer is to prevent damage to the structural component when the roof shingles are nailed in place.

The panels shown in Figures 4.1-3 and 4.1-4 are designed to sustain 90 mph wind loads, and climate III live and dead loads. The roof has a steep 10/12 pitch and the horizontal span from the ridge to the soffit is 20 ft. The insulation depth is 6.9 inches to achieve R-40. The panel structural component is comprised of a 0.036 inch thick interior face sheet and a 0.079 inch thick exterior face sheet. Six 0.045 inch thick steel webs are laser welded at equally spaced intervals, 16 inches on center, over the panel width. The structural depth is 7.25 inches, compatible with 2x8 frame construction. The exterior face sheet is much thicker than the interior face sheet because the magnitude of the live and dead loads for climate III is greater than the 90 mph wind uplift loads. Similarly, a deeper structure (as compared to the designs for climate I loading) is required to sustain the larger live and dead loads from climate III.

For the panel with the integral metal roof (Figure 4.1-3), the integral metal roof is bonded to the PUR as part of the foaming process. The corrugations are evenly spaced such that the longitudinal edges end with corrugations. With this configuration, the joint between adjacent panels can be a simple metal flashing (see section 4.3). The integral metal roof has a PVDF coating. The panel that is compatible with standard roofing materials (Figure 4.1-4) is finished with a 0.4375 (7/16) inch thick OSB sheet. This sheet is bonded to the PUR foam as part of the foaming process: The OSB sheet and the exterior face sheet provide surfaces during the foaming process.

A broad range of truss core panel designs are listed in Table 4.1-1. These panels are specified for roof panels with a horizontal span of 20 ft in all three climates. The corresponding structural and foam features are shown in Figure 4.1-5. Table 4.1-1 reveals several design trends. For all designs, the exterior face sheet thickness is greater than or equal to the interior face sheet thickness: The exterior face sheet is loaded in compression and a thicker sheet is required to sustain buckling loads. The web thickness is greater than or equal to the interior face sheet thickness because the web is subjected to buckling loads. Truss core roof panel designs for all climates and span lengths from 12 to 20 feet can be found in Appendix G.

Table 4.1-1 also lists a truss core ceiling panel design suitable for occupied living space. This panel is designed to span unsupported for 15 ft. Panel loads and deflection limits are as specified in the residential building code for steel ceiling joists (10 psf dead

load, 40 psf live loads and deflection less than the span divided by 360). Either a ceiling panel such as that specified or a traditional set of wood joists can be used with the roof panel. Both options are considered in the case study of section 8.

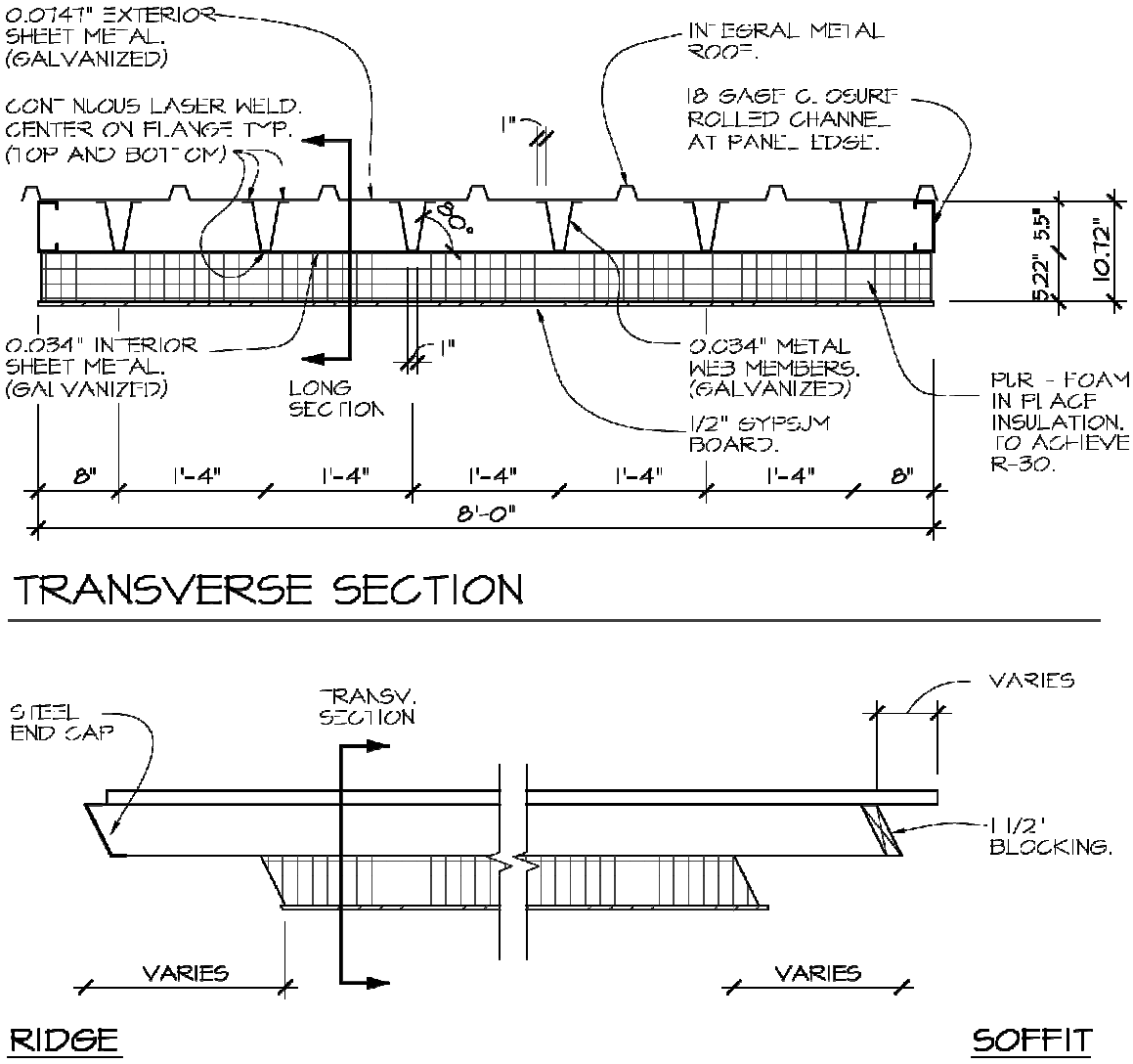

Figure 4.1-1: Engineering drawing of the truss core roof panel for climate I, 6/12 roof pitch with an integral metal roof and foam on the interior.

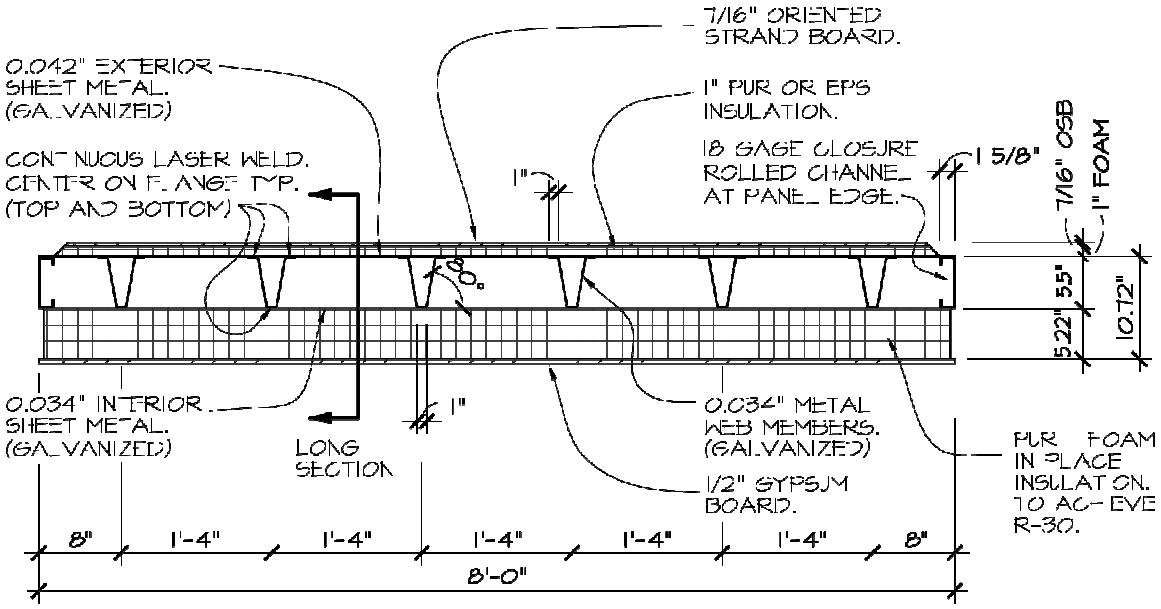

TRANSVERSE SECTION

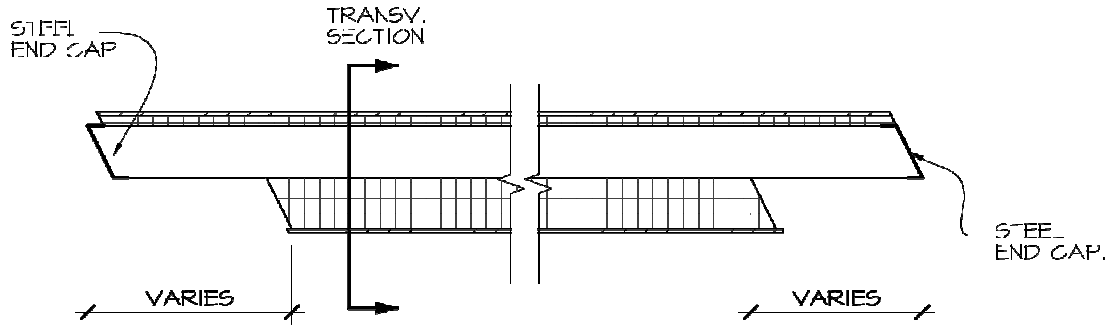

RIDGE SOFFIT

LONGITUDINAL SECTION

TRUSS CORE PANEL - CLIMATE I - 6/12 PITCH

APPLIED ROOF FINISH

Figure 4.1-2: Engineering drawing of the truss core panel for climate I, 6/12 roof pitch with OSB exterior finish and foam on the interior.

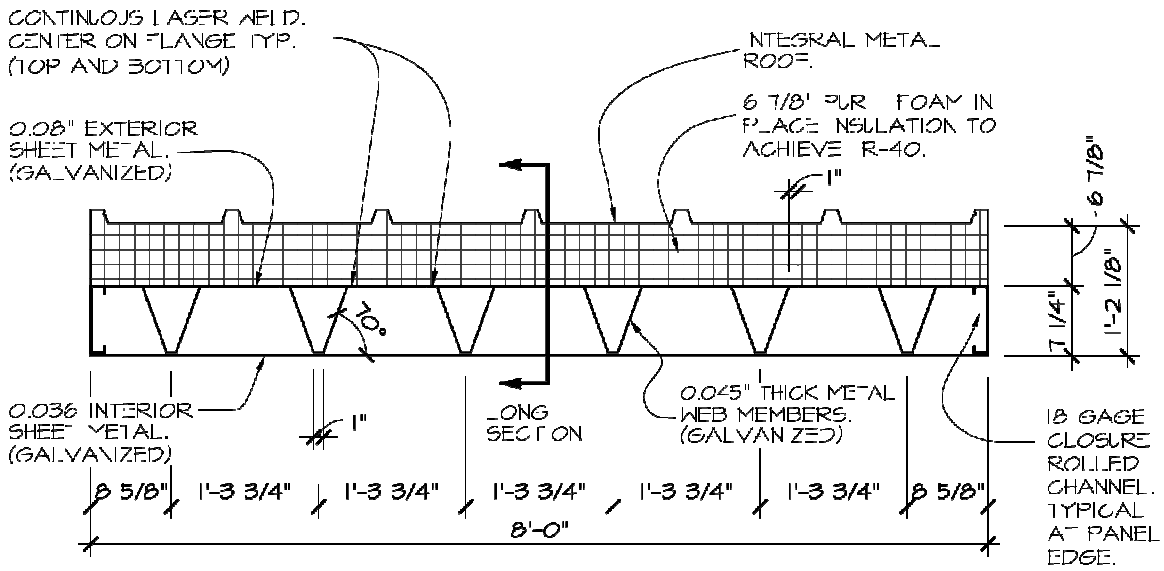

TRANSVERSE SECTION

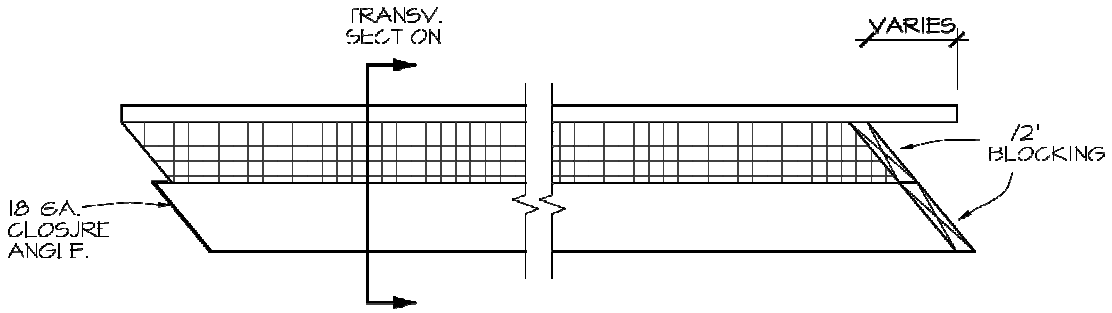

LONGITUDINAL SECTION

TRUSS CORE PANEL - CLIMATE III - 10/12 PITCH

INTEGRAL METAL ROOF

Figure 4.1-3: Engineering drawing of the truss core roof panel for climate III, 10/12 roof pitch with an integral metal roof and foam on the exterior.

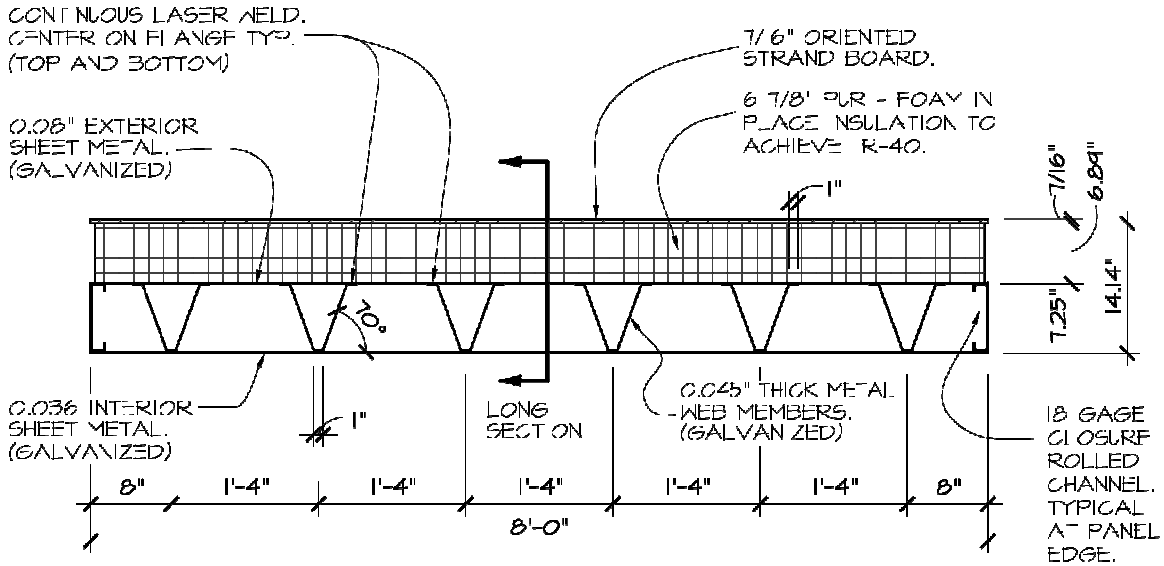

TRANSVERSE SECTION

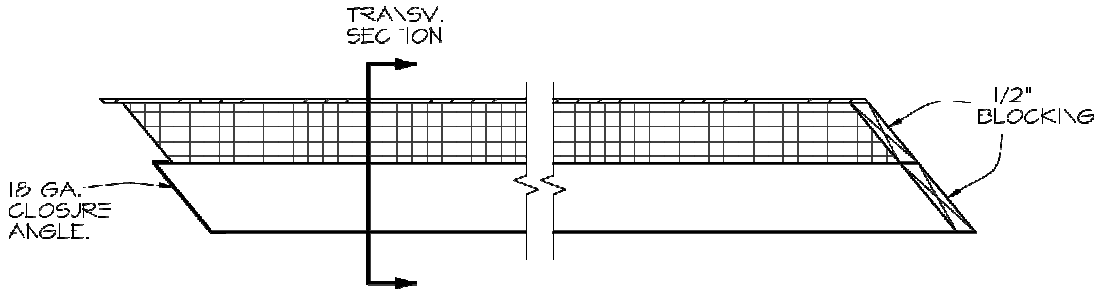

LONGITUDINAL SECTION

TRUSS CORE PANEL - CLIMATE III - 10/12 PITCH

APPLIED ROOF FINISH

Figure 4.1-4: Engineering drawing of the truss core roof panel for climate III, 10/12 roof pitch with OSB exterior finish and foam on the exterior.

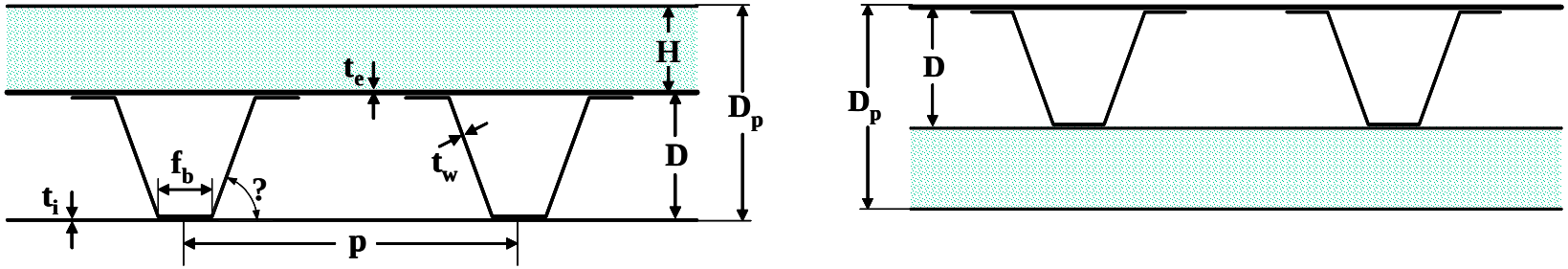

Figure 4.1-5: Truss core geometry.

Table 4.1-1: Specifications for the structural and insulation components of truss-core panels designed for a 6.1 m horizontal span. Panels have been optimized for minimum weight.

Climate and Roof Pitch	Truss Core Structural Component							Foam layer		Panel[1]	
	Structure depth D [in.]	Structure weight [lb/ft^2]	Exterior sheet thickness t_e [in.]	Interior sheet thickness t_i [in.]	Web pitch p [in.]	Web thickness t_w [in.]	Web angle θ [°]	R Value (ft^2-°F-hr/Btu)	Foam Depth H [in.]	Panel depth D_p [in.]	Panel weight [lb/ft^2]
I-6/12	5.5	4.55	0.042	0.033	16	0.033	80	30	5.22	10.72	5.53
I-10/12	7.25	5.05	0.037	0.037	16	0.037	80	30	5.22	12.47	6.04
II-6/12	7.25	4.95	0.037	0.037	16	0.037	85	40	6.89	14.14	6.24
II-10/12	7.25	5.76	0.049	0.039	16	0.039	75	40	6.89	14.14	7.06
III-6/12	7.25	6.10	0.048	0.038	16	0.048	80	40	6.89	14.14	7.39
III-10/12	7.25	7.23	0.079	0.036	16	0.045	70	40	6.89	14.14	8.52
Ceiling panel (15 ft span	7.25	4.57	0.038	0.038	24	0.038	75	N/A	N/A	7.25	4.57

[1] Excluding interior and exterior finish, including roofing materials.

4.2 Connector Details

Connections were considered for the four most common connections in any house—the panel to panel, ridge, soffit and gable end joints. Ridge and soffit joint designs were developed for a ridge joint that has a beam or equivalent support. The use of a ridge beam was selected during Budget Period 2 (Davidson et al., 2007b) to avoid an overly complex connection at the soffit. Connectors for the truss core panel were designed for a simple gable house subjected to climate III loading conditions and either 90 mph or 130 mph wind loads. Two gable roof configurations were considered: a shallow sloped roof (6/12 pitch) with a 20 ft soffit to ridge horizontal span, and a steep sloped roof (10/12 pitch) with a 12 ft soffit to ridge horizontal span. Loads on each connector are detailed in Appendix C. Connectors for the 90 mph steep sloped roof with a 90 mph wind load in climate III are shown in Figures 4.2-1 through 4.2-4 (panel to panel, ridge, soffit and gable end, respectively). A complete set of connector drawings can be found in Appendix H.

The connectors are fabricated from galvanized steel sheet metal. In general, panel to panel connectors are comprised of a single strip of sheet metal. The only exception to this design is for the interior foam panel with in integral metal roof. In this case, the structural connection is made on the top surface of the panel with an integral, lapped self-flashing structural connection (Figure 4.2-5). Ridge, soffit and gable end connectors are comprised of sheet metal assemblies that conform to the angles at the ridge, soffit and gable ends. Panels are attached to the connectors with self tapping sheet metal screws. The connectors are attached to wood framing components at the ridge, soffit and gable end with wood screws. The fastener size and schedule are detailed in each figure.

The connectors shown in Figures 4.2-1 through 4.2-4 are representative of the connectors for the shallow sloped, 20 ft horizontal span and for panels subjected to 90 mph wind loads. In general, the sheet metal thickness and fastening/welding requirements are identical for steeper roof slopes. The primary difference in these connectors is the pitch of the metal components at the ridge and soffit. Compared to connectors designed for 90 mph wind loads, connectors designed for 130 mph wind loads use thicker sheet metal components, and additional fasteners and welds.

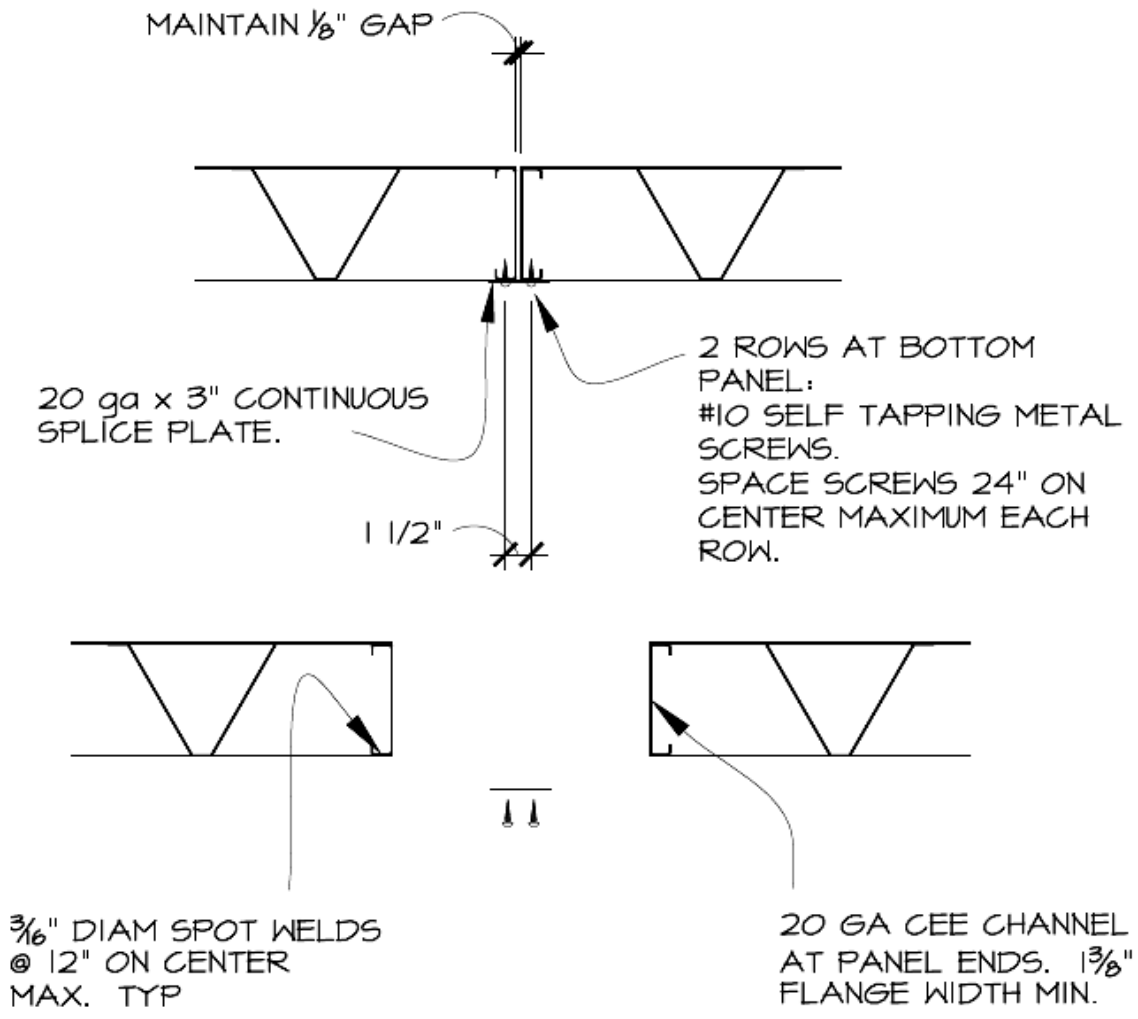

Figure 4.2-1: Truss core panel to panel connectors for climate III and 90 mph.

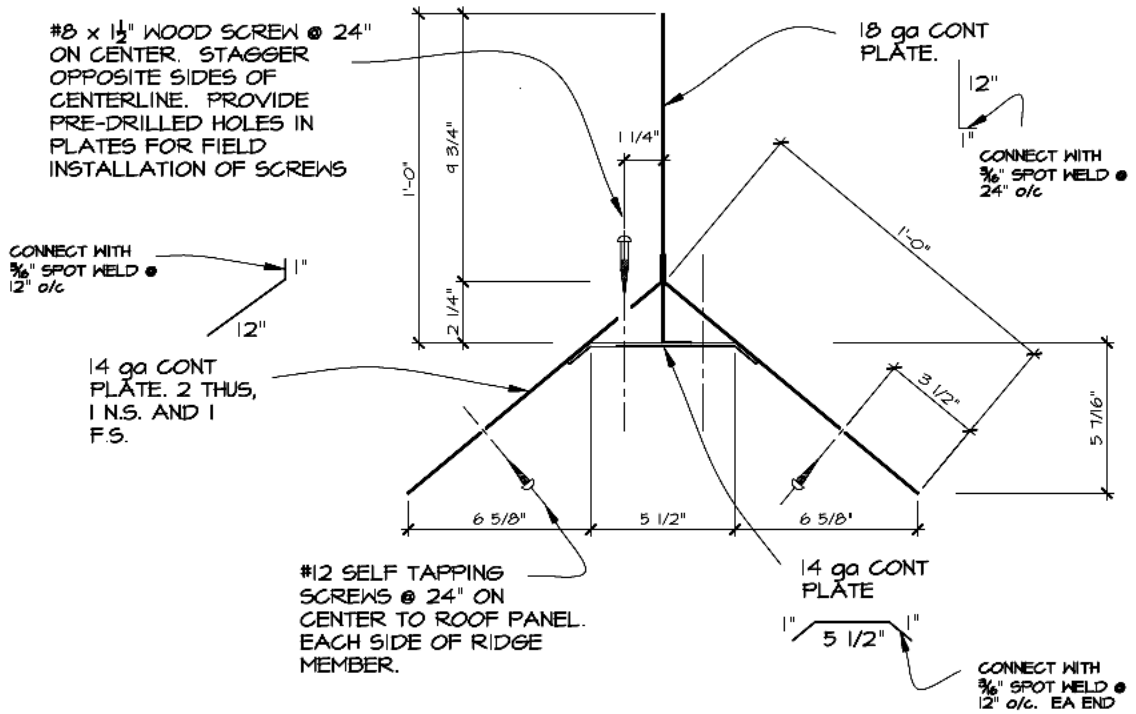

Figure 4.2-2: Truss core ridge connector for steep slope climate III and both 90 and 130 mph.

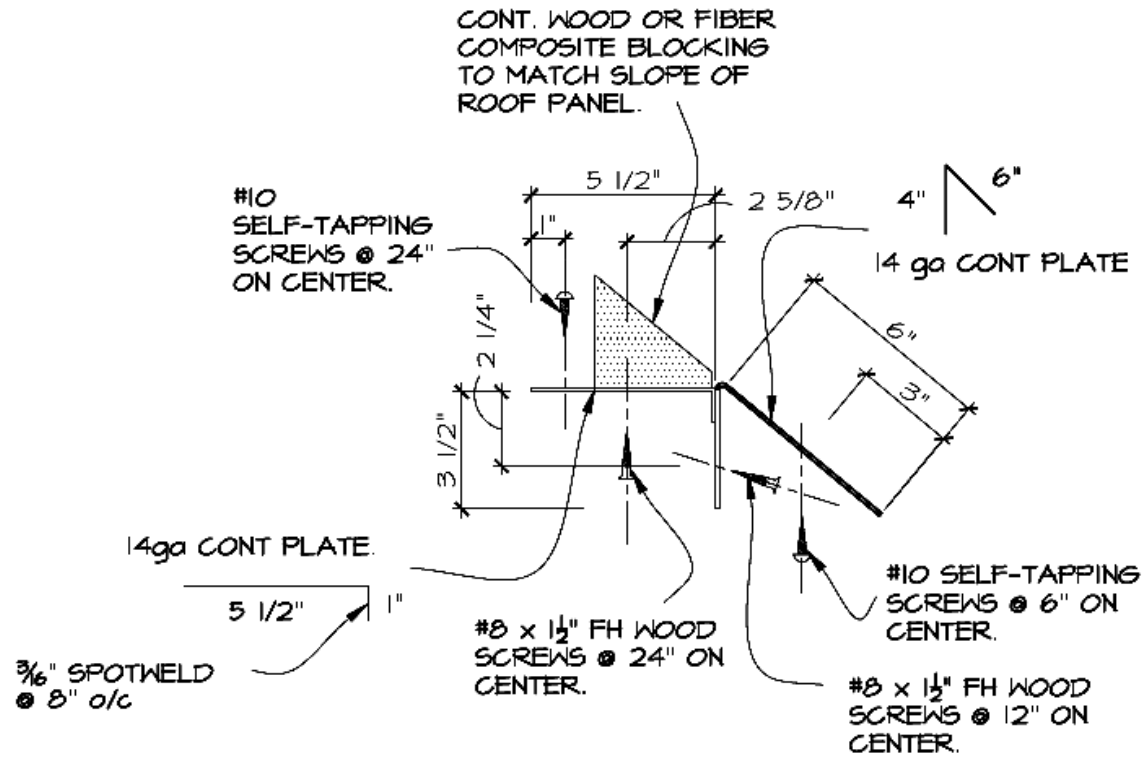

Figure 4.2-3: Truss core soffit connector, steep slope, climate III and 90 mph.

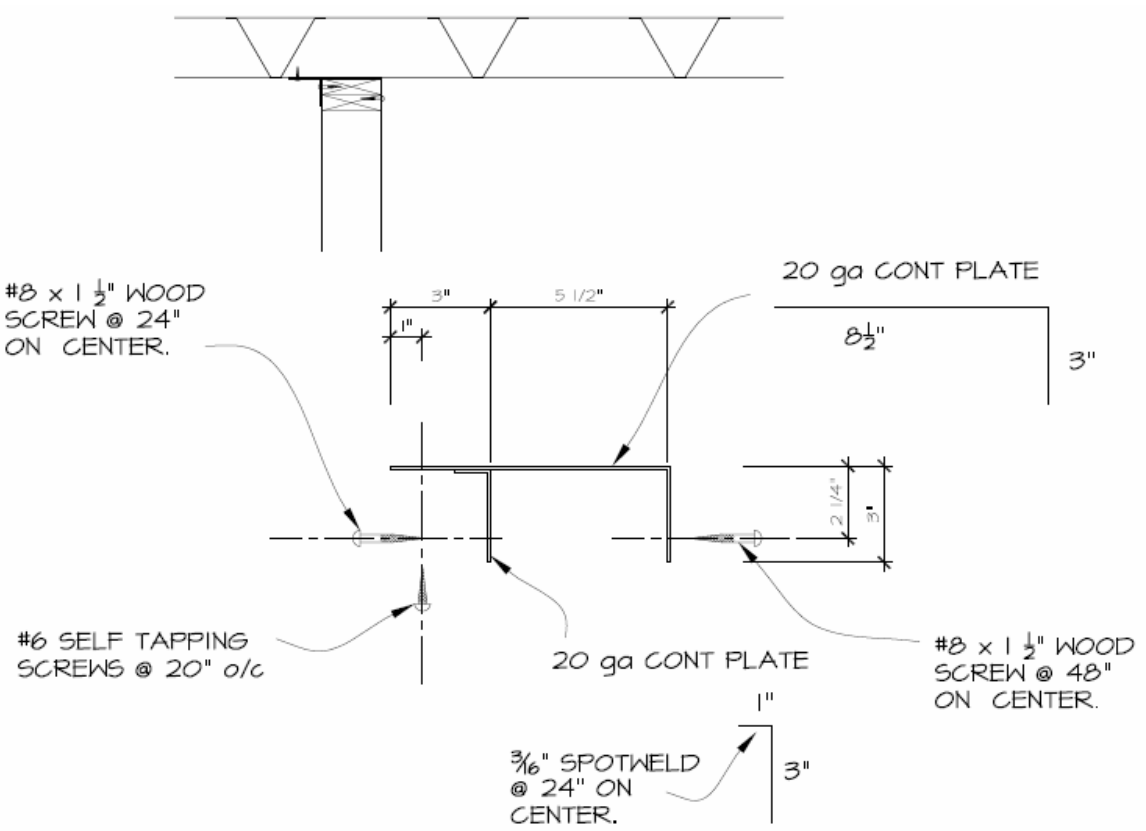

Figure 4.2-4: Truss core gable connector, shallow and steep slope, climate III 90 mph.

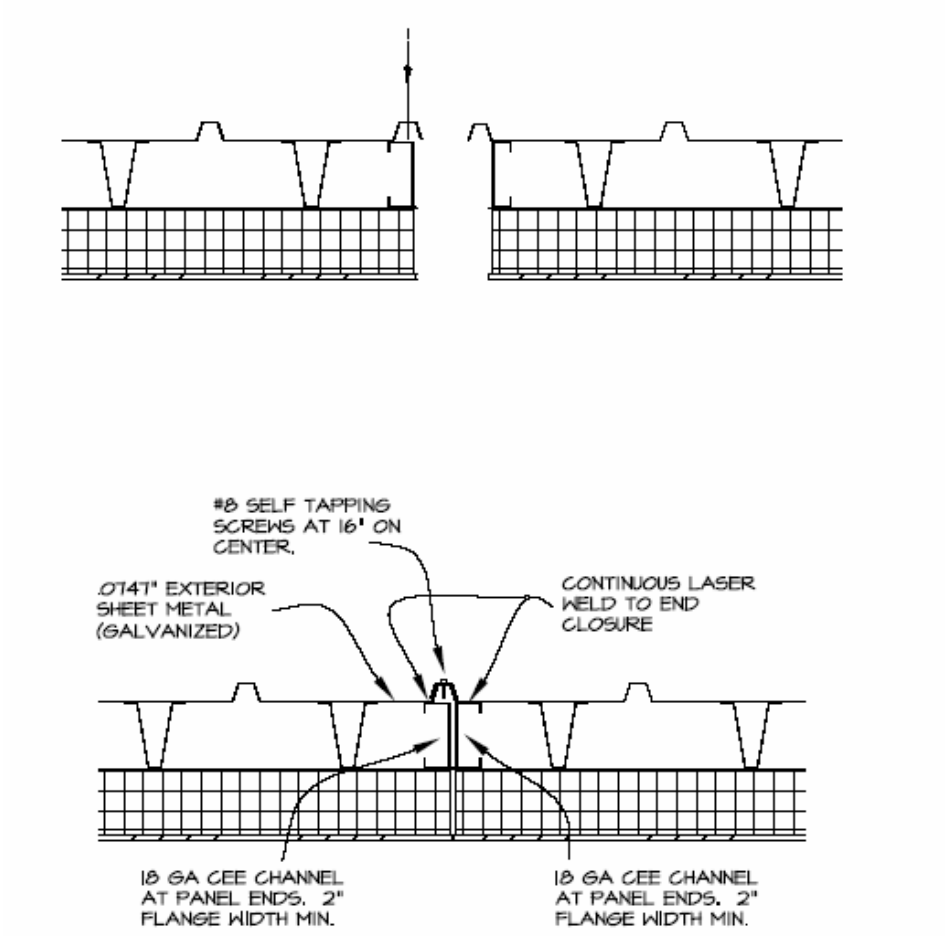

Figure 4.2-5: Truss core panel to panel connector, shallow or steep slope, integral metal roof, climate III and 90 mph.

4.3 Architectural Details

Architectural details for the truss core panel system were developed for panel to panel, ridge, soffit and gable end joints. These four architectural details are applied to eight conditions:

Figure 4.3-1: Exterior insulation, steep slope roof, conventional roofing
Figure 4.3-2: Exterior insulation, steep slope roof, integral metal roofing
Figure 4.3-3: Exterior insulation, shallow slope roof, conventional roofing
Figure 4.3-4: Exterior insulation, shallow slope roof, integral metal roofing
Figure 4.3-5: Interior insulation, steep slope roof, conventional roofing
Figure 4.3-6: Interior insulation, steep slope roof, integral metal roofing
Figure 4.3-7: Interior insulation, shallow slope roof, conventional roofing
Figure 4.3-8: Interior insulation, shallow slope roof, integral metal roofing

See Appendix I for a complete explanation of each detail including which elements of each assembly are part of the manufacturing process and which are part of the field installation.

4.3.1 Panel to Panel Joints

The panel to panel joint running parallel to the V-shaped web within the truss core panel must transfer all loads between adjacent panels. In the structural analysis, wind and live loads, concentrated loads and in plane wind shearing loads are considered. In the panel to panel joint for exterior foam panels (Figures 4.3-1 through 4.3-4), the structural connection between panels is made with a continuous 76 mm (3 in.) wide steel plate. This plate is fastened to the panel edges with sheet metal screws. This connection takes place on the bottom side of the panel, where it also serves to support a self-adhesive membrane vapor seal tape. For the interior foam panel designs that incorporate an integral metal roof (Figures 4.3-6, 4.3-8), the structural connection is made on the top surface of the panel by use of a lapped, self-flashing joint. This joint is fastened with sheet metal screws with integral neoprene or rubber washers. A layer of double-faced butyl sealing tape is placed between the lapped metal layers of the joint as a vapor seal and as a second layer of protection against water intrusion at the fastener penetration. For interior foam panels that employ traditional roof finishes (Figures 4.3-5, 4.3-7), the structural connection is made with a continuous 76 mm (3 in.) wide steel plate fastened to the panel edges with sheet metal screws. This connection takes place on the top structural skin of the truss core panel. The structural spline is fastened after a self-adhesive membrane vapor seal tape is applied to the joint. The field installed insulation foam can be either a one or two part PUR.

4.3.2. Ridge Joints

The ridge joint is made structurally sound by the use of a continuous, welded sheet steel connector. This connector is fastened to a continuous ridge beam. The panels are fastened to the connector with self-tapping sheet metal screws. Steel C-channel end caps are welded to the ends of the structural component of the truss core panel to provide reinforcement and to allow flexibility in locating air and vapor seals.

The ridge joint design for the exterior foam panel (Figures 4.3-1 through 4.3-4) employs field-applied foam insulation to ensure insulation continuity between panels on opposite sides of the ridge. Vapor sealing is accommodated on the structural connector. In the case of the integral metal roof design, vapor sealing also occurs at the ridge cap flashing. This vapor seal isolates the insulation layer from vapor penetration from the exterior, as is required for this approach. Ridge joint design for the interior foam panel (Figures 4.3-5 through 4.3-8) requires field-applied PUR or rigid foam insulation on the interior of the assembly in plane with the panel insulation. Blocking must be included at the ridge to allow attachment of fireproofing and finish materials as required. The ridge beam is a potential thermal bridge in this design, so should be constructed of wood or other low-thermal conductivity material. Vapor sealing is accomplished on the exterior side of the assembly. Figures 4.3-6 and 4.3-8 show a vented option, where air is allowed out of the structural component at the ridge through openings created by cutting back the peaks of the metal corrugations prior to welding the steel cap to the panel end. These

openings are covered by a sheet metal ridge cap and venting is ensured by use of an air-permeable profile filler under the edges of this cap.

4.3.3. Soffit Joints

The soffit connection allows the panel to cantilever beyond the face of the exterior wall of the building. This configuration allows maximum architectural flexibility, and facilitates quick field assembly. A welded sheet steel connector is utilized. In conjunction with a continuous beveled bearing block, this connector serves to support the loads imposed by gravity, uplift forces imposed by wind, and any residual thrust forces encountered at the soffit location. The panel is fastened to the connector with self-tapping sheet metal screws along the length of the connector.

For the exterior foam panel (Figures 4.3-1 through 4.3-4), the crucial concern at the soffit is ensuring the continuity of the insulation layer to avoid thermal bridging through the structural component of the truss core panel. To accommodate fastening of this layer, blocking is installed in the ends of the panels. Additional blocking for finish materials and rigid insulation, or prefabricated insulation/finish assemblies may then be applied as needed. Air and vapor seals are located on the structural connector. Insulation placed to the outside of these seals should be sized appropriately for the climate. This insulation layer must be made airtight with air-sealing tape or other means to avoid air infiltration into the assembly. In the case of the integral metal roof design, blocking in the insulation layer must be vapor-tight, and all edges must be sealed. This vapor seal isolates the insulation layer from vapor penetration from the exterior, as is required for this approach. The soffit design for the interior foam panel (Figures 4.3-5 through 4.3-8) is simpler, due to the interior location of the roof insulation layer. As with the exterior foam panel design, air and vapor seals are located on the structural connector. Blocking is again employed to provide fastening surfaces for finish materials. Figures 4.3-6 and 4.3-8 show a vented option, with perforated blocking used at this location. This accommodation for venting must be designed to drain condensation that may form under some climatic conditions. Continuity of the insulation layer is ensured by use of field-applied foam at the wall/roof joint, as shown. This insulation may be installed through holes drilled into the cavity from below.

4.3.4. Gable End Wall Joints

The gable end wall is structurally fastened to the roof panel by the use of a continuous welded sheet steel connector. Continuous support of the panel is provided by beam or bracket supports at the ridge, and in plane with the exterior bearing wall on the soffit end of the panel. Vapor sealing is accomplished with double-faced butyl tape applied to the top plate of the wall assembly, and to the top of the structural connector.

Gable end wall joint design for the exterior foam panel (Figures 4.3-1 through 4.3-4) requires the use of rigid foam insulation and blocking to wrap the fascia and soffit faces of the panel to avoid thermal bridging. This insulation layer must be made airtight with air-sealing tape or other means to avoid air infiltration into the assembly. In the case

of the integral metal roof design, blocking in the insulation layer must be vapor-tight, and all edges must be sealed. This vapor seal isolates the insulation layer from vapor penetration from the exterior, as is required for this approach. Additional blocking for finish materials and rigid insulation, or prefabricated insulation/finish assemblies may then be applied as needed. The beam or bracket supports are potential locations for thermal bridges or air infiltration. They must be constructed of low thermal conductivity materials and detailed carefully to avoid these potential problems. Gable end wall joint design for the interior foam panel (Figures 4.3-5 through 4.3-8) uses field-applied PUR to ensure insulation continuity at the joint. This insulation may be applied after panel installation by means of holes drilled into the joint cavity from below. If continuous beams are used to support the panel, they must be made of low thermal conductivity materials to avoid thermal bridging. Finish materials may be applied directly to the panel, or to blocking, as required.

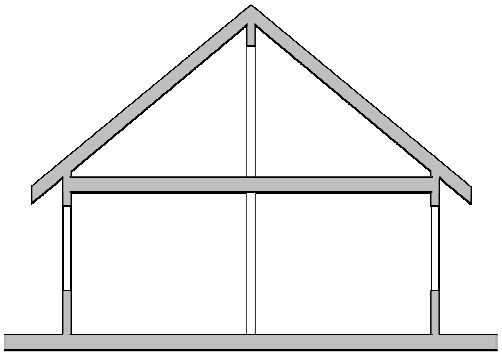

Figure 4.3-1:
Truss core panel, exterior insulation, steep slope, traditional roof finish.

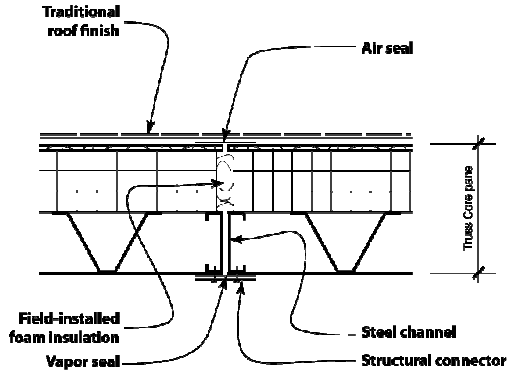

Panel to Panel Joint

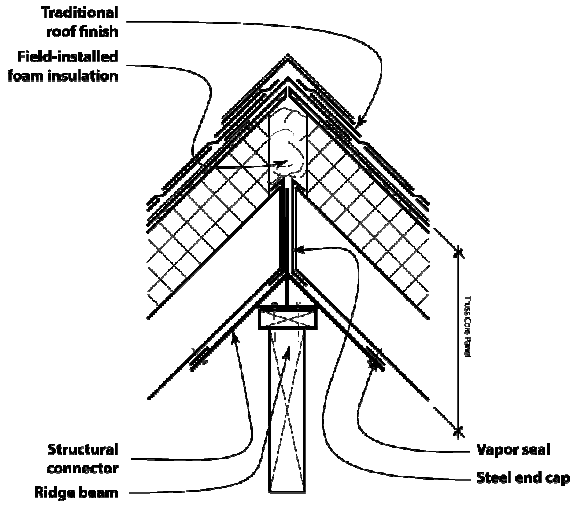

Ridge Joint

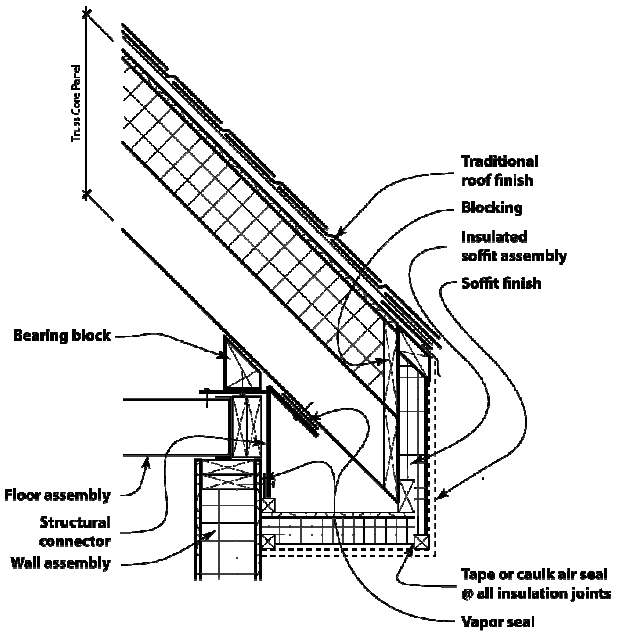

Soffit Joint

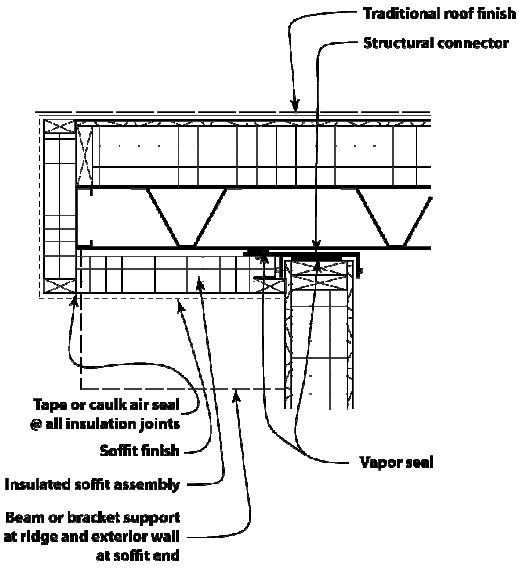

Gable End Wall Joint

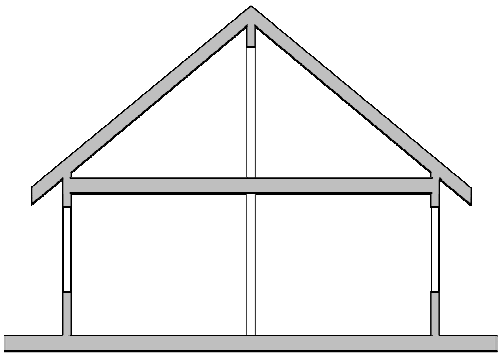

Figure 4.3-2:
Truss core panel, exterior insulation, steep slope, integral metal roof.

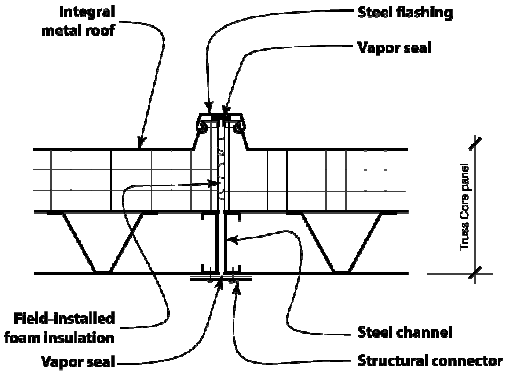

Panel to Panel Joint

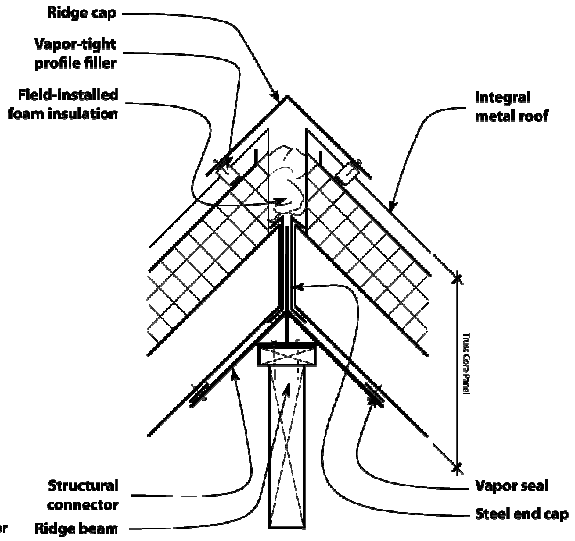

Ridge Joint

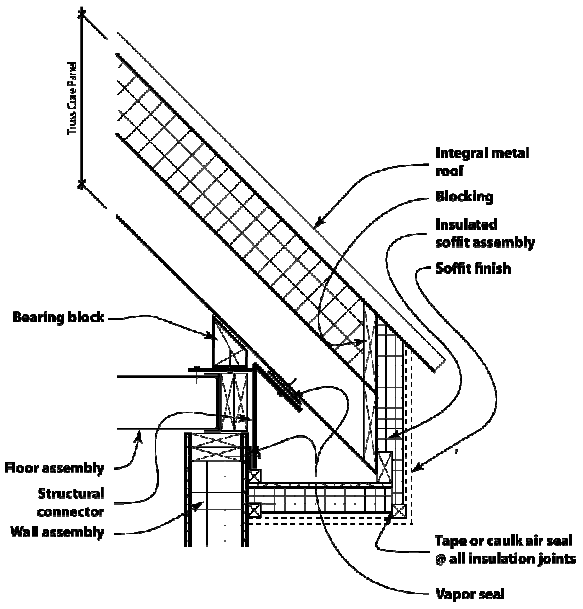

Soffit Joint

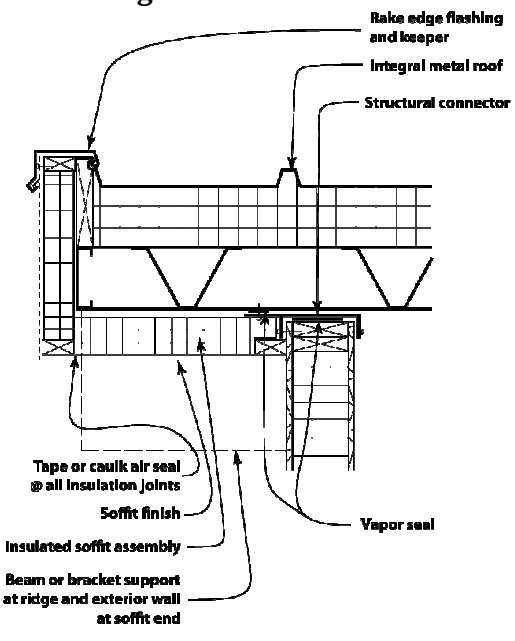

Gable End Wall Joint

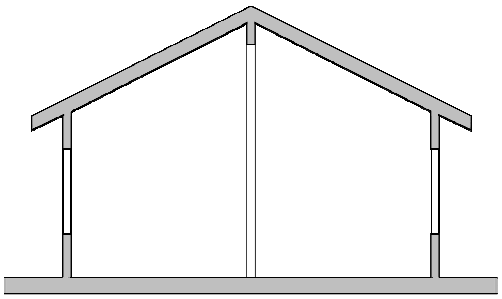

Figure 4.3-3:
Truss core panel, exterior insulation, shallow slope, traditional roof finish.

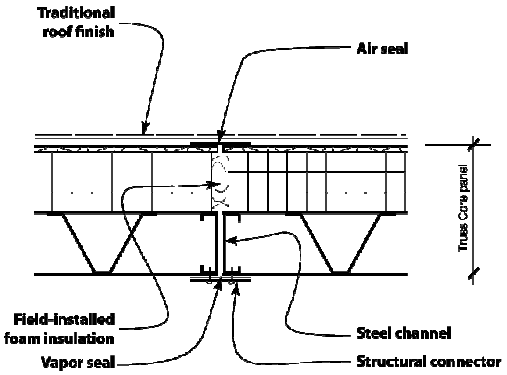

Panel to Panel Joint

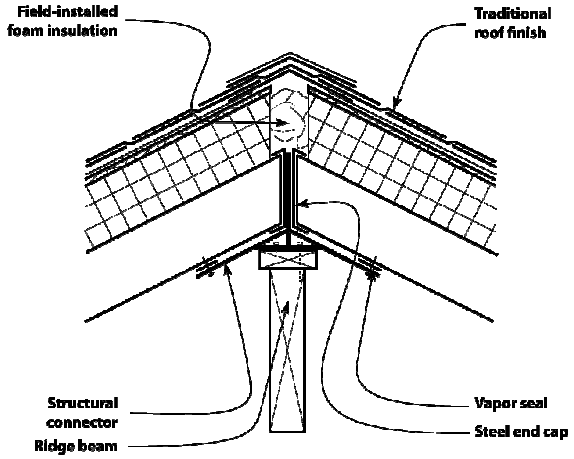

Ridge Joint

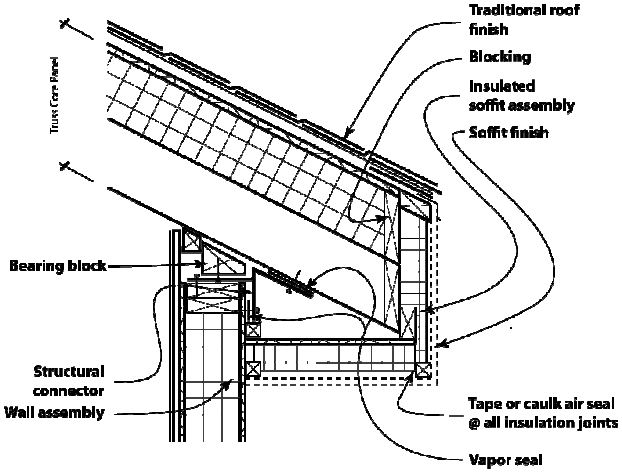

Soffit Joint

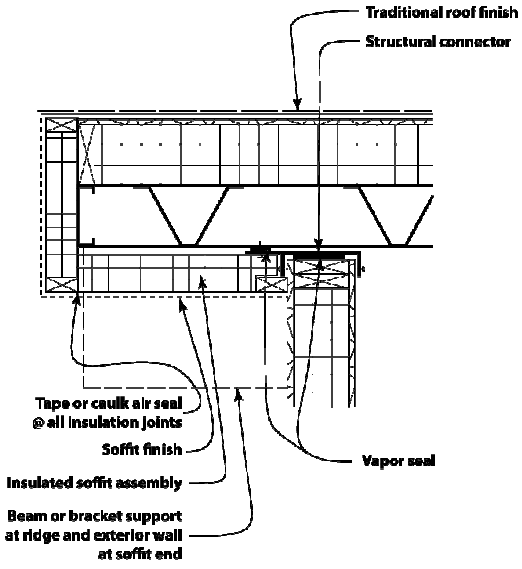

Gable End Wall Joint

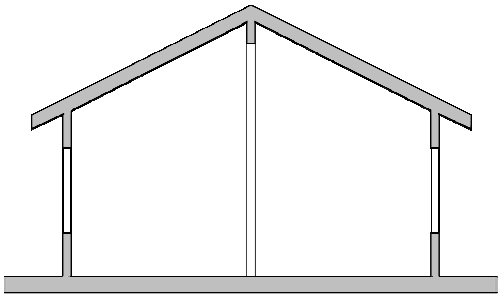

Figure 4.3-4:
Truss core panel, exterior insulation, shallow slope, integral metal roof.

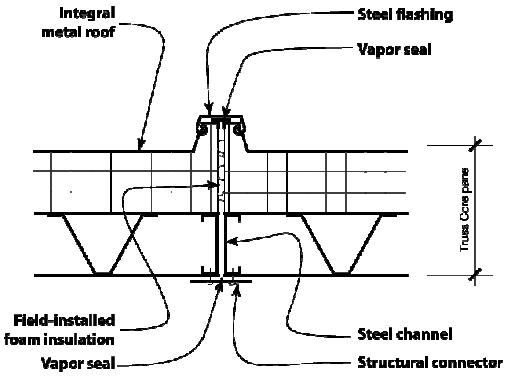

Panel to Panel Joint

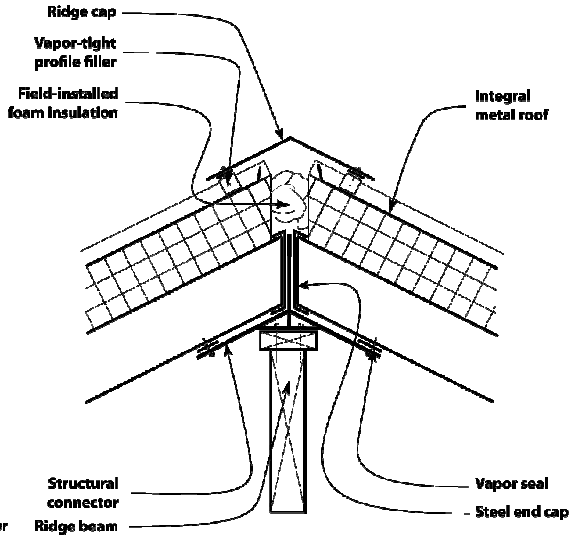

Ridge Joint

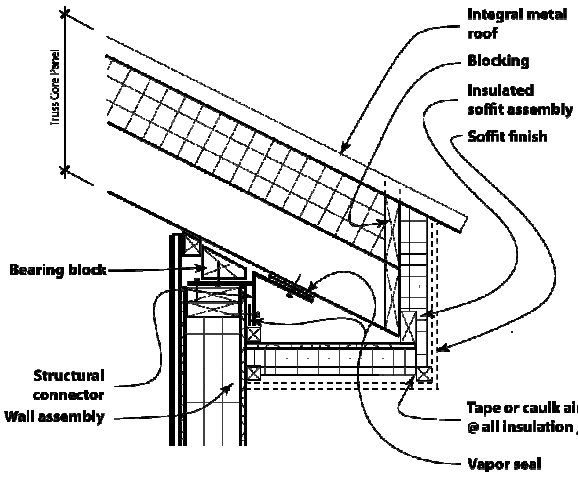

Soffit Joint

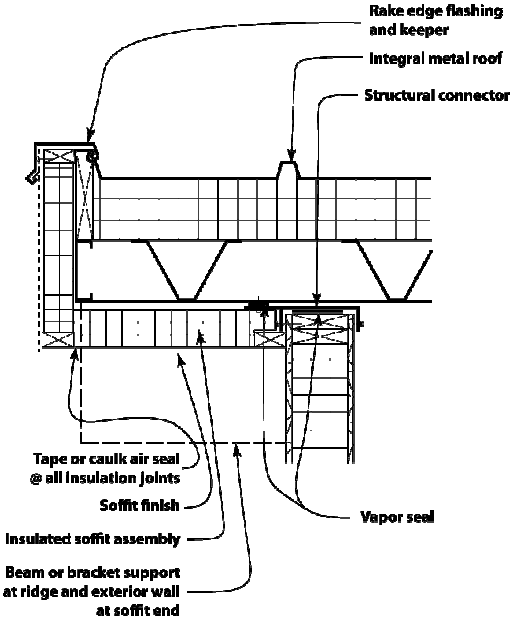

Gable End Wall Joint

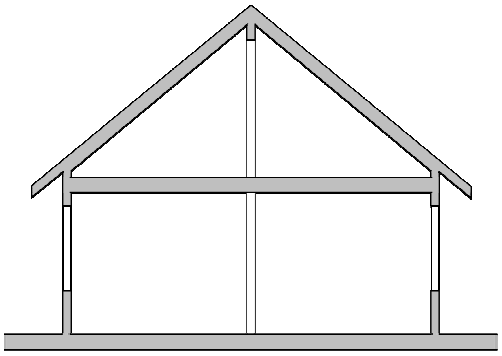

Figure 4.3-5:
Truss core panel, interior insulation, steep slope, traditional roof finish.

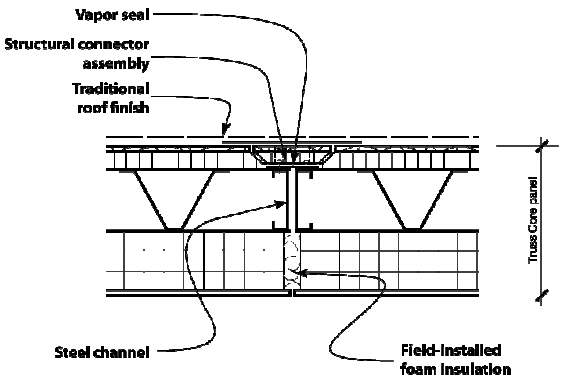

Panel to Panel Joint

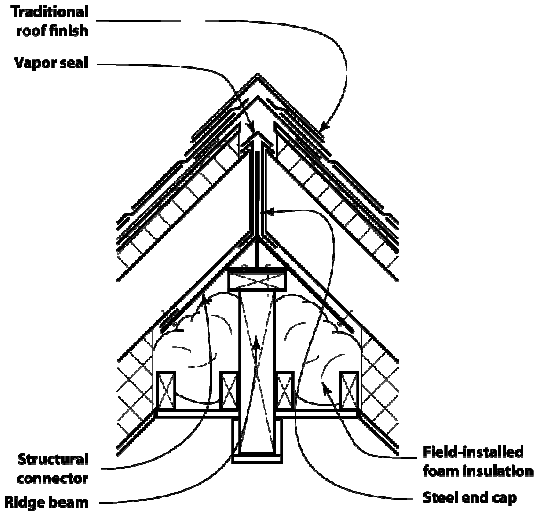

Ridge Joint

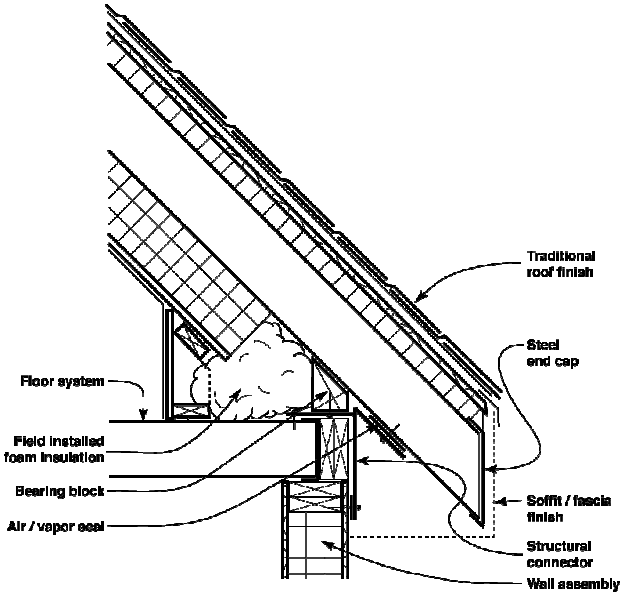

Soffit Joint

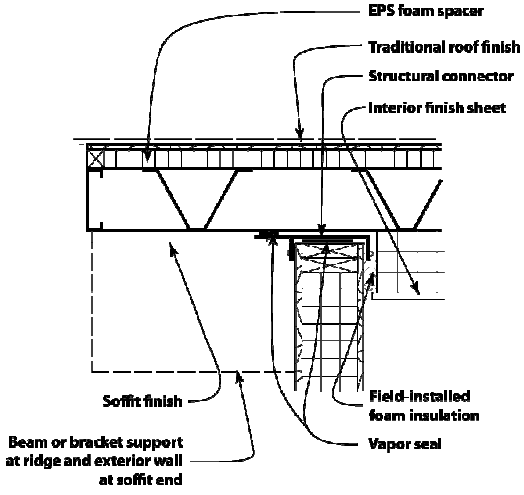

Gable End Wall Joint

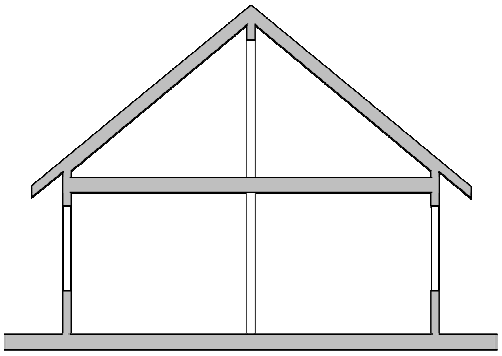

Figure 4.3-6:
Truss core panel, interior insulation, steep slope, integral metal roof.

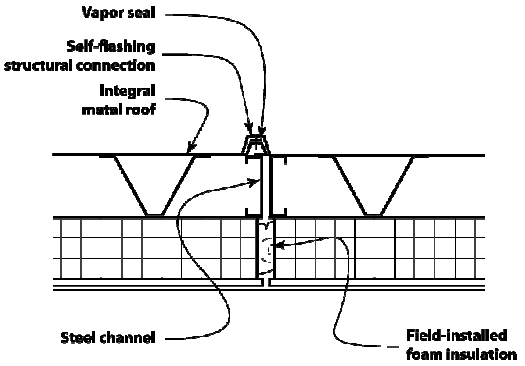

Panel to Panel Joint

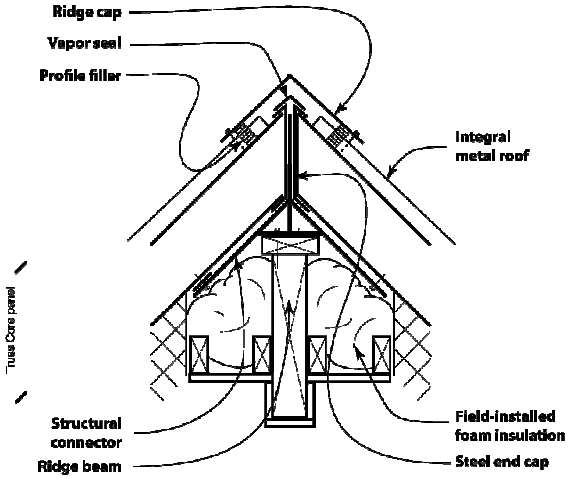

Ridge Joint

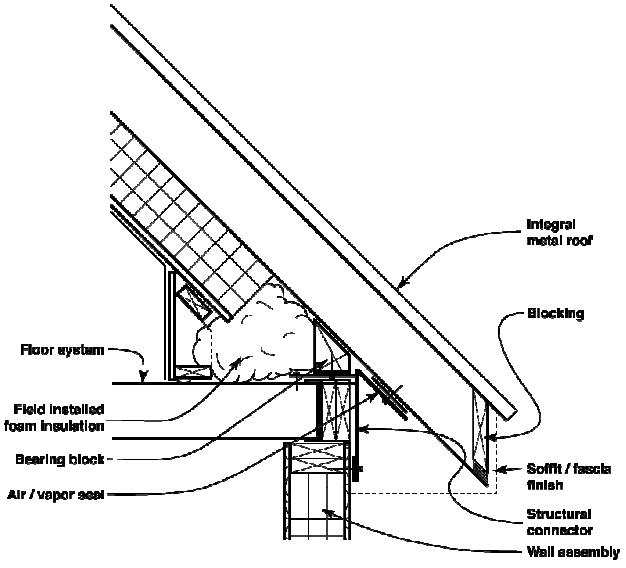

Soffit Joint

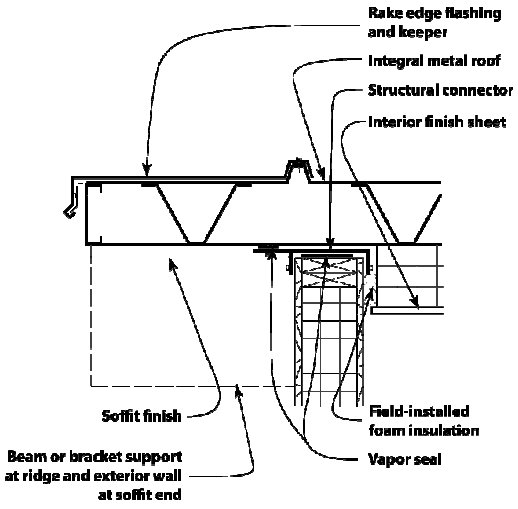

Gable End Wall Joint

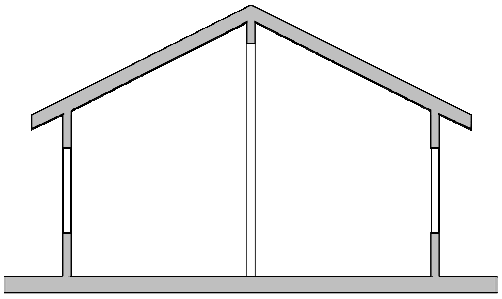

Figure 4.3-7:
Truss core panel, interior insulation, shallow slope, traditional roof finish.

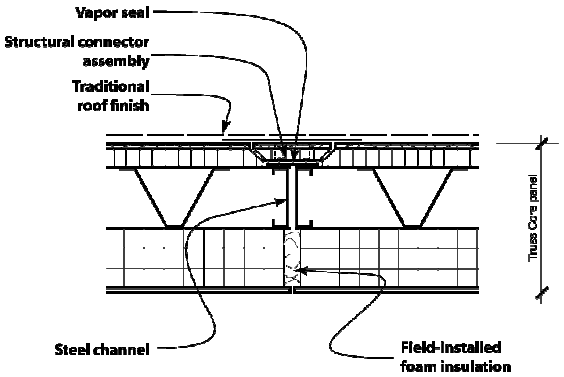

Panel to Panel Joint

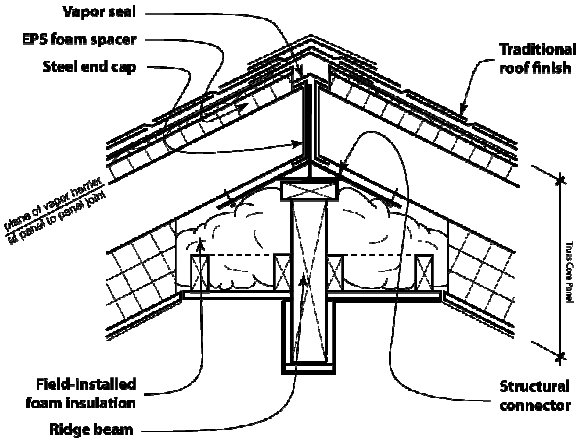

Ridge Joint

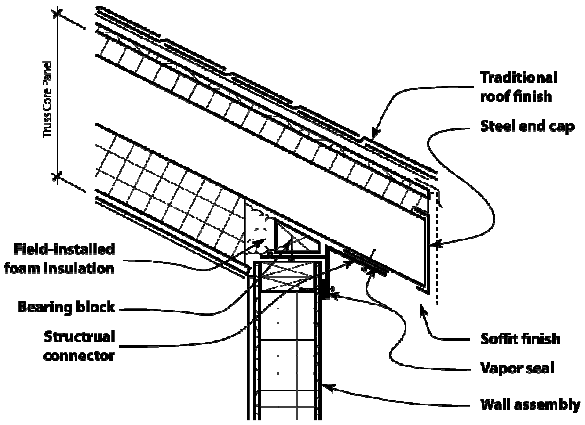

Soffit Joint

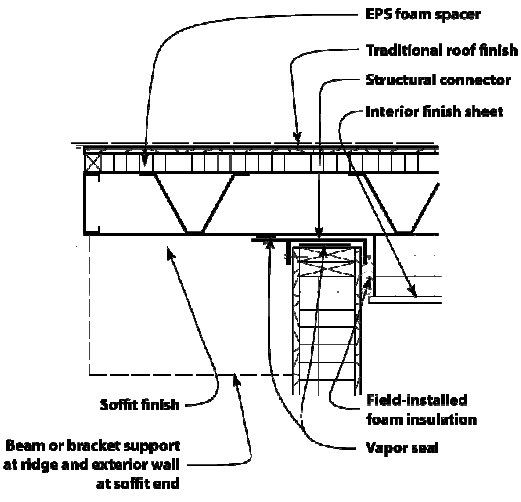

Gable End Wall Joint

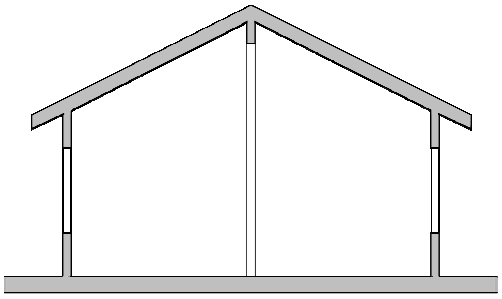

Figure 4.3-8:
Truss core panel, interior insulation, shallow slope, integral metal roof.

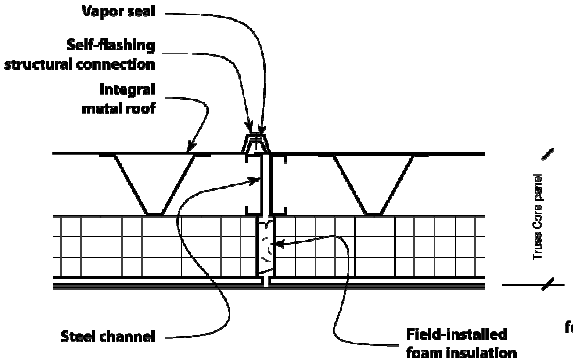

Panel to Panel Joint

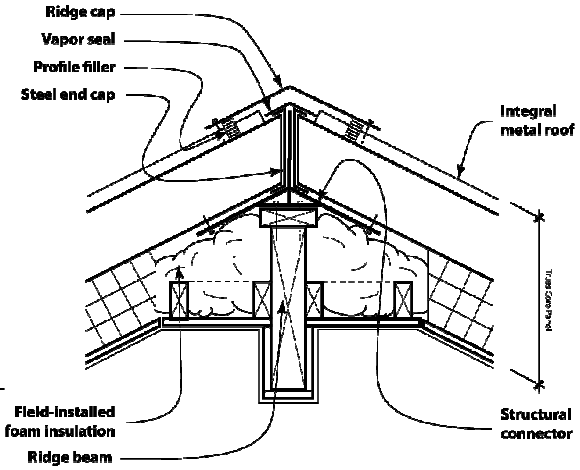

Ridge Joint

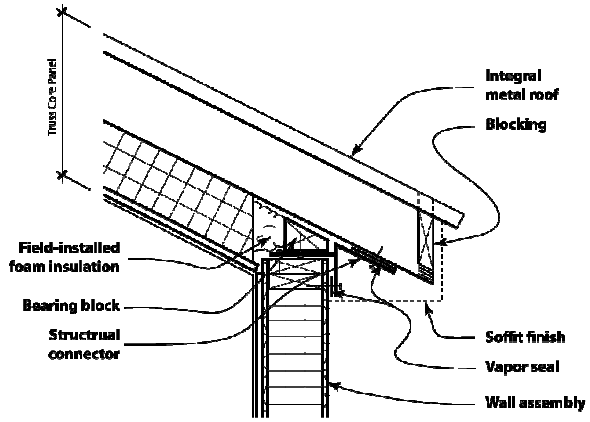

Soffit Joint

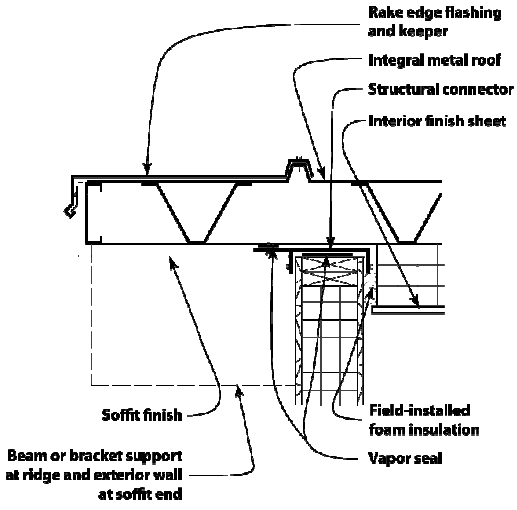

Gable End Wall Joint

4.4 Manufacturing Plan

The key steps in panel manufacture are: 1) form and galvanize the sheet metal components, 2) foam the PUR insulation between the finish face sheet and the truss core face sheet, 3) laser weld the webs and second face sheet, and 4) add interior and exterior finish sheets as required. Figure 4.4-1 illustrates the sequence for the foaming and welding steps. Initially, the project team planned to fabricate the truss core structure first and then foam the PUR. Discussions with BASF, a producer of PUR, revealed the pressure during foaming could cause the truss core panel face sheet to buckle between the V-webs (Figure 4.4-2). The proposed approach, which begins with forming a sandwich panel, eliminates the risk of buckling the structural components during foaming. The process also has the added benefit of ensuring that the face sheet surface will be flat and therefore enabling good contact with the webs during welding.

A production flow chart for manufacturing a truss core panel with an integrated metal roof is shown in Figure 4.4-3. The process of fabricating a roof panel begins with straightening the steel that is delivered in coils. Different sized sheets are cut to produce the top sheet, bottom sheet, V webs and edge channels. The V webs and channel edges are cold formed from the cut sheets. Each of the panel sheet metal components is galvanized. The PUR is foamed between the finish face sheet and one of the truss core face sheets prior to any welding. Once the PUR has cured, the webs and longitudinal edge channels are welded to the truss core face sheet. There is no issue with welding webs to the truss core face sheet after foaming because laser welding heats a small concentrated area. Once the webs are welded to the face sheet, the remaining face sheet is welded to the webs and longitudinal channels. This progressive welding process increases the amount of material handling required in the factory, but has little impact on variable costs as there is no additional equipment required (i.e., same number of welds regardless of sequence). The panel edges are cut to the roof slope and the cut edges are capped as required.

Factory finish of the panel depends on the panel configuration (see Figures 2.1-1 through 2.1-4). For panels with an integral metal roof, the profiled metal roof is coated with PVDF for long term weather resistance. PVDF is applied to the surface like paint.

The biggest challenge in shipping the completed panel to the construction site is minimization of any damage to the sheet rock edges and face. Field repair of small sheet rock damage can be managed with putty and sanding. Significant damage may require rework at the factory, with accompanying increase in shipping cost. To mitigate any sheet rock damage, the BOM and production flow includes provision for attachment of a plastic edge and face protector for the inner surface of the panel.

1. Create sandwich panel with PUR foam. One surface is a finish face sheet, the other surface is a truss core face sheet that has been galvanized prior to foaming.

2. Laser weld channels. Channels are galvanized prior to welding.

3. Laser weld final face sheet. Final face sheet is galvanized prior to welding.

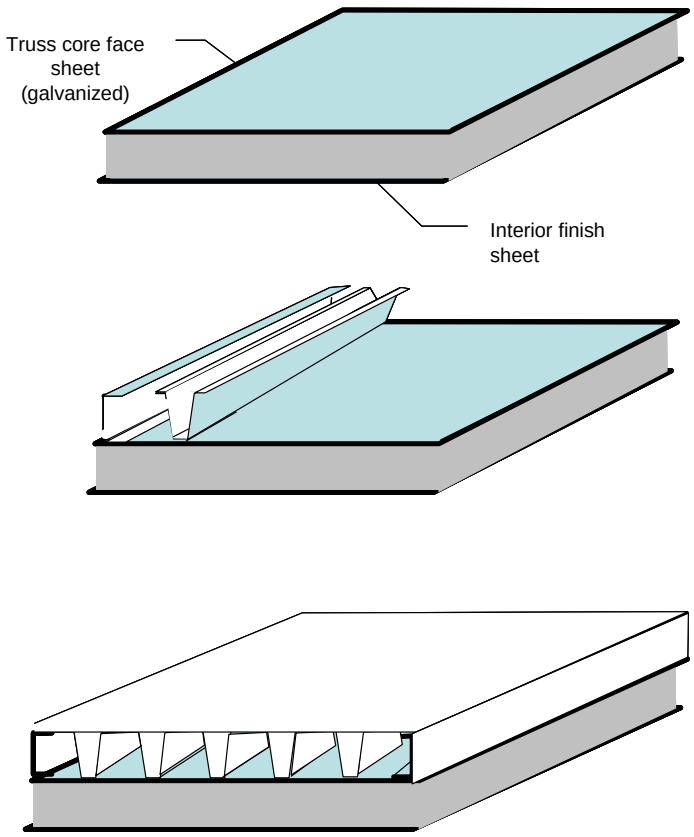

Figure 4.4-1: Illustration of the foaming and welding steps for a truss core panel with exterior foam.

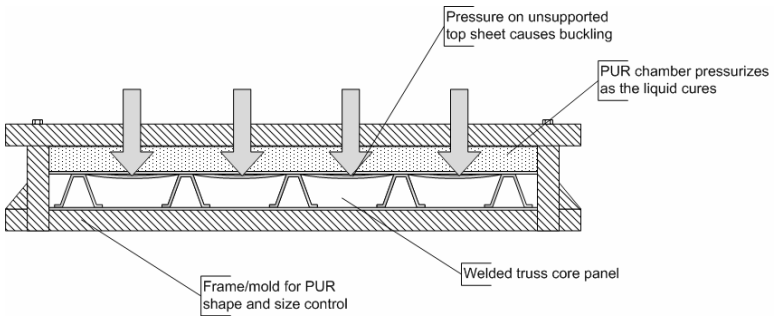

Figure 4.4-2: The pressure during foaming can cause the face sheet of the truss core panel to buckle.

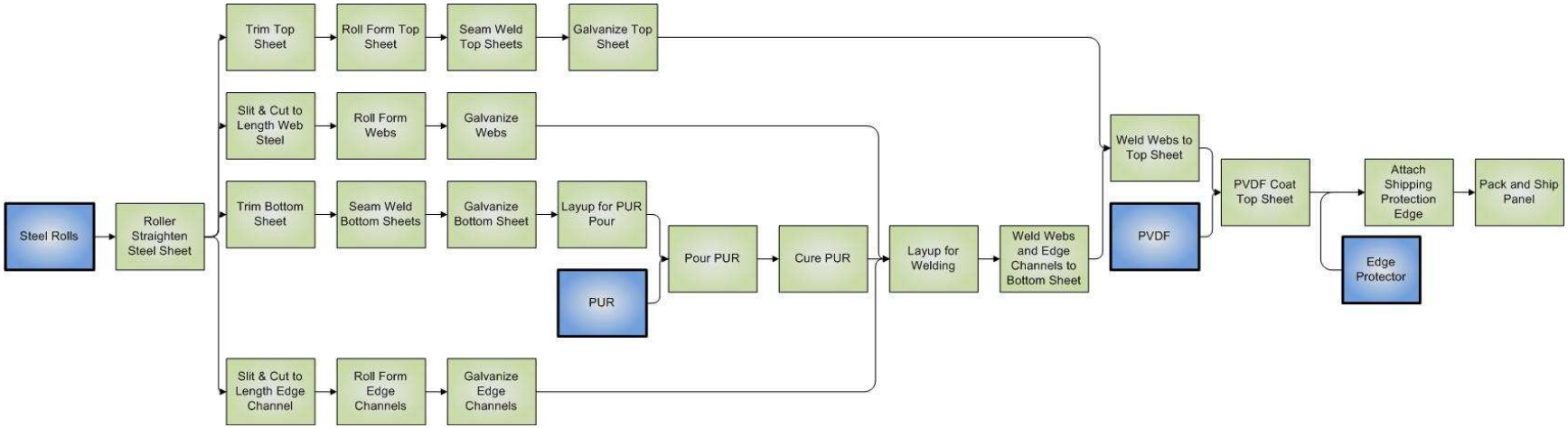

Figure 4.4-3: Production flow for an insulated truss core panel with integral metal roof.

5.0 Stiffened Plate Panel

In this section, stiffened plate panel geometries, connections and architectural details are presented for houses with gable style roofs. The roof slope is either steep or shallow. The details provided in this section are a result of extensive structural and hygrothermal analysis, and careful consideration of architectural constraints.

5.1 Panel Geometries

Examples of stiffened plate panels as delivered to the job site are shown in Figures 5.1-1 and 5.1-2. The stiffened plate panel is configured with either an integral metal roof (Figure 5.1-1) or an OSB exterior for finish with a traditional shingle roof (Figure 5.1-2). The edges at the ridge and soffit are cut at an angle (to accommodate the roof slope) and blocked/capped as required for moisture management. Specific dimensions for the structural and insulation components are also shown. The details regarding stiffened plate structural component geometry and foam depth depend on the climate and desired insulation R-value. Alternate dimensions for the structural or insulating components may be substituted without affecting the roof interior or exterior finish details.

The structural and insulation component dimensions shown in Figures 5.1-1 and 5.1-2 are for a roof panel subjected to climate I loading and 90 mph wind loads. The roof has a shallow 6/12 pitch and a ridge to soffit *horizontal* span of 20 ft. The panel structural component is designed to achieve a minimum weight panel for this particular set of wind, live and dead loads. The panel sheet thickness is 0.033 inches for the interior face sheet and 0.050 in for the webs. The six webs are laser welded to the interior face sheet at equally spaced intervals, 16 inches on center. The webs serve two structural functions: to provide shear stiffness and to sustain compressive or tensile bending loads. This latter function drives the webs to be thicker than the interior face sheet. The depth of the structural component is 7.25 inches, and was selected to be compatible with 2x8 construction. In addition to the foam between the 7.25 inch deep webs, there is a 5.2 inch deep layer of foam on top of the webs. The combination of foam between the webs and the foam depth on top of the webs provides R-43. Insulation beyond the minimum R-30 level is required because there is a risk of condensation at the web surface (see section 3 and appendix F).

For the stiffened plate panel with the integral metal roof (Figure 5.1-1), the integral metal roof is bonded to the PUR as part of the foaming process. The corrugations are evenly spaced such that the longitudinal edges end with corrugations. This configuration allows for a metal flashing joint at the roof surface between adjacent panels (see section 5.3). A PVDF coating is applied to the metal roof exterior surface to provide a durable and architecturally acceptable finish. The panel that is compatible with standard roofing materials (Figure 5.1-2) is finished with a 0.4375 (7/16) inch thick OSB sheet. This OSB nailbase is bonded to the PUR foam as part of the foaming process (see section 5.4).

The stiffened plate panel is limited to climate I and II with 90 mph wind loads. The panel is not recommended for climate III because it is heavier than the truss core panel and, in some cases, the web thickness exceeds the cold roll forming limits (0.1 in. maximum sheet thickness for cold rolling operations). The panel is also not recommended for 130 mph wind loads because both an interior and an exterior face sheet (as in the truss core panel) are required to sustain the wind uplift loads. Architectural and constructability issues restrict the foam application to exterior surfaces (see section 2).

Stiffened plate panel design details are summarized in Table 5.1-1 for climates I and II. In particular, structural and insulating component geometries (Figure 5.1-3) are listed for shallow and steep sloped roof pitches and a 20 ft. horizontal span from ridge to soffit. For each combination of loading, span and roof slope, the minimum weight structural component is detailed in Table 5.1-1. Structure and panel weight increase with increasing slope and/or increasing load. The lightest weight stiffened plate panel designs are typically limited by the web crippling failure criteria. Thus, the web thickness and spacing vary considerably from climate to climate and between roof pitches. The foam depth is selected to prevent condensation. For climate I, the net effect is an insulation level that exceeds the target value of R-30. For climate II, the insulation required to achieve the target minimum of R-40 is nearly sufficient to prevent condensation at the web/foam interface.

Stiffened plate panel designs for horizontal spans (from ridge to soffit) ranging from 12 to 20 ft for climates I and II are presented in Appendix G.

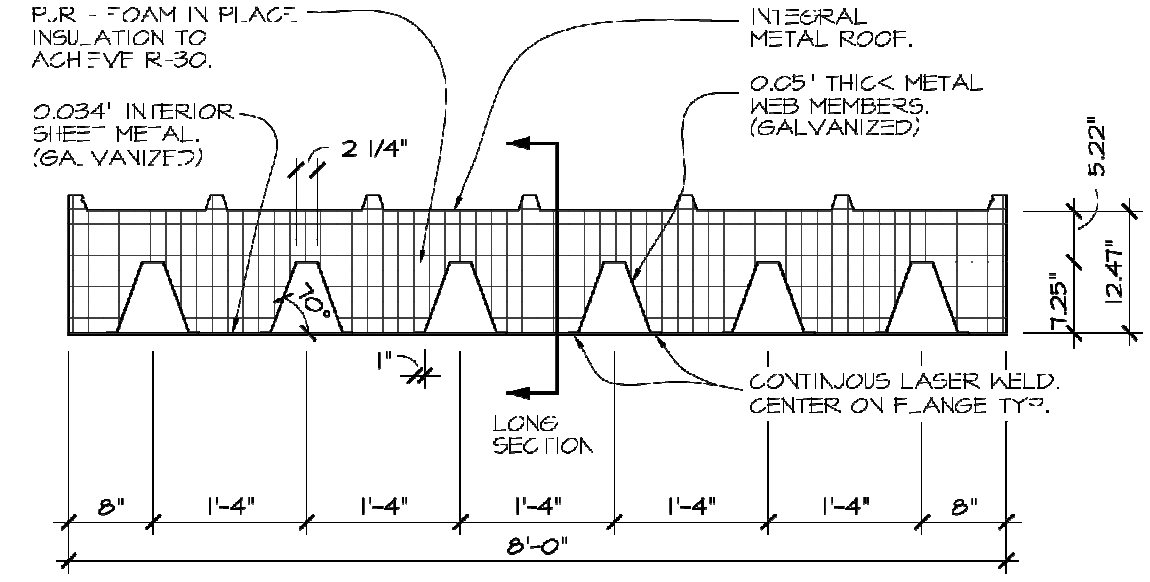

TRANSVERSE SECTION

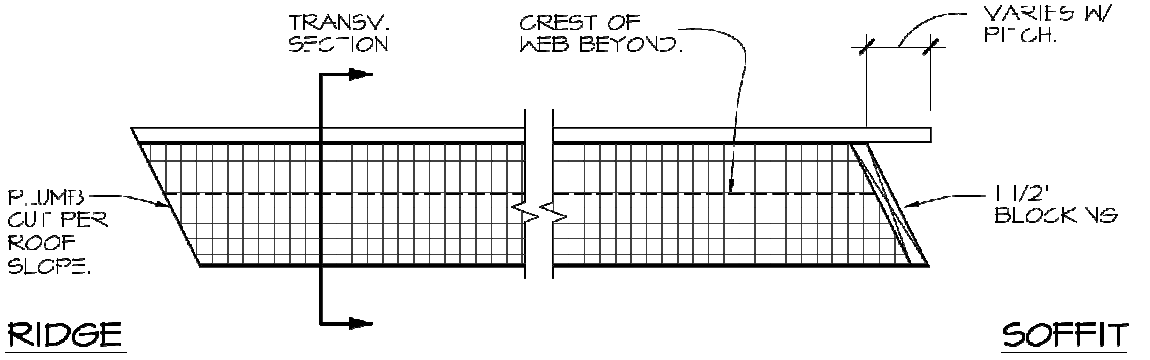

LONGITUDINAL SECTION

STIFFENED PLATE PANEL - CLIMATE I - 6/12 PITCH

INTEGRAL METAL ROOF

Figure 5.1-1: Stiffened plate panel with integral metal roof designed for climate I, 90 mph, 6/12 roof pitch.

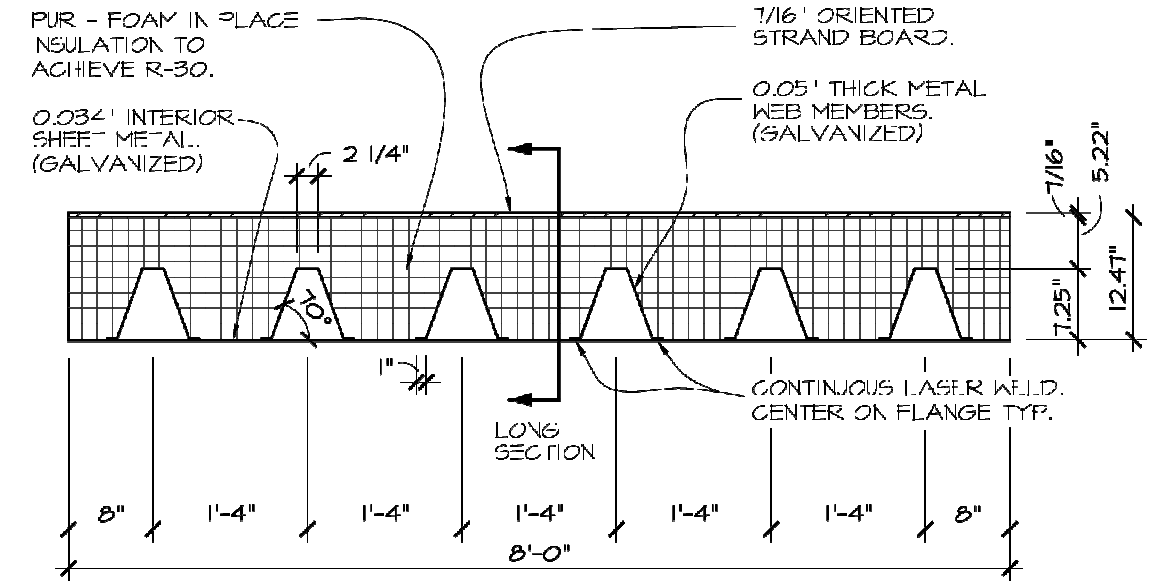

TRANSVERSE SECTION

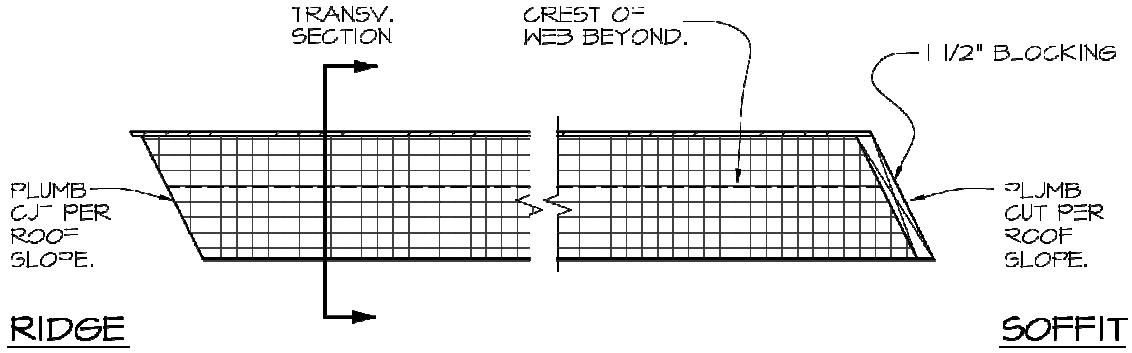

LONGITUDINAL SECTION

STIFFENED PLATE PANEL - CLIMATE I - 6/12 PITCH

APPLIED ROOF FINISH

Figure 5.1-2: Stiffened plate panel with OSB exterior finish sheet designed for climate I, 90 mph, 6/12 roof pitch.

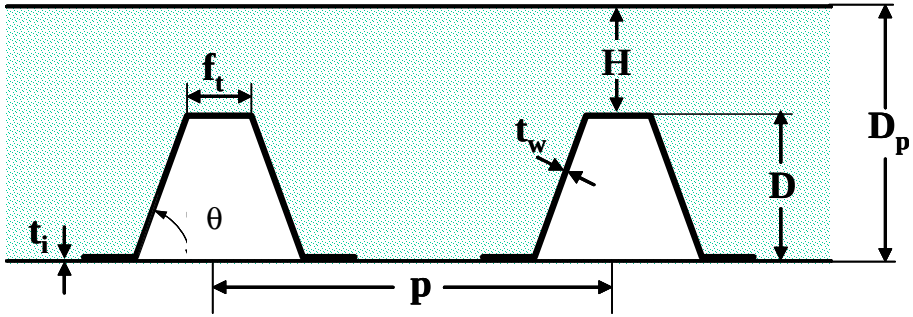

Figure 5.1-3: Stiffened plate panel geometry.

Table 5.1-1: Specifications for the stiffened panel with interior sheet designed for a 6.1 m horizontal span. Panels have been optimized for minimum weight.

Climate and Roof Pitch	Stiffened Plate Structural Component							Foam		Panel[1]	
	Structure depth D [in.]	Structure weight [lb/ft^2]	Interior sheet thickness t_i [in.]	Web pitch p [in.]	Web thickness t_w [in.]	Web angle θ [°]	Exterior flange width f_t [in.]	Foam depth on top of webs H [in.]	R Value (ft^2-°F-hr/Btu)	Panel depth D_p [in.]	Panel weight [lb/ft^2]
I-6/12	7.25	3.95	0.033	16	0.050	70	2.24	5.22	43	12.47	5.84
I-10/12	7.25	4.70	0.038	19	0.066	70	4.53	5.22	39	12.47	6.52
II-6/12	7.25	4.49	0.036	19	0.063	65	4.06	5.22	42	12.47	6.29
II-10/12	7.25	5.64	0.034	24	0.094	60	7.13	5.22	41	12.47	7.31

[1] Excluding interior and exterior finish, including roofing materials.

5.2 Connector Details

Connectors for the stiffened plate panel were designed for the various connection points on a typical roof configuration: panel to panel, ridge, soffit, and gable end. These connectors were designed to sustain the combined live, dead and wind loads (90 mph) for climates I and II as described in Appendix C. Two gable roof configurations were considered: a shallow sloped roof (6/12 pitch) with a 20 ft soffit to ridge horizontal span, and a steep sloped roof (10/12 pitch) with a 12 ft soffit to ridge horizontal span. Because the connector design depends primarily on the wind loading, the connector designs for the stiffened plate ridge, soffit and gable end are identical to the truss core panel joints (for 90 mph wind loading) shown in Figures 4.2-1 through 4.2-4. The panel to panel joint for the stiffened plate panel (Figure 5.2-1) and the truss core panel (Figure 4.2-1) are similar in that both are comprised of a continuous sheet metal strip. However, the panel to panel joint for the stiffened plate panel (Figure 5.2-1) is a thicker (16 ga compared to 20 ga) and wider (6 in. compared to 2 in.) sheet metal strip. The thicker sheet metal is required for the stiffened plate panel to panel joint because the stiffened plate panel edge is a single face sheet, while the truss core panel edge has two face sheets with a C channel stiffener (Figure 4.2-1). A complete set of connector drawings for the stiffened plate panel can be found in Appendix H.

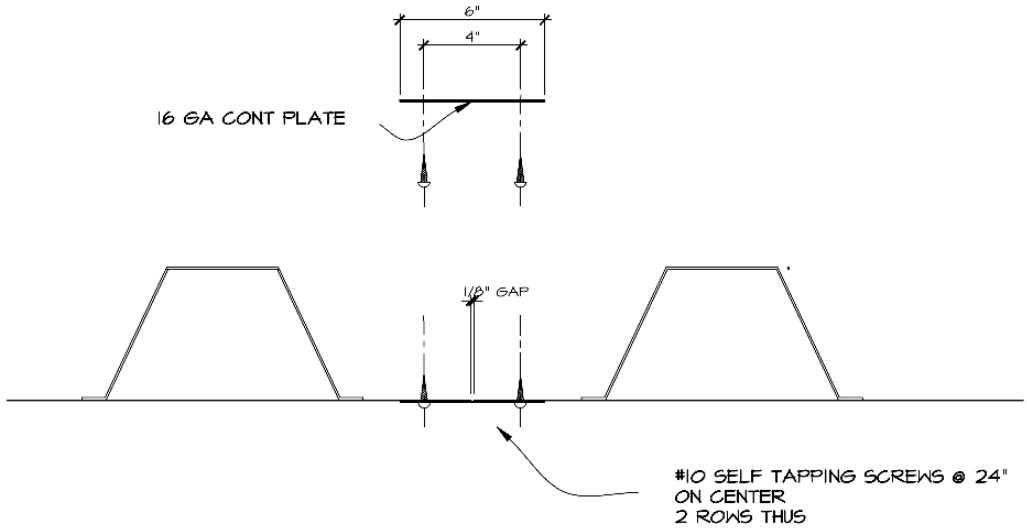

Figure 5.2-1: Stiffened plate panel to panel connector.

5.3 Architectural Details

Architectural details for the stiffened plate panel system were developed for the panel to panel, ridge, soffit and gable end joints. The following four architectural details are applied for the four conditions:

Figure 5.3-1: Steep slope roof, conventional roofing
Figure 5.3-2: Steep slope roof, integral metal roofing
Figure 5.3-3: Steep slope roof, conventional roofing
Figure 5.3-4: Steep slope roof, integral metal roofing

Appendix I includes a complete explanation of each detail including which elements of each assembly are part of the manufacturing process and which are part of the field installation.

5.3.1 Panel to Panel Joints

The panel to panel joint running parallel to the V-shaped stiffener within the stiffened plate panel must transfer all loads between adjacent panels. In the structural analysis, wind and live loads, concentrated loads and in plane wind shearing loads were considered. The structural connection at the panel to panel joint (Figures 5.3-1 through 5.3-4) is made with a continuous 3 in. wide steel plate. This plate is fastened to the panel edges with sheet metal screws. This connection takes place on the bottom side of the panel, where it also serves to support a self-adhesive membrane vapor seal tape. The integral metal roof panels (Figures 5.3-2 and 5.3-4) require an additional vapor seal at the roof surface connection to avoid vapor penetration into the foam insulation. This vapor seal is achieved with self-adhesive flexible flashing, and is covered by a prefabricated metal cap flashing.

5.3.2 Ridge Joints

The ridge joint is made structurally sound by the use of a continuous, welded sheet steel connector. This connector is fastened to a continuous ridge beam. The panels are fastened to the connector with self-tapping sheet metal screws.

The ridge joint design for the stiffened plate panel (Figures 5.3-1 through 5.3-4) employs field-applied foam insulation to ensure insulation continuity between panels on opposite sides of the ridge. Vapor sealing is accommodated on the structural connector. In the case of the integral metal roof design (Figures 5.3-2 and 5.3-4), vapor sealing also occurs at the ridge cap flashing. This vapor seal isolates the insulation layer from vapor penetration from the exterior.

5.3.3 Soffit Joints

The soffit connection allows the panel to cantilever beyond the face of the exterior wall of the building. This configuration allows maximum architectural flexibility, and facilitates quick field assembly. A welded sheet steel connector is utilized. In conjunction with a continuous beveled bearing block, this connector serves to

support the loads imposed by gravity, uplift forces imposed by wind, and any residual thrust forces encountered at the soffit location. The panel is fastened to the connector with self-tapping sheet metal screws along the length of the connector.

For the stiffened plate panel (Figures 5.3-1 through 5.3-4), the crucial concern at the soffit is ensuring the continuity of the insulation layer to avoid thermal bridging through the structural component of the panel structure. To accommodate fastening of this layer, blocking is installed in the ends of the panels, both within the section of the stiffener, and within the insulation layer. Additional blocking for finish materials and rigid insulation, or prefabricated insulation / finish assemblies may then be applied as needed. Air and vapor seals are located on the structural connector. Insulation placed to the outside of these seals should be sized appropriately for the climate. This insulation layer must be made airtight with air-sealing tape or other means to avoid air infiltration into the assembly. In the case of the integral metal roof design (Figures 5.3-2 and 5.3-4), blocking in the insulation layer must be vapor-tight, and all edges must be sealed. This vapor seal isolates the insulation layer from vapor penetration from the exterior, as is required for this approach.

5.3.4 Gable End Wall Joints

The gable end wall is structurally fastened to the roof panel by the use of a continuous welded sheet steel connector. Continuous support of the panel is provided by beam or bracket supports at the ridge, and in plane with the exterior bearing wall on the soffit end of the panel. Vapor sealing is accomplished with double-faced butyl tape applied to the top plate of the wall assembly, and to the top of the structural connector.

Gable end wall joint design for the stiffened plate panel (Figures 5.3-1 through 5.3-4) requires the use of rigid foam insulation and blocking to wrap the fascia and soffit faces of the panel to avoid thermal bridging. This insulation layer must be made airtight with air-sealing tape or other means to avoid air infiltration into the assembly. In the case of the integral metal roof design (Figures 5.3-2 and 5.3-4), blocking in the insulation layer must be vapor-tight, and all edges must be sealed. This vapor seal isolates the insulation layer from vapor penetration from the exterior, as is required for this approach. Additional blocking for finish materials and rigid insulation, or prefabricated insulation / finish assemblies may then be applied as needed. The beam or bracket supports are potential locations for thermal bridges or air infiltration. They must be constructed of low thermal conductivity materials and detailed carefully to avoid these potential problems.

Figure 5.3-1:
Stiffened plate panel, steep slope, traditional roof finish.

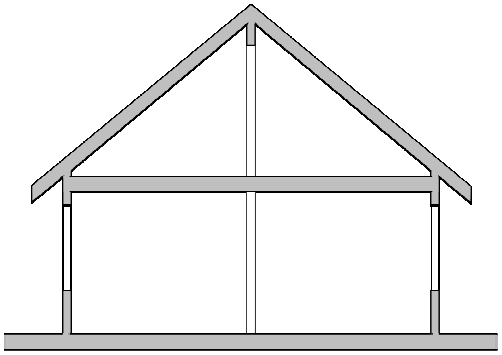

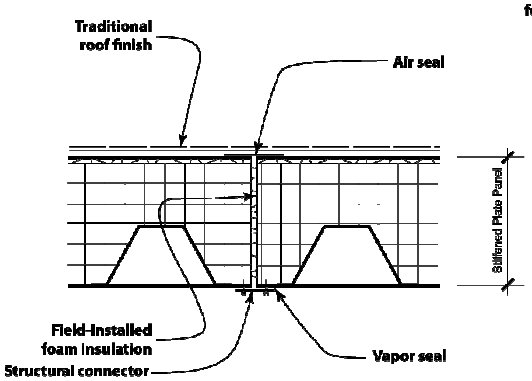

Panel to Panel Joint

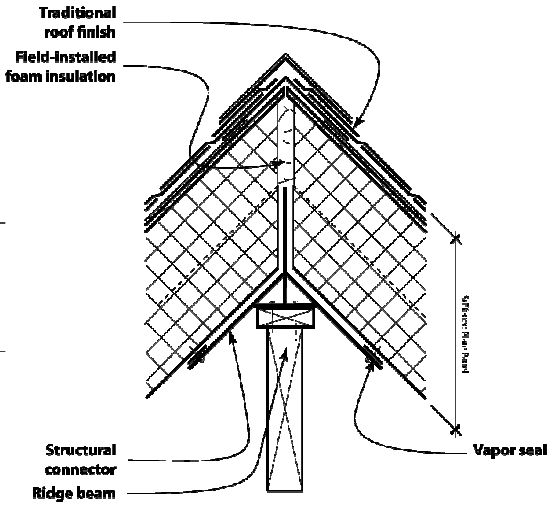

Ridge Joint

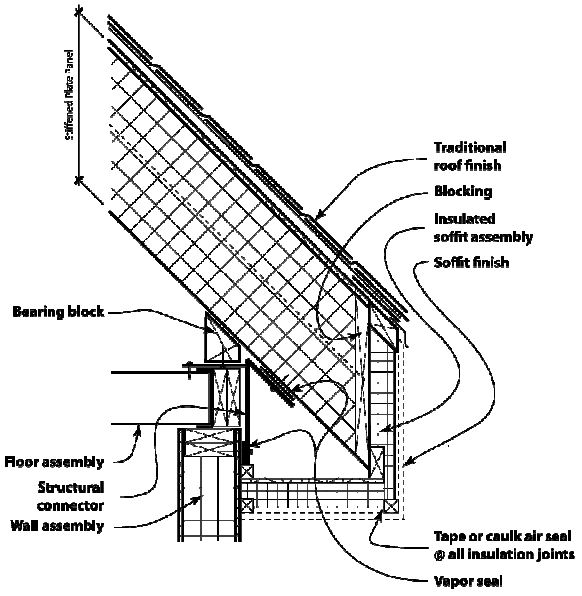

Soffit Joint

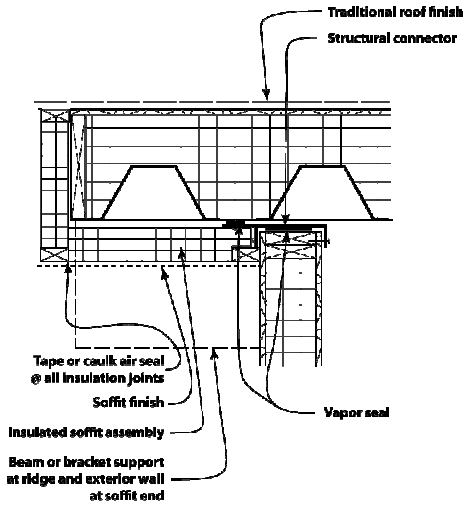

Gable End Wall Joint

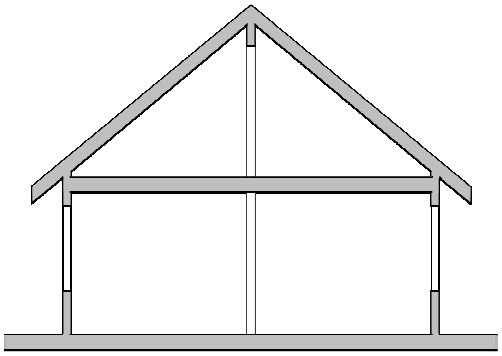

Figure 5.3-2:
Stiffened plate panel, steep slope, integral metal roof.

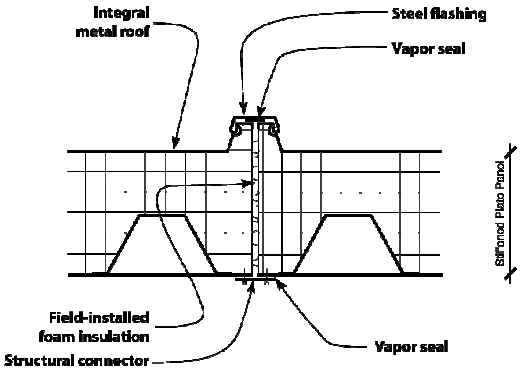

Panel to Panel Joint

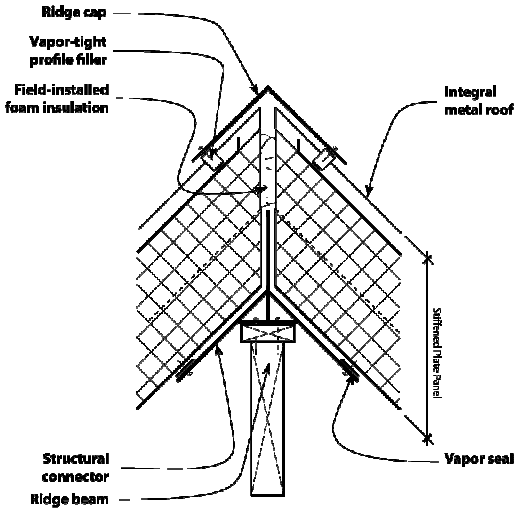

Ridge Joint

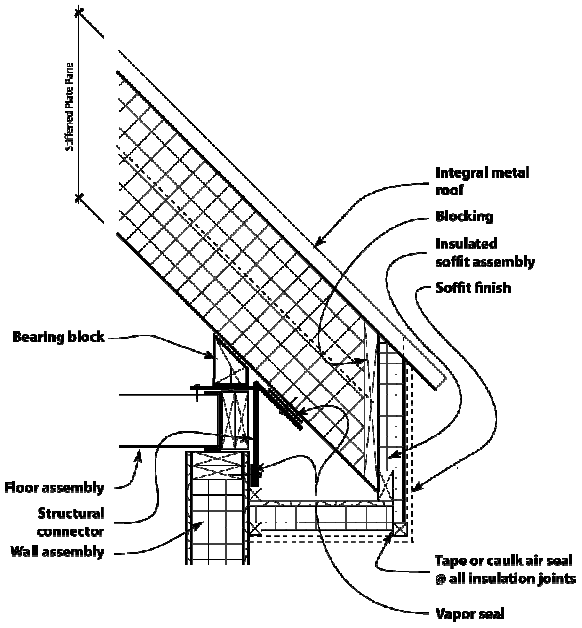

Soffit Joint

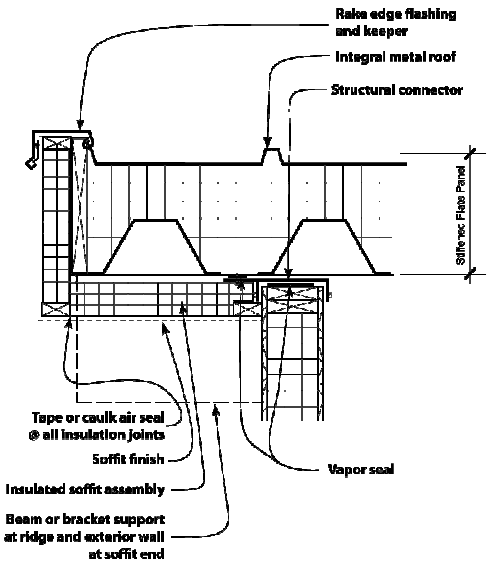

Gable End Wall Joint

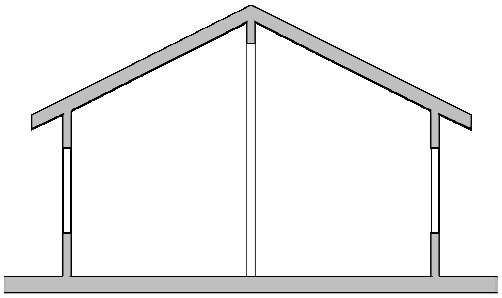

Figure 5.3-3:
Stiffened plate panel, shallow slope, traditional roof finish.

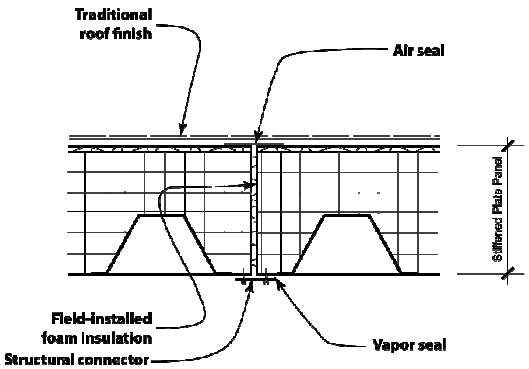

Panel to Panel Joint

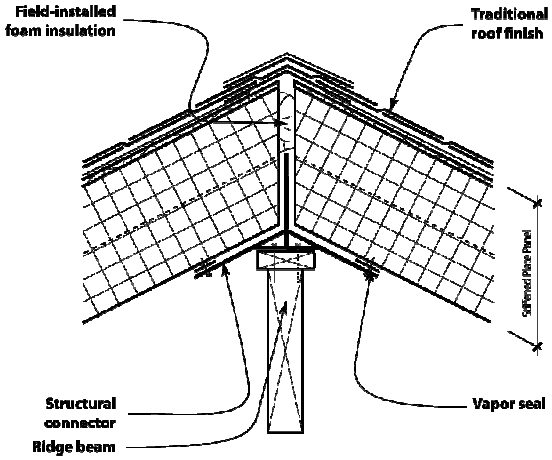

Ridge Joint

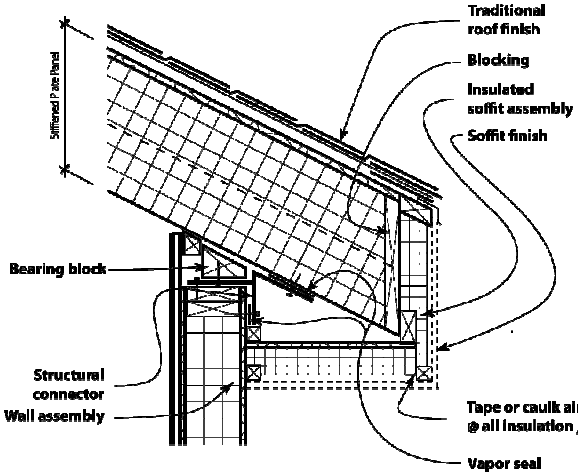

Soffit Joint

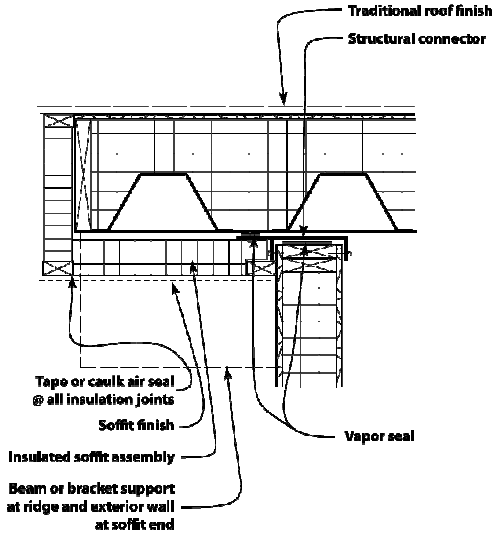

Gable End Wall Joint

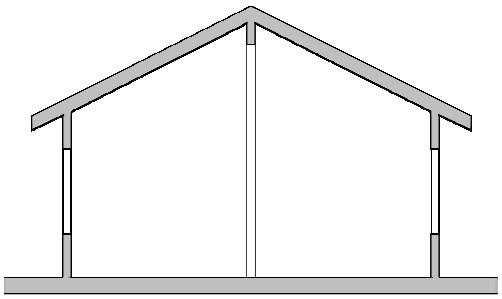

Figure 5.3-4:
Stiffened plate panel, shallow slope, integral metal roof.

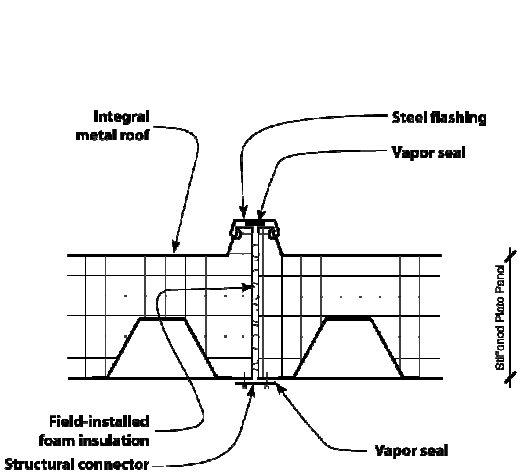

Panel to Panel Joint

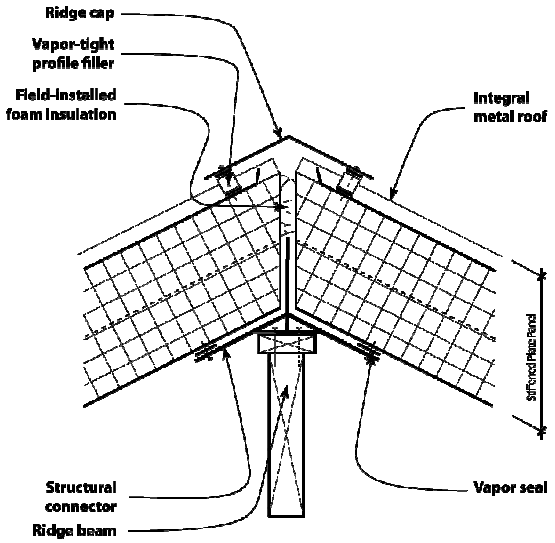

Ridge Joint

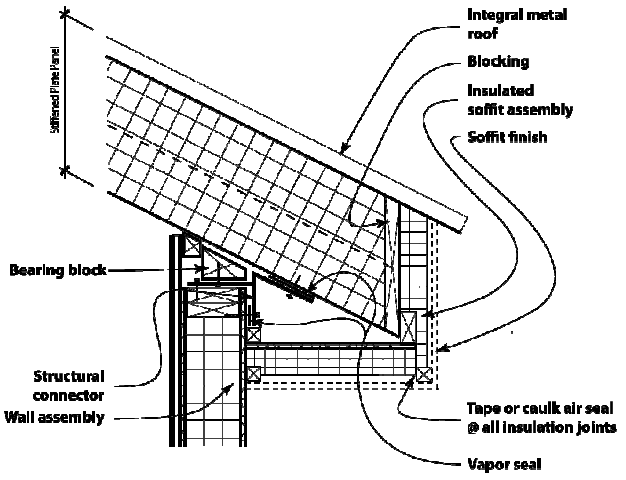

Soffit Joint

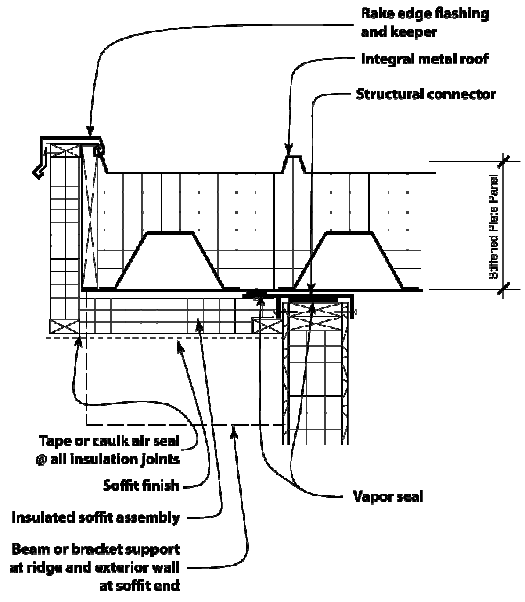

Gable End Wall Joint

5.4 Manufacturing Plan

The manufacturing plan for the stiffened plate panel is similar to the plan for the truss core panel: 1) sheet metal components are formed and galvanized, 2) foam in place the PUR insulation (the finish face sheet and the webs are part of this structure) and 3) laser weld the interior face sheet. Figure 5.4-1 illustrates the manufacturing steps for the stiffened plate panel. This manufacturing sequence ensures that the web shape is maintained during the foaming process.

The process begins with cutting and roll forming steel sheet stock to produce the interior face sheet and V webs. The sheet stock components are galvanized. The V webs are laid up on a mold and the PUR is foamed between the mold/web surface and the exterior finish sheet. Once the PUR has cured, the interior face sheet is laser welded to the webs. The panel edges are cut to the roof slope and the cut edges are capped with an edge channel as required.

Factory finish of the panel depends on the panel configuration (see Figures 2.2-1 and 2.2-2). For panels with an OSB nailbase exterior, there are no additional finish steps. For panels with an integral metal roof, the profiled metal roof is coated with PVDF for long term weather resistance. The panel is protected during shipping with a plastic edge.

1. Create sandwich panel with PUR foam. One surface is a exterior finish sheet (OSB or integral metal roof), the other surface is a mold with webs inserted in the surface

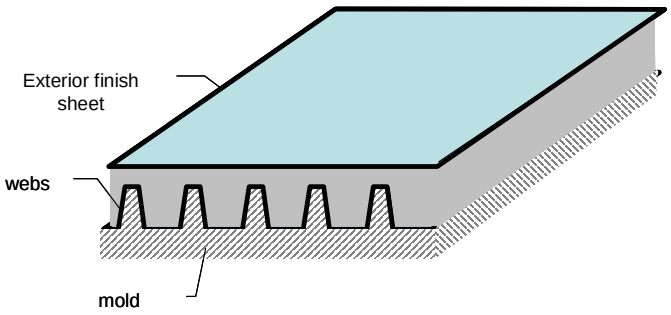

2. Laser weld interior face sheet to webs

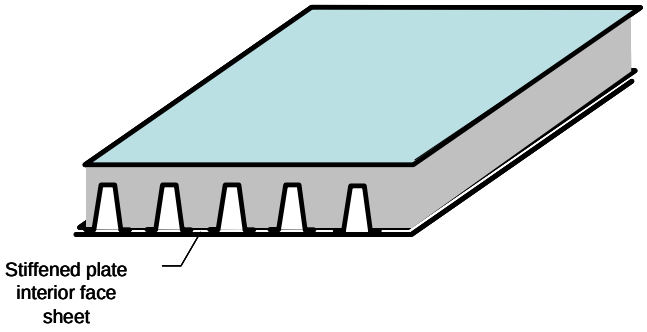

Figure 5.4-1: Illustration of the foaming and welding steps for a truss core panel with exterior foam.

6.0 Solar Integrated Panel

The panelized roof has the potential to improve integration of roof mounted solar technology. Current solar products are manufactured in factories and delivered to construction sites, where highly skilled workers perform installation. To accommodate a variety of roof geometries, these products have rigid frames designed for safe installation on inclined surfaces. The roof panel is produced in a factory, where the use of lower cost labor could reduce the cost and complexity associated with roof mounted solar systems.

Typically, a roof-mounted photovoltaic system will cost $9/kW, with half of that cost related to installation. The goal of this study was to evaluate how much of the installation cost could be eliminated. Design concepts were identified that would eliminate much of the conventional solar mounting hardware, resulting in a lower profile.

The project team held a series of meetings aimed at identifying the requirements for a solar-integrated roof panel. Pulte Home provided the market perspective and defined a model home that served as the base case for design integration. UMN provided details of the roof panels. GE Solar provided information on existing product offerings that could be modified to meet the new application. Of the requirements discussed by the team, five were deemed most critical to the quality (CTQ) of the solution:

1. Any concept evaluated must be producible within a year. This requirement was further clarified to mean that the study would not evaluate any new inventions, relying instead on existing products. This decision was important for two reasons: 1) a solution that looked economically viable would need to be proven in a follow-on project and 2) new inventions imply higher risk.
2. The solar-integrated roof panel must provide a solar solution that was of economic value to the homeowner, meaning that it must have an installation cost lower than other solar market offerings.
3. The roof panel, with solar technology installed, must have a long life. Design concepts must not accelerate the degradation of the roof panel.
4. Solar modules tend to degrade at a significantly higher rate than the underlying roof. As such, it must be possible to replace solar modules during their life. As most solar products allow replacement of individual modules, this study would seek solutions that provided the same serviceability.
5. The solar industry is continually seeking products with improved aesthetics. Many solar products require mounting hardware that lifts the solar module well above the roof surface. Design concepts that moved the plane of the solar panel to the roof surface were to be valued more highly.
6. Solar thermal options must be robust and cost effective. GE made the decision to incorporate commercially available solar thermal collectors (2) rather than an integrated PV/thermal module into the roof panel. At the time GE was evaluating solar thermal options, the availability of robust PV/T solutions was limited. As a result, these products were not considered as part of the analysis.

Figure 6.0-1 shows a schematic showing how requirements drove specific quality goals.

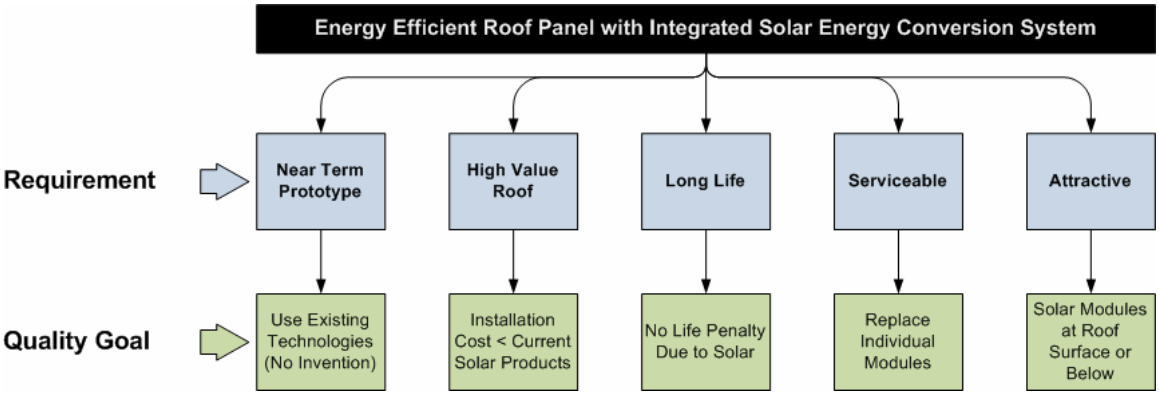

Figure 6.0-1: Requirements and quality goals for the solar integrated roof panel.

6.1 Design Concepts

Each quality goal was "flowed down" to a set of specific design features that are the basis upon which design concepts were compared. A brainstorming session was held with GE Solar to define some alternative concepts for integrating solar technology on the truss core panel. Four of those concepts are summarized in Table 6.1-1.

A "Pugh Matrix" provides a qualitative comparison of the four concepts. In the matrix, each integration concept was evaluated according to strengths and weaknesses against GE's standard roof-rack mounted solar product (referred to, in the Pugh Matrix, as a datum or base concept). Typically, the datum is the best available alternative or current concept.

In the selection matrix developed by the team (Figure 6.1-1), each design feature was associated with its corresponding CTQ. For each feature, a weight is provided – establishing the relative importance of each design feature. A score of 5 indicates high importance, 1 indicates lowest. The datum (roof rack mounted solar product) is indicated in the shaded column. Since it is the base concept, its scores are null. For each of the four integration concepts, there is a score indicating how – on each design feature – that concept compares to the base. Scores are valued as follows: "S" indicates that the comparison concept is equivalent to the base, "++" indicates that the comparison is significantly better than the base, "+" is slightly better, "-" is slightly worse and "--" indicates a much worse comparison to the base.

The overall weighted score was calculated based upon the weighting of each design feature, multiplied by a value associated with each score indicated. The Pugh Matrix was used as a decision support tool, not an accurate comparison of concepts. So the specific values were of less value than the relative values. The conclusion drawn from the Pugh Matrix exercise was that two concepts appeared to be significantly more attractive than the other two. It was on this basis, that the integrated metal roof photovoltaic (PV) and big PV shingle concepts were selected for further evaluation.

Table 6.1-1: Concepts for PV integration.

Integration Concept	Product Configuration	Performance	Assembly/ Installation	Service	Appearance
OSB-Plate:  (end view)	o Roof surface is sheathed with insulation and OSB o Rectangular cutouts in sheath provide space for junction box and wiring o Standard PV modules, without frames, are adhered to the top surface of the OSB sheathing around the edges o Exposed OSB sheath is covered with moisture barrier and shingles	o No provision for solar thermal heat dissipation under panel o Uncertain performance/life of adhesives on OSB o Potential problems with maintaining a water tight roof	o Each recess must be water sealed o Wiring would either be surface mounted on shingles after assembly or passed through penetrations in top sheet of truss core roof panel	o Individual PV modules can be replaced without disturbing adjacent modules o Must break adhesive seal to replace PV modules o Modules that are removed will likely be destroyed/damaged due to the adhesive	o Low profile on roof (virtually in plane with shingles) o Standard blue solar cells deviate from normal look of a shingled roof
Integrated Metal Roof PV:  (end view)	o Standing seam metal roof (no shingles) o PV laminate, without frame, would be glued to the lands o Laminate must be sized to fit an integer multiple of seams o Wires run in gap between bottom of solar module and top surface of truss core panel o Periodic recesses provided on seams to allow each module to sit in a slot – to immobilize panel o Junction box remains attached to the back plane o Solar modules plug into connectors on wire run	o Channels under PV panels present opportunity for heat dissipation o Uncertain performance/life of adhesive on metal seam roof	o Metal on outside of roof panel would be coated to protect from moisture o Wiring would run under the PV panels, up to ridge for house interconnect	o Individual PV modules can be replaced without disturbing adjacent modules o Must break adhesive seal to replace PV modules o Modules that are removed will likely be destroyed/damaged due to the adhesive	o Similar appearance to current roof rack mounted PV modules, except lower profile (closer to roof surface)
PV Channel:  (end view)	o Full length channels with side brackets that hold PV laminates onto roof panel o Channels run full length of the roof panel, from ridge to soffit, with OSB sheath between PV channels o Top edge of each PV laminate would have a molded strip for spacing and to house junction box and wiring interconnect	o Heat from solar panel will (thermal) short to interior of roof panel – where solar thermal heat capture may be possible o Possible problems maintaining a water tight roof	o Metal surfaces within PV channel would be coated to protect from moisture o Channel brackets must be designed to prevent water from penetrating between bracket and OSB/insulation o Wiring would run under the PV panels, down to soffit for house interconnect	o Individual PV modules can be replaced o Modules loaded into channel from the ridge line, so replacement of modules will require disconnection and removal of all panels above	o Recessed panels will appear more like PV shingles than roof rack mounted PV modules due to recessed mounting
Big PV Shingle:  (side view)	o PV laminates are layered on roof from ridge to soffit o Edge rail provides junction between adjacent laminates and channel for junction box and wiring interconnect o At ridge, a strip of insulation and OSB sheathing runs width of panel o At soffit, last panel would overlap an insulated, weather-protected strip of OSB sheath o Embed diodes into the edge separators o Edge separator – between solar modules – is slotted to allow movement of air along truss core panel, from soffit to roof ridge o Slots in separator strip allow connecting wires to run between modules	o Solar thermal energy capture occurs in the gap between the bottom surface of the photovoltaic module and the top surface of the truss core panel	o At ridge and soffit, OSB sheath and insulation will need to be moisture protected o Modules plug into wire run with connectors, simplifying installation and service	o Individual PV modules can be replaced o Modules are layered from bottom of roof panel up to ridge so replacement of lower modules will require disconnection and removal of at least one module above	o Similar appearance to PV shingles, except modules are larger in size

Pugh Concept Selection Matrix

CTQ	Design Features	Criteria Weighting	Concepts: Roof Rack Mount	OSB Plate	Standing Seam PV	PV Channel	Big PV Shingle
Attractive	Appearance	5	0	+	+	+	+
High Value Roof	Ease of Installation - Module to Module	4	0	-	+	-	+
High Value Roof	Allows Integration of Solar Thermal	4	0	S	++	-	++
High Value Roof	Ease of Installation - House Wiring	3	0	-	+	-	+
Long Life	Moisture barrier	5	0	-	S	-	-
Long Life	Reliability	5	0	S	S	S	S
Long Life	Rigidity	4	0	-	-	+	+
Long Life	Live Load (e.g., Vibration)	3	0	S	S	S	S
Long Life	Temperature Load	3	0	-	+	-	+
Long Life	Dead Load (e.g., Weight of Installed Components)	2	0	+	+	+	+
Near Term Prototype	Changes Needed to Off-The-Shelf Solar Products	5	0	-	S	S	-
Near Term Prototype	Modifications Needed to Truss Core Panel Design	5	0	-	S	-	-
Serviceability	Ability to Service Individual PV Modules	5	0	-	+	--	+
	Sum of Positives		0	2	8	3	9
	Sum of Negatives		0	8	1	8	3
	Sum of Sames		13	3	5	3	2
	Weighted Sum of Positives		0	7	30	11	34
	Weighted Sum of Negatives		0	-34	-4	-34	-15
	Overall Weighted Score		**0**	**-27**	**26**	**-23**	**19**

Figure 6.1-1: Pugh Matrix for selection of a solar integration concept.

6.1.1 Standing Seam PV Concept

The structural roof panel with standing metal ridges provides a flexible design platform on which to integrate photovoltaics and takes advantage of the natural air flow beneath the PV to increase solar-to-electric efficiency. Unlike conventional metal seam roofs, the structural roof panel has a single, continuous sheet of roll-formed sheet metal as the top roof surface. This construction is only practical in prefabricated roof panels for the 8 ft width. Assembly of large sheets of metal at the construction site would not be economical. Figure 6.1-2 shows how the integral metal roof PV panel might appear. Each roll-formed ridge provides an indentation in which a photovoltaic laminate could be glued (Figure 6.1-3). In the space bounded by metal seams, the under side of the photovoltaic laminate and the top sheet of the truss core panel, wires would be run between modules. Wires could then be terminated with a connector that would allow quick connect/disconnect of laminates in case of replacement. The wire bundle from each pair of solar modules would run to the ridge of the roof, where they would be collected and run out to the gable and connected to house wiring. The ridge of the house would have a cap to protect the wires from weather.

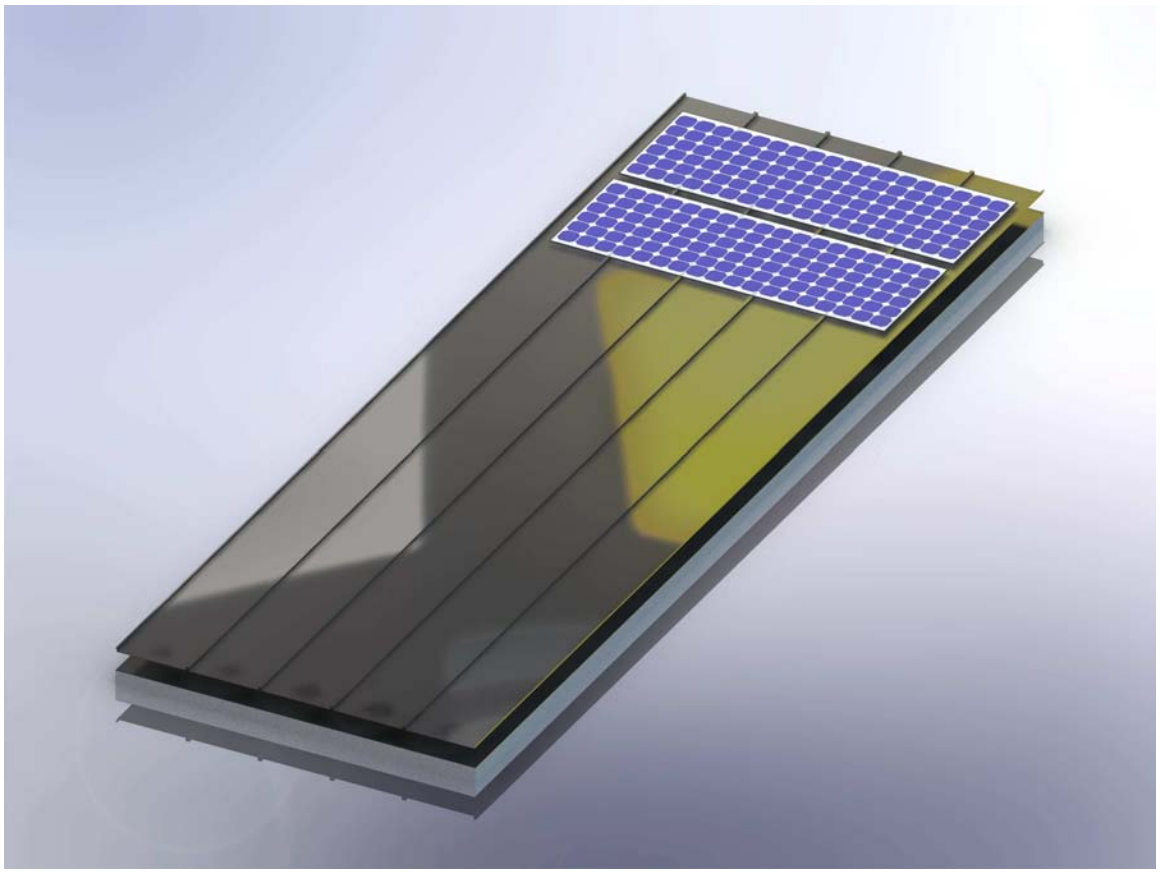

Figure 6.1-2: Integral metal roof panel with PV modules in place.

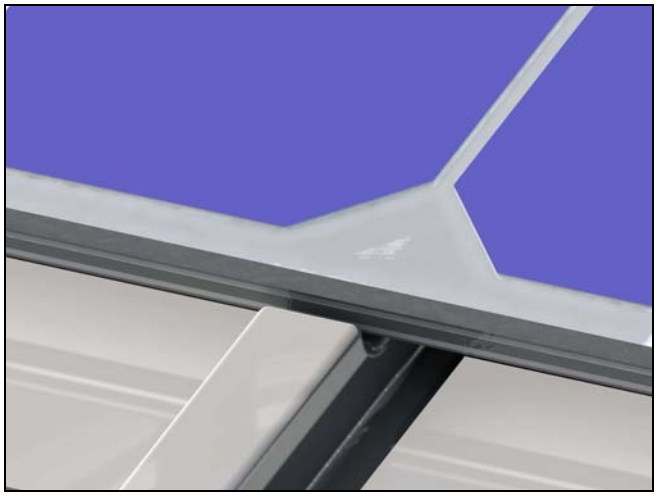

Figure 6.1-3: Formed ridge on integral metal roof, with PV laminate in place.

Cooling can be handled by air flow in the open channel formed by the metal corrugation and the underside of the PV panel. The panels are cooled by radiation and free convection as ambient air rises through the channel. A scale analysis and numerical study of PV modules with a back mounted air channel were conducted to estimate heat transfer rates over a practical range of operating conditions and channel geometries. A generalized correlation for the average channel Nusselt number for the combined convective-radiative cooling was developed for modified channel Rayleigh numbers from 10^2 to 10^8, channel aspect ratios between 15 and 50 and inclination angles between 30 and 90 degrees. This work is described fully in Appendix J.

Passive air flow through the channel underneath the PV module can decrease operating temperature as much as 35° F, resulting in an *absolute* efficiency gain of 1 to 2%, depending on the channel geometry and the solar radiation flux.

6.1.1 Big PV Shingle Concept

The benefit of the PV shingle concept is that it integrates with roof panels sheathed with OSB. The PV laminates are recessed into the OSB so the impact on home appearance is mitigated. The big shingle concept is shown in Figure 6.1-4. The OSB sheathing has two cutouts near the roof's ridge into which the photovoltaic modules would be mounted. Each of the photovoltaic modules overlaps the next adjacent module, much like the overlap of shingles, allowing rainwater to flow down the roof incline without pooling. Modules would be connected to one another with molded strips that provide rigidity and are shaped to allow airflow beneath the modules. See details of the design in Figure 6.1-5. The air flow holes in the "S" connector strip should provide a channel for running wires that connect modules together. The "S" connector would be fastened to the top sheet of the truss core panel with an adhesive.

6.2 Selected PV Concept

The GE team selected the standing seam PV concept for further development. It has the greatest potential for cost savings, takes advantage of the opportunity for passive cooling with the integral metal roof truss core panel, and provides a low profile appearance on the roof.

The most significant drawback of the "big shingle" design is the difficulty providing a water barrier between the PV module and the edge of the OSB sheathing. The GE team evaluated a number of concepts but could not settle on one that would be expected to last the life of the roof. As a result, the big shingle concept was dropped as an alternative and only the standing seam concept was carried forward into the economic analysis.

Figure 6.1-4: "Big shingle" concept showing OSB (without roof covering).

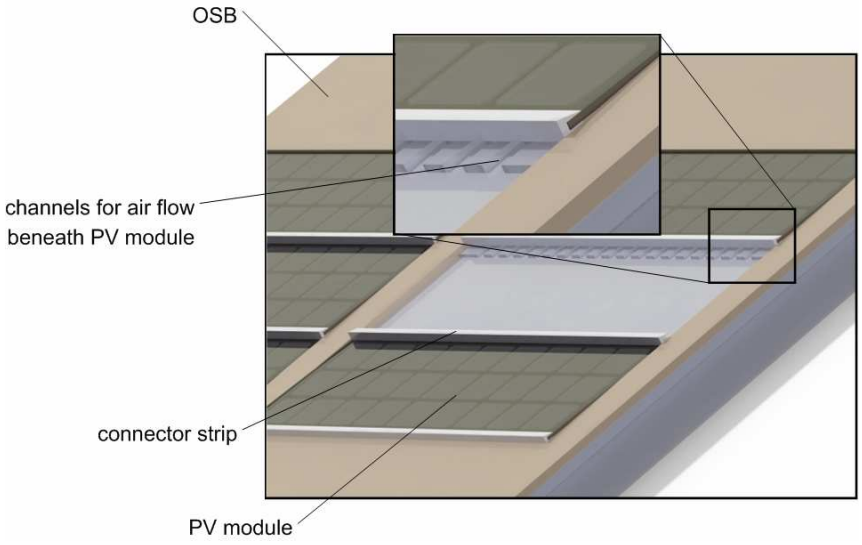

Figure 6.1-5: Detail of PV module and connector strip.

7.0 Comparison of Panel Options

The truss core panel is the recommended panel design. This recommendation is based on a careful evaluation of panel structural and hygrothermal performance along with panel compatibility with architectural practices.

The truss core panel is a versatile design that can be tailored to sustain the structural and thermal loads for all three climate zones (including wind loads up to 130 mph) for a wide range of spans and roof pitch. The insulating foam layer can be placed on the interior or exterior surface as required for moisture management. The exterior roof finish can either be a shingle roof or an integral metal roof. Much of this versatility is a result of the structural component of the panel. This component is comprised of an interior and an exterior face sheet spanned by webs. This balanced design can accommodate wind uplift loads without compromising dead and live load capabilities. The insulating layer can readily be attached to either sheet, and either surface can serve as a vapor barrier. Architectural details, especially as related to establishing vapor barriers at the joints, are fairly straightforward because the interior and exterior face sheet surfaces are flat and parallel.

The stiffened plate panel is limited in use to climates I and II and is projected to cost more than the truss core panel. Although the stiffened plate panel offers the potential advantage of a reduction in the cost of galvanization and welding, the amount and consequently the cost of foam will be higher. The amount of foam is particularly important because it represents 30 percent of the material costs (see section 9). In addition, the foam insulation must be placed on the exterior side of the steel structure and thus the vapor barrier is always on the interior of the panel. In warmer climates, it is preferable to place the vapor barrier on the exterior and thus the stiffened plate panel is not ideal for many locations in climates I and II. Potential moisture problems can be avoided by adding extra foam beyond the depth required to meet R-30, but this solution increases the relative cost even further. In summary, the structural design of the stiffened plate panel leads to limitations in hygrothermal performance and challenges with satisfying architectural requirements.

8.0 Application to Representative Residential Homes

In collaboration with industry partners, a house design was selected to test the applicability of the truss core panel. Design alternatives were created to allow a comparative economic analysis of three variations of the panelized roof system and two variations of conventional construction. The economic analysis is in section 9.

The baseline house is model 1155, designed by Pulte Homes, Inc. It sold for roughly $350,000 in the Las Vegas, NV area during the summer of 2008. The land was valued at $100,000. It is a ranch with a 460 square foot two car garage and has 1155 square feet of living space. The house contains two bedrooms and two baths, with an eat-in kitchen and great room. The attached garage is located at the front of the house. The attic is enclosed and the conventional shingle roof is mounted on sheathing attached to the trusses. Attic insulation is on the floor of the attic and both the electric HVAC unit and electric hot water heater are installed in the attic. Ductwork runs through the unconditioned space within the attic.

The selection of a baseline was driven by a number of factors including:

- Commercial viability: UMN and GE consulted with Pulte Home Builders to identify a home design that was already shown to be attractive to home buyers.
- Energy efficiency: Though the energy efficient panelized roof would compare more favorably to older, less energy efficient home designs, the project team decided that picking a state-of-the-art, commercially available, design would provide a better assessment of the competitiveness of the panelized roof.
- Roof geometry: The rectangular geometry of the roof facilitated installation of the roof panel. Simple, straight line, ridge and soffit configurations simplified the construction.
- Attic alternatives: The baseline house allowed the comparison of shallow and steep roof planes. The steep roof provided sufficient attic space to permit occupancy.
- Solar-technology friendly: The house is intended for a U.S. location with excellent solar resource.

8.1 Overview of Options

Houses of this design in current production utilize roof trusses that span from exterior bearing wall to exterior bearing wall. They are installed at 24 inches on center and then sheathed. Several traditional roof finishes are available. A variety of roof forms are available as options. A simple gable roof with no hips or valleys was selected for the present study due to the ease of adapting this design to suit panelized construction (Figures 8.1-1 through 8.1-3). An energy efficient option of the base house has insulation at the rafter plane of the attic (Figure 8.1-4). Panelized roof solutions for the house were designed to meet the specific requirements of truss core panel roofs. Provisions were made to support a continuous ridge beam on columns. This ridge beam must extend to the outer edge of the panels at gable wall conditions. In addition, beam or bracket

supports that extend to the same panel edge are required at the soffit end. Two roof slopes were selected for panelized construction: a 10/12 pitch, two-story option with an additional two bedrooms and one bath (Figures 8.1-5 through 8.1-8), and a 3/12 pitch, cathedralized ceiling option (Figures 8.1-9 through 8.1-12).

The interior foam panel with an integral metal roof was chosen for application in the panelized designs for the following reasons:

- The integral metal roof reduces field labor and its associated cost and time penalties.
- Industry partners were interested in considering solutions for housing markets in warmer climates, where the interior foam panel displays excellent hygrothermal performance.

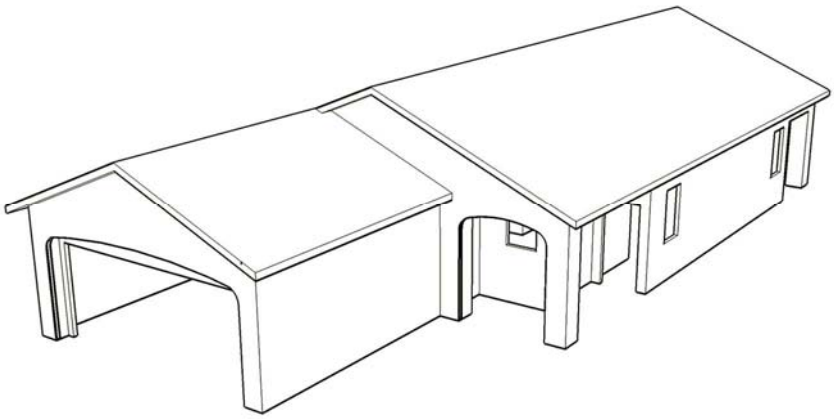

Figure 8.1-1: Base case house truss roof structure, 5/12 pitch (Option A).

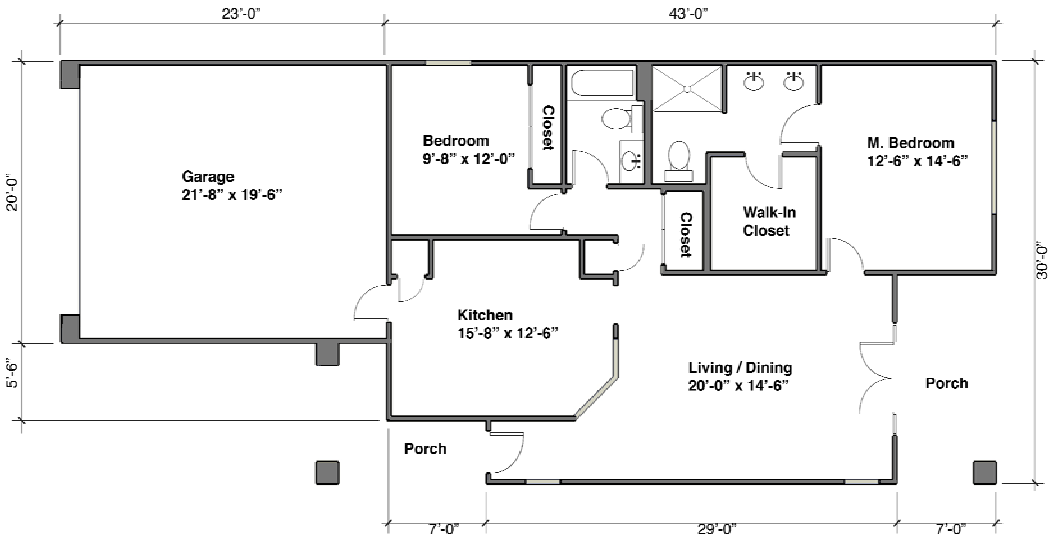

Figure 8.1-2: Base case house, plan (Option A and B).

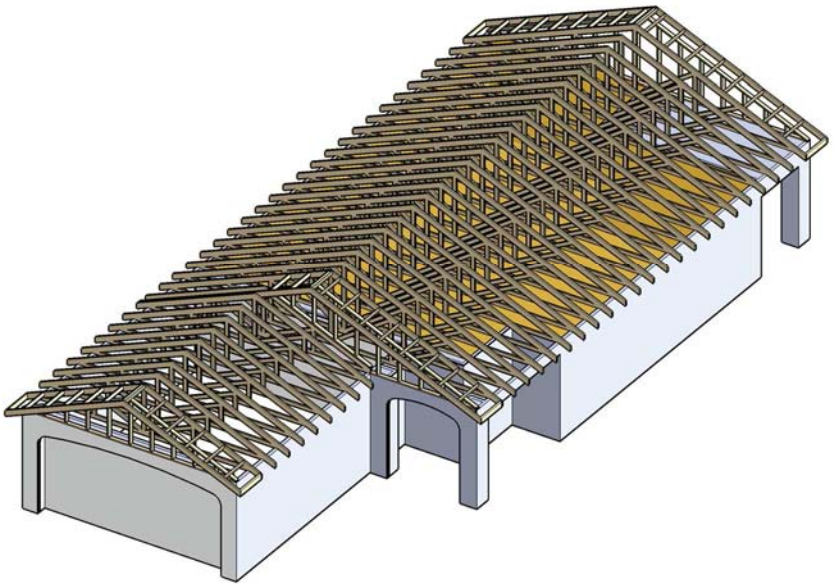

Figure 8.1-3: Base case truss roof structure, 5/12 pitch, attic floor insulation (Option A).

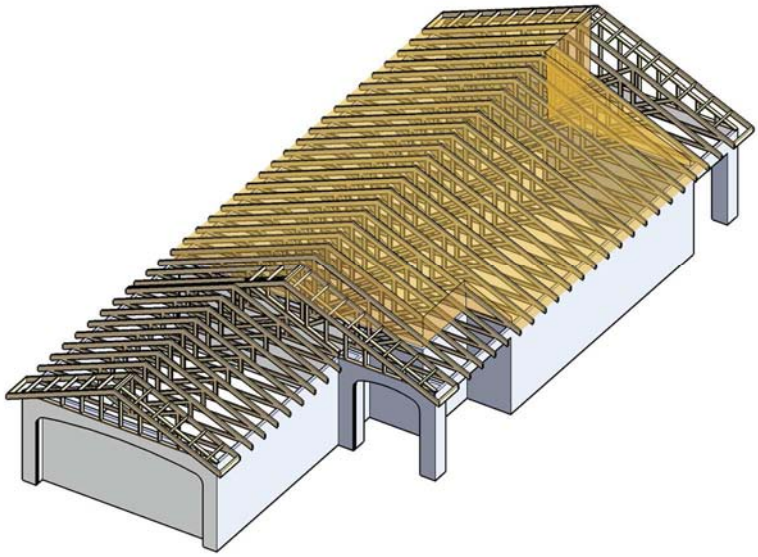

Figure 8.1-4: Truss roof structure, 5/12 pitch, roof plane insulation (Option B).

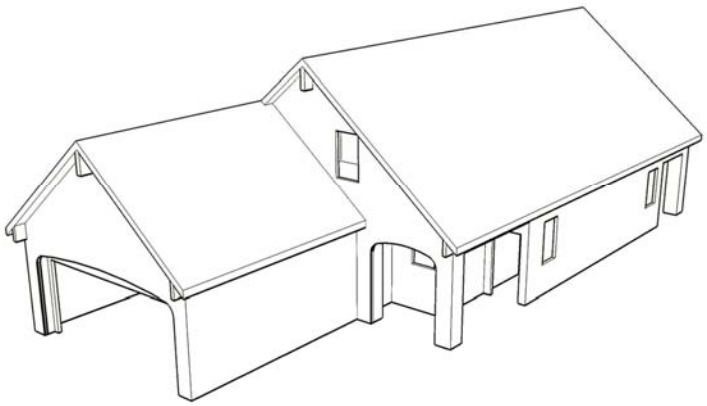

Figure 8.1-5: Panelized roof structure, 10/12 pitch with occupied attic (Option C).

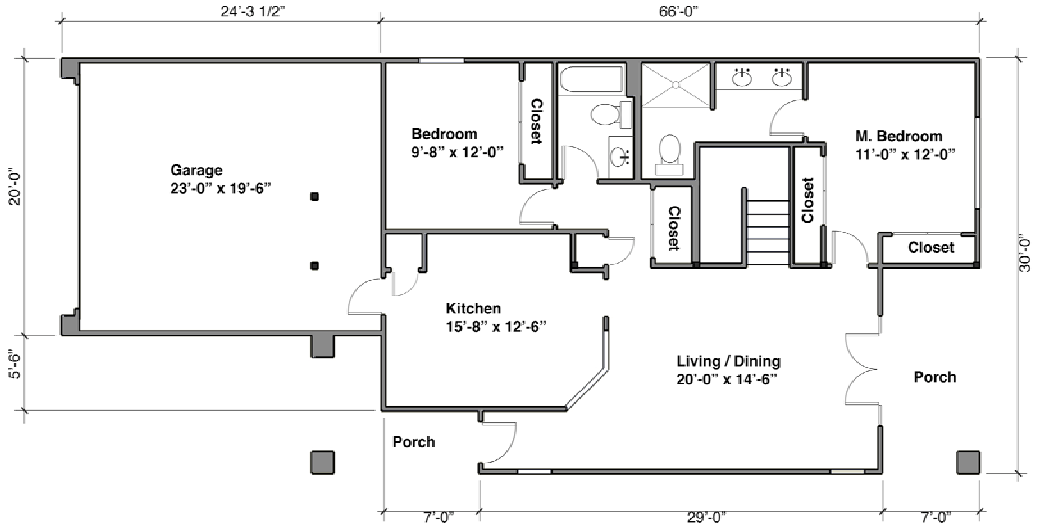

Figure 8.1-6: Panelized roof structure, first floor plan (Option C).

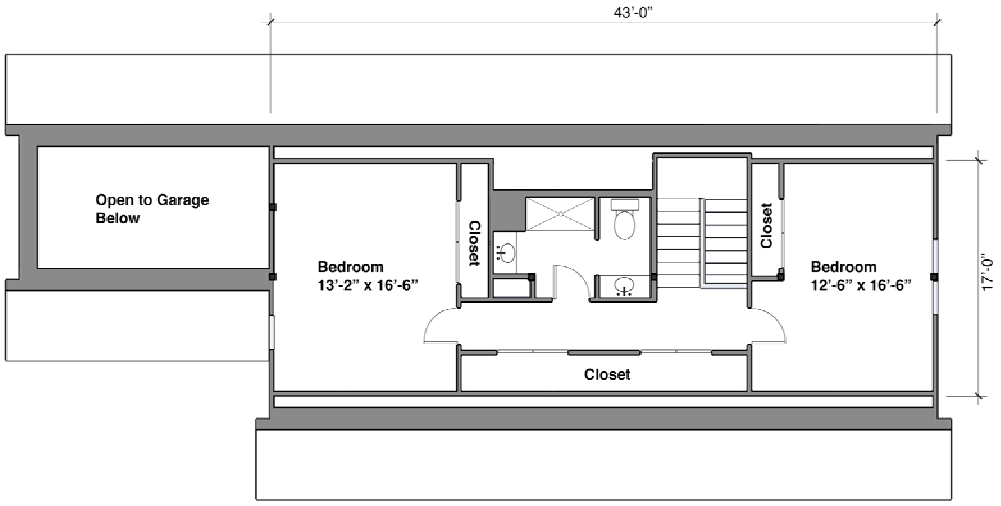

Figure 8.1-7: Panelized roof structure, second floor plan (Option C).

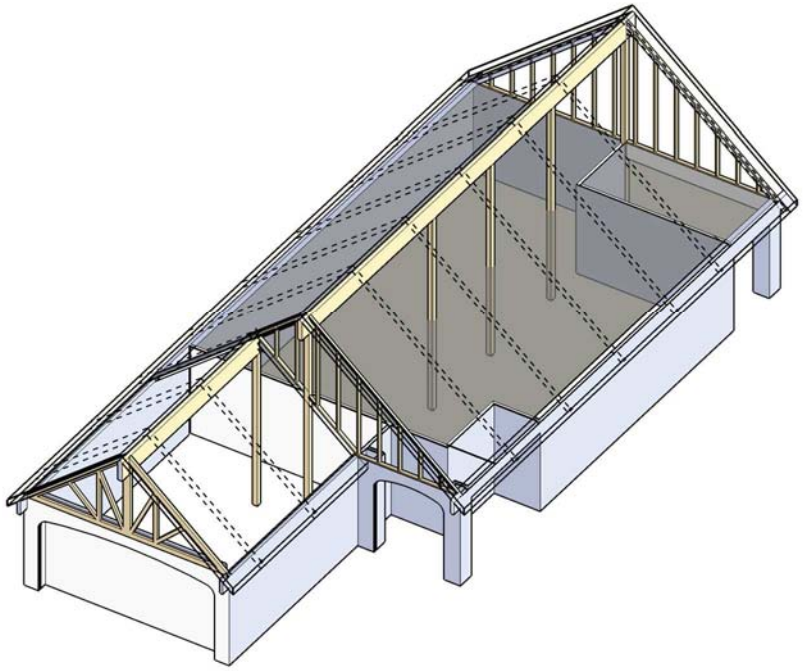

Figure 8.1-8: Panelized roof structure, 10/12 pitch, with occupied attic (Option C).

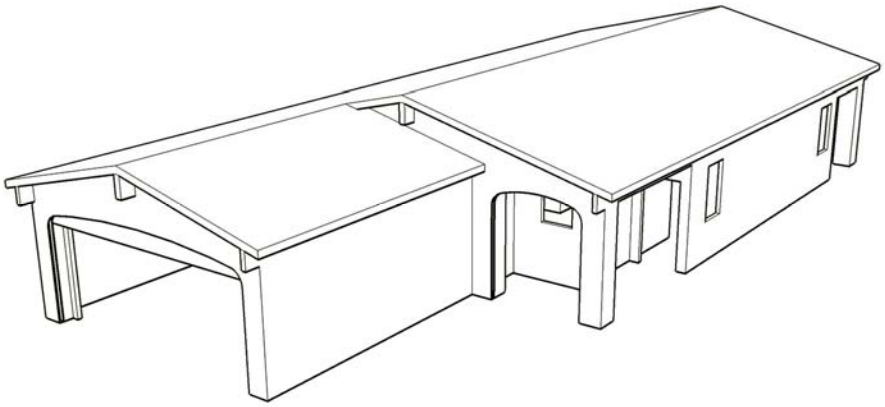

Figure 8.1-9: Panelized roof structure, 3/12 pitch with cathedral; ceiling (Option D).

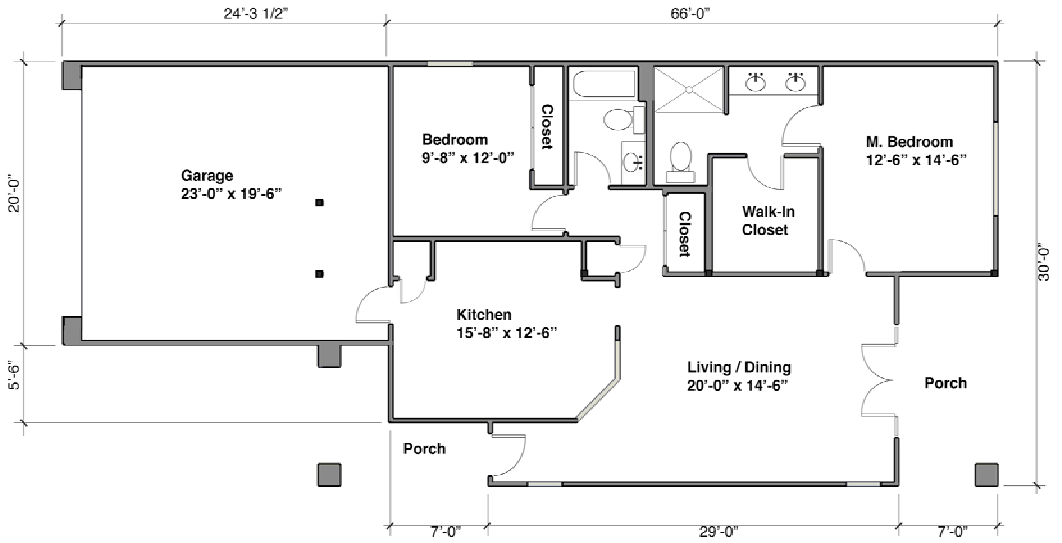

Figure 8.1-10: Panelized roof structure, plan (Option D).

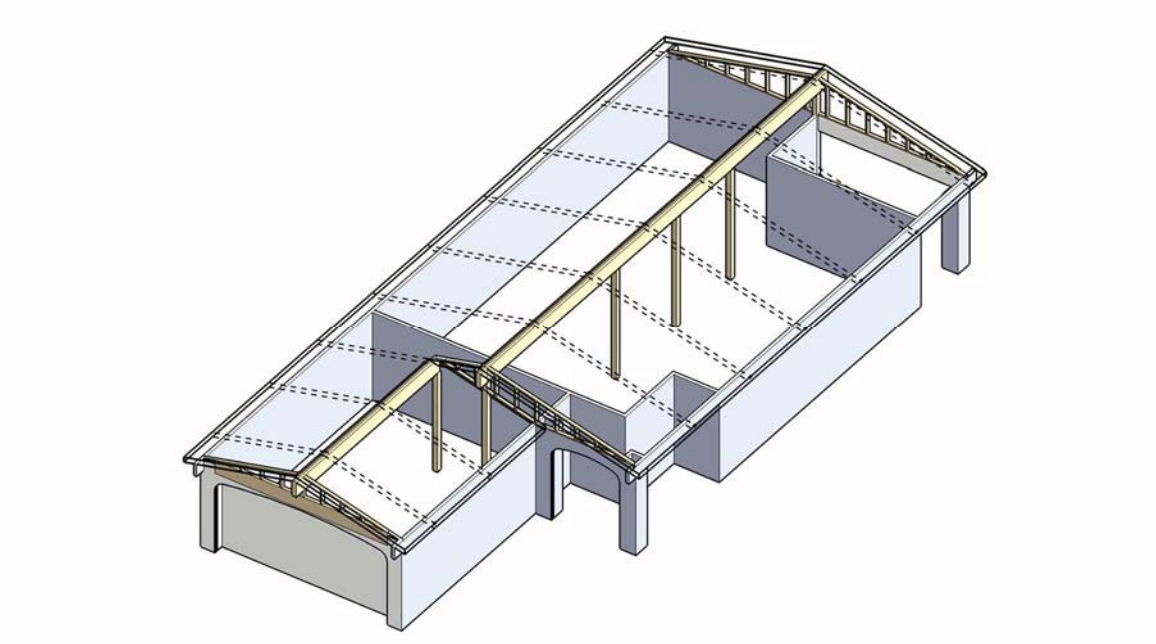

Figure 8.1-11: Panelized roof structure, 3/12 pitch, cathedral ceiling (Option D).

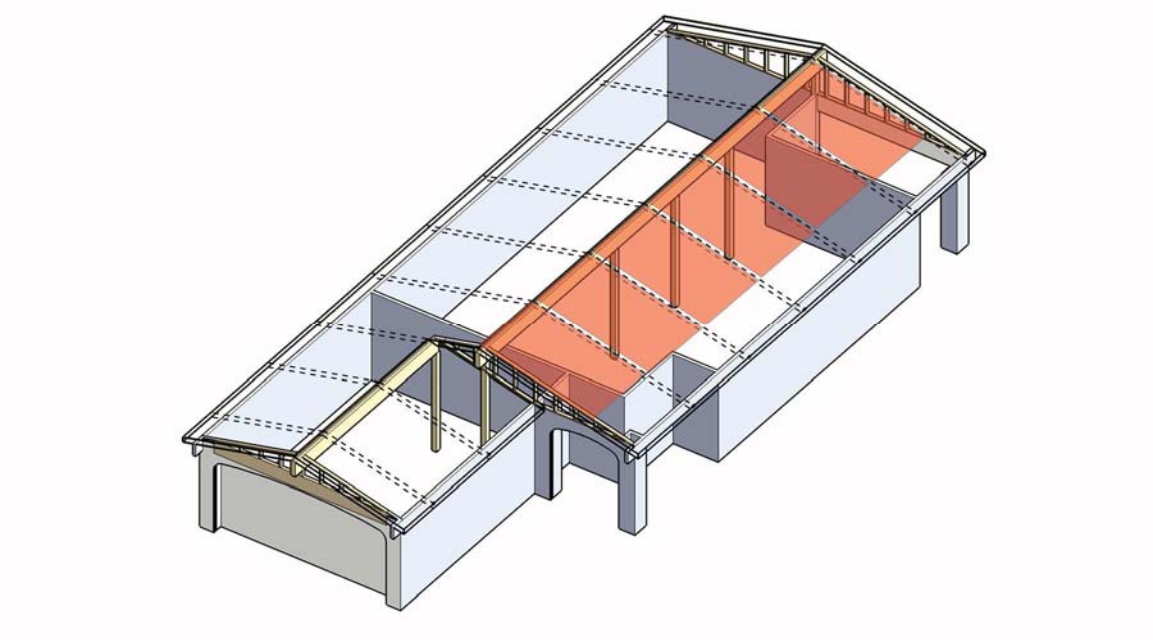

Figure 8.1-12: Solar panelized roof, 3/12 pitch, cathedral ceiling (Option E).

8.2 Option A – Baseline Home, 5 / 12 Pitch, Trusses with Attic Floor Insulation

The option A home (Figure 8.1-1 through 8.1-3), selected to serve as a base case conventional home for the economic analysis, consists of roof trusses spaced 24 inches on center along the length of the house with insulation placed in the plane of the attic floor. The home has 1155 ft^2 of finished area with a 5/12 roof pitch. The garage is 460 ft^2.

8.3 Option B – 5 / 12 Pitch, Trusses with Roof Plane Insulation

The option B home (Figures 8.1-2 and 8.1-4) is also constructed with roof trusses spaced 24 inches on center. In this case, the insulation is placed between the roof sheathing and a layer of netting fixed to the bottom face of the top chord of the trusses. At locations where the exterior wall is not coincident with the bearing plane of the trusses, insulation is installed in vertical planes that correspond with walls below. This option creates a conditioned attic in which mechanical equipment is placed. The insulated area over which heat is lost (or gained) to the ambient is increased to 3236 ft^2 compared to 2469 ft^2 for Option A. Energy modeling (section 9.1.4) shows that the thermal losses due to this increase in insulated surface area offset the gains of placing the mechanical equipment in the conditioned attic.

8.4 Option C – Panelized, 10 / 12 Pitch, Occupied Attic

Option C (Figures 8.1-5 through 8.1-8) uses panels and ridge beam with columns rather than roof trusses. This option increases the finished space to 1878 ft^2 by raising

the pitch of the roof to allow a second story. This option requires the extension of the garage by 1 ft 3½ in. to accommodate adequate parking stall depth when column supports for the ridge beams are brought down in the garage. Columns are located in walls that align vertically on both floors. A secondary beam or truss is required over the garage door to transfer load from the ridge beam around the opening. The ceiling of the first floor may be provided by truss core attic panels with no insulation, or by conventional framing techniques. The availability of structure along the centerline of the house allows the span of this system to be half of the overall width of the house, or about 15 feet. The space utilized by the walk-in-closet in the prior examples is used to accommodate a stair. This closet is replaced by two smaller closets, which reduces the floor area of the master bedroom. No other changes were necessary. The second story contains two large bedrooms and a large bathroom, in addition to three closets. Three windows are added to allow code-required egress paths for both bedrooms.

8.5 Option D – Panelized, 3 / 12 Pitch, Cathedral Ceiling

Option D (Figures 8.1-9 through 8.1-11) represents a panelized roof option that reproduces the plan of the truss-roof option A and B except for the cathedral ceiling and the garage extension. The pitch is reduced to 3/12 to keep the interior ceiling height at 11 ft 9 in. (Ceiling height in option A-C is 9 ft.) Columns are simple to integrate into the existing plan because it features multiple walls located along the centerline of the plan under the ridge beam. Like option C, a secondary beam support is required over the garage door to support the point load induced by the ridge beam above. The ceiling in the main public rooms and the bedrooms is cathedralized. The gypsum board face sheet of the truss core panel is the interior finish layer. In bathrooms and closets, a flat ceiling may be framed in to accommodate mechanical equipment in the attic.

8.6 Option E – Panelized, 3 / 12 Pitch, Cathedral Ceiling, with Solar Thermal and PV

Option E (Figure 8.1-12) is identical to option D except that it includes factory-installed solar thermal and solar photovoltaic panels to offset occupant energy use. All wiring between PV modules would occur in the factory. The only installation required at the construction site is the connection of wires at the ridge and the running of wires down the length of the ridge to the gable where it would penetrate the wall and run through to the electrical panel. Each roof panel would be capable of holding four GEPVp-200-MS photovoltaic modules, rated at 211W. At typical house configuration might have 3 roof panels with PV modules attached (more are possible). The cost model was set up to allow changes to the number of roof panels that have PV modules attached.

9.0 Economics of Panelized Roof System

This section describes the economic model and cost analysis results. The cost model was developed for the integral metal roof truss core panel applied to a home currently sold in Las Vegas (option A described in section 8). The production spreadsheet model is appended to this report in electronic format. An example calculation is provided and the reader is referred to the spreadsheet itself for additional details and parametric study.

9.1 Cost Estimation

9.1.1 Bill of Materials

The first step in estimating production cost is development of a product bill of materials (BOM). The BOM was derived from the panel design described in Table 9.1-1. The steel structural component was design for a 10/12 roof (option C home) and is thus also suitable for the shallow slope roofs of option D and E homes. The economic analysis assumes that the same panel is used in each home, including the garage.

The "Panel Material" tab of the roof panel cost spreadsheet has the BOM. In the cost analysis, it was assumed that the panel would be produced from raw materials. For example, the steel used as top sheet, bottom sheet and webs was sourced as cold-rolled steel – cut and formed to size and shape, galvanized, and laser welded in the factory. The cost model did not take into account any material cost reduction due to changes in order quantities as these cost differences tend to be small in relation to the overall business cost structure.

The BOM table lists the constituent parts of the panel, the unit price, the quantity of each part per panel, and the total cost per panel for each part. Adding total costs for each part provided a total material cost for each panel. The BOM, shown in Figure 9.1-1, provides cost estimates for rafter and ceiling panels. The "rafter panel" is used at the roof line and includes PUR insulation. The ceiling panel does not require insulation or external finish layers. Material costs are $\$6.39/ft^2$ for the rafter panel and $\$3.17/ft^2$ for the ceiling panel.

The BOM also includes costs associated with PV integration, PV balance of system and solar thermal integration. PV components listed in the table are based upon standard GE prices. PV module prices were adjusted to eliminate incremental costs due to assembly of metal frames around each module. The PV balance of system includes all components typically installed in residential systems. These include an LCD meter, an inverter and all wiring required.

The solar thermal panel selected for the cost model is sold by SunEarth. Costs were estimated based upon standard product pricing. Installation costs were not included in the material cost table as those costs were captured under construction costs.

Table 9.1-1: Panel design used for cost analysis.

Product configuration (see Figure 2.1-1)	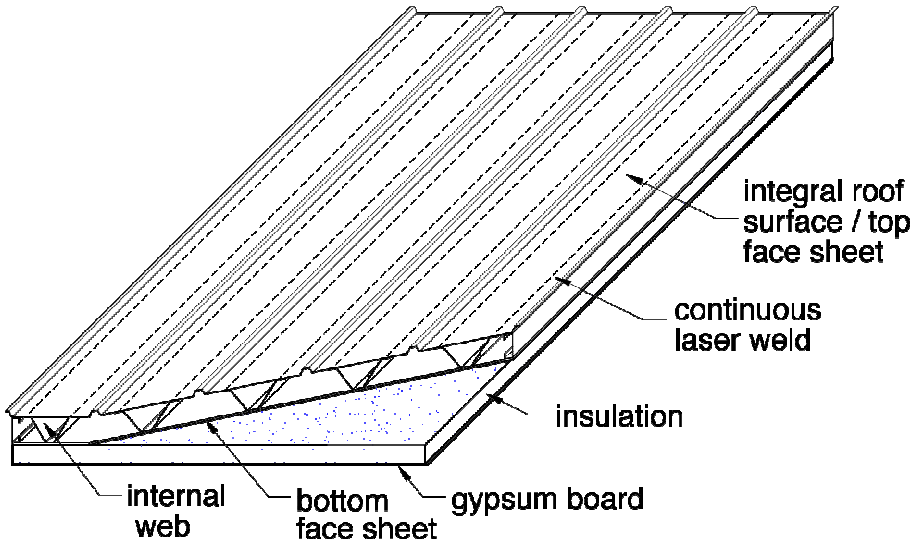
Roof surface	Integrated galvanized metal roof, PVDF coated
Insulation	PUR foamed in-situ
Finish face sheet	1/2 in. Gypsum board
Top sheet , web and bottom sheet material	Galvanized, cold rolled steel
Nominal size	8 ft W x 17.5 ft L x 10.7 in. D
Number of V-channels (webs)	5 (running from soffit to ridge, # across width)
Web angle	65 degrees
Sheet thickness	0.034 in. sheet for interior face sheet and V channels 0.045 in. sheet for exterior integral metal roof

Bill of Materials - Roof Panel		Unit Info		Rafter Panel		PV Rafter Panel		PV+ST Rafter Panel		Ceiling Panel	
Item	**Description/Dimensions**	**Unit Price**	**Unit**	**Qty.**	**Total Cost**	**Qty.**	**Total Cost**	**Qty.**	**Total Cost**	**Qty.**	**Total Cost**
Base Panel											
Top sheet	Steel sheet (from coil)	$ 0.55	sq.ft.	140.0	$ 76.56	140.0	$ 76.56	140.0	$ 76.56	240.0	$ 110.83
Web	Cut from 60" wide steel coil	$ 0.41	sq.ft.	70.0	$ 28.92	70.0	$ 28.92	70.0	$ 28.92	180.0	$ 83.13
Bottom sheet	Steel sheet (from coil)	$ 0.41	sq.ft.	140.0	$ 57.85	140.0	$ 57.85	140.0	$ 57.85	240.0	$ 110.83
Insulation - rafter panel	PUR @ 2.3 lb/cu.ft. and $2/lb	$ 4.60	cu.ft.	60.7	$ 279.07	60.7	$ 279.07	60.7	$ 279.07	-	$ -
Top coat	Hylar 5000 PVDF coating	$ 90.00	gal.	2.3	$ 202.50	2.3	$ 202.50	2.3	$ 202.50	-	$ -
Finished interior surface	Gold Bond® 1/2"x4'x8' Fire-Shield Gypsum Board TPD	$ 0.15	sq.ft.	140.0	$ 21.00	140.0	$ 21.00	140.0	$ 21.00	240.0	$ 36.00
Galvanized coat	Zinc	$ 0.35	lb.	553.0	$ 193.55	553.0	$ 193.55	553.0	$ 193.55	1,096.8	$ 383.88
Packing materials	Plastic edge protector	$ 35.00	ea.	1.0	$ 35.00	1.0	$ 35.00	1.0	$ 35.00	1.0	$ 35.00
PV Integration											
PV Laminate	9x6 array, 211W, glass enclosed, edge sealed, $4.25/W	$ 896.75	ea.	-	$ -	4.0	$ 3,587.00	4.0	$ 3,587.00	-	$ -
Adhesive	Silicone sealant	$ 5.00	ea.	-	$ -	1.0	$ 5.00	1.0	$ 5.00	-	$ -
Conduit mounting brackets	Plastic, clip, glued to panel top sheet	$ 3.50	ea.	-	$ -	8.0	$ 28.00	8.0	$ 28.00	-	$ -
Conduit	PVC pipe	$ 3.00	ft.	-	$ -	12.0	$ 36.00	12.0	$ 36.00	-	$ -
Additonal packing material		$ 50.00	ft.	-	$ -	1.0	$ 50.00	1.0	$ 50.00	-	$ -
PV Balance of System											
GE Meter 2 LCD	Standard meter	$ 380.00	ea.	-	$ -	1.0	$ 380.00	1.0	$ 380.00	-	$ -
Inverter	Standard inverter	$ 1,040.00	ea.	-	$ -	1.0	$ 1,040.00	1.0	$ 1,040.00	-	$ -
30A AC disconnect		$ 42.94	ea.	-	$ -	1.0	$ 42.94	1.0	$ 42.94	-	$ -
M/F extension		$ 0.57	ft.	-	$ -	20.0	$ 11.40	20.0	$ 11.40	-	$ -
Roof connection kit	Penetrate at top of gable	$ 40.00	ea.	-	$ -	1.0	$ 40.00	1.0	$ 40.00	-	$ -
Owners manual		$ 5.00	ea.	-	$ -	1.0	$ 5.00	1.0	$ 5.00	-	$ -
Solar Thermal Integration											
Solar thermal panel	2 SunEarth flat panels	$ 1,100.00	ea.	-	$ -	-	$ -	2.0	$ 2,200.00	-	$ -
Pump	shop.solardirect.com	$ 250.00	ea.	-	$ -	-	$ -	1.0	$ 250.00	-	$ -
Valves	shop.solardirect.com	$ 200.00	ea.	-	$ -	-	$ -	1.0	$ 200.00	-	$ -
Misc. components	shop.solardirect.com	$ 150.00	ea.	-	$ -	-	$ -	1.0	$ 150.00	-	$ -
PVC pipe		$ 110.00	ea.	-	$ -	-	$ -	1.0	$ 110.00	-	$ -
Total					**$ 894.45**		**$ 6,119.79**		**$ 9,029.79**		**$ 759.67**
Total/sqft					**$ 6.39**		**$ 43.71**		**$ 64.50**		**$3.17**

Figure 9.1-1: Bill of materials for roof and ceiling panels.

9.1.2 Production Cost

The manufacturing process (Figure 4.4-3) was encoded into the cost model as a list of processing steps for which equipment cost, labor and floor space were estimated. GE's experience has shown that the exact process flow is less important in cost analysis than ensuring all steps are captured and the degree of automation is properly assessed. This information is in the tab "P&E DL sqft". The model includes production costs for roof panels, for panels with PV attached, and roof panels with PV and solar thermal collectors attached. To determine the amount of equipment needed at each step, an estimate was made of the throughput capacity for each machine. Capacity was captured as number of completed panels per hour per machine. Each capacity was converted to number of panels per year per machine by adjusting for number of hours per shift, number of shifts per day, and number of days per year. This representation of capacity allowed the scaling of the equipment set with different annual production needs from the factory. The number of machines required for each step was simply the annual factory capacity divided by the machine capacity.

Each machine had an estimated unit cost determined by benchmarking industrial machine suppliers or GE purchases. The total machine cost was calculated by multiplying the number of machines by the cost per machine, and summing across all process steps. GE captures "facilitization cost" for each machine. Typically, in an established factory, this cost runs 7 to 15% of the machine cost. In a new factory, infrastructure must be built to support the machinery. A rule of thumb for new facilities is that facilitization runs approximately 50% of equipment cost.

At each process step, an estimate was made of the direct labor required. In many cases, the staff per process step was lower than 1.0, indicating that the labor would be shared between workstations. As the number of machines scaled, to meet annual factory production throughput, the amount of direct labor scaled proportionally. Hence, there is a column in the costing table that indicates direct labor scaled ("DL Scaled").

Finally, a floor space estimate was made for each piece of equipment. This number also scaled with annual factory throughput. Each work area typically requires an additional factory area to cover walkways, offices, restrooms, etc. The multiplier on unit floor space for each workstation was 2.5x, a rule of thumb used in calculating floor space in many new GE facilities.

Assembly of solar components to the roof panel was assumed to be a manual process. The additional process steps would occur after the completion of the roof panel and include:

- Fabricate the wiring harness – This step would be done off-line, and would involve installing connectors on wires that run between PV modules and to the house, cutting wires to length, bundling those wires and inserting them into conduit.
- Attach conduit to roof panel – The prepared conduit would be attached with adhesive-mounted brackets to the top surface of the roof panel.

- Place PV module onto panel – Each formed recess on the roof panel would have a bead of adhesive applied, the PV modules would be connected to the wires in the conduit, and then lowered onto the roof panel.
- Continuity and light table check – An electrical test would be performed on wires to ensure continuity and each roof panel would experience a light check to ensure PV modules are generating electricity as designed.
- Pack and ship – The integration of solar modules to the top surface of the roof panel was expected to increase the complexity of the pack and ship operation as damage could occur in transit. Additional time was assumed in the production cost table – and incremental packing materials were added to the material cost table.

The final contributor to panel cost is estimated overhead. Overheads were estimated for a factory capable of 50,000 panels per year production. Overheads typically scale less continuously than other production costs. The overheads in the panel cost model are valid for annual panel throughputs up to roughly 100,000. Figure 9.1-2 shows overhead costs included in the spreadsheet tap "Panel Mfg Overhead".

All of the contributors to panel production cost are summed in the "Panel Summary Cost" tab within the spreadsheet model (Figure 9.1-3). The summary table is set up to allow changes to key operating parameters and immediate feedback of costing results. At the top of the summary table, there are cells that allow specification of baseline panel dimensions, quantity produced per year and labor shift patterns. Further down the table, there are places where unit labor costs and other assumptions can be entered. Near the bottom of the table, all variable and base costs are summed and displayed separately. A sales margin can be specified by the user. Twenty five percent is specified in the present analysis. The final calculations at the very bottom of the summary table show cost per panel and cost per square foot.

Overhead Costs (Valid Up To 100k Panels/yr)

Manufacturing Overhead Category	Cost ($k/yr)
Energy cost - equipment	$ 1,500
Energy cost - facilities (HVAC, lighting, etc.)	$ 560
Information/communication technology	$ 150
Grounds maintenance	$ 60
Canteen	$ 60
Custodial	$ 100
Equipment maintenance - material	$ 1,500
Equipment maintenance - labor	$ 1,300
Indirect materials	$ 250
Office expenses	$ 150
Travel	$ 200
Total	**$ 5,830**

Salaried Labor	# People
Plant Manager	1
Administrative Assistant/Receptionist	1
Manufacturing Engineer	2
EHS	1
Production Control	1
Sourcing	1
Finance	1
Quality Assurance	1
Total	**9**

Figure 9.1-2: Overhead cost table from the cost model.

Model Summary					
Inputs	**Performance & Operations**	**Ceiling Panel**	**Rafter Panel**	**PV Panel**	**PV+ST Panel**
	Panels Produced (#/yr)	50,000	50,000	50,000	50,000
	Yields (nonrecoverable losses)	99%	99%	99%	99%
	Panel Length (ft)	30	17.5	17.5	17.5
	Panel Width (ft)	8	8	8	8
	Number of Shifts	2	2	2	2
	Hours per Shift	7.5	7.5	7.5	7.5
	Days per Week	5	5	5	5
	Work Weeks per yr	50	50	50	50
	Direct Hourly	**Ceiling Panel**	**Rafter Panel**	**Solar Panel**	**PV+ST Panel**
	DL Headcount Ceiling Panel	46	-	-	-
	DL Headcount Rafter Panel Insulation	-	54	-	-
	DL Headcount Solar Integration	-	-	68	77
	Total DL Headcount	46	54	68	77
	Overall Labor				
	Hourly Wage ($/hr)	$22.00	$22.00	$22.00	$22.00
	Indirect Hourly Wage ($/hr)	$26.00	$26.00	$26.00	$26.00
	Salaried Wage ($/yr)	$85,000	$85,000	$85,000	$85,000
	DL Comp & Benefits (% of Salary)	50%	50%	50%	50%
	Indirect Hourly Percent of DL	15%	15%	15%	15%
	Number of Indirect Hourly	7	9	11	12
	Number of Salaried	9	9	9	9
	Materials				
	Direct Material Cost from BOM ($/unit)	$759.67	$894.45	$6,119.79	$9,029.79
	Effective Direct Material Cost (post yield) ($/unit)	$767.35	$903.48	$6,181.61	$9,121.00
	Consumables ($/unit)	$38.37	$45.17	$309.08	$456.05
	Total DM	**$805.71**	**$948.66**	**$6,490.69**	**$9,577.05**
	Plant Assumptions				
	Total P&E ($)	**$11,205,000**	**$12,405,000**	**$13,897,500**	**$14,347,500**
	Capex Depreciation (yr)	20	20	20	20
	Plant Size (ft^2)	99,000	101,000	105,400	107,700
	Lease / Rent ($/ft^2/yr)	$5.30	$5.30	$5.30	$5.30
Outputs	**Variable Costs**	**$/yr**	**$/yr**	**$/yr**	**$/yr**
	Total Material Cost ($/yr)	$40,285,619	$47,432,955	$324,534,318	$478,852,500
	Total Direct Hourly Cost ($/yr)	$5,690,025	$6,649,088	$8,393,963	$9,507,713
	Total Indirect Hourly Cost ($/yr)	$866,250	$1,113,750	$1,361,250	$1,485,000
	Manufacturing Overhead	$5,830,000	$5,830,000	$5,830,000	$5,830,000
	Total Variable Costs ($/yr)	**$52,671,894**	**$61,025,792**	**$340,119,531**	**$495,675,213**
	Base Costs				
	Total Salaried Comp & Ben ($/yr)	$1,147,500	$1,147,500	$1,147,500	$1,147,500
	Lease / Rent ($/yr)	$524,700	$535,300	$558,620	$570,810
	Capex Depreciation ($/yr)	$560,250	$620,250	$694,875	$717,375
	Insurance & Taxes	$649,329	$748,961	$3,363,660	$4,820,802
	Other Base Support Costs	$2,164,429	$2,496,538	$11,212,199	$16,069,339
	Total Base Costs ($/yr)	**$5,046,207**	**$5,548,549**	**$16,976,854**	**$23,325,825**
	Total Variable + Base Costs ($/yr)	**$57,718,101**	**$66,574,341**	**$357,096,385**	**$519,001,038**
	Total Variable + Base Costs ($/unit)	**$1,154.36**	**$1,331.49**	**$7,141.93**	**$10,380.02**
	Panel Sales Markup (%)	**25%**	**25%**	**25%**	**25%**
	Panel Sales Price ($/unit)	**$1,443**	**$1,664**	**$7,475**	**$10,713**
	Panel Sales Price ($/sq ft)	**$6.01**	**$11.89**	**$53.39**	**$76.52**
	Sales Revenue ($/yr)	**$72,147,626**	**$83,217,926**	**$373,739,970**	**$535,644,623**

Figure 9.1-3: Panel production summary tab.

One of the clear model sensitivities is with panel production volume. As annual volume increases, so must the plant and equipment investment. The scaling of costs happens differently for different cost contributors. Hence, as volume increases, cost per part drops at a changing rate. At lower volumes, the incremental decrease in cost/per part (as volume scales) is greater as the number of parts produced dominates the calculation of cost per part. As base costs are spread over more parts per year, the costs become dominated by materials and the curve flattens out. At 50,000 parts per year, production cost for an 8 by 17.5 ft rafter panel is $9.41 (not shown in Figure 9.1-3 but easily calculated in the panel summary cost spreadsheet by setting "Sales Markup" to 0%) prior to sales markup. Panel cost is not very sensitive to increases in production volume above 50,000. Nearly seventy percent of the production cost is due to materials with the remainder split roughly equally between labor and overhead. As a result, panel costs would expect to fluctuate as material costs change in the commodities market. With a 25% sales markup, the cost of the rafter panel is $11.89/ft^2.

Production cost of the ceiling panel is $4.76. Material costs are 66% of this value. With a sales markup of 25%, the ceiling panel would sell for $6.01/ft^2.

9.1.3 Construction Cost

Construction costs were estimated based upon a cost survey published in the "2008 National Construction Estimator" (Ogershok and Pray, 2008). Only those construction costs that differed between alternatives were tabulated. All other costs were assumed to be identical between house designs.

For instance, each house had an identical foundation size, so the cost of preparing the foundation was not included in the analysis. However, the panelized roof houses requires reinforced footings to support columns that hold up the ridge beam. Hence, reinforced footings were included in the analysis. Also included are the costs of additional interior finishing with panelized construction. The costs of the added bathroom, windows, doors and wall finish in option C are included in the current model. The result was a difference in costs between each alternative and the baseline. This difference was applied to the baseline house cost of $350,000 – yielding a comparative house construction view.

The basic flowchart of the construction process is shown in Figure 9.1-4. Annotations are provided to indicate where differences existed between each alternative house design. For each annotation, there is a corresponding cost entry in the spreadsheet model. The layout of the construction cost table is shown in Figure 9.1-5.

For the house option C, costs are provided for conventional frame construction of the floor of the enclosed attic as well as for use of ceiling panels. The total cost is based on the least expensive option.

The majority of cost increase due to solar integration on the roof panel was embedded in the factory production cost tables. The only cost added to the construction cost table was the labor required to tie in the wiring and plumbing to the house (at the ridge). When the solar thermal switch on the "Summary" tab is turned off, all costs associated with the solar hot water components are disregarded in the tabulation of construction costs.

9.1.4 Energy Cost

The cost model allows estimation of energy savings under different assumptions. A summary of the economic analysis is provided in the spreadsheet in the tab labeled "Summary" (Figure 9.1-6). At the top of the spreadsheet, financial assumptions are listed. These include sales price of the baseline Option A house and financing terms. Energy parameters are listed below the financial information. There is an additional section that specifies government incentive benefits for each home. There are separate benefits for insulation and roofing, so these are separated in the model. The government incentives are subtracted from the house price (mortgage present value), providing small monthly cash flow savings over the life of the mortgage. Parameters that may be changed in the model include HVAC and hot water loads, number and characteristics of solar PV and solar thermal modules, cost of electricity, and value of energy efficiency financial incentives.

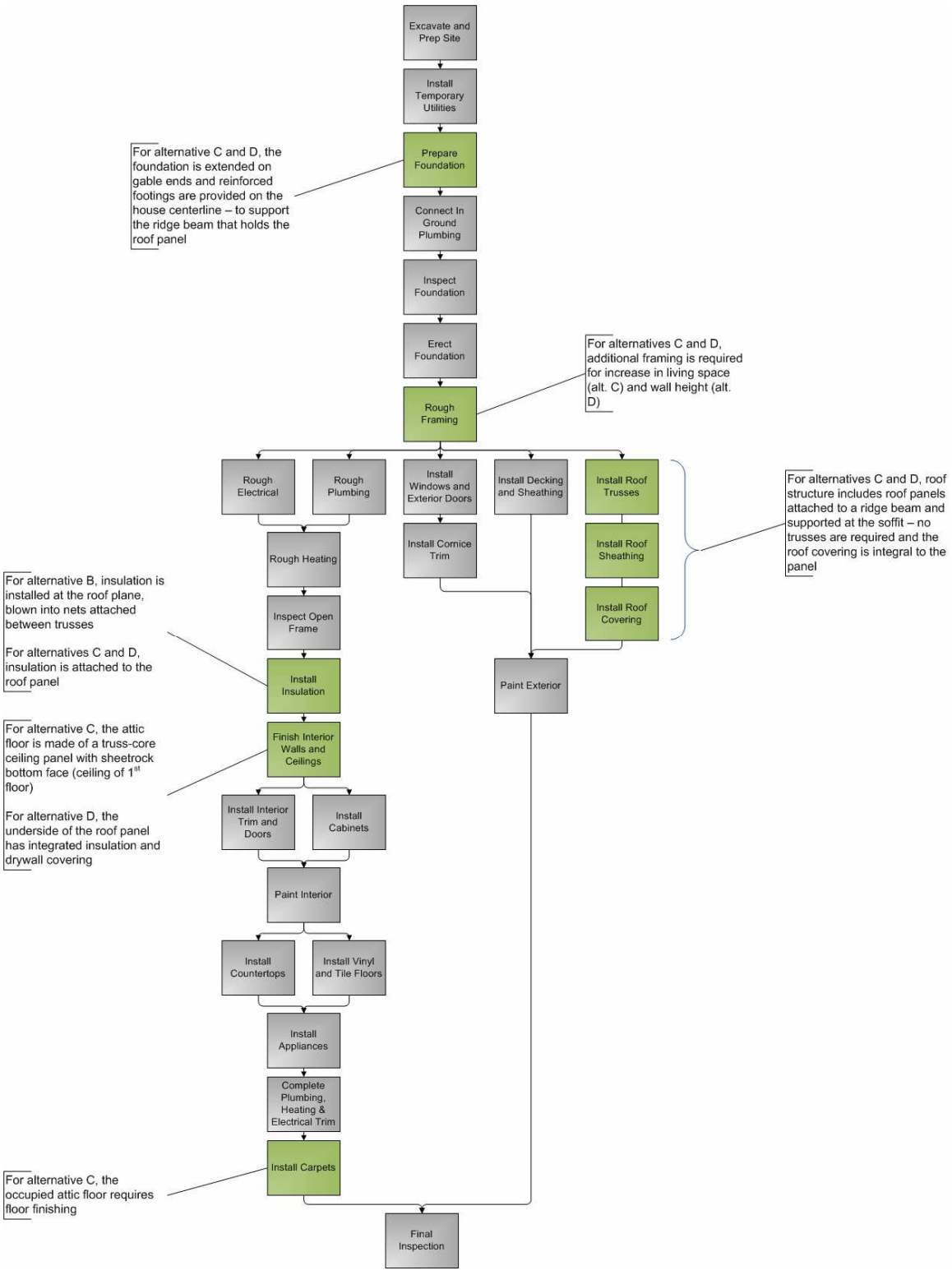

Figure 9.1-4: Home construction flowchart, showing differences between alternative house designs.

Variance Analysis - Construction Costs

House Construction - Process Step	A: Base Case - Conventional House				B: Base Case - Energy Efficient House				C: Panelized, Steep Slope, Occupied Attic				D: Panelized, Shallow Slope, Cathedral				E: Panelized, Shallow Slope, Cathedral, Solar			
	Mat'l	Labor	Eqt	Total	Mat'l	Labor	Eqt	Total	Mat'l	Labor	Eqt	Total	Mat'l	Labor	Eqt	Total	Mat'l	Labor	Eqt	Total
Foundation																				
Column footings (4, to support ridge beam)	$ -	$ -	$ -	**$ -**	$ -	$ -	$ -	**$ -**	$ 703	$ -	$ -	**$ 703**	$ 586	$ -	$ -	**$ 586**	$ 469	$ -	$ -	**$ 469**
Rough Framing																				
Trusses	$ 2,513	$ 981	$ 161	**$ 3,655**	$ 2,513	$ 981	$ 161	**$ 3,655**	$ -	$ -	$ -	**$ -**	$ -	$ -	$ -	**$ -**	$ -	$ -	$ -	**$ -**
Additional wall area inside house	$ -	$ -	$ -	**$ -**	$ -	$ -	$ -	**$ -**	$ 1,321	$ 2,960	$ -	**$ 4,281**	$ 330	$ 741	$ -	**$ 1,071**	$ 330	$ 741	$ -	**$ 1,071**
Ridge beam (2" x 12" x 56' beam)	$ -	$ -	$ -	**$ -**	$ -	$ -	$ -	**$ -**	$ 96	$ 123	$ -	**$ 220**	$ 96	$ 123	$ -	**$ 220**	$ 96	$ 123	$ -	**$ 220**
Support columns (5 1/2 x 5 1/4" Parallel Strand Lumber)	$ -	$ -	$ -	**$ -**	$ -	$ -	$ -	**$ -**	$ 170	$ 58	$ -	**$ 228**	$ 141	$ 48	$ -	**$ 190**	$ 113	$ 39	$ -	**$ 152**
Decking and Sheathing																				
Roof sheathing, 7/16"OSB	$ 1,680	$ 403	$ -	**$ 2,083**	$ 1,680	$ 403	$ -	**$ 2,083**	$ -	$ -	$ -	**$ -**	$ -	$ -	$ -	**$ -**	$ -	$ -	$ -	**$ -**
12. 5 Rafter panels (Steep slope: 12.5x8'x21'; shallow slope: 12.5x8'x17.5' ; insulated with drywall)	$ -	$ -	$ -	**$ -**	$ -	$ -	$ -	**$ -**	$ 24,965	$ 1,081	$ 800	**$ 26,847**	$ 20,804	$ 1,081	$ 800	**$ 22,686**	$ 41,474	$ 1,081	$ 800	**$ 43,355**
5 Garage rafter panels (steep slope: 5x8'x14.5' shallow slope: 5x8'x12', insulated with drywall)	$ -	$ -	$ -	**$ -**	$ -	$ -	$ -	**$ -**	$ 6,895	$ -	$ -	**$ 6,895**	$ 5,706	$ -	$ -	**$ 5,706**	$ 5,706			**$ 5,706**
Attic Floor																				
Ceiling panel (8' x 30', no insulation)	$ -	$ -	$ -	**$ -**	$ -	$ -	$ -	**$ -**	$ 8,658	$ -	$ -	**$ 8,658**	$ -	$ -	$ -	**$ -**	$ -	$ -	$ -	**$ -**
Conventional Framing $5/sqft(1440 sq ft)									$ 7,200	$ -	$ -	**$ 7,200**								
Interior Finishing																				
Additional wall area inside house	$ -	$ -	$ -	**$ -**	$ -	$ -	$ -	**$ -**	$ 1,321	$ 2,960	$ -	**$ 4,281**	$ 330	$ 741	$ -	**$ 1,071**	$ 330	$ 741	$ -	**$ 1,071**
Sheetrock on ceiling (5/8" gypsum)	$ 444	$ 780	$ -	**$ 1,223**	$ 444	$ 780	$ -	**$ 1,223**	$ -	$ -	$ -	**$ -**	$ -	$ -	$ -	**$ -**	$ -	$ -	$ -	**$ -**
Bath, 3 windows and doors for finished attic									$ 8,000			**$ 8,000**								
Rough Electrical																				
PV installation (electrician, 8 hours)	$ -	$ -	$ -	**$ -**	$ -	$ -	$ -	**$ -**	$ -	$ -	$ -	**$ -**	$ -	$ -	$ -	**$ -**	$ -	$ 420	$ -	**$ 420**
Rough Plumbing																				
ST installation (plumber, 6 hours)	$ -	$ -	$ -	**$ -**	$ -	$ -	$ -	**$ -**	$ -	$ -	$ -	**$ -**	$ -	$ -	$ -	**$ -**	$ -	$ 436	$ -	**$ 436**
Roofing																				
Roofing felt	$ 136	$ 274	$ -	**$ 410**	$ 136	$ 274	$ -	**$ 410**	$ -	$ -	$ -	**$ -**	$ -	$ -	$ -	**$ -**	$ -	$ -	$ -	**$ -**
Shingles	$ 877	$ 1,003	$ -	**$ 1,880**	$ 877	$ 1,003	$ -	**$ 1,880**	$ -	$ -	$ -	**$ -**	$ -	$ -	$ -	**$ -**	$ -	$ -	$ -	**$ -**
Insulation (Attic)																				
Fiberglass batts, attic floor	$ 1,223	$ 363	$ -	**$ 1,586**	$ -	$ -	$ -	**$ -**	$ -	$ -	$ -	**$ -**	$ -	$ -	$ -	**$ -**	$ -	$ -	$ -	**$ -**
Netting and blown in at roof plane	$ -	$ -	$ -	**$ -**	$ 482	$ 1,134	$ 300	**$ 1,915**	$ -	$ -	$ -	**$ -**	$ -	$ -	$ -	**$ -**	$ -	$ -	$ -	**$ -**
Carpeting																				
Attic floor (nylon 26 oz, with pad, 149 sq yards)	$ -	$ -	$ -	**$ -**	$ -	$ -	$ -	**$ -**	$ 1,296	$ 894	$ -	**$ 2,190**	$ -	$ -	$ -	**$ -**	$ -	$ -	$ -	**$ -**
Total Cost (from above)	**$ 6,873**	**$ 3,803**	**$ 161**	**$ 10,837**	**$ 6,131**	**$ 4,574**	**$ 461**	**$ 11,166**	**$ 51,967**	**$ 8,077**	**$ 800**	**$ 60,844**	**$ 27,994**	**$ 2,735**	**$ 800**	**$ 31,529**	**$ 48,518**	**$ 3,582**	**$ 800**	**$ 52,900**

Figure 9.1-5: Construction cost comparison table from cost analysis spreadsheet.

House Information					
Model Name	Morgan @ Solera				
Location	Las Vegas, NV				
Type	Ranch				
Number of Floors	Single				

Financial Summary	A: Base Case	B: Base Case, Energy Efficient	C: Panelized, Occupied Attic	D: Panelized, Cathedral Ceiling	E: (Option D) with Solar Technology
Financing					
Sales Price (includes land value of $100,000)	$ 350,000	$ 350,329	$ 400,007	$ 370,692	$ 391,734
Down Payment	$ 30,000	$ 30,000	$ 30,000	$ 30,000	$ 30,000
Mortgage Present Value	$ 320,000	$ 319,829	$ 369,007	$ 339,692	$ 350,404
Term	30	30	30	30	30
Interest Rate	5.00%	5.00%	5.00%	5.00%	5.00%
Monthly P&I	$ 1,718	$ 1,717	$ 1,981	$ 1,824	$ 1,881
Energy					
Number of Roof Panels with PV Installed	NA	NA	NA	NA	3
Include Solar Thermal (y/n)?	NA	NA	NA	NA	y
PV Watts Installed	NA	NA	NA	NA	2532
PV Capacity Factor	NA	NA	NA	NA	19%
PV Efficiency Gain - Backplane Cooling	0	0	0	0	2%
PV Energy Generated (kWh/month)	0	0	0	0	383
HVAC Electricity Usage (kWh/month)	476	486	426	339	339
Hot Water Electricity Usage (kWh/month)	212	212	212	212	212
Hot Water Electricity Savings (%)	-	-	-	-	70%
Total Electricity Use, Net (kWh/month)	688	698	638	551	20
Electricity Cost ($/kWh)	$ 0.10	$ 0.10	$ 0.10	$ 0.10	$ 0.10
Electricity Cost ($/month)	$ 68.80	$ 69.80	$ 63.80	$ 55.10	$ 1.98
Incentives					
Roofing Energy Efficiency Tax Credit	$ -	$ -	$ 500.00	$ 500.00	$ 500.00
Insulation Energy Efficiency Tax Credit	$ -	$ -	$ 500.00	$ 500.00	$ 500.00
Nevada State Solar Rebate ($2.5/kW)	$ -	$ 500.00	$ -	$ -	$ 6,330.00
PV Energy Efficiency Tax Credit	$ -	$ -	$ -	$ -	$ 2,000.00
ST Energy Efficiency Tax Credit	$ -	$ -	$ -	$ -	$ 2,000.00
Homeowner Monthly Expenses - Home Finance + Energy ($/mo)	**$1,787**	**$1,787**	**$2,045**	**$1,879**	**$1,883**
Monthly Savings in Homeowner Expenses Compared to Option A	**NA**	**($0)**	**($258)**	**($92)**	**($96)**
House Sales Price per Finished Sq Ft (Non-Garage) $/sqft. This figure assume that the value of the land is $100,000. Cost of the 460 sq ft garage is $23,000 at $50/sqft.	**$197**	**$197**	**$148**	**$214**	**$233**
HVAC Energy Consumption Compared to Option A (fraction)	**NA**	**0.02**	**(0.11)**	**(0.29)**	**(0.29)**
Annual Reduction in Load for Space Conditioning (kWh/year)	**NA**	**(120)**	**600**	**1,644**	**1,644**
Net Annual HVAC Energy per Living Area (kWh/sqft/yr)	**4.95**	**5.05**	**2.72**	**3.52**	**0.00**
Net Annual HVAC + Hot Water Energy Use Per Living Area (kWh/sqft/yr)	**7.15**	**7.25**	**4.08**	**5.72**	**0.21**

Figure 9.1-6: Summary cost comparison table from cost analysis spreadsheet.

Annual simulations were performed to estimate the heating, cooling, and water heating electric consumption of the five house options. Simulations were run in REM/Rate, version 12.3, using weather data for Las Vegas, Nevada. Houses A, B, C, and D were simulated, with house E being presumed similar in energy consumption to house D. Variables used to model the individual cases can be found in Table 9.1-2. All houses were assumed to use slab-on-grade construction, with R-5 insulation under the slab. Walls were specified according to the architectural drawings supplied by the builder, and consist of 2x4 framing with R-13 cellulose insulation. A layer of 1 in. foam insulation is run continuously over the OSB sheathing, which provides a ground surface for a synthetic stucco finish. The R-value of the foam was modeled as R-4. The specific area of wall included in each model varies by house, and reflects differences in roof slope and the location of the insulation plane. Window size and placement correspond with plans as provided, with the exception of house C, which required additional windows to provide egress paths to the upstairs bedrooms. Window construction is assumed to

Table 9.1-2: Values used to model energy consumption in the five homes.

	Option A	Option B	Option C	Option D	Option E
Plan					
Finished area (ft^2)	1155	1155	1878	1155	1155
Volume of conditioned space (ft^3)	10395	16459	21916	12916	12916
Envelope area[1] (ft^2)	2469	3236	3773	3079	3079
Insulation plane	Attic floor	Attic floor	Roof plane	Roof plane	Roof plane
Area of roof for thermal losses to ambient (ft^2)	1155	1734	2084	1652	1652
Energy					
Attic R-value (h-ft^2-°F/Btu)	25	25	30	30	30
Net air Infiltration[2] (ach)	0.5	0.5	0.28	0.29	0.29
Heat pump capacity (kBtuh)	24	30	24	18	18
Heating Load (kWh/month)	210	244	175[3]	144	144
Cooling Load (kWh/month)	266	242	251	195	195
Total HVAC Load (kWh/month)	476	486	426	339	339
Hot Water Load (kWh/month)	212	212	212	212	212
PV Installed (kW)					2.5
Solar Hot Water (ft^2)					64

[1] The envelope area is the surface area for thermal losses. For option A it includes the area of the floor of the attic. For all other options it includes the roof area.

[2] The net ach is a weighted average based on 0.5 ach for the area considered conventional construction and 0.1 ach for the panelized roof.

[3] Energy loads for the larger home are estimated assuming no change in occupancy.

consist of double-glazed panes in vinyl frames, with a low-e coating. Attic insulation for the conventional home options A and B is R-25. Air infiltration rate was set at 0.5 air changes per hour (ach).

Panelized homes provide improved insulation properties and reduced air infiltration through the roof. Options C, D and E were modeled with R-30 at the roof plane to simulate the panelized construction. For the factory quality panels on Options C, D and E, the air infiltration rate was halved to 0.1 ach for the fraction of the envelope area covered with panels. For the remainder of the envelope area, the air infiltration was set to 0.5 ach consistent with options A and B. The reduction in air infiltration reflects

the enhanced air tightness possible with panelized construction and rigid foam insulation at the roof plane.

The mechanical system, water heater, and ducts were modeled in the unconditioned attic, or in the conditioned attic, as appropriate for a given design. Ducts modeled in unconditioned attic spaces were simulated at 75% thermal efficiency to reflect energy losses to the unconditioned attic, while those run in conditioned spaces were simulated at 95% thermal efficiency.

HVAC systems for all cases consist of a 12 SEER (Seasonal Energy Efficiency Ratio), 7.5 HSPF (Heating Seasonal Performance Factor) electric heat pump. Heat pump capacity varies by house size, and reflects loads modeled for that design. Water heating is provided by a 30-gallon (113 liter) electric water heater.

9.2 Economic Results

Key input parameters to the present model are listed in Table 9.2-1. Results using the assumption in the present study are shown in Figure 9.1-6 and summarized in Table 9.2-1. Assumptions include a 30 year term mortgage at 5% interest rate, an electricity rate of $0.10/kWh, and a 2.5kW rated PV system for option E. All HVAC and hot water loads are met with electricity. Calculation of energy costs assumes net metering and credits the homeowner at the full retail rate for electricity.

Given the assumptions in the cost model, the least expensive home is Option A ($350,000). The cost per square foot of living space is $197/ft^2 (note this value is based on the selling price of the home minus the land cost of $100,000). The average monthly cost for electricity for HVAC and water heating is $69. Per finished area, the annual HVAC energy use is 4.95 kWh/ft^2. With water heating, the annual energy use is $7.15/ kWh/ft^2. The monthly expense of the mortgage plus electricity is $1,787.

Option B is slightly more expensive to purchase than option A due to the cost of installing loose fill insulation at the roof plane ($350,329). The cost per square foot of living space is essentially the same as option A. There is no energy benefit of option B compared to option A because the thermal losses through the roof are greater than through the attic floor in option A. The added thermal losses from the roof offset the benefit of placing the ducts in a conditioned attic space. The HVAC energy consumption for option B is 2% higher than for option A. The average monthly cost for electricity for HVAC and water heating is $70. With a $500 tax credit, the option B house does not increase the monthly expense for the homeowner relative to option A. However because there is no energy savings, the tax credit should not be available. If the tax credit is not given, the monthly cost of Option B increases by $2.

Option C, which has a panelized roof and converts the attic to a second floor living space, costs $400,007, $50,007 more than the conventional option A house. The biggest contributor to this difference is the cost of the roof panels ($26.847 for the attic and $6,895 for the garage). The remaining difference is due to changes in the plan. The cost per square foot of living space is reduced 25% compared to option A to $148/ft^2. The average monthly cost for electricity for HVAC and water heating is $64. Per

finished area, the annual HVAC energy use is reduced 45% to 2.72 kWh/ft^2. This result suggests panelized roofs may be of more economic benefit when the added living space is considered. The added living space in this house is valuable space for the homeowner. The added living space is 723 ft^2 and includes two large bedrooms, a bath and three closets. The larger house results in roughly $258 monthly increase in expenses for the homeowner relative to option A.

Option D also uses a panelized roof but is constructed with a shallow slope roof and is thus a single story home with the same living space as option A. Option D costs $20,692 more than option A. The cost per square foot of living space is $214. The benefit of this home is reduced total energy consumption. Option D has the lowest monthly energy cost of the non solar options ($55/month). Per finished area, the annual HVAC energy use is 3.52 kWh/ft^2, nearly a 30% reduction relative to option A. The monthly expense is increased $92 relative to option A.

Option E uses PV and solar thermal panels to achieve a net zero-energy home. The comparison for energy performance and cost is relative to option D, which is an identical home without solar. One important result of the analysis is the significant projected reduction in PV installation cost. The price difference between house alternative D (roof panel) and E with integrated PV (without solar hot water) is related solely to the material, production and construction costs of the PV system. For a 2.5kW PV system (19% capacity), the difference in house prices is roughly $17,367, or $6.95/W. The cost for PV installation compares favorably to typical residential installed systems that cost $9/kW. The addition of a solar water heater (64 ft^2 of collector area plus balance of system components for a solar fraction of 70%) adds $3674 to the cost of the home. The solar home is essentially net zero energy (only 20 kWh per month). At $0.10/kWh the solar home saves the homeowner $53/month in energy costs over option D. The average monthly electric bill is $2. The monthly expense of the homeowner is increased $14 relative to option D.

In summary, the economic model provides a basis upon which to evaluate panelized roof economics, particularly as market conditions change. All costs assumptions are based on prices available September 2008. As material, energy, labor and construction costs change, model parameters can be modified to provide a new assessment of panel economics. It is likely that the economics of the panelized roof shift in the future. The economic model described herein provides an ongoing tool for understanding those shifts.

Table 9.2-1: Input parameters and results of economic assessment.

	Option A	Option B	Option C	Option D	Option E
Financial					
House Price ($)	350,000	350,329	400,007	370,692	393,615 (with PV and solar thermal)
Price/Area[1] ($/ft^2)	197	197	148	214	234
Down Payment (%)	10%	10%	10%	10%	10%
Term (years)	30	30	30	30	30
Interest Rate (%)	5	5	5	5	5
Energy					
Cost of Electricity ($/kWh)	0.10	0.10	0.10	0.10	0.10
Summary of Results					
Electricity Cost ($/mo)	69	70	64	55	2
Annual HVAC Energy Use per Living Area (kWh/ft^2/yr)	4.95	5.05	2.73	3.52	0
Cost ($/month) [Mortgage+Energy]	1787	1787	2045	1879	1893

[1] Based on selling price of the home minus the cost of land and construction of the garage at $50/ft^2.

10.0 Recommendation

Improvements in the building envelope can reduce energy consumption significantly. Thermal losses (or gains) from the roof make up 14 percent of the building component energy load. Infiltration through the building envelope, including the roof, accounts for an additional 28 percent of the heating loads and 16 percent of the cooling loads. These figures provide a strong incentive to develop and implement more energy efficient roof systems. However, the roof is a challenging component of the building envelope to change because of the wide spread use and cost effectiveness of the engineered roof truss. The energy savings of a new roof system must be balanced with first and life-cycle costs, durability, appearance, and ease of construction.

The objectives of this study were to design and evaluate the ability of a panelized roof system to provide a superior roof for residential buildings. At the onset, the builder partner wanted a completely open conditioned attic space for HVAC equipment and storage space in traditional home styles. Consequently the project team's primary goal was to develop manufactured rafter panels that could provide all the structural support, insulation, and moisture protection without significant change to the architectural style of production and semi-custom homes. From an energy perspective, the goal was to reduce thermal bridging and air infiltration – both problems in truss roof construction. A secondary goal was to integrate the roof panels with solar photovoltaics and solar hot water systems. Market acceptability and cost were important considerations.

A nationwide market assessment that was conducted as part of this study shows there is a broad market opportunity with production and semi-custom builders in the United States for such a system. The market potential is enhanced through construction activity levels in target markets. Southern markets, from Florida to Texas account for 50 percent of the total new construction angled-roof volume. California contributes an additional 13 percent share of market volume. These states account for 2.8 to 3 billion square feet of new construction angled roof opportunity.

In response to these needs and opportunity, the University of Minnesota collaborated with industry to conceive and design a panelized roof system for residential buildings. A number of potential design options and materials were considered and analyzed for their ability to meet applicable standards and codes for structure and hygrothermal performance, manufacturability, constructability, architectural integration, and cost. The outcome of this initial assessment was the selection of cold rolled steel and polyurethane foam as materials. Steel was selected over wood products because it is amenable to a continuous off-site manufacturing process and has the properties required for long spans and roof loads across the U.S. Polyurethane was selected because it can be foamed in-situ and naturally adheres to a number of materials including steel, gypsum board and OSB. Moreover, it is recommended over other insulating foams in the case of fire.

Two panel designs, referred to as the truss core panel and the stiffened plate panel, were down selected from a number of options. The unique aspect of both the truss

core and the stiffened plate panel is that each separate the function of the steel structure from the foam insulation yet can be manufactured as an assembly in a factory. The steel provides the long life desired for residential construction and the foam provides excellent thermal properties and minimizes air infiltration.

Prototypes of both the truss core and the stiffened plate panels were fabricated using laser welding and tested for structural performance. The foaming process and foam properties were also examined. The prototype testing program confirmed the suitability of the materials for the application and validated the design algorithm developed to design panels. Connections and architectural details at panel to panel, ridge, soffit and gable end joints were designed to satisfy structural, hygrothermal performance requirements at these common joints. The ridge and soffit joint connectors were developed for a ridge beam or equivalent support for relatively single gabled homes. The ridge beam leaves a clear attic span and at the same time reduces the complexity of the connectors, particularly at the soffit. GE Global Research and the University of Minnesota developed concepts to integrate solar photovoltaics (PV) into the roof panel.

After evaluation and comparison of the two down selected panels for structural and hygrothermal performance along with their compatibility with architectural practice, the truss core panel was identified as the most versatile design. The truss core panel satisfies thermal and structural loading requirements throughout the United States for wind loads as high as 130 mph and for a range of roof spans and roof slopes. Panel configuration can be tailored for warm and cold climates with different finish options. The panel exceeds the basic criteria of the building envelope including providing insulation without thermal bridging, reducing air infiltration, managing vapor and moisture for a given climate, and accommodating conventional shingle or tile roof finishes or serving as an integral metal roof. The only drawback of using the panel to span between the soffit and the ridge without any intermediate support is the need for a ridge beam to avoid an overly complex connection at the soffit.

Representative panel designs are included in the report. Designs include specification of materials, dimensions, manufacture, connectors, and production and construction costs. Architectural details including field assembly procedures ensure drainage of rainwater, a continuous moisture barrier, minimize infiltration and thermal bridging and ease of field assembly. Panel to panel connectors join adjacent panels very simply at the steel structure and thus avoid conductive paths across the foam. Ridge, soffit and gable end connectors are comprised of sheet metal assemblies that conform to the angles at the ridge, soffit and gable ends. Application of the panelized roof system is described for a $350,000, 1155 square foot home plus 460 square foot garage with a simple gable roof currently built in Las Vegas.

For the panelized roof system to be commercially viable, it must compete economically with existing roof products. Roofing has seen a gradual reduction in installed cost to the point where a new roofing product, like the panelized roof, may struggle to compete in today's market on the basis of first cost. At 50,000 parts per year, production cost for an 8 by 17.5 ft rafter panel is $\$9.41/ft^2$ prior to sales markup. Panel

cost is not very sensitive to increases in production volume above 50,000. Approximately 70 percent of the production cost is due to materials with the remainder split roughly equally between labor and overhead. As a result, panel costs are expected to fluctuate as material costs change in the commodities market.

The benefits to the homeowner of the panelized roof are the savings in energy costs over the lifetime of the home and the added space if the attic is converted to occupied space. In the example Las Vegas home, this conversion to occupied space provides nearly 725 ft^2 of new space with two large bedrooms and a bath. Panelized construction initially costs more than a conventional truss roof system used today.

Without any major change to the house plan, the panelized system adds $20,692 to the cost of the Las Vegas home. The projected energy benefit is a 29% reduction in energy used for space heating and cooling. The energy saving are attributed primarily to reduced air infiltration and to a lesser extent to the higher effective R-value. In addition, there is a significant projected reduction in PV cost when PV modules are integrated with the roof panel during production (the saving are estimated to be $2/W).

The panelized roof has a greater benefit if the roof is steeper and the attic is converted to attractive living space. In this case, the annual HVAC energy is reduced by 45 percent on a per square foot basis. In addition, the cost per square foot of living space is reduced from $197/$ft^2$ to $148/$ft^2$.

In conclusion, the truss core panelized roof system offers a promising technology for achieving a more energy efficient home and offers a superior roof system in many respects. The panelized roof system is designed to be placed on any conventionally-built house and is adaptable to a wide range of house types and styles. Manufacturing processes and on-site erection procedures appear feasible and there are interested manufacturers. The justification for panelized construction is a substantial increase in energy efficiency and for solar integrated panels, lower net cost.

As a follow up to the present study, a key question is can changes to the design reduce cost? One option may be to consider panels spanning shorter distances between beams, trusses or other intermediate supports. This option may prove more economic than the truss core panel, which combined with a ridge beam and columns, is capable of supporting the roof between the soffit and the ridge.

Another option is to consider a redesign of the entire house. The truss core panel was developed independently of the rest of the house. While this makes sense in terms of the broadest possible application and market, it does not permit the synergies that would occur with a whole house panelized system where connection systems and construction methods can be completely optimized. Such a system could lead to further performance enhancements and cost reductions. House designs could be developed that use the system more efficiently while still providing a variety of styles and options.

References

[ASHRAE] American Society of Heating, Refrigerating and Air-Conditioning Engineers. 2005. Thermal and Moisture Control in Insulated Assemblies-Fundamentals, Chapter 23. Atlanta, GA: ASHRAE

[AISI] American Iron and Steel Institute. 2001. North American Specification for the Design of Cold-Formed Steel Structural Members.

Davidson, J. H. et al. 2006. Advanced Energy Efficient Roof System: Topical Report. University of Minnesota.

Davidson, J.H. et al. 2007a. Advanced Energy Efficient Roof System: Topical Report Year 2. University of Minnesota.

Davidson, J.H. et al. 2007b. Advanced Energy Efficient Roof System: Addendum Topical Report Year 2. University of Minnesota.

Davies, J. M. 1994. "Core Materials for Sandwich Cladding Panels." In International Conference on Building Envelope Systems and Technology, pp. 299-306, Singapore.

Desjarlais, A. O., T. W. Petrie, and T. Stovall. 2004. “Comparison of Cathedralized Attics to Conventional Attics: Where and When do Cathedralized Attics Save Energy and Operating Costs?” In Performance of Exterior Envelopes of Whole Buildings IX International Conference. Atlanta, GA: ASHRAE.

Hendron, R., S. Farrar-Nagy, R. Anderson, P. Reeves, and E. Hancock. 2004. “Thermal Performance of Unvented Attics in Hot-Dry Climates: Results from Building America.” ASME Journal of Solar Energy Engineering, **126**, pp. 732-737.

[ICC] International Code Council. 2003a. 2003 International Residential Code for One- and Two-Family Dwellings. Country Club Hills, IL: ICC.

[ICC] International Code Council. 2003b. 2003 International Energy Conservation Code. Country Club Hills, IL: ICC.

[ISO] International Organization for Standardization. 1992a. *ISO 9223 Corrosion of Metals and Alloys -- Corrosivity of Atmospheres Classification.* Geneva, Switzerland: ISO.

[ISO] International Organization for Standardization. 1992b. *ISO 9224 Corrosion of metals and alloys -- Corrosivity of Atmospheres Guiding values for the Corrosivity Categories.* Geneva, Switzerland: ISO.

[ISO] International Organization for Standardization. 2002. *ISO 11303 Corrosion of Metals and Alloys -- Guidelines for Selection of Protection Methods Against Atmospheric Corrosion.* Geneva, Switzerland: ISO.

Künzel, H., M. Holm, A. Zirkelbach, D. and Karagiozis A.N. 2005. “Simulation of Indoor Temperature and Humidity Conditions Including Hygrothermal Interactions with the Building Envelope” *Solar Energy*, **78**, pp. 554-561.

Lstiburek, J. and J. Straube. 2008. “BSP-032: Designs that Work: Hot-Humid Climate (New Orleans, LA),” *www. buildingscience.com.*

Ogershok, D. and R. Pray, Eds. 2008. *2008 National Construction Estimator*. Los Angeles: Craftsman.

Rudd, A. 2005. “Field Performance of Unvented Cathedralized (UC) attics in the USA.” *Journal of Building Physics*, 29(2):145-169.

Timoshenko, S. P. and J. M. Gere. 1961. *Theory of Elastic Stability*. New York: McGraw-Hill.

WUFI 2D-3.0, Institute of Building Physics. 2005. Oberlaindern Germany.

Advanced Energy Efficient Roof System

DE-FC26-04NT42114
Final Report
Volume II: Appendices

to

Parrish Galusky
Marc LaFrance
Department of Energy
National Energy Technology Laboratory
Energy Efficient Buildings Technologies
3610 Collins Ferry Road, P.O. Box 880
Morgantown, WV 26507-0880

Submitted by

University of Minnesota
Technical Contact: Professor Jane H. Davidson
Department of Mechanical Engineering
111 Church St., S. E.
Minneapolis, MN 55455
TEL: 612-626-9850
FAX: 612-625-6069
EMAIL: JHD@me.umn.edu

September 25, 2008

Advanced Energy Efficient Roof system

This report provides the final results of a collaboration of the University of Minnesota and industry partners to develop an innovative residential roof with the primary objective of creating a more energy efficient building envelope. The research and development focused on a panelized roof system. The design approach and examples of panel design and implementation in residential buildings are presented in Volume I. Economic and energy analyses compare the projected cost and savings in energy used for space heating. Volume II includes appendices with additional information on approach as well as supplemental results.

Major contributors to the effort are:

Jane H. Davidson, Susan C. Mantell
G.L. Di Muoio, G. Mittelman, C. Briscoe, B. Schoenbauer, and D. Huang
Department of Mechanical Engineering
University of Minnesota

T. Okazaki, C.K. Shield, B.J. Siljenberg
Department of Civil Engineering
University of Minnesota

John C. Carmody, and G.E. Mosiman
Center for Sustainable Building Research
University of Minnesota

David H. MacDonald
Mattson MacDonald Young
Minneapolis, Minnesota

Peter Kalish
GE Global Research
Niskayuna, NY 12309

Additional contributors include Jim Petersen, Pulte Home Sciences, Larry Wrass, formerly with Pulte Homes, and Ducker Worldwide. Mike Krupa, BASF, provided valuable expertise on foam properties and manufactured components for the prototypes with foam. Kennotech of Finland provided valuable expertise on laser welding and fabricated the truss core panel prototypes.

This report was prepared with the support of the U.S. Department of Energy, under Award No. DE-FC26-04NT42114. However, any opinions, findings, conclusions, or recommendations expressed herein are those of the author(s) and do not necessarily reflect the views of the DOE.

Table of Contents

Volume II

Appendix A: Marketing Study

DUCKER WORLDWIDE

University of Minnesota

Panelized Roof System

– Pricing and Opportunity Analysis –

Table of Contents

1.0 Executive Summary

There is a defined market opportunity for the panelized roof system with production and semi-custom builders in the South and West regions of the United States. Furthermore, the panelized roof system installation attributes provide a compelling case for adoption with builders and contractors in Central and Northern regions of the country where labor rates account for a an average of 43 percent more in construction cost based on U.S. Bureau of Labor statistics. Senior personnel at top builders including; Centex Homes, Lennar Corporation, Kimball Hill Homes and others express interest in the performance attributes and indicate long-term opportunity exists if the system can deliver a clear value proposition. The market potential is further enhanced through construction activity levels in target regions. Southern markets, from Florida to Texas account for 50 percent of the total new construction angled-roof volume. California contributes an additional 13 percent share of market volume. These states, demonstrating the greatest needs for energy efficient building systems, account for 28 to 30 million squares (2.8 to 3 billion square feet) of new construction angled roof opportunity.

Positioning

In order to capitalize on system advantages, participants in the construction channel require a value proposition that maximizes tangible and measurable benefits for adoption. Specifically, the drivers for use are 1) reducing construction cycle time (cost) and 2) offering increased energy efficiency to the homebuyer. These two system attributes resonate with builders and provide measurable performance features necessary for undertaking the adoption process. Although other attributes offer value to builders and homebuyers over the long-term, they present challenges in defining initial interest and often complicate the evaluation process.

Production, and in many ways, custom-home construction is a highly refined and optimized process. Builders demonstrate resistance to altering from established procedures and need to fully understand all of direct and in-direct implications in doing so before they will undertake a change initiative. To ensure the panelized roof system presents viable conditions for adoption, its introduction to market will require minimizing process change requirements and streamline system attributes to include only those features of greatest value to the builder/contractor and his customer. This positioning element is consistent across builders and regions and was concisely summarized by a production builder in the Dallas market.

"Any product or system we would consider has to live within our business model and the market expectations. We won't create a house for a product. The product needs to be created for the house".

To accurately position the panelized roof system for successful introduction, its final design, positioning and marketing communication all need to maximize the top two priority features and minimize costs and complexity from others. The message that offers the most compelling reason for adoption is that the system presents builders with the opportunity to reduce cycle time [cost] in the construction process and offer an innovative systems-approach for energy management.

Requirements for Adoption

Based on the need to live within the builder business model and overcome cost pressure in the short and medium-term, system design must be optimized to deliver on the two core value premises. Builders are unwilling to incur any added costs or change requirements that don't support 1) the largest cycle time reduction and 2) the highest energy efficiency improvement. With these features serving as the foundation for adoption, design and communication efforts should avoid distraction away from this core premise.

Across all builders and markets analyzed, the uncertainty factor of incorporating new design and construction elements into the construction process presents the greatest concern for derailing the system success. Regardless of type or degree of roof system advantage, builders indicate that uncertainty in their process can quickly erode potential benefit. Issues such as "cutting through metal layer for vent stacks" or "needed specialized tools" will require simple and concise communication solutions. Whether or not an issue presents an actual challenge in system installation, the perception of uncertainty is sometimes a greater barrier to overcome than the reality itself. Incorporating simple design solutions into an initial presentation will alleviate uncertainty and enable builders to focus on achieving the greatest possible advantage.

Entry level and step up homes in the markets typically have construction cycle times of 50 to 70 days and carrying costs of approximately $600 per day. Although variation exists based on a number of factors (design, demand, etc) creating measurable improvement in these areas is of interest to builders. Existing cost structures play a critical role in benchmarking the roof system attractiveness and determining the cost-to-value opportunity. Average material and labor pricing from the markets under analysis are provided in the table below. Texas, Arizona and Nevada demonstrate very similar pricing conditions. Southern California and areas of Northern and Northeast markets often have

higher priced home values and demonstrates costs in excess of those summarized below:

Conventional Roof System Costs

Roof Component	Material & Labor
Trusses	$3,350
Decking (including vents)	$1,600
Insulation	$950
Roofing (tile)	$4,000
Conventional Roof Cost (No roofing)	**$5,900**
Total Conventional Roof Cost	**$9,900**

The average cost of a conventional roof system to a builder in these markets is currently $4.10 per square foot for material and labor. Truss systems in these markets often range in material cost from $2.50 to $3.50 per square foot, with an additional $0.85 per square foot for installation. Several participants anticipate the cost to come down further in the near-term. When adding the roofing material and installation, the average cost is $6.88 per square foot. These costs represent the benchmark upon which builders evaluate the cost-to-value trade-off in Southern markets for panelized roof system adoption. These numbers are lower than those previously reported in the "Advanced Energy Efficient Roof System" report and reflect the current state of the construction industry and continued pricing pressure.

Construction material and labor rates are relatively consistent within the markets analyzed during this program. However, when widening the view to include Northern markets, differences in labor rates impact conventional roof system pricing. The U.S. Bureau of Labor Statistics provides "mean construction hourly labor rates by MSA (Metropolitan Statistical Area). These numbers, consistent with those found in the analysis, illustrate the impact from labor cost by market.

Dallas is report by the Bureau as having the lowest mean hourly rate of markets studied, as found in the field interviews. At $15.52 per hour, this market average is close to half of that found in Chicago, which reports a mean hourly rate of $27.44 per hour. Although differences in material and design preference exist between these markets, the result of labor expense alone is an additional 10 percent to the total system cost, as shown in the following chart:

Conventional Roof System Costs

- By Region -

MSA	Mean Hourly Wage
Chicago	$27.44
Detroit	$24.39
San Diego	$22.19
Las Vegas	$21.49
Phoenix	$17.05
Dallas	$15.52

Labor Cost	Material Cost	Total	
$2,232	$8,662	$10,894	Labor is 25 to 30% of total cost
$1,238	$8,662	$9,900	Labor is 15 to 20% of total cost

Despite the fact that builders acknowledge that labor rates influence conventional roof system costs, they typically do not view material and labor as separate cost items. Instead, they use total installed cost (including material, labor) and cycle time to negotiate their subcontractor expense.

Although the market is expected to rebound, cost pressure has forced pricing to extreme lows. The conventional roof system pricing analysis, in conjunction with builders' aversion to uncertainty, create a market condition where the roof system will need to be streamlined to maximize cycle time reduction and energy efficiency, without adding costs for other options. Without specific homebuyer demand, builders view any cost increases as unacceptable.

Over the long-term, opportunities for promoting addition system benefits, such as conditioned attic space or offering integrated solar panels may evolve, but will require demand creation. Builders demonstrate varying levels of understanding of roof system options, but most have previous experience in their evaluation. Most notably, builders in these markets have experimented with conditioned attic space, often referred to as "cocoon systems" and found increased cost and low homebuyer interest as deterrents for offering. Although a smaller air conditioning unit can be utilized due to efficiency gains, there is typically a 15 to 20 percent overall material and labor increase due to "sealed unit" requirements and additional componentry.

For the integrated solar panels options, builders and homebuyers alike recognize the long-term value for incorporating into the roof system design. However, adding an emerging technology onto an innovative roof structure is viewed as taking on more change than is acceptable at a given point. The necessary approach will be to "proven out" the roof system performance in initial market launch and then integrate this and other options as knowledge and confidence matures.

Tailoring system design to market requirements

Based on the market needs and system features, a three-phased commercialization approach is recommended and summarized below:

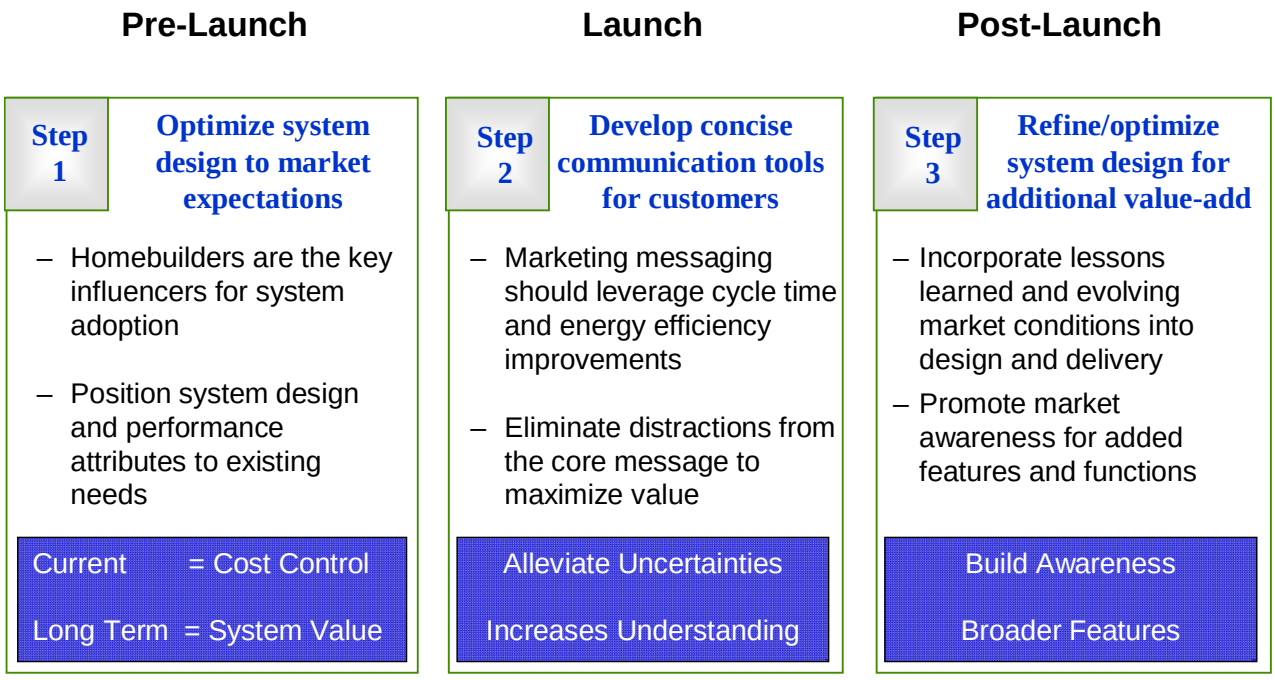

The objective of commercialization approach is to align the panelized roof system with existing conditions for market penetration as noted in Step 1. Builders are the primary adoption decision influencers and efforts should be coordinated to optimize system performance to create the strongest case for system adoption. Once the system has been optimized, a clear communication tool will assist builders, contractors and other channel partners in understanding the system advantages and reducing the disadvantages from uncertainties, as noted in Step 2. The more concise the marketing communication and education package, the greater the likelihood of overcoming resistance. As market demand grows in post-launch Step 3, the roof system can be expanded to offer a broader portfolio of features or tailored to meet the demands of more specific market categories.

Although the current conditions of the construction industry present challenges in commercializing the innovative roof system, a definite need and market fit has been identified. Eight percent of program participants indicate that they are either “very willing” or “moderately willing” to consider adopting the roof system once ready for market introduction. Several participates also comment that down-turns in the industry afford time to evaluate new products or practices. By coordinating efforts to enhance the drivers for adoption and minimize the

barriers, the panelized roof system stands to capitalize on a growing market demand for energy efficient building alternatives and create a compelling case for market adoption.

2.0 Roofing Industry Overview

Size, Organization and Value

The 2007 residential and light commercial angled roofing market is estimated at 180 to 190 million squares; with one square equaling 100 square feet. The industry experienced a decrease of approximately 7 percent from the 2006 size of 195 to 205 million squares. New construction recorded a decline of approximately 25 percent, while remodeling expenditure grew slightly. In terms of the total angled roof market, remodel or re-roof applications represent over three-quarters of the total volume. The new construction angled roof size provides a foundation for understanding the panelized roof system potential.

Within the new construction volume of 45 to 48 million squares or 4.5 to 4.8 billion square feet, the South and West regions account for 63 percent of the total volume. These markets, controlling the majority of U.S. construction share, also represent the greatest overall demand and opportunity for energy efficient building products and systems. The market potential is summarized in the following graphic:

2007 Angled Roof Market
(by Application)

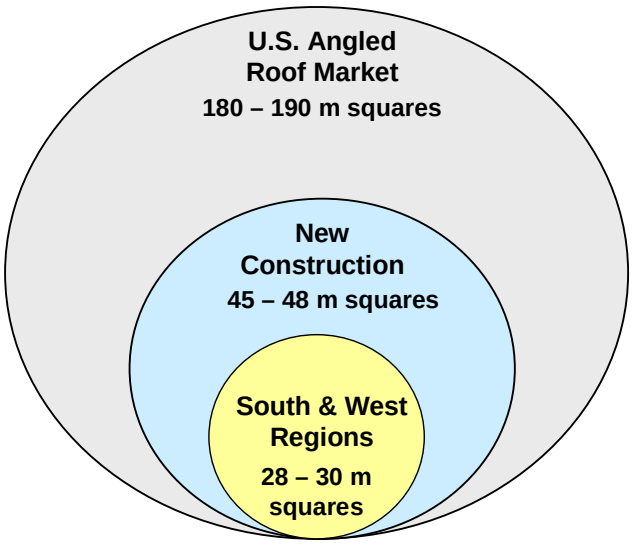

New construction, angled roof applications can also be segmented by residential and commercial projects. During the peak of the housing boom, residential projects accounted for 90 percent of new pitched roof installations. With the recent construction slow-down however, residential pitched roof installations have slide in their overall share, now accounting for approximately 80 percent of the market, as shown in the following chart:

2007 U.S. Pitched Roofing Market
(by Application)

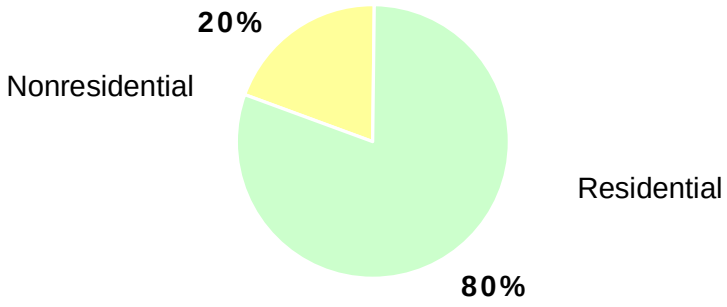

Total = 45 to 48 Million Squares

With the South and West regions controlling 63 percent share, they account for an estimated 2.2 to 2.4 billion square feet of residential, new construction angled roofing opportunity. The North central, often referred to as Heartland area accounts for an additional 15 percent share or roughly 550 million square feet of new construction, residential area. The Northeast region rounds out the U.S. pitched roof market, with 22 percent share or an additional 800 million square feet.

Further segmentation illustrates construction activity by home type. The market for new application roofing can be further segmented into four key types of housing. Each of the following home types represents a different degree of household income and spending on construction materials. Although asphalt shingles are the dominant roofing material at the national level, the South and Western markets represent a disproportionately high rate of concrete tile utilization. Concrete tile is the preferred material by builders participating in the program and considered a requirement for use on their roofing systems.

Roofing Product Positioning by Home Type

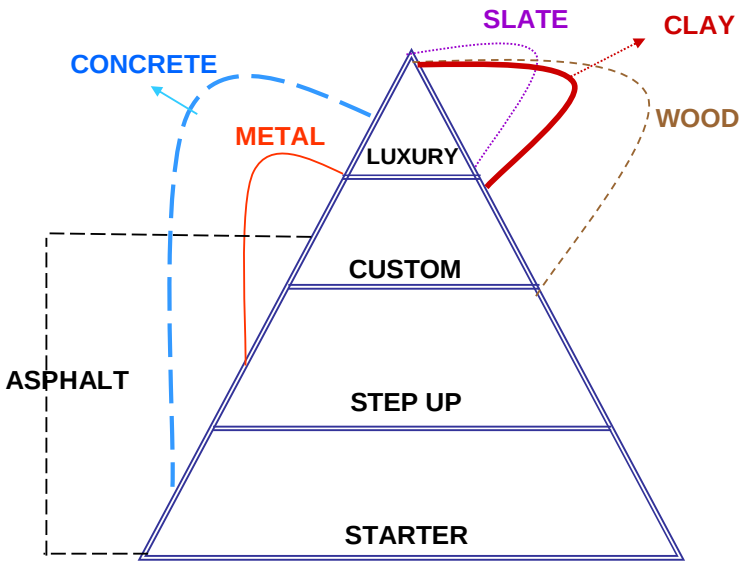

Luxury home is the highest and most exclusive construction and household income levels. Represents very small percentage of total housing starts in the US.

Custom homes are built by truly custom builders, single construction, not part of full developments. Use multitude of roofing product styles.

Step Up homes are the most changing segment in the past several years. Step up includes semi-custom and lower priced community developments. Typically asphalt-based market except in FL and CA where metal and lightweight concrete are used.

Starter homes are track home style construction, little or no customization, with lowest income buyers and greatest price sensitivity.

Product segmentation, usage and route-to-market

Asphalt shingles dominate the angled roofing market, though specialty materials continue to gain share. In total, asphalt shingles represent nearly 85 percent of the market, down from 90 percent six years ago. Although overall volume of concrete roof tile is down, it continues slow growth at the expense of other specialty roofing materials such as clay, slate, metal, composites, and traditional asphalt shingles. Concrete tile usage is strong in the South and West, where it capitalizes on greater production, supply and distribution success. This has allowed concrete to take some share from clay. Product segmentation for the 2007 angled roof market is provided below:

2007 Angled Roof Market

(by Product Type)

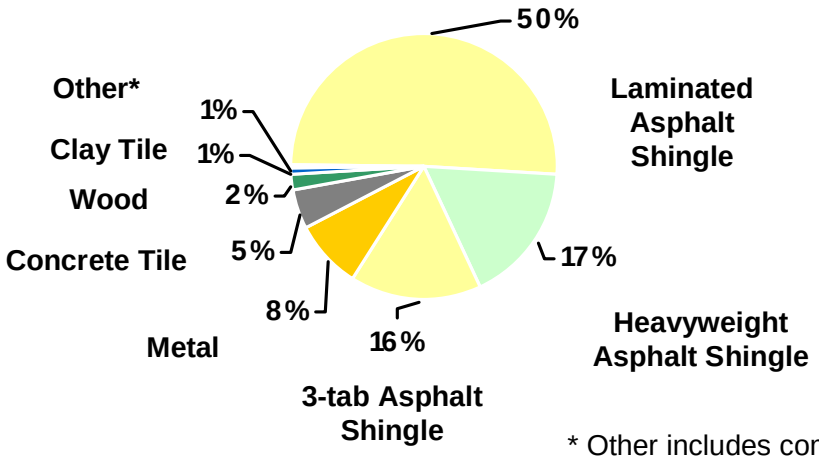

* Other includes composites, slate

Total = 180 to 190 Million Squares

Asphalt Shingles

Although asphalt shingles represent 85 percent of the U.S. roofing products share, their use can vary greatly by region. In the Northcentral and Northeast, their share is estimated at nearly 94 percent of material usage, where low cost and harsh weather durability drive demand. Differing performance requirements in other regions of the country create conditions where asphalt underperforms market expectations. In the Southwest for example, extreme temperatures and aesthetic preferences limit asphalts penetration to an estimated average of 75 percent and as low as 50 percent in certain markets. Of importance, is the finding that production and semi-custom homebuilders interviewed in these markets indicate that offering a tile roofing option will be important to market acceptance, as many of their community as designed exclusively with this roofing material.

Purchase location for asphalt singles has shifted during the last five years, with production and large homebuilders increasingly buying directly from the manufacturer. It is estimated that only 6 percent of material was sourced directly from the manufacturer in 2002, whereas direct supply increased to nearly 20 percent in 2007. A series of one and two-step roofing distributions account for the largest share of asphalt purchase location, with organizations such as ABC Supply and Allied Building Products Supply dominating share in the category. Lumberyard and Big Box represent the smallest segment of purchase location, as shown in the following chart:

Asphalt Roofing Purchase Location

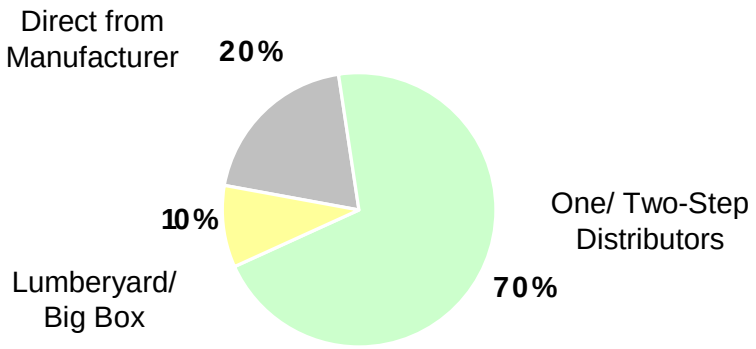

Metal Roofing

Metal roofing products are now estimated as representing nearly 5 percent of the residential roofing market in squares (including both new construction and re-roof) and 15 to 20 percent in revenue. For nonresidential applications, metal share accounts for approximates 35 percent of volume (squares).

The metal roofing market uses a wide variety of distribution partners; however unlike other conventional roofing material, such as shingles, over 50 percent of the market is distributed directly to builders, contractors and end users. Traditional residential and nonresidential building products channels, including lumberyards, big box store, and building products distributors, constitute the remainder of the market, as summarized in the following chart:

Metal Roofing Purchase Location

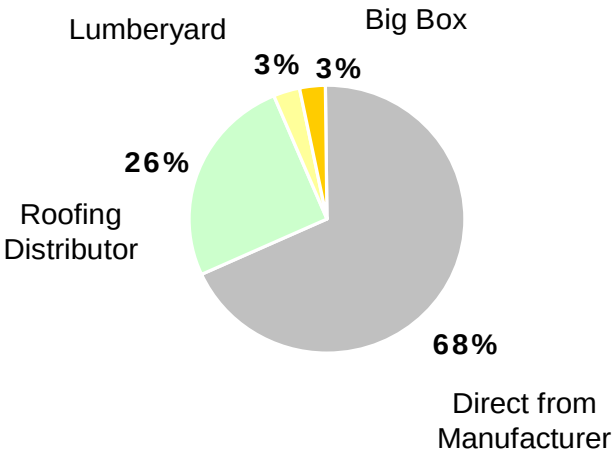

Concrete Tile

Concrete roof tile is popular due to its aesthetics, weatherability, long life, and comparative low cost to other tile roofing options (clay and slate). The majority of concrete tile is for new construction applications due to the cost and weight of the product as well as its longevity. It is also used primarily in residential applications due to weight and pitch requirements. Eighty percent of concrete tile is used in new construction projects.

While most manufacturers sell a small amount of tile directly to roofing contractors, the vast majority of contractors purchase through distributors. Manufacturers and distributors do not currently have a network of authorized or preferred roofing contractors as in other specialty roofing materials.

Concrete Tile Purchase Location

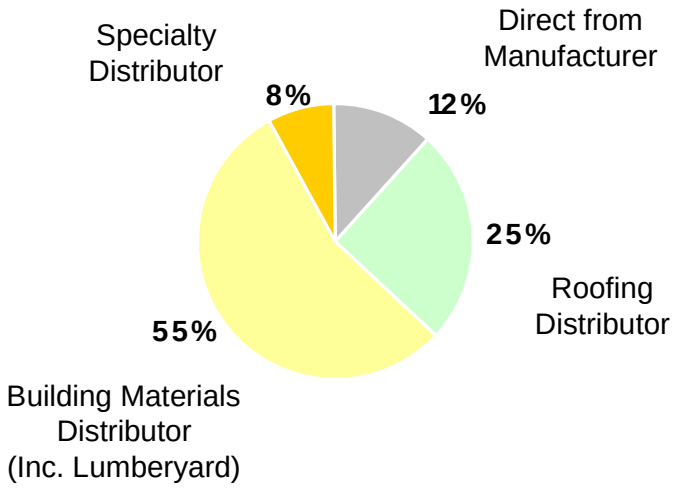

Target Market Conditions

As a component of the market research process, target markets were profiled to determine current and evolving construction conditions and the requirements for system adoption. This step is critical in understanding the factors for adoption as they exist today, but also as they emerge in the coming years. In-person interviews were conducted by Ducker personnel with key respondents at top builders and construction firms to define the opportunity. Interviews included discussions of the current construction climate, but were positioned to capture long-term potential. This was done to alleviate the “cost is king” mentality reported by many to describe the 2008 construction climate and instead place emphasis on corporate and divisional strategies for selling homes in stabilizing and growing housing markets. Summaries are provided below:

Dallas

New home construction in Dallas has contracted from approximately 45,000 homes in 2006 to a forecasted 32,000 to 34,000 homes in 2008. As a result, builders are cost sensitive in the short and medium-term. In the long-term, several builders communicate a sales strategy toward product differentiation and are looking for ways of distinguishing their homes. When asked how willing they are to consider using new products or processes in their construction, respondents have mixed reactions.

> *"It is now more acceptable to consider [energy efficient products] that we have time to evaluate our processes for the future and research new products"* – Semi Custom Builder

> *"Products need to have a proven track record before we are willing to use them in our homes. Pioneers are the ones that are out in front when it comes to trying new products. They also run the risk of getting shot in the back and we can't afford to take that risk"* – Production Builder

Phoenix

New home construction permits decreased 16 percent in 2007, from approximately 44,000 in 2006 to 37,000 in 2007. Continued decreases are predicated for 2008, prompting builders to place even greater emphasis on cost containment. However, despite the current down-turn, builders in this market express a willingness to evaluate new product or process options. This trend is driven by openness to process improvements and future home differentiation.

Builders have corporate commitments to energy star compliance and invest resources in collaborating with Arizona's water and power utility (SRP) in programs to seek 'green' alternatives. Design and purchase decision processes for entry and step-up homes are typically cost-driven.

San Diego

New home construction decreased by approximately 9 percent in 2007, with builders reporting low profitability and slow sales for 2008. The availability of low cost labor has impaired builders and contractors from many process or product improvements as turn-over is high and crews are generally unfamiliar with specialized equipment. There is also a negative perception regarding usage of panelized products driven by supply problems.

> *"We don't use panelized products because suppliers are not reliable in delivery [too far away, not on time] as well as because the labor is relatively cheap*".

Legislation and increasing home buyer interest are the two driving factors for energy efficiency and "green" initiatives. Although homes meet Energy Star compliance, builders report that benefits adopting additional products or practices have not materialized.

> *"The only way we are generally willing to incur additional cost for these options is if it is regulated by law. For instance, when they increased the SEER rating (for air conditioning) from 10 to 13, our costs increased about $1000 per home and the price increase to the customer was $1,500".*

Las Vegas

Las Vegas has seen 14,500 foreclosures year-to-date, with 19,000 pre-foreclosures. Some builders have halted production altogether due to 14 months worth of housing inventory. The usage of SIPS (Structural Insulated Panels) for walls and ceilings is somewhat common and manufacturers of these systems report they are able to offset material price increase through large, standardize orders. A new state-of-the-art SIPS production facility has recently been built to supply regional demand.

Detroit / Chicago

Detroit and Chicago experienced new home construction decline of 47 percent and 37 percent respectively. During this downturn, remodeling of homes has remained relatively flat. High labor costs represent a main area of concern for builders and new product/system adoption is met with concern as builders often require market acceptance and validation before adopting.

> "*I need to see laboratory test results, authority approval and compliance with current codes that dictate wind lifting and snow load metrics before I would consider using".*" – Framing Contractor

<u>Energy Efficiency Contributions</u>

The U.S. Green Building Council has been setting the standards in the green building industry with their LEED (Leadership in Energy and Environmental Design) program. LEED is a scoring system for rating the "greenness" of a building, taking into account categories such as energy management, material use, innovation and design process, among others. Although LEED certifications have primarily been focused on public buildings, it is a good barometer regarding overall trends in environmentally-friendly and energy efficiency construction practices, because it is the primary standard for

measuring performance in these areas today. LEED certifications also present an opportunity to track and forecast share increases in energy efficient building systems, and will become important in benchmarking the panelized roof system following its commercialization. The following chart depicts the number of LEED projects and approximate market share since 2002 and forecasted through 2010:

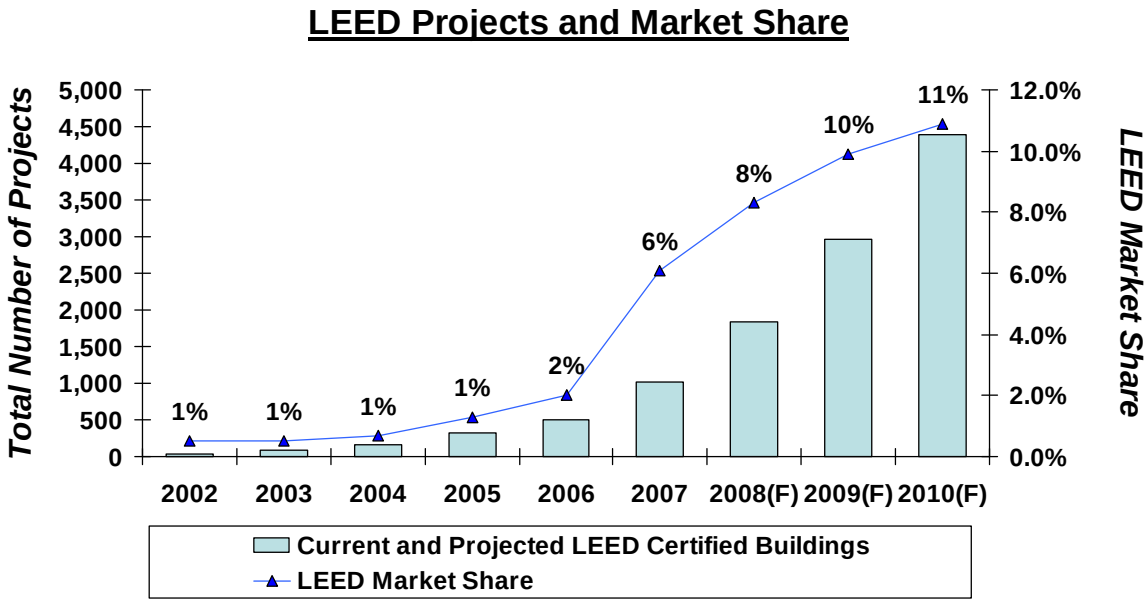

3.0 Production and Semi-Custom Builder Analysis

To systematically determine the range of opportunity for the panelized roof system, in-depth interviews and field research has been conducted with production and semi-custom builders, framing, roofing and other general contractors and industry participants in five U.S. markets. Quality research methods and expert analysis have been utilized to develop an understanding of the drivers of acceptance as well as limitations in adopting. The analysis also focused on relative pricing levels and cost justification elements for the innovative roof system versus conventional construction practices. The discussion guide used in the interviews is included in the Appendix. To maintain confidentiality of information and to alleviate participant concern around sharing proprietary cost and construction information, data points are reported in aggregate value. This component of the research methodology is necessary in encouraging an open dialogue during interviews, as well as ensuring sensitive information cannot be directly attributable to individual participants or their organizations. Secondary sources and internal Ducker Worldwide industry databases have also been utilized in the analysis.

A sample of the companies and respondents participating in the program is provided below. Typically, multiple individuals were included in each interview to elicit feedback and insight from a broader scope of business responsibilities. Several "Top 10 Production Builders" were interviewed in multiple markets to enable understanding of market differences, as these firms account for larger shares of home construction.

Program Participants	
Company	Description
A K Services	Framing Contractor
Alliance Builders	Semi-custom/Remodelers
Centerline Construction	General Contractor
Centex Homes	Production Home Builder
Douglas Scott Homes	Semi/Custom Builder
Galaco Carpentry Plus	Framing Contractor
Highland Homes	Production Home Builder
Holiday Builders	Production Home Builder
KB Homes	Production Home Builder
Kimball Hill Homes	Production Home Builder
Lennar Corporation	Production Home Builder
PAC	Production Home Builder
Quantum Homes	Production Home Builder
Shea Homes	Production Home Builder
Unicor	Semi/Custom Builder

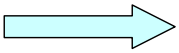

Sample of Respondents
Construction Foreman
Division Manager
Prinicipal/Owner
Project Manager
Purchasing Manager
Roofing Manager
Sales Manager
VP of Operations
VP of Purchasing

Metropolitan Statistical Area (MSA) data has been utilized to provide insight into construction activity in target markets and program participants share. The following table summarizes new home permits by market and the relative size of builders.

Metropolitan Statistical Area (MSA)	Phoenix	Dallas	Las Vegas	San Diego	Chicago	Detroit
Total Permits	36,963	28,807	24,039	7,458	31,084	8,939
Centex Homes	3.6%	5.3%	3.0%	-	2.2%	3.4%
KB Home	3.7%	-	9.2%	-	-	-
Lennar Corporation	4.7%	-	5.7%	3.6%	2.8%	-
Shea Homes	3.7%	-	-	5.0%	-	-
Kimball Hill Homes	-	-	1.7%	-	1.4%	-
Highland Homes	-	4.5%	-	-	-	-
TOTAL SHARE OF MSA	15.7%	9.8%	19.6%	8.6%	6.4%	3.4%

Construction process and design

Historically, truss placement & extreme temperature have been the dominant attic conditions in the primary markets under analysis. Builders have investigated opportunities with panelized systems for using this area, referred to as "cocoon systems", but found cost and low homebuyer interest as deterrents. Respondents demonstrate varying degrees of corporate sophistication, but all communicate efforts in streamlining processes, optimizing design/planning procedures, implementing cost control measures and better understanding home buyer needs.
Builders utilize these previous experiences as evaluative tools to gauge interest and feasibility in pursuing opportunities. The most common approach discussed during interviewing in evaluating the specific merit of a product or process alternative is a Return on Investment model. However, before arriving at the point of formal evaluation, initial interest criteria need to be met. In particular, is the present opportunity worth the time and effort to investigate?

As is typically the case when considering a new product or process, builders' first response is to probe areas of uncertainty. With a process as refined as production home building [and in many ways semi-custom homebuilding] builders often have little tolerance deviation from approved procedures.

Most builders participating in the program indicate that they would likely have to use the panelized system on all homes in a particular category/ community or none at all. The rationale is that the design elements of communities are locked well in advance of construction and builders report reluctance to deviating from the master plan. Respondents indicate that the panelized system would need to be designed into the community at the early planning stages; during CAD drawings.

> *"We would have to make the decision to use a panelized roof system early in the process, from the blueprint stage. This needs to be done to account for any implications to the construction cycle (costs, schedule changes, etc). It may simplify my process if the ordering and scheduling of all roof components are handled by a single vendor and then streamlined"* – Production Builder, Phoenix

Although process variation and decision requirements exist between builders, all program participants state that panelized roof system performance would need to live within the corporate and community requirements. As such, a summary of the process steps for adoption is provided below, detailing key milestones along the path to approval and installation:

Decision Process for System Approval

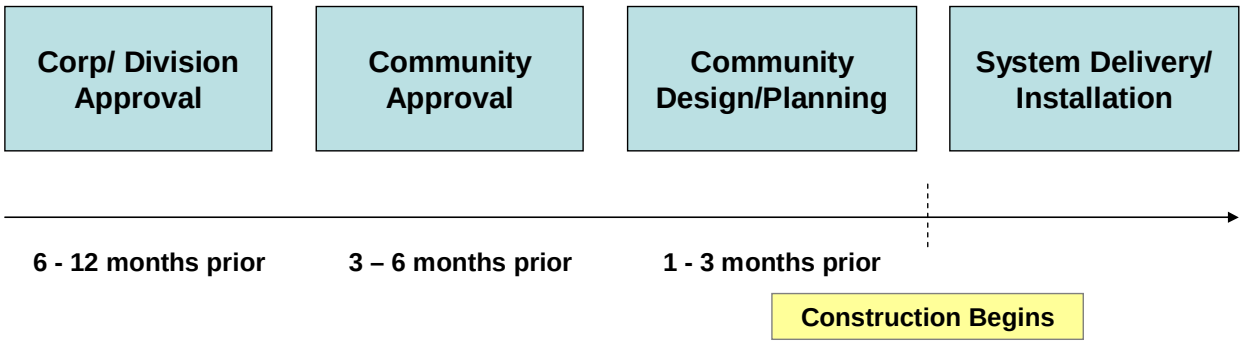

As noted, specific requirements at each stage of approval often differ by builder. However, addressing the "permission-to-play" factors within their process steps is critical. A summary of typical milestones is provided below:

Corporate/Division Approval and sign-off is required at the senior organizational level. Typically, approval at the high level involves satisfying cost and performance expectations (Purchasing Department), delivery and warranty expectations (Operations Department) and design and appearance expectation (Planning/Architectural Services). Corporate interests for roof system procurement suggest that having a sole source may be perceived as a negative, should problems arise in the ability to supply systems and/ or in maintaining competitive pricing terms.

Community Approval involves aligning system attributes with Home Owner Association (HOA) and community design needs. Principally, understanding if the panelized system adds value or in some way enhances the community over existing methods needs to be validated. This added value must offset any process change or cost increases.

Community Design/Planning involves determining the overarching design elements and finalizing the Computer Aided Design (CAD) and blueprints for construction. This stage often begins further in advance, but is typically frozen at a certain point prior to construction start-date. Changing design past this point on a house or building creates multiple downstream implications that need to be addressed.

System Delivery/Installation requires a supplier to contractually meet planned schedules. Builders demonstrate a high degree of sensitivity around logistics planning, often because any reduction in cycle time erodes when steps are not completed on schedule. Past experiences with SIPS and panelized systems have increased awareness of these issues.

Living within these process elements is commonly viewed as the first and most crucial step in determining feasibility of the system. Without formalized and specific policies to reduce uncertainty, most participants indicate they would be hesitant to consider adopting.

Home differentiation potential

Qualitative and quantitative research methods were utilized to gauge builder preferences of system attributes and the corresponding value to the homes. Respondents were asked to describe their corporate views on each of six factors. Using this information as a foundation, respondents were then asked to rate the value of improvement in each area; on a scale of 1 to 5, with 1 indicating no value in improvement, 3 indicate moderate value and 5 indicating the highest possible value in improving.

It is important to note that the conversations were focused on long-term strategy for home differentiation and value. Most respondents, as holding senior positions in the organization and having tenure in the industry, have experienced construction industry cycles and provided the strategic, long-range view. Where conversation shifted to short-term reactions and decisions within the current economic cycle, the information was captured but not integrated when defining the long-term system value (as this would dilute overall potential). Importance ratings from builders and contractors participating in the program are summarized below.

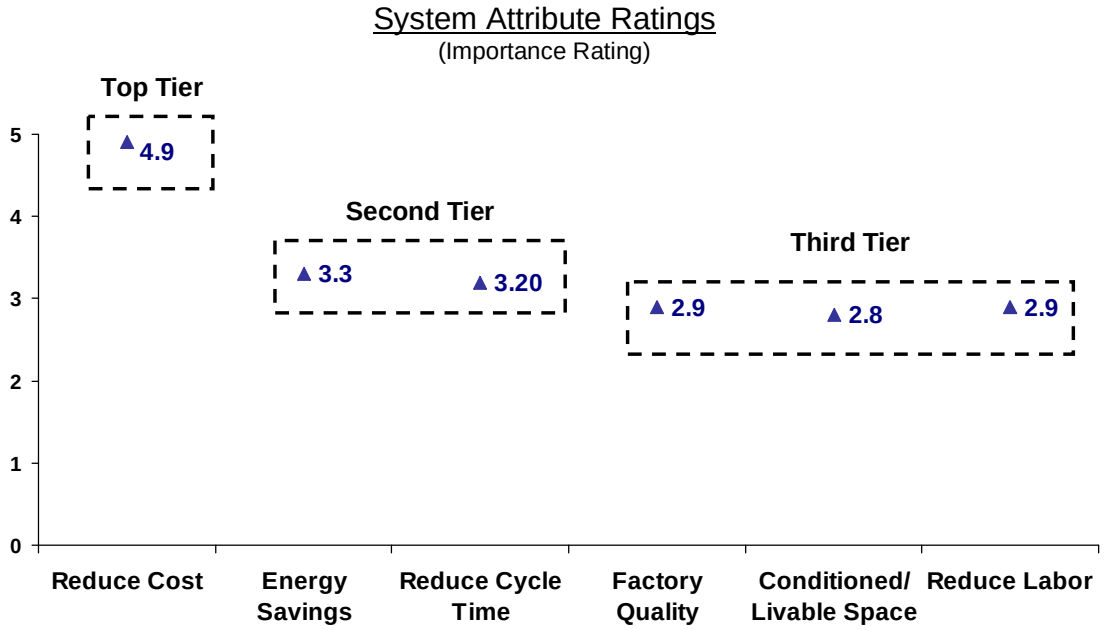

When analyzing the importance ratings, three tiers of importance categories emerge. Most notably, reducing overall cost (Top Tier) is the primary driver in construction decision making. From the builder perspective, overall cost includes the direct (material, labor) costs, as well as indirect (process change, downstream impacts, service & warranty risk) and is the overarching factor in evaluating fit.

Second tier importance factors offer the most compelling, measurable factor for system adoption and include; increased energy efficiency over conventional roof design and reducing the construction cycle time. Whereas reducing cycle time [cost] offers builders internal value, energy efficiency and meeting market demand offer external drivers for considering. The pairing of these two factors affords the most succinct, direct-line benefit to the builder business and their homebuyer needs. When discussing these factors, builders report interest in capitalizing on growing demand for energy efficiency and in placing homebuyers in their homes sooner.

> *"The system attributes [reduced cycle time, improved energy efficiency] have a lot of good, sellable value. But, they need to live within the cost/value equation. We are value builders, meaning everything we include in the home has a specific value to us or the homebuyer"* – Home builder, Dallas

Third tier system factors, including factory quality fabrication, conditioned/ livable space and reduction in field labor offer value, but are generally not perceived as compelling drivers for adoption. Taken in order of importance rating, descriptions include:

Factory quality fabrication offers some value in increasing roof system quality, but presents difficulty in measuring. Builders do not allow unsatisfactory installations from their subs (meeting code and performance regulations) and often state that "sub contractors meet these standards now, or come back to correct if done wrong, how much does factory quality add"?

Conditioned attic space/livable area are factors that many of the respondents have investigated previously, often referred to as "cocoon systems". Experiences in placing mechanicals in conditioned attic space have often had negative implications, as commented by a Las Vegas builder: *"Air conditioning equipment requires additional investment to be in conditioned space, such as air circulation, etc. This drives added costs of HVAC about 15-20 percent per home and homebuyers are not willing to incur this expense".* There is also a consistently reported inability to monetize their features, as low homebuyer interest paired with increased overall cost offer obstacles in overcoming.

Without a direct line between added value and market interest, selling the attribute becomes difficult.

> *"Communicating these benefits to our customers is going to be tough"* – Builder, San Diego

> *The conditioned attic space would not be a type of square foot that is sellable to consumers. And for the extended life of mechanicals, customers expect all their equipment to run excellent for a long time. Potential extension of life of mechanicals is often met with more confusion than advantages"* – Home Builder, Phoenix

Two ultimate questions emerge when evaluating a potential fit for the panelized roof system; 1) will it save us [builder] money, and 2) will it make our homes more attractive to buyers? To appropriately assess the level of differentiation potential, participants were asked if they believe that a house/building with an energy efficient - panelized roof system would sell faster than one with a conventional roof system.

Twenty percent of participants speculate that once market awareness begins to occur, the panelized roof system may help differentiation a home to the point that it would sell faster than one without the system. None of the participants across the different regions were willing to state definitively that they believe the system would help sell a home faster. Responses to this question are summarized in the following chart:

Ability to Sell Faster – Differentiation

(Percent of Respondents)

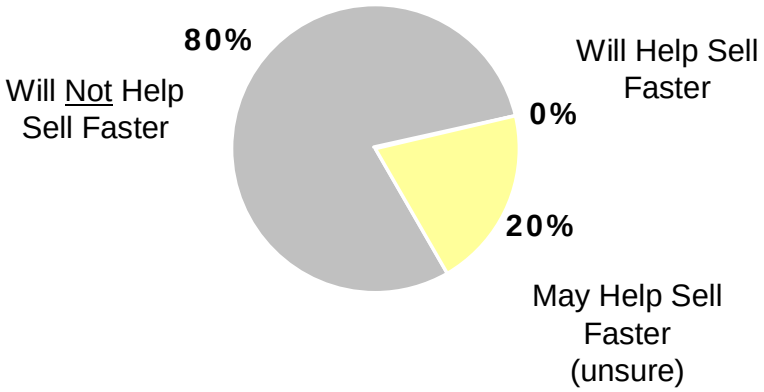

Builders typically indicate that demand creation will be needed in the market prior to the panelized system offering them a distinct selling or marketing

advantage. With the multitude of design options already in the buying process, including additional factors that have low awareness require builders to educate the buyer. Without a specific and measurable margin-advantage, there is limited value in the effort.

> *"There are local and municipal programs that would encourage the use of this system, however, it is still not enough. In order for a legislation to encourage me to use this it would have to give me better economical conditions. To really advance acceptance of this system, you would have to target HOA's [Home Owners Associations] and municipalities to approve and help them get this product to market"* – Production Builder, San Diego

> *"Everything is about the cost structure, and this is not expected to change in the future. Unless we are in a super hot market we don't add costs to our construction. If it's minimally higher than our current costs its ok [max $500 per house]. However, if it is significant [doubles our roof cost]) there is no way we're adopting it"* – Production Builder, Phoenix

Integrated Solar Panel Option

Few builders perceive solar panel integration as a near-term advantage. Most cite concern for solar panel integration with Homeowner Association (HOA) and civil regulations. Current solar specifications mandate placement of panels in areas of the home where they are not visible from certain points. Although integrated solar provides an alternative approach to roof-mounted systems, they would still face similar HOA and civil code investigations and approvals. These conditions will need to be addressed at the community and/or county level and require approval prior to builders' willingness to adopt. Reported concerns over complying with aesthetic regulations and the associated cost factors have become a deterrent to use for many builders in the South and West regions. Production builders participating in the program report that HOA approval is a significant component of their evaluation process and would need to be addressed early in the community design process. Semi-custom builders can be considered somewhat less sensitive in this area as they do not always have the same HOA conditions as production builders. However, cost justification remains the primary decision factor. In addition to the direct and indirect costs associated with design approval and sign-off, solar panel integration is perceived as a costly option, which is ultimately passed along to the homebuyer and needs to be justified in the budgeting process. Builders report being acutely sensitive to adding costs for solar options in their sales process, as commented below:

"Solar panel acceptance for instance is down because they are costly systems. They can cost $15,000 and get you a rebate of only $5,000, which still makes it a significant expense" – Production Builder, San Diego

4.0 Acceptable and Relevant Price Ranges

Existing methods and cost assessment

Construction material and labor expense are typically determined through a negotiation process with subcontractors and are often considered confidential. To maintain confidentiality, material and labor expenses are reported in aggregate for each component in the roof system. The following assessment summarizes average builder costs for a conventional roof system on a 2,250 square foot, production home, with approximately 1,440 square feet of roof area. Although current information suggests the panelized roof system may be targeted to single story structures due to installation requirements, most builders need to evaluate cost on a two-story structure for true comparability with the majority of home layouts.

Reported values are representative of 2008 pricing arrangements for Phoenix, Dallas and Las Vegas markets. These areas have high levels of available labor, increasing buyer (builder) purchase power and creating hyper-competitive bid situations. Findings are summarized below:

Roof Component	Material & Labor
Trusses	$3,350
Decking (including vents)	$1,600
Insulation	$950
Roofing (tile)	$4,000
Conventional Roof Cost (No roofing)	**$5,900**
Total Conventional Roof Cost	**$9,900**

The average cycle time for the roof construction is 1.5 to 3 days, with crew size generally ranging from 5 to 13 people. Average price of the conventional system per square foot of roof area is $4.10 without roofing material and $6.88 with roofing. More than half of the builders state that they were unwilling to incur any increases over current costs to adopt a panelized roof system. Some are willing to incur small additional costs (no more than $500 per home).

"I wouldn't pay anything above my current costs to use this system. The only way I would is if it is regulated by law, for instance, when they increased the SEER rating (for air conditioning) from 10 to 13, our costs increased about $1000 per home, and the price increase to the customer was $1,500" – Production Builder, San Diego

Respondents provided detail regarding their evaluation processes to determine feasibility of a new product or process. The results from analysis are provided below:

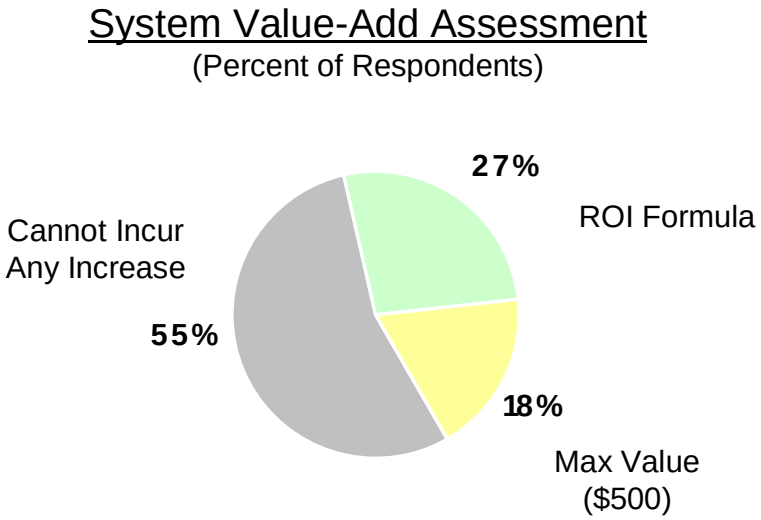

Slightly more than one-quarter of builders report that a detailed Return on Investment analysis will determine their likelihood for adoption once final cost figures are known. In this analysis, a cycle time reduction is perceived favorably due to the potential to reduce $600 per day carrying costs.

Direct and indirect switching costs

Within the pricing/performance evaluation, direct and indirect switching costs were captured and profiled. Direct switching costs are reported in four categories, including; equipment requirements, implications resulting from construction material changes [use of steel], planning & design modifications & approval and process implications. Indirect costs are primarily viewed as a function of undertaking a change initiative. These costs include future/unknown considerations that emerge as installations get underway. Builders commonly report that, regardless of the thoroughness in planning, change always creates unexpected impacts further in the process. The interaction of different trades, schedules and delivery management, city approval process and construction interruptions are unknown and will likely require management attention in

resolving. Builders report that the known factors for use need to be presented once finalized and that formal cost evaluations will take place to determine feasibility of use. These factors are summarized in the following chart:

Direct and Indirect Switching Requirements

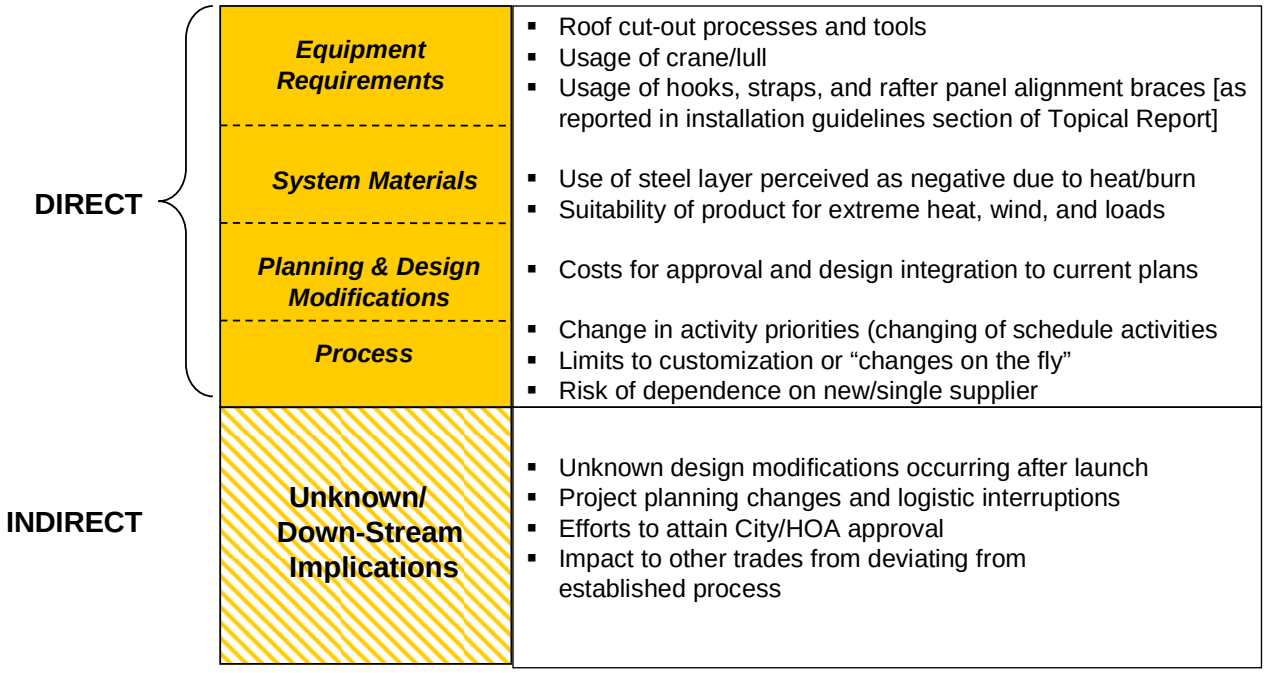

"The change involves costs of seeking approval of structure and design from city council, which could be a challenge in adopting the system" – Builder, Las Vegas

5.0 Advantages and Disadvantages of System Attributes

As a final step in the information collection process, interviews focused on compiling and quantifying perceptions of the panelized roof system attributes. Each of the conditions were identified are a system advantages that would encourage adoption or a system limitation that may create a barrier for adoption. The last step in the assessment was to rate the degree of advantage or disadvantage on a scale of High, Medium or Low. Findings are summarized below by major category and provide further insight into builders' and their customers' decision processes:

Advantages for System Adoption

(In order of significance)

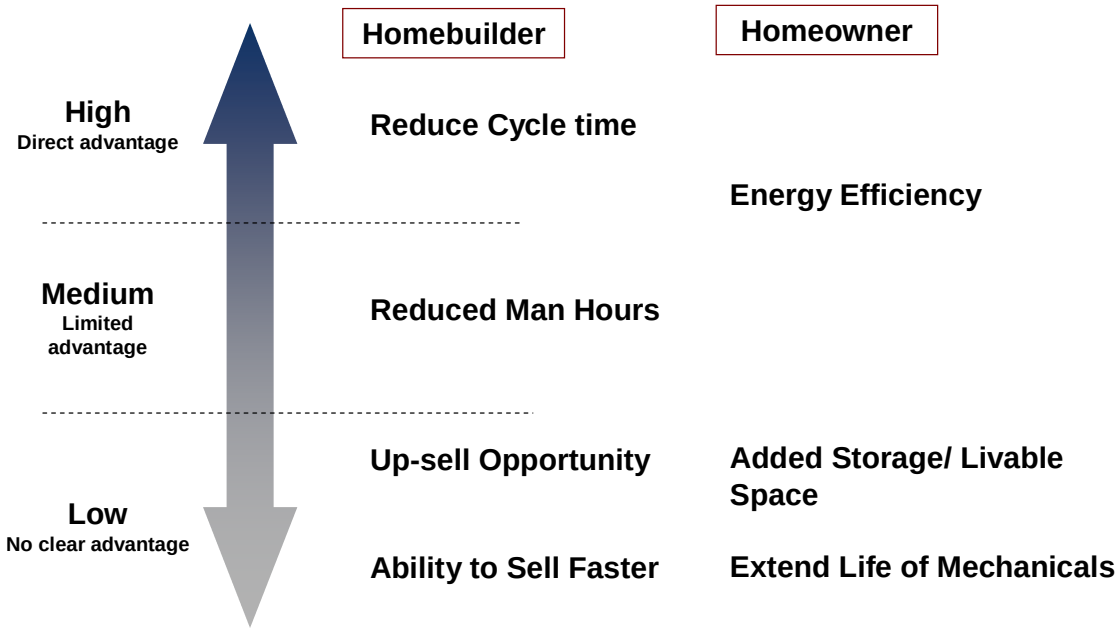

Barriers for System Adoption

(In order of significance)

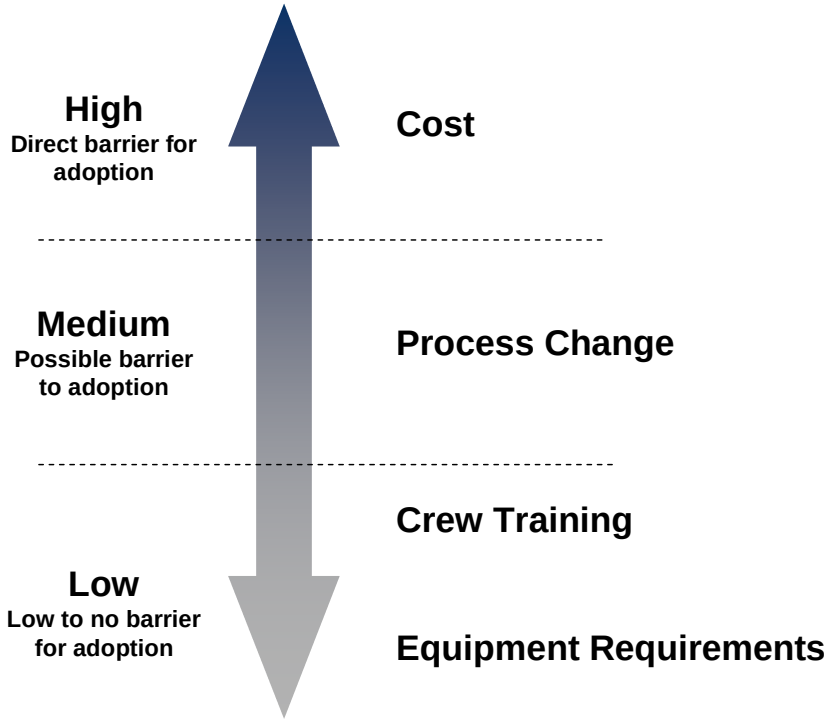

The majority of respondent perceptions are consistent across the markets analyzed. One notable are of difference did emerge in regards to the impact of additional equipment needed for system installation. The Dallas market represents the only area where a crane or construction lull requirement would create a High barrier to adoption. Respondents in other markets report this consideration as an issue requiring attention, but not something that would derail efforts. In contrast, builders in Dallas are acutely sensitive to larger equipment, requiring skilled operators, on small lot sizes. These factors create a higher than average degree of concern in formally pursuing use of the roof system.

Impact of additional equipment

Additional equipment requirements and their implications were then explored at a deeper level. Nearly 60 percent of program participants across markets report that using a crane or construction Lull is of "little to no concern" for them. Most suggest that this is not an issue that would be ignored, but rather it does not present a significant barrier in the efficient use of the system. Responses in this area are summarized below, with only 6 percent or respondents reporting a significant concern in needing this equipment:

Builder Perspective of Crane/Lull Requirement

(Percent of Respondents)

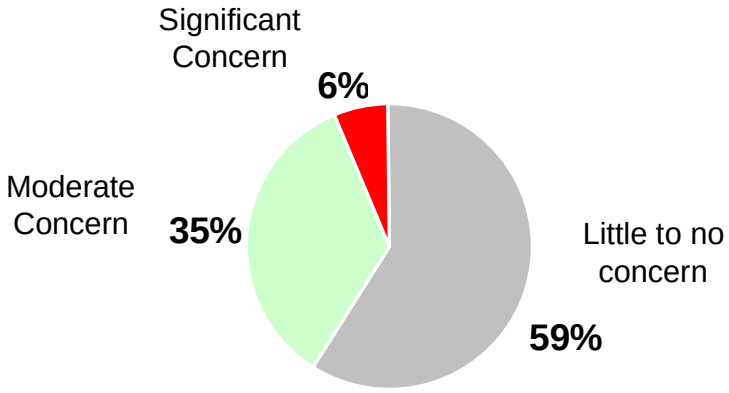

The added expense or scheduling requirements will ultimately need to be considered in a costing assessment and balanced against the return on investment for using. All other equipment requirement responses have been accounted for in previous sections, presenting only a need for a simple solution, but no significant areas of concern.

Upon conclusion of the interview sessions, respondents were posed the question, "assuming that the panelized roof system delivers on its value proposition, how willing are you/your company to formally consider adoption"? Responses are summarized in the following chart:

Willingness to Formally Consider System

(Percent of Respondents)

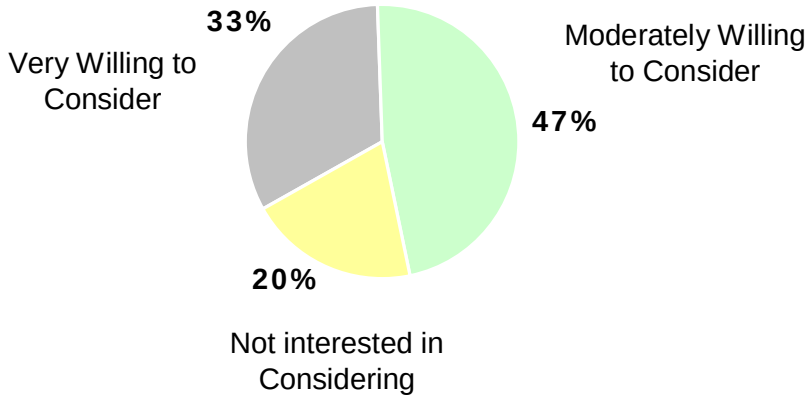

Twenty percent of builders indicate that the panelized roof system would not fit within their construction interests and that they do not see potential for adoption. The remaining 80 percent believe that the roof system is of interest in formally considering once market introduction occurs. Although they express specific requirements for use, this group of respondents if generally optimistic about the stated opportunities and would welcome additional system information.

> *"I think the concept is great. If it improves our construction process and offers homebuyers a real advantage, the opportunity is worth pursuing"* – Production Builder, Las Vegas

The Panelized Roof System Pricing and Opportunity Analysis program has been guided by three primary goals. The intention of these goals has been:

- *To determine, through quality research methods and expert analysis, the range of opportunity for the innovative roof system*
- *To develop an understanding of the drivers of acceptance and use as well as limits or barriers from production and semi-custom builder perspectives*
- *To determine relative pricing levels and cost justification elements for the innovative roof system versus traditional construction practices*

Program findings and recommendations confirm a distinct opportunity within the current 2.8 to 3 billion square feet segment of the angled-roof construction market. Existing and near-term industry conditions require commercialization within specific cost and performance boundaries, but once market validation occurs, the long-term potential broadens greatly. The existing construction slow-down has also created the need to consider innovative solutions and presents the opportunity to lock-in potential users as the panelized roof system nears market readiness. A construction rebound may offer the potential to incorporate other value-add features to the system design and ultimately capitalize on higher margin or home differentiation opportunities. Tailoring the panelized roof system attributes to the market needs will play the largest role in its level of acceptance and long-term opportunity potential.

6.0 Supplemental Slides

DUCKER WORLDWIDE

OPPORTUNITY EVALUATION WITH HOME BUILDERS FOR PANELIZED ROOFING SYSTEM

JUNE, 2008

TRANSPORTATION * CONSTRUCTION * INDUSTRIAL * MATERIALS * FINANCIAL

DUCKER WORLDWIDE
ducker.com

Construction Information

	Total Home	Framing Segment	*Roof System*	*Insulation in Ceiling*
Cost				
Cycle Time				
Avg. Crew Size	N/A			
Total Man Hrs				
Disposal Cost				
Builder Margin				

Comparison of convention vs. PR	Conventional	PR System (3,764 sq ft)
Total Cycle Time		2 days
Total Labor Time (in man hours)		48.75 hours
Total Labor Expense (avg. $28.27/hr)		$1,378
Crane Rental	N/A	$800
Insulation for Ceiling		N/A
Waste/Disposal Cost		N/A
Total Roof Structure Cost		

Current Framing & Roofing Considerations

- What types of equipment do your framing and roofing crew currently use (crane/Lull)
- How sophisticated are your framing crews? Not at all, moderately, very sophisticated?
- Have your crews adopted any new products or technologies in recent years that demand a process change?
  - Please describe the process of managing the learning curve
  - Does/Do these experience impact your willingness to try new products? How?
- What options have you investigated for cost reduction or product differentiation (short and long-term)
- Do you currently use any panelized products? If so, what have been some of the key advantages/disadvantages of these?

Energy Efficiency Trends

- What energy efficient products have you adopted lately and what type of impact did it have to your costs and ability to sell?

Product	What has been **Cost Impact**	What has been **Selling Impact**
Windows		
Energy Star Compliant Machines		
HVAC systems		
Other:_____		
Other:_____		

- What has driven these changes?
  - Homebuyer interest
  - Cost consideration
  - Legislation/regulations
  - Other_____
  - Other_____
- How do you manage the costs or savings (i.e. pass on to homebuyer, other)?
- What is the status or market demand for energy efficiency? Has there been an increase in the acceptance of any energy efficient products lately?

Value to the Builder and Homeowner

Builder Value
The Panelized Roof System offers builders the opportunity to capture efficiencies in roof construction and performance. Compared to conventional roof systems, the PR system installs faster, requires less labor and is a better quality product (factory production quality). In addition, the energy saving features of the PR system offer builds the ability to promote "green" construction materials and practices, a factor that may likely have multiple positive impacts, including reputation and product differentiation.

Homeowner Value
Due to innovative insulating properties, the PR system reduces a home's energy consumption for heating and cooling, achieving cost savings for the homeowner. HVAC and other mechanicals can also be placed in conditioned space, reducing wear and tear and potentially extending operating life and efficiency. Furthermore, the homeowner has the option of integrating solar panels with the PR system, enabling another means for energy savings.

PR System - Process Considerations

- The PR system will require the installing contractor to use a crane or construction Lull. How significant is this issue to utilizing a panelized roof system?
  - How able are you/your crews to invest in new products or processes to reduce labor costs?
  - Why? (cheap labor, expensive investments, etc)
- Besides the use of a Crane/construction Lull, what additional resources or change requirements do you believe you will have with a PR system installation?
  - Would it change the roofing activity priority?
  - Would it have an impact on project planning and execution? If so, at which points?
  - What type of decrease in activity or time do you anticipate the PR system would offer over your current process? (framing time reduction. Compare with time of roofing section and framing time related to roofing)
  - What impact do you believe it will have on the design and planning processes?

PR System - Cost considerations

- Assuming that the PR system will reduce cycle time, offer home differentiation and energy savings advantages, how interested are you in offering the system?
  - How would you evaluate the cost and value to your business?
  - What percent cost above your current roof system expense would prevent you form offering a PR system?
- What type of service and support would you expect for a PR system?
  - What details need to be addressed in an informational presentation?
- Are there any other advantages or benefits that you may be able to leverage with the system?
- Are there any other cost or process concerns that the PR system raises?

Selling Advantage

- What value do you perceive the following system attributes would have in your ability for premium/up-sell opportunity in your construction
  - Additional square feet
  - Conditioned attic/ storage area
  - Energy saving features
  - Potential to extend the life of mechanicals
- How would you communicate these benefits to your customers?
- Do you believe using a PR system will have a positive impact in your company's image?
- Do you believe a house with a PR system will sell faster? If so, what is the average time reduction you would might expect?
- Is there any legislation that would encourage you to use a PR system (i.e. tax break, program)?

Benefits & Drawbacks

- From the list of system attributes and others we've discussed, please indicate whether there is an advantage or disadvantage and rate the degree or importance/significance on a 1 to 5 scale (with 1 = low/no significance, 3 = moderate significance and 5 = strongest significance)

Adv/Dis		1 to 5	Please Describe
_____	Reduce cycle time	_____	
_____	Reduce man hours	_____	
_____	Energy efficiency benefits	_____	
_____	Up-sell/premium opportunity	_____	
_____	Sell home faster	_____	
_____	Conditioned storage	_____	
_____	Additional living space	_____	
_____	Extend life of mechanicals	_____	
_____	Upfront/added cost	_____	
_____	Process change/ learning curve	_____	
_____	Crew/ installer training	_____	
_____	Equipment requirements	_____	(what else changes)
_____	Suitability for snow loads	_____	
_____	Other_____	_____	
_____	Other_____	_____	

TRANSPORTATION * CONSTRUCTION * INDUSTRIAL * MATERIALS * FINANCIAL
DUCKER WORLDWIDE
ducker.com

This concludes our discussion. Thank you.

For over 45 years, Ducker Worldwide has enabled clients to navigate and thrive in a dynamic, global marketplace. Our unique and proven combination of custom market intelligence, critical thinking and strategic consulting create valuable opportunities that deliver critical results. For more information regarding our strategic services, expertise and to learn how Ducker Worldwide can help you, please contact one of our team members at 248-644-0086 or visit our website at www.ducker.com

Appendix B: Material Properties and Selection

Properties for structural and insulating materials are summarized in this section. Material selection criteria for roof panel applications are described and material recommendations are provided. Commercially available materials were considered.

1.0 Structural Materials

Structural materials considered are steel and three types of fiber-reinforced plastics (FRP). Oriented strand board was not considered as it is not compatible with the truss core and stiffened plate designs. Density, coefficient of thermal expansion, thermal conductivity, modulus, and tensile strength are reported for each material in Table 1. Steel properties used for designing the panel structural component are representative of a low carbon cold rolled steel such as AISI 1020 carbon steel. Cold rolled steel with a galvanized coating is recommended to prevent corrosion. This material is well suited for production manufacturing and is compatible with laser welding.

The fiber-reinforced plastic materials have different modulii and coefficients of thermal expansion. Compared to the other FRP materials, the chopped fiber reinforced plastic (CP), a thermoplastic, has the highest coefficient of thermal expansion and the lowest material modulus. The uni-directional plastic (UD), a thermoset, provides the benefit of a coefficient of thermal expansion comparable to steel, but has the highest cost of the structural materials considered. All fibers are continuous and oriented lengthwise. A similar thermal expansion benefit is provided by multi-directional plastic (MD) (also a thermoset) that is composed of alternating layers of unidirectional rovings and random-orientation continuous strand mat.

Table 1: Properties of structural materials

Material	**Density** (kg/m^3)	**Coef. of thermal expansion** ($10^{-6}/K$)	**Thermal conduc-tivity** (W/m-K)	**Modulus** (GPa)	**Strength** (MPa)	**Cost** ($/m^2$)
Steel, 1020 cold-rolled, galvanized	7870	11.7	51.7	205.0	230	8.31
FRP: Chopped fiber (CF), Noryl 30% glass fill	1290	30.6	0.173–0.415	9.2	116	50
Uni-directional (UD), Glass/Epoxy, 45% glass fill	1794	8.6		38.6	610	
Multi-directional (MD), Pultruded flat sheet	1794	14.4		12.4	138	

Cost estimates based on typical steel thickness: 16 ga (1.6 mm); and FRP thickness: 5 mm

2.0 Insulating Materials

Polymer foams are well-suited for insulating materials for residential roof applications. Foam hygrothermal properties are superior to those of traditional insulating materials such as fiberglass (ASHRAE, 2005): The mechanical properties of foam allow for use on the exterior of the roof where there are exterior loads. As with any insulating material, however, several considerations must guide the selection of foam material and placement. These considerations include structural and hygrothermal requirements, building code compliance, and manufacturability issues.

For this application, the range of polymer foams considered can be grouped into three categories: polystyrenes, urethanes, and other foams. The latter category consists of a broad variety of materials, none of which are currently thought to be viable options for residential insulation. Polystyrenes are thermoplastic foams, and urethanes are thermoset foams. With few exceptions, almost all of the other foams are thermoplastic as well. In this section, the foam performance requirements that are specific to the truss core and stiffened plate panel concepts are described, material properties are presented for the foams considered, and foam selection recommendations are provided.

The important properties relevant to the use of foams in roof applications can be divided into several categories: mechanical properties, hygrothermal properties and performance in fire or at high temperatures. The mechanical properties relate to structural performance. The important mechanical properties are stiffness and strength; specifically, the compressive modulus, shear modulus, compressive strength, and shear strength. The tensile and flexural properties of foams are not important for roof panels because the foam contributes negligibly to the structural performance of the panels. Instead, analysis of the structural performance of the foam is focused mainly on its ability to withstand external loads. To ensure adequate thermal and moisture performance for the roof, several hygrothermal properties of the foam must be considered as well. The hygrothermal properties relate to the thermal insulating value of the foam and to its effectiveness as a water vapor retarder. These properties include the thermal conductivity, specific heat, and water vapor permeability.

High temperature performance and flammability are also critical for roof applications. Depending on several factors (such as R-value, roof orientation and slope, roofing color, and the presence of solar panels) the outer surface of the roof may reach temperatures of 80 °C or higher (Davies 1997; Davies 2001). These temperatures are approaching the glass transition temperature for many polymer materials and therefore can have important implications for foam material selection. Foams should not be used in applications where the maximum service temperature will routinely be reached. Fire performance of thermoplastic foams (such as polystyrene) differs from that of thermoplastic foams (such as polyurethane). Several authors (Abbott 1986; Davies 1996; Davies 1997; Davies 2001; Rakic 2003) have reported on the behavior of polystyrene foam sandwich cores under medium- and large-scale fire tests. When exposed to high temperatures, the foam melts and draws away from the heated panel surface, creating voids within the panel. Substantial bowing of the affected panels is

accompanied by failure of the panel-to-panel joints and eventually leads to rapid spread of fire. Urethane foams do not melt at high temperatures; instead, a stable char is formed that prevents flame spread and provides a small amount of thermal protection to the surrounding foam (Davies 1997; Davies 2001; Rakic 2003).

Typical mechanical and hygrothermal property values for the commonly used foams are summarized in Table 2. The maximum service temperature and fire performance are also included. The focus is on polystyrene and urethane foams because these are the materials commonly used for commercial or residential building insulation. These foam types also have associated ASTM material standards ([ASTM] 2004; [ASTM] 2008a; [ASTM] 2008b), thus, indicating that the foams have been accepted for use in structural applications. Properties from these materials have been obtained from the ASTM standards and manufacturers data sheets. Specific sources of data for each material are noted in the table. In the case of the thermal conductivity of PUR, there is a significant difference between the ASTM standard specification and the manufacturers' data. The ASTM standard for PUR foam ([ASTM] 2004) specifies thermal conductivity for this material ranges from 0.036–0.037 W/m-K. This value for thermal conductivity is substantially higher than the values (0.023-0.033 W/m-K) reported in vendors' data sheets. The specific heat values, which are not typically available from vendors, are taken from the ASHRAE Fundamentals ([ASHRAE] 2005). The remaining mechanical properties not specified by ASTM standards are taken from vendors' data sheets.

Table 2 indicates the range of densities over which the ASTM standards apply and in which the foams are typically available for use as building insulation. With the exceptions of specific heat and maximum service temperatures, the physical properties vary with foam density. Because higher density foams are more "solid" than lower density foams, most of the properties increase as density increases. The primary exception is water vapor permeance, which is partly a function of the porosity of the foam and therefore decreases as density increases. Also, because of the large cell sizes typically associated with polystyrene foams (the optimum density for insulation is approximately 50 kg/m^3 (Gibson and Ashby 1997)), thermal conductivity decreases with density over the range indicated in the table. For clarity, all of the property values in Table 2 are reported as a range with the initial value corresponding to the lowest density and the second range limit corresponding to the highest density.

Note that polystyrene foams come in a lower density range than urethane foams. This difference does not significantly affect panel weight (since steel, with a density of 7870 kg/m^3, far dominates the total weight), but it may have other implications. For example, the cost of a foam is, in general, proportional to the density (Klempner and Frisch 1991; Landrock 1995; Lee and Ramesh 2004). Given that the foams in Table 2 are all currently produced in large volumes for various applications (Klempner and Frisch 1991), a reasonable first cost comparison of the foams can be made based on density. In situations where other considerations do not rule out the use of a particular foam, it may be more economical to use the material with the lowest possible density.

Referring to Table 2, polystyrene foams tend to have higher strength and stiffness than urethane foams at a given density, but they also tend to have higher thermal conductivity and water vapor permeability. A tradeoff thus exists between structural and hygrothermal performance. Significantly, polystyrene foams definitely have a lower maximum service temperature than urethane foams. In applications where roof temperatures are expected to exceed 70°C for any appreciable lengths of time, PS foams should not be used.

The property data provided in Table 2 are nominal values. That is, long-term effects such as creep and thermal aging are not included. Foam stiffness (compressive modulus and shear modulus) must be reduced to account for the dead loads and the live loads. Foam strength (tensile, compressive, shear and adhesive strengths) must be reduced to account for fatigue loads. These properties are reduced following the procedures described in the Topical Report for Year 1 (Davidson et al., 2006).

Table 2: Typical nominal properties of foams commonly used for thermal insulation.

	EPS[1]	**XPS[1]**	**PUR[2]**	**PIR[3]**
Density (kg/m^3)	15–29	21–48	32–64	29–96
Compressive modulus (MPa)	1.4–3.3[6]	9.3–26[7]	2.9–5.8[8]	3.4–20[9]
Shear modulus (MPa)	2.1–4.3[6]	2.9–6.2[7]	1.3–4.5[8]	1.2–3.9[9]
Compressive strength (kPa)	69–73	104–690	172–448	137–862
Shear strength (kPa)	140–240[6]	100–280[7]	172–276	110–441[9]
Thermal conductivity (W/m-k)	0.040–0.034	0.029	0.023–0.033[8]	0.029–0.032
Specific heat[4] (J/kg-K)	1214	1214	1591	1591
Vapor permeance (ng/Pa-m^2-s)	287–143	86–63	92–23[4]	230–115
Max service temperature[5] (°C)	75–85	75–90	90–120	90–120
Fire performance	Melts	Melts	Forms char	Forms char

Notes:

1. All values specified by ASTM C-578-08 unless otherwise noted.
2. All values specified by ASTM E-1730-04 unless otherwise noted.
3. All values specified by ASTM C-591-08 unless otherwise noted.
4. Typical values as provided by the ASHRAE Fundamentals ([ASHRAE] 2005).
5. Typical values as provided by Davies (1994).
6. Typical values as provided in manufacturer's data sheets (Diversifoam, 2008).
7. Typical values as provided in manufacturer's data sheets (Owens Corning, 2008).
8. Typical values as provided in manufacturers' data sheets (General Plastics, 2006; BASF, 2006; BASF, 2008).
9. Typical values as provided in manufacturer's data sheets (Elliott Company, 2008).

3.0 Material Selection

Panel design dictates selection of structural and insulation materials.

For the truss core and stiffened plate panel designs, the insulation bears none of the structural loads. In this case, material selection can be based on the cost required to obtain a particular bending stiffness. A convenient measure for this adjusted cost $\bar{c}$ is:

$$\bar{c} = \frac{c}{E / \rho g} \tag{1}$$

where c is the material cost per unit weight (i.e. $/kg). The term in the denominator is referred to as the specific stiffness and has units of length (i.e. meters). The ratio of the adjusted cost for the steel panel to that of the composite panel is 0.14. Based on this result, a steel panel can be designed to meet the structural requirements at a significant cost savings over a fiber reinforced plastic panel. From the structural materials considered, the adjusted cost of steel is the least.

PUR is the recommended foam for residential roof applications. PUR has several advantages over EPS and XPS. The primary advantage is in the high temperature and fire performance. PUR can be used at higher service temperatures that EPS or XPS: the maximum service temperature for PUR and PIR, 90-120°C, exceeds the expected service temperature of 80°C. During flammability tests, PUR forms a char while EPS and XPS melt. The melting can lead to rapid spread of fire. Moreover, PUR can be foamed in place, whereas EPS and XPS must be glued to the panel. While both PUR and PIR have similar high temperature and fire performance and can be foamed in place, PUR is a lower cost material.

For the analyses performed in this report, a 36 kg/m^3 (2.25 pcf) PUR foam is considered. This PUR formulation is manufactured by BASF and designed to be foamed *in-situ*. Table 3 shows nominal and the predicted PUR foam properties after 100,000 hours (the standard for European sandwich panels ([ECCS] 1991)) and 50 years (the design life for the truss core and stiffened plate panels). The properties at 50 years were used in the analysis of panel performance. Nominal structural properties are as reported by BASF. Hygrothermal properties are those found in WUFI.

Table 3: Design values for the mechanical properties of *in-situ* foamed PUR at 36 kg/m^3 (BASF, 2006; BASF, 2008) to account for creep and fatigue

Property	Nominal	11.4 years (10^5 hours)	50 years
Density (kg/m^3)	36		
Compressive modulus (MPa)	2.99	1.00	0.83
Shear modulus (MPa)	1.29	0.43	0.36
Tensile strength (kPa)	231	162	152
Compressive strength (kPa)	138	97	91
Shear strength[1] (kPa)	>173	>121	>114
Adhesive strength (kPa)	124	87	82
Thermal conductivity (W/m-K)	0.025		
Specific heat[2] (J/kg-K)	1470		
Vapor permeance[2] (ng/Pa-m^2-s)	60		

Notes:

1. Adhesive failure occurred during shear testing at the indicated strength
2. Property values used for analysis as specified by WUFI

References:

[ASHRAE] American Society of Heating, Refrigerating and Air-Conditioning Engineers. 2005. *2005 ASHRAE Handbook: Fundamentals*. Atlanta, GA: ASHRAE.

[ASTM] ASTM International. 2004. *ASTM E-1730-04: Standard Specification for Rigid Foam for Use in Structural Sandwich Panel Cores*. West Conshohocken, PA: ASTM.

[ASTM] ASTM International. 2008a. *ASTM C-591-08: Standard Specification for Unfaced Preformed Rigid Cellular Polyisocyanurate Thermal Insulation*. West Conshohocken, PA: ASTM.

[ASTM] ASTM International. 2008b. *ASTM C-578-08: Standard Specification for Rigid, Cellular Polystyrene Thermal Insulation*. West Conshohocken, PA: ASTM.

[ECCS] European Convention for Constructional Steelwork. 1991. *European Recommendations for Sandwich Panels: Part I Design*. Brussels, Belgium: ECCS.

Abbott, J. G. 1986. "Standard Laboratory Tests: How Meaningful Are They in Assessing Fire Performance of Insulation Materials?" In *Conference on Fire and Cellular Polymers*, pp. 199-218.

BASF Chemical Company (2006). "ELASTOPOR® P17226R Resin/ELASTOPOR® P1046U Isocyanate Rigid Urethane Foam System." Data Sheet.

BASF Chemical Company (2008). "University of Minnesota Panel Results: Physical Testing Results of Panel Made at BASF in May, 2008." Data Sheet.

Davidson, J.H. et al. 2006. Advanced Energy Efficient Roof System: Topical Report. University of Minnesota.

Davies, J. M. 1994. "Core Materials for Sandwich Cladding Panels." In *International Conference on Building Envelope Systems and Technology*, pp. 299-306, Singapore.

Davies, J. M. 1996. "Performance of Sandwich Panels in Fire 1. Onshore Applications." In *Sandwich Construction 3*, pp. University of Southampton.

Davies, J. M. 1997. "Design Criteria for Sandwich Panels for Building Construction." In *Proceedings of the 1997 ASME International Mechanical Engineering Congress and Exposition, Nov 16-21 1997*, pp. 273-284, Dallas, TX: ASME.

Davies, J. M., Ed. 2001. *Lightweight Sandwich Construction*. Oxford: Blackwell Science.

DiversiFoam Products (2008). "Physical Properties of RayLite EPS Insulation." Online data sheet, www.diversifoam.com.

Elliott Company (2008). "ELFOAM® Polyisocyanurate Foam." Online Data Sheets, www.elliottfoam.com.

General Plastics Manufacturing Company (2006). "Nominal Physical Property Data for LAST-A-FOAM FR-6700 Rigid Foam." Online data sheet, www.generalplastics.com.

General Plastics Manufacturing Company (2006). "Nominal Physical Property Data for LAST-A-FOAM FR-7100 Rigid Foam." Online data sheets, www.generalplastics.com.

Gibson, L. J. and M. F. Ashby. 1997. *Cellular solids: structure and properties*. New York: Cambridge University Press.

Klempner, D. and K. C. Frisch, Eds. 1991. *Handbook of Polymeric Foams and Foam Technology*. New York: Hanser.

Landrock, A. H., Ed. 1995. *Handbook of Plastic Foams: Types, Properties, Manufacture and Applications*. Park Ridge, NJ: Noyes.

Lee, S. T. and N. S. Ramesh, Eds. 2004. *Polymeric Foams: Mechanisms and Materials*. Boca Raton, FL: CRC Press.

MatWeb (2006). "AISI 1020 Steel, As Rolled." Online data sheet, www.matweb.com.

MatWeb (2006). "AISI Type 317 Stainless Steel, Annealed Sheet." Online data sheet, www.matweb.com.

Owens Corning (2008). "Foamular 400/600/1000 High Compressive Strength Rigid Foam Insulation Product Data Sheet." Online data sheet 58307-D, www.owenscorning.com.

Rakic, J. 2003. "Fire Rated Insulated (Sandwich) Panels" *Fire Australia*, pp. 33-37.

Appendix C: Panel and Joint Loads

Panel and joint loads will depend on roof live, dead and wind loads. These loads conditions can be found in the residential building code for various geographic locations in the US. However, interpretation of these codes requires specification of the roof size and slope. In section 1.0, we describe two roof configurations that were considered in panel and joint designs. Roof live, dead and wind loads in the US and the method for combining these roof loads are presented in sections 2 and 3 respectively. Panel loads will depend on the roof slope and climate conditions. Joint loads will depend on the roof slope, span length from ridge to soffit, and climate conditions. Panel loads are presented in section 4 and joint loads are presented in section 5.

1.0 Roof Configuration

Panels and joints were designed for a simple gable style roof with a ridge beam. The connection points for such a configuration are at the ridge, soffit, gable end and panel to panel. Two roof configurations were considered: a and 6/12 (26.5 degree pitch) with a 6.1 m (20 ft.) span from ridge to soffit and a 10:12 (40 degree pitch) with a 3.6 m. (12 ft.) span from ridge to soffit (Figures 1 and 2 respectively). The panel for the shallower roof is referred to as the long span panel. The panel for the steep slope is referred to as the short span panel. The panels were oriented to span parallel to the 12.1 m (40 ft) building dimension.

The building system included the placement of a structural supporting member at the ridge of each roof. Previous joint designs considered the absence of a ridge support and the complexity of the subsequent joint designs led to the rejection of a self supporting roof system. The placement of the supporting ridge member is illustrated in Figures 3 and 4. Possible ridge beam configurations are shown in Figure 5 and a possible truss configuration is shown in Figure 6.

The ridge support members are shown for illustrative purposes. Numerous options for member size, material and support locations are possible and depend in large part on the configuration of the room partition layout in the building below. The ridge beams and the truss shown in the Figures 5 and 6 have been designed to support the maximum anticipated loads for the most severe roof load condition. A commercial truss supplier was contacted and retained to provide a design to confirm that a standard commercial truss could be used for this design.

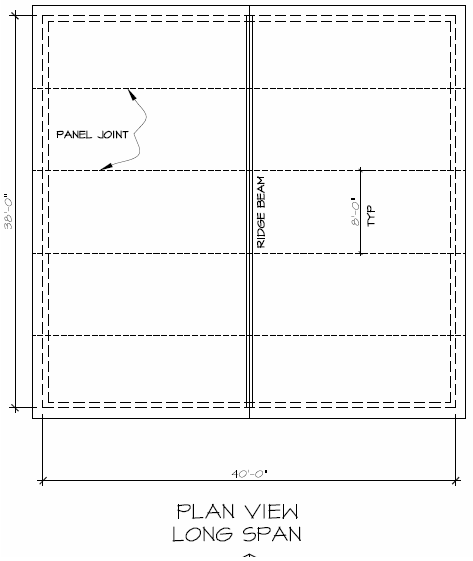

Figure 1: Configuration – Shallow slope (long span) roof.

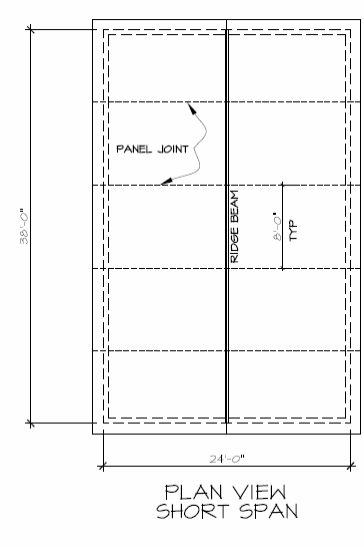

Figure 2: Configuration – steep slope (short span) roof.

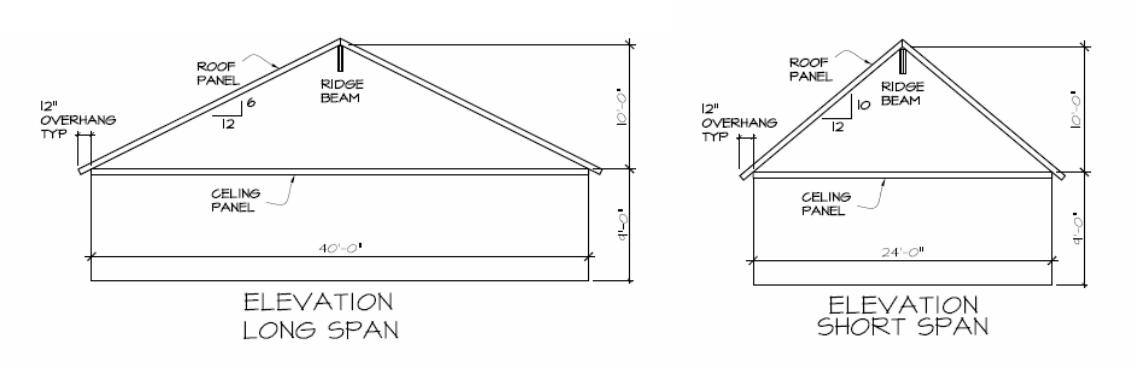

Figure 3: Building Configuration – Ridge Beam Support.

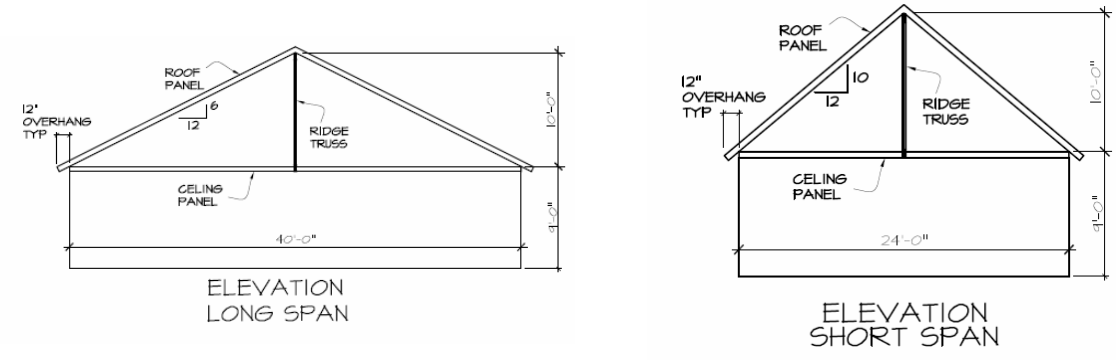

Figure 4: Building Configuration – Truss Support.

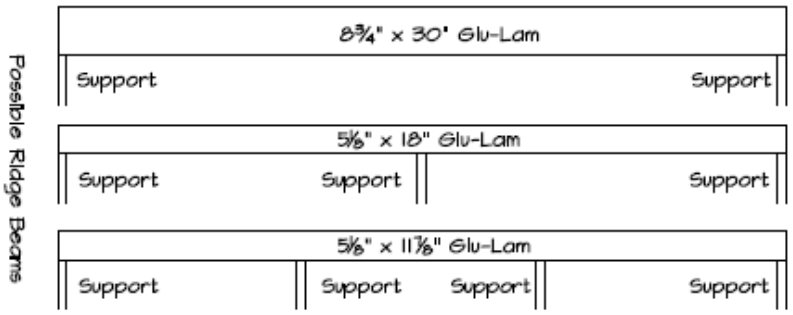

Figure 5: Possible ridge beam configurations.

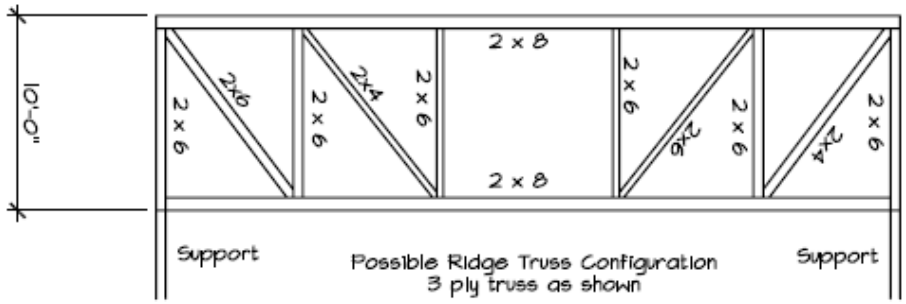

Figure 6: Possible Truss Configuration.

2.0 Dead, Live and Wind Loads

The loads considered for the design of the panels and joints are the dead load of the panel plus the weight of any additional building materials such as roofing and insulation, live loads resulting from rain or snow and wind loads acting on the roof surface.

Dead Loads

Dead loads are based on estimates of the panel weight (including insulation) and exterior and interior finish weights. The interior and exterior finish materials are estimated to weigh 328 N/m^2 (329 psf). This weight includes shingles, felt vapor barrier, an interior gypsum board face sheet and fasteners. Over the range of designs considered, the combined structure and insulation weight is generally less than 350 N/m^2 (7.3 psf) for climates I and II and 630 N/m^2 (13.2 psf) for climate III. An approximate insulation weight is obtained by assuming 36 kg/m^3 (2.25 pcf) PUR with a thermal conductivity of 0.025 W/m-K (0.014 Btu/hr-ft-°F). The R value for climates I and II is R_{SI}-5.3 (R-30) and for climate III the R value is R_{SI}-7.0 (R-40). Thus, the total dead loads are

approximated as 718 N/m^2 (15 psf) for climates I and II, and 958 N/m^2 (20 psf) for climate III (see Table 1). Dead loads are defined relative to the panel length.

Live Loads

Roof live loads were determined following the method described in the document ASCE 7, "Design Loads for Buildings and Other Structures" published as a design standard by the American Society of Civil Engineers. The code defines the snow loads with respect to a horizontal surface. Thus distributed loads normal to the panel will depend on the roof pitch. Sloped roof balanced and unbalanced loads were determined as illustrated in Figures 7 and 8. The live loads are based on a minimum roof load of 958 N/m^2 (20 psf) for climate I, a ground snow load of 1915 N/m^2 (40 psf) for climate II or a ground snow load of 3352 N/m^2 (70 psf) for climate III.

Wind Loads

The lateral wind loads considered for the panel and joint designs were chosen to be the result of either a 40.2 m/s (90 mph) or a 58.1 m/s (130 mph) wind speed. Wind speeds of 40.2 m/s (90 mph) are typical of climates I, II and III. Wind speeds of a 58.1 m/s (130 mph) and above can be found in regions along the East coast and Southern/Gulf coasts. Wind loads are defined as an inward or outward pressure component (i.e. perpendicular to the roof surface) whose value depends on wind speed and roof inclination. These loads will vary on the roof surface and will be greater at corners and edges. In Figure 9 three roof zones are identified: zone one consists of the center of the roof, zone two consists of the edges and zone three consists of the corners. Wind loads are greatest in zone three. These loads are calculated following the components and cladding section of the International Residential Building code. In Table 2 loads for a wind speed of 40.2 m/s (90 mph), defined as pressure perpendicular to the roof plane, are shown for roof pitches of 6/12 and 10/12. In Table 3 loads for a wind speed of 58.1 m/s (130 mph) are shown for roof pitches of 6/12 and 10/12. Positive loads act inward and negative loads act outward. The inward load does not vary across the roof and is greatest for the steep sloped roof. The outward wind load is greatest at the corners of the shallow sloped roof.

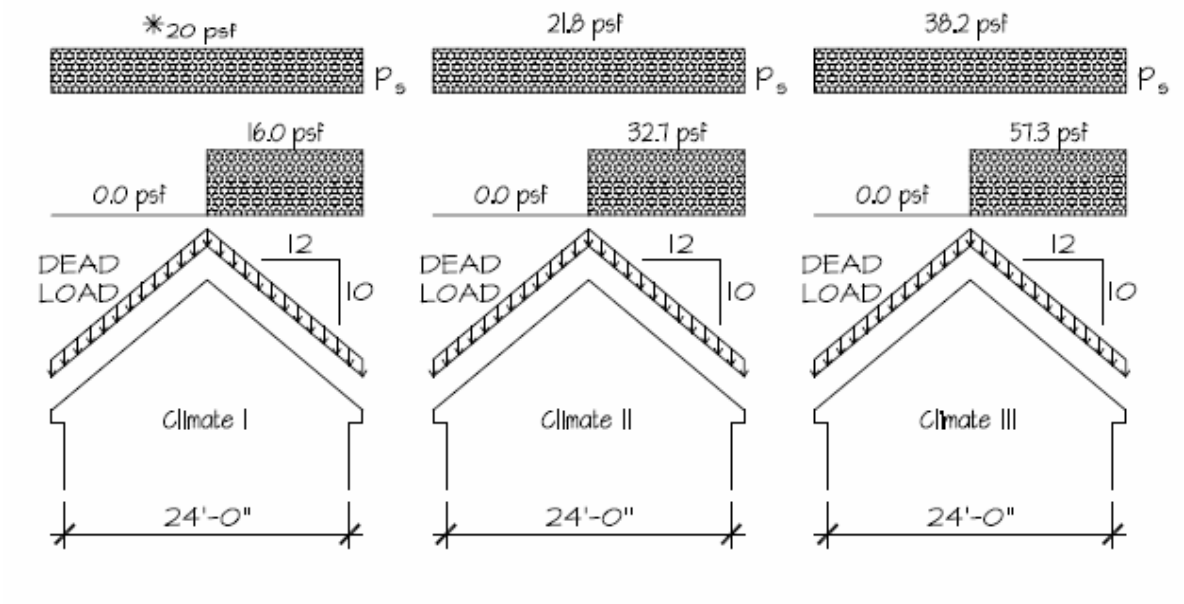

	Climate I	Climate II	Climate III
Ground Snow Load	20 psf	40 psf	70 psf
Basic Flat roof (pf)	14.0 psf	28.0 psf	49.0 psf
Roof Design Values			
Sloped Roof Load (ps)	*10.8 psf	21.8 psf	38.2 psf
Unbalanced Loading			
Leeward Roof	16.0 psf	32.7 psf	57.3 psf
Windward Roof	0.0 psf	0.0 psf	0.0 psf

Ce=1.0 Ct=1.0 I=1.0

* Minimum Roof Live Load = 20 psf

Figure 7: Roof live loads for the steep slope roof. Nominal ground snow loads were considered in the panel and joint design.

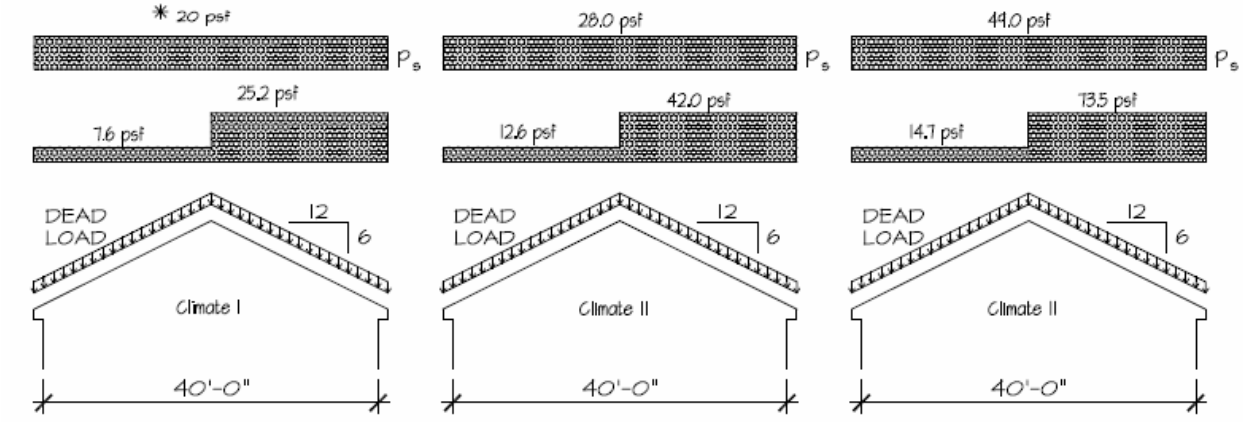

	Climate I	Climate II	Climate III
Ground Snow Load	20 psf	40 psf	70 psf
Basic Flat roof (pf)	14.0 psf	28.0 psf	49.0 psf
Roof Design Values			
Sloped Roof Load (ps)	*14.0 psf	28.0 psf	49.0 psf
Unbalanced Loading			
Leeward Roof	25.2 psf	42.0 psf	73.5 psf
Windward Roof	7.6 psf	12.6 psf	14.7 psf

Ce=1.0 Ct=1.0 I=1.0

* Minimum Roof Live Load = 20 psf

Figure 8: Roof live loads for the low slope roof. Nominal ground snow loads were considered in the panel and joint design.

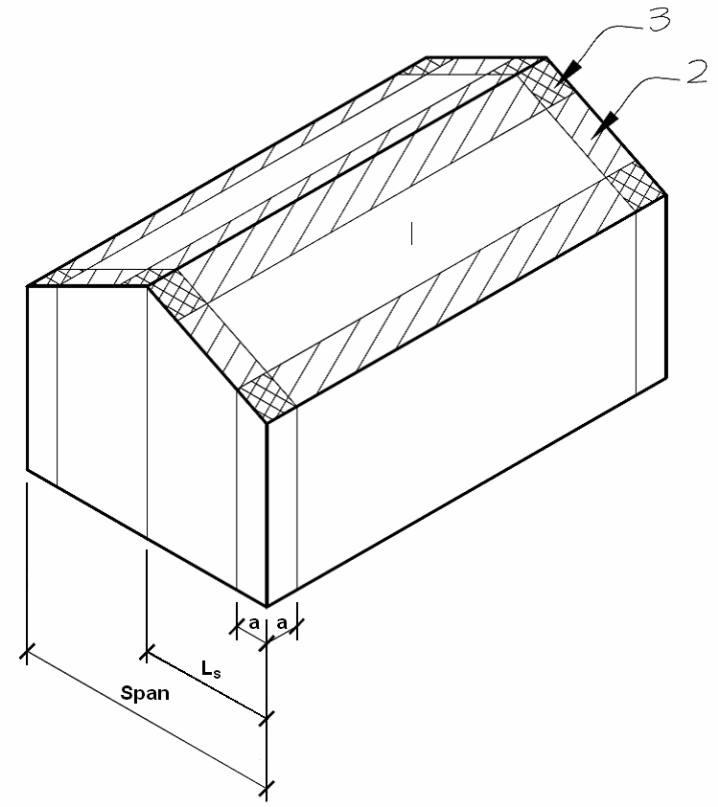

Figure 9: Roof zones corresponding to wind loads reported in Table 1.2 [ASCE 2005].

Table 1: Vertical roof dead load components, defined with respect to the panel length.

	Climate		
	I (R_{US}-30) (R_{SI}-5.3)	II (R_{US}-30) (R_{SI}-5.3)	III (R_{US}-40) (R_{SI}-7.1)
Structure [N/m^2, psf]	**340, 7.1**	**340, 7.1**	**570, 11.9**
Insulation [N/m^2, psf]	**50, 1.0**	**50, 1.0**	**60, 1.2**
Int. and Ext. Finish [N/m^2, psf]	**328, 6.9**	**328, 6.9**	**328, 6.9**
Total Dead Load [N/m^2, psf]	**718, 15.0**	**718, 15.0**	**958, 20.0**

Table 2: Wind loads for a wind speed of 40.2 m/s (90 mph) defined as pressure perpendicular to the roof plane, positive loads act inward and negative loads act outward [ASCE 2005].

Loads for wind speed of 40.2 m/s (90 mph)				
Roof Slope	**Ratio a/L_s**	**Zone Wind Pressure [N/m^2, psf]**		
		1	**2**	**3**
6/12	0.2	479, 10.0 – 747, -15.6	479, 10.0 – 1049, -21.9	479, 10.0 – 1662, -34.7
10/12	0.25	- 771, 16.1 – 790, -16.5	771, 16.1 – 943, -19.7	771, 16.1 – 943, -19.7

Table 3: Wind loads for a wind speed of 58.1 m/s (130 mph) defined as pressure perpendicular to the roof plane, positive loads act inward and negative loads act outward [ASCE 2005].

Loads for wind speed of 58.1 m/s (130 mph)				
Roof Slope	**Ratio a/L_s**	**Zone Wind Pressure [N/m^2, psf]**		
		1	**2**	**3**
6/12	0.2	986, 20.6 – 1666, -34.8	986, 20.6 – 2753, -57.5	986, 20.6 – 4137, -86.4
10/12	0.25	1748, 36.5 – 1867, -39.0	1748, 36.5 – 2198, -45.9	1748, 36.5 – 2198, -45.9

3.0 Combined Dead, Live and Wind Loads

The dead loads, live or snow loads, and out of plane wind loads were combined as recommended in [AISI 2001] and [ASCE 2005] in order to determine the maximum load conditions on the roof. The load combinations used were as follows:

For Climate I Loads

1. Dead + Live
2. Dead + Wind
3. Dead + .75(Wind + Live)
4. .6 Dead + Wind

For Climate II and III Loads

1. Dead + Snow
2. Dead + Wind
3. Dead + .75(Wind + Snow)
4. .6 Dead + Wind

(Nominal Ground Snow loads were considered.)

The load combinations were applied in order to determine the maximum distributed loads on the panels and the corresponding end reactions. These reactions are then used to design the connector elements for each of the panel joints, for the truss core panels and the stiffened plate panel. The load conditions considered for the truss core panel and panel joints were climates I, II and III with wind speeds of 40.2 m/s (90 mph) and 58.1 m/s (130 mph). Joints for the stiffened panel were designed for climates I and II with a wind speed of 40.2 m/s (90 mph). These limitations for the stiffened plate panel design are based on the predicted performance of the panel and are unrelated to the joints.

4.0 Panel Loads

The transverse distributed load on a panel (load perpendicular to the panel surface) were calculated following the combinations of live, dead and wind loads described in section 2. The dead, live and wind loads listed in Tables 1–4 are resolved into transverse distributed loads for each panel slope (Table 4). The combined loads are reported in Table 5. The greatest distributed transverse loads are highlighted in grey in Table 5 and summarized in Table 6. Transverse load increases with climates (due to the increasing snow load) and decreases with increasing roof pitch. For example considering a 6/12 roof pitch, the transverse load q is 1576 N/m^2 (32.9 psf) for climate I and increases to 3537 N/m^2 (73.9 psf) for climate III. For a roof pitch of 10/12, the transverse load is 1554 N/m^2 (32.5) for climate I and increases to 2798 N/m^2 (58.4) for climate III.

Table 4: Transverse dead, live (snow) and wind loads defined perpendicular to the roof panel surface.

	Slope	Climate		
		I	II	III
Dead Load q_D [N/m^2, psf]	**β=0°**	718, 15.0	718, 15.0	958, 20.0
	6/12 - β=26.6°	642, 13.4	642, 13.4	857, 17.9
	10/12 - β=39.8°	552, 11.5	552, 11.5	736, 15.4
Live Load q_V [N/m^2, psf]	**β=0°**	958, 20.0	1915, 40.0	3352, 70.0
	6/12 - β=26.6°	766, 16.0	1531, 32.0	2680, 56.0
	10/12 - β=39.8°	565, 11.8	1130, 23.6	1979, 41.3
Wind Load q_w [N/m^2, psf]	**β=0°**	0	0	0
	6/12 - β=26.6°	479, 10.0	479, 10.0	479, 10.0
	10/12 - β=39.8°	771, 16.1	771, 16.1	771, 16.1
Wind Uplift q_w [N/m^2, psf]	**β=0°**	0	0	0
	6/12 - β=26.6°	–1290, -26.9	–1290, -26.9	–1290, -26.9
	10/12 - β=39.8°	–943, -19.7	–943, -19.7	–943, -19.7

Table 5: Transverse distributed load combinations following the ASD procedure.

Transverse distributed loads combinations for ASD procedure [N/m^2, psf]				
Roof pitch	**Combination**	**Climate**		
		I	**II**	**III**
6/12 -	**q_D+q_L**	1408, 29.4	2173, 45.4	3537, 73.9
	q_D+q_W	1121, 23.4	1121, 23.4	1336, 27.9
	$q_D+0.75(q_L+q_W)$	1576, 32.9	2150, 44.9	3226, 67.4
	q_D+q_{WU}[1]	–648, -13.5	–648, -13.5	–433, -9.0
10/12 -	**q_D+q_L**	1117, 23.3	1682, 35.1	2715, 56.7
	q_D+q_W	1323, 27.6	1323, 27.6	1507, 31.5
	$q_D+0.75(q_L+q_W)$	1554, 32.5	1978, 41.3	2798, 58.4
	q_D+q_{WU}[1]	–391, 8.2	–391, -8.2	–207, -4.3

[1] WU stands for wind uplift

Table 6: Transverse distributed load used for panel design.

	Transverse distributed loads [N/m^2, psf]		
Slope	**Climate I**	**Climate II**	**Climate III**
6/12	1575, 32.9	2173, 45.4	3537, 73.9
10/12	1554, 32.5	1978, 41.3	2798, 58.4

5.0 Joint Loads

Panel to panel joints

The load combinations indicated in section 2 produced the maximum reactions needed for the design of the roof system joints. However there are additional loads which are unique to the panel to panel joint. The panel to panel joint must be designed to sustain point loads placed on one panel adjacent to the joint and diaphragm loads caused by wind.

Point loads

Point loads on one panel adjacent to the joint can cause a differential deflection of the panels across the panel to panel joint. ASCE 7-05 [ASCE 2005], "Design Loads for Buildings and Other Structures", indicates that the concentrated load to be used in the design of a roof is a load of 1334 N (300 lb) applied to an area of 0.76 m x 0.76 m (2'-6" x 2'-6"). It is implied in the document that this is the design load that will occur as the result of maintenance workers or equipment on the roof. In considering various scenarios, we deemed it possible to have up to two workers standing next to each other on one panel in close proximity to a panel joint. Further, it may be possible that these workers are carrying roofing materials or equipment. We judged that the presence of two 1334 N (300 lb) loads is an extreme load condition that is likely only during the construction and could be considered a temporary construction load. This distinction is important as it will affect the required factor of safety used in the design of the panel joint to resist these loads. Therefore, we established two design criteria for the panel joint point loads (Figure 10):

1. A single 1334 N (300 lb) load applied to a 0.76 m x 0.76 m (2'-6" x 2'-6") area and located where it would produce the greatest forces on the joint connection. Since this load is described as a normal design requirement of ASCE 7 for roofs, this load is considered a long term building load and the design would include the normal factor of safety used for permanent loads.
2. Two 1334 N (300 lb) point loads, each applied on an area approximately equal to the surface area of a normal shoe and located where they would produce the greatest forces on the joint connection. This load is considered a temporary construction load and the design would allow for a reduction in the normal factor of safety.

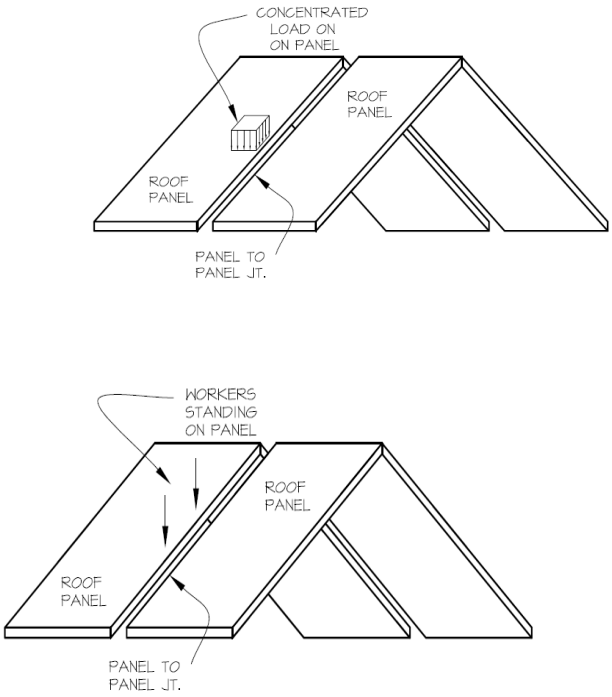

Figure 10: Models for Load Cases 1 and 2 – Temporary Construction Load

Diaphragm loads

In addition to analyzing the panel joints for out of plane dead, snow and wind loads, it is also important to review the affects of the lateral in plane wind loads on the panel to panel joint. The panel to panel joint is critical for this condition since the roof system must act as a diaphragm when resisting the wind loads applied to the building (Figure 11). The lateral loads considered for the design of the panels were chosen to be the result of a 40.2 m/s (90 mph) and a 58.1 m/s (130 mph) design wind velocity. The loads imposed on the building have been determined for this criterion using the method for determining the wind loads given in the document ASCE 7, "Design Loads for Buildings and Other Structures" provided as a design standard by the American Society of Civil Engineers.

The wind condition that induces the most severe loading on the roof diaphragm is a wind parallel to the building ridge (Figure 12). This wind will cause a positive pressure on the windward wall of 575 N/m^2 (12 psf) and a negative pressure on the leeward wall of 814 N/m^2 (17 psf). The net pressure acting on the building which must be resisted in part by the roof diaphragm is therefore 1389 N/m^2 (29 psf). This was rounded to 1440 N/m^2 (30 psf) total pressure on the building for analysis purposes. The results of this wind force were used in the design of the panel to panel connection.

The wind load that is transferred to the roof diaphragm is the result of the wind in the gable endwall. Due to the varying height from the ceiling level to the roof, the load

applied to the roof panels from the wind on the gable endwall will vary from 0 N at the eave line to 667 N (150 lb) at the ridge (Figure 13). The total resultant load to the roof diaphragm is therefore 7560 N (1700 lb). The diaphragm load is transferred to the wall system at the building eaves and for the building under consideration, having a total length of 11.6 m (38 ft), the shear at the eave is calculated as 651.7 N/m (45 pounds per linear foot) (Figure 14). The panels must transfer this shear to each adjacent panel to perform as a roof unit and effectively act as a diaphragm. The panels will resist the tendency to "rack" if the connection between panels is adequately strong. The panels must resist a force of 651.7 N/m (45 pounds per linear foot) along the panel to panel connection to transfer the shear force to the adjacent panel and allow the panels to act properly as a complete diaphragm (Figure 15).

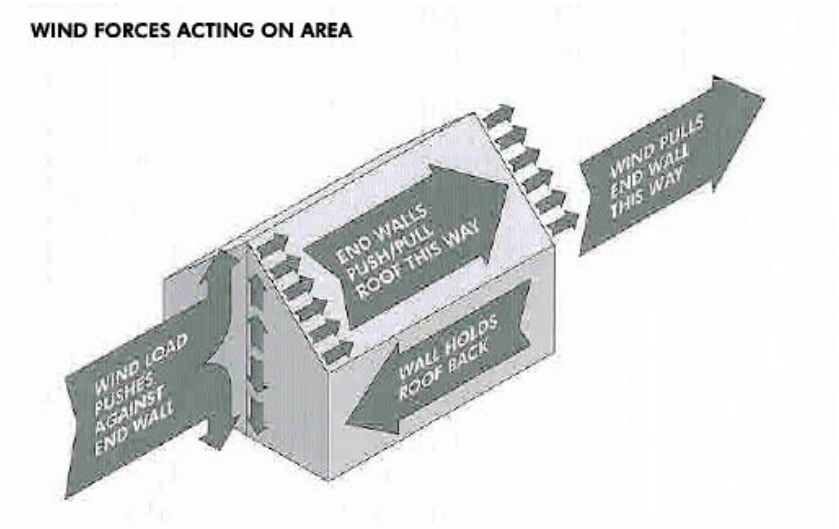

Figure 11: Wind forces acting on the building.

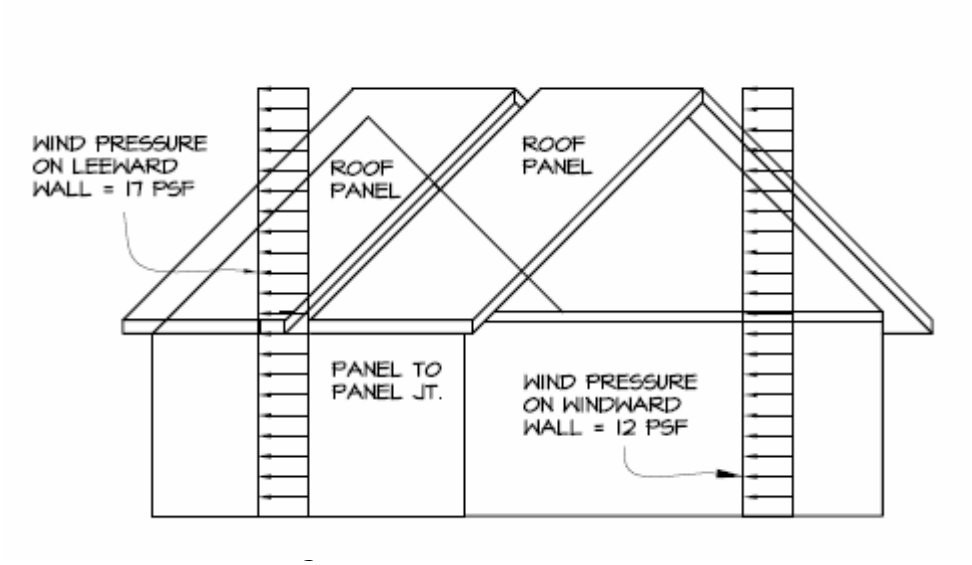

Figure 12: Wind loads on the building.

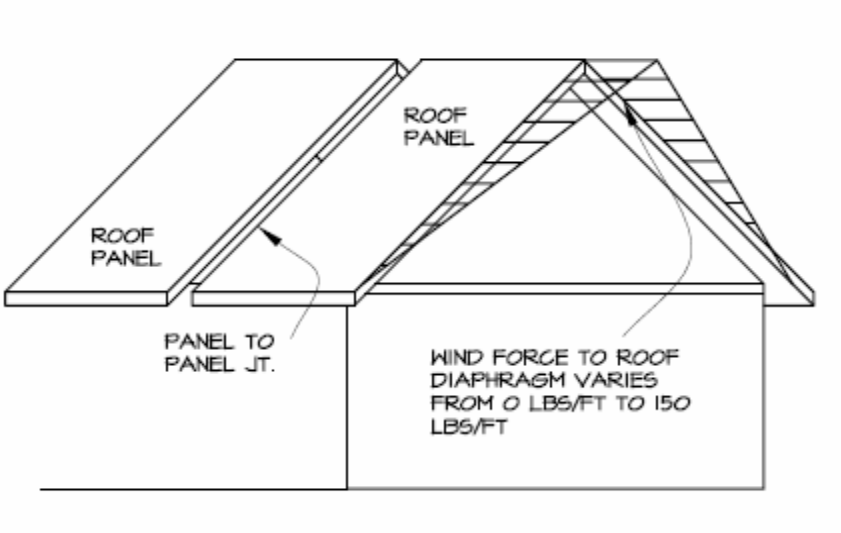

Figure 13: Wind loads transferred from the gable endwall to the roof panel.

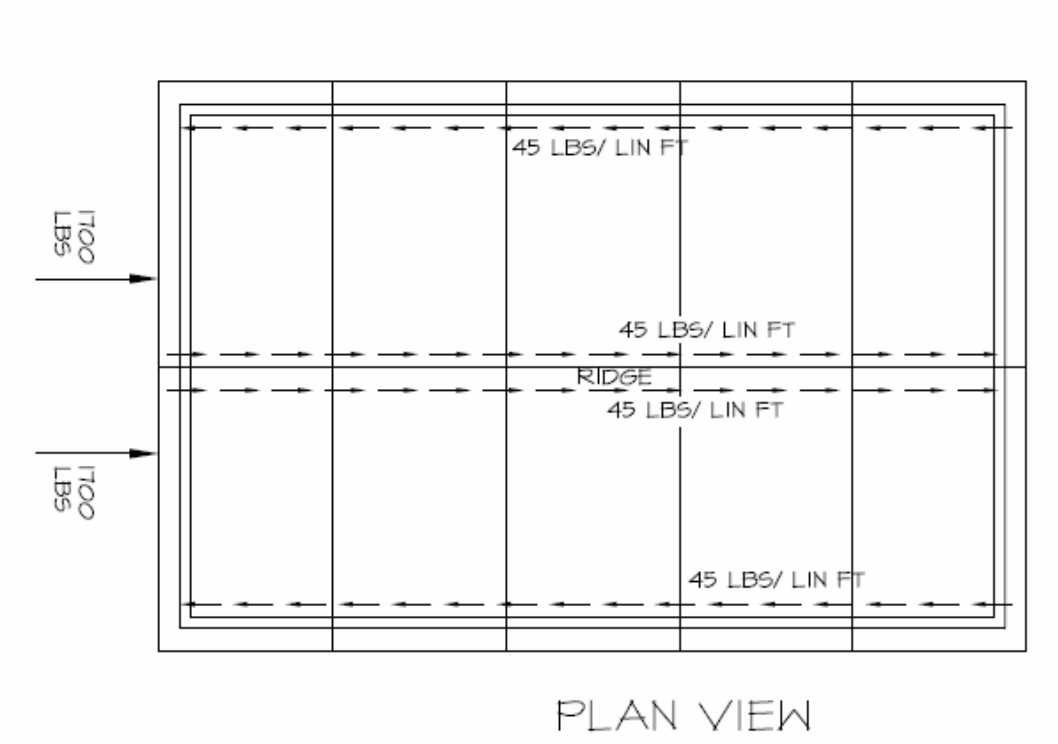

Figure 14: Transfer of wind loads to the eaves.

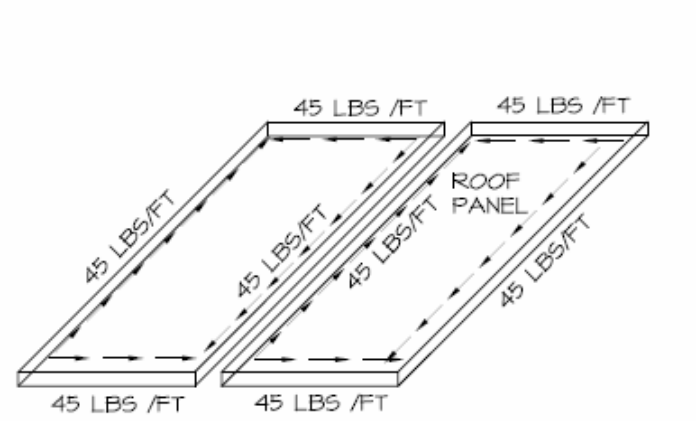

Figure 15: Diaphragm loads in the panel.

Load summary for panel to panel joints

The panel to panel joint must resist gravity loads when an unusual load condition occurs such as the weight of workers or when equipment is placed on the roof. The normal gravity loads due to dead weight of the roof system and snow or out of plane wind loads do not create a significant load differential across the joint. In plane wind loads create a shear load that must be resisted across the joint to allow the roof system to

act as a proper diaphragm. Representative combined joint loads for the steep slope panel and the shallow slope panel are summarized in Figures 16 and 17.

Ridge Joints

The highest magnitude reaction determined from the load combinations was used for the design of the ridge connection for both panel configurations; long span and short span. The reaction was resolved into forces perpendicular and parallel to the panel span and the components of the ridge joint connector were analyzed for bending stresses, shear stresses, tension and compression. Connectors were designed to resist shear and uplift forces on the connection.

Soffit Joints

The highest magnitude reaction determined from the load combinations was used for the design of the soffit connection for both panel configurations; long span and short span. The reaction was resolved into forces perpendicular and parallel to the panel span and the components of the joint connector were analyzed for bending stresses, shear stresses, tension and compression. Connectors were designed to resist shear and uplift forces on the connection.

Gable End Joints

The highest magnitude reaction determined from the load combinations was used for the design of the gable end connection for both panel configurations; long span and short span. The reaction was resolved into forces perpendicular and parallel to the panel span and the components of the joint connector were analyzed for bending stresses, shear stresses, tension and compression. Connectors were designed to resist shear and uplift forces on the connection.

Short Panel Frame w/ Supported Ridge

Short Panel Frame Reactions		Loads in Founds per ft of panel length		
Load Condition		Reaction RL	Reaction Rc	Reaction RR
Climate I	Vert	196	526	196
	Horiz	28	0	-28
Climate II Balanced	Vert	247	664	247
	Horiz	36	0	-36
Unbalanced	Vert	316	526	76
	Horiz	28	0	-28
Climate III Balanced	Vert	359	967	359
	Horiz	52	0	-52
Unbalanced	Vert	482	733	62
	Horiz	39	0	-39
Wind +Dead Transverse	Vert	114	255	76
	Horiz	-92	0	-116
Wind +Dead Longitudinal	Vert	48	101	48
	Horiz	51	0	-51
Wind on Panel Only				
Windward Face	Vert	141	282	
	Horiz	-17	0	
Leeward Face	Vert	76	-74	
	Horiz	-180	0	

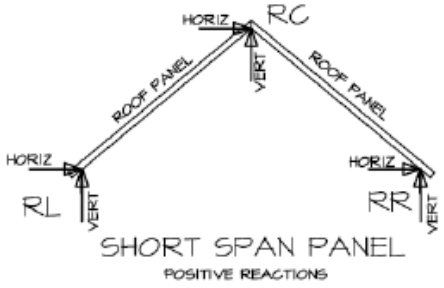

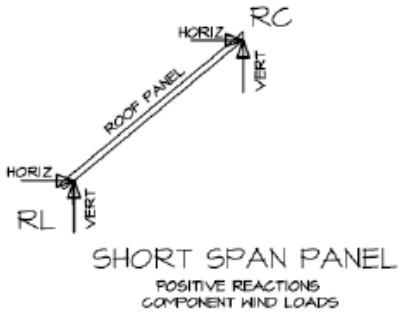

Figure 16: Representative combined joint loads for the steep sloped (short span) roof panel.

Long Panel Frame w/ Supported Ridge

Long Panel Frame Reactions		Loads in Pounds per ft of panel length		
Load Condition		Reaction RL	Reaction Rc	Reaction RR
Climate I	Vert	294	882	294
	Horiz	37	0	-37
Climate II Balanced	Vert	382	1146	382
	Horiz	48	0	-48
Unbalanced	Vert	494	882	94
	Horiz	37	0	-37
Climate III Balanced	Vert	566	1698	566
	Horiz	71	0	-71
Unbalanced	Vert	764	1242	64
	Horiz	52	0	-52
Wind +Dead Transverse	Vert	59	151	58
	Horiz	54	0	-55
Wind +Dead Longitudinal	Vert	59	152	59
	Horiz	54	0	-54
Wind on Panel Only				
Windward Face	Vert	243	293	
	Horiz	-100	0	
Leeward Face	Vert	40	-45	
	Horiz	170	0	

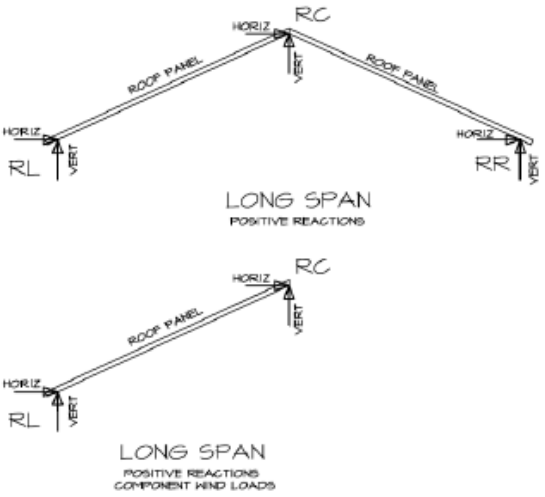

Figure 17: Representative combined joint loads for the shallow sloped (long span) roof panel.

References

[ICC] International Code Council. 2003. 2003 International Residential Code for One- and Two-Family Dwellings. Country Club Hills, IL: ICC.

[AISI] American Iron and Steel Institute. 2001. North American Specification for the Design of Cold-Formed Steel Structural Members.

[ASCE] American Society of Civil Engineers. 2005. ASCE/SEI 7-05, Minimum Design Loads for Buildings and Other Structures.

Appendix D: Panel Structural Design Methodology

1.0 Overview of Approach

In evaluating structural panel performance, four failure modes were considered: deflection, bending moment capacity, web crippling, and foam failure. The first three failure modes are illustrated in Figure 1 for the truss core panel and in Figure 2 for the stiffened plate panel. The limit on allowable deflection is set by the International Residential Code (ICC 2003) at $L_s/240$, where L_s is the horizontal span of the panel. Bending moment capacity is the strength required to support the bending moment acting on the panel, accounting for postbuckling behavior and material yielding. Web crippling strength refers to the force that the web can support at the panel supports. Although the foam is not used as a structural material, it must transmit loads to the structural panel without failure. The analytical and empirical equations used to assess panel performance are provided in this appendix.

2.0 Deflection

Global and local deflection are evaluated. For both calculations, the approach used is described by Timoshenko and Gere [1997] for beams with standard sections and adopted by the AISI specification for cold rolled light gage steel members [AISI 2001a]. For global deflection the panel is modeled as a simply supported beam with an effective moment of inertia I_{eff} that depends on the postbuckling behavior of the panel (determination of I_{eff} is described further in sections 3.2 to 3.4). Local deflection is considered for the stiffened plate panel design (Figure 2), where the bottom face sheet is directly subjected to the distributed transverse load. In this case the bottom face sheet is treated as a beam with clamped edges.

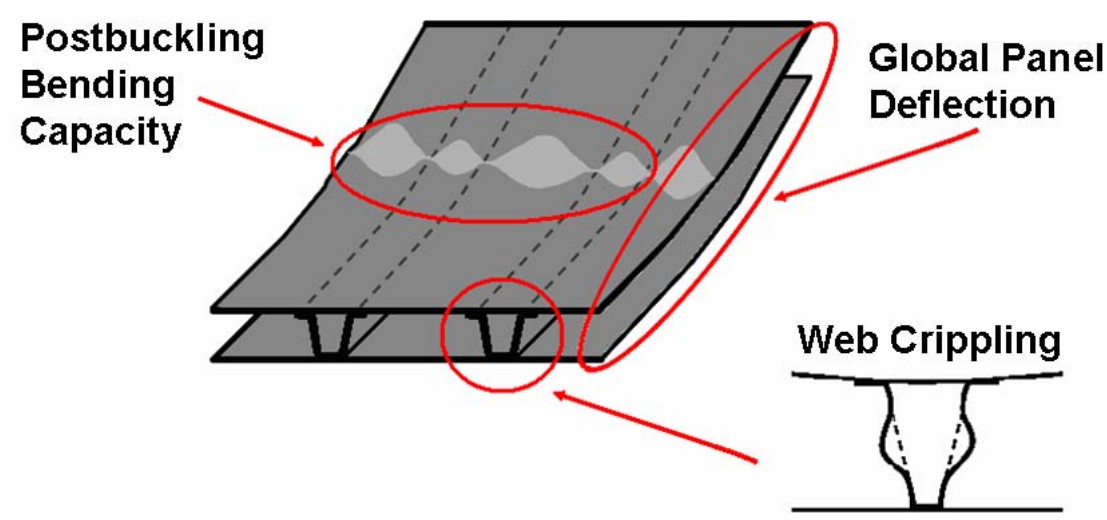

Figure 1: Truss-core panel structural failure modes.

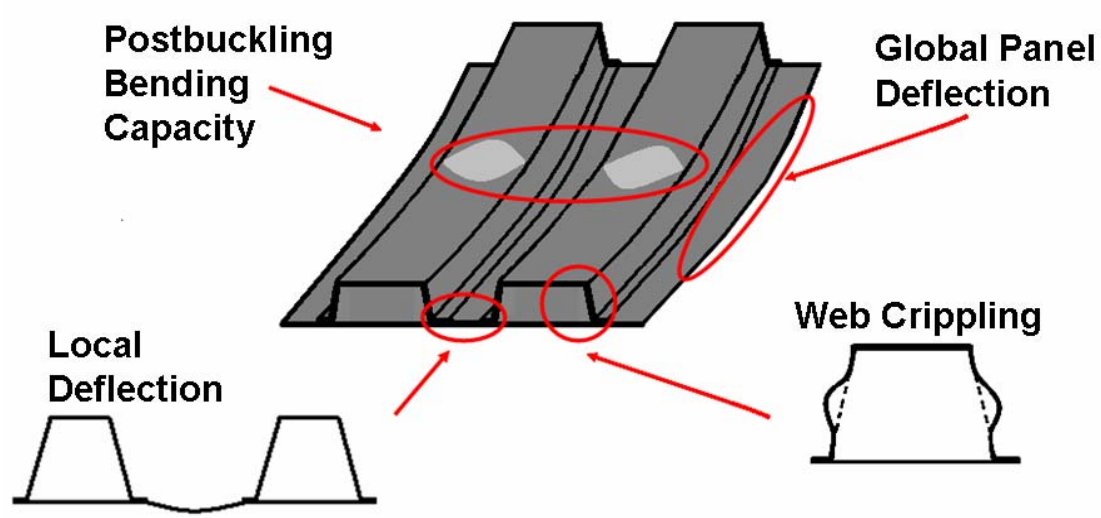

Figure 2: One-sided panel structural failure modes.

2.1 Global Deflection

The total global deflection (displacement in the direction perpendicular to the panel) of the panel is:

$$w_g = w_b + w_s \tag{1}$$

where w_b is the deflection due to the transverse distributed load q:

$$w_b = \frac{5}{384}\frac{qba^4}{EI_{eff}}. \tag{2}$$

The effective moment of inertia I_{eff}, is a non linear quantity computed following the iterative procedure for deflection described in sections 3.3 and 3.4. The deflection due to the shear w_s is computed as:

$$w_s = \frac{\alpha qpa^2}{8GA_{tot,eff}}. \tag{3}$$

The shear coefficient α is defined as [Timoshenko and Gere 1997]:

$$\alpha = \frac{A_{tot,eff}}{A_{webs,eff}}, \tag{4}$$

where $A_{tot,eff}$ and $A_{webs,eff}$ refer to the effective total and web cross-section area respectively. The maximum admissible deflection $w_{g,max}$ defined relative to the panel horizontal span length L_s is:

$$w_{g,max} = \frac{L_s}{240}. \quad (5)$$

The safety factor for global deflection is defined as:

$$\Omega_{def,g} = \frac{w_{g,max}}{w_g}. \quad (6)$$

The computed safety factor $\Omega_{def,g}$ must be greater than or equal to the required safety factor for deflection $\Omega_{def,req}$:

$$\Omega_{def,g} \geq \Omega_{def,req}. \quad (7)$$

In the present analysis, the required safety factor for deflection is 1.0.

2.2 Local Deflection (stiffened plate panel only)

Assuming clamped boundary conditions for a plate of length $f_{0,b}$, the local deflection of the one-sided panel with interior face sheet is computed as:

$$w_{loc} = \frac{qaf_{0,b}^{\ 4}}{384EI_{b,t}}, \quad (8)$$

where

$$I_{b,t} = \frac{at_b^{\ 3}}{12} \quad (9)$$

is the transverse moment of inertia of the bottom face sheet. The maximum admissible local deflection is set equal to the bottom sheet thickness, i.e.

$$w_{loc,max} = t_b, \quad (10)$$

to ensure small deformation and validity of linear theory. The safety factor for the local deflection is defined as:

$$\Omega_{def,loc} = \frac{w_{loc,max}}{w_{loc}}. \quad (11)$$

The computed safety factor $\Omega_{def,loc}$ must be greater than or equal to the required safety factor for deflection $\Omega_{def,req}$:

$$\Omega_{def,loc} \geq \Omega_{def,req}. \quad (12)$$

The required safety factor for local deflection is 1.0.

3.0 Bending Moment Capacity

For a simply supported beam subjected to a uniformly distributed transverse load q the maximum generated bending moment is

$$M_u = \frac{ql^2}{8}. \quad (13)$$

The nominal bending moment capacity M_n, computed considering initiation of yielding at the highest stressed location in the cross section is given by

$$M_n = \frac{I_{eff}}{y_{max}} \sigma_Y , \qquad (14)$$

where y_{max} is the distance between the neutral axis and the highest stressed location in the section, and σ_Y is the material yield strength. The effective moment of inertia I_{eff} is a nonlinear quantity and is computed following the iterative procedure described in sections 3.3 and 3.4. The safety factor for bending moment capacity is computed as:

$$\Omega_{BM} = \frac{M_n}{M_u} . \qquad (15)$$

The computed safety factor Ω_{BM} must be greater than or equal to the required safety factor for bending moment $\Omega_{BM,req}$:

$$\Omega_{BM} \geq \Omega_{BM,req} \quad . \qquad (16)$$

The required safety factor for bending moment capacity is 1.67.

3.1 Additional Requirement for Stiffened Plate Panel

For the stiffened plate panel design with interior face sheet, the highest state of stress may occur in proximity of the welds in the bottom face sheet (Figure 3), due to the presence of stresses in the longitudinal (x) and transverse (y) directions. The equivalent stress at this location must be less than the material yield strength.

Considering the loads applied to the panel, the stress in the longitudinal direction σ_x at the weld is a function of the safety factor $\Omega_{BM,req}$:

$$\sigma_x = \frac{M_u \Omega_{BM,req} \hat{y}_{max}}{\hat{I}_{eff}} , \qquad (17)$$

where $\hat{y}_{max}$ and $\hat{I}_{eff}$ are computed following the effective width method using the procedure for deflection described in section 3.4 and applying the bending moment $M_u \Omega_{BM,req}$ instead of M_u (the output relevant in this case is the effective moment of inertia and not the deflection). The stress σ_y in the transverse direction is a result of the pressure applied to the face sheet. The region between the webs is modeled as a beam

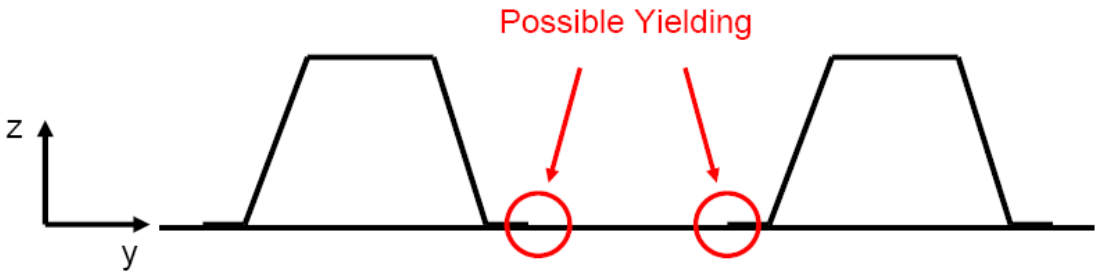

Figure 3: Possible yielding location due to biaxial state of stress in the interior face sheet for one-sided panel design.

with fixed edges, the welds, subjected to a uniform pressure q. Thus,

$$\sigma_y = \frac{q f_{0,b}^2 \Omega_{BM,req}}{2 t_b^2}. \quad (18)$$

Equation (18) can be written in a form similar to equation (17):

$$\sigma_y = \frac{M_y \Omega_{BM}}{S_{bot}}, \quad (19)$$

where the section modulus of the bottom face sheet S_{bot} is

$$S_{bot} = \frac{a t_b^2}{6}, \quad (20)$$

and the bending moment M_y in the transverse direction is

$$M_y = \frac{q a f^2_{0,b}}{12}. \quad (21)$$

Given the present loading, τ_{xy} is small. The equivalent Von Mises stress $\sigma_{VM,}$ with the plane stress assumption, is then

$$\sigma_{VM} = \sqrt{\sigma_x^2 + \sigma_y^2 - \sigma_x \sigma_y}. \quad (22)$$

The equivalent Von Mises stress σ_{VM} at the weld location must be less than the material yield strength, i.e.

$$\sigma_{VM} < \sigma_y. \quad (23)$$

Note the safety factors have been included in the stress calculations in equations (18) and (19).

3.2 Effective Moment of Inertia Determination

3.2.1 Postbuckling behavior and effective moment of inertia

Elements of the panel cross section, such as the webs, or face sheet sections between welds are modeled as plates with simply supported edges (along the welds). These plate sections have a width to thickness ratio, w/t, that can be very high (>250). When loaded in compression, the sections can exhibit local buckling. However, due to the support conditions (i.e. welds), stress redistribution can occur, leading to considerable postbuckling strength. The load carrying capacity of such members is higher than that computed using the critical linear elastic buckling stress.

Due to the stress redistribution, only a fraction of the buckled plate width near the supports is effective in resisting further compressive loads. The effective width method is a technique commonly utilized in structural analysis of light gage steel members. In this technique, an equivalent width is developed such that the stress acts uniformly over two strips near the plate edges while the central region of the plate is unstressed. Figure 4 shows the effective width b and the real stress distributions for two different levels of

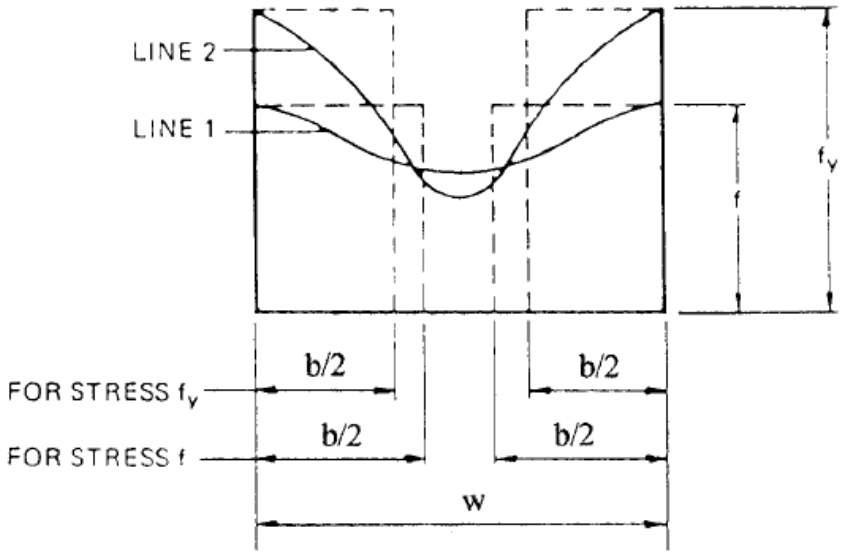

Figure 4: Two real stress distributions and the two relative effective widths are shown for stress levels f and f_v [AISI 2001b].

stress in a compressed element of width w. The effective width b is substituted for the actual width w in determining the section properties.

Equations to compute the effective width are described by the AISI specification for cold rolled steel members [AISI 2001a,2001b,2002]. These equations provide the effective width as a nonlinear function of the maximum stress allowed in the compressed element. The computation of the effective section properties such as the effective moment of inertia I_{eff} may require iterative procedures. Such procedures are not described by the AISI specification and are therefore reported in the following sections. Figure 5 shows the moment of inertia of a structure characterized by post buckling behavior. In this case, the moment of inertia is a function of the maximum stress allowable in the section. The moment of inertia is greatest for low stresses, before buckling occurs. For higher stresses (and therefore loads), the moment of inertia decreases. The minimum value occurs when the highest-stressed location in the section yields.

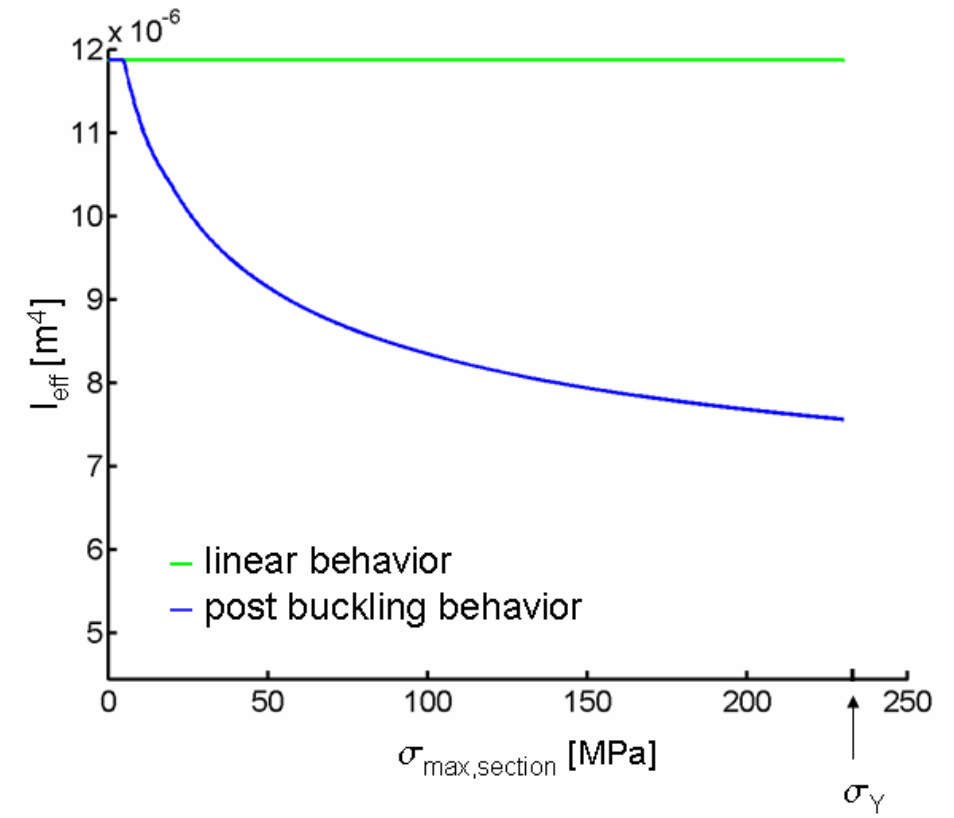

Figure 5: Effective moment of inertia of a two-sided truss core structure characterized by post buckling behavior as a function of maximum stress allowed in the section. A structure with linear behavior has a constant moment of inertia up to failure.

3.3 Procedure for Evaluating the Bending Moment Capacity

The bending moment capacity M_n is computed using equation (14) where the effective moment of inertia I_{eff} of the section is computed when the highest-stressed location in the section (compression or tension) reaches the yield strength σ_Y. The stresses on the panel are implicitly related to the effective moment of inertia, i.e. the value of each depends on the value of the other. For this reason, it is typically necessary to determine I_{eff} through an iterative process.

In computing the effective moment of inertia (for the purpose of evaluating the bending moment capacity), the following procedure is implemented (see Figure 6):

1 Initialization:

- choose section geometry and the yield strength σ_Y to be allowed in the section.

2 Full effective properties determination:

- compute the neutral axis e, the compressed depth of the panel $h_{compression}$, and the tensioned depth of the panel $h_{tension}$.

3 Iteration:

- impose the stress σ_Y in the highest stressed location of the panel (tension if $h_{tension} > h_{compression}$ or compression if $h_{tension} < h_{compression}$).

- compute the stress in the remaining part section assuming a linear strain diagram with the highest stress as σ_Y.
- compute the effective widths of the different compressed elements (compression flanges and webs)
- compute a new neutral axis e, compressed depth of the panel $h_{compression}$, and tensioned depth of the panel $h_{tension}$.
- check if the relative error on neutral axis position is less than 0.05%. If not repeat step 3 using the new neutral axis e and depths h.

4 Strength determination:

- using the effective section properties found at the last iteration compute the effective moment of inertia I_{eff} and the nominal section strength M_n.

The error value limit of 0.05% on the neutral axis location e was chosen to guarantee good accuracy in the computation of the effective moment of inertia I_{eff}.

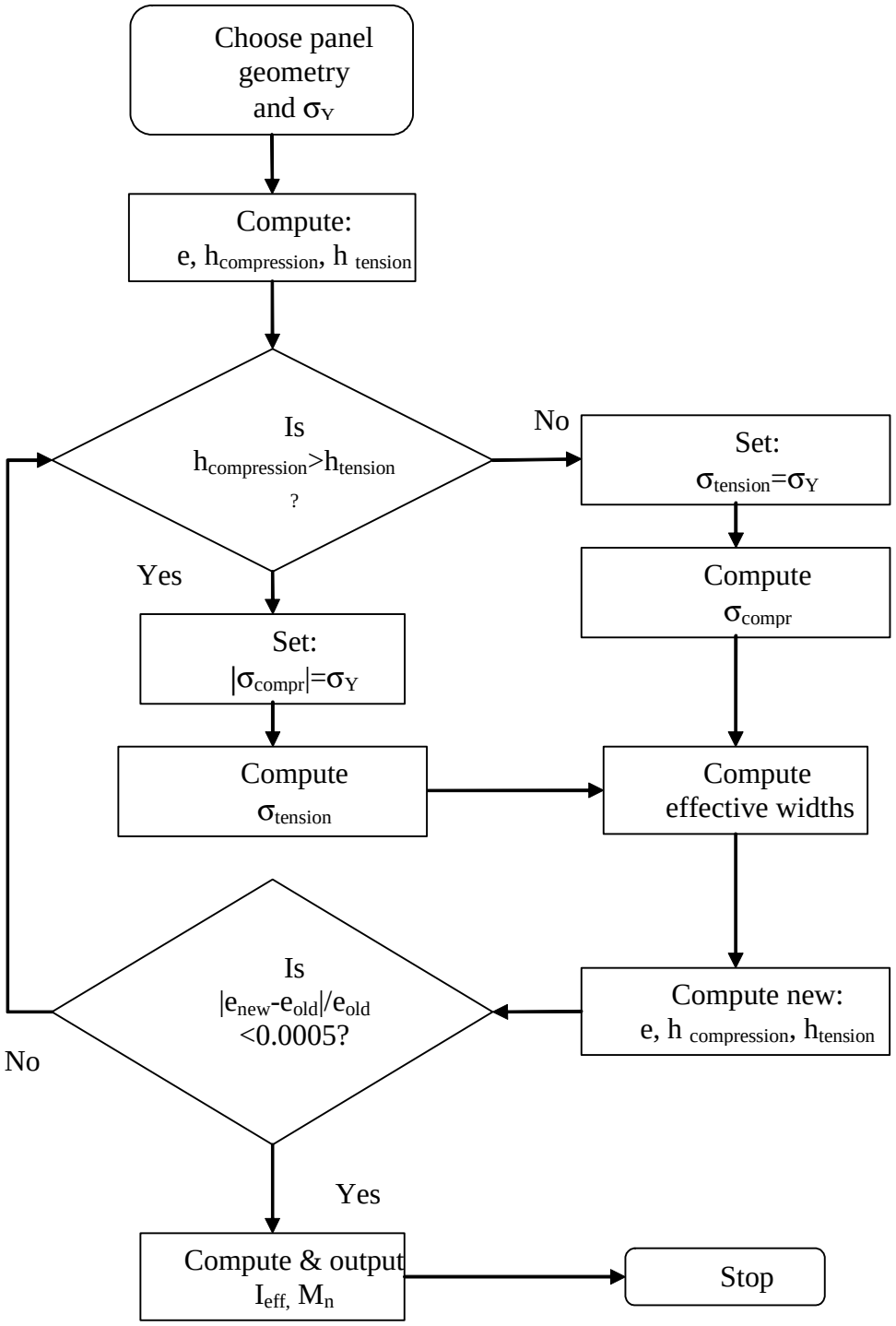

Figure 6: Flow chart for bending moment capacity determination procedure.

3.3 Procedure for evaluating the deflection (accounting for I_{eff})

Panel deflection is determined using the effective moment of inertia for a structure subjected to the imposed bending moment M_u (i.e. not the bending capacity M_n). As with the moment capacity calculations, the stresses are implicitly related to the effective moment of inertia M_u.

The value of M_u can be determined using a modification of the procedure described in Section 3.2. Rather than imposing a stress and determining the resulting bending moment and effective moment of inertia, the bending moment is imposed. From the bending moment, the resulting stresses and effective moment of inertia are determined. The algorithm is described below and a flow chart is shown in Figure 7:

1 Initialization:
- choose section geometry and the imposed bending moment M_u at which the effective moment I_{eff} is to be computed.

2 Guess:
- guess a maximum stress $\sigma_{max,\ imposed,}$ to be allowed at the highest stresses location of the panel, equal to half of the material yield strength.

3 Iterations:
- compute the section strength $M_{n,iter}$ at the imposed level of stress using the procedure described in section 3.2
- if the computed strength $M_{n,iter}$ is less than required bending moment M_u increase the stress $\sigma_{max,\ imposed}$ (using a bisection algorithm) and repeat step 3
- If $M_{n,iter}$ is greater than M_u, decrease the stress $\sigma_{max,\ imposed}$ (using a bisection algorithm) and repeat step 3
- Continue until the relative error of M_u is less than 0.1%.

4 Compute deflection:
- Compute the deflection using the effective moment of inertia I_{eff} determined in the last iteration.

5 Output:
- Output the computed strength $M_{n,iter}$, the maximum stress imposed $\sigma_{max,\ imposed}$, the effective moment of inertia I_{eff} at the last iteration and deflection.

The 0.1% error limit in the computation of the moment was chosen as a reasonable value considering the level of approximation typically required in structural analyses. This procedure converges only if the required bending strength M_u is less than the nominal section strength M_n (or if the imposed stress $\sigma_{max,imposed}$ is less than the material yield strength $\sigma_{yielding}$). Therefore, the bending capacity is checked prior to starting the procedure in order to ensure that the panel has sufficient structural strength.

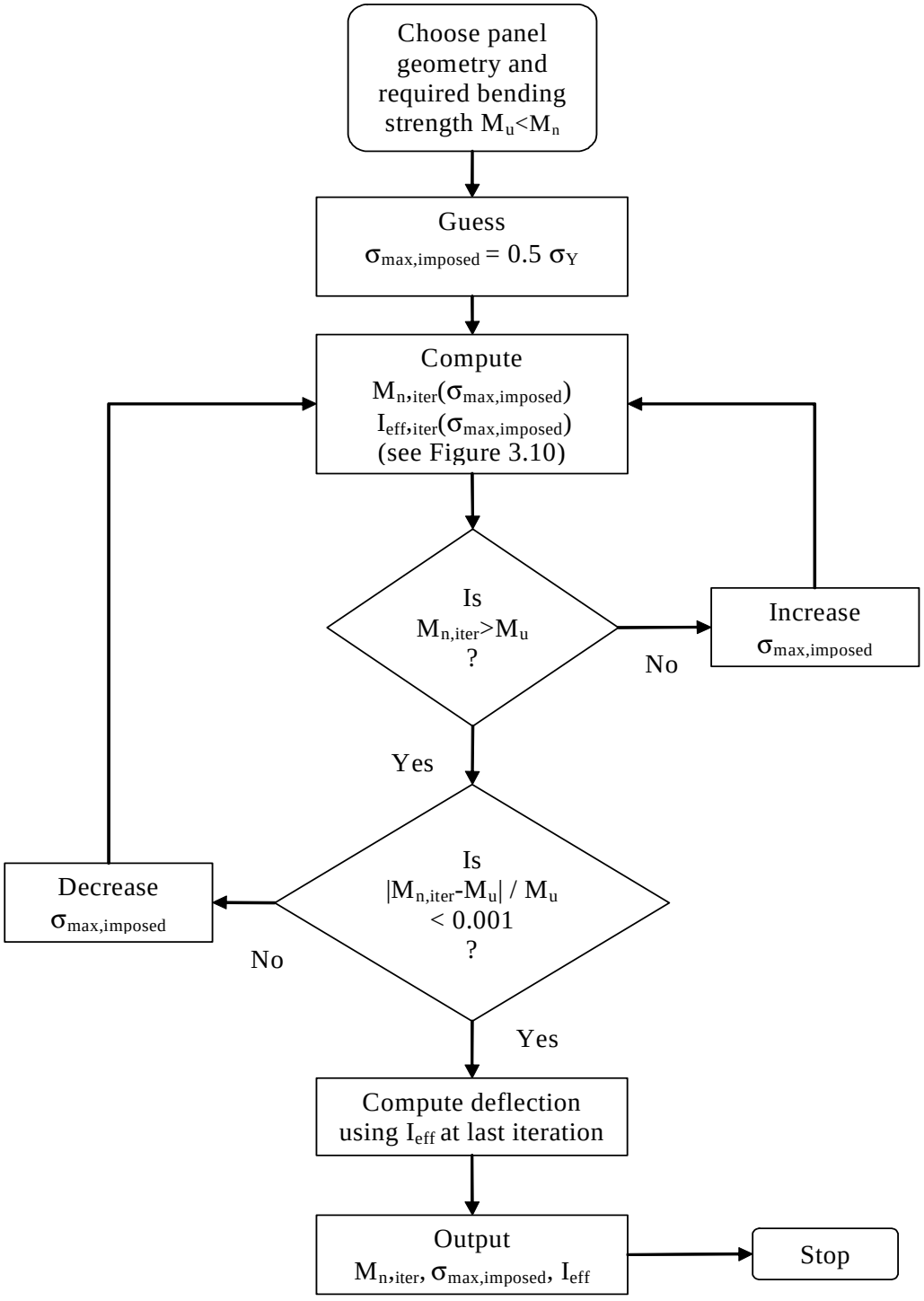

Figure 7: Flow chart for evaluating the deflection and the corresponding I_{eff}.

4.0 Web Crippling

Web crippling is a form of web instability that results from several factors, including load eccentricity and local edge phenomena. Crippling strength is influenced by web and section geometry, material properties, and support conditions. An exact theoretical analysis would have to account for non uniform stress distributions, elastic and inelastic instability, local yielding, bending produced by the eccentric load, initial imperfections, various edge restraints and web inclination [AISI 2001a, 2001b]. An empirical expression for the web crippling strength is of the form [AISI 2002]

$$P_n = Ct_w^2\sigma_Y \sin\theta\left(1-C_R\sqrt{\frac{R}{t_w}}\right)\left(1+C_N\sqrt{\frac{N}{t_w}}\right)\left(1-C_h\sqrt{\frac{h}{t_w}}\right), \quad (24)$$

where C is a coefficient that depends on the type of loading and support position, C_R is the inside bend radius coefficient, C_N is the bearing length coefficient, C_h the web slenderness coefficient, h is the flat width of the web and N is the bearing length. Each term in parenthesis (Equation 24) represents a factor that influences the web crippling strength. The first term accounts for the effect of the bending radius R. The second term accounts for the effect of the bearing length N. The third accounts for the effect of the slenderness ratio h/t_w of the web.

The reaction that each web must carry is

$$P_u = \frac{qab}{2N_{web}}, \quad (25)$$

where a and b are the panel length and width and N_{web} is the number of webs in the panel. The safety factor for web crippling is

$$\Omega_{wc} = \frac{P_n}{P_u}. \quad (26)$$

The computed safety factor Ω_{wc} must be greater or equal to the required safety factor for web crippling $\Omega_{wc,req}$:

$$\Omega_{wc} \geq \Omega_{wc,req} \quad (27)$$

The value of the required safety factor for web crippling is 2.25 [AISI 2001a].

The constants for web crippling are determined empirically. Constants for the case in which the webs are unstrapped and unfastened are provided in the AISI standard [2004]. Physically, the unstrapped case represents a situation in which the webs are free to expand, there is no face sheet constraining the webs (Figure 8). The unfastened case corresponds to a situation in which the panel is supported at the edges, but not fastened to the support (Figure 9). Web crippling constants for the fastened and strapped cases were evaluated from published data for cold formed steel structures with geometries similar to the truss core and stiffened plate panels.

Validation of the crippling predictions was obtained through testing on prototype truss core and stiffened plate panels. The results indicate that web crippling in the truss core and stiffened plate panels can be predicted with the empirical constants for the

strapped case. The empirical constants for the strapped case (evaluated by the University of Minnesota) and the unstrapped case (from the AISI standard) are listed in Table 1. A detailed description of the determination of these empirical constants can be found in the supplement to this appendix.

Table 1: Web crippling constants.

Web Crippling Constants		
	strapped[1]	**unstrapped**[2]
General coefficient C	5.271	3.000
Inside bend radius coefficient C_R	0.170	0.400
Bearing length coefficient C_N	0.369	0.290
Web slenderness coefficient C_h	0.014	0.028
Bend radius to web thickness ratio R/t_w	1	
Bearing Length N [mm]	78.1 mm (for 6/12 roof pitch) 90.9 mm (for 10/12 roof pitch)	

[1] coefficients determined by UMN and used to evaluate web crippling in the two-sided truss-core and stiffened plate panel designs

[2] coefficients listed in AISI 2004, found empirically for cold formed sections that are unstrapped and unfastened

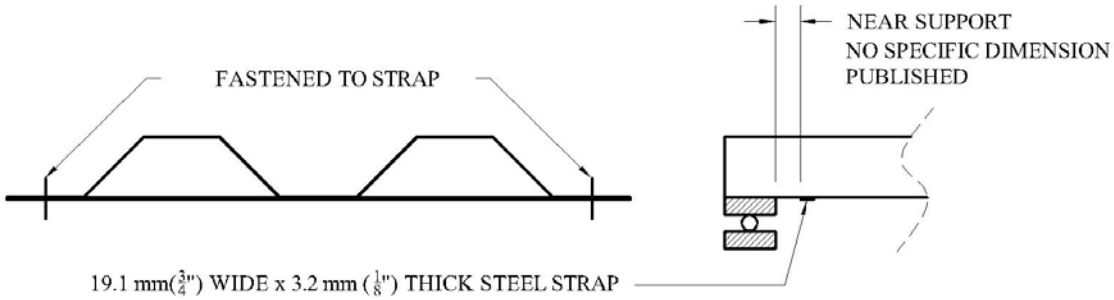

Figure 8: Web crippling tests on a multideck section in which the webs are fastened to a strap.

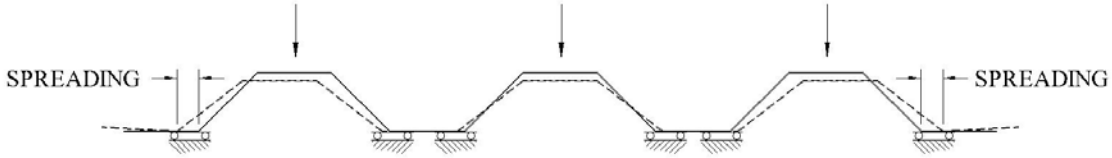

Figure 9: Unfastened multi-web deck section subject to lateral spreading under vertical web crippling load at the end of the section

5.0 Foam Structural Performance

In truss core and stiffened plate panels, the foam attached to the structure must not fail under the applied loading. The foam may be attached on either the exterior or the interior of the panel. If the foam is placed on the exterior, then the foam transmits the external loads to the underlying panel. If the foam is attached to the interior, then the foam is not subjected to any loading other than the dead weight of the gypsum and any finishing materials or fixtures attached to it. In either case, the foam will be subjected to stresses resulting from the curvature of the structural panel under load. Two failure modes of the foam are considered: stress failure of the foam itself, and adhesive failure between the foam and the structure.

The locations where the stresses are evaluated are indicated in Figure 10. For the panel with exterior foam, stresses are evaluated at the *center* and at the soffit *support*. The location marked *center* is subject to the live (snow) loading plus the bending stresses imposed on the foam by its attachment to the panel. The location marked *support* is subjected to wind uplift forces. For the panel with interior foam, the location marked *interior* is subject to the bending stresses plus the dead weight of the foam and the gypsum layer beneath.

In order to establish the performance of the foam under the worst case scenario, the analysis was performed assuming Climate III loading with R-7.0 insulation under 90 mph winds, on a roof with a 6/12 slope. The material properties of the foam are reduced to account for the effects of aging over a life of 50 years. The strength of the foam is reduced to account for fatigue, and the stiffness is reduced to account for creep. The applied loads and material properties are provided in Appendix A. Interpretation of the panel loads for the exterior and interior foam cases is provided, followed by the results for the present case.

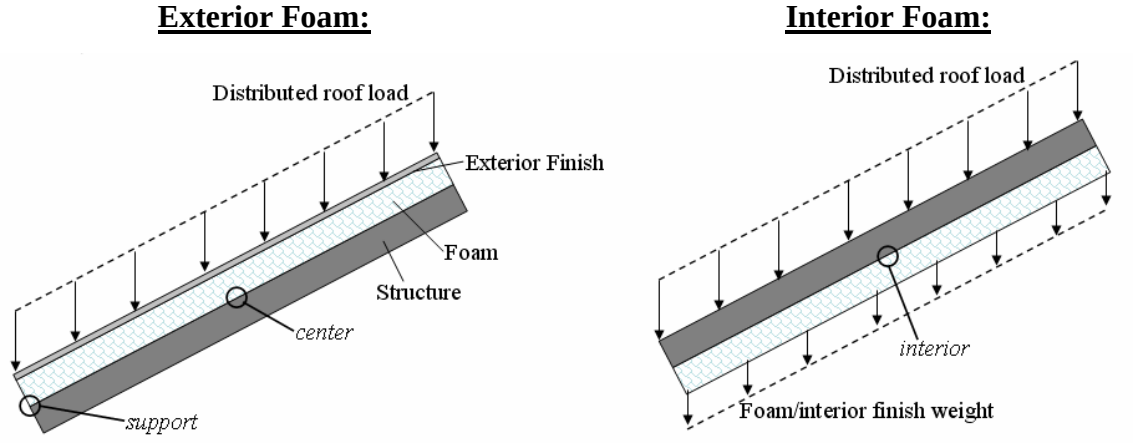

Figure 10: Approximation of the loading on the foam for a truss core panel showing the possible locations of highest stress

5.1 Exterior Foam

As illustrated in Figure 10, two locations must be considered when the foam is applied to the exterior of truss core and stiffened plate panels. At the *center* of the panel, the foam is subjected to snow loading and to stresses resulting from panel curvature. At the *support*, the foam is subjected to wind uplift loading. The two cases are described below.

At the *center* of the panel, the foam is subjected to the maximum snow loading and to stresses resulting from panel curvature. The snow load is a gravity load, so it acts in the vertical direction as illustrated in Figure 10. Because the panel is oriented at a 6/12 roof pitch, the snow load is resolved into normal and tangential components with respect to the panel. The load is defined in terms of stress, so the resolved loads are directly applied to the foam. The normal component of the load becomes a compressive stress of 2680 Pa, and the tangential component becomes a shear stress of 1342 Pa (see appendix A, Table 4).

The stress resulting from panel curvature is determined based on the total deflection of the loaded panel. A conservative approximation is made by assuming sufficient curvature to cause yielding of the face sheets, i.e. a 0.2% strain. Foams typically yield at higher strains; therefore, the stress on the foam can be found using linear elasticity. The stress is $E_c\varepsilon$, with the foam modulus E_c reduced as necessary to account for creep. The initial stress in the foam is 5980 Pa. Given the estimated foam compressive modulus after 50 years, the stress under constant panel curvature is 1660 Pa.

At the *support*, the foam is subjected only to wind uplift loads. The loads act normal to the panel and cause a tensile stress of 1662 Pa (corresponding to the wind uplift load).

5.2 Interior Foam

When the foam is placed on the *interior* side of the panel (as is the case for the truss core panel), the maximum stress occurs at the center. At this location, the foam is subjected to panel curvature as described for the *center* case in the analysis for the case of exterior foam. The panel is also subjected to dead loads resulting from the weight of the foam and interior finish. The dead load is based on the amount of PUR at 36 kg/m^3 required to achieve R-7.0 (63 N/m^2 for 175 mm foam), plus the weight of the gypsum (105 N/m^2, 2.2 psf), plus an allowance of 105 N/m^2 for fixtures or other interior finish. The total weight of 273 Pa is resolved into a normal stress of 122 Pa and a shear stress of 244 Pa.

5.3 Analysis and Conclusions

The stresses described in the preceding sections are listed along with analysis of the foam performance in Tables 2 and 3. Table 2 shows the stresses in the foam initially, i.e. with no reductions for creep or fatigue. Table 3 shows the stresses on the foam when the properties are reduced to account for 50 years of loading. These two cases establish

limits on the expected foam performance: the first case represents a state of constant stress, and the second case represents constant panel curvature. Both cases must be examined because, as the foam ages, both the applied stresses and the available strengths go down. The foam was analyzed using two different failure criteria: maximum principle stress and maximum shear stress. Adhesive failure of the foam was evaluated by comparing the maximum shear or tensile principle stress to the adhesive strength of the foam. Under the maximum principle stress criterion, the strength of the foam is either the compressive or tensile strength (depending on the sign of the largest principle stress), reduced for fatigue. Under the maximum shear stress criterion, the shear strength of the foam is used with reductions for fatigue.

Tables 2 and 3 show that the foam will not fail in any expected loading scenario. The lowest safety factor for stress failure of the new foam is 21 (in the *center* element), and the lowest safety factor for adhesion is 21 (in the *interior* element). The lowest safety factor for stress failure of the aged foam is 25, and the lowest safety factor for adhesive failure is 48 (both in the same elements as with the new foam). From the results of this study, we conclude that structural failure of the foam will not occur under any of the cases for which panels have been designed.

Table 2: Stresses acting on the foam with no aging effects and corresponding safety factors

	Exterior Foam panel		***Interior Foam Panel***
	center	***support***	***interior***
σ_x **(Pa)**	-5980 (curvature)	0	5980 (curvature)
σ_y **(Pa)**	-2680 (live loads)	1662 (wind uplift)	122 (dead loads)
τ_{xy} **(Pa)**	-1342 (live loads)	0	244 (dead loads)
σ_{max} **(Pa)**	-6457	1662	5990
σ_u **(Pa)**	-138000	231000	231000
SF	21	139	39
τ_{max} **(Pa)**	2127	831	2939
τ_u **(Pa)**	173000	173000	173000
SF	81	209	59
Adhesive SF	58	75	21

Table 3: Stresses acting on the foam after 50 years and corresponding safety factors.

	Exterior Foam panel		***Interior Foam Panel***
	center	***support***	***interior***
σ_x **(Pa)**	-1660 (curvature)	0	1660 (curvature)
σ_y **(Pa)**	-2680 (live loads)	1662 (wind uplift)	122 (dead loads)
τ_{xy} **(Pa)**	-1342 (live loads)	0	244 (dead loads)
σ_{max} **(Pa)**	-3606	1662	1698
σ_u **(Pa)**	-91000	152000	152000
SF	25	91	90
τ_{max} **(Pa)**	1436	831	807
τ_u **(Pa)**	114000	114000	114000
SF	79	137	141
Adhesive SF	57	49	48

References

[AISI] American Iron and Steel Institute. 2001a. *North American Specification for the Design of Cold-Formed Steel Structural Members*.

[AISI] American Iron and Steel Institute. 2001b. *Commentary on North American Specification for the Design of Cold-Formed Steel Structural Members*.

[AISI] American Iron and Steel Institute. 2002. *AISI Manual: Cold-Formed Steel Design*.

[AISI] American Iron and Steel Institute. 2004. *Supplement 2004 to the North American Specification for the Design of Cold-Formed Steel Structural Members*.

[ICC] International Code Council. 2003. *2003 International Residential Code for One- and Two-Family Dwellings*. Country Club Hills, IL: ICC.

Gere, J.M. and S.P. Timoshenko. 1997. *Mechanics of Materials*. Boston: PWS.

Supplement to Appendix D: Determination of Web Crippling Coefficients for the Truss Core and Stiffened Plate Panels

The *2001 AISI Specification* and *2004 AISI Supplement* prescribe the web crippling strength of cold-formed steel structural sections by a unified equation (here after referred to as the unified web crippling equation). The unified web crippling equation contains four coefficients, C, C_N, C_R, and $C_{h,}$ which reflect the cross section, geometry, loading condition, and boundary conditions of interest. The unified web crippling equation prescribed in the *2004 AISI Supplement* consistently under predicts the web crippling strength of the truss core panel subjected to end of flange (EOF) loading with values of P_{test}/P_n between 2.2 and 2.6 for the unfastened condition. Consequently a study was conducted to reevaluate the coefficients in the unified web crippling equation. In this study, web crippling coefficients that are applicable to the truss core and stiffened plate panel geometry were determined. These coefficients were found by curve fitting (calibrating) the web crippling constants to web crippling data for multideck sections with unstrapped and unfastened deck (i.e. web) restraint conditions.

1.0 Fastening and strapping

The *2001 AISI Specification* provides different sets of coefficients for the unified web crippling equation depending on (a) the cross section, (b) the loading condition, and (c) the condition of fastened/unfastened to the support. While (a) and (b) are clearly defined, the fastened condition is not specifically defined in the *2001 AISI Specification*. Past research including EOF loading indicates that fastening to the support is achieved by connecting the bottom flange to the support using screws or bolts, or by welding. Although not explicitly addressed by the 2001 AISI Specification, the transverse boundary condition which eliminates the possibility of spreading of the section also has a large input on the result of web crippling tests. In applications, adjacent panels can prevent multi-web deck sections from spreading. Some researchers have simulated this restraint in their experimental setups by strapping their specimen, while others have not. An attempt is made to clarify the significance of the fastened/unfastened and strapped/unstrapped conditions, and to determine their relevance to the truss core and stiffened plate panel.

1.1 Fastening to support condition

While the *AISI Specification* does not directly define the terms fastened and unfastened to the support, it may be inferred that fastening is defined as a screw, bolt, or weld through the bottom flange to the support reaction, as has been the case for all tests of fastened multi-web deck sections. However, the Commentary sheds light on the physical effect that fastening has on the section: “What is important is that the flange elements [and thus the web elements] are restrained from rotating at the location of load application (2001 AISI Comm.).” For this study, the fastened condition is interpreted as a connection where the bottom of the web is restrained against rotation. The truss core

and stiffened plate panels were observed to behave as an unfastened section regardless of any mechanical fastening between the bottom flange and support because there was not sufficient rotational restraint observed at the base of the web.

1.2 Strapping condition

Unless lateral spreading of the cross section is prevented, a multi-web deck section with angled webs subject to EOF loading is likely to fail due to flattening of the cross section, as reported by Wallace (2003), Wallace and Schuster (2004) and Bhakta (1992), and as illustrated in Figure. The failure is caused by opening of the angle at the flange-to-web junction. Resistance against this failure mode comes from the bending strength of the flange-to-web junction and the friction force between the flange and support reaction surface.

For typical multi-web deck sections in service conditions, the lateral spreading failure mode is avoided by the restraint supplied by adjoining sections and structural components to which the sections are connected. Lateral section spreading occurs when the horizontal component of force at the bottom of the section caused from the inclined webs overcomes friction at the interface between the bottom flange and the reaction surface. The cold-formed bend then unfolds producing a drop in load. If this failure mode is prevented, the web will fail under web crippling loads by buckling along the web length as shown in Figure 2. A fundamental difference exists in the tests which were used to calibrate the web crippling equation in the *2001 AISI Specification*. Some researchers strapped their specimens against transverse spreading, while others did not. Consequently, in order to exclude the unrealistic lateral spreading mode, Yu (1981), Wu (1997), Avci (2002) and Avci and Easterling (2004) strapped the specimen using transverse straps producing the failure mode of web buckling shown in Figure 2. In the truss core panel, the lateral spreading mode of failure is inhibited by the top and bottom face sheets, thus the web fails by buckling.

The *2001 AISI Specification* does not make a clear distinction between the different failure modes caused by EOF loading: lateral spreading of the cross section versus the failure driven by local buckling of the web. Both failure modes are referred to as a web crippling failure. Furthermore, the unified web crippling strength equation in the *2001 AISI Specification* does not recognize the distinction between the strapped (lateral spreading prevented) and unstrapped (lateral spreading permitted) condition.

The web crippling coefficients for multi-web deck sections in the 2001 AISI Specification were calibrated using tests that were performed in the unstrapped condition; therefore, these coefficients are not applicable to the truss core or stiffened plate panel. The inclusion of spreading as a failure mode on the AISI web crippling equation is the likely reason for the significant unpredictability of the web crippling strength using the AISI web crippling equation for multi-web deck sections.

2.0 Criteria for selecting parameters similar to the truss core panel

Because of the lack of restraint against spreading in the tests used to calibrate the 2001 AISI web crippling equation for multi-web deck sections, the web crippling coefficients were calibrated using the selected data from the literature that most closely approximated the geometry and behavior of the truss core panel. Prior to calibration of the *2001 AISI Specification* web crippling equation, a list of criteria was formed which was used to collect test results applicable to the truss core or stiffened plate panels. The parameters accounted for in the *2001 AISI Specification* web crippling equation are the yield stress (F_y), web thickness (t_w), web inclination angle (θ), bend radius divided by the web thickness (R/t_w), bearing length divided by the web thickness (N/t_w), and the web height divided by the web thickness (h/t_w). Additionally, the *2001 AISI Specification* accounts for the fastened/unfastened condition.

Criteria of the test specimen:

1. Only multi-web deck sections were investigated. In the literature some authors have indicated that sections having only two webs are multi-web deck sections. To clarify for this study, only multi-web deck sections with four or more webs were considered.
2. Inclination angles of webs must be equal to or less than 90° where the inclination angle is defined as the angle at which the corner is bent. Some testing programs involved specimens which had re-entrant corners (Figure 3); in other words, the web inclination angle was greater than 90 degrees. Because the truss core panel specimens all had a web inclination angle of 60 degrees and are never expected to contain webs with web inclination angles greater than 90 degrees, the data resulting from these programs were disregarded.
3. The observed behvaior must not be affected by embossments and stiffeners on the web. Some testing programs used specimens with embossments in the webs. Because such embossments traditionally reduce the capacity of the section against web crippling and, moreover, the truss core panel webs were clear of such irregularities, only data from specimens that were either clear or that did not demonstrate a reduction in web crippling capacity from embossments were used.
4. For sections with yield strengths higher than 451 MPa (60 ksi), the section must be composed of the proportion of steel yield strength and bend radius discussed in Section 3.4. The Commentary on the *2001 AISI Specification* advises against the use of sections containing high yield steel and small corner radii. Because the

truss core panel contains mild steel and average corner bend radii, only sections with reasonable proportions of yield strength to corner bend radii were used.

Aside from the specimens used in the web crippling testing, the test setup varied among different testing programs as well. This variability may have been a result of parameters accounted for in the *AISI Specification* or a result of a lack of clarity in the *AISI Specification*.

Criteria of the test setup:

5. Section must be unfastened to the reaction support. An initial test of truss core panel prototypes showed that the truss core panels behave as a section which is unfastened to the support, or lack rotation restraint at the bottom of the webs regardless of the presence of mechanical fasteners, only test results of unfastened specimens were used. It was inferred that this "unfastened" condition applies to the stiffened plate panels as well.
6. The section must be strapped against lateral spreading and thus fail by buckling of the web. Because the truss core and stiffened plate panels have face sheets which restrained lateral spreading of the section, only results of tests on multi-web deck sections which restrained the section from spreading were used in determining the web crippling coefficients.
7. The section must not span beyond the reaction plate supporting the failed end. Because EOF loading is performed on the truss core and stiffened plate panels with no portion of the section resting past the exterior edge of the reaction, only results of tests with a similar loading condition were used.

3.0 Available test data for equation calibration

The test results of the testing programs available in the literature are described in the following sections.

3.1 Yu (1981)

Yu (1981) tested 18 multi-web deck sections which met the criteria 1 through 6 listed. The specimens were tested in four-point bending targeting crippling failures over both reactions. The specimens were placed on steel reactions which were allowed to rotate. The specimens were reinforced at the loading points and in the constant moment region by attaching an overlapping section to the specimen. The edge-to-edge distance between the reaction plate and loading plate was 1.5 times the distance between the inside edges of the face sheet along the plane of the web (h^*). However, photographs

included in Yu (1981) indicate that the reinforcement attached to the middle portion of the specimen extended into the region within 1.5h^* of the reaction edge. While it is possible that the reinforcing section may have increased the measured web crippling capacity of the section, photographs indicate that the buckling of the web occurred away from the reinforcing section and thus appeared to be unaffected by the reinforcing section. As shown in Figure , all specimens were strapped just inside the support by a 3.2 mm x 19.0 mm ($^1/_8$ in. x $^3/_4$ in.) steel strap connected to the bottom of the section.

3.2 Studnicka (1991)

Studnicka tested 76 multi-web deck sections under non-symmetric three-point bending. As shown in Figure 5, the fixed reaction support was placed at a 1:20 slope. The specimens were strapped near the support using metal straps. Two different sections having an overall depth of 50 mm and 80 mm respectively were tested. Four parameters in the test setup were evaluated for each of the two different section types as shown in Figure 5: (a) standard/inverted orientation, (b) the distance between the end of the section and the exterior edge of the reaction support (ranging from 0.4h^* to 4.0h^*), (c) the edge-to-edge distance between the reaction and load point (ranging from 1h^* to 3h^*), and (d) the bearing length (ranging from N/t_w = 10 to N/t_w = 80).

The test data obtained by Studnicka (1991) was omitted from this study because the specimen over hung the reaction, violating Criteria 7. This length was zero for all EOF loading tests performed on the truss core panel. Additionally, the interior bend radius of the cold-formed bend, which is a parameter in the unified web crippling strength equation, was not published in Studnicka's paper.

3.3 Bhakta (1992)

Bhakta tested four multi-web deck sections in a symmetric three-point bending test arrangement. Both ends of the specimen were considered test ends. Two specimens were fastened to the support reaction by connecting the bottom flange to the support using one 14 mm (1/2 in.) diameter A307 bolt half way between each web. The other two specimens were not fastened to the support. The specimens were reinforced near the loading point with an overlapping section of identical geometry. This overlapping section was placed at a distance greater than 1.5h^* from the inside edge of the reaction point. The specimens were not strapped to prevent transverse spreading.

Bhakta noted that all four specimens (fastened and unfastened to the support) failed under the same mode of buckling of the web with some curling of the interior flanges. No significant differences in failure mode between the fastened and unfastened conditions were described. However, photographs of the unfastened tests show spreading of the exterior two webs rather than buckling. On average, the measured capacities of the fastened tests were 21% higher than the measured capacities of the unfastened tests.

The two fastened test results were not included in this study because they violated Criteria 4. The two unfastened test results were not included because the lack of strapping caused lateral translation of the exterior webs, violating Criteria 5.

3.4 Wu and Yu (1997)

Wu and Yu (1997) tested 21 multi-web deck sections under symmetric three-point bending. Both ends of the specimen were considered test ends. The specimens were composed of Grade 80 steel. They were restrained against lateral spreading using straps clamped to the bottom exterior flange. Local failure at the loading point was controlled by placing wood blocks between the webs or by placing an overlapping section on the specimen. The load and the straps were placed at a minimum distance of 1.5h* from the interior face of each reaction. For specimens with webs at inclinations less than 90 degrees, the lateral strapping was placed directly inside the interior edge of the reaction at a distance less than 1.5h* to prevent excess warping of the section.

A schematic interpretation of the web crippling mode observed by Wu and Yu (1997) is shown in Figure 6. The web buckled in the direction to decrease the angle between the top flange and web and increase the angle between the bottom flange and web, while the bottom flange bent upwards.

The specimens tested by Wu and Yu (1997) were composed of high yield strengths in combination with low R/t_w ratios. Figure 7 shows the relationship between the R/t_w ratio and yield strength for the specimens tested by Yu (1981), Wu and Yu (1997), Avci (2002), Avci and Easterling (2004), and the test results of the truss core panel. The test data collected by Wu and Yu (1997) exhibits similar values of R/t_w as other sections; however, the yield strengths are substantially higher. Figure 7 shows the typical linear trend between R/t_w and yield strength observed in the data obtained by Yu (1997) Avci (2002) and Avci and Easterling (2004). The data obtained by Wu and Yu (1997) were from specimens with tighter bend radii for the strength of steel. Because of the small R/t_w in combination with high yield strength, this data was excluded from the current study.

3.5 Avci (2002) and Avci and Easterling (2004)

Avci and Easterling conducted tests on 78 multi-web deck sections under symmetric three-point bending. Load was applied at midspan of the specimen leaving an edge-to-edge distance greater than 1.5h between the loading plate and reaction plate. Both ends of the specimen were considered test ends. Thirty-nine of the specimens were fastened to the supports using self tapping screws and 39 tests contained specimens which were not fastened to the supports. As shown in Figure 8, all specimens were strapped across the width of the section at a distance greater than 1.5h from the edge of the support. At this location a 25mm (1 in.) wide steel strap was fastened to the top and bottom of the section using sheet metal screws. At the loading point, the test specimen was reinforced by attaching an overlapping section in order to avoid an interior web cripple and/or flexural failure at the loading point. The observed failure mode was very similar to the failure mode observed by Wu and Yu (Figure 6 (a)).

Nine of the specimens were composed of steel with yield strengths higher than 410 MPa (60 ksi). While test data from Wu and Yu (1997) was rejected because of a combination of high yield strengths and tight bend radii, the high yield strength

specimens tested by Avci and Easterling had large values of R/t_w (Figure 7) as suggested by the Commentary to the *2001 Specification*. All of unfastened data collected by Avci (2002) and Avci and Easterling (2004), including specimens with large yield strengths, was considered in this study because it met all of the criteria. The fastened specimens were not included in the current study because they violated Criteria 5.

3.6 Wallace (2003) and Wallace and Schuster (2004)

Wallace and Schuster tested 149 multi-web deck sections under non-symmetric three-point bending. Seventy-four of the specimens were unfastened to the support while the remaining 75 specimens were fastened to the support using 11 mm (7/16 in.) bolts without a washer. All specimens were unstrapped because the researchers felt that the strapped condition tends to provide a higher web crippling strength.

The fastened tests performed by Wallace and Schuster (Wallace, 2003; Wallace and Schuster 2004) were not included in the current study because they violated Criteria 5. Because the multi-web deck sections tested did not contain any strapping, thus violating Criteria 4, the unfastened test results were not included as well. Therefore, none of the data collected by Wallace and Schuster (Wallace 2003; Wallace and Schuster 2004) was considered applicable to the truss core panels.

3.7 Selected data

Six experimental studies on EOF loading of multi-web deck sections were reviewed. The unfastened test data obtained by Yu (1981), Avci (2002) and Avci and Easterling (2004) were selected as a basis to calibrate the coefficients for the unified web crippling strength equation for truss core like panels. Table 1 presents the data obtained by Yu (1981). Table 2 presents the data obtained by Avci (2002) and Avci and Easterling (2004). Both tables present all the input parameters required to compute P_n using the unified web crippling equation with the proposed coefficients, the test results, and nominal web crippling capacity using the coefficients proposed All other data was not included in this study because the test sections or testing methods failed to meet the list of criteria. Table 3 shows the ranges of parameters covered by the test specimens included in the selected set of data for the calibration of the web crippling coefficients for truss core panels, as well as values of these parameters for the truss core panel.

4.0 New Coefficients for the unified equation

4.1 Range of parameters in the selected test data

The test data by Yu (1981) and Avci (2002) was selected to calibrate the coefficients of the uniform web crippling equation applicable to the truss core or stiffened plate panels. A series of histograms are presented in Figure 9 through Figure 13 to study the distribution of geometric and material parameters (N/t_w, R/t_w, h/t_w, F_y, and θ) covered in the data set. The histograms also show the parameters from test on truss core panel

prototypes in order to illustrate how applicable the newly calibrated coefficients are to the tested truss core panels.

Figure 9 shows the distribution of the bearing length divided by the web thickness (N/t_w). The value of N/t_w used in the truss core panel tests is within the range of calibration source data. Figure 10 shows the distribution of the bend radii divided by the web thickness (R/t_w) in the specified data. The R/t_w values for the truss core panel were on the low end of the distribution. The truss core panel had h/t_w values slightly higher than the specified maximum ratio of 200 specified by the *2004 AISI Supplement* for unreinforced webs. Figure 11 shows the truss core panels contained web slenderness values between 1.6 and 2.2 times larger than the most slender webs in the data set. Figure 12 shows the distribution of measured yield strength values in the specified data. The truss core panel exhibited yield strengths which were approximately 20% smaller than the lowest value in the data set. Figure 13 shows the distribution of web inclination values in the data set. The truss core panel web inclinations were near the middle of the range represented in the data set.

Of the five geometric and material parameters considered in the uniform equation, the h/t_w and F_y of the truss core panel lie outside of that covered in tests by Yu (1981) and Avci (2002). The selected set of data for Yu and Avci were used to calibrate the coefficients in the unified web crippling equation for truss core and stiffend plate panels.

4.2 Calibration method

The values C, C_N, C_R, and C_h were calibrated using a generalized reduced gradient (GRG) optimization method. Using this method, the coefficient of variation of the test-to-nominal strength (P_{test}/P_n) was minimized while constraining the mean of P_{test}/P_n to be one. To solve for these coefficients the add-in statistical package of Microsoft Excel employing the generalized reduced gradient non-linear optimization (GRG) method was used. The GRG solves multi-variable problems computationally by making small changes to each of the independent variables until an optimized solution is obtained. The magnitude and direction of change to each variable are based on the gradient, or the derivative with respect to each variable, of the function at that position. More information on the GRG method can be found in Lasdon (1978). No additional restraints were placed on the coefficients.

4.3 Results

Table 4 shows the coefficients calibrated using the data and method described. Table 5 shows the input parameters for the six truss core panel tests. Also included in the table is the measured capacity per web (P_{test}/web), the nominal capacity based on the *AISI Specification* web crippling equation using the coefficients proposed in this study, and the value of P_{test}/P_n.

Using the proposed coefficients, Figure 14 through Figure 18 show the test-to-nominal strengths for panel test and the calibration source data as functions of N/t_w, R/t_w, h/t_w, yield stress, and web inclination angle, respectively. In Figure 18 there is a subtle

decreasing trend in the value of P_{test}/P_n with increasing θ in the Yu data, however the Avci and Easterling data does not show a similar trend. There is no clear trend in the values of P_{test}/P_n to any other parameter indicating the proposed coefficients are capturing the effect of each of the variables.

Values of P_{test}/P_n are between 0.9 and 1.1 for data collected by Avci (2002) and Avci and Easterling (2004). However, data collected by Yu (1981) contains a somewhat larger spread from $P_{test}/P_n = 0.66$ to $P_{test}/P_n = 1.29$. Twelve of the 18 tests have values of P_{test}/P_n between 0.8 and 1.2. There were almost twice as many data points from Avci (2002) and Avci and Easterling (2004) as Yu (1981) (39 versus 18) used to obtain the proposed coefficients. As a result, the data obtained from Avci (2002) and Avci and Easterling (2004) was more influential than the data obtained from Yu (1981), thus resulting in a higher scatter of the Yu (1981) data. This is further reinforced by the higher COV from Yu's data (Table 1) than from Avci and Easterling's data (Table 2).

4.4 Contribution of R/t_w, N/t_w, h/t_w on P_n

Values of h/t_w and F_y in the truss core panels were outside the range of the data sets used to calibrate the web crippling coefficients. Specifically, the slenderness of the truss core panel webs (h/t_w) was between 1.6 and 2.2 times larger than the largest h/t_w in the calibration data set (Figure 11). If the coefficients which were used on a range of parameters did not accurately capture the trend of parameters outside that range, the value of P_n could be incorrect.

However, P_n is not only a function of the geometric parameters, but also the coefficients C, C_R, C_N, and C_h. The sensitivity of P_n, using the proposed coefficients, to changes in the three parameters, R/t_w, N/t_w, and h/t_w, can be investigated by dividing the uniform web crippling equation into three dimensionless terms, Term I, Term II, and Term III.

$$P_n = Ct_w^2 F_y \sin(\theta) \overbrace{\left(1 - C_R\sqrt{\frac{R}{t_w}}\right)}^{\text{I}} \overbrace{\left(1 + C_N\sqrt{\frac{N}{t_w}}\right)}^{\text{II}} \overbrace{\left(1 - C_h\sqrt{\frac{h}{t_w}}\right)}^{\text{III}} \quad (1)$$

Each term, I, II, and III, represents the total contribution of R/t_w, N/t_w, and h/t_w, respectively, to the nominal capacity P_n. Figure 19 shows the distribution of Term I for each of the data sets from Yu (1981), from Avci (2002) Avci and Easterling (2004), and the truss core panel test results. Because the truss core panel had relatively small radii, Term I is slightly larger than the same term for other data in the calibration set. The range of Term I (i.e. a factor of two) indicates that a change in the R/t_w ratio alone from the lowest value of the calibration data to the largest value in the calibration data could more than double the capacity.

Figure 20 shows the distribution of values for Term II for all the specified data. The range of Term II is from ~3 to ~6 (i.e. a factor of two). Similar to the parameter R/t_w, the range of Term I (i.e. a factor of two) indicates that a change in the N/t_w ratio alone from the lowest value of the calibration data to the largest value in the calibration data could more than double the capacity. The bearing length used for the testing of the truss

core panel resulted in a relatively large positive influence on the nominal web crippling capacity, P_n. However, the value of N/t_w was still within the values represented by the calibration data set.

Figure 21 shows the distribution of Term III for the specified data. Because the truss core panel contained slender webs it can be seen that Term III is smaller than the data used to obtain the coefficients. The range of Term III shown in Figure 21 is from ~0.8 to ~0.93 indicating that the changes in web slenderness in the data set did not substantially change the nominal capacity. In other words, where the most slender truss core panel was multiplied by a factor of 0.8, the stockiest section in the calibration data was multiplied by a factor of 0.93. If the truss core panel would have had webs with half the slenderness, the nominal capacity would only increase by less than 10%.

Using the proposed coefficients, the parameters of R/t_w and N/t_w had approximately the same influence considering the range of parameters in the calibration data set. The parameter h/t_w had a substantially smaller influence. The situation to be avoided is parameters in the panel which were past the range in the calibration data set and also highly sensitive as a result of the coefficients. The most sensitive parameters, R/t_w and N/t_w, were small and large, respectively, relative to the calibration data set range for the truss core panel. However, these parameters were within the range of parameters in the calibration data range.

On the other hand, the truss core panel contained values of h/t_w between 1.6 and 2.2 times the larges values in the calibration data set. However, the proposed coefficients result in a low sensitivity to h/t_w, and therefore the large h/t_w does not cause concern. Because the most influential parameters were average and the least influential parameter was the single most extreme for the truss core panel, it is concluded that the resulting values of P_{test}/P_n (Table 4) computed using the proposed coefficients are appropriate.

5.0 Conclusions

A comparison of the measured capacity of the truss core panel under EOF loading with the nominal capacity using the *2004 AISI Supplement* suggested that the nominal capacity was excessively conservative. As a result, the background of the unified web crippling strength equation was examined through the literature study. The literature study suggested that the coefficients for the unified equation prescribed in the *2004 AISI Supplement* was overly conservative because the current coefficients are based on the test data from unstrappped specimens which were allowed to spread laterally, while the continuous top and bottom face sheets of the truss core panel prohibit the spreading failure mode. Consequently, it was deemed necessary to establish a new set of coefficients for the unified equation based on specimens tested under conditions that reflect the service condition of the truss core panels.

Test data selected according to the criteria were used to calibrate the coefficients of the unified web crippling strength equation for use on truss core panels. The calibrated unified equation was found to produce a reasonable estimate of the web crippling

capacity measured for tests. The value of P_{test}/P_n was 1.16 on average with a coefficient of variation of 0.093.

The geometry of the truss core panel lies outside the range of test specimens from previous studies used to establish the new coefficients. Specifically, the truss core panel had a very high value of h/t_w. However, the proposed coefficients resulted in a low sensitivity to the parameter h/t_w. As a result, it was concluded that the high value of h/t_w did not have a large effect on the average value of P_{test}/P_n and thus the results presented in Table 4 were deemed appropriate.

References

[AISI] American Institute of Steel and Iron. 2001. *North American Specification for the Design of Cold-Formed Steel Structural Members.* Washington, D.C.

[AISI] American Institute of Steel and Iron. 2004. *Supplement to the North American specification for the design of cold-formed stee structural members.* Washington, D.C.

Avci, O. 2002. "Web-Crippling Strength of Multi-Web Cold-Formed Steel Deck Sections Subjected to End One Flange (EOF) Loading," thesis, presented to Virginia Polytechnic Institute and State University in partial fulfillment of the requirements for the degree of Master of Science in Civil Engineering.

Avci, O., Easterling, S. 2004. "Web Crippling Strength of Steel Deck Subjected to End One Flange Loading." *Journal of Structural Eng*., 130(5), 697-707.

Bhakta, B.H. 1992. "The effect of flange restraint on web crippling strength," thesis, presented to University of Missouri-Rolla in partial fulfillment of the requirements for the degree of Master of Science in Civil Engineering.

Lasdon, L.S., Waren, A.D., Jain, A., and Ratner, M. 1978. "Design and testing of a generalized reduced gradient code for nonlinear programming." *AMC Transactions on Mathematical Software*, 4(1), 34-50.

Studnicka, J. 1991. "Web crippling of multi-web deck sections." *Thin-Walled Structures*, (11), 219-231.

Wallace, J.A. 2003. "Web Crippling of Cold Formed Steel Multi-Web Deck Sections Subjected to End One-Flange Loading," thesis, presented to University of Waterloo in partial fulfillment of the requirements for the degree of Master of Science in Civil Engineering.

Wallace, J.A., Schuster, R.M. 2004. "Web Crippling of Cold Formed Steel Multi-Web Deck Sections Subjected to End One-Flange Loading." *Proc. 17th Int. Specialty Conf. on Cold-Formed Steel Structures*, 2004, 171-185.

Wu, S., Yu, W.W. 1997. "Strength of Flexural Members Using Structural Grade 80 of A653 Steel (Web Crippling Tests)" *Third Progress Report*, American Iron and Steel Institute, Washington D.C.

Yu, W. 1981. "Web Crippling and Combined Web Crippling and Bending of Steel Decks." Civil Engineering Study 81-2, University of Missouri-Rolla, Rolla, MN

TABLES

Table 1: Unfastened test results from Yu (1981)

	#Webs	Angle (°)	t_w (mm)	R/t_w	N/t_w	h/t_w	F_y (Mpa)	P_{test}/web (kN)	P_n/web (kN)	P_{test}/P_n
EOF-1A	4	62.4	0.74	6.85	102.0	62.7	299	2.117	1.781	1.189
EOF-1B	4	61.6	0.74	6.83	102.0	62.1	299	2.140	1.771	1.208
EOF-2A	4	62.1	0.76	6.98	197.0	59.5	299	2.616	2.439	1.072
EOF-2B	4	62.7	0.75	7.09	200.0	61.1	299	2.571	2.384	1.078
EOF-3A	4	63.7	1.12	4.52	67.4	40.3	296	5.293	4.110	1.288
EOF-3B	4	63	1.14	4.47	66.7	39.8	296	5.338	4.232	1.261
EOF-4A	4	64.4	1.20	4.45	126.0	38.1	296	5.516	6.100	0.904
EOF-4B	4	64.5	1.20	4.46	126.0	38.0	296	5.427	6.102	0.889
EOF-5A	4	69.5	0.79	6.43	95.8	88.7	332	1.770	2.328	0.761
EOF-5B	4	70	0.81	6.31	94.0	87.4	332	1.815	2.457	0.739
EOF-6A	4	70.5	0.74	6.83	202.0	92.2	332	2.682	2.710	0.990
EOF-6B	4	70	0.75	6.80	202.0	93.5	332	2.696	2.777	0.971
EOF-7A	4	71.3	1.24	3.89	61.1	55.7	284	4.448	5.042	0.882
EOF-7B	4	72.2	1.22	3.97	62.2	57.2	284	4.448	4.906	0.907
EOF-8A	4	71.3	1.17	4.57	129.0	58.0	284	6.361	5.732	1.110
EOF-8B	4	71.3	1.22	4.38	124.0	54.8	284	6.272	6.228	1.007
EOF-19A	10	75.9	0.73	4.86	103.0	57.6	284	1.463	2.052	0.713
EOF-19B	10	75.1	0.73	4.88	104.0	56.4	284	1.348	2.052	0.657
									Average	0.98
									COV	0.19

Note: P_n is computed using the proposed coefficients in the unified web crippling equation

Table 2: Unfastened test results from Avci (2002) and Avci and Easterling (2004)

	#Webs	Angle (°)	t_w (mm)	R/t_w	N/t_w	h/t_w	F_y (MPa)	P_{test}/web (kN)	P_n/web (kN)	P_{test}/P_n
U-P1-22-1	6	70	0.75	6.90	50.8	42.7	316	1.530	1.606	0.953
U-P1-22-2	6	70	0.75	6.90	50.8	42.7	316	1.517	1.606	0.945
U-P1-22-3	6	70	0.75	6.90	50.8	42.7	316	1.539	1.606	0.958
U-P2-26-1	6	58	0.46	14.60	82.4	42.8	658	0.805	0.861	0.935
U-P2-26-2	6	58	0.46	14.60	82.4	42.8	658	0.836	0.861	0.971
U-P2-26-3	6	58	0.46	14.60	82.4	42.8	658	0.814	0.861	0.945
U-P3-26-1	6	50	0.46	17.10	82.0	75.9	717	0.716	0.694	1.032
U-P3-26-2	6	50	0.46	17.10	82.0	75.9	717	0.703	0.694	1.013
U-P3-26-3	6	50	0.46	17.10	82.0	75.9	717	0.747	0.694	1.077
U-P4-22-1	6	75.5	0.76	6.80	50.0	56.6	331	1.717	1.754	0.979
U-P4-22-2	6	75.5	0.76	6.80	50.0	56.6	331	1.744	1.754	0.994
U-P4-22-3	6	75.5	0.76	6.80	50.0	56.6	331	1.748	1.754	0.997
U-P5-28-1	6	58	0.39	11.20	98.0	29.2	724	0.903	0.913	0.990
U-P5-28-2	6	58	0.39	11.20	98.0	29.2	724	0.903	0.913	0.990
U-P5-28-3	6	58	0.39	11.20	98.0	29.2	724	0.890	0.913	0.975
U-C1-16-1	6	63	1.52	3.10	25.1	31.8	321	6.112	6.396	0.956
U-C1-16-2	6	63	1.52	3.10	25.1	31.8	321	5.881	6.396	0.919
U-C1-16-3	6	63	1.52	3.10	25.1	31.8	321	6.183	6.396	0.967
U-C1-18-1	6	63	1.20	4.00	31.6	40.6	341	4.448	4.266	1.043
U-C1-18-2	6	63	1.20	4.00	31.6	40.6	341	4.250	4.266	0.996
U-C1-18-3	6	63	1.20	4.00	31.6	40.6	341	4.497	4.266	1.054
U-C1-20-1	6	63	0.91	5.20	41.9	54.3	359	2.797	2.595	1.078
U-C1-20-2	6	63	0.91	5.20	41.9	54.3	359	2.718	2.595	1.047
U-C1-20-3	6	63	0.91	5.20	41.9	54.3	359	2.600	2.595	1.002
U-C1-22-1	6	63	0.75	6.40	50.8	66.2	372	1.853	1.803	1.028
U-C1-22-2	6	63	0.75	6.40	50.8	66.2	372	2.026	1.803	1.124
U-C1-22-3	6	63	0.75	6.40	50.8	66.2	372	1.977	1.803	1.096
U-C2-16-1	6	67	1.52	3.10	25.1	48.4	241	4.893	4.874	1.004
U-C2-16-2	6	67	1.52	3.10	25.1	48.4	241	4.987	4.874	1.023
U-C2-16-3	6	67	1.52	3.10	25.1	48.4	241	4.559	4.874	0.936
U-C2-18-1	6	67	1.20	4.00	31.6	61.5	331	4.373	4.177	1.047
U-C2-18-2	6	67	1.20	4.00	31.6	61.5	331	4.255	4.177	1.019
U-C2-18-3	6	67	1.20	4.00	31.6	61.5	331	4.300	4.177	1.030
U-C2-20-1	6	67	0.91	5.20	41.9	82.1	369	2.891	2.685	1.077
U-C2-20-2	6	67	0.91	5.20	41.9	82.1	369	2.804	2.685	1.044
U-C2-20-3	6	67	0.91	5.20	41.9	82.1	369	2.822	2.685	1.051
U-C2-22-1	6	67	0.75	6.40	50.8	100.0	362	1.735	1.758	0.987
U-C2-22-2	6	67	0.75	6.40	50.8	100.0	362	1.621	1.758	0.922
U-C2-22-3	6	67	0.75	6.40	50.8	100.0	362	1.680	1.758	0.956
									Average	1.00
									COV:	0.05

Note: P_n is computed using the proposed coefficients in the unified web crippling equation

Table 3: Range of parameters for test data available in the literature and the truss core panel

Data Set	F_y (MPa)	Angle, degrees	t_w, mm	R/t_w	N/t_w	h/t_w
Yu (1981)	284 - 332	61.6 - 75.9	0.73 - 1.24	1.3 - 1.7	61.1 - 202	38.0 - 93.5
Wu (1997)	717 - 772	59.8 - 62.8	0.43 - 0.74	2.2 - 5.5	34.5 - 58.8	29.5 - 208
Avci (200) and Avci and Easterling (2004)	241 - 724	50 - 75.5	0.39 - 1.52	3.1 - 17.1	25.1 - 98.0	29.2 - 100
Truss core Panel	192 - 197	60	.75 - 1.00	1.3 - 1.7	114.3 - 152.4	161.3 - 215.1

Table 4: Mean and COV of P_{test}/P_n for truss core panel test results and calibration data set

Data Set:	Coefficient	Proposed
	C	5.271
	C_R	0.17
	C_N	0.369
	C_h	0.014
Truss core Panel	Mean	1.16
	COV	0.093
Yu, Avci and Easterling	Mean	1.00
	COV	0.11

Table 5: Test results from the truss core panel

	#Webs	Angle (°)	t_w (mm)	R/t_w	N/t_w	h/t_w	F_y (MPa)	P_{test}/web (kN)	P_n/web (kN)	P_{test}/P_n
A.1-1CR	4	60	0.75	3.20	152	204	192	1.70	1.523	1.116
A.1-4CR	4	60	0.75	3.20	152	204	192	1.61	1.523	1.057
C.1-1CR	4	60	0.75	3.20	152	205	192	1.57	1.522	1.031
D.2-1CR	4	60	1.00	2.40	114	153	197	3.39	2.706	1.253
D.1-1CR	4	60	1.00	2.40	114	153	197	3.48	2.706	1.286
D.1-2CR	4	60	1.00	2.40	114	153	197	3.31	2.706	1.223
									Average	1.16
									COV	0.093

Note: P_n is computed using the proposed coefficients in the unified web crippling equation

FIGURES

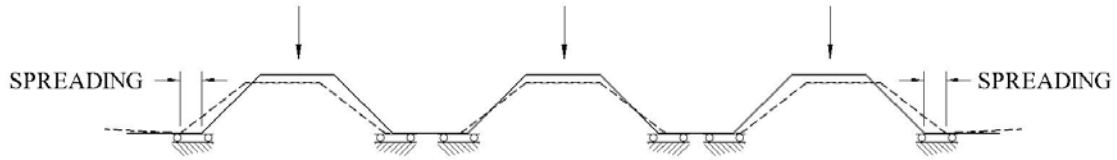

Figure 1: Unfastened multi-web deck section subject to lateral spreading under vertical web crippling load at the end of the section

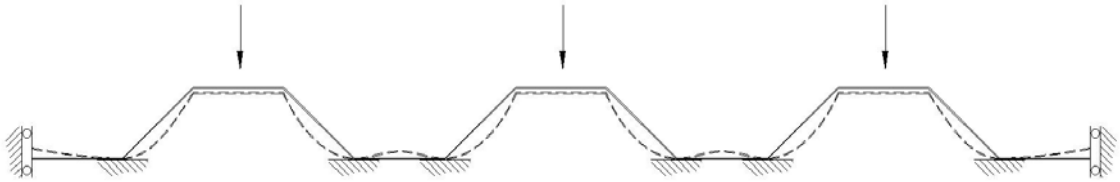

Figure 2: Unfastened multi-web deck section laterally restrained by neighboring deck sections; Loading condition for Yu (1981) and Avci (2002) unfastened tests

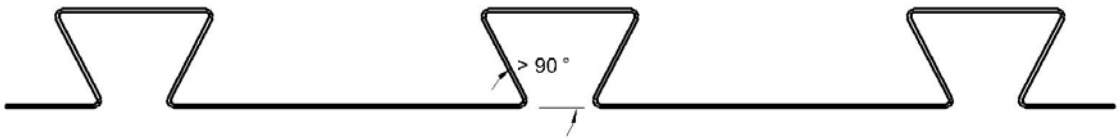

Figure 3: Multi-web deck section with reentrant corners (i.e. web inclination angle greater than 90 º

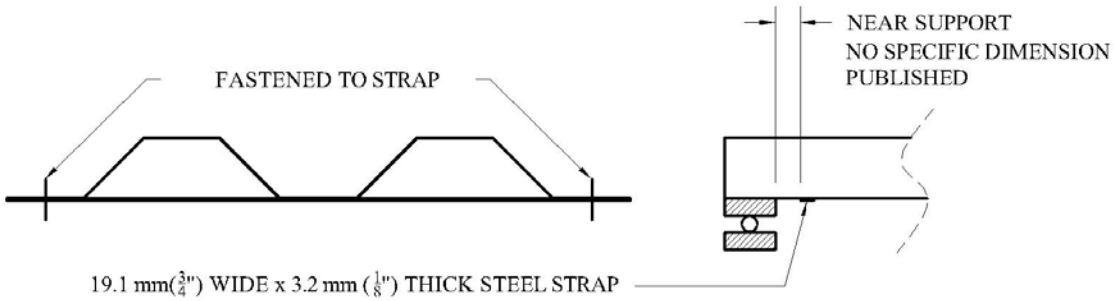

Figure 4: EOF web crippling tests conducted Yu (1981)

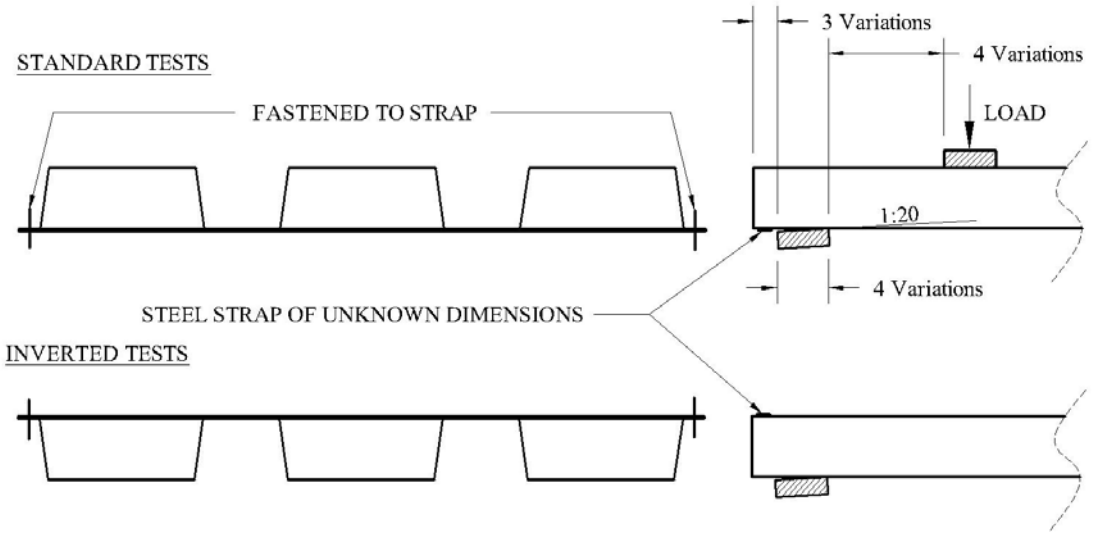

Figure 5: EOF web crippling tests conducted Studnicka (1991)

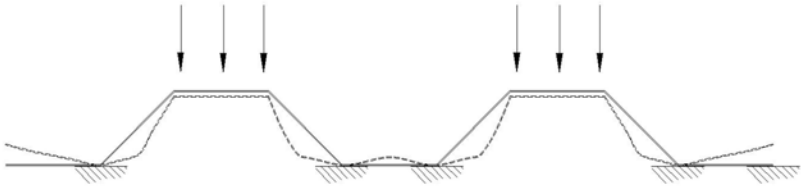

Figure 6: Failure modes (shown as dashed lines) observed by Wu for EOF loading of multi-web deck sections with angled webs

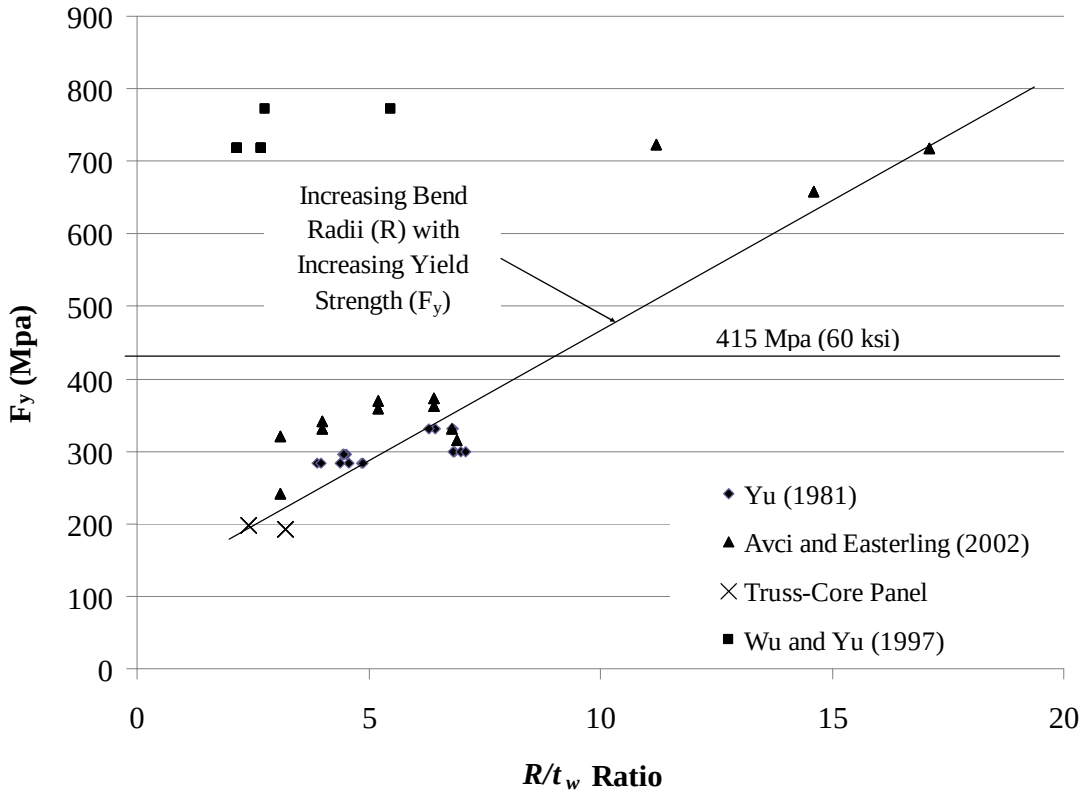

Figure 7: Yield strength of each specimen graphed with respect to R/t ratio for the specimens used by Yu (1981), Wu (1997), Avci (2002), and the truss core

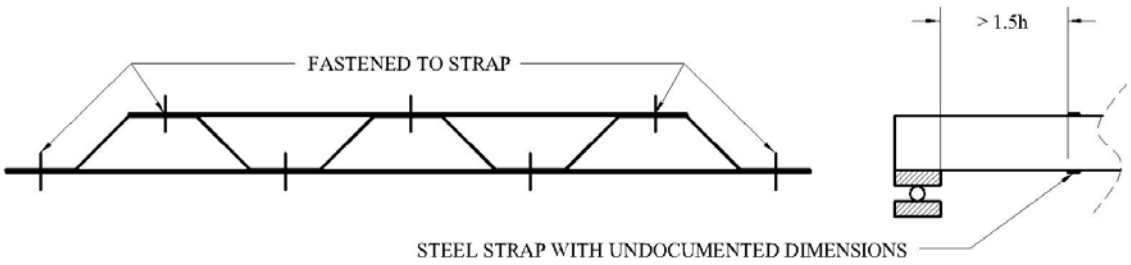

Figure 8: EOF web crippling tests conducted Avci (2002)

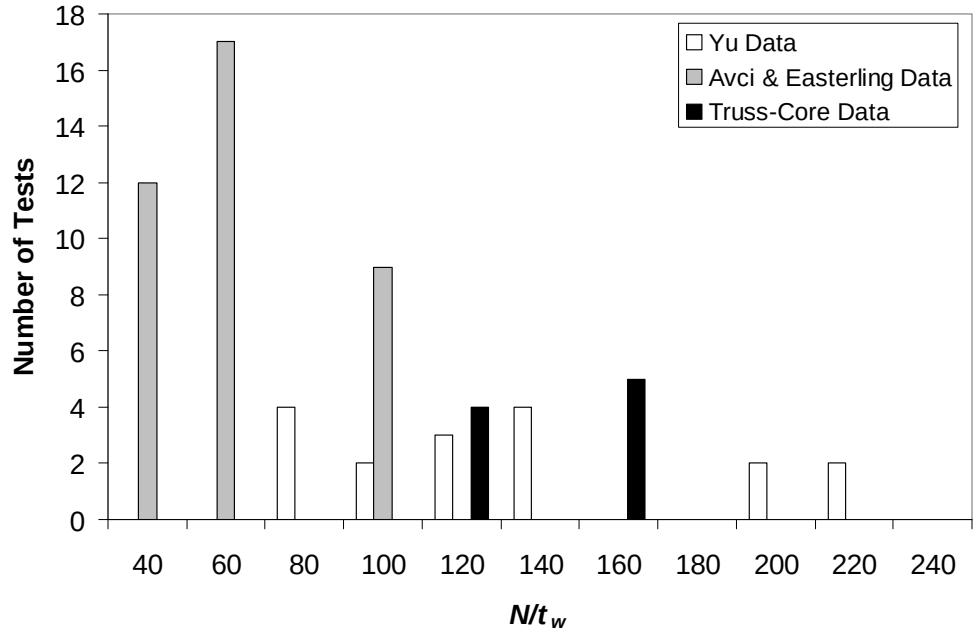

Figure 9: Distribution of N/tw values in the Yu, Avci and Easterling, and truss core panel test results

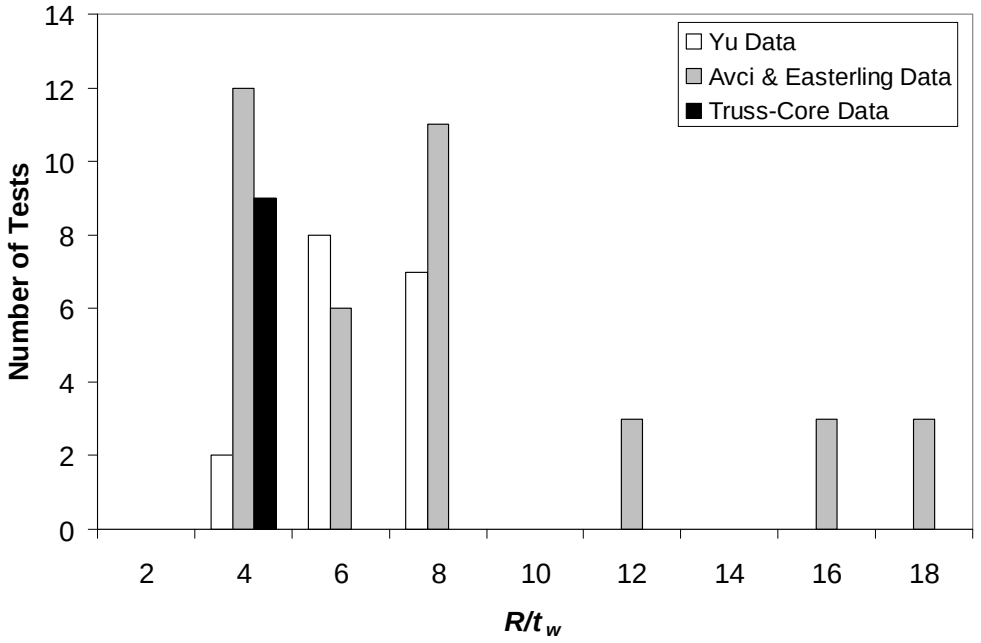

Figure 10: Distribution of R/tw values in the Yu, Avci and Easterling, and truss core panel test results

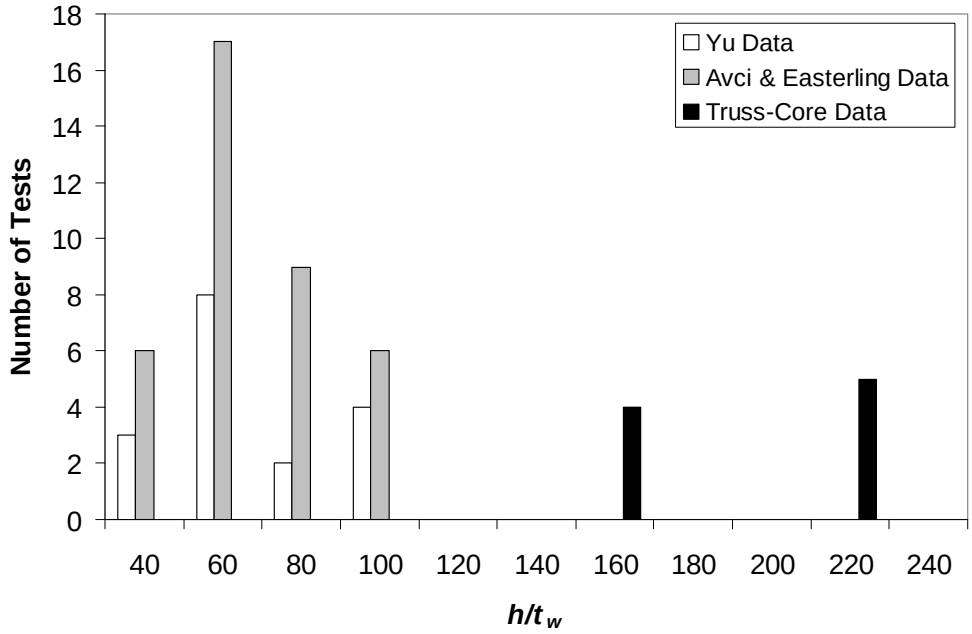

Figure 11: Distribution of h/t_w values in the Yu, Avci and Easterling, and truss core panel test results

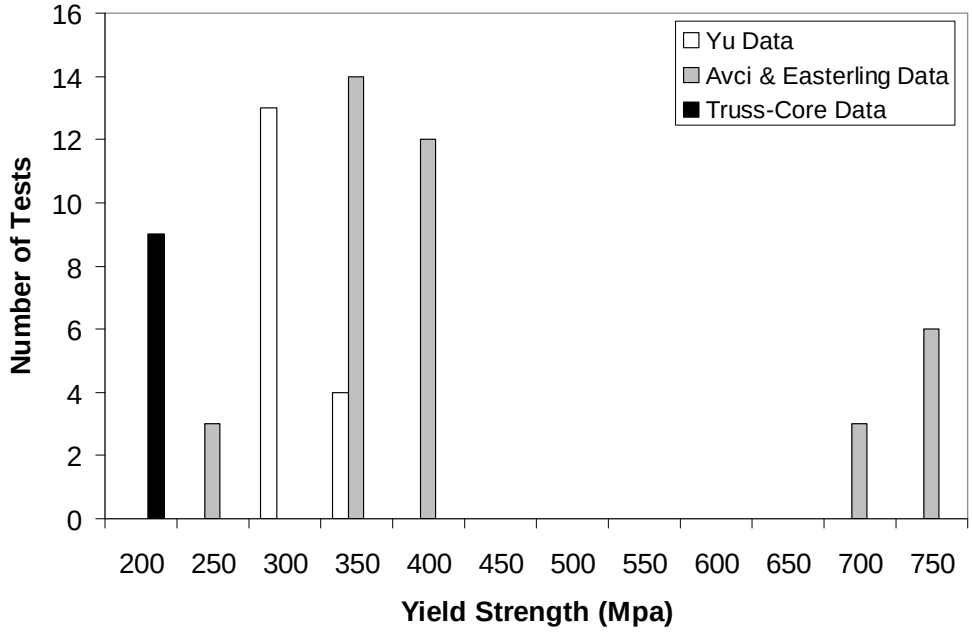

Figure 12: Distribution of yield strength values in the Yu, Avci and Easterling, and truss core panel test results

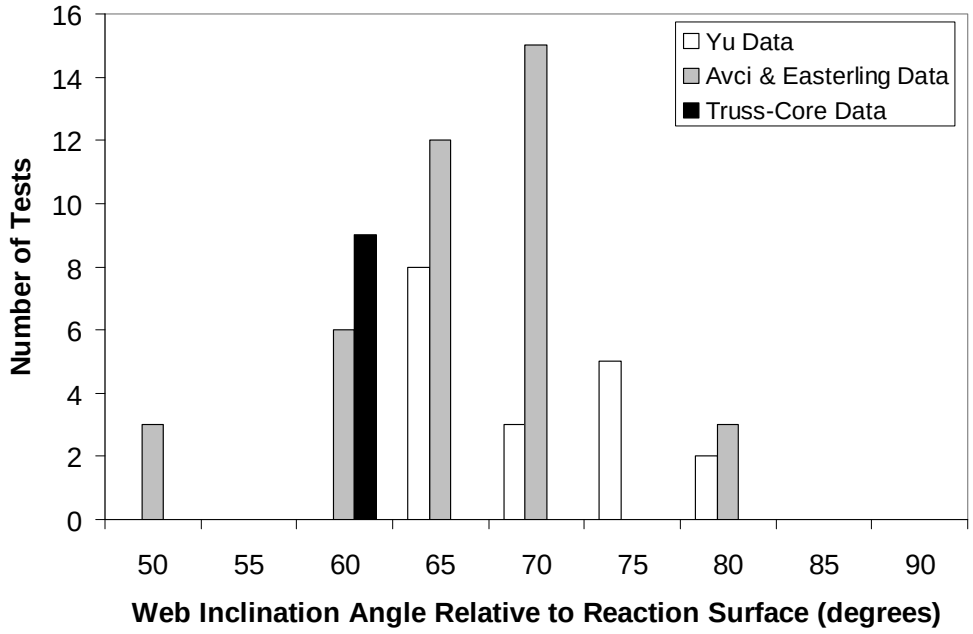

Figure 13: Distribution of web inclination values in the Yu, Avci and Easterling, and truss core panel test results

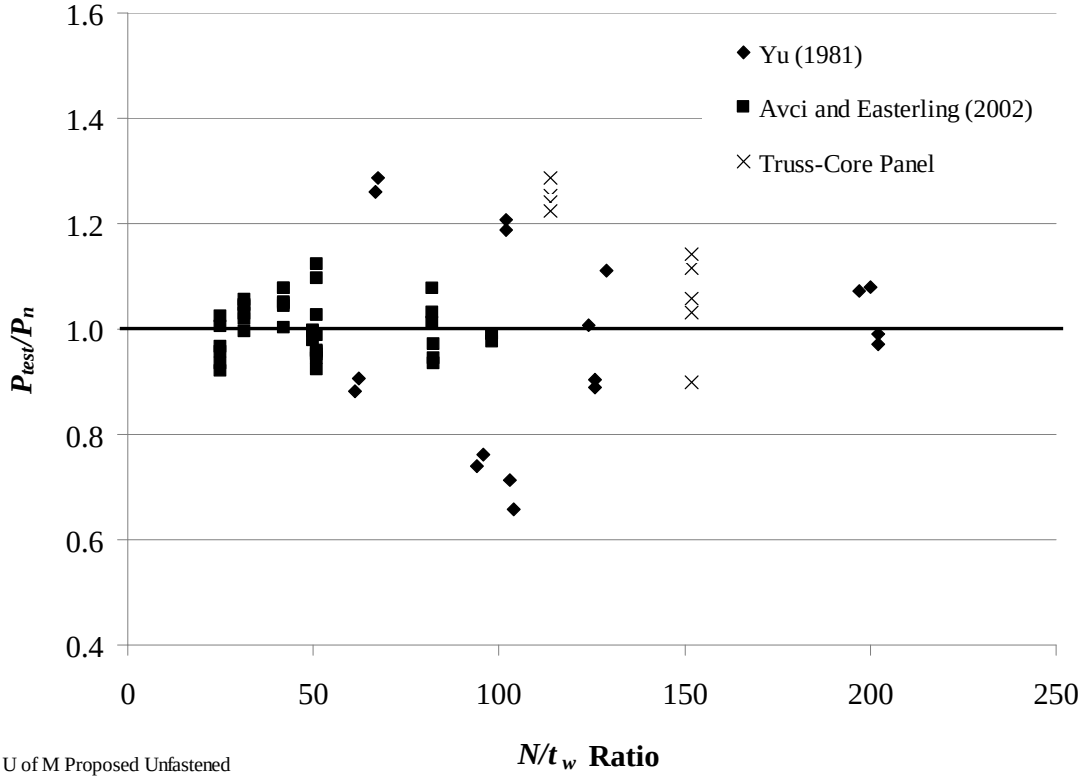

Figure 14: Yu, Avci and Easterling, and truss core panel data graphed with respect to N/t_w

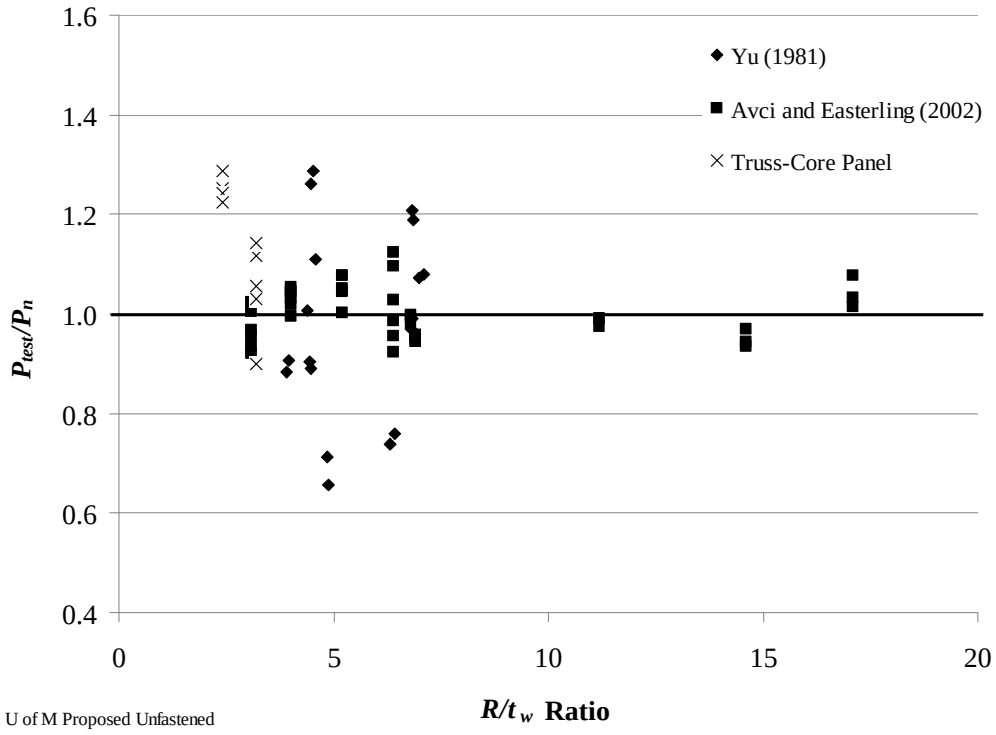

Figure 15: Yu, Avci and Easterling, and truss core panel data graphed with respect to R/t_w

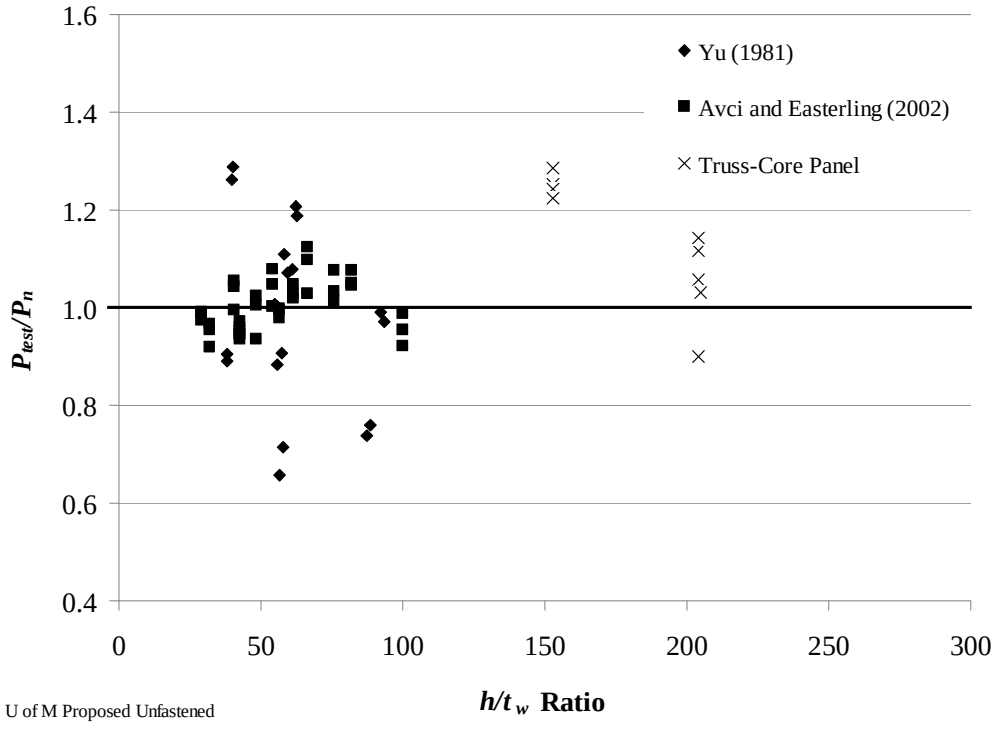

Figure 16: Yu, Avci and Easterling, and truss core panel data graphed with respect to h/t_w

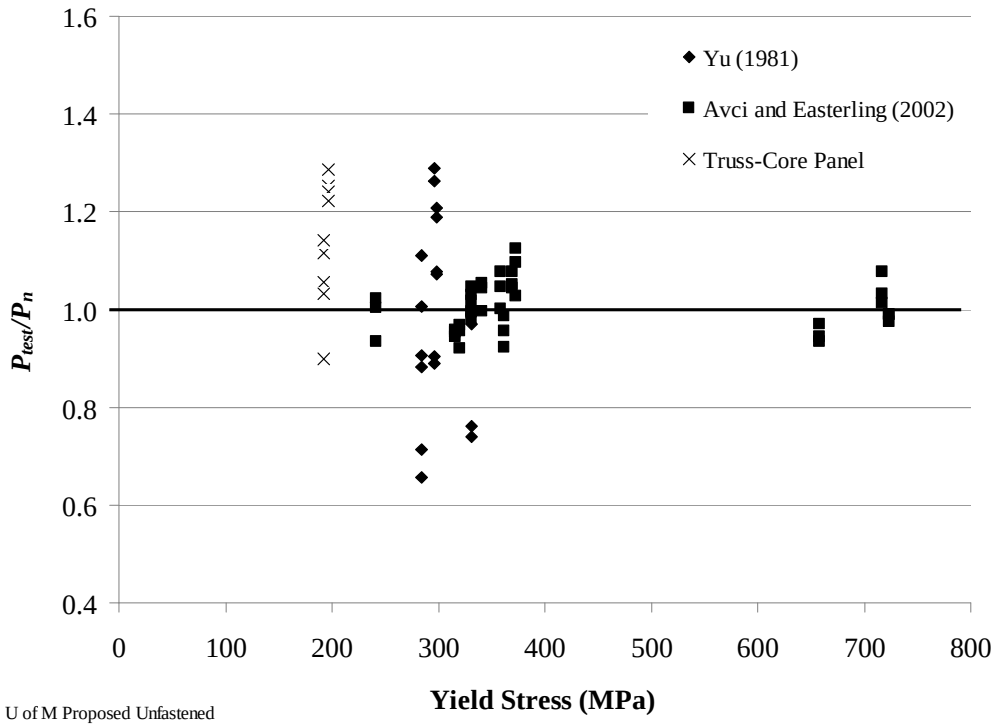

Figure 17: Yu, Avci and Easterling, and truss core panel data graphed with respect to steel yield stress

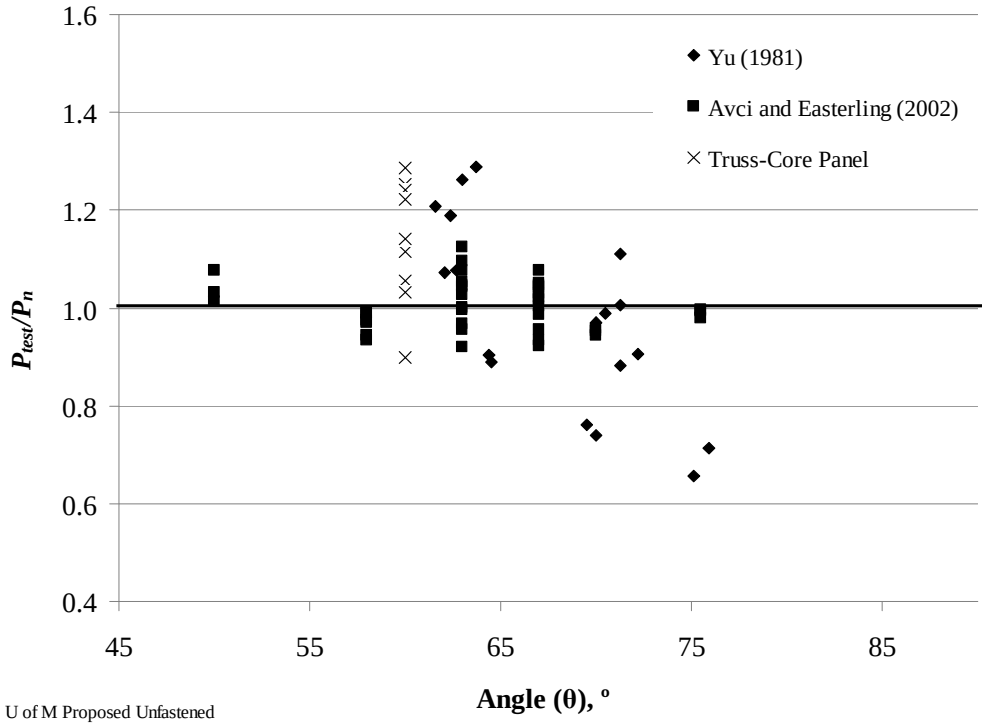

Figure 18: Yu, Avci and Easterling, and truss core panel data graphed with respect to web inclination angle

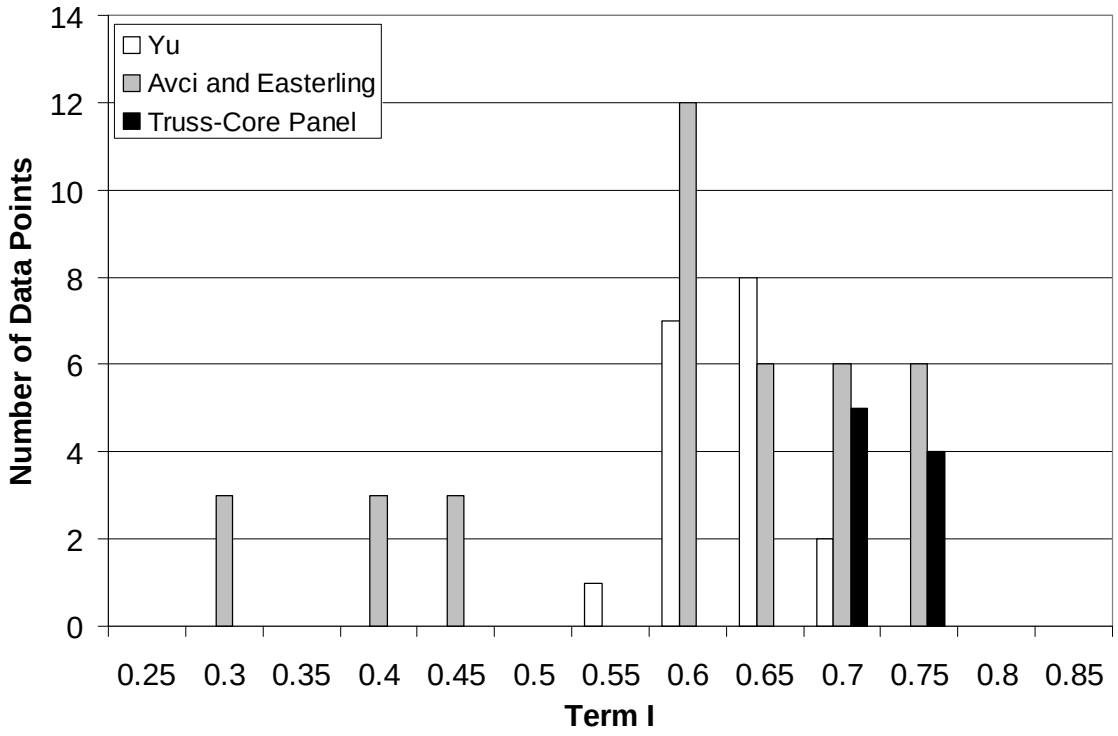

Figure 19: Distribution of term I in Equation (5.1) for the data from Yu (1981), Avci (2002), Avci and Easterling (2004), and the truss core panel

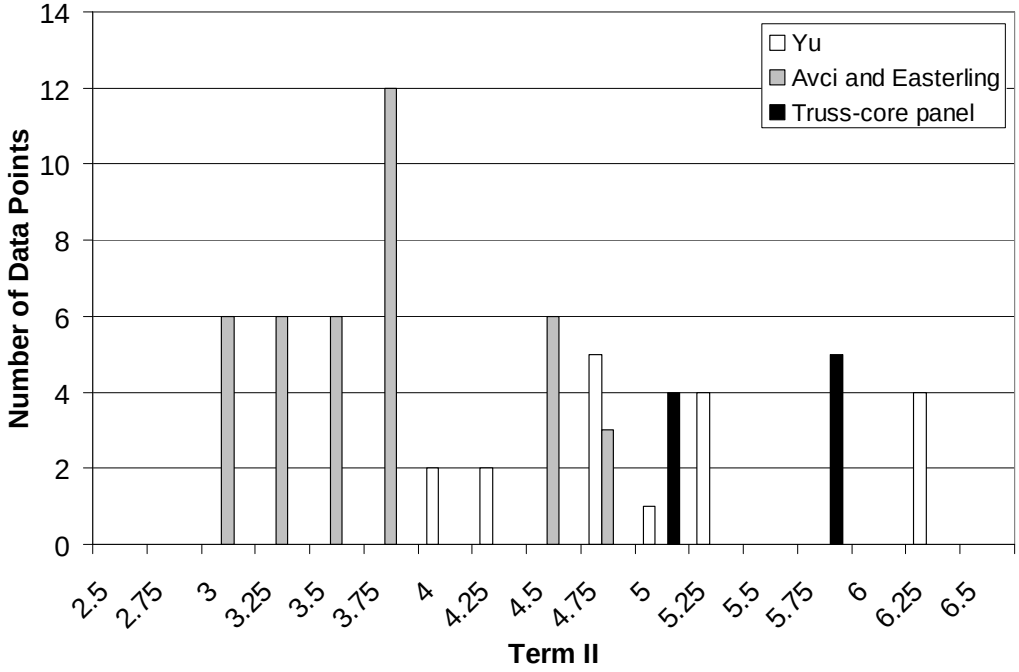

Figure 20: Distribution of term II in Equation (5.1) for the data from Yu (1981), Avci (2002), Avci and Easterling (2004), and the truss core panel

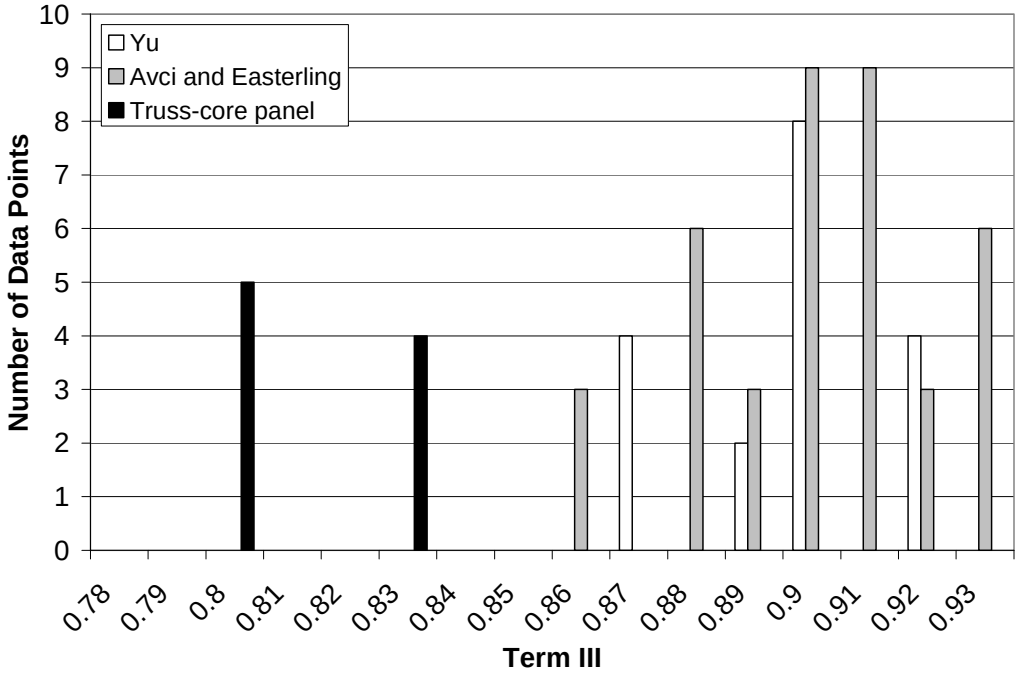

Figure 21: Distribution of term III in Equation (5.1) for the data from Yu (1981), Avci (2002), Avci and Easterling (2004), and the truss core panel

Appendix E: Panel Test Results

1.0 Overview

Prototype truss core and stiffened plate panels were tested to evaluate structural performance. Two types of tests were performed: flexural tests and web crippling tests. Panel stiffness (deflection)[1] and moment capacity were evaluated in the flexural tests. End of flange failure of the webs was evaluated in the web crippling test. The model for structural performance predicts structure stiffness/deflection, moment capacity and web crippling. This model is applicable to either geometry. For this reason, the bulk of the testing was performed on the truss core prototypes, for a range of face sheet and web thicknesses. Because there was excellent agreement between the model predictions and test data for truss core prototypes, limited testing was performed on the stiffened plate prototype. In the sections which follow, the test procedures and data are presented for the truss core and stiffened plate panel prototypes.

2.0 Test Specimens (prototype panels)

Truss core and stiffened plate prototypes were specifically designed to validate the model of panel structural performance. A total of five different test panel geometries were tested, four truss core panel designs and one stiffened plate panel design. Dimensions are reported in Table 1 for the truss core structural component (Figure 1a) and in Table 2 for the stiffened plate panel structural component (Figure 1b). A total of 7 truss core prototype panels (2 panels for each of three designs, A, B, and C and 1 panel for design D) were fabricated. One stiffened plate panel prototype, design E, was fabricated. Prototype panel depths, sheet thicknesses and web geometries were selected to be consistent with roof panel designs. (See section 4.1 and 5.1 for truss core and stiffened plate roof panel designs, respectively.)

The truss core panels were fabricated in Finland at KennoTech. This vendor had experience with laser welding. Thus the prototyping process provided insight into the quality and durability of the laser welds between the face sheets and webs. Cold formed, ‘V’ shaped web flutes were continuously welded to the face sheets along the middle of a 25 mm (1 in.) flange at the top and bottom of the web flute. The web inclination angle was 60° to accommodate manufacturer limitations. The exterior face sheet was between 1.5 and 2 times thicker than the interior face sheet. A combination of the thicker exterior face sheet and reduced clear span between web connection points resulted in lower slenderness ratios of the exterior face sheet. Prototype width was either 0.75 m or 2.19 m. The narrow width was selected to fit within a hydraulic load frame. The wide width (specimen D) was designed to be a full scale prototype. Long panel lengths are desirable to simulate planar loading conditions expected in roof applications. The prototype length was limited to 5 m due to shipping constraints. Because the panels were long and the

[1] Stiffness and deflection are interchangeable. The deflection is the load divided by the stiffness.

fabricated from sheet stock, splicing of the webs and the bottom face sheet was necessary. Figure 2 shows metal inert gas (MIG) welds used to splice the webs together. Figure 3 shows a lap splice with a double laser weld that spanned the entire width of the bottom face sheet of the truss-core panel. The exterior (top) face sheet (compressed face sheet) contained no splicing or welding of any sort.

The stiffened plate panel prototype was fabricated by Bergh Steel fabricators in Minnesota. Because the laser welding process had been validated with the truss core prototypes, the stiffened plate prototype was purchased from a local vendor. In this panel, a single steel web was spot welded (at approximately 75 mm on center) to a steel face sheet. The thickness of the face sheet was greater than that of the webs. This configuration was selected to verify the moment capacity in the case where the compressed sheet (i.e. the webs) yields. The stiffened plate prototype panel was 0.45 m wide and approximately 3 m long. The prototype length was limited by the manufacturer's press brake size. Figure 4 shows the stiffened plate panel cross section and figure 5 shows the panel spot welds.

Table 1: Panel dimensions for the truss core structural component shown in Figure 1a.

Panel	Sheets thickness			Number of channels N_c	Web inclination angle θ[°]	Flange width [mm]			Panel width b [mm]	Panel length a [mm]	Panel depth D [mm]
	Top t_t [mm]	Web t_w [mm]	Bottom t_w [mm]			f_e	f_v	f_0			
A	2	0.75	0.75	2	60	38	184	305	750	5000	140
B	2	0.75	0.75	5	60	51	184	298	2190	5000	140
C	1.5	0.75	0.75	2	60	38	184	305	750	5000	140
D	2	1	1	2	60	38	184	305	750	5000	140

Table 2: Specimens dimensions for the stiffened plate prototype shown in Figure 1b.

Panel	Sheets thickness		Number of channels N_c	Web inclination angle θ [°]	Flange width [mm]				Panel width b [m]	Panel length a [mm]	Panel depth D [mm]
	Web/Top t_w [mm]	Bottom t_w [mm]			f_e	$f_{v,b}$	$f_{0,b}$	f_t			
E	0.91	1.21	1	60	31	388	N/A *	260	450	3050	89

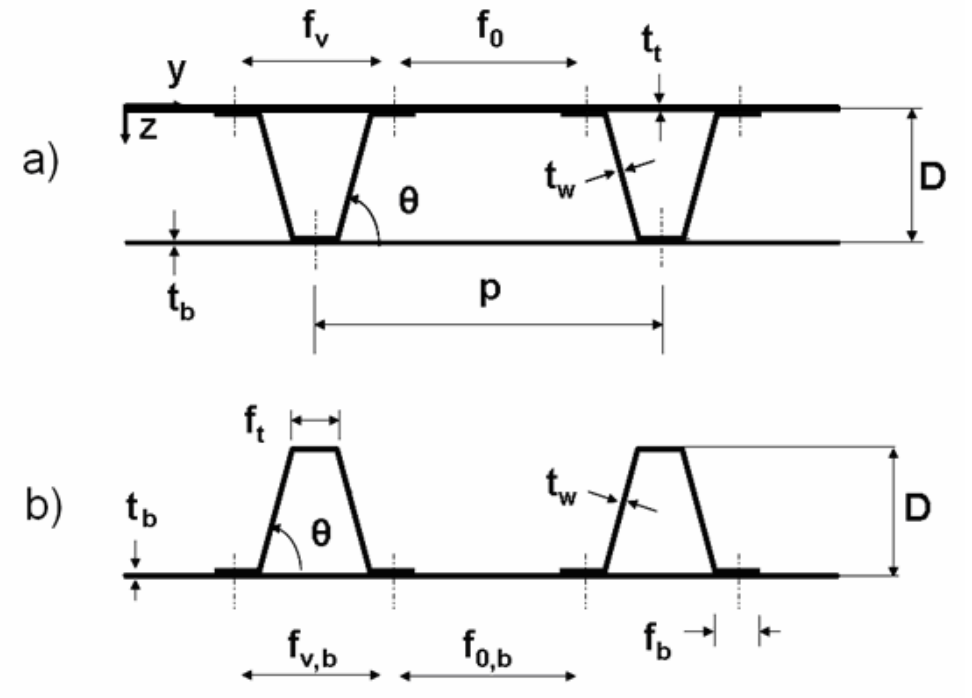

Figure 1: Prototype geometries for the: a) truss core panel, and b) the stiffened plate panel.

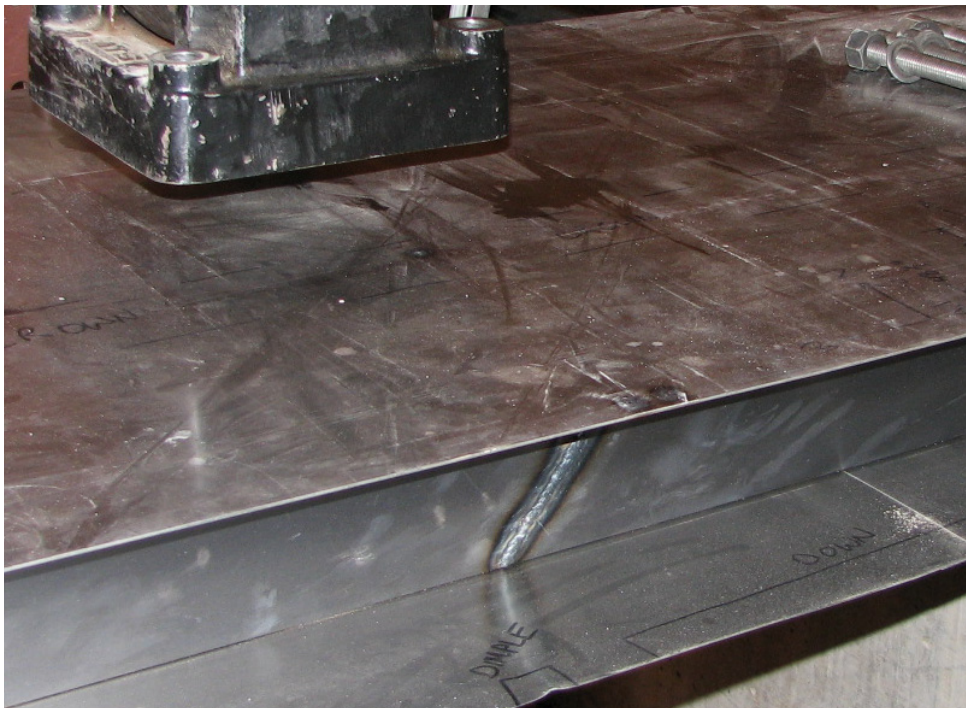

Figure 2: MIG weld splicing web flutes together below load point.

Figure 3: Bottom face sheet lap splice using a double laser weld.

Figure 4: Stiffened plate prototype panel.

Figure 5: Stiffened plate prototype panel showing spot welds.

3.0 Model Parameters for Validation of Design Equations

The truss-core and stiffened plate panels were designed to meet deflection (stiffness, EI), flexural moment capacity and web crippling requirements. The theoretical models for these structural performance measures were developed from basic mechanics theory, previous literature, and the 2001 *AISI Specification*. To demonstrate that these models accurately predict the panel behavior, experimental data for prototype panels were compared with model predictions. Input parameters to the model include panel geometry, material properties and loading conditions. Prototype panel geometry is listed in Tables 1 and 2. The material properties required to predict performance are modulus and yield strength. For this reason, tensile test coupons were prepared from material samples taken from the prototype panels. Tensile test data, including the material yield strength and modulus, were obtained from these samples. Table 3 shows the measured yield strength, ultimate strength which resulted from the testing. The material properties vary by sheet thickness. This variation, however, is not necessarily a function of the sheet thickness, but more a function of the heat treatment and lot for that particular panel.

Table 3: Material properties of the steel sheets used for the prototypes.

Sheet Thickness [mm]	Elastic Modulus [GPa]	Yield Stress $\sigma_{Y,0.2\%}$ [MPa]	Ultimate Strength [MPa]
0.75	201	192	304
0.91	159	211	
1.0	164	197	325
1.21	156	184	
1.5	159	158	281
2.0	202	176	299

4.0 Flexural Testing

The purpose of the flexural testing was to validate the model predictions of panel stiffness, moment capacity and strains. In the distributed load test, sand is uniformly distributed over the prototype panel surface (a frame is constructed to contain the sand) and the panel deflection is recorded as a function of the weight of the sand load. The load at panel failure is the moment capacity. Panel deflection, load and strain are recorded throughout the test.

4.1 Distributed Load Test

Truss core panel design D and stiffened plate panel design E were subjected to the distributed load test. In a distributed load test, the test specimen was loaded with a uniformly distributed sand load. The distributed load was applied by placing sand on the surface of the specimen in load steps. At the end of each load step the sand was smoothed to a uniform depth across the width and length of span relative to vertical rulers

which are attached to the surface of the panel. Each load step is 50 mm (2 in.) deep of sand for the first 460 mm (18 in.). Load steps are 13 mm (0.5 in.) deep of sand there after.

Figures 6 shows the vertical frame used to contain the sand on the truss core prototypes. For the stiffened plate panel, PUR foam was cut to fit the contoured surface of the web (Figure 7). The loading frame was built above the foam layer (Figure 8). In each case, the frame was supported at the four corners of the prototype and did not touch the specimen at any location along the span. Therefore the container frame did not affect the measurement of load or displacement. At each of the two ends, the specimen rested on 76 mm (3 in.) x 102 mm (4 in.) x 8 mm (5/16 in.) HSS (hollow square section) steel tubes. The 102 mm (4 in.) side was the bearing edge. These tubes were placed on load cells. This arrangement provided sufficient rotational freedom to the panel at the reaction ends. This method of testing produced a load control condition which eliminated the ability to carefully watch the propagation of failure.

For the truss core panel, two 111 kN (25 kip) capacity load cells were placed under each reaction tube as shown in Figures 9 and 10. The dial gages, with a 0.001 in., resolution which were placed at the midspan and at 152 mm (6 in.) from the inside face of each reaction. Two gages were placed at each longitudinal position at 203 mm (8 in.) in from the exterior longitudinal edge of the panel. The readings of each pair of gages were averaged for data analysis. Instrumentation for the stiffened plate panel was similar to the truss core panel (Figures 11 and 12). Load cells and dial gages were placed under each reaction tube. Dial gages were also placed along the exterior edge of the panel. Strain gages were bonded to the surfaces of the webs and the bottom face sheet at the midspan of the specimen (truss core and stiffened plate prototypes) as shown in Figure 13.

Measurements of load, displacement, and strain were taken after the sand was leveled at the end of each load step.

Figure 6: Distributed load testing of the truss core prototype panel.

Figure 7: PUR foam was cut to fit the surface of the stiffened plate panel. Sand loads were applied directly to this surface.

Figure 8: Distributed load testing of the stiffened plate prototype panel.

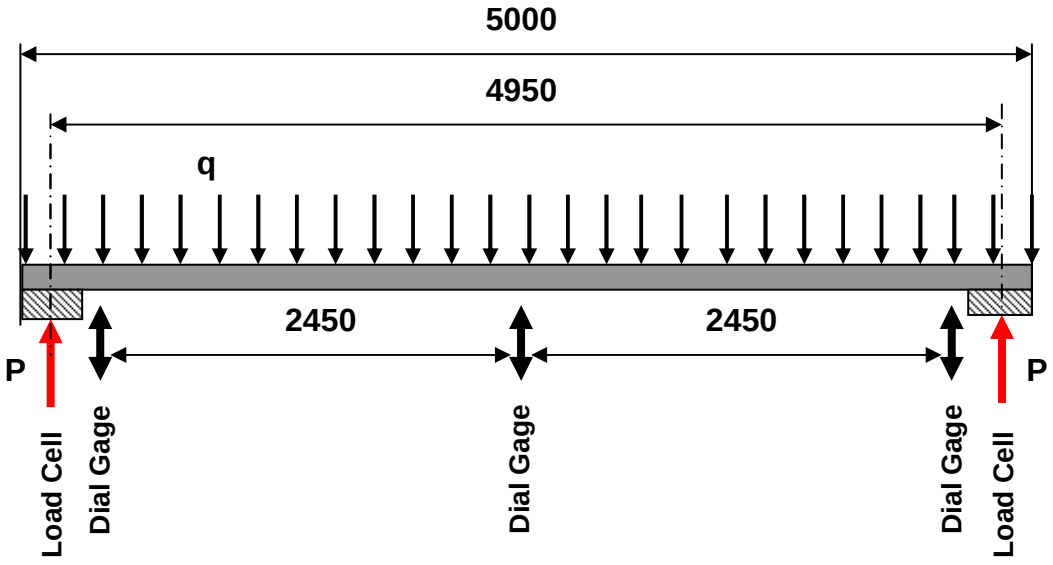

Figure 9: Transducer positions for the truss-core distributed load test. All dimensions in mm.

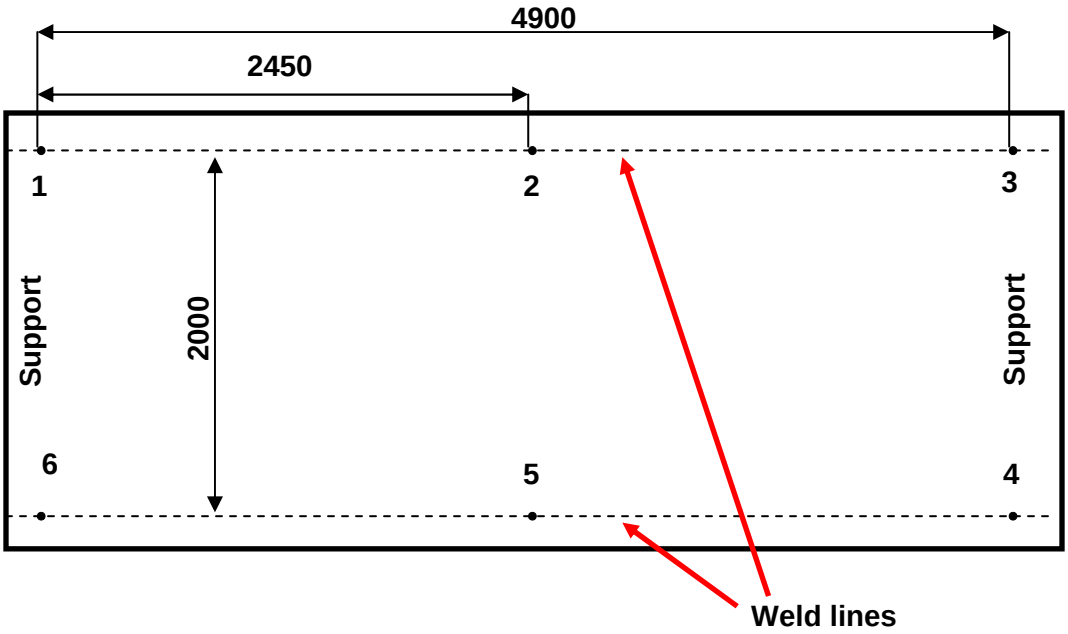

Figure 10: Dial gage placement for the truss-core panel distributed load test. Dial gages are placed in a grid pattern in correspondence to the welds. Dimensions in mm.

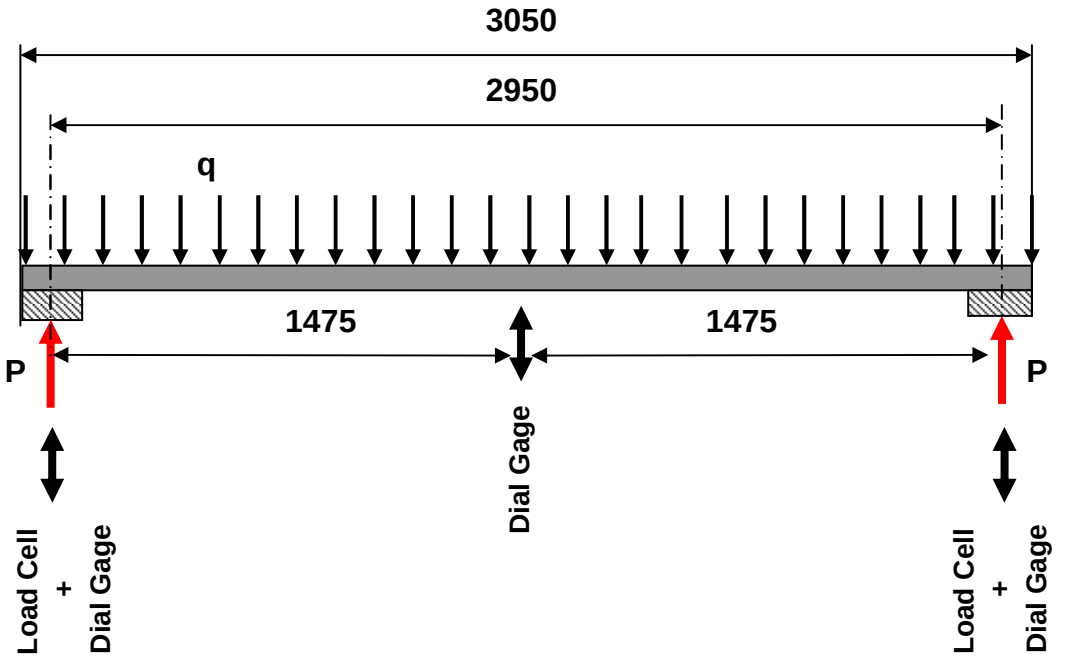

Figure 11: Transducer positions for the stiffened plate panel distributed load test. All dimensions in mm.

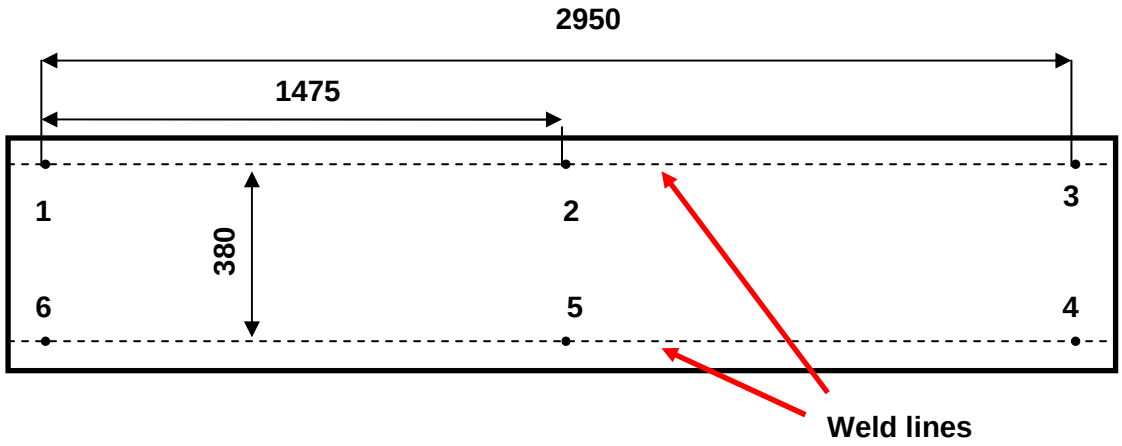

Figure 12: Dial gage placement for the stiffened plate panel distributed load test. Dial gage are placed in a grid pattern in correspondence to the welds. Dimensions in mm.

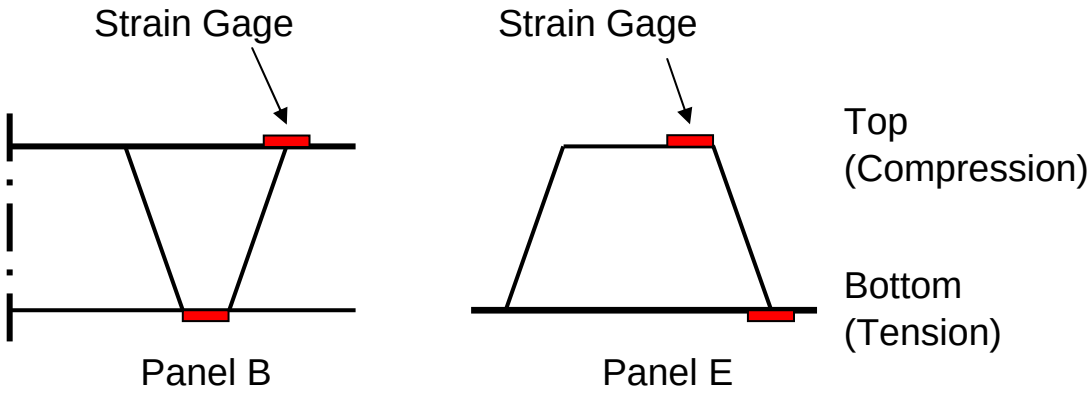

Figure 13: Strain gage positions for distributed load tests.

4.2 Truss Core Panel Flexure Test Results

The ultimate failure occurred at midspan very suddenly. Figure 14 shows the failure at midspan that was composed of several smaller buckles across the width of the panel. Strain gages indicated that the bottom face sheet yielded prior to failure and the top face sheet did not yield until after failure. Once the bottom face sheet yielded, the top face sheet of the section buckled under the additional compressive stress. The failure could have been propagated by the following events: (1) the top face sheet may have buckled resulting from a lack of restraint from the top web flute tabs, or (2) the web may have buckled under the stress gradient, eliminating restraint to the top face sheet. It is impossible to know the order of failure because of the suddenness of the failure.

Figure 15 shows the load-displacement history. Trend lines are presented assuming both the gross cross section and effective cross section. It is initially observed that the trend of the measured deflection is slightly stiffer than theoretical predictions.

The stiffness starts to reduce around 4,000 Pa of applied load. The measured load-displacement curve clearly softens with increasing load matching the trend of the nominal deflection obtained using the effective width method.

Figure 16 shows the strain measurements. The strain on the bottom face sheet exceeded the yield strain at approximately 43,300 N-m (384,000 lb-in) while the ultimate moment capacity was 53,200 N-m (471,000 lb-in). Theoretical load-strain relationships using the effective section are plotted in Figure . At low loads before substantial buckling occurred, the measured strains are in reasonable agreement with beam theory predictions using either the gross or effective section. The bottom face sheet, however, shows substantially higher strain than predicted for applied moments above approximately 3,000 Pa (62 psf).

The measured flexural capacity correlated very well (M_{test}/M_n = 1.00) with the nominal value predicted the AISI effective width method using the measured material properties. The flexural stiffness (EI) was determined by a least squares fit to the load-displacement curve between 0.20 M_{max} and 0.70 M_{max}. The ratio of the measured EI to the predicted EI_{gross} was found to be one, based on an assumed E of 203 GPa (29,500 ksi) and an I_{gross} calculated geometrically assuming all thin elements were infinitely thin (i.e. no moment of inertia about their in-plane axis) as recommended by the *2002 AISI Manual of Cold-Formed Steel Design* (AISI Manual 2002).

In summary, the flexural capacity and elastic stiffness of the truss-core panels were examined by one distributed load test. Deflections, strains, and applied load were monitored during testing. The predominant failure for the panels was the propagation of buckling across the entire width of the compressed face sheet. The web flute tabs unfolded at the cold-formed bend permitting upward deformation of the face sheet. The single distributed load test which did not contain any local point loads, resulted in an M_{test}/M_n = 1.00. Strain measurements showed good agreement with the yielded failure mode of bottom face sheet yield as predicted by the effective width method.

Figure 14: Compressive face sheet buckle

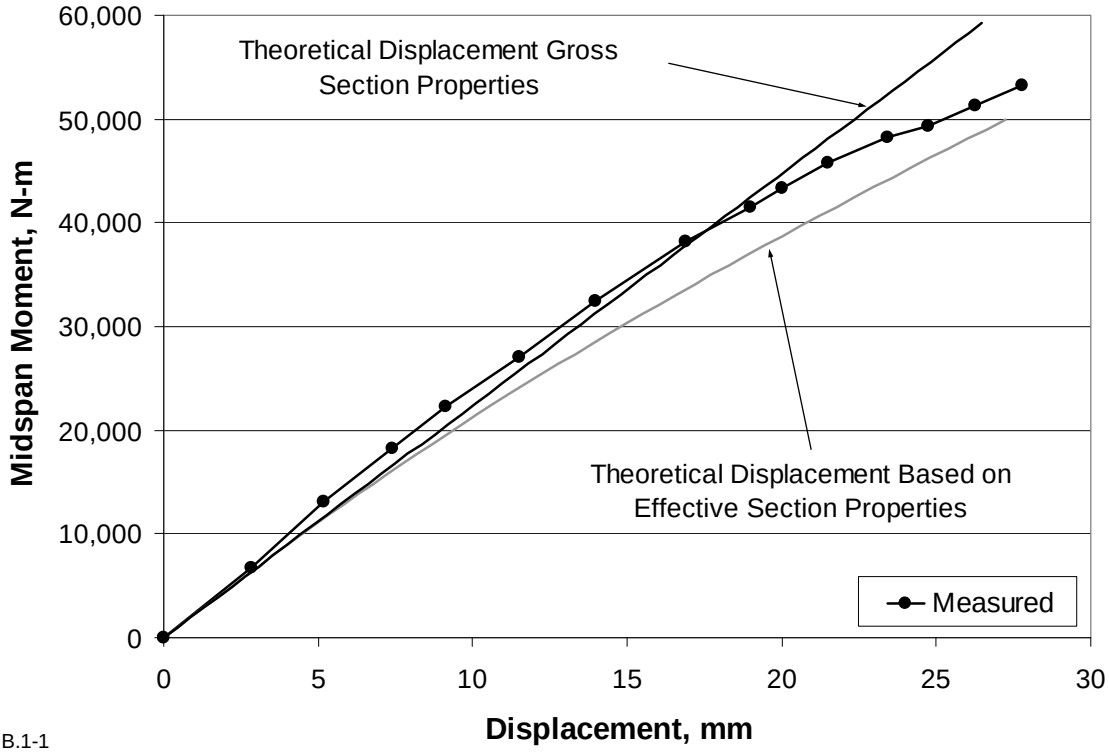

Figure 15: Load displacement curve for truss core panel prototype subjected to a uniformly distributed load.

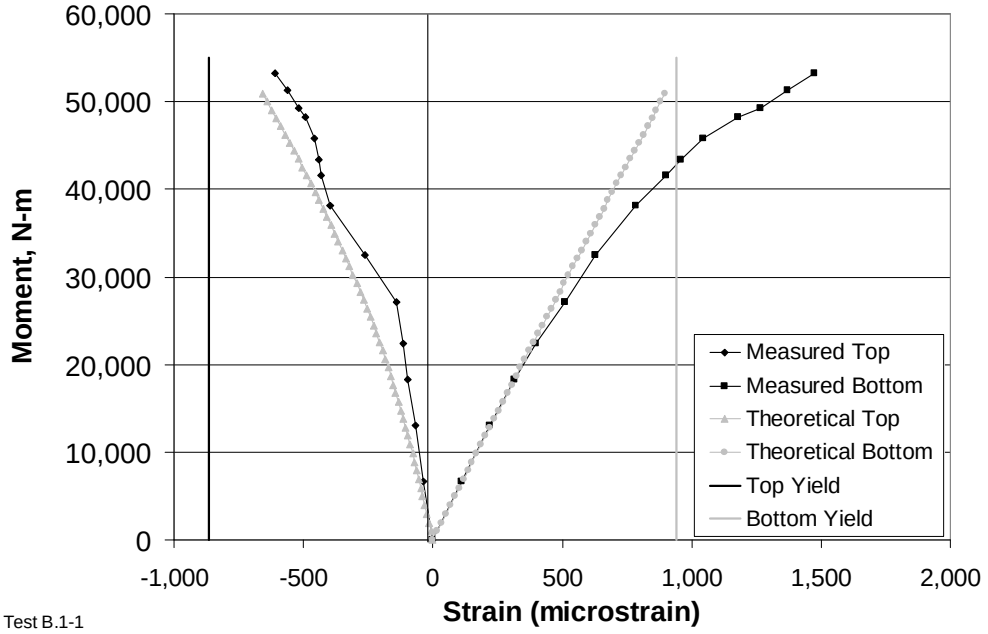

Figure 16: Midspan strain gage data for the truss core prototype panel subjected to a distributed load.

4.3 Stiffened Plate Panel Flexure Test Results

As with the truss core panel, the ultimate failure of the stiffened plate panel occurred at midspan very suddenly. The web lateral surfaces and top surface buckled at midspan (Figure 17). There was no failure in the spot welds. The strain gage data (Figure 18) show that the compressive strain in the top surface of the web exceeded the yield limit at an applied moment of approximately 1500 N-m. The strain gage data indicate that the strain in the bottom face sheet was well under the yield limit throughout the test. Because failure occurred suddenly, it is assumed that the web top surface and lateral (side) surfaces buckled simultaneously.

Figure 19 shows the load-displacement history. Model predictions of load displacement behavior are indicated by the line labeled “analytic”. The measured moment capacity is 1840 N-m while the predicted moment capacity is 1560 N-m. The data indicate that the prototype panel is stiffer than predicted by the model. Up to a loading of approximately 1000 N-m, the data and model predict linear behavior. As the loading increases beyond 1000 N-m, the web begins to yield (see the strain data in Figure 18) and effective section properties must be considered. Although the predicted strains for the web and the bottom face sheet agree well with the experimental data, the model underpredicts the moment capacity (by 15%) and stiffness. This discrepancy may be caused by the interaction during yielding between the web top and lateral surfaces. This interaction leads to additional post buckling stiffness that is not captured by the model. The model provides a conservative estimate of the stiffened plate panel flexural performance.

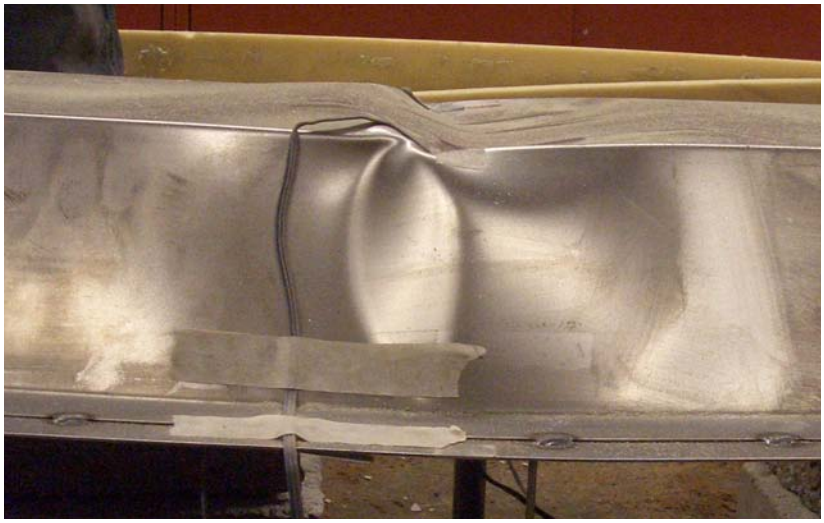

Figure 17: Failure of the stiffened plate panel in the distributed load test.

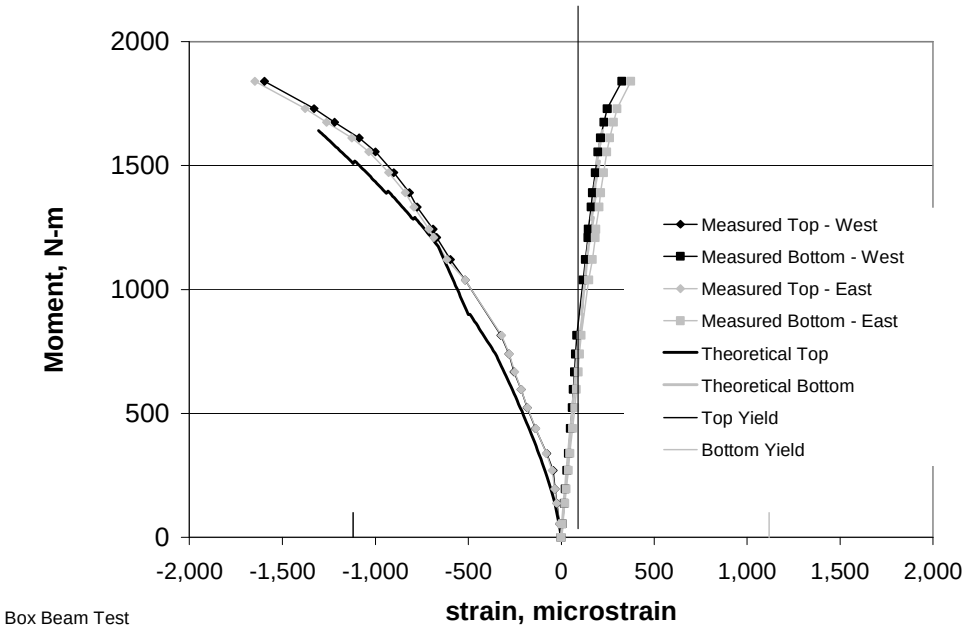

Figure 18: Midspan strain gage data for the stiffened plate panel in the distributed load test. The notation "top" refers to the strain gage located on the top surface of the web, "bottom" refers to a strain gage located on the bottom face sheet. Strain yield limits are shown at -1100 and 1100 microstrain.

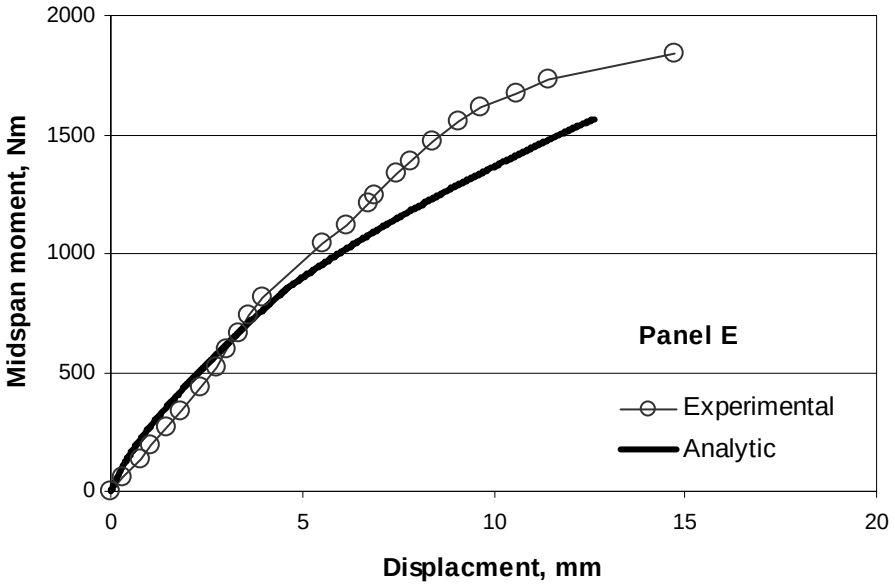

Figure 19: Load displacement curve for the stiffened plate panel prototype (E) subjected to a uniformly distributed load.

5.0 Web Crippling

The purpose of the web crippling test is to validate the model predictions of the load carrying capability of the panel at the panel supporting edges. The roof panels are simply supported at the ridge and soffit. Excessive loading can cause the webs to buckle at these edge supports. The web crippling test is a 3 point loading test which is designed to cause failure at the support. The prototype panel is supported at the two ends and subjected to a transverse line load near one of the end supports. The loading condition is such that the webs will fail at the support nearest the load application point. Strain, displacement and the applied load are measured during the test. The load at failure is compared to the model prediction of the web crippling load.

Model predictions of the web crippling loads for the prototype panels are based on an empirical model that can be found in the *AISI Specification* (see Appendix D). The *2004 AISI Supplement* includes an empirically calibrated equation for the nominal web crippling capacity for both fastened and unfastened conditions of multi-web deck sections subject to EOF loading. Two characteristics separate the truss-core and stiffened plate panels from the five standard cold-formed steel sections that are defined in the *AISI Specification* First, the panels have at least one continuous face sheet that connect all webs. The continuous face sheet(s) restrain the webs against lateral translation and prevents spreading of the cross section (thereby achieving a condition referred to as "strapped" in the literature). Second, the panels are assembled by laser welding the V shaped web flutes to the face sheet(s). It is unclear whether the laser welded assembly should be modeled by a fastened or unfastened condition.

In many applications, cold-formed steel sections have the lower flange fastened to a supporting component in order to keep the section in position, or in the case of a multi-web section, to engage the section in diaphragm action. This condition is referred to in the literature and in the *AISI Specification* as the "fastened (to support)" condition. Researchers observed that the fastened condition, which is inherent in many cold-formed steel sections in service condition, have the added benefit of increasing the web crippling strength of the section (Bahkta 1992, Prabahkaran 1998, Beshara 2000, Wallace and Schuster 2004, Avci and Easterling 2004). As observed by Bhakta (1992), the increased web crippling capacity is a result of added rotational restraint provided to the web by the bottom flange fastened to the support. As a result, the effect of the fastened condition on web crippling has been an area of research in cold-formed steel since Bahkta's research in 1992.

While it was assumed that strapped conditions apply to the truss core and stiffened plate panels, it was unclear whether the fastened or unfastened conditions are appropriate. Thus, web crippling tests were performed on truss core prototypes in both the fastened and unfastened configuration. These tests included additional data related to the deformation of the web sections. The conclusion of these web crippling tests on the truss core panel indicated that the panel web crippling behavior is best modeled by the strapped, unfastened condition. Stiffened plate panel tests were performed in the

unfastened condition. Tests on the stiffened plate prototype were limited, because much of the model validation was established through the tests on the truss core prototypes.

For both the truss core and stiffened plate panel prototypes, there was good agreement between the web crippling data and model predictions with the strapped, unfastened condition. With the AISI Specification web crippling coefficients for the unstrapped condition (unfastened or fastened), the web crippling model underpredicts the web crippling load by 100% or more. The web crippling model with the strapped, unfastened coefficients underpredicts the web crippling load by 5 to 25 %.

5.1 Web Crippling Test Procedure

The prototype panels were tested under non-symmetric three-point bending that simulated an EOF loading condition. The critical location of the specimen (the test end) was near the reaction closer to the loading point. Figures 20 and 21 show a schematic representation of the test arrangement for the truss core and stiffened plate panel prototypes, respectively. Figure 22 is a photograph showing the typical test set up for a truss core panel. The two ends of the specimen rested on wood reaction blocks which were composed of three 38 mm x 140 mm (1.5 in. x 5.5 in.) pine timbers. The spreader beam between the actuator foot and specimen was composed of three 38 mm x 152 mm pine timbers and a 235 mm x 45 mm (9.25 in. x 1.75 in.) glue laminated (GluLam) manufactured beam. The bearing width for the truss core specimens was 114 mm (4.5 in.) The stiffened plate prototype test set up (Figure 23) is comparable to the truss core prototype set up. The load application beam and reaction block support widths are 76 mm (3 in.) wide for the stiffened plate prototypes.

To allow for rotation in the primary bending plane of the specimen at the reactions (simulating a pinned support condition), a 13mm (½") thick neoprene pad was placed between the load/reaction beams and the specimen for tests on panels A, C; and E, and between the wood reaction block and rigid support for tests on panels D. Past web crippling tests typically placed the loading point at a distance greater than 1.5 *h* from inside face of the critical reaction plate (Wallace and Schuster 2004; Avci and Easterling 2004). As shown in Figures 20 and 21, all specimens used a distance greater than 2.5*h* between the inside edge of the loading beam and inside edge of the reaction beam for EOF loading of prototype. This was specified to mitigate any interaction between the applied load stress concentration and the reaction stress concentration (i.e. arching action between the load and reaction). The loading beam was carefully aligned in the center of the section and parallel to the reaction beam prior to loading.

Load was applied using a 340 kN (77 kip) capacity actuator. The load rate was set between 0.25 and 0.75 mm/min. (0.01 and 0.03 in./min). A 360 kN (80 kip) capacity load cells was placed between the actuator piston and the actuator foot. A 36 kN (8 kip) per 10 volt calibration setting was used for these tests to get the best load precision out of the relatively large capacity load cell. Maximum loads obtained during testing were between 20% and 38% of the calibrated range. Loading was applied by monotonically increasing displacement until a drop in load was observed. Actuator stroke and actuator

load was recorded for all web crippling tests. Additional data were recorded for truss core panels. These data included distortion of the cross section and strain data at the webs.

Distortion of the cross section at the test end was measured in two tests (on panels A and D) using the Metris optical based coordinate measurement system to study the effect of face sheet modifications. The Metris system is composed of light emitting diodes (LEDs) which are placed on the test specimen. Figure 24 shows the location of the LEDs placed on the web and face sheet edges. Five LEDs were positioned on each web and seven LEDs were placed along the top face sheet so that the rotation of the web and face sheet could be computed at the web-to-face sheet intersection. Using triangulation, three specialized cameras determine the position of the LEDs in a three dimensional coordinate system. Using a predefined relative coordinate system, data obtained from the Metris system was used to isolate out-of-plane displacement of the web and face sheet elements.

Strain data were obtained for web crippling tests performed on truss core panel prototypes A, C, and D. These data were used to establish whether yielding had occurred prior to failure. One 45 degree strain gage rosette was placed on each web at mid height ($d/2$) and half way between the reaction and loading points. As a means of strain verification, the shear stress at the section estimated based on the shear strain component (termed as 'the shear stress acting on the vertical plane) was compared with the measured load. The rosettes were positioned with the center gage aligned vertically and the other two gages positioned at ± 45 degrees from vertical.

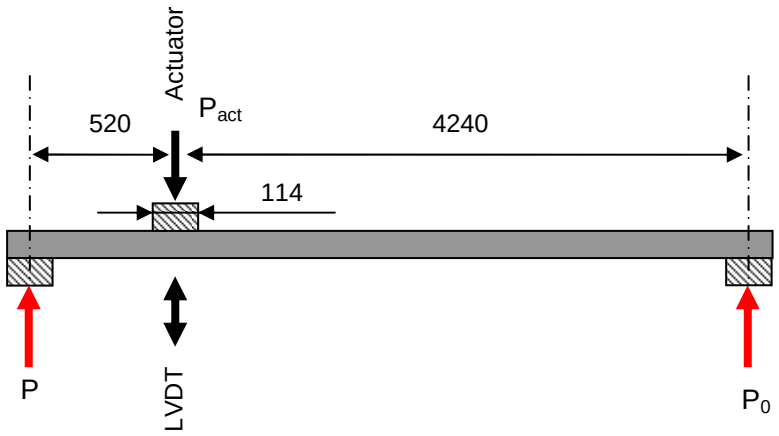

Figure 20: Three-point bending test arrangement for web crippling for the truss core panel. Dimensions (in mm) shown are typical.

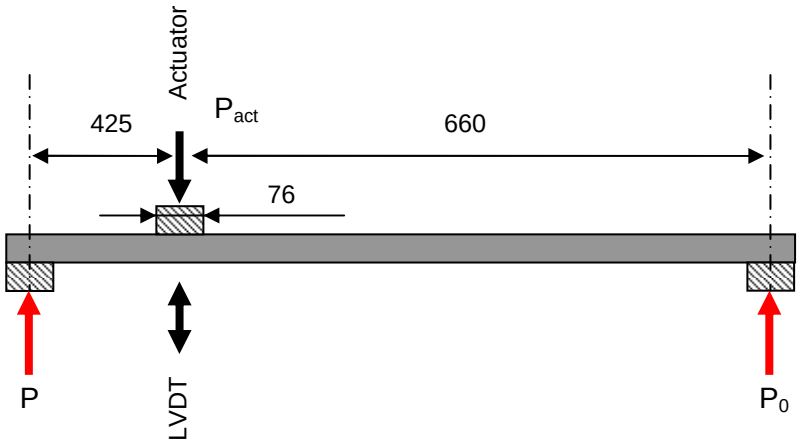

Figure 21: Three-point bending test arrangement for web crippling for the truss core panel. Dimensions (in mm) shown are typical.

A: Actuator foot
B: Wood spreader beam
C: Test specimen
D: 13mm (½") thick neoprene rubber pad
E: Wood reaction block resting on rigid steel beam
h: The distance of the flat portion of the web along the plane of the web
N: Reaction bearing distance

Figure 22: Test set up for a web crippling test of the truss core panel.

Figure 23: Test set up for a web crippling test of the stiffened plate panel.

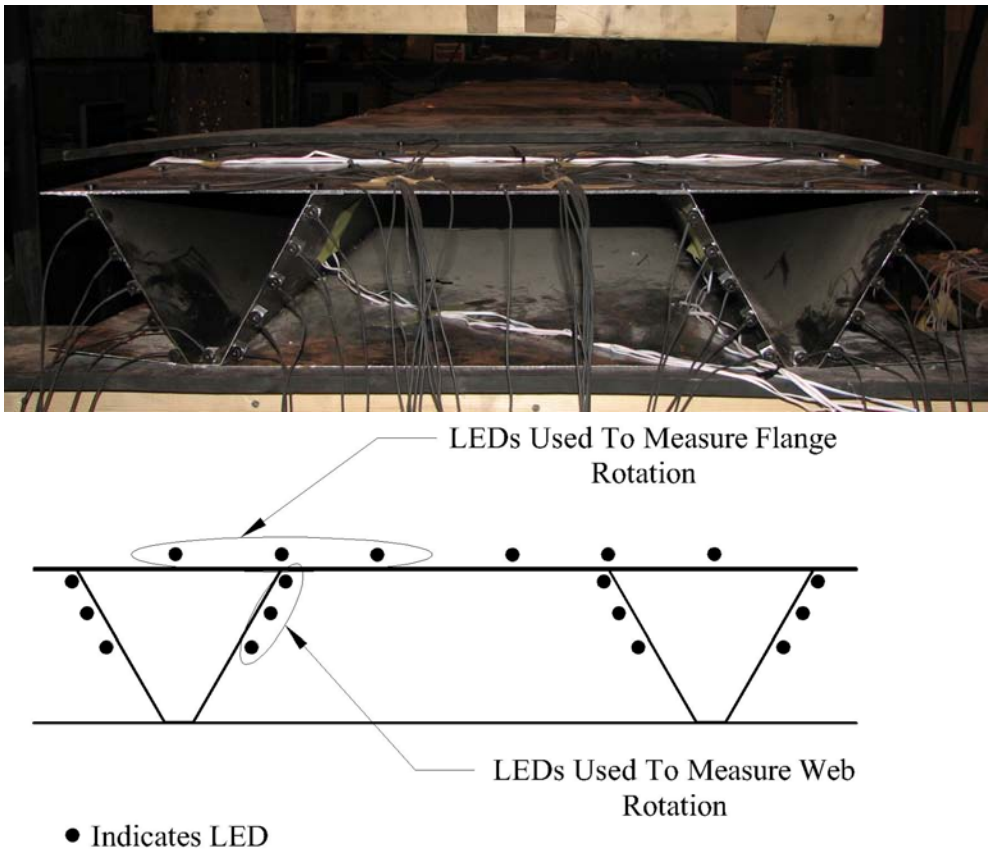

Figure 24: LED Sensors to measure element rotations. This instrumentation was used in two web crippling tests (on Panels A and D).

5.2 Truss Core Panel Web Crippling Results

A total of six truss-core panel specimens were tested under an end one-flange (EOF) loading condition to investigate the effect of two different test parameters (Table 4). First, the specimens included two different web slenderness ratios (h/t_w): three specimens with $h/t_w = 204$ and three specimens with $h/t_w = 153$. Second, three specimens were fastened to the support while three specimens were not fastened to the support. The web crippling behavior of the truss-core panel was studied using load versus displacement response and local strain response. In addition, distortion of the cross section was measured directly above the supports. In the discussion which follows, test observations are presented and web crippling loads are compared with predicted values obtained for the unstrapped conditions (from the 2004 AISI Standard) and the strapped, unfastened condition (derived by UMN and described in the Supplement to Appendix D).

5.2.1 Test Observations

5.2.1.1 Failure mode

Figure 25 shows a plot of reaction force versus total actuator stroke for test A.1-1CR ($h/t_w = 204$). In addition to the deflection of the panel and the deformation of the section, the actuator stroke contains the rigid body motion associated with settling of the elastomeric pads at the reactions; therefore the slope is shallower at lower loads. A drop in load is observed just after the ultimate load indicating failure. Figure 26 shows a plot of reaction force versus lateral web displacement at mid depth. While an idealized perfect member under compression or shear would have no lateral displacement until buckling, initial imperfections in each web caused small displacements from the beginning of loading. A smaller initial slope indicates larger imperfections in the web. The gradually increasing displacement with increased load indicates amplification of the imperfection. The rapid increase in lateral web displacement at ultimate capacity is indicative of an elastic failure because the web buckled while sustaining load. After the web yielded at the extreme fiber as a result of the buckle, a plastic hinge formed and a drop in load was observed.

Figure 27 shows a plot of reaction load versus actuator stroke for test D.2-1CR ($h/t_w = 153$), which was a specimen with a stockier web than Specimen A.1-1CR. The behavior was similar to test A.1-1CR. Figure 28 shows a plot of reaction load versus lateral web displacement at mid depth. The variation in load-displacement trend amongst the four webs is a result of initial imperfections affecting load distribution amongst the webs. For example, the particularly large displacement observed in web II is indicative of substantial imperfections in that web. The horizontal load-displacement trend at the ultimate load is again an indication of elastic buckling of the web followed by the formation of a plastic hinge.

The general behavior to failure may be summarized as follows. As the load was increased, the webs gradually bowed outward from the straight ‘V’ shape, as illustrated in Figure 29a. In all six tests, elastic buckling of the web resulted in the formation of a

plastic hinge approximately $^1/_3$ of the section depth (*d*) above the reaction surface (Figure 29b) at the end of the section. Figure 30 shows the end profile of one web flute of specimen A.1. Figure 31 shows the web flute in Figure 30 significantly after ultimate capacity was reached. The yield line at the end of the section was evident at a height of approximately *d*/3. Figure 32 shows a side profile view of the same web flute prior to loading. Figure 33 shows this web after ultimate capacity was reached. The photograph also shows how folding of the web along the yield lines led to substantial reduction in the depth of the section. A yield line is observed extending from the section end at *d*/3 down to the bottom face sheet approximately 2 *N* from the end of the section. Two additional yield lines were formed between the bottom yield line and the top face sheet. All of the observed yield lines resulted from buckling of the web and were not the cause of buckling as described earlier.

5.2.1.2 Observations from measured strain

Principle stress and principle angle

Figure 34 shows the orientation of the two principle stresses at the middle of the web, σ_A and σ_B, which were calculated from the three measured strains of the strain gage rosette. The principle direction associated with compressive stress, σ_A, roughly coincided with the line connecting the reaction edge and the support edge. Figure 35 shows a graph of the principle stress, σ_A, measured in each of the four webs (denoted I – IV) during test D.2-1CR as a function of reaction load. The principle compressive stress was equal between the four webs until the load reached 1/3 of the ultimate load. It is evident that the stress was not uniformly distributed between the webs from this part of the test on.

Figure 36 shows the principle stress angle in each web, γ, as defined in Figure 34. The gage titles were kept consistent with their orientation on the test specimen. In other words, if all the webs responded identically, the angles would all be identical as well regardless of which side of the web the gage was placed.

The maximum measured von Mises stress is recorded in Table 5 for all tests containing strain gages. During all tests, the measured von Mises did not exceed the yield stress. However, the yield lines did not form close to a strain gage rosette in any of the tests. Therefore, the strain measurements were not affected by the local deformation associated with the yield lines. The stress at the yield lines was certainly at yield, however, the yield lines were a result of buckling of the web.

Shear stress acting on the vertical plane

The shear stress acting on the vertical plane was used to confirm that the shear stress acting through the web computed by dividing the shear force (based on load cell reading) by the number of webs, multiplying by the arccosine of the inclination angle of the web (θ) then dividing by the web area (assuming uniform shear stress distribution) agreed with the shear stress computed based on the strain gage readings and an assumed elastic modulus, *E*, and Poisson's Ratio, ν.

Tests of specimen A.1 (h/t_w = 204)

Figure 37 compares the shear stress in each web from test A.1-1CR. The horizontal axis shows the average shear stress acting on the vertical plane computed using the load cell reading. The vertical axis shows the shear stress acting on the vertical plane computed based on the strain gage readings. In other words, the figure compares shear stress in each web computed from independent measurements. Identical measurements of stress as derived from the load cell readings and strain gage readings would result in a 1-to-1 slope. A large variability exists between the shear stress in the different webs which is most likely the result of initial imperfections. Figure 38 shows the average of the measured shear stress in the four webs. Despite the variability observed in Figure 37 the average of the shear stress agrees with the expected value based on the load cell reading.

Tests of specimen D.2 (h/t_w = 153)

Figure 39 compares the shear stress acting on the vertical plane of each web from test D.2-1CR. The figure suggests that the shear stress in webs III and IV (right-half of the specimen as viewed in the figure) concentrated increasingly more to web IV as the specimen approached failure. Webs I and II (left-half of the specimen) continued to share the load evenly throughout the test. Figure 40 compares the average of the shear stresses computed based on strain gage readings in the four webs against the shear stress computed based on load cell readings. Because a 1-to-1 slope is observed in the figure, strain gage measurements correlated well with load cell measurements for test D.2-1CR indicating reliability of the instrument system.

The shear distribution among the four webs was more uniform for webs with lower slenderness (h/t_w = 154 in test D.2-1CR) than in tests of specimens with higher slenderness (h/t_w = 204 in tests A.1-1CR). This trend is most likely the result of initial imperfections having a larger impact on the more slender webs.

5.2.1.3 Web rotations

Figure 41 shows the deformed shape of the cross section at the reaction associated with web crippling. The face sheet angles, α, and web rotation angles, β, were determined using differential displacements measured at the locations indicated in Figure 24.

Figure 42 plots the relationship between reaction and web and face sheet rotations evaluated for test A.1-1CR. The same information is plotted in Figure 43 for tests D.2-1CR. In both Figure 42 and Figure 43 it can be observed that the face sheet rotations (α) were lower than the web rotations (β) at the web-face sheet intersection by more than an order of magnitude. A perfectly rigid connection at the web-to-face sheet intersection would result in the rotations at α and β having the same magnitude. Considering the position at which the displacements were measured to calculate the rotation (at the mid point of the face sheet between web-to-face sheet intersections) it could be argued that a much larger bending stiffness in the top face sheet than the bending stiffness of the web would cause a difference between rotations. However, while slenderness of the face

sheet was 0.47 and 0.72 times the slenderness of the web for each side of the web, respectively (for specimen A.1), the difference in rotation observed in Figure 42 and Figure 43 is more than an order of magnitude. Therefore, it is concluded that the connection at the web-to-face sheet intersection is essentially pinned.

5.2.2 Web Crippling Capacity

Table Table 6 shows the fastening condition, tested capacity, and nominal capacity for each of the web crippling tests. The right columns show the ratio of P_{test}/P_n where P_n is the nominal capacity calculated following the *2004 AISI Supplement*. Several ratios are reported: (1) P_n is the nominal capacity calculated in accordance with the *2004 AISI Supplement* using the coefficients for unstrapped, unfastened and unstrapped, fastened multi-web deck sections and (2) P_n is the nominal capacity calculated with the UMN derived coefficients for the strapped, unfastened condition. The tests are separated into two groups, tests with specimens composed of webs with an $h/t_w = 204$, and tests with specimens composed of webs with an $h/t_w = 153$.

5.2.2.1 Evaluation of the Fastened Condition

Specimens A.1-1CR, A.1-4CR, and C.1-1CR shared the same h/t_w ratio and were under the same loading condition. The web crippling strengths measured for these specimens were fairly consistent, measuring 220 to 238 percent of the nominal value computed according to the *2004 AISI Supplement*. Similar consistency was observed between specimens D.2-1CR, D.1-1CR, and D.1-2CR, which had slightly stockier webs with measured web crippling strengths of 257 to 264 percent of the nominal value. Three specimens, A.1-4CR, C.1-1CR, and D.1-1CR were fastened to the wood support using fasteners, while the remaining three specimens were unfastened (Table 4). The average measured capacity for all tests with specimens having webs with $h/t_w = 204$ and $h/t_w = 153$ are reported in Table 6.

Tests A.1-4CR and C.1-1CR resulted in values of P_{test}/P_n of 2.25 and 2.20, respectively. The average value of P_{test}/P_n of tests of specimens with identical slenderness without fastening to the support was 2.24. Test D.1-1CR resulted in a value of P_{test}/P_n of 2.71. This value is 4 percent higher than the average value of P_{test}/P_n of tests with specimens unfastened to the support. A 4 percent increase in P_{test}/P_n indicates a small increase in capacity as a result of fastening. It is speculated that stockier webs may benefit slightly from fastening as previously observed for cold-formed 'Z' sections (Yu 2000). For each web slenderness, the value of P_{test}/P_n was consistent regardless of whether the specimen was fastened to the support or not. Therefore, fastening to the support has a negligible effect on the web crippling strength of the truss-core panel.

The fixity of the connection between the web and face sheet was observed to be pinned as discussed. Figure 44a and Figure 44b show the observed web deformation shape for unfastened to the support and fastened to the support tests, respectively. The deformed shapes of the fastened and unfastened conditions are not significantly different

from each other. More specifically, the location of the yield line at the section's end does not change as it likely would with increased rotational restraint at the base of the web.

The Commentary on the *2001 AISI Specification* indicates that restraint provided to the flange, and thus the web, is what is important when considering the fastened to the support versus unfastened to the support cases. The observations and measured strength data strongly suggest that the truss-core panel behaves as an unfastened section regardless of whether the panel is fastened to the support. It is additionally noted that the *2004 AISI Supplement* provides a smaller web crippling strength for unfastened sections compared to fastened.

5.2.2.2 Evaluation of the Empirical Constants for Web Crippling

Measured strength values were between 2.2 and 2.6 times the nominal strength using the coefficients for the unstrapped, unfastened case from the *2004 AISI Supplement*. Using the coefficients for the unstrapped, fastened case, the measured strength values were between 1.7 and 2.1 times nominal values. Consequently, the *2004 AISI Supplement* unified web crippling strength equation with the strapped condition coefficients does not accurately predict the web crippling strength of the truss-core panel. However, the coefficients developed by UMN for the strapped, unfastened condition accurately predict the measured strength values. The measured strength values were between 1.03 and 1.29 times the nominal strength found by using the coefficients for the strapped, unfastened condition. Note these coefficients were determined from published data (see the Supplement to Appendix D). None of the test data from the truss core (or stiffened plate) prototypes was considered.

Table 4: Truss core web crippling specimens.

	Panel and Test	**Fastened to support**	R/t_w	N/t_w	h/t_w	t_f/t_w	**Web Yield strength (MPa)**
h/t_w = 204	A.1-1CR	No	3.20	152	204	2.67	192
	A.1-4CR	Yes	3.20	152	204	2.67	192
	C.1-1CR	Yes	3.20	152	205	2.00	192
h/t_w = 153	D.2-1CR	No	2.40	114	153	2.00	197
	D.1-1CR	Yes	2.40	114	153	2.00	197
	D.1-2CR	No	2.40	114	153	2.00	197

Table 5: Measured von Mises stress in each web, kPa (psi).

Test	Web Yield Stress	Web I	Web II	Web III	Web IV
A.1-1CR	192,000 (27,800)	106,200 (15,400)	59,300 (8,600)	124,800 (18,100)	134,400 (19,500)
D.2-1CR	197,000 (28,600)	60,700 (8,800)	49,600 (7,200)	140,000 (20,300)	44,800 (6,500)

Table 6: Truss core web crippling results.

	Test	P_{test} per web, kN (lb)	Unfastened P_n[1] per web, kN (lb)	P_{test} /P_n	Fastened P_n[1] per web, kN (lb)	P_{test} / P_n	Strapped, Unfastened P_n per web, kN (lb)	P_{test} / P_n
h/t_w = 204	A.1-1CR	1.70 (380)	0.71 (160)	2.38	0.91 (210)	1.86	1.52 (342)	1.12
	A.1-4CR	1.61 (360)	0.71 (160)	2.25	0.91 (210)	1.77	1.52 (342)	1.06
	C.1-1CR	1.57 (350)	0.71 (160)	2.20	0.91 (210)	1.72	1.52 (342)	1.03
			Average:	2.23	Average:	1.75	Average:	1.07
h/t_w = 153	D.2-1CR	3.39 (760)	1.28 (290)	2.64	1.62 (365)	2.09	2.71 (608)	1.25
	D.1-1CR	3.48 (780)	1.28 (290)	2.71	1.62 (365)	2.14	2.71 (608)	1.29
	D.1-2CR	3.31 (740)	1.28 (290)	2.57	1.62 (365)	2.04	2.71 (608)	1.22
			Average:	2.63	Average:	2.09	Average:	1.25

[1] Nominal values calculated following the 2004 AISI Supplement using the coefficients for unstrapped, unfastened and unstrapped, fastened multi-web deck sections.

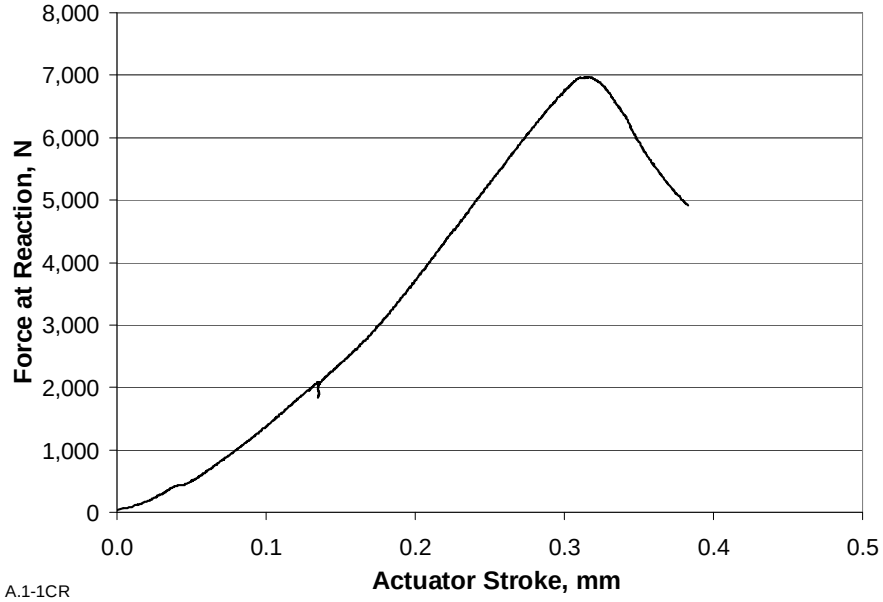

Figure 25: Actuator stroke vs. reaction force for test A.1-1CR

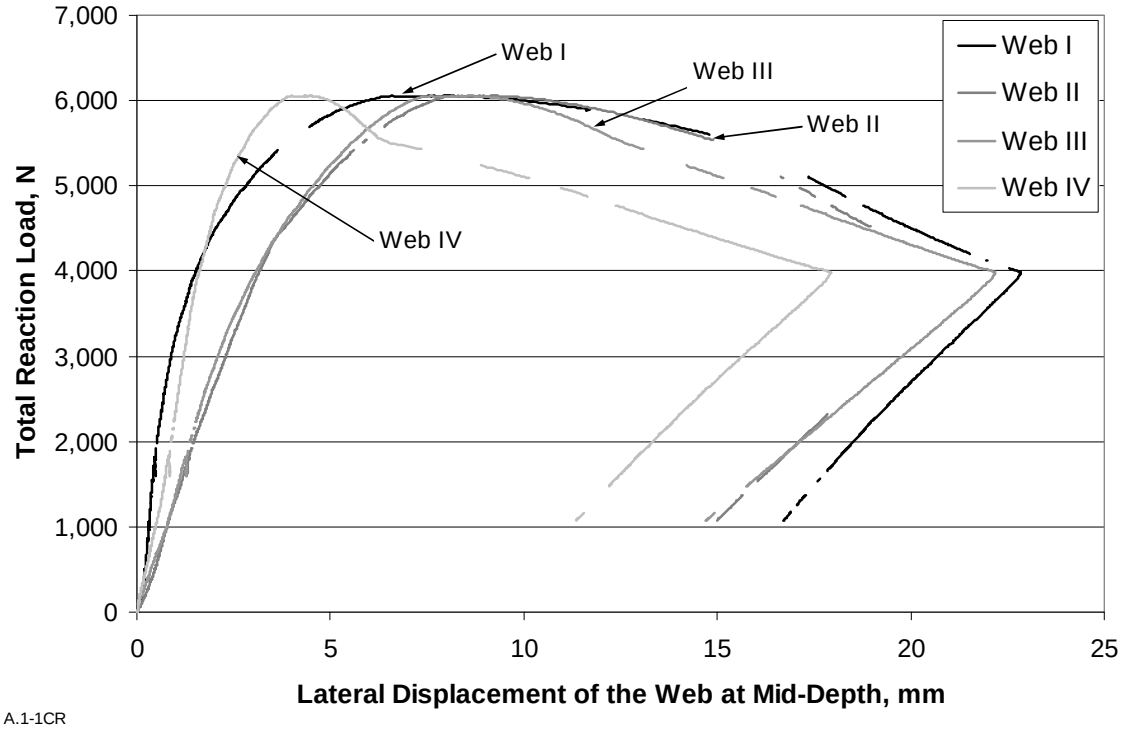

Figure 26: Lateral web displacement vs. reaction force for test A.1-1CR

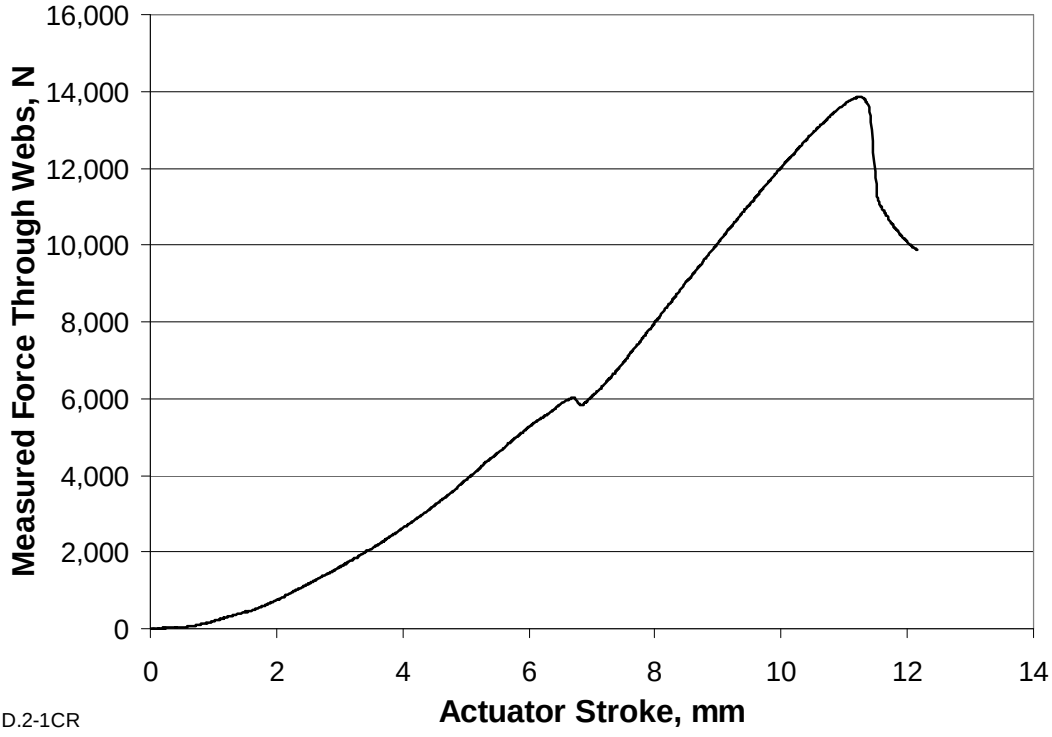

Figure 27: Actuator stroke vs. reaction force for test D.2-1CR

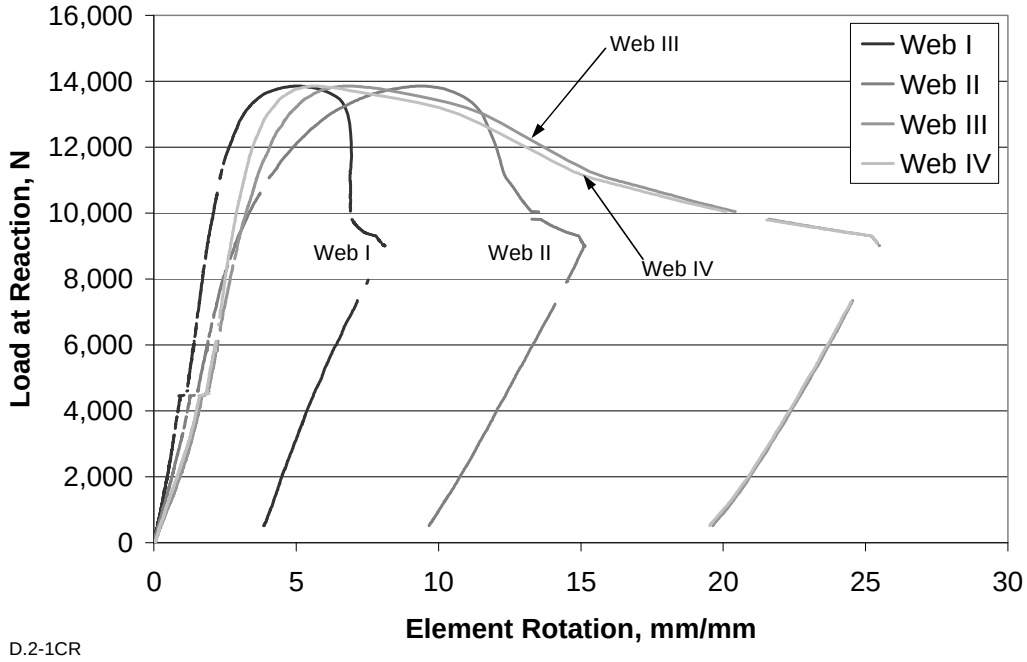

Figure 28: Lateral web displacement vs. reaction force for test D.2-1CR

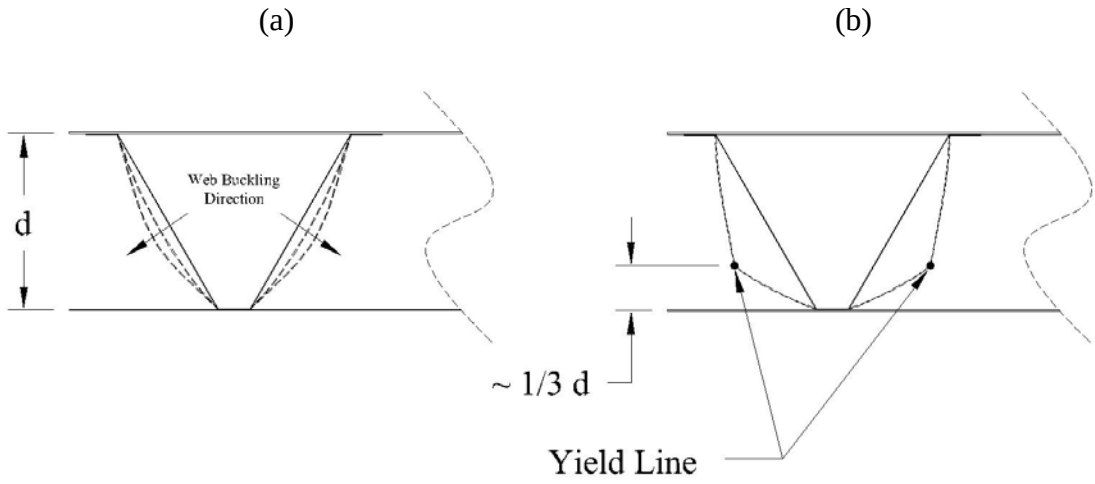

Figure 29: Deformed shape of web observed at end of the: (a) Amplification of deformed shape to ultimate load and (b) formation of yield lines after ultimate load

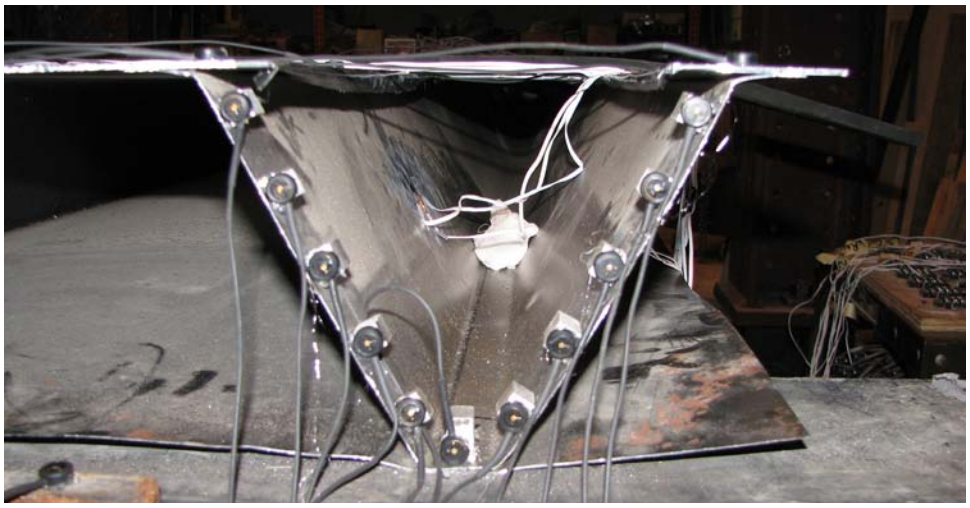

Figure 30: End profile view of truss-core panel specimen prior to EOF loading

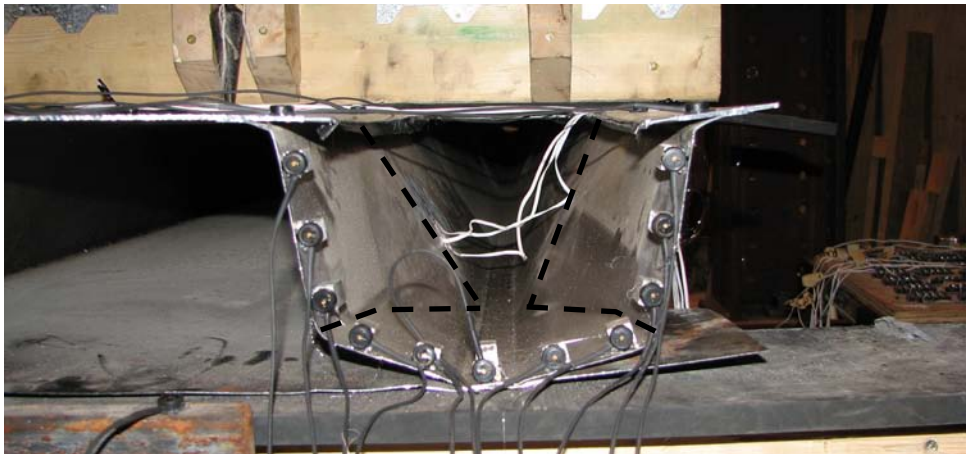

Figure 31: End profile view of failure at end of the truss-core panel specimen from EOF loading substantially after ultimate capacity was established (dashed lines indicate yield lines resulting from buckling)

Figure 32: Side profile view of truss-core panel specimen prior to EOF loading

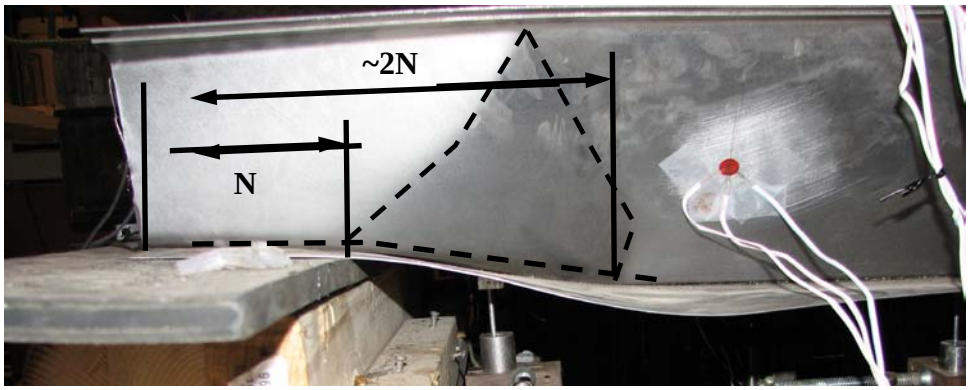

Figure 33: Side profile view of failure at end of the truss-core panel specimen from EOF loading substantially after ultimate capacity was established (dashed lines indicate yield lines resulting from buckling)

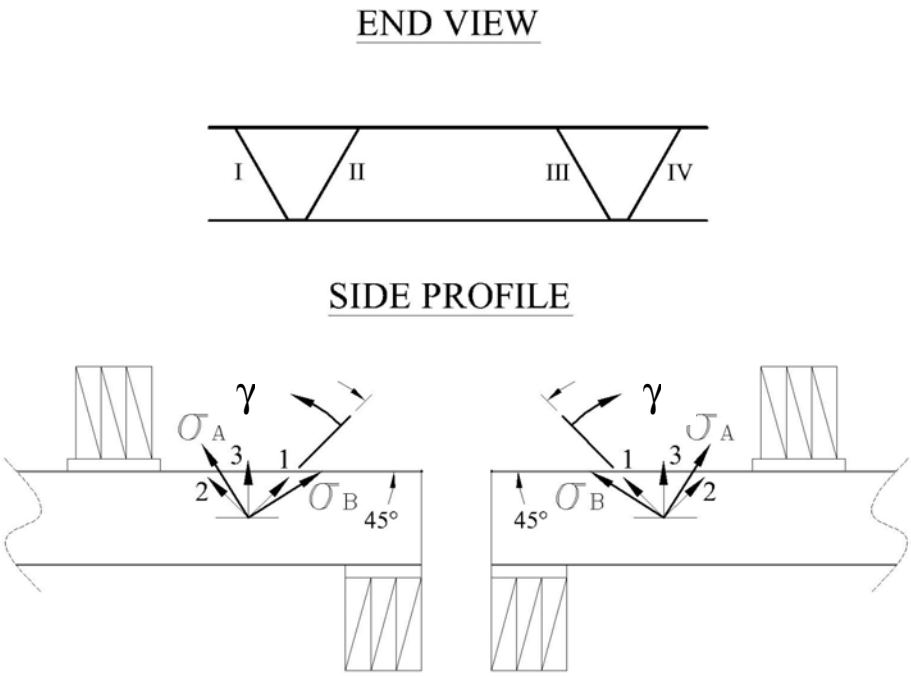

Figure 34: Stress magnitude and direction labels used for strain analysis

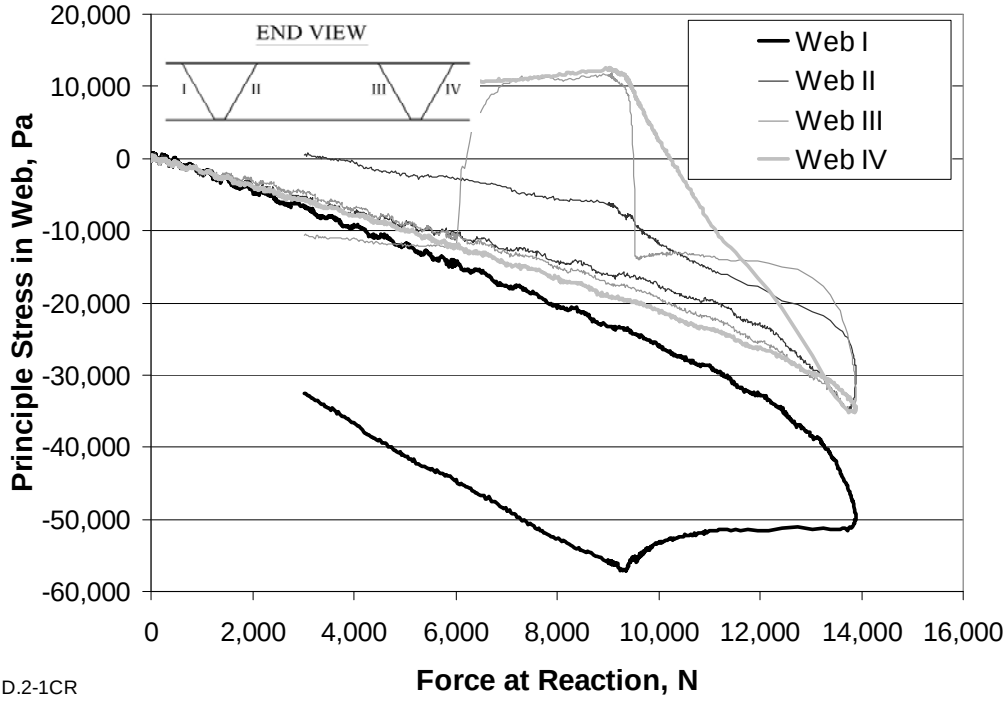

Figure 35: Measured principle compressive stress in each web of test D.2-1CR (F_y=197 MPa)

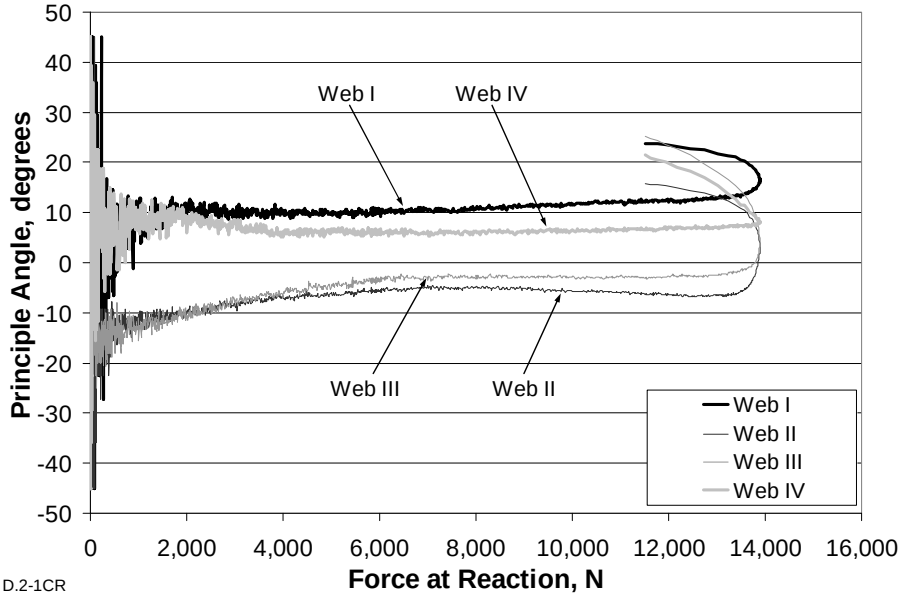

Figure 36: Measured principle stress angle in test D.2-1CR

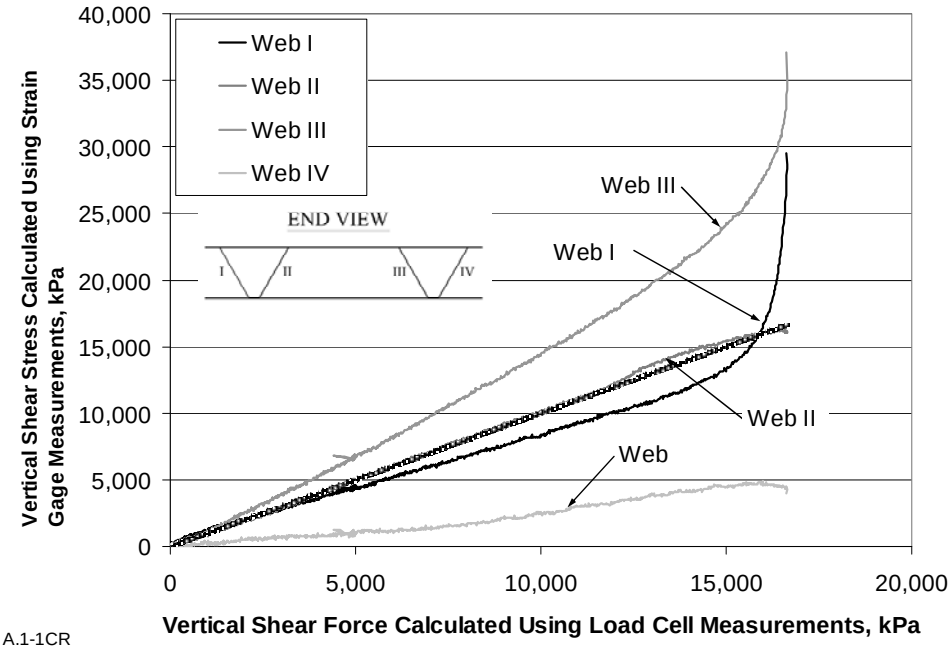

A.1-1CR

Figure 37: A.1-1CR vertical shear stress in each web

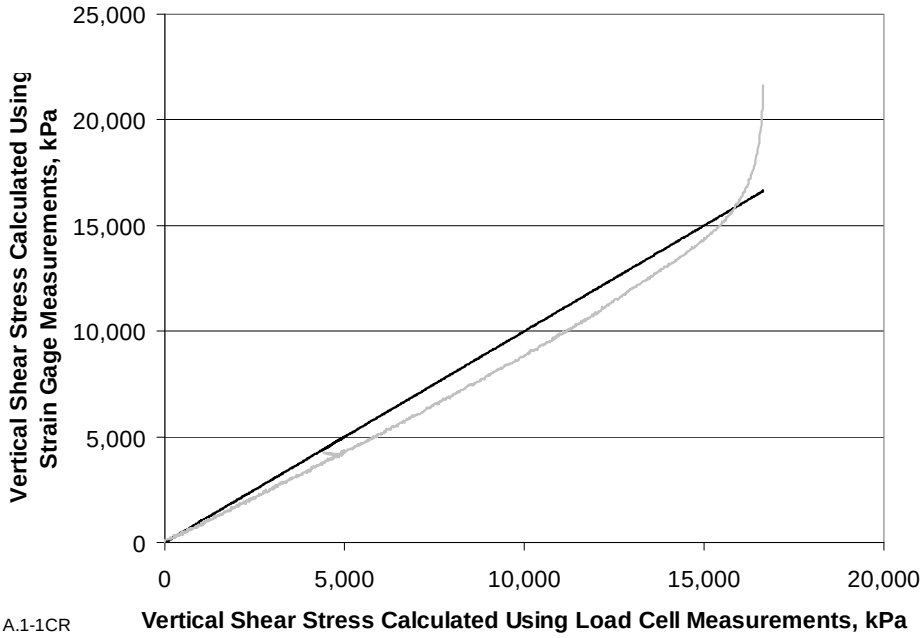

A.1-1CR

Figure 38: A.1-1CR total vertical shear stress

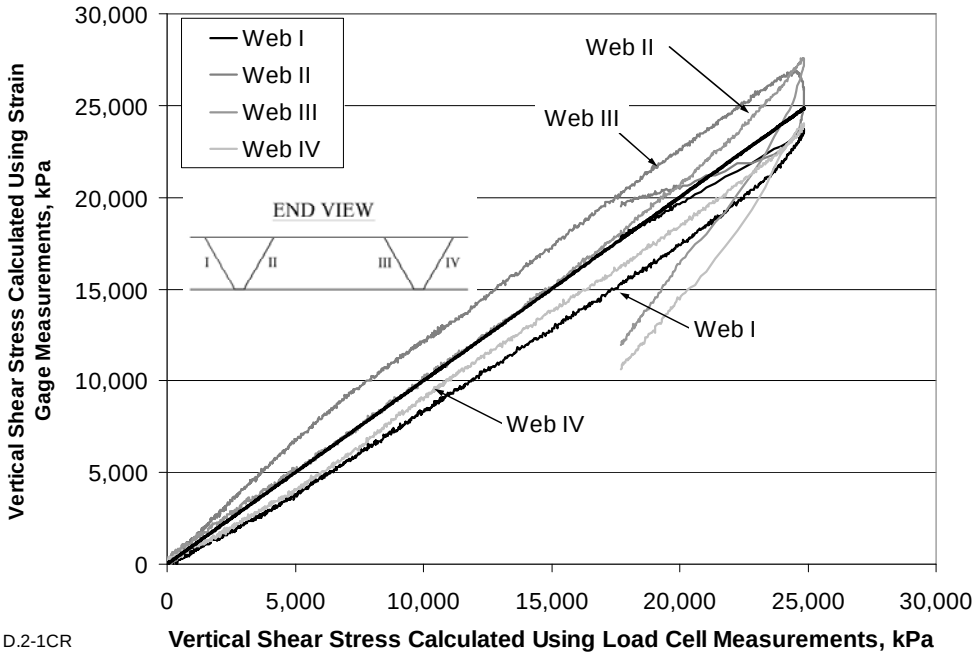

Figure 39: D.2-1CR vertical shear stress in each web

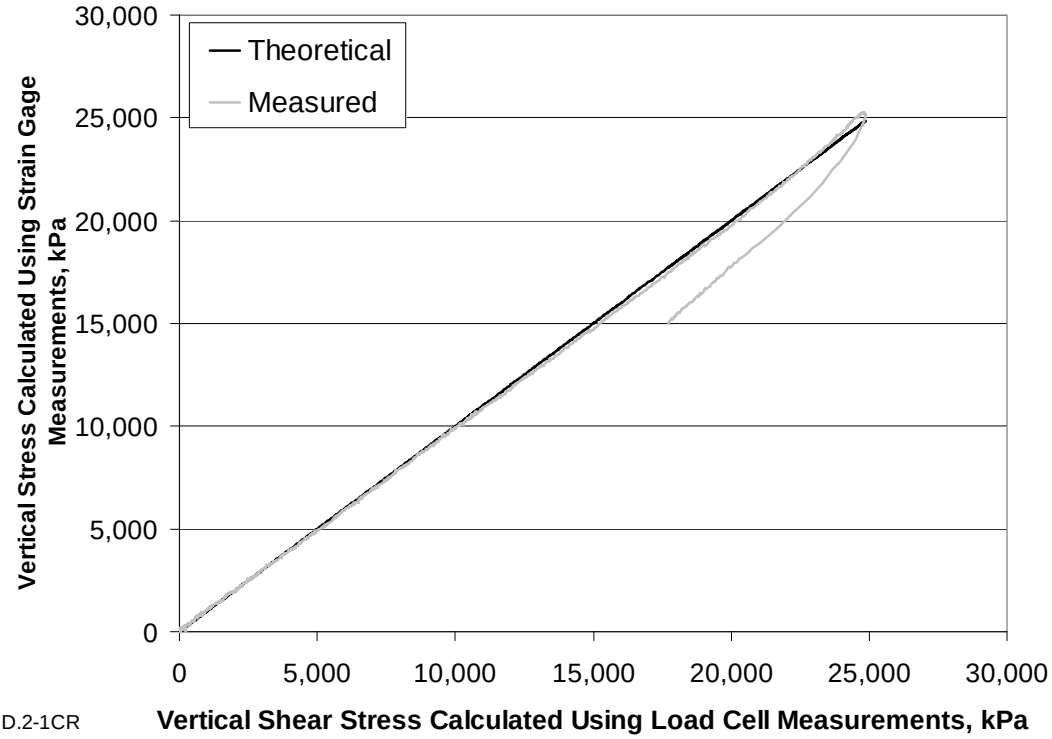

Figure 40: D.2-1CR average vertical shear stress

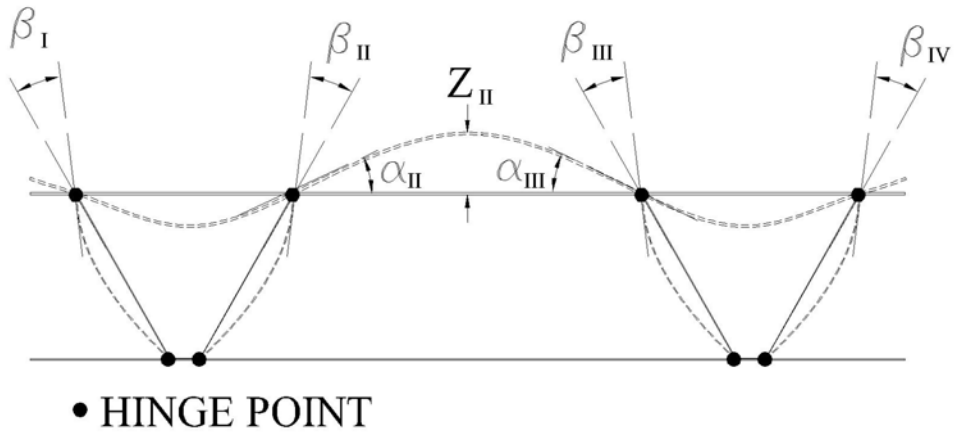

Figure 41: Schematic interpretation of deformed shape of the cross section at the crippling end prior to ultimate capacity (deformations not to scale)

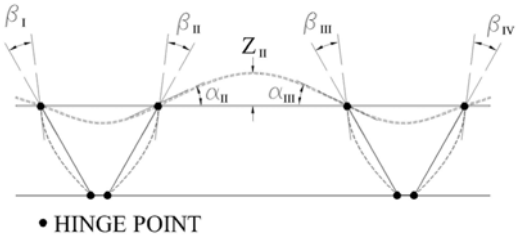

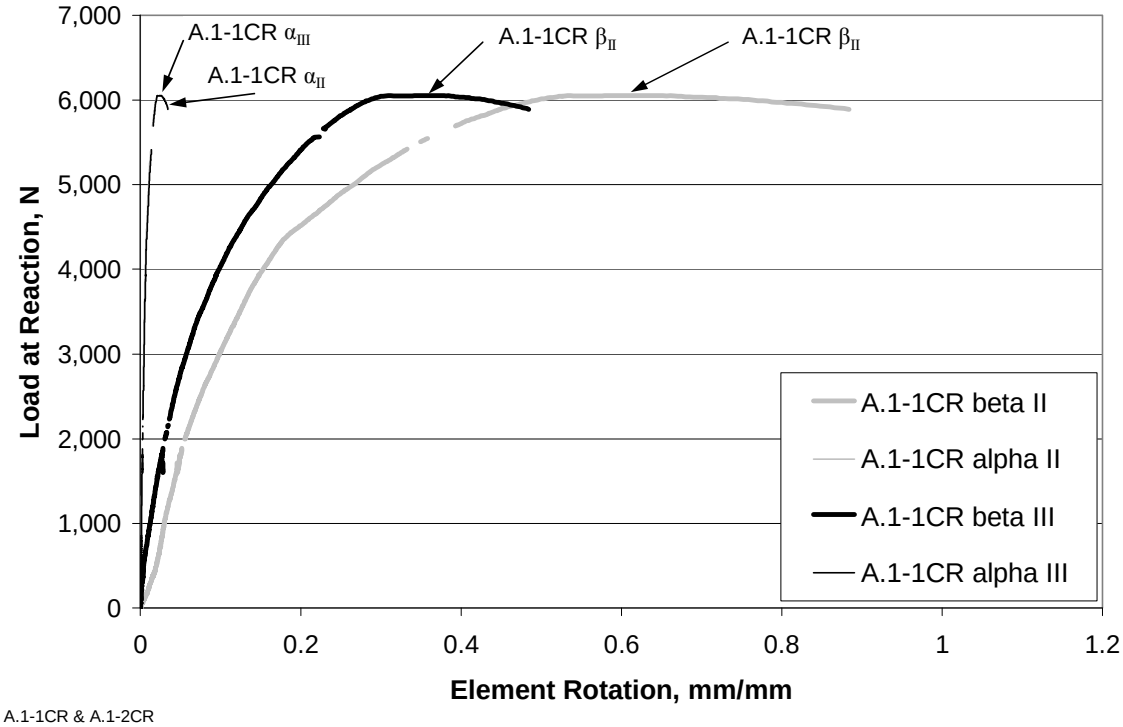

A.1-1CR & A.1-2CR

Figure 42: Measured web and face sheet rotations at the intersection points for tests A.1-1CR

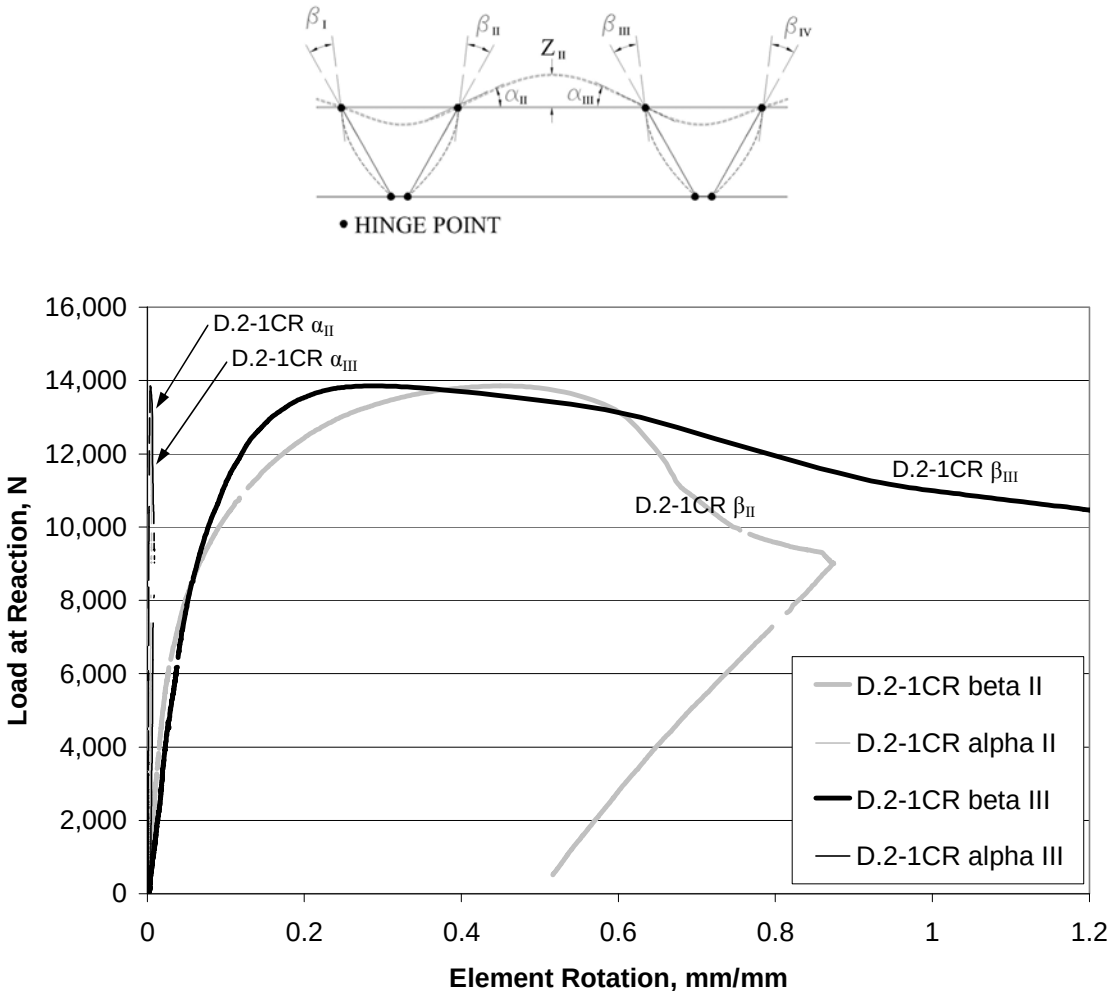

Figure 43: Measured web and face sheet rotations at the intersection points for tests D.2-1CR

(a)

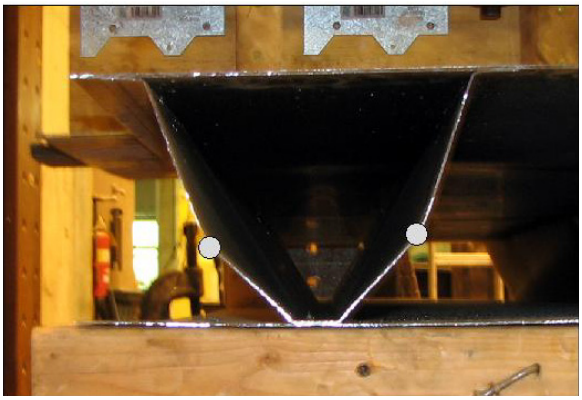

(b)

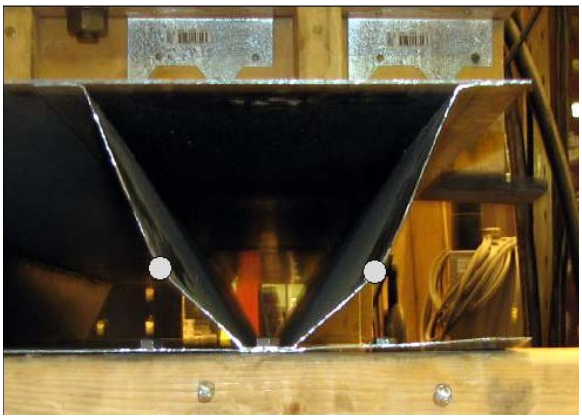

Figure 44: Observed web crippling failure for an (a) unfastened and (b) fastened specimen

5.3 Stiffened Plate Panel Web Crippling Results

Three stiffened plate web crippling tests were performed using Panel E (see Table 2). Web crippling tests were performed on each end. The panel was cut to provide a third sample. The relevant geometric features and material properties for these samples are noted in Table 7. For each stiffened plate web crippling test, reaction force vs. actuator displacement was recorded. The measured web crippling capacity corresponds to the ultimate load divided by the number of flutes (two, in the case of the stiffened plate prototype).

5.3.1 Test Observations

Reaction force vs. total actuator stroke for Test E.1-1CR (h/t_w = 107) is shown in Figure 45. This plot is typical of the data obtained for the three tests, and is similar to that obtained for the truss core panel prototypes. The initial slope is shallow, corresponding to compression of the elastomeric pads. Failure is indicated by a sharp drop in the load. Because the reaction force is the total load supported by the cross section, the web crippling force corresponds to the ultimate load divided by the number

of web flutes (two, in the case of the stiffened panel prototype). For tests E.1-1CR and E.1-2CR, the loss of load carrying capability is immediate after the peak load was achieved. For test E.1-3CR, the loss of load is more gradual (Figure 46).

Photographs of the buckled shapes indicate differences in the buckled shapes for the three tests. The buckled shape for tests E.1-1CR and E.1-2CR is similar. Figure 47 shows the buckled shape of the web for test E.1-1CR. In this figure, one of the webs has buckled inward (towards the center of the web). The buckled shape shows a plastic hinge, similar to that noted in the truss core web crippling tests, located approximately 1/3 of the section depth above the reaction surface. Folding of the cross section on this buckled side is evident. Figure 47 shows the side profile of the buckled web flute. A yield line is noted beginning at the plastic hinge and extending down to the face sheet at approximately 2N (N is the width of the bearing support). This feature is similar to that observed in the truss core web crippling test. For test E.1-3CR, both web flutes begin to deform towards the center of the specimen. Because there is no spot weld at the sample edge, the web flange lifts up from the bottom face sheet (Figures 48 and 49). The deformation of the web flute is gradual and does not exhibit the folded yield line observed in tests E.1-1CR and E.1-2CR.

5.3.2 Web Crippling Capacity

Measured and nominal web crippling capacity for each test is noted in Table 8. The measured web crippling capacity for tests E.1-1CR and E.1-2CR is 2.27 and 2.15 kN, respectively, while the capacity for test E.1-3CR is 1.81 kN. All three tests should have nearly the same web crippling capacity because these samples are from the same panel. However, the measured web crippling capacity for test E.1-3CR is approximately 20% lower. This reduction in strength is attributed to the weld condition at the end: there is no spot weld at the sample edge. As the earlier study of web crippling in truss core samples indicated, the bond between the web and face sheet is critical, leading to a "strapped" condition. The web crippling capacity for strapped conditions is much higher than for the unstrapped condition.

5.3.3 Evaluation of the Empirical Constants for Web Crippling

The ratios between the measured web crippling capacity P_{test} and nominal web crippling capacity P_n are also reported in Table 8. The measured crippling capacity is significantly greater than that predicted by the model for the unstrapped condition. For tests E.1-1CR and E.1-2CR, the measured capacity is nearly double that predicted by the model: P_{test}/P_n is 2.14 and 2.03 respectively. For test E.1-3CR, the measured capacity is 76% larger (P_{test}/P_n is 1.76).

Model predictions based on the strapped, unfastened condition more accurately predict the web crippling capacity. For tests E.1-1CR and E.1-2CR, the measured capacity is 9% and 4% greater than that predicted by the strapped, unfastened condition (P_{test}/P_n is 1.09 and 1.04 respectively). For test E.1-3CR, the measured web crippling capacity is less than that predicted by the strapped, unfastened condition. In this case the

strength is 87% of the model prediction (P_{test}/P_n is 0.87). This result is as expected because there is only one spot weld (for each web flute) along the bearing length for test sample E.1-3CR. The joint between the web and face sheet does not reflect a strapped condition.

Table 7: Stiffened plate panel web crippling specimens.

	Panel and Test	**Fastened to support**	***R/t*$_w$**	***N/t*$_w$**	***h/t*$_w$**	**Web Yield strength (MPa)**
h/t_w = 107	E.1-1CR	No	4.0	83	106.6	211
	E.1-2CR	No	4.0	83	106.6	211
	E.1-3CR	No	4.04	83	106.6	211

Table 8: Stiffened plate panel web crippling specimens.

	Test	P_{test} per web, kN (lb)	Unfastened P_n[1] per web, kN (lb)	P_{test} /P_n	Fastened P_n[1] per web, kN (lb)	P_{test} / P_n	Strapped, Unfastened P_n per web, kN (lb)	P_{test} / P_n
h/t_w = 107	E.1-1CR	2.27 (510)	1.06	2.14	1.38	1.65	2.08	1.09
	E.1-2CR	2.15 (483)	1.06	2.03	1.38	1.56	2.08	1.04
	E.1-3CR	1.81 (407)	1.06	1.71	1.38	1.31	2.08	0.87

[1] Nominal values calculated following the 2004 AISI Supplement using the coefficients for unstrapped, unfastened and unstrapped, fastened multi-web deck sections.

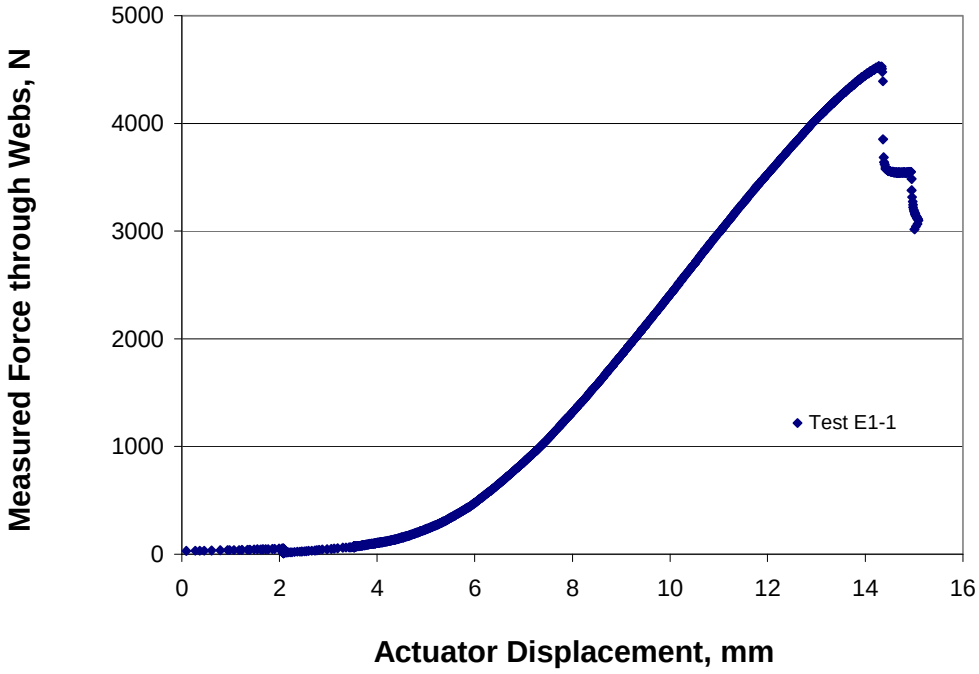

Figure 45: Measured force as a function of actuator displacement for Test E.1-1CR.

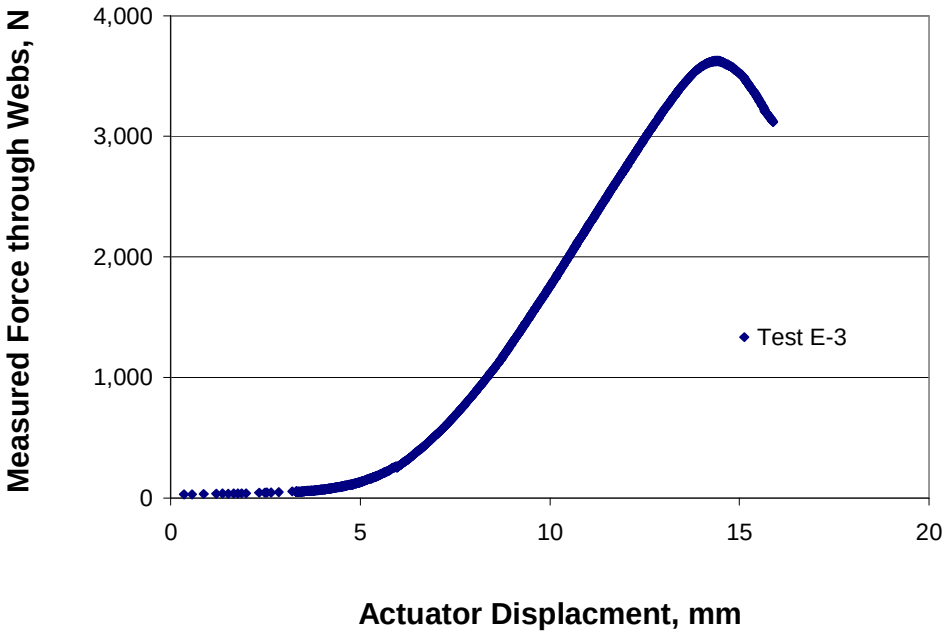

Figure 46: Measured force as a function of actuator displacement for Test E.1-3CR.

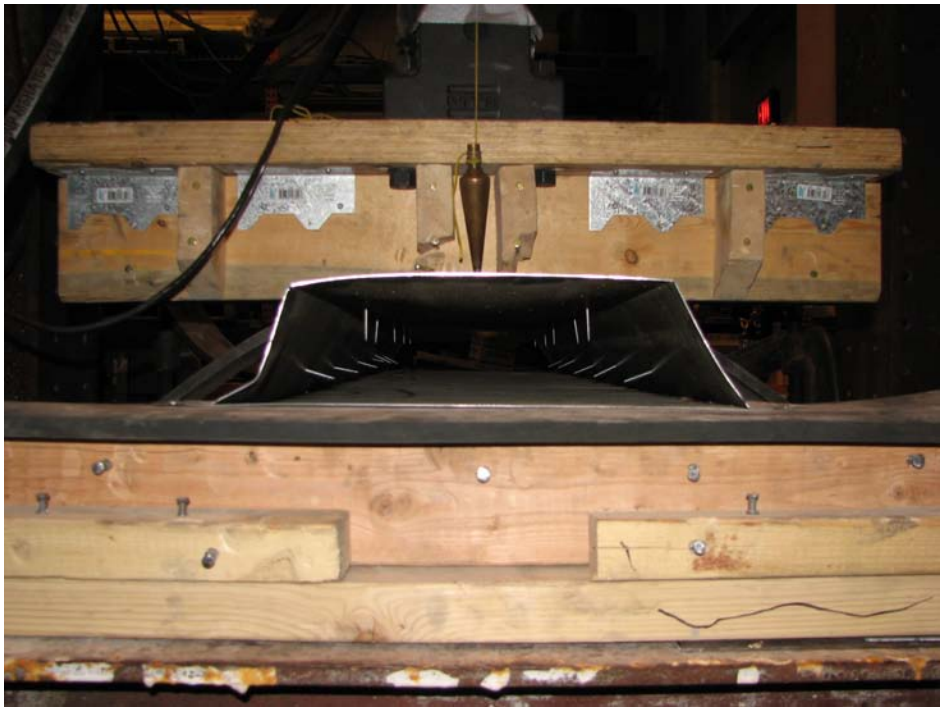

Figure 47: End profile view of failure for a stiffened plate panel specimen (from test E.1-1CR).

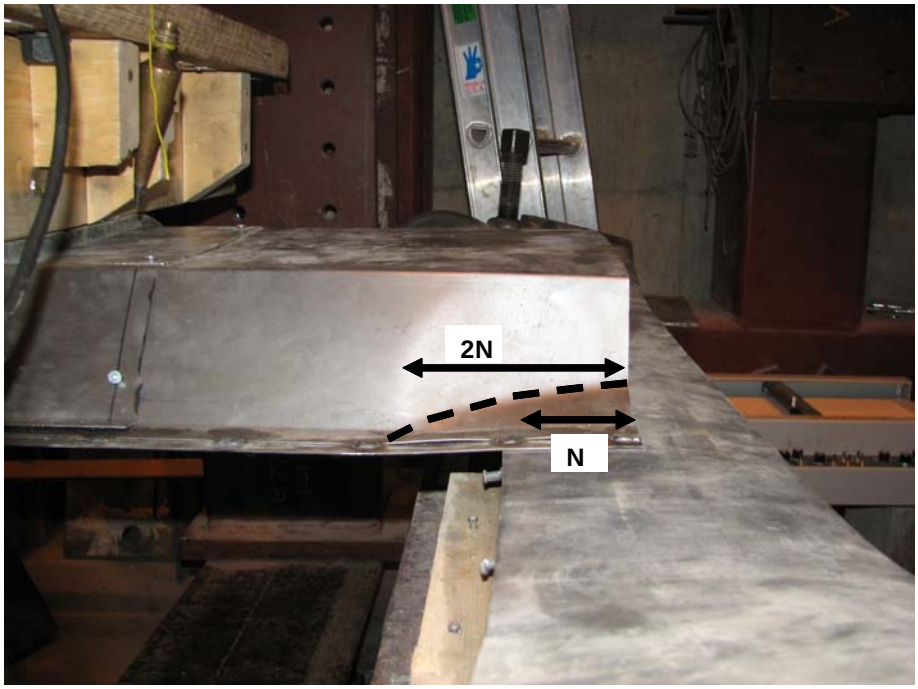

Figure 48: Side view of failure for a stiffened plate panel specimen (from test E.1-1CR). The dashed lines show the line of yielding.

Figure 49: End profile view of the spot weld region for test specimen E.1-3CR.

Figure 50: End profile view of failure for a stiffened plate panel specimen (from test E.1-3CR).

References

[AISI] American Institute of Steel and Iron. 2001. *North American Specification for the Design of Cold-Formed Steel Structural Members*. Washington, D.C.

[AISI] American Institute of Steel and Iron. 2002. *Cold-Formed Steel Design Manual.* Washington, D.C.

[AISI] American Institute of Steel and Iron. 2004. *Supplement to the North American specification for the design of cold-formed steel structural members*. Washington, DC.

Avci, O., Easterling, S. 2004. "Web Crippling Strength of Steel Deck Subjected to End One Flange Loading." *Journal of Structural Eng*., 130(5), 697-707.

Bhakta, B.H. 1992. "The effect of flange restraint on web crippling strength," thesis, presented to University of Missouri-Rolla in partial fulfillment of the requirements for the degree of Master of Science in Civil Engineering.

Beshara, B. and Schuster, R.M. 2000. "Web crippling data and calibrations of cold formed steel members." *Final Report*, American Iron and Steel Institute, Washington D.C.

Prabakaran, K., and Schuster, R.M. 1998. "Web crippling of cold formed steel members." *Fourteenth International Specialty Conference on Cold-Formed Steel Structures*, AISI, St. Louis, Missouri, 151-164.

Wallace, J.A., Schuster, R.M. 2004. "Web Crippling of Cold Formed Steel Multi-Web Deck Sections Subjected to End One-Flange Loading." *Proc. 17th Int. Specialty Conf. on Cold-Formed Steel Structures*, 2004, 171-185.

Yu, Wei-Wen. 2000. *Cold-Formed Steel Design*. John Wiley & Sons, Inc., New York, New York.

Appendix F: Hygrothermal Performance

1.0 Truss Core Panel

1.1 Thermal Performance

The thermal performance of the truss core panel is reported as the clear wall R-value. Both the United States Department of Energy (2002) and the International Energy Conservation Code (ICC, 2003) provide guidelines and suggestions for R-value for different building envelopes and climates. The ICC recommends R-5.3 m^2-K/W (R-30) for any site with less than 4500 heating degree days (HDD) and R-7.0 m^2-K/W (R-40) for sites with more than 6000 HDD. We assigned R-7.0 m^2-K/W for all sites with HDD greater than 4500. Table 1 lists the cities simulated with WUFI along with their heating and cooling degree days and required R-value. The required thickness of PUR (D_{ins}) was determined from the required R-value and the bulk thermal conductivity (k_{ins}) of PUR as reported by the manufacturer (0.025 W/m-K):

$$D_t = R(k_{ins}), \quad (1)$$

The contribution of the structural component and the additional sheathing to the R-value was neglected.

1.2 Moisture Transport

Moisture transport in the truss core panel is modeled for the assemblies which have a steep vapor barrier on only one side of the foam. The arrangement with steel on both sides of the foam is not modeled. Cities selected for this analysis are Atlanta, Boston, Houston, Los Angeles, International Falls, Miami, Phoenix, and Seattle.

The moisture performance of the panel was modeled with WUFI 2D-3.0 (Künzel and Kiessl, 1997; Künzel et al., 2005) using the cold year, WUFI-ORNL/IBP database. The WUFI simulations were carried out for a period of 3 years to ensure independency of the results on the initial conditions and to observe the seasonal as variations in moisture transport. Data from year 3 are used to assess the potential for failure due to i) condensation, ii) mold or mildew, iii) wood decay, and iv) metal corrosion. Because the model assumes local thermal equilibrium between the foam matrix and the air, it cannot be used to assess condensation within the foam. The risk of condensation at the PUR/steel interface was assessed based on the temperature difference between the metal surface of the truss core structural component and the dew point temperature of the air within the adjacent PUR. In all simulated cases, this temperature difference was insufficient to drive condensation. Gypsum and OSB are susceptible to mold at RH > 80%. Brief periods of high RH are acceptable as long as the monthly average is less than 80%. OSB is also susceptible to decay. The maximum allowable moisture content in the OSB layer is 20% (ASHRAE, 2005). A variety of criteria have been suggested to assess

the risk and rate of corrosion of carbon steel and other metals. Corrosion of carbon steel can begin at RH = 60%, but the rate of corrosion is very low for RH < 80%. ISO standards (9223 and 9224) specify that corrosion is likely if relative humidity at the metal surface is greater than 80% and the temperature is above freezing. The number of hours for which a metal surface is exposed to these conditions is termed the Time of Wetness (TOW). The ISO 9223 and 9224 standards provide corrosion rates based on the material and TOW (Table 2). We report the TOW at the interface of the truss core metal face sheet and the PUR. Although there are situations for which the TOW is low or zero, many climates pose some risk of corrosion and thus we recommend a protective coating be applied during manufacture.

The computational domains for WUFI models of the exterior and interior foam panels are shown in Figure 1a and b. The depth of foam was specified in each simulation to match the requirements of the site. The metal structure was treated as an impermeable boundary by setting the porosity of steel to a very low value (0.00001). WUFI does not include provisions for an impermeable material. For the panel with foam on the outside of the structure, the exterior finish of the panel is 12.5 mm (0.5 in.) OSB that adheres to the PUR and is put in place at the factory as part of the foaming process. A variety of roof finishes are possible. In the present study, we assumed that asphalt roof paper and shingles are attached to the OSB finish sheet. For the panel with foam on the inside of the structure, the interior face sheet is 0.5 in. gypsum board with primer and an acrylic paint finish. The integral metal roof is not included in the model because the interior face sheet of the steel structure provides an impermeable boundary condition for moisture transport.

The interior surface boundary conditions were set within WUFI to represent typical conditions. The interior temperature is 20 to 22 °C and the relative humidity has a mean value of 50 ±10%. Exterior temperature and relative humidity were specified within WUFI for each site. Convective thermal boundary conditions were specified at both exterior and interior surfaces. The specified heat transfer coefficients are 18 and 9 W/m^2-K, respectively. These values represent forced convection and long wave emission on the exterior and natural convection on the interior. The sky temperature and the ambient temperature were assumed equal. Symmetry boundary conditions were set at the edges of the panel. The initial temperature and relative humidity were set to 20°C and 80%, respectively. The material properties required by the model are listed in Table 3.

The results of the simulations are summarized in Tables 4 and 5 for the exterior and interior foam panels, respectively. For the exterior foam panel, the steel structure provides a vapor barrier at the interior of the panel. Moisture transport is from the exterior and thus outdoor conditions control hygrothermal performance. Based on conventional building practice, this panel was expected to perform best in cold climates. The conventional rule of thumb is in severe cold climates building assemblies need to be protected from moisture transport from the interior while in hot and humid climates, building assemblies need to be protected from moisture transport from the exterior (Lstiburek, 2002, Künzel, 2005). The present study shows that the exterior foam panel

performs well in cold climates and in warm, dry climates. It has excellent hygrothermal performance in Boston, International Falls, Los Angeles, Phoenix and Seattle. On the other hand, in Atlanta, Houston, and Miami, there is risk of corrosion of the steel at the PUR/metal interface unless the steel is adequately protected by galvanization. Transport of warm, humid outdoor air through the foam in these cities yields undesirably high humidity levels at the PUR/metal interface during portions of the year. The high RH at the PUR/metal interface is due to cooling of warm moist air as it diffuses through the foam layer. To illustrate the annual variation of RH and temperature at the PUR/metal interface, data for Miami are plotted throughout the year in Figure 2. The temperature at the interface is relatively constant reflecting the indoor temperature. The RH at the interface fluctuates depending on outdoor conditions. RH exceeds 80% except for brief periods during the winter; TOW = 8345 hr/year. In Houston an unprotected metal face sheet will be at risk of corrosion from May to January; TOW = 5045 hr/year. In Atlanta, TOW= 2248 hr/year. We recommend galvanization of the metal structure to slow corrosion in all climates. The risk of mold and mildew in the OSB finish sheet in Houston can be alleviated by use of a borate or copper treated OSB.

For the interior foam panel, the steel structure provides a vapor barrier at the exterior of the panel. Moisture transport is from the interior conditioned space. Based on conventional building practice, the panel was expected to perform best in warm climates. The WUFI data show that the interior foam panel has excellent hygrothermal performance in Los Angeles, Miami, and Phoenix. In Atlanta, Houston, and Seattle, the only potential problem is corrosion of unprotected metal at the PUR/steel interface. This potential problem is attributed to periods of cool weather in these cities. During the winter months, water vapor is cooled as it moves from the conditioned space through the gypsum and foam insulation and thus the RH at the PUR/metal interface can reach levels that pose a risk of corrosion of unprotected steel. To illustrate the annual variation of RH and temperature at the PUR/metal interface, data for Houston are plotted throughout the year in Figure 3. The temperature at the interface reflects outdoor conditions. The RH at the interface fluctuates inversely with outdoor temperature. RH exceeds 80% during the winter months. Unprotected steel will be at risk of corrosion for 850 hr/year. In Seattle and Atlanta where ambient temperatures are lower, an unprotected metal face sheet will be at risk of corrosion for much of the year. In Seattle, TOW = 8596 hr/yr. In Atlanta, TOW = 2626 hr/year. As in the exterior foam panel, we recommend galvanization of the steel structure to lessen the risk of corrosion in all climates.

2.0 Stiffened Plate Panel

As with the truss core panel, the structural portion of the stiffened plate panel forms an impermeable boundary for moisture transport. Because the foam is always located on the exterior side of the stiffened plate panel, the moisture performance of the stiffened plate panel is similar to that of the truss core panel with exterior foam. Differences in hygrothermal performance arise due to the fact that the stiffened plate structure extends into the foam layer. In the truss core panel, a uniform layer of foam is

applied in order to achieve the required R-value. In the stiffened plate panel, the foam depth is variable.

2.1 Thermal Performance

The PUR foam fills space between each web and extends above the structural panel as required to achieve R-5.3 m^2-K/W for Climate I and R-7.0 m^2-K/W for Climate II. The steel webs provide a conductive path through the foam and consequently the portion of the foam between the webs is less effective per unit depth than the foam above the hat sections.

The overall depth of foam required to achieve the target R-values for Climates I and II for representative panels was determined from a two-dimensional finite element model of conduction in the metal/foam assembly. The computational domain is a symmetric section comprised of one hat section as illustrated in Figure 4. The dimensions of the modeled panels are listed in Table 6. Isothermal boundary conditions were applied at the top and bottom surfaces. The specified temperature gradient is 25 ºC. Symmetry conditions were applied at the lateral edges. Thermal conductivity was assumed constant within each material (k_{steel} = 51.9 W/m-K for cold rolled steel, and k_{PUR} = 0.025 W/m-K). The objective was to determine the minimum depth of foam *H* required above the hat sections to achieve the desired R-value.

The space within the hat sections was assumed to contain air. In cases where the temperature inside the house is warmer than the temperature outside, natural convection will increase the rate of heat transfer in the air space compared to conduction in air. To account for this effect, an effective thermal conductivity k_e defined as the value for which the heat transfer by conduction would be equal to the heat transfer from natural convection, i.e.

$$q'' = h\Delta T = k_e \frac{\Delta T}{L}, \tag{2}$$

where h is the film coefficient for natural convection and L is an appropriate length scale defined here as height of the hat section (184 mm). Using the Nusselt number for natural convection,

$$k_e = Nu k_{air}, \tag{3}$$

where k_{air} is the thermal conductivity of air at the average temperature within the hat. The Nusselt number is estimated from the published correlation for horizontal cavities:

$$Nu = 0.069 Ra^{1/3} Pr^{0.074} \quad 3x10^5 < Ra < 7x10^9. \tag{4}$$

A temperature gradient of 5 K was assumed between the two surfaces of the cavity, yielding Ra = 3×10^6, Nu = 9.57 and $k_e = 0.239$ W/m-K.

The geometry was modeled in ANSYS using PLANE55 elements with a maximum edge length of 10 mm along each of the steel surfaces. The nodal spacing was refined until the computed R-value differed by less than 1×10^{-3}. The R-value was determined from numerical integration of heat flux along the bottom surface of the panel. The depth of foam required to achieve R-5.3 and R-7.0 m^2-K/W was determined iteratively. The R-value resulting from an initial guess for *H* was calculated, from which the required change ΔR to meet the given value was determined. *H* was then varied according to $\Delta H = k_{PUR}\Delta R$. The process was repeated until the *R* was within ±0.03 of the desired value.

To achieve R-5.3 m^2-K/W requires 82 mm of foam on top of the 184 mm deep webs. To achieve R-7.0 m^2-K/W requires 124 mm of foam on top of the webs. These results indicate that the part of the panel containing the hat sections provides about R-2.0 m^2-K/W. The stiffened plate panel therefore requires more foam than the truss core panel to meet a given R-value. In cases where the stiffened plate panel provides no clear structural benefit over the truss core panel, the truss core is likely to be more economical in terms of foam use.

Representative results from the FE analysis are presented in Figures 5 and 6. Figure 5 is a plot of the temperature distribution within the foam layer of the Climate II-10/12 stiffened panel design with R-7.0 m^2-K/W. The temperatures close to the web are nearly equal to the indoor air temperature, thus demonstrating the thermal bridging caused by the webs. The figure shows that the temperature difference between the two surfaces of the hat section is about 3 K. The assumption of a 5 K gradient in calculating the Nusselt number is therefore reasonable. Figure 6 is a plot of the heat flux through the same panel. Note that the heat flux through the webs is orders of magnitude larger than the flux anywhere else in the panel, once again indicating the thermal penalty imposed by the webs.

2.2 Moisture Performance

A moisture analysis was performed for the stiffened plate design in Phoenix and Houston. These two sites were selected to represent warm, dry and warm, humid climates, respectively. As with the truss core panel, four potential failure modes were examined: condensation, mold or mildew, wood decay, and metal corrosion.

The computational domain for the WUFI model is shown in Figure 7. The geometry is the climate I design for a 6/12 roof slope (see Table 6). A climate I panel was selected for this analysis because it has the thinnest foam layer and is thus most susceptible to moisture problems. The hat sections were designed to be trapezoidal; the modeling capabilities of WUFI, however, are limited to rectangular elements with edges oriented in the *xy*-coordinate directions. Therefore, the webs were approximated at rectangular hats of width equal to the average width of the (actual) trapezoidal hats. The

air layer within the hats was modeled using material properties built into WUFI. Several options were available for air; the one chosen has an effective thermal conductivity of 0.23 W/m-K, which is close to the effective thermal conductivity (0.239 W/m-K) calculated for natural convection. The roof finish was assumed to be asphalt roof paper and shingles attached to a layer of OSB.

The internal surface boundary conditions in the stiffened plate analysis were the same as for the truss core analysis. As with the truss core analysis, convective boundary conditions were applied to the interior and exterior surfaces with heat transfer coefficients of 9 and 18 W/m^2-K respectively. Symmetry boundary conditions were set at the edges of the panel. The simulation was run for three years with one hour time steps, and assessments of the performance were based on data from the third year. The initial temperature and relative humidity were 20°C and 80% everywhere in the panel.

The stiffened plate panel has no anticipated moisture risks in Phoenix. The annual variation in RH and temperature at the interface between the PUR and the metal hat section is plotted in Figure 8. The RH fluctuates with outdoor conditions. Because the indoor air is cooler than the outdoor air for much of the year, the RH at the interface tends to be slightly higher than the outdoor RH but it never exceeds 60%. The temperature of the steel is close to the indoor temperature.

In Houston, the stiffened plate panel with R-5.3 m^2-K is at risk for metal corrosion, with a TOW of 5351 hr, slightly greater than that of the truss core panel in Houston. This result was anticipated from the analysis of the truss core panel. The variation in temperature and RH for Houston at the interface between the hat and the adjacent PUR is plotted in Figure 9. The RH exceeds 80% for much of the year; TOW =. 5351 hr/yr. Corrosion is slowed by galvanization. However additional steps are required to prevent condensation along the top surface of the hat section during the months of August and September. Contour plots of the temperature and relative humidity within the panel for August 1 at 5:00 PM are shown in Figure 10. The temperature and relative humidity at the top of the hat section are higher than at the other steel surfaces.

Condensation is prevented by increasing the depth of foam beyond that required for R-5.3 m^2-K. To show that the use of a thicker foam layer solves the condensation problem, the analysis was repeated for a panel foamed to 132 mm above the hats. This depth of insulation above the hats is the same as that used for the truss core panel. The total depth of foam is 316 mm, which provides R-7.3 m^2-K/W. The annual temperature/RH variation for this panel is plotted in Figure 11. Note that the variations in RH are slightly attenuated with the use of thicker foam. The maximum RH at the interface decreases from 96% to 92%, while the temperature remains almost unchanged. The result is that the occurrence of condensation is eliminated.

Table 8 includes the required R-values to prevent moisture problems in panels designed for climate I and II. Values are presented in S.I. and English units for the convenience of the reader.

Table 1: Sites simulated with WUFI

Site	Heating degree days (HDD)[1]	Cooling degree days (CDD)[2]	R-value (m^2-K/W)
Atlanta	2827	1810	5.3
Boston	5630	777	7.0
Houston	1525	2893	5.3
International Falls	10,264	233	7.0
Los Angeles	1274	679	5.3
Miami	149	4361	5.3
Phoenix	1027	1226	5.3
Seattle	4797	173	7.0

[1] http://www.ncdc.noaa.gov/oa/climate/online/ccd/nrmhdd.txt

[2] http://www.ncdc.noaa.gov/oa/climate/online/ccd/nrmcdd.txt

Table 2: Corrosion rates for steel from ISO standards 9223 and 9224

	First year (ISO 9223)		Average for the first 10 years (ISO 9224)		Steady state (ISO 9224)	
Atmospheric pollution level	Low[1]	High[2]	Low	High	Low	High
TOW [hr/yr]						
≤10	<1.3	1.3 - 25	<0.5	0.5 - 5	<0.1	0.1 – 1.5
10 to 250	<1.3	50 - 80	<0.5	12 - 30	<0.1	6 - 20
250 to 2500	1.3 - 50	80 - 200	0.5 - 12	30 - 100	0.1 – 6	20 - 90
2500 to 5500	25 - 50	80 - 200	5 - 12	30 - 100	1.5 – 6	20 - 90
> 5500	25 - 80	80 - 200	5 - 30	30 - 100	1.5 - 20	20 - 90

[1] Low pollution level = deposition rate of SO_2 and chloride are less than 10 and 3 mg/(m^2d), respectively.

[2] High pollution level = deposition rate of SO_2 is between 80 and 200 mg/(m^2d) and deposition rate of chloride is between 300 and 1500 mg/(m^2d).

Table 3: Material property values specified in WUFI

	Density [kg/m^3]	Porosity	Specific heat [J/kg·K]	Thermal conductivity [W/m·K]	Water vapor diffusion resistance dry
Asphalt roof paper	909	0.001	1500	10	2014
OSB	650	0.95	1880	0.092	813
Gypsum	625	0.7	870	0.16	7
PUR	39	0.99	1470	0.025	88.9
Steel	7870	0.00001	486	40	10^6
Air	1.3	1	1000	0.23	0.38

Table 4: Summary of moisture risks for the exterior foam truss core panel

Site	Potential risk	
Boston International Falls Los Angeles Phoenix Seattle	None	
Atlanta	Corrosion (Aug-Oct) TOW=2248 hr/yr	
Houston	Corrosion (May-Dec) TOW=5045 hr/yr	Mold/Mildew in OSB (Dec-May)
Miami	Corrosion TOW=8345 hr/yr	

Table 5: Summary of moisture risks for the interior foam truss core panel

Site	Potential risk
Los Angeles Miami Phoenix	None
Atlanta	Corrosion (Dec-Apr) TOW=2626 hr/yr
Houston	Corrosion (Jan-Mar) TOW = 850 hr/yr
Seattle	Corrosion TOW=8596 hr/yr

Table 6: Geometry of the stiffened plate designs used for the thermal analysis

Application	**Horizontal Roof Span (m)**	***P* (mm)**	**t_w (mm)**	**t_b (mm)**	**f_t (mm)**	**Θ**
Climate I-6/12	6.1	400	1.28	0.85	57	70°
Climate I-10/12	6.1	480	1.68	0.96	115	70°
Climate II-6/12	6.1	480	1.60	0.91	103	65°
Climate II-10/12	6.1	600	2.40	0.87	181	60°

Table 8: Summary of moisture risks for the stiffened plate panel

Site	Potential risk	
Phoenix	None	
Houston	Corrosion (April–Dec) TOW = 5351 hr/yr	Condensation (Aug–Sept)
Houston (thick foam layer)	Corrosion (April–Dec) TOW = 5348 hr/yr	

Table 8: Specifications of foam depth and R-value for the stiffened panel with interior sheet designed for a 20 ft (6.1 m) horizontal span.

Climate and roof slope	Structure depth D [in., mm]	Foam depth on top of webs H [in., mm]	R Value (ft^2-°F-hr/Btu, m^2-K/W)	Panel depth D_p [in., mm]
I-6/12	7.25, 184	5.22, 133	43, 7.6	12.47, 317
I-10/12	7.25, 184	5.22, 133	39, 7.4	12.47, 317
II-6/12	7.25, 184	5.22, 133	42, 6.9	12.47, 317
II-10/12	7.25, 184	5.22, 133	41, 7.2	12.47,317

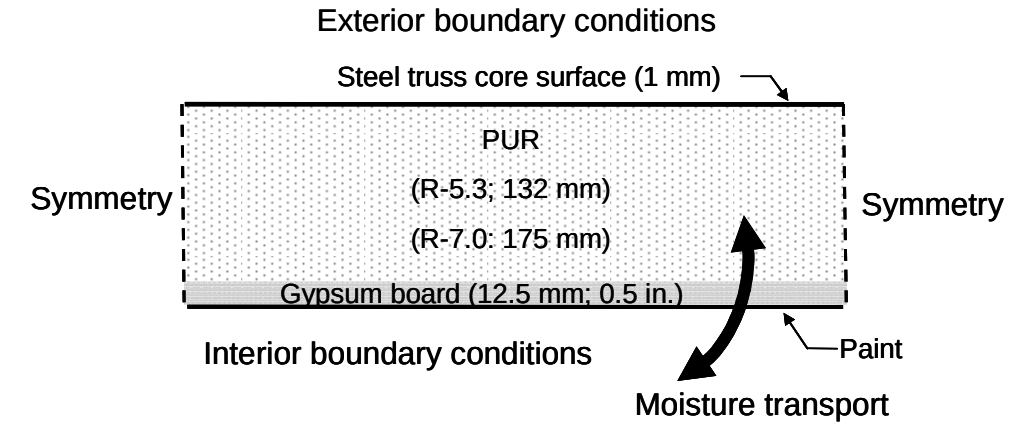

(a)

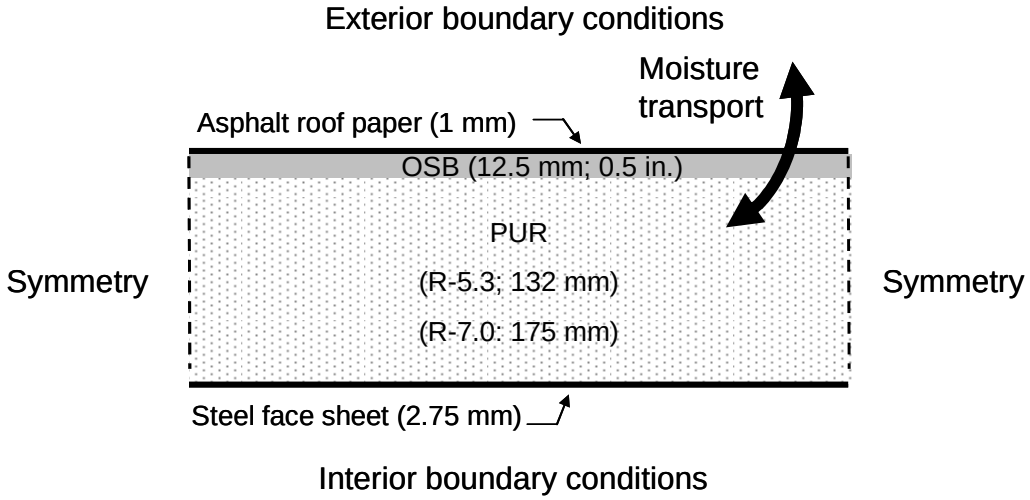

(b)

Figure 1: Hygrothermal model of truss core panel assemblies (not to scale) (a) exterior foam panel and (b) interior foam panel

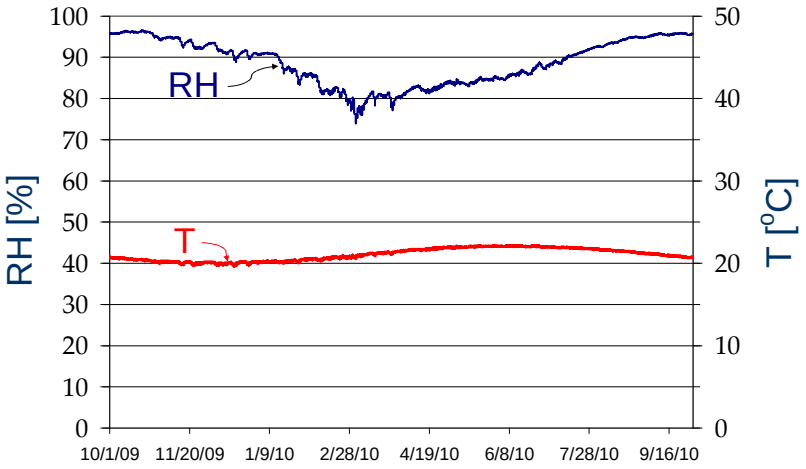

Figure 2: Relative humidity and temperature at the PUR/steel interface of a truss core panel with exterior foam in Miami

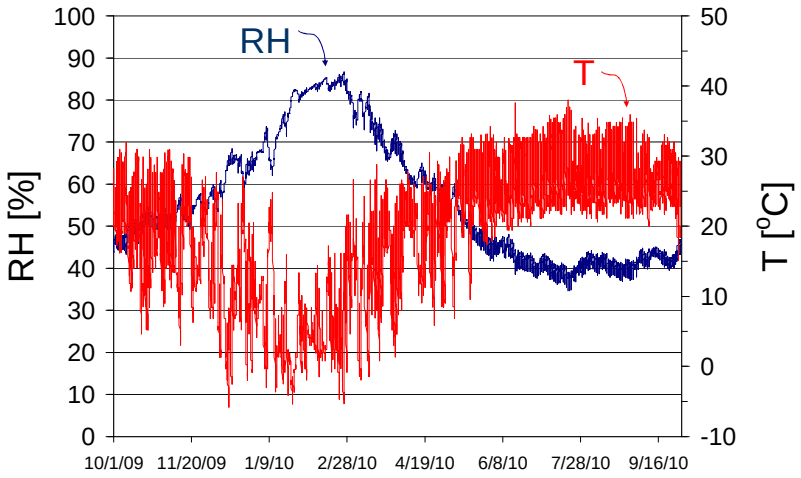

Figure 3: Relative humidity and temperature at the PUR/steel interface of a truss core panel with interior foam in Houston

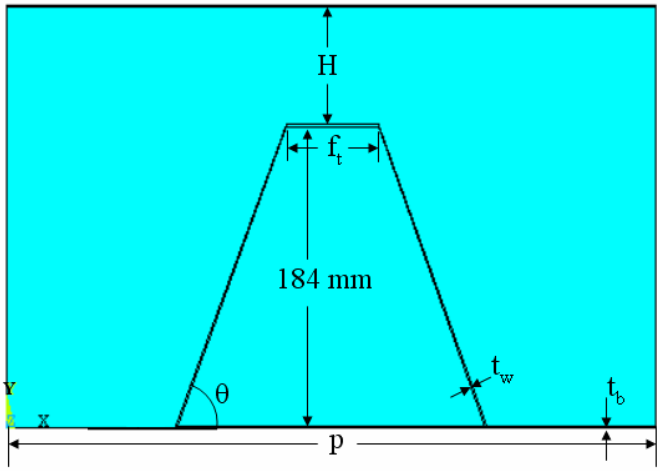

Figure 4: Geometry of the stiffened plate for thermal analysis

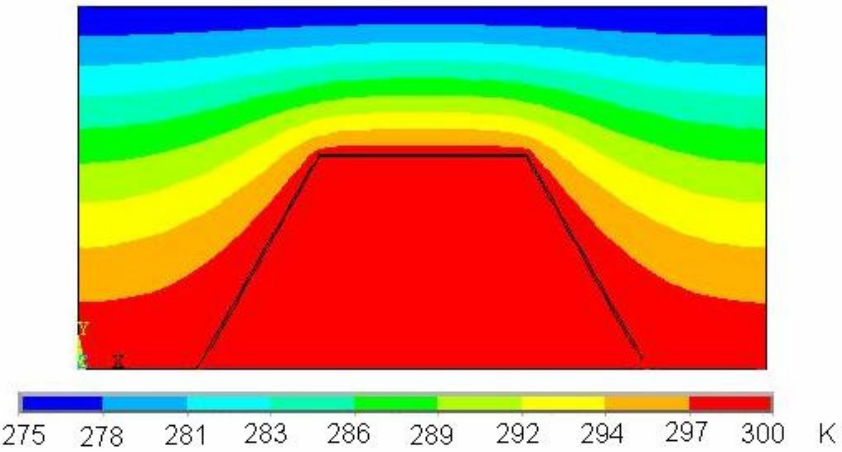

Figure 5: Temperature iso-contours for the Climate II-10/12 stiffened panel design with R-7.0 m^2-K/W

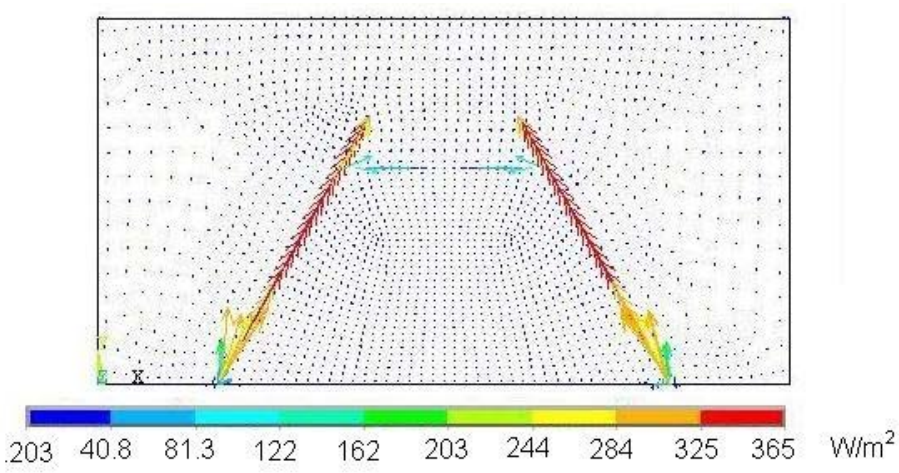

Figure 6: Vector plot of the heat fluxes for the Climate II-10/12 stiffened panel design with R-7.0 m^2-K/W

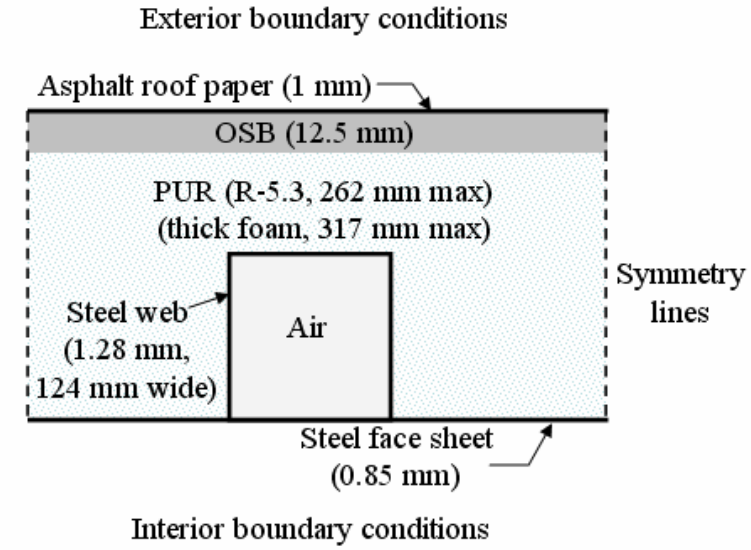

Figure 7: Hygrothermal model of the stiffened plate panel assembly (not to scale)

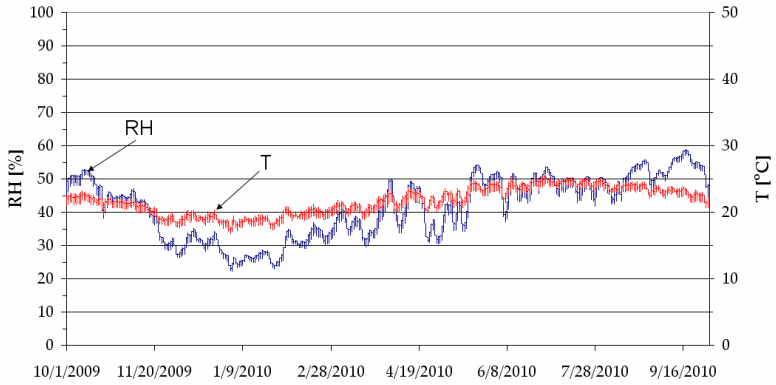

Figure 8: Relative humidity and temperature at the PUR/steel interface of the stiffened foam panel designed for climate I and a 6/12 roof pitch in Phoenix

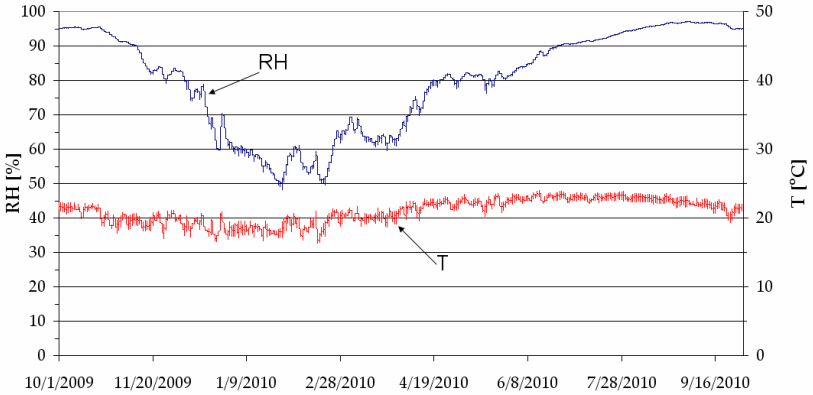

Figure 9: Relative humidity and temperature at the PUR/steel interface of a stiffened foam panel designed for climate I and a 6/12 roof pitch in Houston. R = 5.3 m^2-K/W

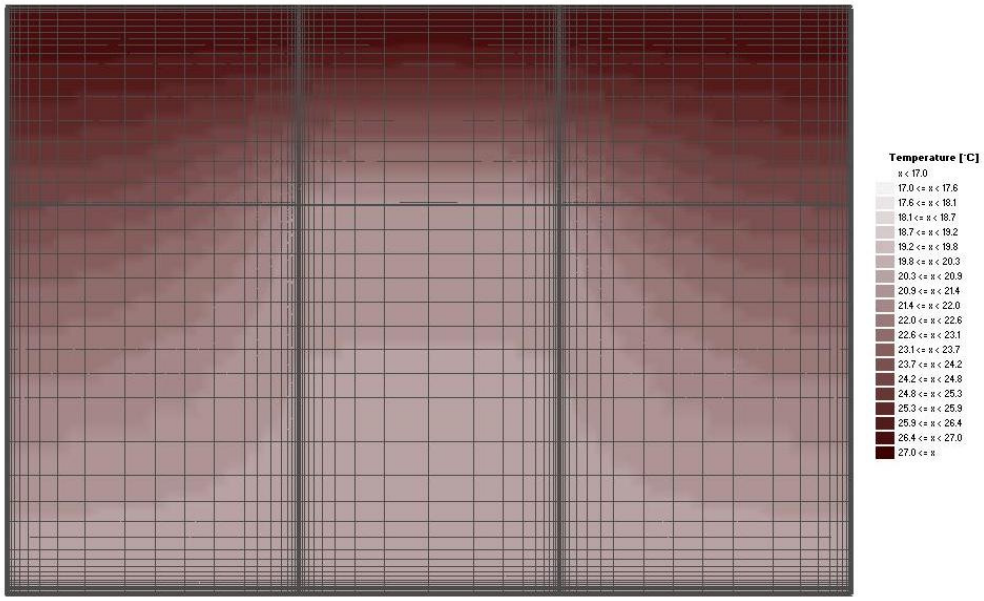

(a)

(b)

Figure 10: Moisture analysis for an R-5.3 m^2-K/W **stiffened plate panel in Houston on Aug 1 at 5:00 PM (a) contour plot of the temperature distribution and (b) contour plot of the relative humidity**

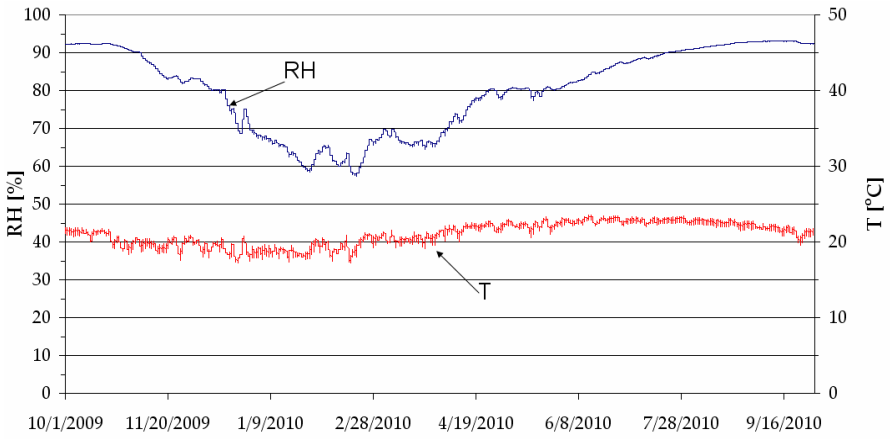

Figure 11: Relative humidity and temperature at the PUR/steel interface of a stiffened plate panel designed for climate I and a 6/12 roof pitch in Houston. R = 7.3 m^2-K/W.

Appendix G: Parametric Design Study

1.0 Overview

In this appendix the results of a parametric study of truss core and stiffened plate panel designs are presented. The purpose of this parametric study is to (1) determine which of the design criteria most affect the panel design, and (2) compare truss core and stiffened plate panel designs for a range of typical house geometries and for the three climate zones. The study focuses on the impact of design parameters on the structural component of the panel.

Panels were designed for a gable roof house with soffit to ridge horizontal spans ranging from 3.0 to 8.0 m (at discrete lengths of 3, 3.6, 4, 5, 6.1, 7 and 8 m). Two roof slopes were considered: a 6/12 pitch and a 10/12 pitch. Two structural component depths were considered, 140 mm and 184 mm. These depths correspond to standard lumber depths for a 2X6 or 2X8, respectively. Face sheet thickness and web thickness t_w ranging from 0.85 mm to 2.5 mm were considered. The minimum sheet thickness, 0.85 mm, was selected to reduce the risk of panel damage during handling and transportation. The maximum sheet thickness was based on the limitations of cold forming of the sheet metal webs. To limit the number of welds, the minimum pitch (web spacing) p was set to 0.4 m. Panels are manufactured in 2.4 m widths. A web spacing of 0.4 m is equivalent to 6 webs for a 2.4 m wide panel. The support length (bearing surface for web crippling) at the ridge and soffit is 78.1 mm for a roof pitch of 6/12 and 90.9 mm for a roof pitch of 10/12. These values are based on a horizontal bearing length of 69.8 mm provided by the ridge and soffit beams. The maximum allowable structural component weight is 340 N/m^2 for climates I and II and 570 N/m^2 for climate III. These weight limits are established to ensure that panel design weights are comparable to typical roof weights.

The weight of the panel structural component is chosen as the objective function to be minimized. The lightest weight panel for each combination of span length and slope was determined by using the custom MATLAB program (see section 3.1). Feasible designs are those that can support the loading imposed and satisfy the constraints imposed. The constraints include limits established by failure modes and limits on geometry (such as panel sheet thicknesses or slenderness ratios) and structural component weight. The safety factors for the various failure modes were selected following the AISI recommendations for light gage steel structures: 1.0 for flexure (deflection); 1.67 for moment capacity/buckling; and 2.25 for web crippling. Panel loading is as described in Appendix C for the case of 90 mph wind loads. Material properties are summarized in Appendix B.

The results of the parametric study are presented as follows: (1) a study of the relative importance of the various failure criteria for truss core panels, (2) a comparison of truss core and stiffened plate panels, and (3) a listing of weight optimized designs of truss core and stiffened plate panels for gable roof houses with ridge to soffit horizontal spans ranging from 3.0 m to 8.0 m.

2.0 Evaluation of Failure Criteria in Truss Core Panel Designs

In this section designs of truss core panels for the three climate zones are presented for a range of horizontal span lengths. In addition, a series of plots which show the relative importance of the failure criteria are presented for each panel design. The trends identified are common to the stiffened plate panel designs. The design details for both types of panels are presented in section 4 of this appendix.

Figure 1 shows truss core minimum weight panel designs for each climate zone and roof pitch for horizontal spans that range from 3 to 8 m. Panel structural component weights range from 186 N/m^2 for a panel designed for a 3 m horizontal span in climate I with a 6/12 roof pitch to 487 N/m^2 for a panel designed for an 8 m horizontal span in climate III with a 6/12 roof pitch. For each combination of climate and roof pitch there is a region of "short" spans in which the panel weight increases gradually followed by a "long" spans region in which the panel weight sharply increases with the horizontal span. For climate I and II (circles and squares) and a roof pitch of 6/12 (dark lines), panel spans up to 5 m are considered short and the panel weight is under 202 N/m^2 (corresponding to a panel designed for a 5 m horizontal span in climate II with a 6/12 roof pitch). Panel weight increases with increasing roof pitch. So for climate I and II and a roof pitch of 10/12, the short span region is only 4 m and the panel weight is under 191 N/m^2 (corresponding to a panel designed for a 4 m horizontal span in climate II with a 10/12 roof pitch). For both roof pitches considered and climate III, the short span region extends only to 3.66 m and the panel weight is under 204 N/m^2 (corresponding to a panel designed for a 3.66 m horizontal span in climate III with a 6/12 roof pitch).

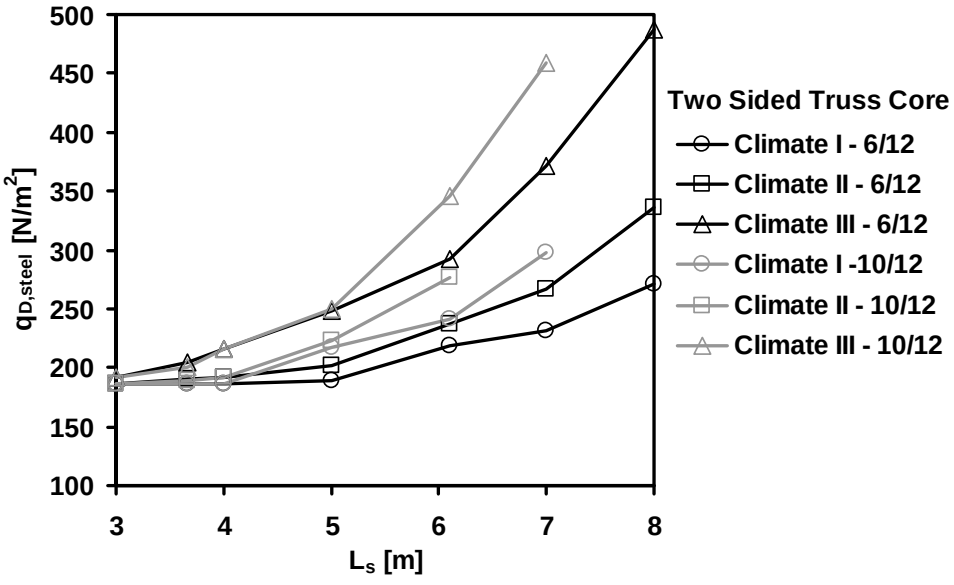

Figure 1: Minimum weight of the steel structural component for the truss core panel. Panel span L_s from 3 to 8 m, roof pitches of 6/12 and 10/12, and three climate zones are considered.

For short horizontal spans, panel weight increases as the loading increases with each climate and there is little or no difference in panel weight between the 6/12 and 10/12 roof pitch. For example a panel designed for a 3.66 m horizontal span in climate II with a 6/12 roof pitch weighs 191 N/m^2, and for a 10/12 roof pitch weighs 189 N/m^2. The weight increases to 204 N/m^2 for a climate III design with a 6/12 roof pitch. For long spans, panel weight increases as the loading increases with each climate. Steep (10/12) roof pitch designs result in substantially greater weights than panels for the 6/10 roof pitch. For example a panel designed for a 7 m horizontal span in climate I with a 6/12 roof pitch weighs 231 N/m^2, and with a 10/12 roof pitch weighs 297 N/m^2. For a climate III design with a 6/12 roof pitch, the weight increases to 371 N/m^2.

In some cases it is not possible to find an optimized design due to constraints on maximum metal sheet thickness or weight. For example there is no optimized design for a panel span of 8 m, roof pitch of 10/12 and climate I loading that has a weight under 340 N/m^2. For the same reason the maximum allowable panel span for a roof pitch of 10/12 and climate II is 6.1 m. For climate III with a roof pitch of 10/12 and a span of 8 m the design would result in sheet thicknesses greater the 2.5 mm.

Figure 2 shows the ratios between required safety factors Ω_{req} and computed safety factors Ω for the three considered failure modes (deflection, moment capacity and web crippling) for the minimum weight two-sided truss-core panel as a function of horizontal span L_s from 3 to 8 m. Results for a roof pitch of 6/12 with climate I loading are shown. A ratio equal to one means that the failure mode is satisfied with the required safety factor, a ratio less than one means that the failure mode considered is satisfied with a safety factor greater than the required (conservative design).

The dominant failure mode for the short span region is web crippling and in the long span region the dominant failure modes are deflection and moment capacity. The ratio for the web crippling safety factor is greater than the ratios for the other two failure modes up to a span length of 5 m. For example for a span length of 3 m the ratio for web crippling safety factors is 0.62 and the ratios for moment capacity and deflection are respectively 0.37 and 0.14. At a span length of 5 m, moment capacity and web crippling are the governing failure modes with ratios equal to one. For spans equal to or longer than 6.1 m, deflection is the governing failure mode.

For spans up to 4 m (short span region) the safety factors ratios are less than one. Panel designs, in which all of the safety factor ratios are less than one, are overdesigned. For the truss core panel designs in climate I, panels designs for horizontal spans less than 4m are limited by the minimum sheet thickness constraint of 0.85 mm. If other climate and slopes are to be considered, the span length at which the transition between web crippling and deflection as governing failure modes decreases but the trend is the same as that described herein.

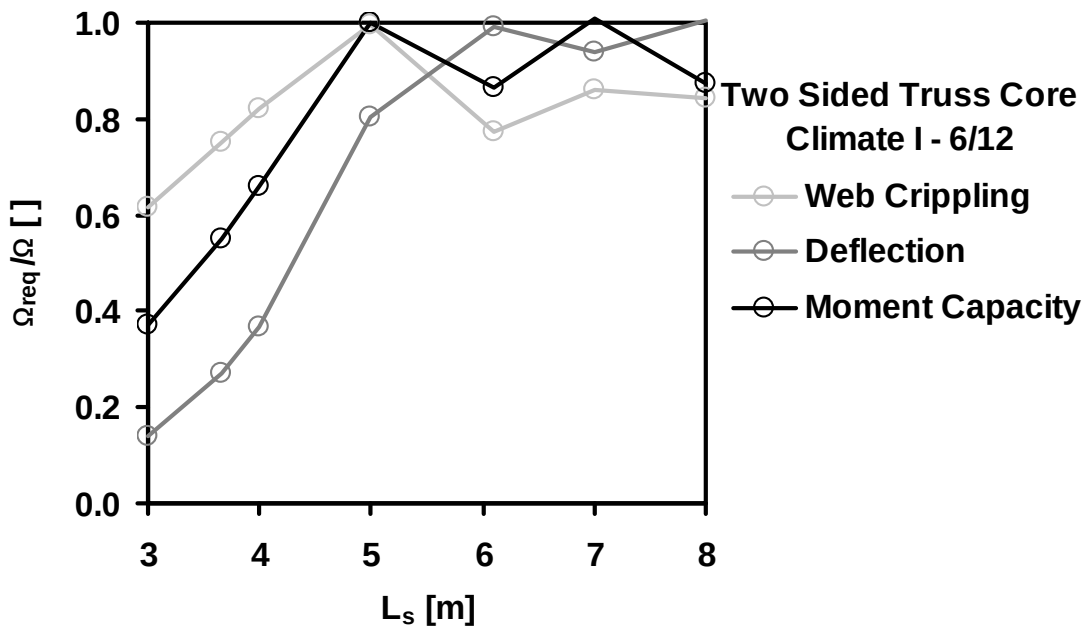

Figure 2: Ratios between required safety factor Ω_{req} and computed safety factor Ω for minimum weight truss core designs as a function of panel span L_s from 3 to 8 m. Results for a roof pitch of 6/12 with climate I loading are shown.

Figure 3 shows panel depth for minimum weight two-sided truss-core designs as a function of panel span L_s from 3 to 8 m, for roof pitches of 6/12 and 10/12, and the three climate zones considered. For span lengths less than 4 m, all the panel depths are 139.7 mm, while for spans length greater than 7 m the depth increases to 184.2 mm. The transition from a depth of 139.7 mm to a depth of 184.2 mm occurs for lower lengths when the load or the slope is increased. For example for a slope of 6/12 and climate I, the transition from a depth of 139.7 mm to a depth of 184.2 mm occurs for a span between 6 and 7 m. While for a slope of 10/12 and a climate III, the transition occurs for spans between 4 and 5 m. Lower depth panels have less slender webs and therefore greater web crippling strength (dominant failure modes for the short span designs). The higher depth panels have a higher moment of inertia and therefore lower deflection (dominant failure mode for long span designs).

Figure 4 shows the thicknesses of the exterior sheet, of the web and of the interior sheet for the minimum weight truss-core designs as a function of panel span L_s from 3 to 8 m. The results reported are for a roof pitch of 6/12 with climate I loading and for a roof pitch of 10/12 for a climate III loading.

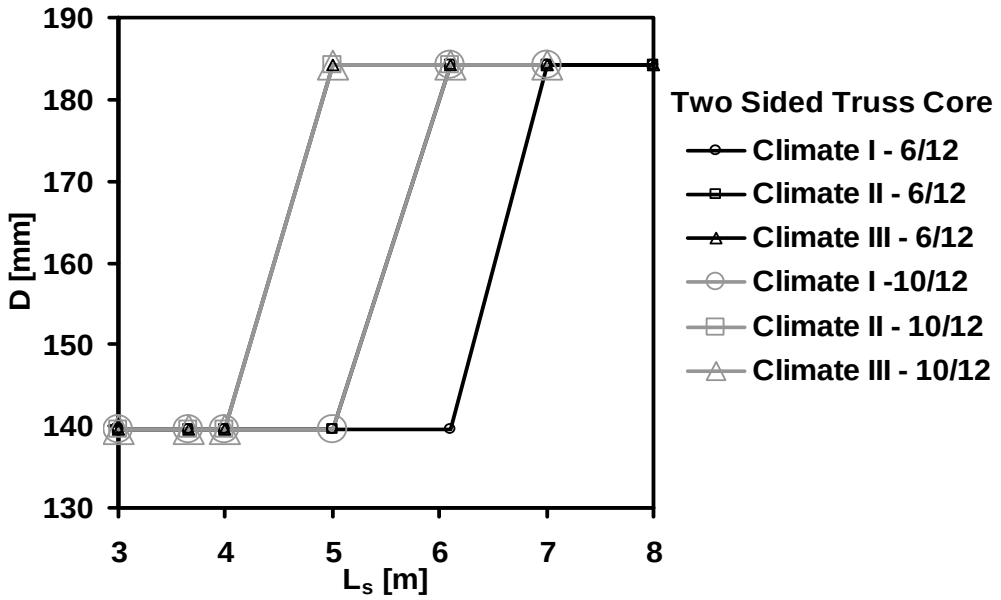

Figure 3: Panel depth for minimum weight truss core panels as a function of panel span L_s from 3 to 8 m. Results for two roof pitch 6/12 and 10/12, and three climate zones are shown.

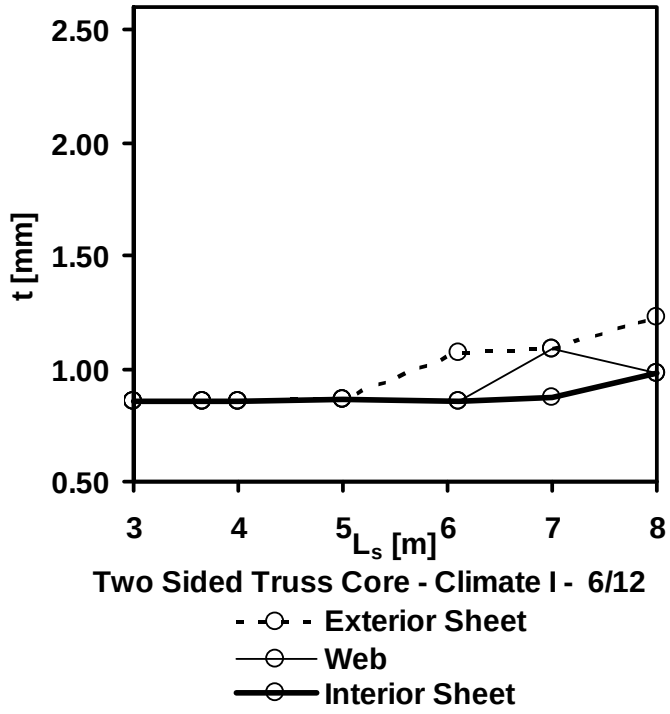

Figure 4: Thicknesses of exterior sheet, web and interior sheet for minimum weight truss core designs as a function of panel span L_s from 3 to 8 m. Results for a roof pitch of 6/12 with climate I loading are shown.

For the short span regions, where web crippling is the dominant failure mode, the increase in thickness with length and load is small. For example the exterior sheet thickness t_t of a panel designed for climate I with a 6/12 roof pitch is 0.85 mm for a 3 m horizontal span and increases only to 0.87 mm for a 5 m span. The reaction force that the web must carry increases linearly with panel length so small increases in thickness are needed to reach the required strength. For longer horizontal spans, where the design is dictated by deflection, the panel weight increases rapidly with increasing horizontal span, reflecting the fact that the deflection increases with length raised to the fourth power. For example, the exterior sheet thickness t_t of a panel designed for climate I with a 6/12 roof pitch is 0.87 mm for a 5 m horizontal span and increases to 1.23 mm for a 8 m span.

The exterior sheet is usually thicker than the interior sheet and the web sheet in order to compensate for the decrease in strength and stiffness caused by local buckling of the compressed exterior sheet. As a consequence, the interior sheet thickness ranges from 0.85 mm to 1.00 mm, while the exterior sheet thickness can reach the a value of 1.21 mm. The web sheet thickness is generally greater than the interior and less than the exterior sheet thickness.

In summary, for each combination of climate and roof pitch there is a region of "short" spans in which the panel weight increases gradually followed by a "long" spans region in which the panel weight sharply increases with the horizontal span. In the short span region panel designs are limited by web crippling and by the minimum sheet thickness criteria. In the "long span" region, panel designs are limited by the deflection and moment capacity criteria. For some loading conditions, panel weight and maximum sheet thickness criteria limit panel designs.

3.0 Comparison of Truss Core and Stiffened Plate Panel Designs

In this section a comparison between the two panel configurations considered in this study are presented. Six plots (three climates and two roof pitches) are presented. In each plot the minimum weight for the three structural components are shown as a function of the horizontal span L_s. Figure 5 shows the optimized weight designs for the two roof slopes and horizontal span lengths (from soffit to ridge) of 3 to 8 m. Truss core panel designs are represented by the open circle and stiffened plate panel designs by the open square.

For several combinations of climate and horizontal span there are no feasible panel designs: There are no stiffened plate panel designs shown for lengths greater than 6.1 meters for the 10/12 roof pitch and for the climate III 6/12 roof pitch. There are also no stiffened plate panel designs for the 8 m span length for the 6/12 roof pitch subjected to climate II loads. Stiffened panel design web thickness exceeds 2.5 mm for these designs. Truss core panel designs are limited for the 10/12 roof pitch. Designs for the climate I and II loads are limited to horizontal span lengths under 7m and 6.1 m (respectively) by the maximum structural component weight (of 340 N/m^2). Because the maximum structural weight limit for climate III is 570 N/m^2, there are feasible truss core panel designs through an 8 m horizontal span.

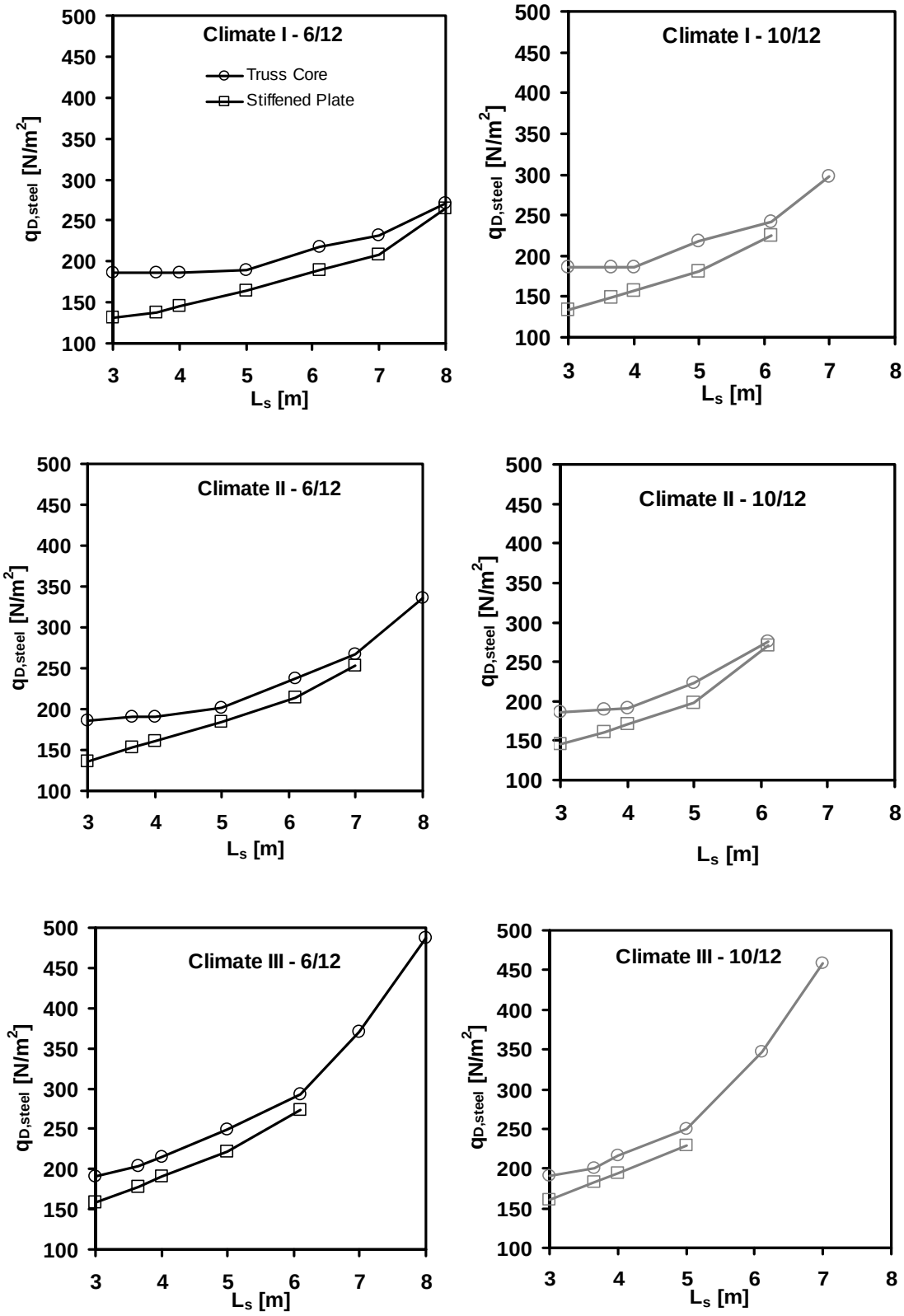

Figure 5: Optimized weight designs for truss core and stiffened plate panels.

Figure 5 also shows several trends. The weight of the truss core panel is slightly greater than that of the stiffened plate panel for all climates and slopes. As the horizontal span length increases, the difference between the panel weights decreases. For horizontal span lengths of 6.1 m, there is typically 10% or less difference in the panel weight. Typical panel weights for the 6.1 m span range from 200 N/m^2 for climate I to 275 N/m^2 for climate III.

The truss core panel is recommended over the stiffened plate panel because the truss core panel can be designed to accommodate all climates. Although the stiffened plate structural component can be optimized to achieve a lighter weight than the truss core structural component, this benefit is offset by the additional foam required in the stiffened plate panel designs to achieve the desired R value.

4.0 Truss Core and Stiffened Plate Panel Designs

In this section the design details for the weight optimized panels discussed in sections 2 and 3 of this appendix are presented. Designs that exceed the limit for structural component weight (340 N/m^2 for climate I and II, and 570 N/m^2 for climate III) or the limit on sheet thickness (2.5 mm max) are highlighted in grey. Panel configurations are presented as follows:

Truss core structural component, 6/12 roof pitch: Tables 1-3,
Truss core structural component, 10/12 roof pitch: Tables 4-6,
Stiffened plate structural component, 6/12 roof pitch: Tables 7-9, and
Stiffened plate structural component, 6/12 roof pitch: Tables 10-12.

Table 1: Complete optimization results for the truss core configuration for climate I, roof slope of 6/12 and panel horizontal span from 3 to 8 m.

Truss-core - Climate I - 6/12							
L_s [m]	3.00	3.660	4.000	5.000	6.100	7.000	8.000
D [mm]	139.7	139.7	139.7	139.7	139.7	184.2	184.2
M_n [kNm]	24.005	24.005	24.005	24.703	42.422	48.034	72.359
N_c	4.000	4.000	4.000	4.000	6.000	4.000	6.000
$q_{D,steel}$ [N/m^2]	186	186	186	189	218	231	272
f_b [m]	0.025	0.025	0.025	0.025	0.025	0.025	0.025
f_t [m]	0.051	0.051	0.051	0.051	0.051	0.051	0.051
f_0 [m]	0.413	0.413	0.413	0.413	0.325	0.476	0.276
$\Omega_{BM,\,req}/\Omega_{BM}$	0.370	0.551	0.658	0.999	0.866	1.007	0.873
$\Omega_{def,\,req}/\Omega_{def}$	0.138	0.270	0.365	0.804	0.993	0.939	1.005
t_b [mm]	0.852	0.852	0.852	0.867	0.854	0.870	0.981
t_c [mm]	0.852	0.852	0.852	0.867	0.854	1.087	0.981
t_t [mm]	0.852	0.852	0.852	0.867	1.067	1.087	1.226
θ [°]	60.000	60.000	60.000	60.000	80.000	75.000	75.000
$\Omega_{WC,\,req}/\Omega_{WC}$	0.616	0.751	0.821	0.996	0.773	0.862	0.842

Table 2: Complete optimization results for the truss core configuration for climate II, roof slope of 6/12 and panel horizontal span from 3 to 8 m.

Truss-core - Climate II - 6/12							
L_s [m]	3.000	3.660	4.000	5.000	6.100	7.000	8.000
D [mm]	139.7	139.7	139.7	139.7	184.2	184.2	184.2
M_n [kNm]	24.005	24.938	28.653	33.932	50.573	73.722	125.015
N_c	4.000	4.000	5.000	6.000	6.000	5.000	6.000
$q_{D,steel}$ [N/m^2]	185.762	190.018	191.361	202.140	236.786	267.148	335.479
f_b [m]	0.025	0.025	0.025	0.025	0.025	0.025	0.025
f_t [m]	0.051	0.051	0.051	0.051	0.051	0.051	0.051
f_0 [m]	0.413	0.413	0.405	0.300	0.342	0.356	0.241
$\Omega_{BM,\,req}/\Omega_{BM}$	0.511	0.731	0.760	1.003	1.002	0.905	0.697
$\Omega_{def,\,req}/\Omega_{def}$	0.204	0.385	0.485	0.887	0.833	0.992	0.998
t_b [mm]	0.852	0.872	0.852	0.852	0.927	0.866	0.888
t_c [mm]	0.852	0.872	0.852	0.852	0.927	1.082	1.110
t_t [mm]	0.852	0.872	0.852	0.852	0.927	1.353	1.942
θ [°]	60.000	60.000	80.000	75.000	85.000	75.000	70.000
$\Omega_{WC,\,req}/\Omega_{WC}$	0.849	0.997	0.818	0.895	0.943	0.999	0.966

Table 3: Complete optimization results for the truss core configuration for climate III, roof slope of 6/12 and panel horizontal span from 3 to 8 m.

Truss-core - Climate III - 6/12							
L_s [m]	3.000	3.660	4.000	5.000	6.100	7.000	8.000
D [mm]	139.7	139.7	139.7	184.2	184.2	184.2	184.2
M_n [kNm]	28.653	31.760	37.289	55.165	82.518	145.521	211.296
N_c	5.000	6.000	6.000	4.000	6.000	6.000	6.000
$q_{D,steel}$ [N/m^2]	191.361	203.964	215.639	249.032	292.422	370.696	487.313
f_b [m]	0.025	0.025	0.025	0.025	0.025	0.025	0.025
f_t [m]	0.051	0.051	0.051	0.051	0.051	0.051	0.051
f_0 [m]	0.405	0.375	0.350	0.510	0.310	0.276	0.276
$\Omega_{BM,\,req}/\Omega_{BM}$	0.696	0.935	0.951	1.004	0.999	0.746	0.671
$\Omega_{def,\,req}/\Omega_{def}$	0.332	0.613	0.697	0.737	0.997	1.000	1.005
t_b [mm]	0.852	0.867	0.916	0.910	0.971	1.056	1.903
t_c [mm]	0.852	0.867	0.916	1.366	1.214	1.320	1.428
t_t [mm]	0.852	0.867	0.916	1.024	1.214	1.979	2.498
θ [°]	80.000	90.000	85.000	80.000	80.000	75.000	75.000
$\Omega_{WC,\,req}/\Omega_{WC}$	0.998	0.997	0.996	0.912	0.974	0.988	0.986

Table 4: Complete optimization results for the truss core configuration for climate I, roof slope of 10/12 and panel horizontal span from 3 to 8 m.

Truss-core - Climate I - 10/12							
L_s [m]	3.000	3.660	4.000	5.000	6.100	7.000	8.000
D [mm]	139.7	139.7	139.7	139.7	184.2	184.2	184.2
M_n [kNm]	24.005	24.005	24.005	38.685	52.902	96.338	152.714
N_c	4.000	4.000	4.000	5.000	6.000	5.000	6.000
$q_{D,steel}$ [N/m^2]	185.762	185.762	185.762	217.347	241.541	297.377	383.812
f_b [m]	0.025	0.025	0.025	0.025	0.025	0.025	0.025
f_t [m]	0.051	0.051	0.051	0.051	0.051	0.051	0.051
f_0 [m]	0.413	0.413	0.413	0.324	0.310	0.321	0.203
$\Omega_{BM,\ req}/\Omega_{BM}$	0.495	0.736	0.879	0.852	0.928	0.671	0.553
$\Omega_{def,\ req}/\Omega_{def}$	0.264	0.518	0.726	1.004	1.004	0.999	1.006
t_b [mm]	0.852	0.852	0.852	0.877	0.942	0.983	1.400
t_c [mm]	0.852	0.852	0.852	0.877	0.942	0.983	1.050
t_t [mm]	0.852	0.852	0.852	1.097	0.942	1.720	2.100
θ [°]	60.000	60.000	60.000	65.000	80.000	70.000	65.000
$\Omega_{WC,\ req}/\Omega_{WC}$	0.666	0.813	0.888	0.837	0.728	0.956	0.869

Table 5: Complete optimization results for the truss core configuration for climate II, roof slope of 10/12 and panel horizontal span from 3 to 8 m.

Truss-core - Climate II - 10/12							
L_s [m]	3.000	3.660	4.000	5.000	6.100	7.000	8.000
D [mm]	139.7	139.7	139.7	184.2	184.2	184.2	184.2
M_n [kNm]	24.005	24.703	28.653	43.141	74.403	137.504	170.278
N_c	4.000	4.000	5.000	5.000	6.000	6.000	6.000
$q_{D,steel}$ [N/m^2]	185.762	188.954	191.361	223.497	275.990	350.160	466.348
f_b [m]	0.025	0.025	0.025	0.025	0.025	0.025	0.025
f_t [m]	0.051	0.051	0.051	0.051	0.051	0.051	0.051
f_0 [m]	0.413	0.413	0.405	0.422	0.276	0.203	0.203
$\Omega_{BM,\ req}/\Omega_{BM}$	0.629	0.910	0.938	0.973	0.840	0.598	0.631
$\Omega_{def,\ req}/\Omega_{def}$	0.354	0.702	0.846	0.856	1.001	1.007	1.002
t_b [mm]	0.852	0.867	0.852	0.927	0.996	1.031	2.237
t_c [mm]	0.852	0.867	0.852	0.927	0.996	1.031	1.118
t_t [mm]	0.852	0.867	0.852	0.927	1.245	2.061	2.237
θ [°]	60.000	60.000	80.000	85.000	75.000	65.000	65.000
$\Omega_{WC,\ req}/\Omega_{WC}$	0.848	1.004	0.816	0.901	0.861	1.000	0.992

Table 6: Complete optimization results for the truss core configuration for climate III, roof slope of 10/12 and panel horizontal span from 3 to 8 m.

Truss-core - Climate III - 10/12							
L_s [m]	3.000	3.660	4.000	5.000	6.100	7.000	8.000
D [mm]	139.7	139.7	139.7	184.2	184.2	184.2	184.2
M_n [kNm]	28.653	33.114	37.965	59.167	129.524	208.409	324.465
N_c	5.000	6.000	6.000	5.000	6.000	6.000	6.000
$q_{D,steel}$ [N/m^2]	191.361	200.694	216.034	249.604	346.442	458.768	625.043
f_b [m]	0.025	0.025	0.025	0.025	0.025	0.025	0.025
f_t [m]	0.051	0.051	0.051	0.051	0.051	0.051	0.051
f_0 [m]	0.405	0.350	0.300	0.356	0.241	0.203	0.276
$\Omega_{BM, req}/\Omega_{BM}$	0.746	0.961	1.001	1.003	0.682	0.558	0.468
$\Omega_{def, req}/\Omega_{def}$	0.484	0.844	0.980	0.982	1.003	0.987	1.002
t_b [mm]	0.852	0.852	0.911	0.877	0.917	1.674	2.774
t_c [mm]	0.852	0.852	0.911	1.097	1.146	1.255	1.387
t_t [mm]	0.852	0.852	0.911	1.097	2.006	2.510	3.467
θ [°]	80.000	85.000	75.000	75.000	70.000	65.000	75.000
$\Omega_{WC, req}/\Omega_{WC}$	0.866	0.894	0.902	0.986	0.985	1.006	0.902

Table 7: Complete optimization results for the stiffened plate panel for climate I, roof slope of 6/12 and panel horizontal span from 3 to 8 m.

Stiffened plate - Climate I - 6/12							
L_s [m]	3.000	3.660	4.000	5.000	6.100	7.000	8.000
D [mm]	139.7	139.7	139.7	139.7	184.2	184.2	184.2
M_n [kNm]	10.738	13.235	16.279	24.901	36.790	48.090	79.095
N_c	6.000	6.000	5.000	5.000	6.000	5.000	4.000
$q_{D,steel}$ [N/m^2]	131.477	137.847	146.166	164.703	189.432	208.266	264.367
f_b [m]	213.288	186.207	191.930	212.459	208.925	205.506	285.506
f_t [m]	25.400	52.481	53.626	106.229	57.025	102.753	142.753
f_0 [m]	374.600	347.519	426.374	373.771	342.975	377.247	457.247
$\Omega_{stress, req}/\Omega_{stress}$	0.439	0.386	0.445	0.597	0.603	0.650	0.695
$\Omega_{locdef, req}/\Omega_{locdef}$	0.921	0.506	0.605	0.902	0.844	0.678	0.920
$\Omega_{BM, req}/\Omega_{BM}$	0.827	0.999	0.970	0.991	0.998	1.006	0.799
$\Omega_{def, req}/\Omega_{def}$	0.342	0.493	0.570	0.760	0.774	0.932	1.003
t_b [mm]	0.853	0.865	0.852	0.854	0.854	0.887	1.142
t_c [mm]	0.853	0.865	1.065	1.281	1.281	1.553	2.284
θ [°]	60.000	60.000	50.000	60.000	70.000	65.000	65.000
$\Omega_{WC, req}/\Omega_{WC}$	0.513	0.610	0.640	0.508	0.486	0.498	0.365

Table 8: Complete optimization results for the stiffened plate panel for climate II, roof slope of 6/12 and panel horizontal span from 3 to 8 m.

Stiffened plate - Climate II - 6/12							
L_s [m]	3.000	3.660	4.000	5.000	6.100	7.000	8.000
D [mm]	139.7	139.7	139.7	139.7	184.2	184.2	184.2
M_n [kNm]	12.903	18.298	21.861	33.802	50.937	76.540	117.173
N_c	6.000	5.000	6.000	5.000	5.000	5.000	4.000
$q_{D,steel}$ [N/m^2]	135.935	153.348	160.806	184.180	214.620	253.707	342.783
f_b [m]	186.207	189.575	212.061	189.575	205.506	230.633	245.675
f_t [m]	52.481	94.787	57.652	94.787	102.753	115.317	220.275
f_0 [m]	347.519	385.213	342.348	385.213	377.247	364.683	379.725
$\Omega_{stress,\ req}/\Omega_{stress}$	0.481	0.539	0.626	0.707	0.735	0.817	0.813
$\Omega_{locdef,\ req}/\Omega_{locdef}$	0.738	0.712	0.980	0.767	0.829	0.963	0.809
$\Omega_{BM,\ req}/\Omega_{BM}$	0.950	0.997	0.997	1.007	0.995	0.872	0.744
$\Omega_{def,\ req}/\Omega_{def}$	0.376	0.503	0.616	0.909	0.823	1.000	1.003
t_b [mm]	0.853	0.876	0.905	0.860	0.914	0.989	1.100
t_c [mm]	0.853	1.095	1.131	1.505	1.600	1.977	3.024
θ [°]	60.000	55.000	65.000	55.000	65.000	70.000	70.000
$\Omega_{WC,\ req}/\Omega_{WC}$	0.707	0.715	0.551	0.564	0.569	0.435	0.297

Table 9: Complete optimization results for the stiffened plate panel for climate III, roof slope of 6/12 and panel horizontal span from 3 to 8 m.

Stiffened plate - Climate III - 6/12							
L_s [m]	3.000	3.660	4.000	5.000	6.100	7.000	8.000
D [mm]	139.7	139.7	184.2	184.2	184.2	184.2	184.2
M_n [kNm]	20.526	30.071	35.623	56.993	85.678	133.002	192.443
N_c	6.000	6.000	5.000	5.000	4.000	4.000	4.000
$q_{D,steel}$ [N/m^2]	158.917	178.526	190.789	220.864	274.056	372.566	512.208
f_b [m]	159.126	179.809	178.241	178.241	183.757	226.829	296.589
f_t [m]	79.563	89.905	89.121	89.121	158.357	201.429	271.189
f_0 [m]	320.437	310.095	390.879	390.879	441.643	398.571	328.811
$\Omega_{stress,\ req}/\Omega_{stress}$	0.629	0.821	0.739	0.917	0.967	0.931	0.774
$\Omega_{locdef,\ req}/\Omega_{locdef}$	0.642	1.002	0.837	1.009	0.746	0.672	0.352
$\Omega_{BM,\ req}/\Omega_{BM}$	0.972	0.987	0.995	0.972	0.963	0.817	0.737
$\Omega_{def,\ req}/\Omega_{def}$	0.412	0.608	0.454	0.726	1.004	1.003	0.998
t_b [mm]	0.852	0.862	0.894	0.853	0.948	1.201	1.847
t_c [mm]	1.065	1.293	1.340	1.706	2.370	3.303	4.155
θ [°]	60.000	65.000	60.000	60.000	55.000	65.000	85.000
$\Omega_{WC,\ req}/\Omega_{WC}$	0.784	0.652	0.868	0.714	0.653	0.378	0.262

Table 10: Complete optimization results for the stiffened plate panel for climate I, roof slope of 10/12 and panel horizontal span from 3 to 8 m.

Stiffened plate - Climate I - 10/12							
L_s [m]	3.000	3.660	4.000	5.000	6.100	7.000	8.000
D [mm]	139.7	139.7	184.2	184.2	184.2	184.2	184.2
M_n [kNm]	11.869	17.653	21.925	33.140	56.895	99.879	143.870
N_c	5.000	5.000	5.000	5.000	5.000	4.000	4.000
$q_{D,steel}$ [N/m^2]	133.628	148.794	157.263	181.237	225.234	304.321	417.147
f_b [m]	224.268	212.459	210.102	205.506	230.633	226.829	280.229
f_t [m]	60.094	106.229	57.260	102.753	115.317	201.429	254.829
f_0 [m]	419.906	373.771	422.740	377.247	364.683	398.571	345.171
$\Omega_{stress,\ req}/\Omega_{stress}$	0.458	0.517	0.491	0.567	0.638	0.654	0.524
$\Omega_{locdef,\ req}/\Omega_{locdef}$	0.930	0.877	0.855	0.779	0.769	0.664	0.266
$\Omega_{BM,\ req}/\Omega_{BM}$	1.000	1.001	0.963	0.995	0.863	0.647	0.587
$\Omega_{def,\ req}/\Omega_{def}$	0.533	0.676	0.568	0.746	0.999	1.003	1.001
t_b [mm]	0.892	0.857	0.853	0.854	0.962	0.981	1.523
t_c [mm]	0.892	1.071	1.066	1.281	1.683	2.698	3.427
θ [°]	55.000	60.000	60.000	65.000	70.000	65.000	80.000
$\Omega_{WC,\ req}/\Omega_{WC}$	0.656	0.548	0.624	0.539	0.395	0.261	0.180

Table 11: Complete optimization results for the stiffened plate panel for climate II, roof slope of 10/12 and panel horizontal span from 3 to 8 m.

Stiffened plate - Climate II - 10/12							
L_s [m]	3.000	3.660	4.000	5.000	6.100	7.000	8.000
D [mm]	139.7	184.2	139.7	184.2	184.2	184.2	184.2
M_n [kNm]	16.279	22.820	26.686	41.941	85.165	129.122	183.593
N_c	5.000	5.000	5.000	5.000	4.000	4.000	4.000
$q_{D,steel}$ [N/m^2]	146.166	160.788	170.822	198.551	269.721	369.452	514.708
f_b [m]	191.930	210.102	212.459	210.102	206.381	263.357	312.700
f_t [m]	53.626	57.260	106.229	57.260	180.981	237.957	287.300
f_0 [m]	426.374	422.740	373.771	422.740	419.019	362.043	312.700
$\Omega_{stress,\ req}/\Omega_{stress}$	0.506	0.568	0.661	0.701	0.779	0.722	0.514
$\Omega_{locdef,\ req}/\Omega_{locdef}$	0.760	0.996	0.979	0.989	0.932	0.744	0.181
$\Omega_{BM,\ req}/\Omega_{BM}$	0.928	0.986	1.007	1.001	0.734	0.637	0.585
$\Omega_{def,\ req}/\Omega_{def}$	0.549	0.542	0.862	0.908	1.003	1.002	1.001
t_b [mm]	0.852	0.872	0.886	0.874	0.871	1.176	1.988
t_c [mm]	1.065	1.090	1.329	1.529	2.396	3.233	3.976
θ [°]	50.000	60.000	60.000	60.000	60.000	75.000	90.000
$\Omega_{WC,\ req}/\Omega_{WC}$	0.662	0.699	0.527	0.531	0.373	0.227	0.175

Table 12: Complete optimization results for the stiffened plate panel for climate III, roof slope of 10/12 and panel horizontal span from 3 to 8 m.

Stiffened plate - Climate III - 10/12							
L_s [m]	3.000	3.660	4.000	5.000	6.100	7.000	8.000
D [mm]	139.7	184.2	184.2	184.2	184.2	184.2	184.2
M_n [kNm]	21.374	32.724	38.053	61.338	123.719	175.945	254.180
N_c	6.000	5.000	4.000	4.000	4.000	4.000	4.000
$q_{D,steel}$ [N/m^2]	160.754	182.323	194.017	228.369	355.973	495.153	697.124
f_b [m]	179.809	178.241	193.973	183.757	245.675	296.589	225.400
f_t [m]	89.905	89.121	96.987	158.357	220.275	271.189	374.600
f_0 [m]	310.095	390.879	503.013	441.643	379.725	328.811	225.400
$\Omega_{stress,\ req}/\Omega_{stress}$	0.632	0.660	0.737	0.875	0.862	0.605	0.462
$\Omega_{locdef,\ req}/\Omega_{locdef}$	0.775	0.794	0.956	0.903	0.896	0.228	0.020
$\Omega_{BM,\ req}/\Omega_{BM}$	1.000	0.972	0.999	0.968	0.714	0.661	0.598
$\Omega_{def,\ req}/\Omega_{def}$	0.580	0.535	0.629	1.003	0.997	0.997	1.003
t_b [mm]	0.867	0.854	0.887	0.853	1.142	1.941	2.725
t_c [mm]	1.083	1.281	1.553	1.918	3.140	3.882	4.768
θ [°]	65.000	60.000	50.000	55.000	70.000	85.000	90.000
$\Omega_{WC,\ req}/\Omega_{WC}$	0.629	0.747	0.838	0.674	0.303	0.226	0.180

Appendix H: Connector Details

Panel to panel, soffit, ridge and gable end connectors were designed for the truss core and stiffened plate panels designed for a shallow, 6/12 pitch, roof and a steep, 10/12 pitch, roof. For the truss core panels, connectors were designed to sustain 90 mph and 130 mph wind loads for climate III. For the stiffened plate panels, connectors were designed to sustain 90 mph wind loads for climate II. With the exception of the panel to panel connectors, the connector designs for the truss core and stiffened plate panels are identical (particularly the 90 mph wind loading conditions). In addition, connectors at the ridge (or slope) for the two different slopes have identical sheet metal thickness and fastening schedule. Gable end and panel to panel connectors do not depend on roof pitch. This similarity among designs is a benefit in terms of cost, manufacturability and constructability. Table 1 is a listing that maps connector detail drawings to the corresponding panel design. Soffit connector details are shown in Figures 1 through 4. Ridge connector details are shown in Figures 5 through 7. Gable end connector details are shown in Figures 8 and 9. Panel to panel connector details are in Figures 10-13.

Table 1: Connector detail drawings for truss core and stiffened plate panels.

Connector	Figure	Panels					
		Truss Core (90 mph)		Truss Core 130 mph		Stiffened Plate 90 mph	
Soffit							
		6/12	10/12	6/12	10/12	6/12	10/12
S90-6/12	1	X				X	
S90-10/12	2		X				X
S130-6/12	3			X			
S130-10/12	4				X		
Ridge							
		6/12	10/12	6/12	10/12	6/12	10/12
R90-6/12	5	X				X	
R90-10/12	6		X		X		X
R130-6/12	7			X			
Gable End							
G90	8	X				X	
G130	9			X			
Panel to panel							
TC90	10	X					
TC130	11			X			
TC90-IM	12	Integral metal roof					
SP90	13					X	

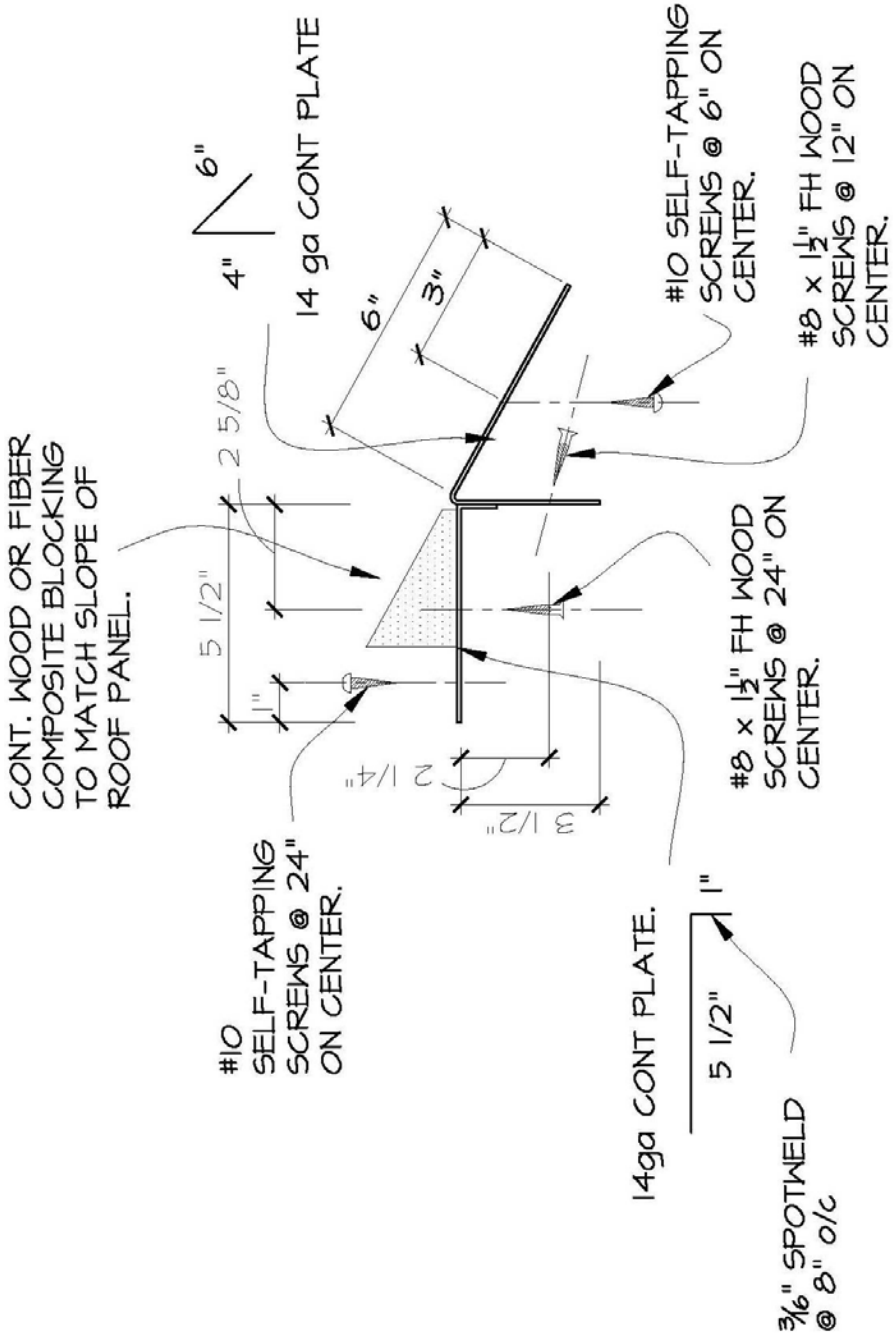

Figure 1: Soffit connector for 6/12 slope roof, 90 mph.

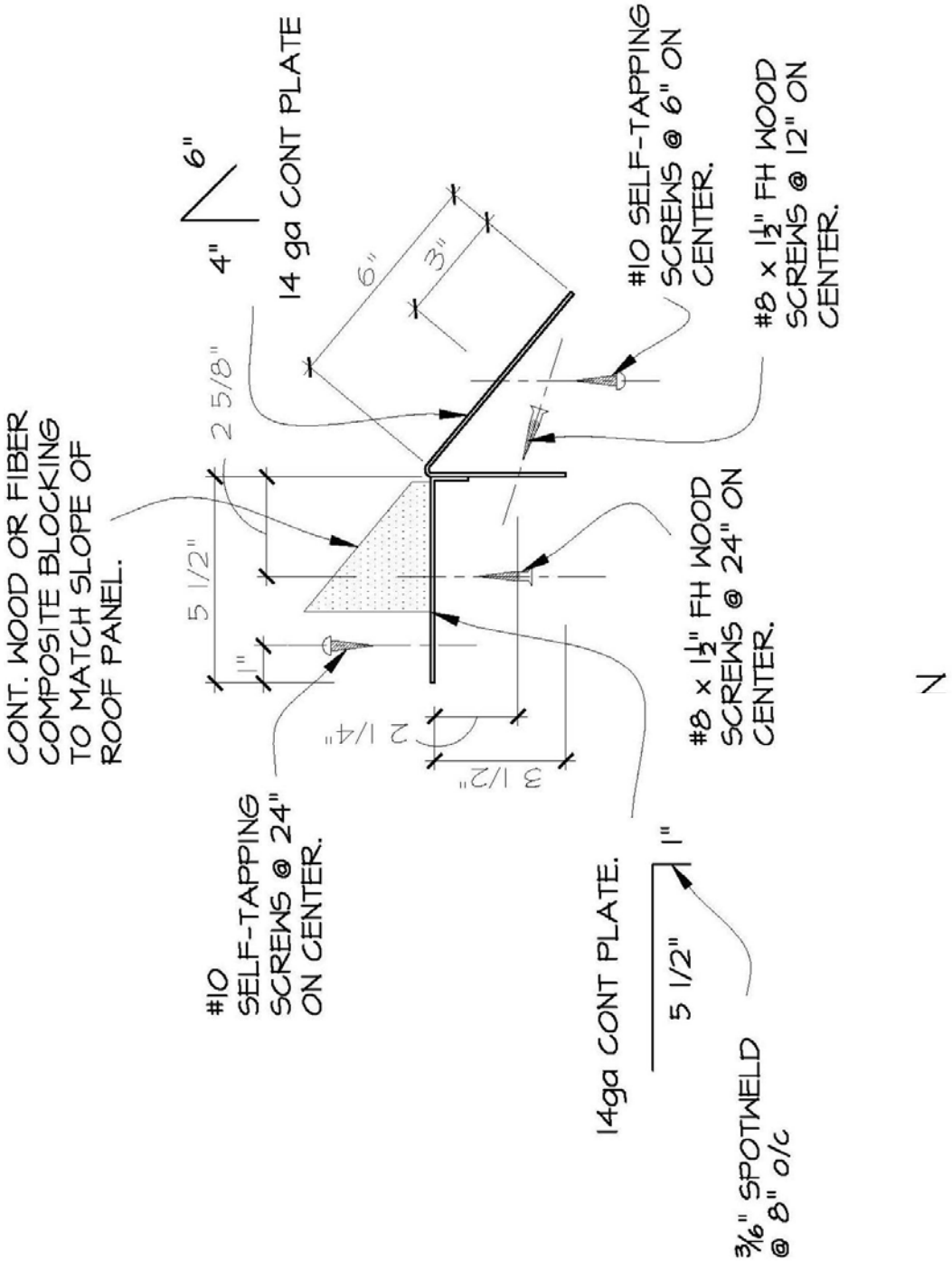

Figure 2: Soffit connector for 10/12 slope roof, 90 mph.

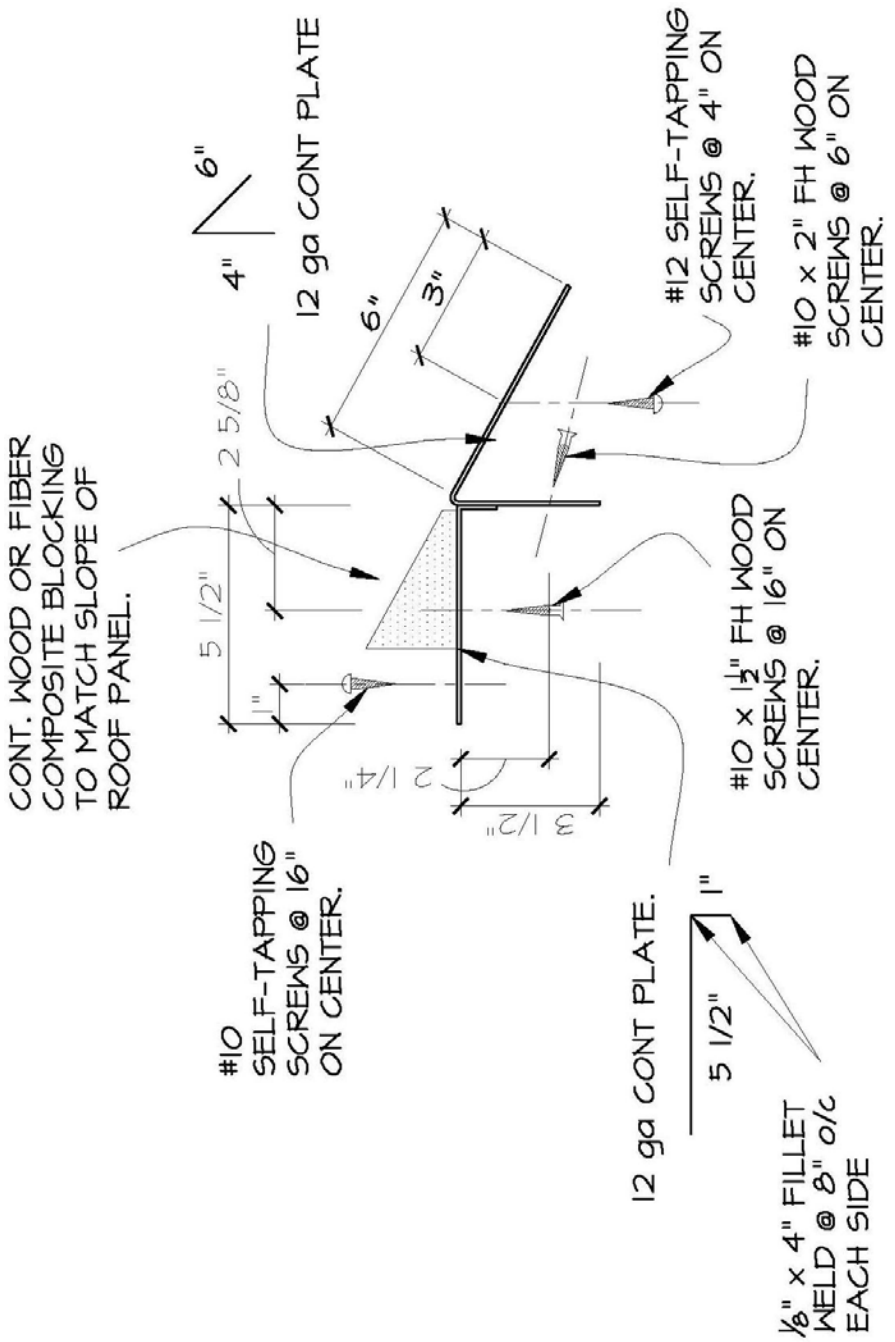

Figure 3: Soffit connector for 6/12 slope roof, 130 mph.

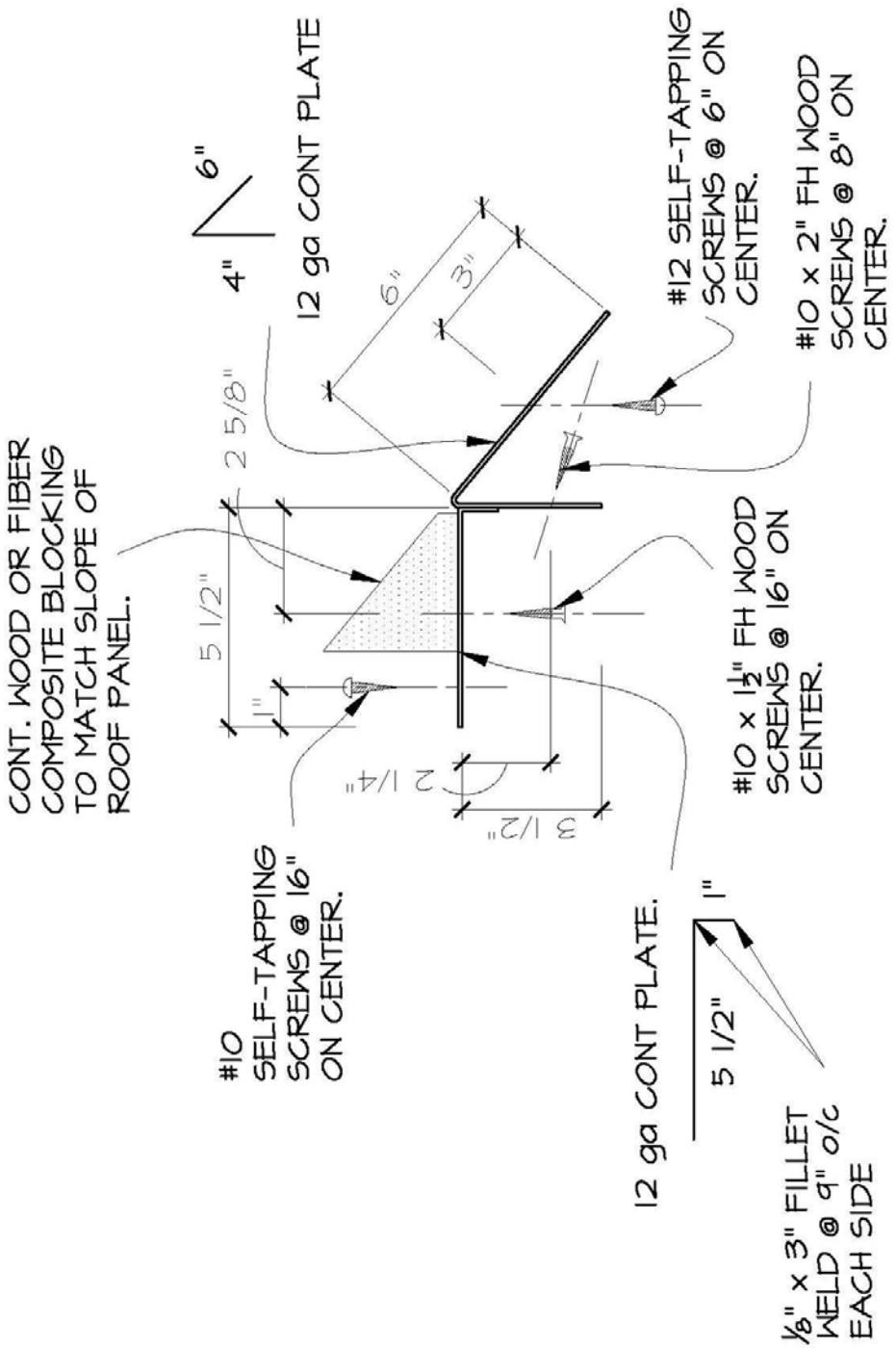

Figure 4: Soffit connector for 10/12 slope roof, 130 mph.

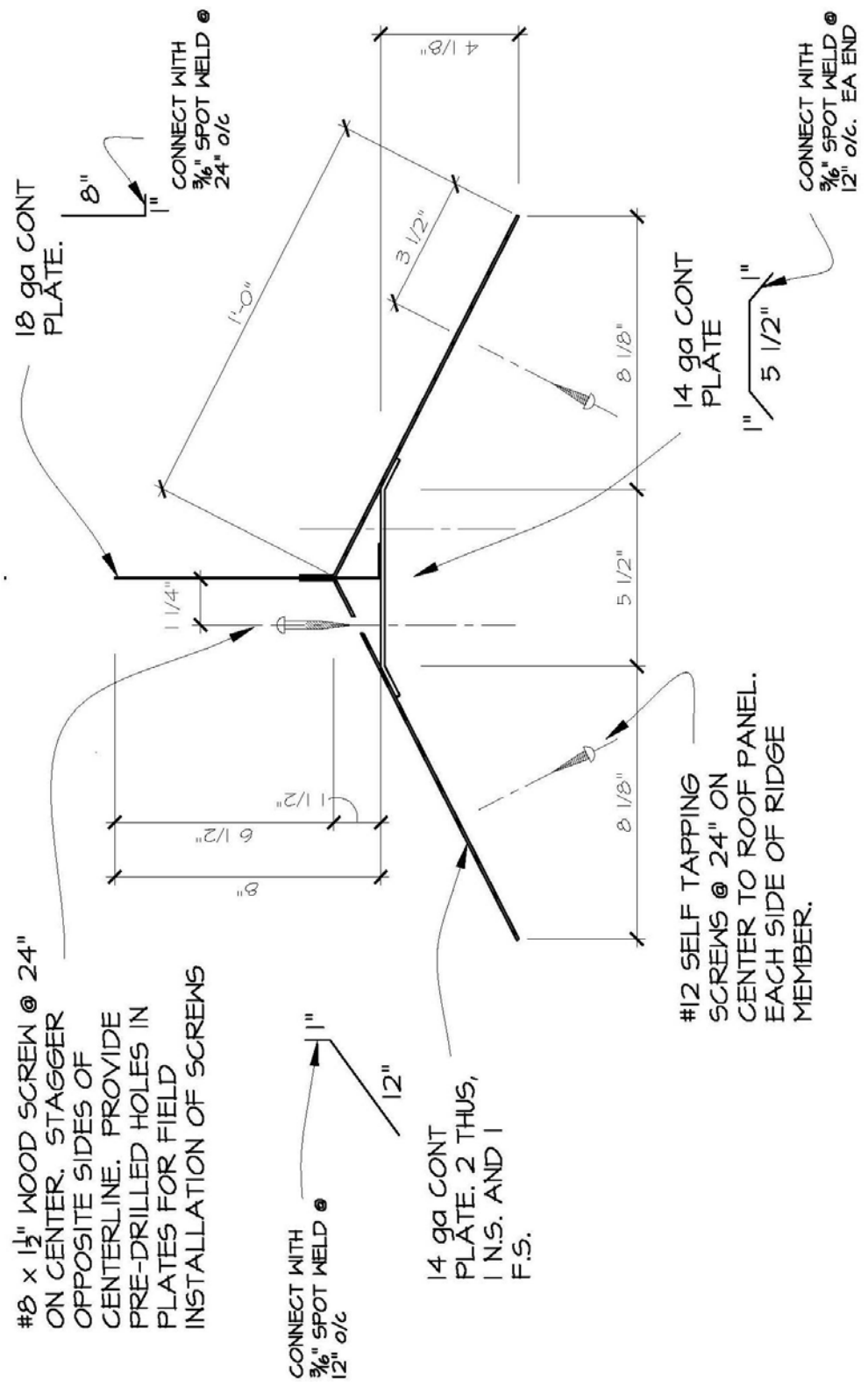

Figure 5: Ridge connector for 6/12 slope roof, 90 mph.

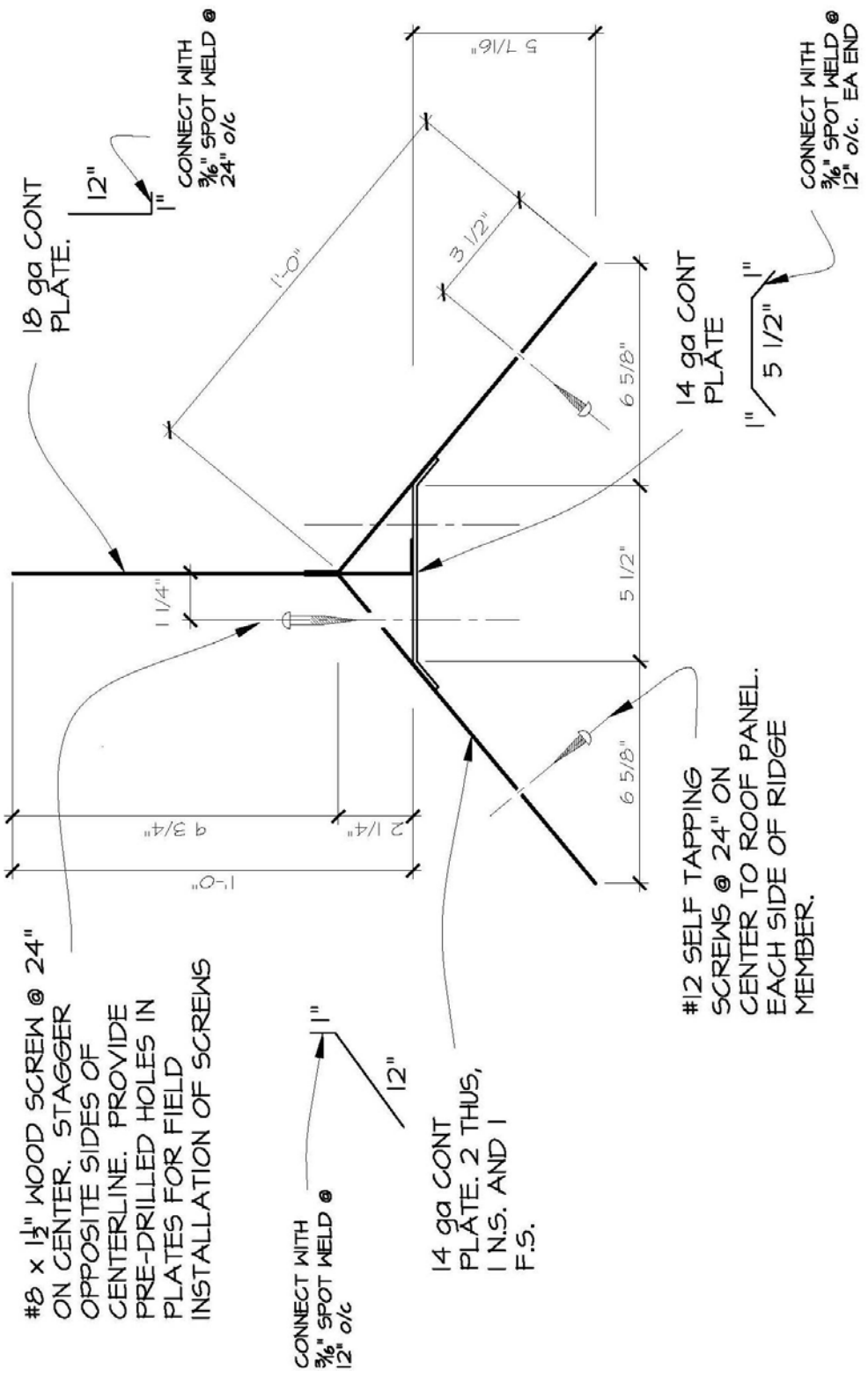

Figure 6: Ridge connector for 10/12 slope roof, 90 mph and 130 mph.

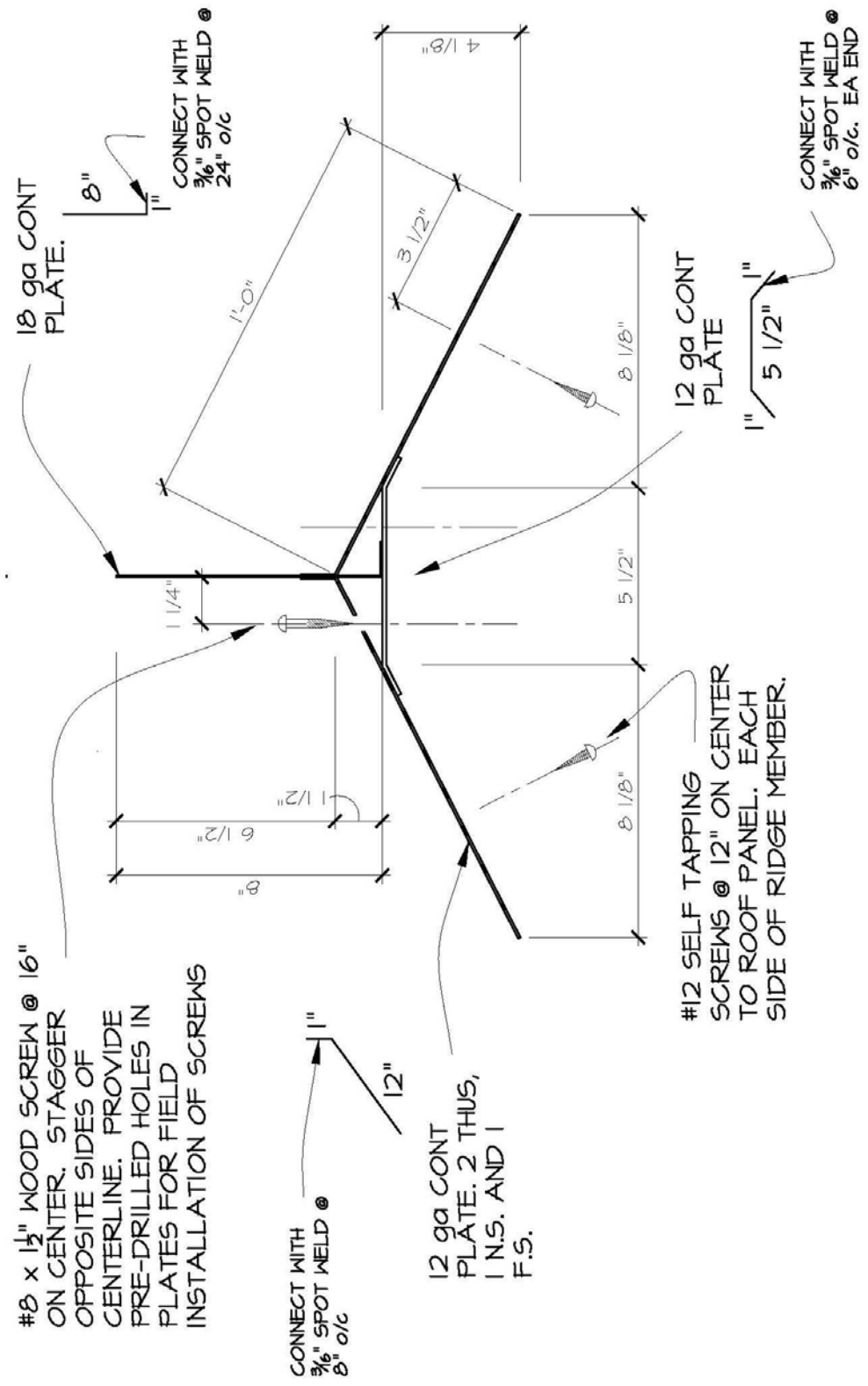

Figure 7: Ridge connector for 6/12 slope roof, 130 mph.

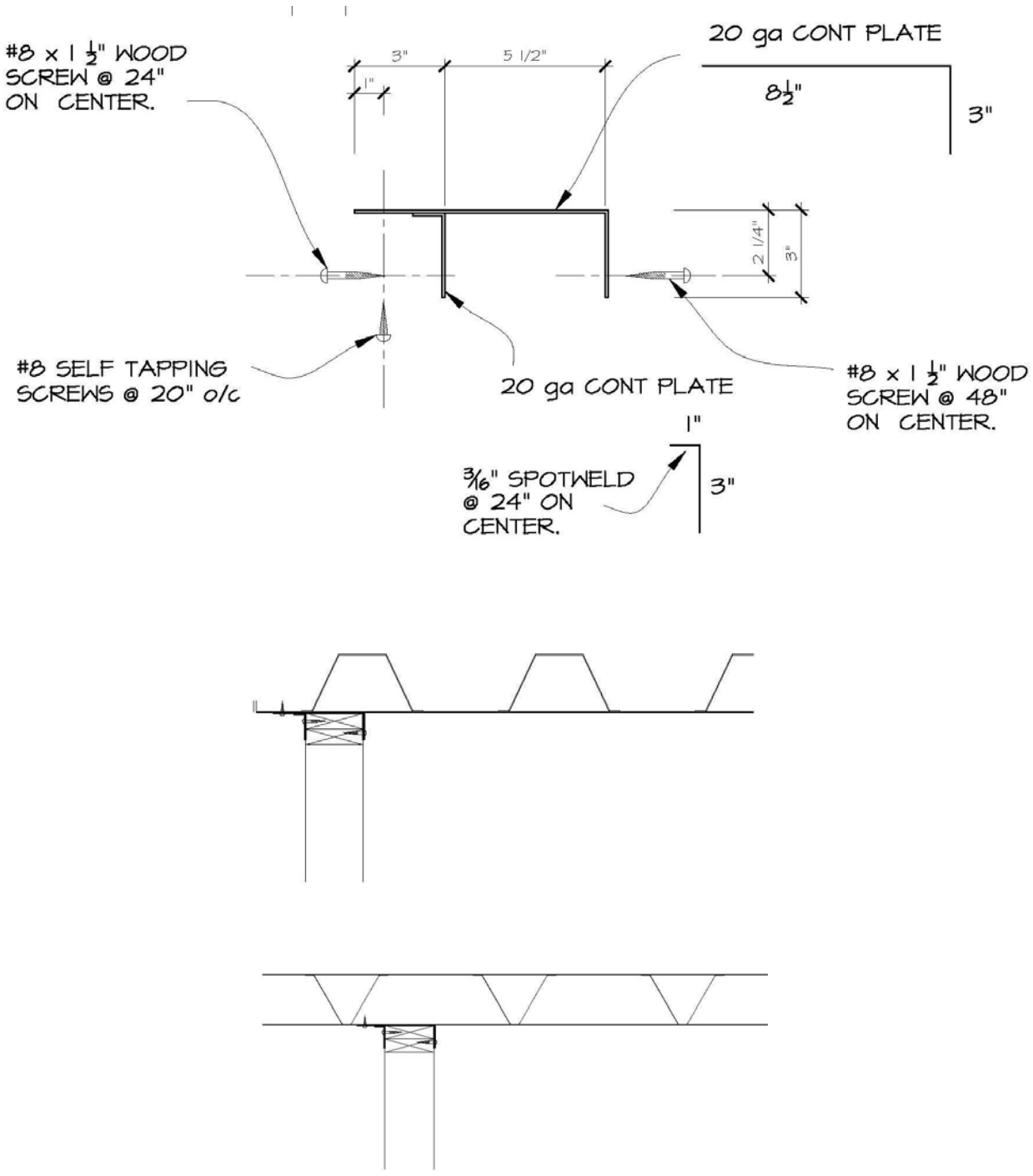

Figure 8: Gable end connector for truss core (top) and stiffened plate panels (bottom), 90 mph.

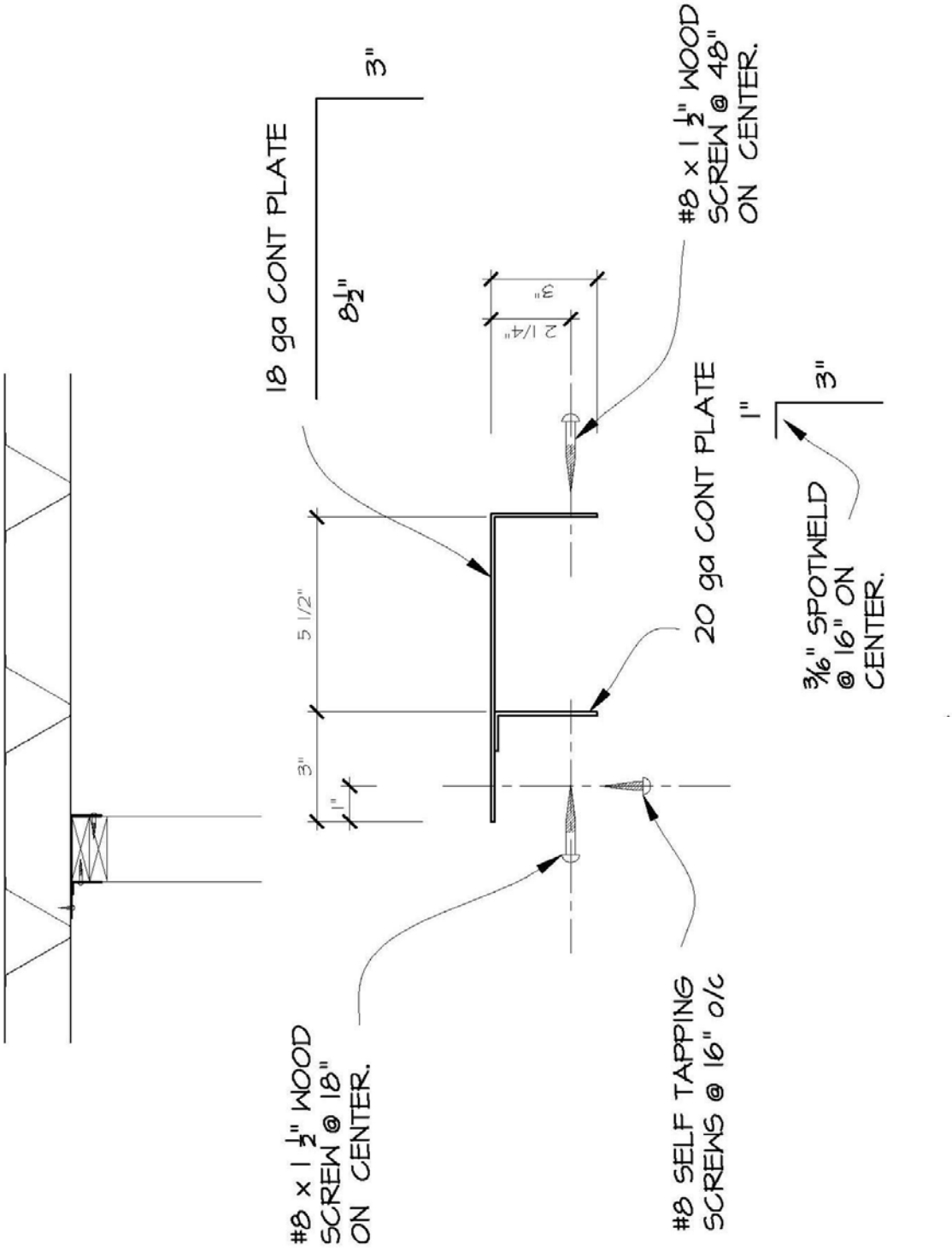

Figure 9: Gable end connector for truss core panels, 130 mph.

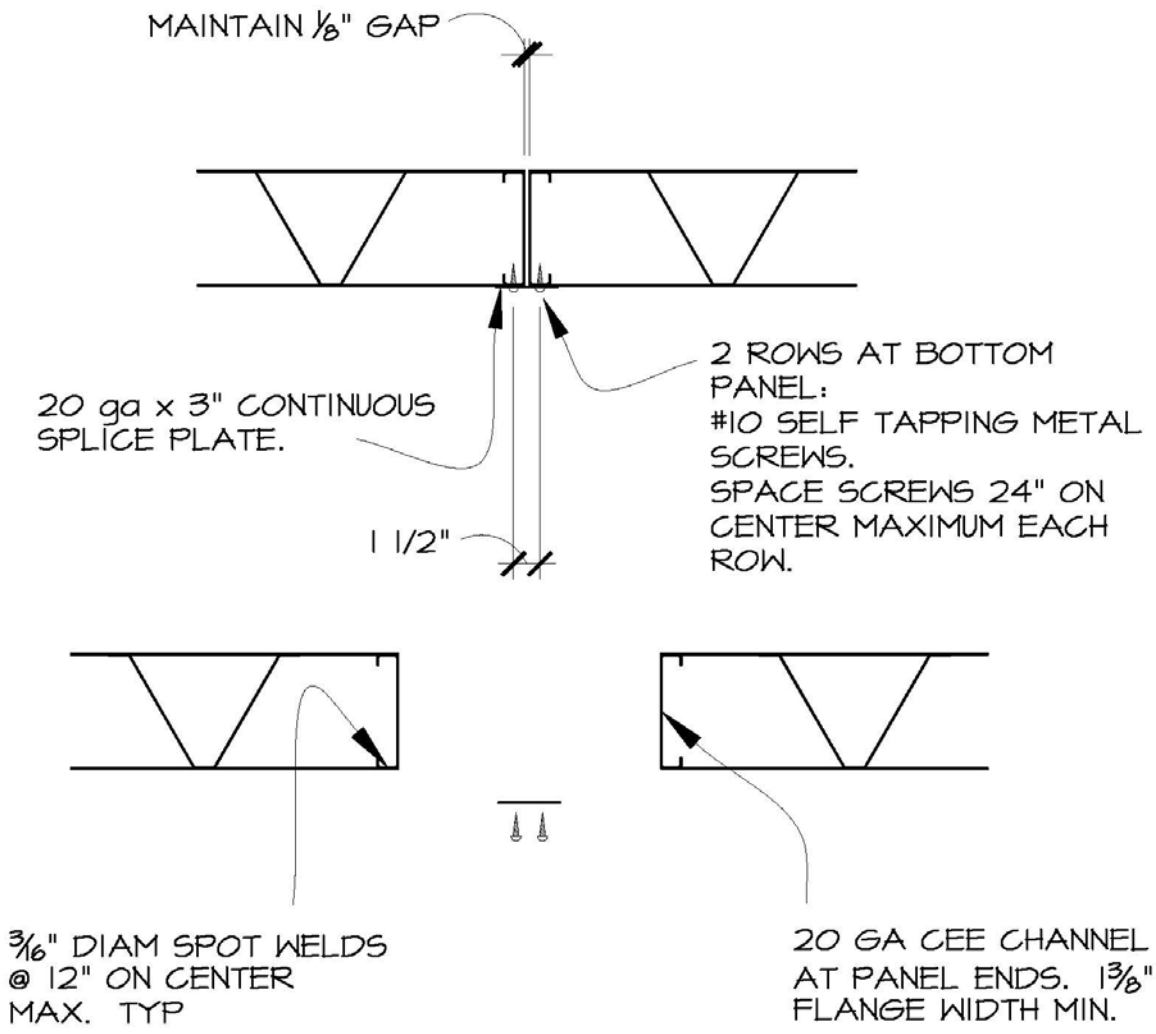

Figure 10: Panel to panel connector for truss core panels, 90 mph.

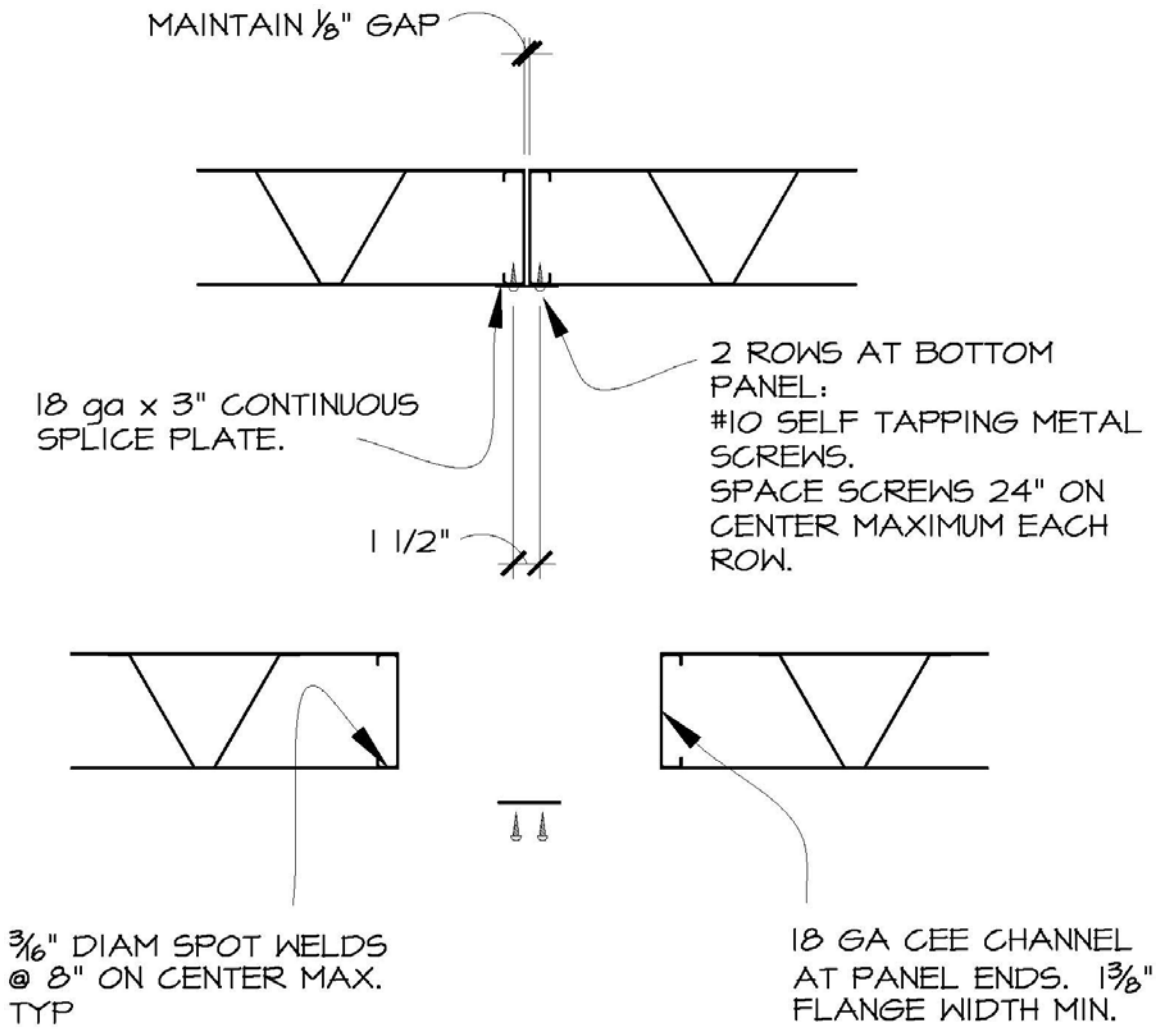

Figure 11: Panel to panel connector for truss core panels, 130 mph.

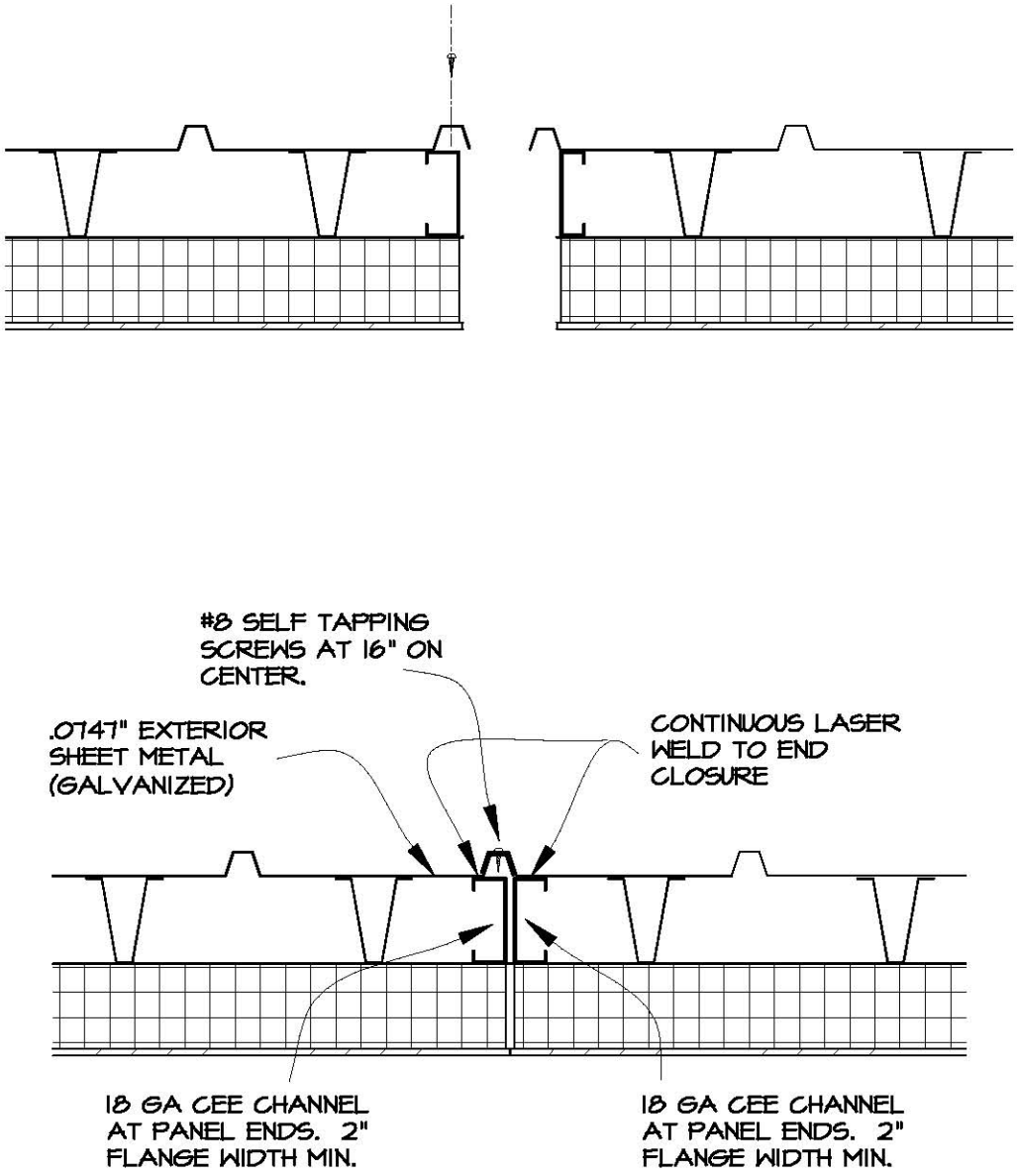

Figure 12: Panel to panel connector for truss core panels, integral metal roof, 90 mph, climate I.

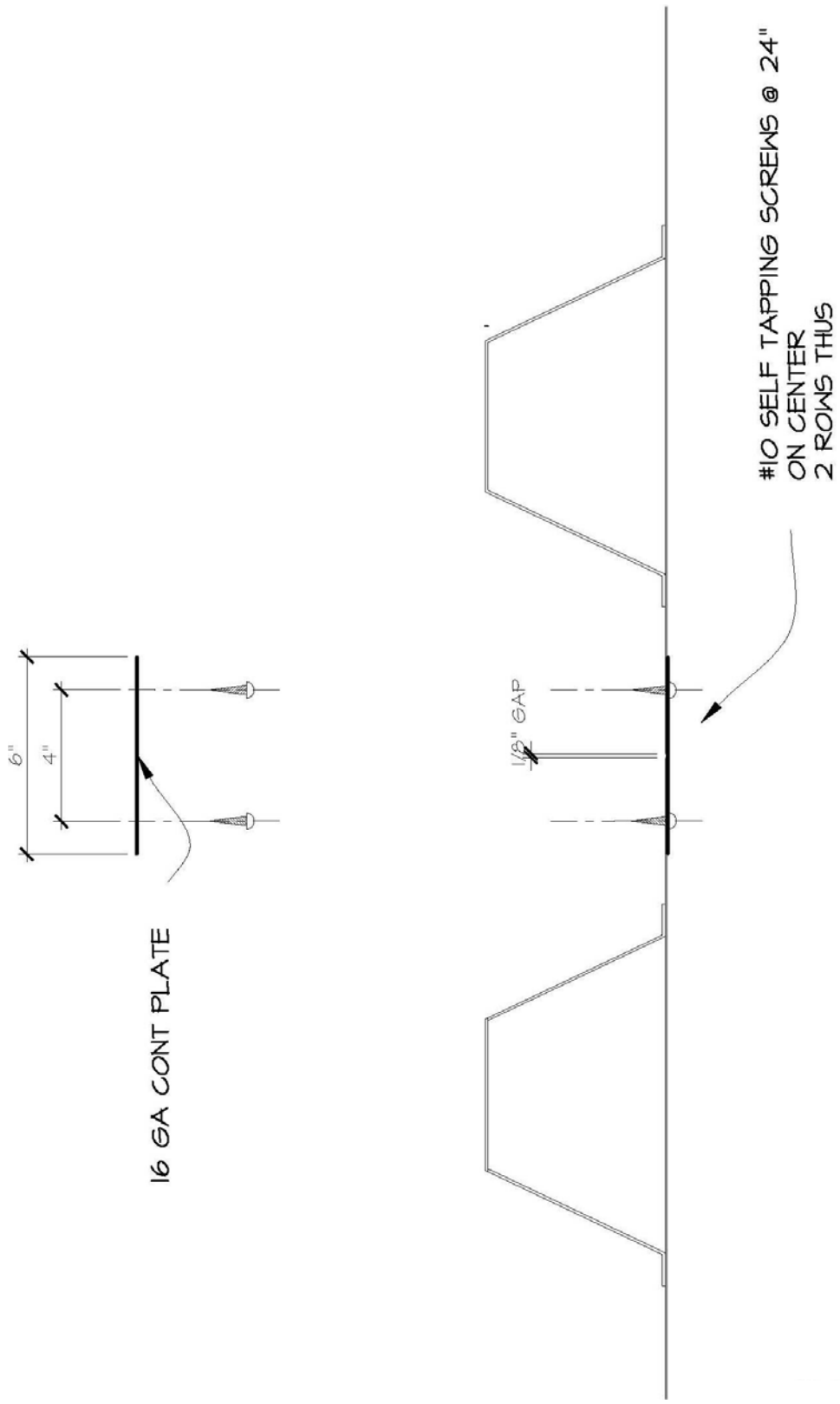

Figure 13: Panel to panel connector for stiffened plate panels, 90 mph.

Appendix I: Architectural Details

This appendix contains architectural details describing the four types of joints (panel-to-panel, ridge, soffit, and gable end - fascia) for four truss core panel configurations and two stiffened plate panel configurations. Discussion of these joints is in section 3.6 for truss core panels, and in section 4.6 for stiffened plate panels. The notes on each detail describe the manufacturing steps (M1, M2, etc.) and field installation steps (F1, F2, etc.).

Figures 1 through 16 refer to the truss core panel. Figures 1 through 4 describe exterior insulation, traditional roof panel joints. Figures 5 through 8 describe exterior insulation, integral metal roof panel joints. Figures 9 through 12 describe interior insulation, traditional roof panel joints. Figures 13 through 16 describe interior insulation, integral metal roof panel joints.

Figures 17 through 20 describe stiffened plate panel joints with a traditional roof. Figures 21 through 24 describe stiffened plate panel joints with an integral metal roof.

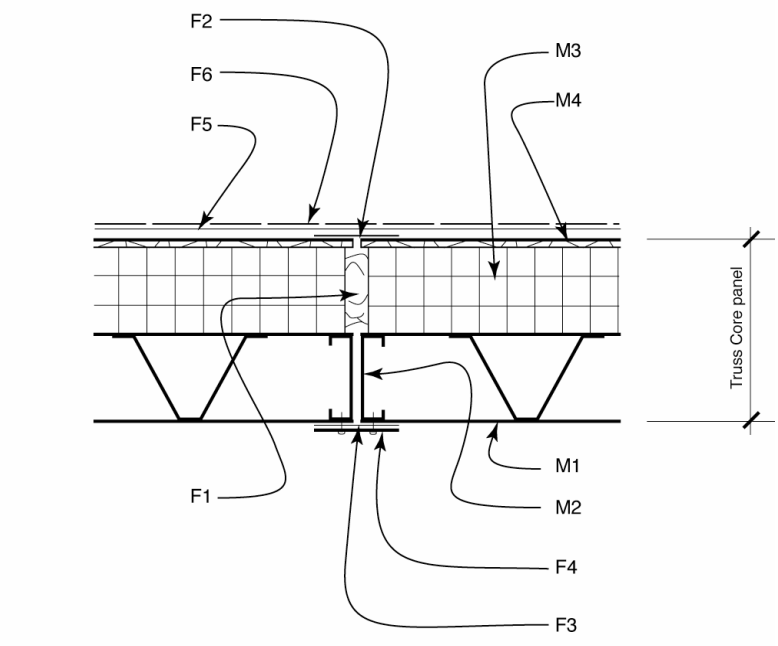

Factory-Installed Components

M1. Truss core structural section
M2. Steel channel panel edge.
M3. Polyurethane foamed-in-place insulation, installed at panel manufacturing facility. Prepare wood and metal surfaces per foam manufacturer specification prior to foam installation. Foam plastic to comply with ICC-ES AC12: "Acceptance criteria for foam plastic insulation" requirements for foam used as a part of roof assembly.
M4. APA-rated, 7/16" Oriented Strand Board (OSB) sheathing, adhered to PUR core during foam-in-place panel manufacturing operation.

Field-Installed Components

F1. Field-applied 1-part or 2-part polyurethane foam sealant. Fill void between panels and remove excess after foam cures.
F2. 1/8" gap between panel skins to allow for expansion, typ. Seal gap with polyethylene-backed, rubberized asphalt roof detailing membrane. Install membrane immediately following panel installation, to prevent potential entry of water.
F3. Polyethylene backed, butyl rubber self adhesive flexible flashing applied to panel joint before installation of steel spline. Flashing material to comply with ICC-ES criteria AC148 "Acceptance criteria for Flexible Flashing."
F4. Steel structural connector / vapor seal backup.
F5. 30# asphalt-saturated felt underlayment, installed per manufacturer specification. Felt material to comply with ICC-ES criteria AC188 "Acceptance criteria for roof underlayments."
F6. Steel or composition shingles, per architect's specification. Attach per manufacturer specification.

Figure 1: Truss Core Panel, Outside Foam, Traditional Roof. Panel-to-Panel Joint

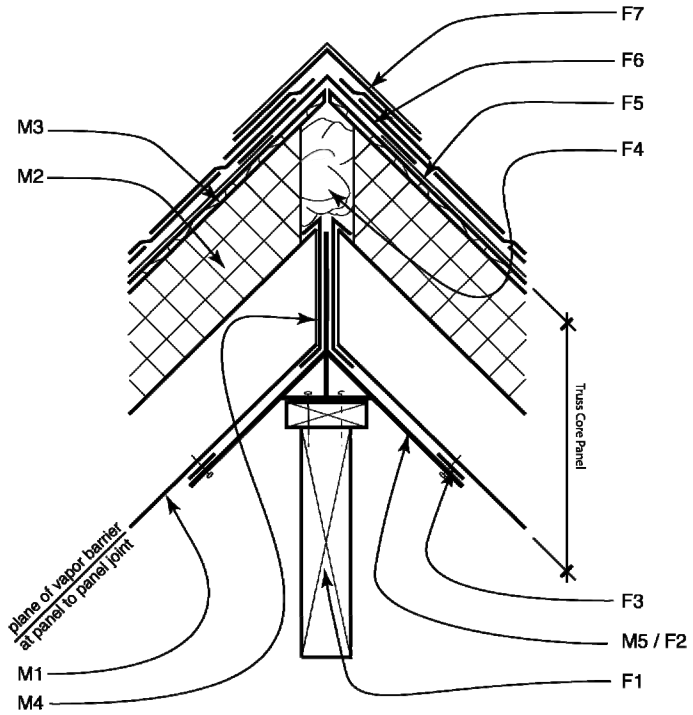

Factory-Installed Components

M1. Truss core structural section
M2. Polyurethane foamed-in-place insulation, installed at panel manufacturing facility. Prepare wood and metal surfaces per foam manufacturer specification prior to foam installation. Foam plastic to comply with ICC-ES AC12: "Acceptance criteria for foam plastic insulation" requirements for foam used as a part of roof assembly.
M3. APA-rated, 7/16" Oriented Strand Board (OSB) sheathing, adhered to PUR core during foam-in-place panel manufacturing operation.
M4. Factory-cut bevel, angle dependent on roof pitch. After panel is cut to length, machine foam to allow space for installation of metal cap. Laser weld cap to truss core structural component. Fold end cap around corners and weld to longitudinal channels, typ.
M5. Metal ridge connector, continuous.

Field-Installed Components

F1. Ridge beam or ridge truss, per structural engineer's specification.
F2. Fasten ridge connector to beam.
F3. Apply continuous strip of double-faced butyl tape as a vapor seal. Ensure vapor seal continuity at joints between connector segments with field-applied sealant. Fasten panels to ridge connector.
F4. Field-applied 1-part or 2-part polyurethane foam sealant. Fill void between panels from above, and remove excess after foam cures.
F5. 30# asphalt-saturated felt underlayment, installed per manufacturer specification. Felt material to comply with ICC-ES criteria AC188 "Acceptance criteria for roof underlayments."
F6. Steel or composition shingles, per architect's specification. Attach per manufacturer specification.
F7. Ridge detail per architectural specification.

Figure 2: Truss Core Panel, Outside Foam, Traditional Roof. Ridge Joint

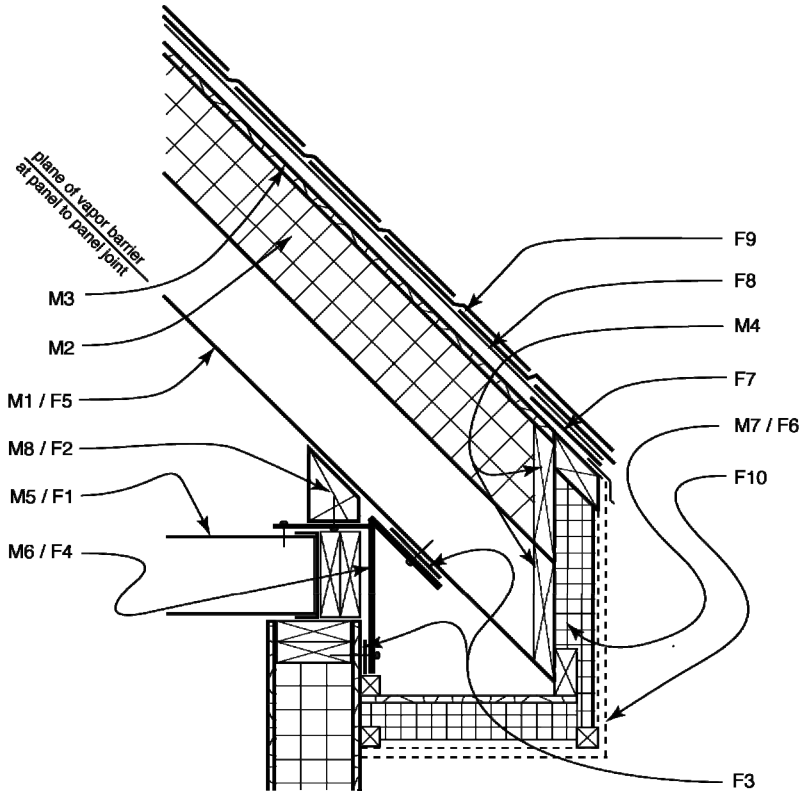

Factory-Installed Components

M1. Truss core structural section.
M2. Polyurethane foamed-in-place insulation, installed at panel manufacturing facility. Prepare wood and metal surfaces per foam manufacturer specification prior to foam installation. Foam plastic to comply with ICC-ES AC12: "Acceptance criteria for foam plastic insulation" requirements for foam used as a part of roof assembly.
M3. APA-rated, 7/16" Oriented Strand Board (OSB) sheathing, adhered to PUR core during foam-in-place panel manufacturing operation.
M4. Factory-cut bevel, angle dependent on roof pitch. After panel is cut to length, machine foam to allow space for installation of blocking. Fasten blocking in place and seal all joints with caulk or tape.
M5. Truss core attic panel or floor assembly
M6. Steel structural connector.
M7. Factory-assembled or site built, insulated soffit / fascia assembly.
M8. Wood bearing block.

Field-Installed Components

F1. Truss core attic panel or floor assembly, set on top of wall top plate. Provide appropriate blocking at rim condition.
F2. Fix bearing block to structural connector with screws driven through connector into bottom surface of block, as shown.
F3. Install continuous double-faced butyl tape as a vapor seal.
F4. Install steel structural connector and bearing block. Fasten connector to top plate of wall and exterior top of wall panel with screws as per structural design. Ensure vapor seal continuity at joints between connector segments with field-applied sealant.
F5. Crane panel into place, locating it as accurately as possible to avoid deforming vapor seals. Fasten panel to connector with screws, as shown.
F6. Soffit / fascia assembly. Install insulation to soffit and fascia. Alternately, install prefabricated soffit / fascia assembly. Ensure continuity of air sealing at insulation joints with caulk or tape, as needed.
F7. Self-adhesive flashing vapor seal. Lap over leading edge of drip edge.
F8. 30# asphalt-saturated felt underlayment, installed per manufacturer specification. Felt material to comply with ICC-ES criteria AC188: "Acceptance criteria for roof underlayments.
F9. Steel or composition shingles, per architect's specification. Attach per manufacturer specification.
F10. Soffit / fascia finish materials, per architect's specification. May be integral with soffit / fascia assembly.

Figure 3: Truss Core Panel, Outside Foam, Traditional Roof. Soffit Joint

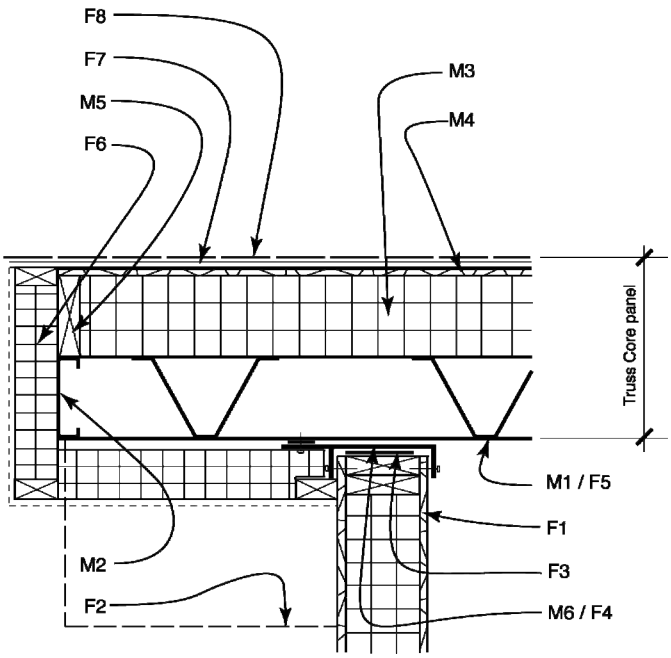

Factory-Installed Components

M1. Truss core structural section
M2. Steel channel panel edge.
M3. Polyurethane foamed-in-place insulation, installed at panel manufacturing facility. Prepare wood and metal surfaces per foam manufacturer specification prior to foam installation. Foam plastic to comply with ICC-ES AC12: "Acceptance criteria for foam plastic insulation" requirements for foam used as a part of roof assembly.
M4. APA-rated, 7/16" Oriented Strand Board (OSB) sheathing, adhered to PUR core during foam-in-place panel manufacturing operation.
M5. Factory-installed blocking. machine foam to allow space for installation of blocking. Fasten blocking in place and seal all joints with caulk or tape.
M6. Steel structural connector

Field-Installed Components

F1. Set perimeter bearing walls.
F2. Dashed line indicates beam or bracket support at ridge and soffit
F3. Install double-faced butyl tape vapor seal at wall top.
F4. Set steel structural connector on top of wall, and fasten with screws driven into top plate. Install butyl tape vapor seal on top surface, as shown. Ensure vapor seal continuity at joints between connector segments with field-applied sealant.
F5. Install roof panel and fasten to structural connector.
F6. Install insulation and finish materials to soffit and fascia. Alternately, install prefabricated soffit / fascia assembly. Ensure continuity of air sealing at insulation with caulk or tape, as needed.
F7. 30# asphalt-saturated felt underlayment, installed per manufacturer specification. Felt material to comply with ICC-ES criteria AC188: "Acceptance criteria for roof underlayments.
F8. Steel or composition shingles, per architect's specification. Attach per manufacturer specification.

Figure 4: Truss Core Panel, Outside Foam, Traditional Roof. Gable End Wall Detail

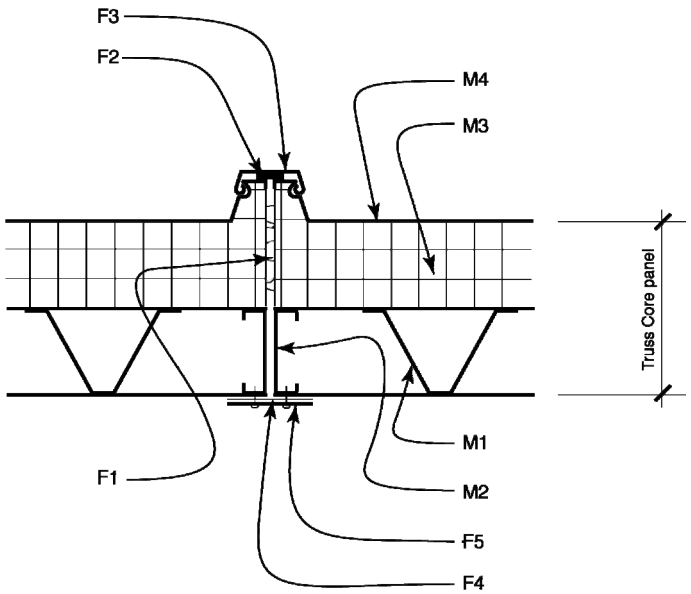

Factory-Installed Components

M1. Truss core structural section
M2. Steel channel panel edge.
M3. Polyurethane foamed-in-place insulation, installed at panel manufacturing facility. Prepare metal surfaces per foam manufacturer specification prior to foam installation. Foam plastic to comply with ICC-ES AC12: "Acceptance criteria for foam plastic insulation" requirements for foam used as a part of roof assembly.
M4. Metal top sheet / integral roof surface. Metal type and finish per architectural specification. Metal skin bonded to PUR core during foam-in-place manufacturing operation.

Field-Installed Components

F1. Field-applied 1-part or 2-part polyurethane foam sealant. Fill void between panels from above, and remove excess after foam cures.
F2. Seal joint with continuous . polyethylene backed, butyl rubber self-adhesive flexible flashing.
F3. Cap flashing, Engage with mating surfaces on adjoining panels.
F4. Polyethylene backed, butyl rubber self adhesive flexible flashing applied to panel joint before installation of steel spline. Flashing material to comply with ICC-ES criteria AC148 "Acceptance criteria for Flexible Flashing."
F5. Install steel structural connector / vapor seal backup.

Figure 5: Truss Core Panel, Outside Foam, Integral Metal Roof. Panel-to-Panel Joint

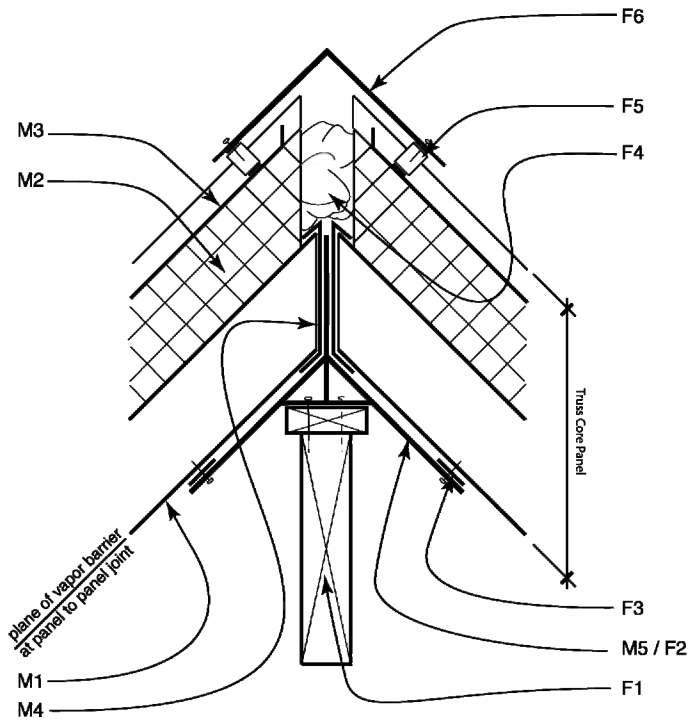

Factory-Installed Components

M1. Truss core structural section
M2. Polyurethane foamed-in-place insulation, installed at panel manufacturing facility. Prepare metal surfaces per foam manufacturer specification prior to foam installation. Foam plastic to comply with ICC-ES AC12: "Acceptance criteria for foam plastic insulation" requirements for foam used as a part of roof assembly.
M3. Metal top sheet / integral roof surface. Metal type and finish per architectural specification.
M4. Factory-cut bevel, angle dependent on roof pitch. After panel is cut to length, machine foam to allow space for installation of metal cap. Laser weld cap to truss core structural component. Fold end cap around corners and weld to longitudinal channels, typ.
M5. Metal ridge connector, continuous

Field-Installed Components

F1. Ridge beam or ridge truss, per structural engineer's specification.
F2. Fasten ridge connector to beam.
F3. Apply continuous strip of double-faced butyl tape as a vapor seal. Ensure vapor seal continuity at joints between connector segments with field-applied sealant. Fasten panels to ridge connector.
F4. Field-applied 1-part or 2-part polyurethane foam sealant. Fill void between panels from above, and remove excess after foam cures.
F5. Vapor-impermeable profile filler. Apply double-faced butyl tape to top and bottom surfaces, and set in place.
F6. Ridge flashing, per architectural design. Fasten to profile filler with self-drilling sheet metal screws with neoprene washers. Ensure fastener engagement with integral metal roof below.

Figure 6: Truss Core Panel, Outside Foam, Integral Metal Roof. Ridge Joint

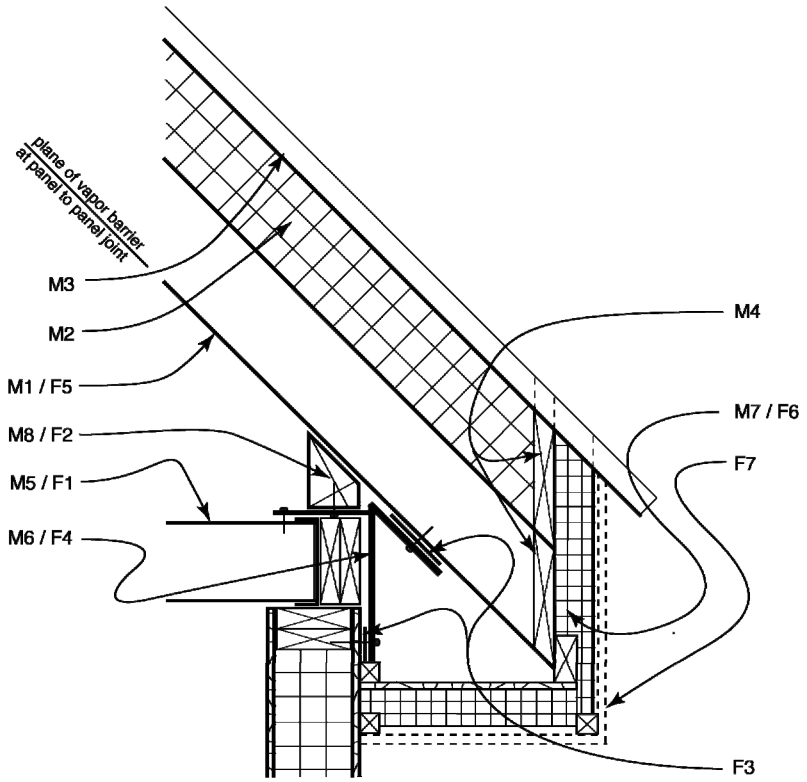

Factory-Installed Components

M1. Truss core structural section
M2. Polyurethane foamed-in-place insulation, installed at panel manufacturing facility. Prepare metal surfaces per foam manufacturer specification prior to foam installation. Foam plastic to comply with ICC-ES AC12: "Acceptance criteria for foam plastic insulation" requirements for foam used as a part of roof assembly.
M3. Metal top sheet / integral roof surface. Metal type and finish per architectural specification.
M4. Factory-cut bevel, angle dependent on roof pitch. After panel is cut to length, machine foam to allow space for installation of blocking. Fasten blocking in place and seal all joints with caulk or tape.
M5. Truss core attic panel or floor assembly
M6. Steel structural connector.
M7. Factory-assembled or site built, insulated soffit / fascia assembly.
M8. Wood bearing block.

Field-Installed Components

F1. Truss core attic panel or floor assembly, set on top of wall top plate. Provide appropriate blocking at rim condition.
F2. Fix bearing block to structural connector with screws driven through connector into bottom surface of block, as shown.
F3. Install continuous double-faced butyl tape as a vapor seal.
F4. Install steel structural connector and bearing block. Fasten connector to top plate of wall and exterior top of wall panel with screws as per structural design. Ensure vapor seal continuity at joints between connector segments with field-applied sealant.
F5. Crane panel into place, locating it as accurately as possible to avoid deforming vapor seals. Fasten connector to panel bottom skin, as shown.
F6. Soffit / fascia assembly. Install insulation to soffit and fascia. Alternately, install prefabricated soffit / fascia assembly. Ensure continuity of air sealing at insulation joints with caulk or tape, as needed.
F7. Soffit / fascia finish materials, per architect's specification. May be integral with soffit / fascia assembly.

Figure 7: Truss Core Panel, Outside Foam, Integral Metal Roof. Soffit Joint

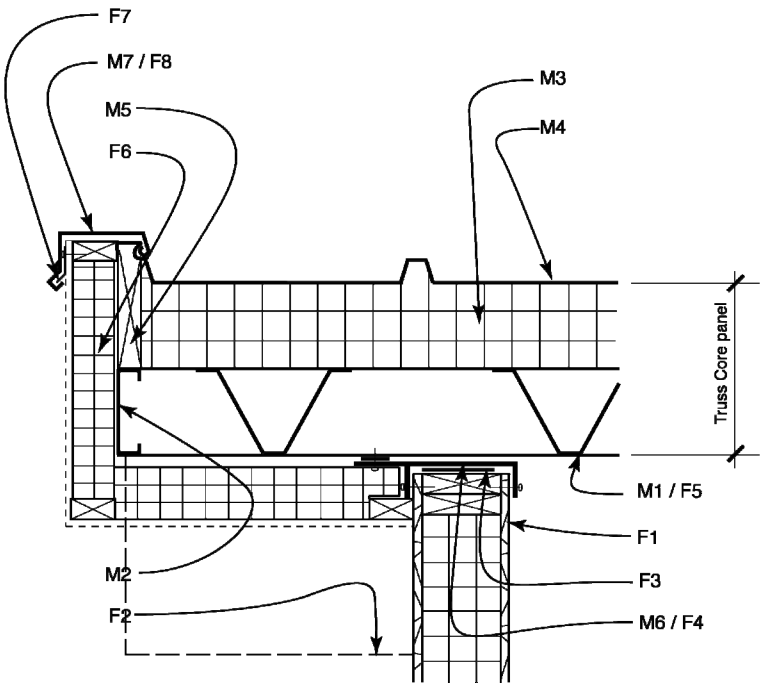

Factory-Installed Components

M1. Truss core structural section
M2. Steel channel panel edge.
M3. Polyurethane foamed-in-place insulation, installed at panel manufacturing facility. Prepare metal surfaces per foam manufacturer specification prior to foam installation. Foam plastic to comply with ICC-ES AC12: "Acceptance criteria for foam plastic insulation" requirements for foam used as a part of roof assembly.
M4. Metal top sheet / integral roof surface. Metal type and finish per architectural specification.
M5. Continuous blocking. Ensure vapor tightness by sealing all edges, or tape with self-adhesive flashing.
M6. Steel structural connector
M7. Preformed roof edge flashing and keeper.

Field-Installed Components

F1. Set perimeter bearing walls.
F2. Dashed line indicates beam or bracket support at ridge and soffit
F3. Install double-faced butyl tape vapor seal at wall top.
F4. Set steel structural connector on top of wall, and fasten with screws driven into top plate. Install butyl tape vapor seal on top surface.
F5. Install roof panel and fasten to structural connector.
F6. Install insulation and finish materials to soffit and fascia. Alternately, install prefabricated soffit / fascia assembly. Ensure continuity of air sealing at insulation with caulk or tape, as needed.
F7. Install keeper to solid blocking.
F8. Hook flashing to keeper and engage with mating surface on panel edge.

Figure 8: Truss Core Panel, Outside Foam, Integral Metal Roof. Gable End Wall Detail

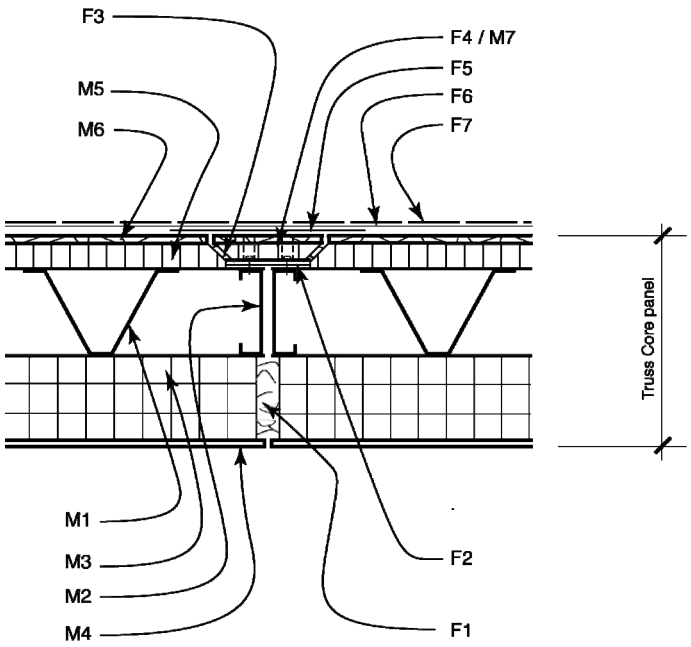

Factory-Installed Components

M1. Truss core structural section
M2. Steel channel panel edge.
M3. Polyurethane foamed-in-place insulation, installed at panel manufacturing facility. Prepare gyp. bd. and metal surfaces per foam manufacturer specification prior to foam installation. Foam plastic to comply with ICC-ES AC12: "Acceptance criteria for foam plastic insulation" requirements for foam used as a part of roof assembly.
M4. Gypsum board.
M5. EPS or PUR insulation. EPS to be adhered to steel and wood layers with 2-part polyurethane laminating adhesive. PUR to be foamed in place, and integrally adhered. Prepare wood and metal surfaces per foam or adhesive manufacturer specification.
M6. APA-rated, 7/16" Oriented Strand Board (OSB) sheathing.
M7. Spline consisting of:

- steel structural connector. Drill pilot holes for #10 sheet metal screws.
- 1" thk. EPS rigid insulation.
- 7/16" OSB sheathing.
- Components bonded with 2-part polyurethane laminating adhesive. Ensure that installed spline OSB surface matches adjacent sheathing. Counterbore foam and sheathing for fasteners.

Field-Installed Components

F1. Field-applied 1-part or 2-part polyurethane foam sealant. Fill void between panels and remove excess after foam cures.
F2. Seal joint with polyethylene-backed, rubberized asphalt roof detailing membrane. Install membrane immediately following panel installation, to prevent potential entry of water.
F3. Field-applied 1-part or 2-part polyurethane foam sealant. Install foam prior to spline installation; ensure that foam has not "skinned over" and will bond to spline surface.
F4. Composite spline. Verify fastening pattern.
F5. 1/8" gap between panel skins to allow for expansion, typ. Seal gap with backed-backed, rubberized asphalt roof detailing membrane. Install membrane immediately following spline installation, to prevent potential entry of water.
F6. 30# asphalt-saturated felt underlayment, installed per manufacturer specification. Felt material to comply with ICC-ES criteria AC188 "Acceptance criteria for roof underlayments."
F7. Steel or composition shingles, per architect's specification. Attach per manufacturer specification.

Figure 9: Truss Core Panel, Interior Foam, Traditional Roof. Panel-to-Panel Joint

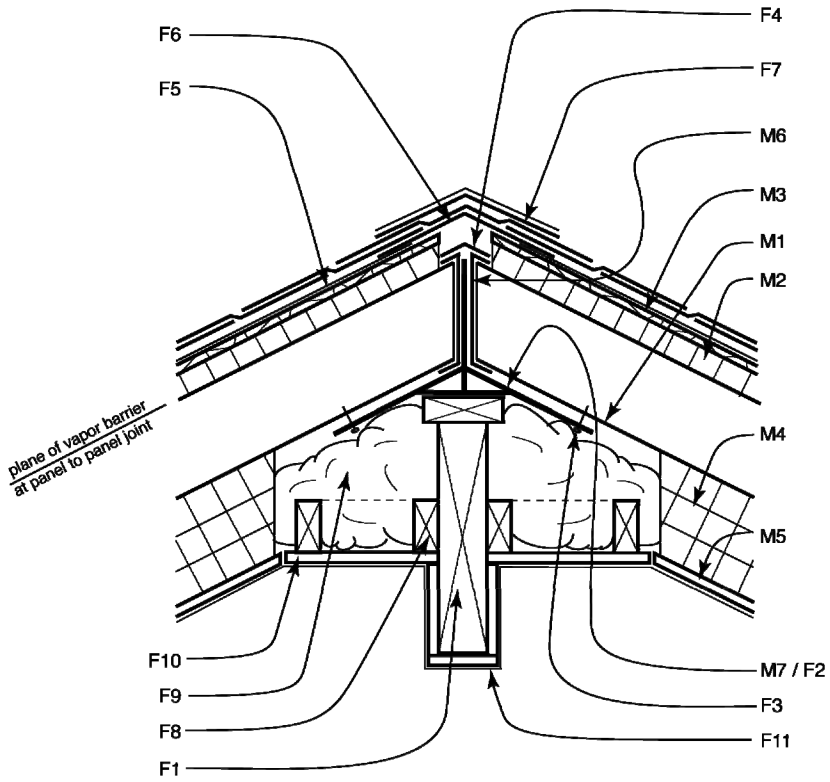

Factory-Installed Components

M1. Truss core structural section.
M2. EPS or PUR insulation. EPS to be adhered to steel and wood layers with 2-part polyurethane laminating adhesive. PUR to be foamed in place, and integrally adhered. Prepare wood and metal surfaces per foam or adhesive manufacturer specification.
M3. APA-rated, 7/16" Oriented Strand Board (OSB) sheathing, adhered to PUR or EPS insulation.
M4. Polyurethane foamed-in-place insulation, installed at panel manufacturing facility. Prepare gyp. bd. and metal surfaces per foam manufacturer specification prior to foam installation. Foam plastic to comply with ICC-ES AC12: "Acceptance criteria for foam plastic insulation" requirements for foam used as a part of roof assembly.
M5. Gypsum board
M6. Factory-cut bevel, angle dependent on roof pitch. After panel is cut to length, machine foam to allow space for installation of metal cap. Laser weld cap to truss core structural component. Fold end cap around corners and weld to longitudinal channels, typ.
M7. Metal ridge connector, continuous. Fasten to ridge beam.

Field-Installed Components

F1. Ridge beam or ridge truss, per structural engineer's specification.
F2. Fasten ridge connector to beam.
F3. Fasten panels to ridge connector .
F4. Rubberized asphalt roof detailing membrane used as a vapor seal
F5. 30# asphalt-saturated felt underlayment, installed per manufacturer specification. Felt material to comply with ICC-ES criteria AC188 "Acceptance criteria for roof underlayments."
F6. Rubberized asphalt roof detailing membrane
F7. Steel or composition shingles, per architect's specification. Attach per manufacturer specification.
F8. Blocking
F9. Field applied, 2-part polyurethane foam. Ensure continuity of insulation within the cavity.
F10. Install gypsum board over blocking.
F11. Latex paint over minimum 1 layer joint tape and 2 layers drywall compound.

Figure 10: Truss Core Panel, Interior Foam, Traditional Roof. Ridge Joint

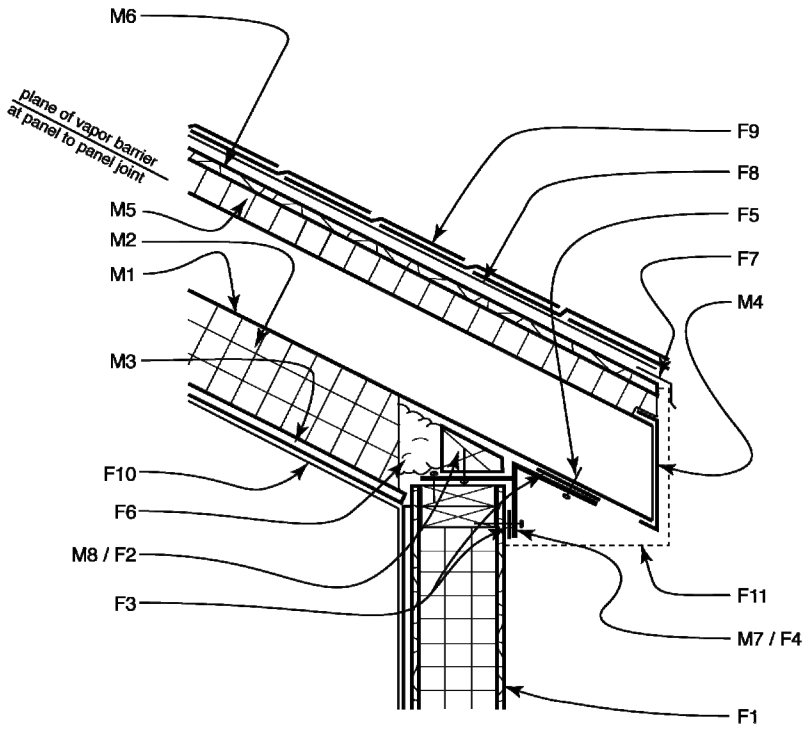

Factory-Installed Components

M1. Truss core structural section.
M2. Polyurethane foamed-in-place insulation, installed at panel manufacturing facility. Prepare gyp. bd. and metal surfaces per foam manufacturer specification prior to foam installation. Foam plastic to comply with ICC-ES AC12: "Acceptance criteria for foam plastic insulation" requirements for foam used as a part of roof assembly.
M3. Gypsum board
M4. Steel end cap. Machine foam back after panel is cut to finished length, and laser weld cap to truss core structural component. Fold end cap around corners and weld to longitudinal channels, typ.
M5. EPS or PUR insulation. EPS to be adhered to steel and wood layers with 2-part polyurethane laminating adhesive. PUR to be foamed in place, and integrally adhered. Prepare wood and metal surfaces per foam or adhesive manufacturer specification.
M6. APA-rated, 7/16" Oriented Strand Board (OSB) sheathing, adhered to PUR or EPS insulation.
M7. Steel structural connector.
M8. Wood bearing block.

Field-Installed Components

F1. Set perimeter bearing walls.
F2. Fix bearing block to structural connector with screws driven through connector into bottom surface of block, as shown.
F3. Install continuous double-faced butyl tape as a vapor seal.
F4. Install steel structural connector and bearing block. Fasten connector to top plate of wall and exterior top of wall panel with screws as per structural design. Ensure vapor seal continuity at joints between connector segments with field-applied sealant.
F5. Crane panel into place, locating it as accurately as possible to avoid deforming vapor seals. Fasten connector to panel bottom skin, as shown.
F6. Field applied, 1-part or 2-part polyurethane foam. Ensure continuity of insulation within the cavity.
F7. Drip edge
F8. 30# asphalt-saturated felt underlayment, installed per manufacturer specification. Felt material to comply with ICC-ES criteria AC188: "Acceptance criteria for roof underlayments.
F9. Steel or composition shingles, per architect's specification. Attach per manufacturer specification.
F10. Latex paint over minimum 1 layer joint tape and 2 layers drywall compound.
F11. Soffit and fascia per architectural design

Figure 11: Truss Core Panel, Interior Foam, Traditional Roof. Soffit Joint

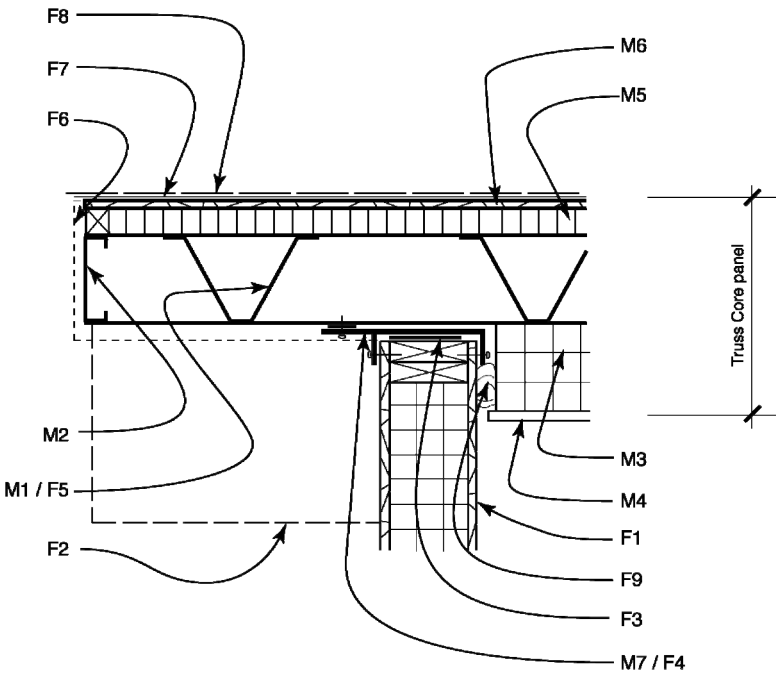

Factory-Installed Components

M1. Truss core structural section
M2. Steel channel panel edge.
M3. Polyurethane foamed-in-place insulation, installed at panel manufacturing facility. Prepare steel and gypsum board surfaces per foam manufacturer specification prior to foam installation. Foam plastic to comply with ICC-ES AC12: "Acceptance criteria for foam plastic insulation" requirements for foam used as a part of roof assembly.
M4. Gypsum board
M5. EPS or PUR insulation. EPS to be adhered to steel and wood layers with 2-part polyurethane laminating adhesive. PUR to be foamed in place, and integrally adhered. Prepare wood and metal surfaces per foam or adhesive manufacturer specification.
M6. APA-rated, 7/16" Oriented Strand Board (OSB) sheathing, adhered to PUR or EPS insulation.
M7. Steel structural connector.

Field-Installed Components

F1. Set perimeter bearing walls.
F2. Dashed line indicates beam or bracket support at ridge and soffit
F3. Install double-faced butyl tape vapor seal at wall top.
F4. Set steel structural connector on top of wall, and fasten with screws driven into top plate. Install butyl tape vapor seal on top surface.
F5. Install roof panel and fasten to structural connector.
F6. Install finish materials to soffit and fascia. Alternately, install prefabricated soffit / fascia assembly.
F7. 30# asphalt-saturated felt underlayment, installed per manufacturer specification. Felt material to comply with ICC-ES criteria AC188: "Acceptance criteria for roof underlayments.
F8. Steel or composition shingles, per architect's specification. Attach per manufacturer specification.
F9. Field applied, 1-part or 2-part polyurethane foam. Ensure continuity of insulation within the cavity.

Figure 12: Truss Core Panel, Interior Foam, Traditional Roof. Gable End Wall Joint

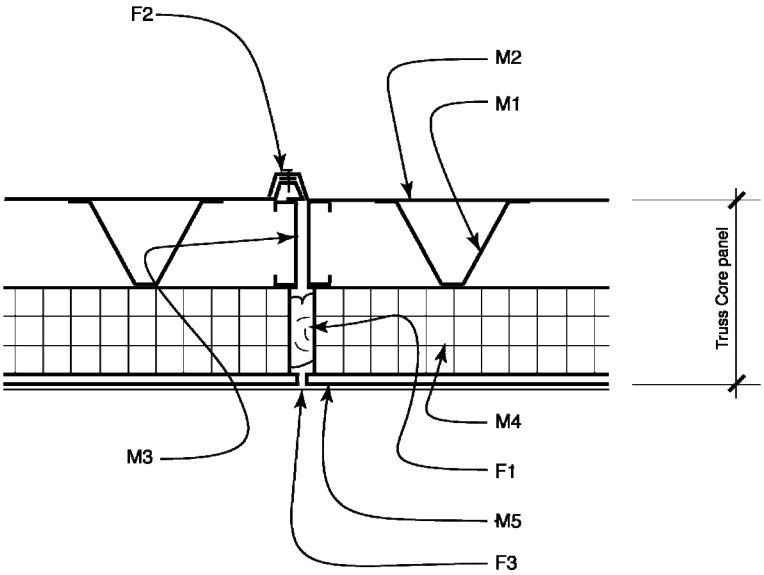

Factory-Installed Components

M1. Truss core structural section
M2. Metal top sheet / integral roof surface. Metal type and finish per architectural specification.
M3. Steel channel panel edge.
M4. Polyurethane foamed-in-place insulation, installed at panel manufacturing facility. Prepare gyp. bd. and metal surfaces per foam manufacturer specification prior to foam installation. Foam plastic to comply with ICC-ES AC12: "Acceptance criteria for foam plastic insulation" requirements for foam used as a part of roof assembly.
M5. Gypsum board

Field-Installed Components

F1. Field-applied 1-part or 2-part polyurethane foam sealant. Fill void between panels and remove excess after foam cures.
F2. Integral self-flashing joint @ metal roof surface. Seal with 1-inch wide butyl rubber double-faced tape, continuous at crest of corrugation between roof layers. Fasten roof layers with galvanized self-drilling roofing screws with integral neoprene washers.
F3. Latex paint over minimum 1 layer joint tape and 2 layers drywall compound.

Figure 13: Truss Core Panel, Interior Foam, Integral Metal Roof. Panel-to-Panel Joint

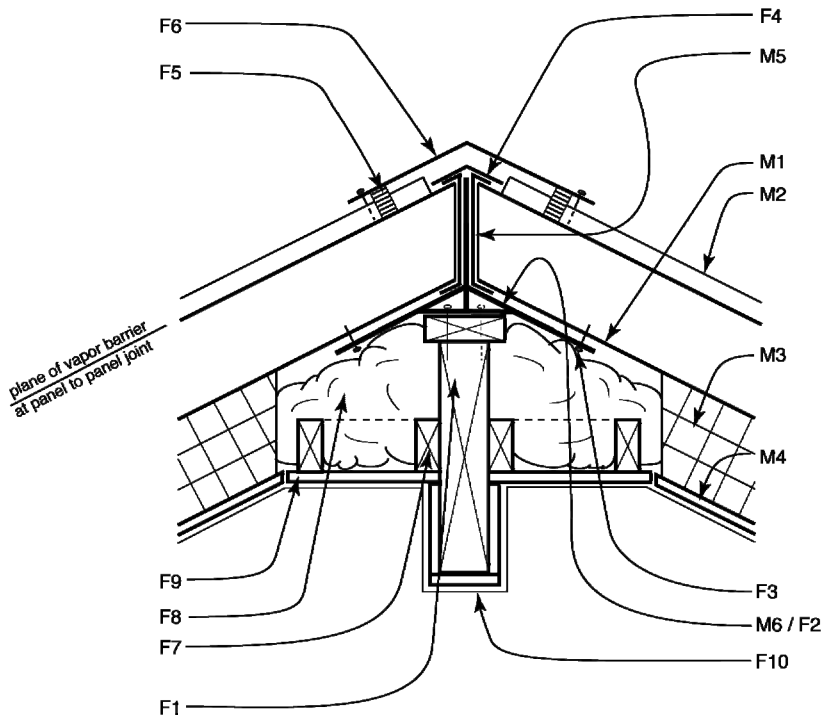

Factory-Installed Components

M1. Truss core structural section.
M2. Top structural skin / roof finish sheet. Arrow indicates crest of corrugation beyond.
M3. Polyurethane foamed-in-place insulation, installed at panel manufacturing facility. Prepare gyp. bd. and metal surfaces per foam manufacturer specification prior to foam installation. Foam plastic to comply with ICC-ES AC12: "Acceptance criteria for foam plastic insulation" requirements for foam used as a part of roof assembly.
M4. Gypsum board
M5. Factory-cut bevel, angle dependent on roof pitch. After panel is cut to length, machine foam and gyp. bd. back as shown. Machine corrugations back as shown, to allow installation of steel end cap and to expose structural cavity for optional ventilation. Laser weld cap to truss core structural component. Fold end cap around corners and weld to longitudinal channels, typ.
M6. Metal ridge connector, continuous.

Field-Installed Components

F1. Ridge beam or ridge truss, per structural engineer's specification.
F2. Fasten ridge connector to beam.
F3. Fasten panels to ridge connector.
F4. Rubberized asphalt roof detailing membrane used as a vapor seal
F5. Perforated or impermeable profile filler, depending on venting option
F6. Fasten sheet metal ridge flashing to crests of corrugations.
F7. Blocking
F8. Field applied, 2-part polyurethane foam or rigid foam. Ensure continuity of insulation within the cavity.
F9. Install gypsum board over blocking.
F10. Latex paint over minimum 1 layer joint tape and 2 layers drywall compound.

Figure 14: Truss Core Panel, Interior Foam, Integral Metal Roof. Ridge Joint

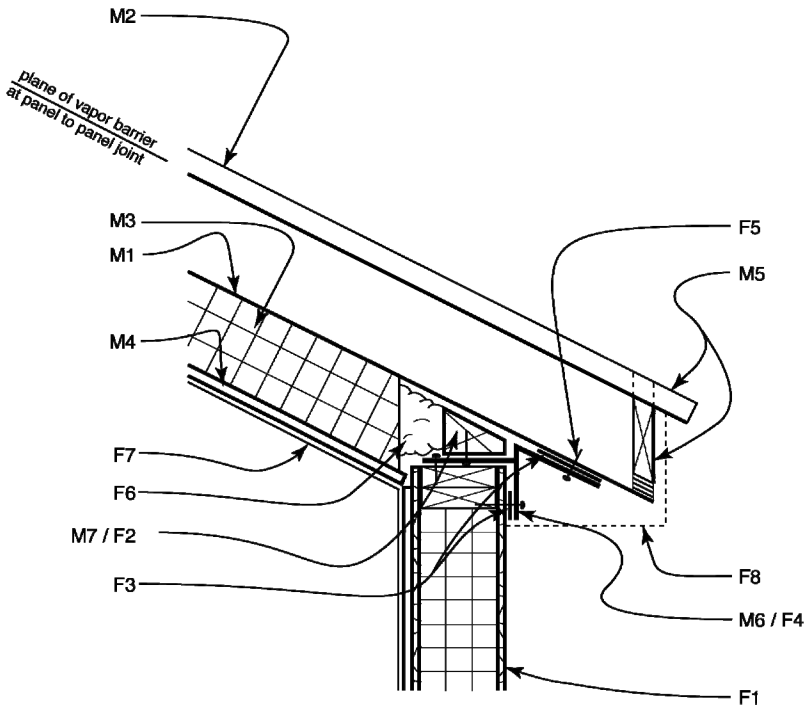

Factory-Installed Components

M1. Truss core structural section.
M2. Top structural skin / roof finish sheet. Arrow indicates crest of corrugation beyond.
M3. Polyurethane foamed-in-place insulation, installed at panel manufacturing facility. Prepare gyp. bd. and metal surfaces per foam manufacturer specification prior to foam installation. Foam plastic to comply with ICC-ES AC12: "Acceptance criteria for foam plastic insulation" requirements for foam used as a part of roof assembly.
M4. Gypsum board
M5. Machine panel end as shown, leaving top sheet long to create a drip edge. Provide for ventilation and drainage with perforated blocking, or use impermeable blocking if venting is not desired. Seal all around web filler materials to prevent insect entry.
M6. Steel structural connector.
M7. Wood bearing block.

Field-Installed Components

F1. Set perimeter bearing walls.
F2. Fix bearing block to structural connector with screws driven through connector into bottom surface of block, as shown.
F3. Install continuous double-faced butyl tape as a vapor seal.
F4. Install steel structural connector and bearing block. Fasten connector to top plate of wall and exterior top of wall panel with screws as per structural design. Ensure vapor seal continuity at joints between connector segments with field-applied sealant.
F5. Crane panel into place, locating it as accurately as possible to avoid deforming vapor seals. Fasten connector to panel bottom skin, as shown.
F6. Field applied, 1-part or 2-part polyurethane foam. Ensure continuity of insulation within the cavity.
F7. Latex paint over minimum 1 layer joint tape and 2 layers drywall compound.
F8. Soffit and fascia per architectural design.

Figure 15: Truss Core Panel, Interior Foam, Integral Metal Roof. Soffit Joint

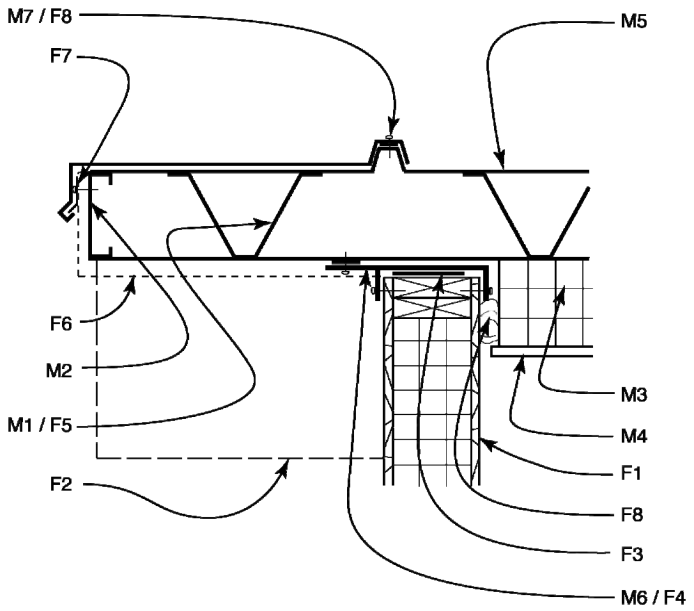

Factory-Installed Components

M1. Truss core structural section
M2. Steel channel panel edge.
M3. Polyurethane foamed-in-place insulation, installed at panel manufacturing facility. Prepare steel and gypsum board surfaces per foam manufacturer specification prior to foam installation. Foam plastic to comply with ICC-ES AC12: "Acceptance criteria for foam plastic insulation" requirements for foam used as a part of roof assembly.
M4. Gypsum board
M5. Metal top sheet / integral roof surface. Metal type and finish per architectural specification.
M6. Steel structural connector.
M7. Preformed roof edge flashing and keeper.

Field-Installed Components

F1. Set perimeter bearing walls.
F2. Dashed line indicates beam or bracket support at ridge and soffit
F3. Install double-faced butyl tape vapor seal at wall top.
F4. Set steel structural connector on top of wall, and fasten with screws driven into top plate. Install butyl tape vapor seal on top surface.
F5. Install roof panel and fasten to structural connector.
F6. Install finish materials to soffit and fascia. Alternately, install prefabricated soffit / fascia assembly.
F7. Install keeper to solid blocking.
F8. Install double-faced butyl tape as a backup waterproof layer. Hook flashing to keeper and fasten to corrugation with self-drilling roofing screws with neoprene washers.

Figure 16: Truss Core Panel, Interior Foam, Integral Metal Roof. Gable End Wall Joint

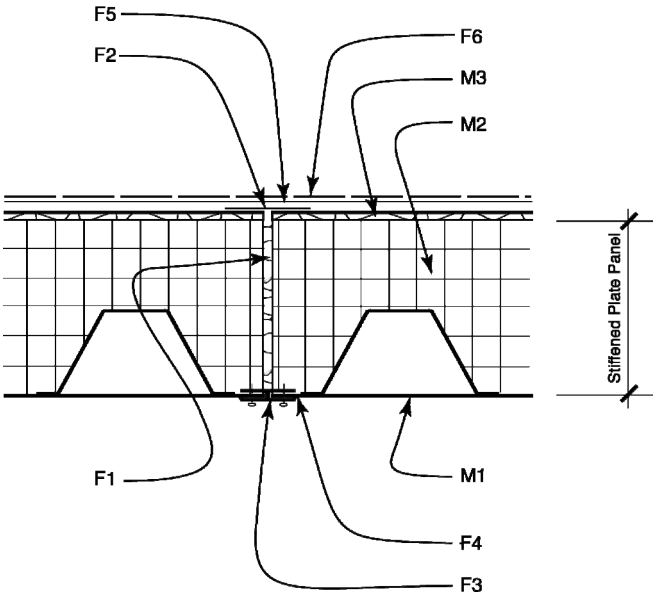

Factory-Installed Components

M1. Stiffened plate structural section
M2. Polyurethane foamed-in-place insulation, installed at panel manufacturing facility. Prepare wood and metal surfaces per foam manufacturer specification prior to foam installation. Foam plastic to comply with ICC-ES AC12: "Acceptance criteria for foam plastic insulation" requirements for foam used as a part of roof assembly.
M4. APA-rated, 7/16" Oriented Strand Board (OSB) sheathing, adhered to PUR core during foam-in-place panel manufacturing operation.

Field-Installed Components

F1. Field-applied 1-part or 2-part polyurethane foam sealant. Fill void between panels and remove excess after foam cures.
F2. 1/8" gap between panel skins to allow for expansion, typ. Seal gap with polyethylene-backed, rubberized asphalt roof detailing membrane. Install membrane immediately following panel installation, to prevent potential entry of water.
F3. Steel structural connector. Place one panel, and fasten connector to panel edge with sheet metal screws. Then engage second panel with connector as it is placed, and fasten with sheet metal screws.
F4. Polyurethane caulk vapor seal, continuous along both edges of connector.
F5. 30# asphalt-saturated felt underlayment, installed per manufacturer specification. Felt material to comply with ICC-ES criteria AC188 "Acceptance criteria for roof underlayments."
F6. Steel or composition shingles, per architect's specification. Attach per manufacturer specification.

Figure 17: Stiffened Plate Panel, Traditional Roof.
Panel-to-Panel Joint

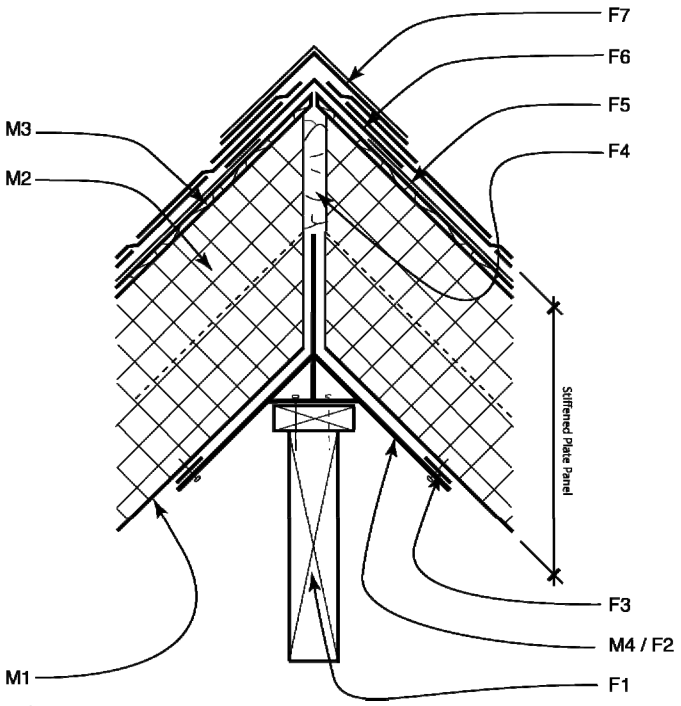

Factory-Installed Components

M1. Stiffened plate structural section
M2. Polyurethane foamed-in-place insulation, installed at panel manufacturing facility. Prepare wood and metal surfaces per foam manufacturer specification prior to foam installation. Foam plastic to comply with ICC-ES AC12: "Acceptance criteria for foam plastic insulation" requirements for foam used as a part of roof assembly.
M3. APA-rated, 7/16" Oriented Strand Board (OSB) sheathing, adhered to PUR core during foam-in-place panel manufacturing operation.
M4. Metal ridge connector, continuous.

Field-Installed Components

F1. Ridge beam or ridge truss, per structural engineer's specification.
F2. Fasten ridge connector to beam.
F3. Apply continuous strip of double-faced butyl tape as a vapor seal. Ensure vapor seal continuity at joints between connector segments with field-applied sealant. Fasten panels to ridge connector.
F4. Field-applied 1-part or 2-part polyurethane foam sealant. Fill void between panels from above, and remove excess after foam cures.
F5. 30# asphalt-saturated felt underlayment, installed per manufacturer specification. Felt material to comply with ICC-ES criteria AC188 "Acceptance criteria for roof underlayments."
F6. Polyethylene backed, butyl rubber self adhesive flexible flashing
F7. Steel or composition shingles, per architect's specification. Attach per manufacturer specification.
F8. Ridge detail per architectural specification.

Figure 18: Stiffened Plate Panel, Traditional Roof. Ridge Joint

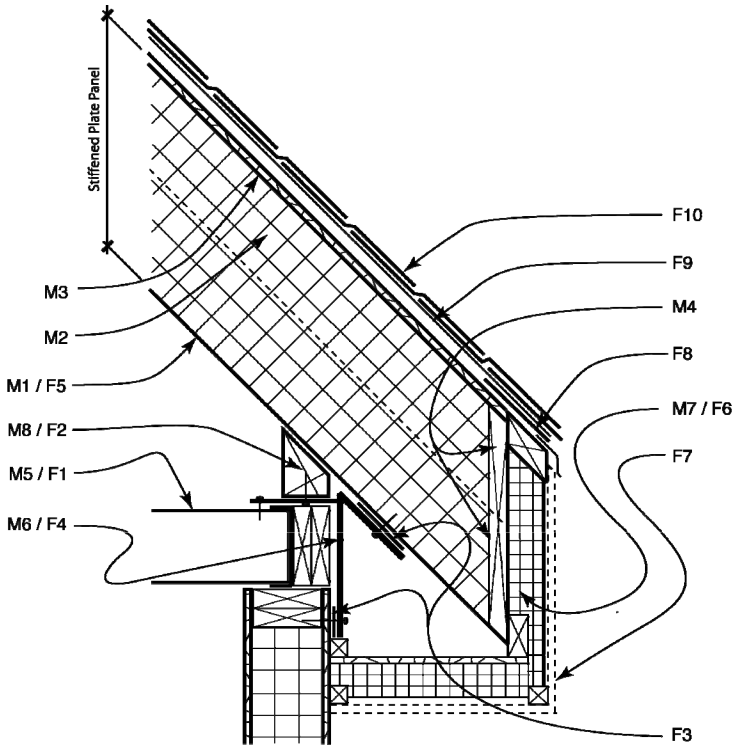

Factory-Installed Components

M1. Stiffened plate structural section.
M2. Polyurethane foamed-in-place insulation, installed at panel manufacturing facility. Prepare wood and metal surfaces per foam manufacturer specification prior to foam installation. Foam plastic to comply with ICC-ES AC12: "Acceptance criteria for foam plastic insulation" requirements for foam used as a part of roof assembly.
M3. APA-rated, 7/16" Oriented Strand Board (OSB) sheathing, adhered to PUR core during foam-in-place panel manufacturing operation.
M4. Factory-cut bevel, angle dependent on roof pitch. After panel is cut to length, machine foam to allow space for installation of blocking. Install blocking in insulation layer and in structural channels, then seal all joints with caulk or tape.
M5. Truss core attic panel or floor assembly
M6. Steel structural connector.
M7. Factory-assembled or site built, insulated soffit / fascia assembly.
M8. Wood bearing block.

Field-Installed Components

F1. Truss core attic panel or floor assembly, set on top of wall top plate. Provide appropriate blocking at rim condition.
F2. Fix bearing block to structural connector with screws driven through connector into bottom surface of block, as shown.
F3. Install continuous double-faced butyl tape as a vapor seal.
F4. Install steel structural connector and bearing block. Fasten connector to top plate of wall and exterior top of wall panel with screws as per structural design. Ensure vapor seal continuity at joints between connector segments with field-applied sealant.
F5. Crane panel into place, locating it as accurately as possible to avoid deforming vapor seals. Fasten panel to connector with screws, as shown.
F6. Soffit / fascia assembly. Install insulation to soffit and fascia. Alternately, install prefabricated soffit / fascia assembly. Ensure continuity of air sealing at insulation joints with caulk or tape, as needed.
F7. Soffit / fascia finish materials, per architect's specification. May be integral with soffit / fascia assembly.
F8. Self-adhesive flashing vapor seal. Lap over leading edge of drip edge.
F9. 30# asphalt-saturated felt underlayment, installed per manufacturer specification. Felt material to comply with ICC-ES criteria AC188: "Acceptance criteria for roof underlayments.
F10. Steel or composition shingles, per architect's specification. Attach per manufacturer specification.

Figure 19: Stiffened Plate Panel, Traditional Roof. Soffit Joint

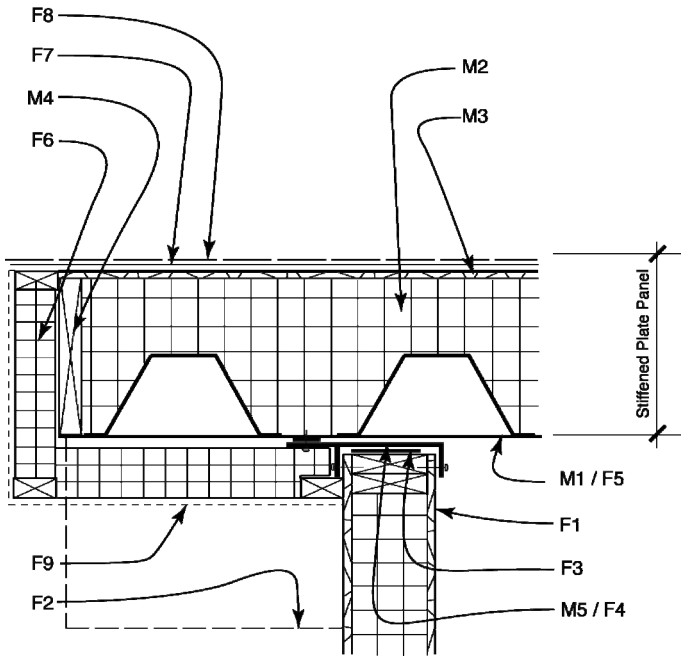

Factory-Installed Components

M1. Stiffened plate structural section
M2. Polyurethane foamed-in-place insulation, installed at panel manufacturing facility. Prepare wood and metal surfaces per foam manufacturer specification prior to foam installation. Foam plastic to comply with ICC-ES AC12: "Acceptance criteria for foam plastic insulation" requirements for foam used as a part of roof assembly.
M3. APA-rated, 7/16" Oriented Strand Board (OSB) sheathing, adhered to PUR core during foam-in-place panel manufacturing operation.
M4. Factory-installed blocking. machine foam to allow space for installation of blocking. Fasten blocking in place and seal all joints with caulk or tape.
M5. Steel structural connector

Field-Installed Components

F1. Set perimeter bearing walls.
F2. Dashed line indicates beam or bracket support at ridge and soffit
F3. Install double-faced butyl tape vapor seal at wall top.
F4. Set steel structural connector on top of wall, and fasten with screws driven into top plate. Install butyl tape vapor seal on top surface, as shown. Ensure vapor seal continuity at joints between connector segments with field-applied sealant.
F5. Install roof panel and fasten to structural connector.
F6. Install insulation and finish materials to soffit and fascia. Alternately, install prefabricated soffit / fascia assembly. Ensure continuity of air sealing at insulation with caulk or tape, as needed.
F7. 30# asphalt-saturated felt underlayment, installed per manufacturer specification. Felt material to comply with ICC-ES criteria AC188: "Acceptance criteria for roof underlayments.
F8. Steel or composition shingles, per architect's specification. Attach per manufacturer specification.

Figure 20: Stiffened Plate Panel, Traditional Roof. Gable End Wall Joint

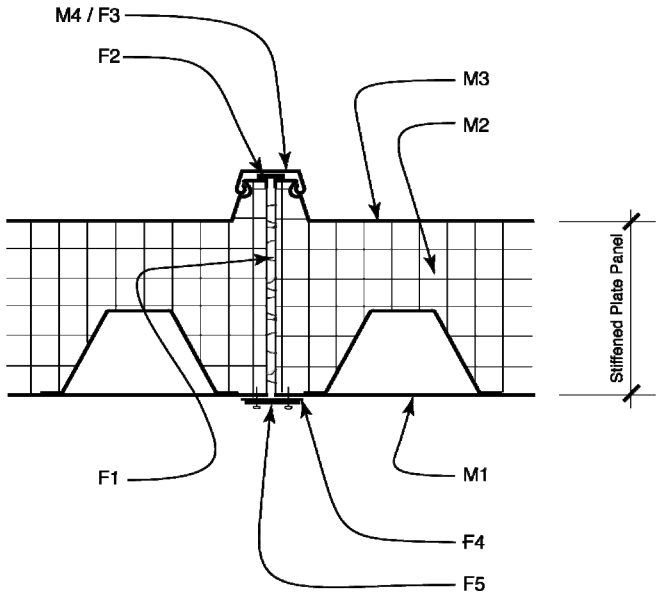

Factory-Installed Components

M1. Stiffened plate structural section.
M2. Polyurethane foamed-in-place insulation, installed at panel manufacturing facility. Prepare metal surfaces per foam manufacturer specification prior to foam installation. Foam plastic to comply with ICC-ES AC12: "Acceptance criteria for foam plastic insulation" requirements for foam used as a part of roof assembly.
M3. Metal top sheet / integral roof surface. Metal type and finish per architectural specification. Metal skin bonded to PUR core during foam-in-place manufacturing operation.
M4. Prefabricated cap flashing

Field-Installed Components

F1. Field-applied 1-part or 2-part polyurethane foam sealant. Fill void between panels from above, and remove excess after foam cures.
F2. Seal joint with continuous . polyethylene backed, butyl rubber self-adhesive flexible flashing.
F3. Cap flashing, Engage with mating surfaces on adjoining panels.
F4. Steel structural connector. Place one panel, and fasten connector to panel edge with sheet metal screws. Then engage second panel with connector as it is placed, and fasten with sheet metal screws.
F5. Polyurethane caulk vapor seal, continuous along both edges of connector.

Figure 21: Stiffened Plate Panel, Integral Metal Roof. Panel-to-Panel Joint

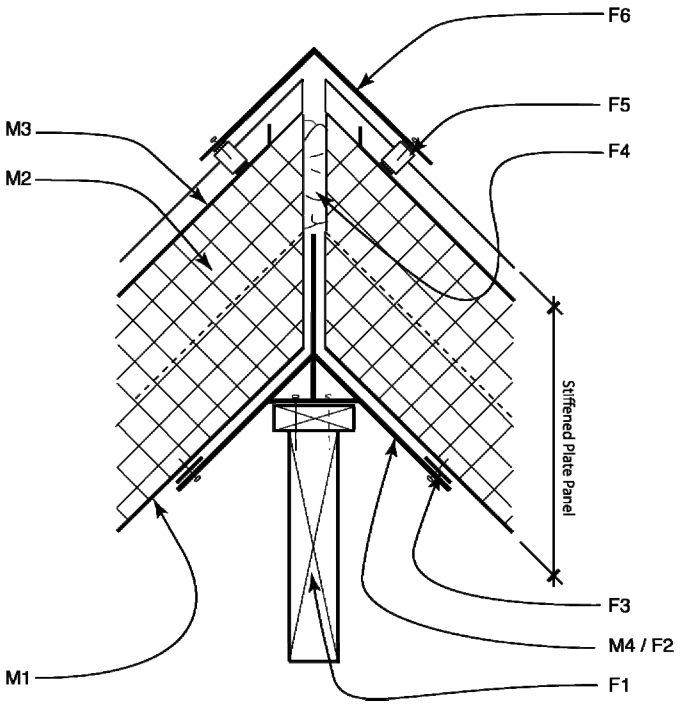

Factory-Installed Components

M1. Stiffened plate structural section
M2. Polyurethane foamed-in-place insulation, installed at panel manufacturing facility. Prepare metal surfaces per foam manufacturer specification prior to foam installation. Foam plastic to comply with ICC-ES AC12: "Acceptance criteria for foam plastic insulation" requirements for foam used as a part of roof assembly.
M3. Metal top sheet / integral roof surface. Metal type and finish per architectural specification.
M4. Metal ridge connector, continuous

Field-Installed Components

F1. Ridge beam or ridge truss, per structural engineer's specification.
F2. Fasten ridge connector to beam .
F3. Apply continuous strip of double-faced butyl tape as a vapor seal. Ensure vapor seal continuity at joints between connector segments with field-applied sealant. Fasten panels to ridge connector.
F4. Field-applied 1-part or 2-part polyurethane foam sealant. Fill void between panels from above, and remove excess after foam cures.
F5. Vapor-impermeable profile filler. Apply double-faced butyl tape to top and bottom surfaces, and set in place.
F6. Ridge flashing, per architectural design. Fasten to profile filler with self-drilling sheet metal screws with neoprene washers. Ensure fastener engagement with integral metal roof below.

Figure 22: Stiffened Plate Panel, Integral Metal Roof. Ridge Joint

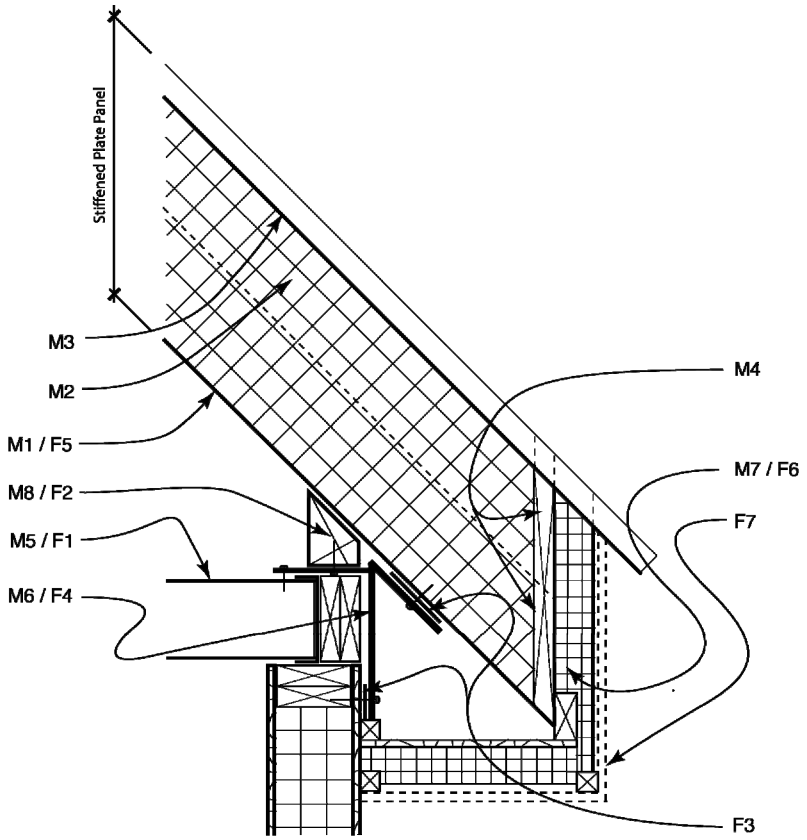

Factory-Installed Components

M1. Stiffened plate structural section
M2. Polyurethane foamed-in-place insulation, installed at panel manufacturing facility. Prepare metal surfaces per foam manufacturer specification prior to foam installation. Foam plastic to comply with ICC-ES AC12: "Acceptance criteria for foam plastic insulation" requirements for foam used as a part of roof assembly.
M3. Metal top sheet / integral roof surface. Metal type and finish per architectural specification.
M4. Factory-cut bevel, angle dependent on roof pitch. After panel is cut to length, machine foam to allow space for installation of blocking. Install blocking in insulation layer and in structural channels, then seal all joints with caulk or tape.
M5. Truss core attic panel or floor assembly
M6. Steel structural connector.
M7. Factory-assembled or site built, insulated soffit / fascia assembly.
M8. Wood bearing block.

Field-Installed Components

F1. Truss core attic panel or floor assembly, set on top of wall top plate. Provide appropriate blocking at rim condition.
F2. Fix bearing block to structural connector with screws driven through connector into bottom surface of block, as shown.
F3. Install continuous double-faced butyl tape as a vapor seal.
F4. Install steel structural connector and bearing block. Fasten connector to top plate of wall and exterior top of wall panel with screws as per structural design. Ensure vapor seal continuity at joints between connector segments with field-applied sealant.
F5. Crane panel into place, locating it as accurately as possible to avoid deforming vapor seals. Fasten connector to panel bottom skin, as shown.
F6. Soffit / fascia assembly. Install insulation to soffit and fascia. Alternately, install prefabricated soffit / fascia assembly. Ensure continuity of air sealing at insulation joints with caulk or tape, as needed.
F7. Soffit / fascia finish materials, per architect's specification. May be integral with soffit / fascia assembly.

Figure 23: Stiffened Plate Panel, Integral Metal Roof. Soffit Joint

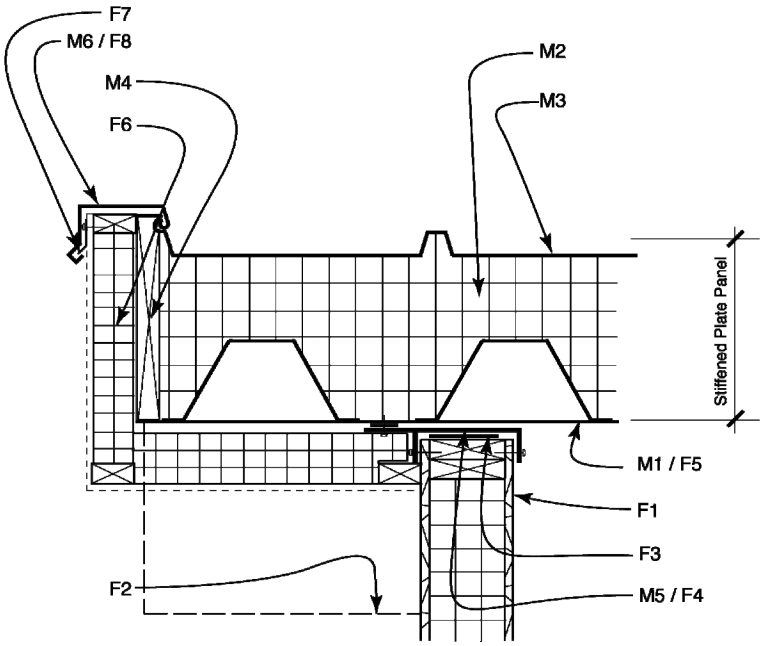

Factory-Installed Components

M1. Stiffened plate structural section.
M2. Polyurethane foamed-in-place insulation, installed at panel manufacturing facility. Prepare metal surfaces per foam manufacturer specification prior to foam installation. Foam plastic to comply with ICC-ES AC12: "Acceptance criteria for foam plastic insulation" requirements for foam used as a part of roof assembly.
M3. Metal top sheet / integral roof surface. Metal type and finish per architectural specification.
M4. Continuous blocking. Ensure vapor tightness by sealing all edges, or tape with self-adhesive flashing.
M5. Steel structural connector
M6. Preformed roof edge flashing and keeper.

Field-Installed Components

F1. Set perimeter bearing walls.
F2. Dashed line indicates beam or bracket support at ridge and soffit
F3. Install double-faced butyl tape vapor seal at wall top.
F4. Set steel structural connector on top of wall, and fasten with screws driven into top plate. Install butyl tape vapor seal on top surface.
F5. Install roof panel and fasten to structural connector.
F6. Install insulation and finish materials to soffit and fascia. Alternately, install prefabricated soffit / fascia assembly. Ensure continuity of air sealing at insulation with caulk or tape, as needed.
F7. Install keeper to solid blocking.
F8. Hook flashing to keeper and engage with mating surface on panel edge.

Figure 24: Stiffened Plate Panel, Integral Metal Roof. Gable End Wall Joint

Appendix J: PV Thermal Management

This appendix provides a full description of the method and results of our analysis of the thermal performance of PV panels attached directly to the truss core panel. The University of Minnesota advocates a passive approach for thermal management of PV integrated truss core panels used in southern climates (where the foam insulation is placed below the metal structural component. Cooling can be handled by air flow in the channel formed by the standing metal seam or other suitable standoff from the top face sheet. The material presented in this appendix is in the form of a paper submitted to the scientific journal *Solar Energy*.

A Model and Heat Transfer Correlation for Rooftop Integrated Photovoltaics with a Passive Air Cooling Channel

Gur Mittelman, Aiman Alshare, Jane H. Davidson*
Department of Mechanical Engineering
University of Minnesota
111 Church St., S.E.
Minneapolis, MN 55455

Abstract

Photovoltaic (PV) panels can experience undesirably high temperatures due to the heat input by that part of the absorbed solar radiation which is not converted into electricity. Regulation of the temperature rise is necessary to maintain maximum solar to electric conversion. One approach for temperature regulation, suitable for rooftop integrated PV, involves fitting an open channel beneath the PV module. The panels are cooled by radiation and free convection as ambient air rises through the channel. A scale analysis and numerical study of PV modules with a back mounted air channel provides heat transfer rates over a practical range of operating conditions and channel geometries. A generalized correlation for the average channel Nusselt number for the combined convective-radiative cooling is developed for modified channel Rayleigh numbers from 10^2 to 10^8, channel aspect ratios between 15 and 50 and inclination angles between 30 and 90 degrees. The usefulness of a passive cooling channel to improve PV efficiency is illustrated by system analyses of typical PV modules.

Keywords: photovoltaic, inclined channel, natural convection, radiation, building integrated

1. Introduction

One potentially cost effect method to regulate the temperature of rooftop integrated photovoltaic (PV) panels is to provide an open air channel beneath the panel. This approach is illustrated in Figure 1. The upper surface of the inclined channel represents the PV module. This surface will experience a uniform heat flux that depends on several factors including the incident solar radiation, the efficiency and optical properties of the PV module, and the ambient conditions. The lower surface of the channel is integral with the roof. The channel geometry is specified by the overall length L, the spacing S between the upper and lower surfaces of the channel, and the inclination angle, ϕ. Ambient air will rise naturally through the asymmetrically heated channel. The PV panel is cooled by the combination of natural convection and radiation heat transfer. The objective of the present study is to develop a generalized approach to determine the PV surface temperature (T_1) for the range of operating conditions and channel geometries that might be encountered in residential applications.

There are a number of prior studies of natural convection vertical channels (e.g, Aung, 1972a,b; Bar-Cohen and Rosenhow, 1984; Webb and Hill, 1989), but more relevant for PV applications is the prior work on natural convection in inclined channels, and particularly studies that include radiative heat transfer. Manca et al. (1992) and Bianco et al. (2000) measured laminar free convection in channels inclined between 30 and 90 degrees. Symmetric (both channel walls heated) and asymmetric heating (top wall heated) were considered. The effects of radiation were not discussed. In both studies, regression of the data provides an

* Corresponding author: 612-626-9850, jhd@me.umn.edu

expression for the Nusselt number as a function of the modified channel Rayleigh number ($g\beta q_1'' S^5/\alpha\nu kL$). Brinkworth et al. (2000a) proposed an approximate method to predict free convection heat transfer in inclined channels with top heating. Their approach estimates the mass flow rate in the channel from a force balance and then treats heat transfer as forced convection. The second step decouples the velocity and the temperature fields and assumes the velocity profile is always symmetric. The error in heat transfer created by this approximation increases at higher heat flux. Predictions obtained with this technique compared favorably to measured data for $Ra''<10^3$ (Brinkworth et al., 2000b), but are less accurate for $Ra''>10^5$ (Brinkworth et al., 2000a; Brinkworth and Sandberg, 2005, 2006). Tonui and Tripanagnostopoulos (2008) calculated the air mass flow rate in a similar way but evaluated the PV temperature using a correlation for free convection in a vertical enclosure maintained at uniform wall temperature. This approach is inappropriate because the flow fields in an enclosure and open ended channels are substantially different. A composite expression for the average Nusselt number for natural convection developed using the prior data is

$$\overline{Nu} = \left[\frac{6.25}{Ra'' \sin\phi} + \frac{1.64}{(Ra'' \sin\phi)^{2/5}} \right]^{-1/2} \qquad 1 \le Ra'' \le 10^5 \text{ and } 30 \le \phi \le 90^\circ . \tag{1}$$

For the application of interest, equation (1) is not sufficient to predict cooling rates because it neglects radiative heat transfer. Moutsogolou and Wong (1989) predict the radiative cooling rate in case of black vertical walls can be as high as 35 to 40% of the total cooling rate for $Ra'' \le 10^4$. Brinkworth (2002) and Brinkworth and Sandberg (2006) proposed an approximate procedure to treat the combined convective and radiative heat transfer based on an energy balance on each of the channel walls using local convective and radiative heat transfer coefficients. The effect of radiation between the walls and the surroundings was estimated by dividing the channel into segments and modeling radiation of segments differently depending on their position relative to the inlet and outlet of the channel where radiation effects are most important (Brinkworth and Sandberg, 2006). This approach is difficult to apply in practice because the appropriate segment lengths depend on both thermal and geometrical parameters that are unknown a priori.

Bianco et al. (2006) conducted an experimental and numerical investigation of vertical channels with symmetric heating for modified channel Rayleigh numbers as high as 10^8 and channel aspect ratios (L/S) from 10 to 58. The ambient temperature was 300K and the emissivity of both walls was 0.8. Bianco et al. (2000) tested inclined channels with a wall emissivity of 0.8, modified channel Rayleigh numbers as high as 10^6 and channel aspect ratios between 10 and 32. Lin and Harrison (2003) measured heat transfer and temperature distribution in asymmetrically heated channels at inclination angles from 10 to 30 degrees, modified Rayleigh numbers from 10 to 5.6×10^4 and aspect ratios between 44 and 220. For an inclination angle of 18 degrees and a surface emissivity of 0.95, a correlation based on $Ra''\sin\phi$ was suggested. Despite the existence of radiation, the above mentioned studies correlated the Nusselt number with a single parameter, $Ra''\sin\phi$. This dimensionless encompasses the channel length and spacing, L and S; however, because the radiation exchange rate depends on the viewing field between the channel walls and the surroundings, the separate effect of the aspect ratio on the Nusselt number must be considered.

2. Problem Statement and Approach

In the present work, a scale analysis and numerical study of the combined convective and radiation heat transfer in inclined channels with asymmetric heating are presented for the range of conditions applicable for temperature regulation of rooftop mounted PV panels. The effects of the channel aspect ratio and the radiation driving force are studied and a generalized Nusselt number correlation is provided. Using that relation, a system analysis is performed to evaluate the PV module temperature and efficiency under a range of situations.

The desire is to determine the temperature of the PV module represented by the top surface of the channel as sketched in Figure 1. An energy balance on the panel module provides an expression for the average PV temperature $\overline{T_1}$ (or $\overline{T_{PV}}$):

$$\alpha_{PV} G[1-\eta_{PV}(\overline{T_{PV}})] = \varepsilon_{PV}\sigma(\overline{T_{PV}}^4 - T_{sky}^4) + h_{top}(\overline{T_{PV}} - T_o) + q_1'' . \tag{2}$$

The PV conversion efficiency depends on temperature:

$$\eta_{PV} = \eta_o + \beta_{PV}(\overline{T_{PV}} - 25°C) + \gamma \log(\frac{G}{1000}) , \tag{3}$$

where η_o is the efficiency at standard temperature (25°C) and β_{PV} and γ are the temperature and solar irradiance coefficients, respectively. The top convective heat transfer coefficient is assumed to be due to wind and is modeled as h_{top}=2.8+3V, where V is the wind speed (Gordon, 2001). A relation between the channel cooling rate, q_1'', and $\overline{T_{PV}}$ is developed from solution of the governing conservation equations assuming two-dimensional steady flow, uniform heat flux, and diffuse gray channel surfaces. Free openings are modeled as black. Once this relationship is known, equation (2) is solved iteratively to determine $\overline{T_{PV}}$ and the PV conversion efficiency.

The governing two dimensional conservation equations for laminar flow in an open ended inclined channel, subject to the Boussinesq approximation are

$$\frac{\partial u}{\partial x} + \frac{\partial v}{\partial y} = 0 \tag{4}$$

$$u\frac{\partial u}{\partial x} + v\frac{\partial u}{\partial y} = -\frac{1}{\rho_o}\frac{\partial P}{\partial x} + \nu(\frac{\partial^2 u}{\partial x^2} + \frac{\partial^2 u}{\partial y^2}) + g\beta \sin\phi\theta \tag{5}$$

$$u\frac{\partial v}{\partial x} + v\frac{\partial v}{\partial y} = -\frac{1}{\rho_o}\frac{\partial P}{\partial y} + \nu(\frac{\partial^2 v}{\partial x^2} + \frac{\partial^2 v}{\partial y^2}) + g\beta \cos\phi\theta \tag{6}$$

$$u\frac{\partial \theta}{\partial x} + v\frac{\partial \theta}{\partial y} = \alpha(\frac{\partial^2 \theta}{\partial x^2} + \frac{\partial^2 \theta}{\partial y^2}) \tag{7}$$

where the modified pressure $P \equiv p - p_e + \rho_o g \sin\phi(x-L)$ and $\theta \equiv T - T_o$. The boundary conditions at the channel walls are

$$u = v = 0,\ -k\frac{\partial T}{\partial y} - q''_{r1} = q''_{1} \text{ at } y = 0 \tag{8a}$$

and

$$u = v = 0,\ k\frac{\partial T}{\partial y} + q''_{r2} = 0 \text{ at } y = S \tag{8b}$$

Note the lower wall (roof surface) is assumed adiabatic as it is beneath the channel. Ambient temperature and total pressure are assumed at the inlet: the magnitude of the inlet velocity is determined via Bernoulli's equation:

$$T = T_o,\ P = -\frac{1}{2}\rho_o u_m^2 \text{ at } x = 0, \tag{9}$$

where u_m is the mean fluid velocity in the channel, i.e. $u_m S = \int_0^S u dy$. The inlet streamwise velocity profile, u(0,y), is found by an iterative process using the pressure constraint of equation (9). At the exit, only the pressure is specified:

$$P = 0 \text{ at } x = L. \tag{10}$$

The net radiative flux from each surface is the sum of the emitted flux and reflected fraction of the incident flux:

$$q''_{r1} = \varepsilon_1 \sigma T_1^4 + (1-\varepsilon_1) q''_{i1} \tag{11a}$$

$$q''_{r2} = \varepsilon_2 \sigma T_2^4 + (1-\varepsilon_2) q''_{i2} \tag{11b}$$

The radiative incident fluxes are given by:

$$q''_{i1} = \frac{1}{dA_1}\{\int_{A_2} [\varepsilon_2 \sigma T_2^4 + (1-\varepsilon_2) q''_{i2}] dF_{d2-d1} dA_2 + \sigma T_o{}^4 (\int_{A_i} dF_{di-d1} dA_i + \int_{A_e} dF_{de-d1} dA_e)\} \tag{12a}$$

$$q''_{i2} = \frac{1}{dA_2}\{\int_{A_1} [\varepsilon_1 \sigma T_1^4 + (1-\varepsilon_1) q''_{i1}] dF_{d1-d2} dA_1 + \sigma T_o{}^4 (\int_{A_i} dF_{di-d2} dA_i + \int_{A_e} dF_{de-d2} dA_e)\} \tag{12b}$$

where i and e denote the channel inlet and exit, respectively. The part of the roof which is uncovered by the PV panels is not neglected entirely in this analysis because the free openings (channel inlet and outlet) are modeled as black bodies at ambient temperature and emit radiation accordingly. This assumption is also used in previous studies (e.g., Brinkworth and Sandberg, 2006). The viewing field between the uncovered roof is always smaller than the viewing field between the channel openings and the top wall. The sky radiation will dominate in case of most residential panel installations, making the above approximation reasonable. The problem is therefore represented by the conservation equations (4)-(7) along with the boundary conditions given by equations (8)-(10) coupled to the radiative equations (11) and (12). In the present work, the emissivity of both channel walls is set to 0.9, in agreement with prior studies (Moshfegh and Sandberg, 1996, Brinkworth et al., 1997, Brinkworth and Sandberg, 2006).

The governing equations are non dimensionalized by introducing the following scales:

$$x^* = \frac{x}{L}; y^* = \frac{y}{S}; u^* = \frac{u}{u_o}; v^* = \frac{v}{u_o}; P^* = \frac{P}{\rho_o \beta \theta_{be} g L \sin\phi}; \theta^* = \frac{\theta}{q_1'' S/k}; \Theta = \frac{T}{q_1'' S/k} \tag{13a}$$

where u_o is the characteristic velocity of the flow and θ_{be} is the difference between the mean (bulk) exit fluid temperature, T_{be}, and the ambient temperature, T_o. The velocity and temperature scales are:

$$u_o = \frac{\alpha}{S}(S/L)^{-1}[Ra'' \sin\phi]^{1/2} \tag{13b}$$

and

$$\theta_{be} = \frac{q_1'' S}{k}\left[\frac{1}{Ra'' \sin\phi}\right]^{1/2}. \tag{13c}$$

Using the scales defined in equation (13), the dimensionless conservation equations become

$$\frac{\partial u^*}{\partial x^*} + (S/L)^{-1}\frac{\partial v^*}{\partial y^*} = 0 \tag{14a}$$

$$u^*\frac{\partial u^*}{\partial x^*} + (S/L)^{-1} v^*\frac{\partial u^*}{\partial y^*} = -\frac{Pr}{(Ra'' \sin\phi)^{1/2}}\frac{\partial P^*}{\partial x^*} + \frac{Pr}{(Ra'' \sin\phi)^{1/2}}[(S/L)^2\frac{\partial^2 u^*}{\partial x^{*2}} + \frac{\partial^2 u^*}{\partial y^{*2}}] + Pr\,\theta \tag{14b}$$

$$u^*\frac{\partial v^*}{\partial x^*} + (S/L)^{-1} v^*\frac{\partial v^*}{\partial y^*} = -\frac{(S/L)^{-1} Pr}{(Ra'' \sin\phi)^{1/2}}\frac{\partial P^*}{\partial y^*} + \frac{Pr}{(Ra'' \sin\phi)^{1/2}}[(S/L)^2\frac{\partial^2 v^*}{\partial x^{*2}} + \frac{\partial^2 v^*}{\partial y^{*2}}] + Pr\cot\phi\,\theta^* \tag{14c}$$

$$u^*\frac{\partial \theta^*}{\partial x^*} + (S/L)^{-1} v^*\frac{\partial \theta^*}{\partial y^*} = \frac{1}{(Ra'' \sin\phi)^{1/2}}[(S/L)^2\frac{\partial^2 \theta^*}{\partial x^{*2}} + \frac{\partial^2 \theta^*}{\partial y^{*2}}] \tag{14d}$$

The dimensionless boundary conditions are

$$1 = -\frac{\partial \Theta}{\partial y^*} - \frac{q_{r1}''}{q_1''} \quad \text{at } y^*=0 \tag{15a}$$

$$0 = \frac{\partial \Theta}{\partial y^*} + \frac{q_{r2}''}{q_1''} \quad \text{at } y^*=1 \tag{15b}$$

$$\theta^* = 0, \quad P^* = -\frac{u_m^2}{2\beta\theta_{be} g L \sin\phi} \quad \text{at } x^* = 0. \tag{15c}$$

$$P^* = 0 \quad \text{at } x^* = 1. \tag{15d}$$

The dimensionless form of equations (11a) and (11b) are

$$\frac{q''_{r1}}{q''_1} = \varepsilon_1 R\Theta_1^4 + \frac{(1-\varepsilon_1)q''_{i1}}{q''_1} \tag{16a}$$

$$\frac{q''_{r2}}{q''_1} = \varepsilon_2 R\Theta_2^4 + \frac{(1-\varepsilon_2)q''_{i2}}{q''_1}. \tag{16b}$$

The dimensionless form of equations (12a) and (12b) are

$$\frac{q''_{i1}}{q''_1} = \frac{1}{dA_1}\{\int_{A_2}[\varepsilon_2 R\Theta_2^4 + (1-\varepsilon_2)q''_{i2}/q''_1]dF_{d2-d1}dA_2 + R\Theta_o^4(\int_{A_i} dF_{di-d1}dA_i + \int_{A_e} dF_{de-d1}dA_e)\} \tag{17a}$$

$$\frac{q''_{i2}}{q''_1} = \frac{1}{dA_2}\{\int_{A_1}[\varepsilon_1 R\Theta_1^4 + (1-\varepsilon_1)q''_{i1}/q''_1]dF_{d1-d2}dA_1 + R\Theta_o{}^4(\int_{A_i} dF_{di-d2}dA_i + \int_{A_e} dF_{de-d2}dA_e)\} \tag{17b}$$

These equations introduce the dimensionless radiation number

$$R \equiv \frac{\sigma q''^3_1 S^4}{k^4}. \tag{18}$$

The two temperature scales θ^* and Θ are related by $\Theta = \theta^* + \Theta_o$.

The scale analysis of the combined convection/radiation problem suggests that the average Nusselt number will depend on the modified Rayleigh number where the gravitational constant is multiplied by sinϕ, the channel aspect ratio, the radiation parameter R, and the dimensionless ambient temperature, Θ_o:

$$Nu^* = Nu^*(Ra''\sin\phi, L/S, R, \Theta_o). \tag{19}$$

In equation (19), the asterisk indicates combined convection/radiation heat transfer.

3. Numerical Model

Solution of the governing conservation equations and boundary conditions is carried out using FLUENT 6.2. The segregated solution method was chosen to solve the governing equations, which were linearized implicitly. The second order upwind scheme was chosen for the energy and momentum equations. The Semi-Implicit Method for Pressure-Linked Equations (SIMPLE) scheme couples pressure and velocity. All surfaces are treated as gray, diffuse. The code divides the flow domain into control volumes. The numerical scheme integrates the governing equations over each control-volume to construct a set of algebraic equations, after linearization of the results (Patankar, 1980). The set is then solved iteratively by the Gauss-Seidel linear equation solver for algebraic multigrid systems (AMG) until convergence is achieved. For convergence determination, the dimensionless residual term of each equation is calculated after iteration. Convergence is achieved when the residual terms of the continuity and momentum equations are less than 10^{-5}, and less than 10^{-8} for the energy equation. A grid refinement study is performed using a mesh size of 20x100, 40x200, 80x300, and 200x400. The velocity profile at selected location in the channel, the dimensionless local wall temperature of the heated wall and the channel Nusselt number showed that a grid of 80x300 is adequate for the all the computations. The numerical solution was validated using

experimental data for both pure convection (Aung 1972b) and combined convection-radiation (Lin and Harrison, 2003).

4. Results

Results are presented for the range of dimensional parameters expected for rooftop integrated PV panels. Channel cooling rates, $q_1^{"}$, are in the range of 0 to 500W/m^2. The channel length, L, is varied between 1 and 10m. The channel spacing, S, is varied between 2 and 20cm. The channel orientation, ϕ, is varied between 90^o (vertical) and 30^o with respect to horizontal. The assumed ambient temperature is 300K. Accordingly, $Ra"\sin\phi \le 10^8$, $15 \le L/S \le 50$ and $1.2\times10^{-11} \le R \le 2.8\times10^4$, $0.1 \le \Theta_o \le 5420$.

Numerical predictions of the global average channel Nusselt number $\overline{Nu^*}$ as a function of $Ra"\sin\phi$ for aspect ratios L/S=15, 30 and 50 are presented in Figure 2 for both pure convection (solid symbols) and combined convection-radiation (open symbols lines). The average Nusselt number is determined from the numerical data as

$$\overline{Nu^*} = \frac{q_1^{"}}{\overline{T_1} - T_o}\frac{S}{k} \tag{20}$$

where the average wall temperature is $\overline{T_1} = \frac{1}{L}(\int_0^L T_1 dx)$. The solid (pure convection) line represents the correlation presented in equation (1). The dashed lines represent a correlation developed for combined convection/radiation and presented in equation (21).

Figure 2 shows that for pure convection, Nusselt number depends solely on $Ra"\sin\phi$. With radiative heat transfer included, Nusselt numbers are higher and also depend on the aspect ratio (L/S). For $Ra"\sin\phi = 7\times10^5$ and L/S=15, the effect of radiation is most pronounced. Nusselt number is 21.4 when radiation is included compared to 9.8 for pure convection. For $Ra"\sin\phi = 7\times10^5$ and L/S=30, the combined convection/radiation Nusselt number is 16.2.

For specified $Ra"\sin\phi$ and L/S and within the frame of dimensional parameters considered here, the Nusselt number is relatively insensitive to changes in the values of R and Θ_o. The most significant change is felt at low aspect ratio, L/S=15, (when the radiation effect is high) and $Ra"\sin\phi = 10^6$. In this case, for L=1m, R=24. For L=1.8m, R= 0.22. Corresponding values of Θ_o are 0.54 and 3.16. The change in Nusselt number from L=1m to L=1.8m is from 17.2 to 16. The Nusselt number is therefore well correlated over a wide range of practical geometries by $Ra"\sin\phi$ and L/S.

Based on the numerical data the following correlation is suggested for the global Nusselt number:

$$\overline{Nu^*} = F(\frac{L}{S})\cdot(Ra"\sin\phi)^{0.203} \qquad \begin{bmatrix} \varepsilon_1 = \varepsilon_2 = 0.9 \\ Ra" \le 10^8 \\ 15 \le L/S \le 50 \\ 30^o \le \phi \le 90^o \end{bmatrix} \tag{21a}$$

where the function F depends on the aspect ratio L/S and is given by

$$F(L/S) = -3.38\times10^{-6}(L/S)^3 + 0.000687(L/S)^2 - 0.04419(L/S) + 1.833 \tag{21b}$$

The average and maximum deviation between equation (21) and the numerical data are 6.5% and 13.2%, respectively.

Figure 3 is a plot of dimensionless temperature difference between the top wall and ambient, θ_1^*, along the length of the channel. In this plot channel length is indicated by x/L where the inlet is located at $x/L=0$ and the outlet is located at $x/L=1$. The shape of the temperature distribution near the inlet and outlet of the channel is affected by the radiation heat transfer as shown by the difference in the curves for convection and combined convection/radiation. This result agrees with data from Moutsogolou and Wong (1989) and Bianco et al. (2006). As expected, the impact of radiation on the temperature profile is most significant at the exit where the viewing angle between the channel and the ambient is highest.

Equations (1) and (21) suggest that both the convective and radiative cooling rates increase with increasing channel spacing, S. The convective and global heat transfer coefficients, $Nu \cdot k/S$ and $\overline{Nu}^* \cdot k/S$, increase monotonically with S. At very small channel spacing, the flow is fully developed (unfavorable) and the small viewing angle to the openings results in poor radiation exchange between the walls and the surroundings. At very large channel spacing, the flow is developing (boundary layer flow) and the view factor between the walls to the surroundings is close to 1.

To illustrate the mechanisms for cooling, two-dimensional temperature and velocity profiles within the channel are presented for $Ra''=10^6$, L=2.4m, S=0.08m, $q_1''=210 W/m^2$, and ϕ=45 degrees. Velocity and temperature profile plots at increasing distance from the channel inlet (x/L=0, 0.25, 0.50, 0.75, 1) are shown in Figures 4 and 5, respectively. The heated top wall is at $y/S=0$.

In the case of pure convection, the uniform heat flux at the upper wall results in a boundary layer flow along the lower surface of the PV module as shown in Figure 4(a). The boundary layer grows along the wall and the maximum surface temperature and air velocity are achieved near the channel exit ($0.95 \bullet x/L \bullet 1$). The maximum velocity is 1.085m/s near the channel top wall ($y/S=0.065$). There is a region of backflow near the adiabatic wall at the channel exit similar to that observed by Azevedo and Sparrow (1985). Figure 5(a) shows the development of the air temperature profile within the channel. The developing thermal boundary layer spans about one-third the gap between the walls. The maximum temperature is 381K at $y/S=0$ and $x/L=1$. The average wall temperature is 368K. Despite the existence of backflow adjacent to the top part of the adiabatic wall the average Nusselt number is well correlated with the $Ra''\sin\phi$ group.

When radiation is incorporated into the model, the lower wall of the channel is heated. The resulting flow field and temperature profiles are shown in Figures 4(b) and 5(b). In contrast to the velocity profile for pure convection, a hydrodynamic boundary layer develops along both walls of the channel. Velocity near the channel walls increases with increasing axial location. The maximum velocity near the top and bottom walls is 0.86 and 0.73m/s, respectively. As illustrated in Figure 5(b), radiation heat transfer accounts for a significant drop in the temperature of the PV module represented here as the top wall of the channel. Temperature decreases about 5K near both walls from $x/L=0.75$ to $x/L=1$. The maximum and the average top wall temperatures are 349K (at $x/L=0.993$) and 342K, respectively.

The average air and the top wall temperatures along the length of the channel are presented in Figure 6. When radiation is included in the model, heat is radiated directly from the walls to the surroundings and as a result the rise in air temperature is less than when radiation is neglected (13K compared to 26K). In the pure convection case, the air temperature decreases slightly (1.6K) near the exit due to reverse flow of cold ambient air in the vicinity of

the bottom wall. The radiation effect is significant in terms of reducing the PV temperature. The average temperature of the top wall is 342K with radiation and 367K for pure convection. The corresponding Nusselt numbers are 15.3 and 9.6.

5. Discussion

The usefulness of a passive cooling channel to improve PV efficiency is evaluated for representative residential applications. The input parameters are listed in Table 1 and include the roof slope, the ambient conditions, the surface properties and module efficiency coefficients. The effect of the channel geometry on the panel's performance is considered in a parametric study. The sensitivity of the PV efficiency to the channel spacing for a channel length of 3 m and an inclination of 30 degrees is shown in Figure 7 at solar radiation levels of 500 and $1000 W/m^2$,. The reference efficiencies without cooling channel ($q_1'' = 0$, base case) are plotted as well. For the fixed channel length, the PV performance is always improved by increasing the channel spacing. Increasing the channel spacing from 5 to 20cm increases the efficiency by 0.3% at $500 W/m^2$ and 0.5% at $1000 W/m^2$. The modified channel Rayleigh number, Ra'', lies between 2455 ($500 W/m^2$, S=3cm) and 0.998×10^8 ($1000 W/m^2$, S= 20cm).

The sensitivity of the PV efficiency to the channel (panel) length for channel spacing of 20cm and inclination of 30 degrees is shown on Figure 8 at solar radiation levels of $500 W/m^2$ and $1000 W/m^2$. Shorter channels (higher aspect ratios) are preferable to a longer channels primarily because of increased radiative loses. Decreasing the length from 10 to 3m results in production drop of 0.5% at $500 W/m^2$ and 0.8% at $1000 W/m^2$. The trends in Figure 8 are more moderate for longer panels because the dependence of the channel radiative cooling rate on the aspect ratio (L/S) is weaker (see Figure 2).

The effect of the solar radiation is depicted in Figure 9, where the electrical production rate ($\eta_{PV}\cdot G$) and the average panel temperature, $\overline{T_{PV}}$ are plotted versus the solar radiation flux for channel dimensions of 3m × 20cm. Due to the large spacing (20cm), the Ra'' numbers in Figure 9 are relatively high and lie between 3.55×10^7 ($G=150 W/m^2$) and 0.998×10^8 ($G=1000 W/m^2$). Without the channel, the PV temperature (which dictates the efficiency) is depends strongly on the solar radiation flux. From 900 to $1000 W/m^2$, PV efficiency decreases slightly. With the channel, the sensitivity of the PV temperature to the solar radiation is much less because some of the excess heat is removed by the channel. As a result, the production rate is nearly proportional to the solar radiation flux.

6. Conclusion

A scale analysis and numerical study have been conducted to predict the passive air cooling rate of an open channel beneath PV panels. The results illustrate the effect of the Rayleigh number and channel aspect ratio on the channel Nusselt number for combined convection-radiation heat transfer. A correlation for the combined heat transfer coefficient is presented in equation (21). The influence of radiative heat transfer is greatest at low aspect ratios (or for short channels). System analysis shows that the inclusion of the channel behind the PV panels can decrease their temperature as much as 10 to 20K, resulting in an absolute efficiency gain of 1 to 2%, depending on the channel geometry and the solar radiation flux. The channel cooling rate increases monotonically with the channel spacing and decreases monotonically with the panel length. However, significant power production enhancement can be achieved even if the channel dimensions are not ideal. These findings suggest that the passive cooling configuration is a sound approach for controlling the temperature of rooftop integrated PV.

Acknowledgments

The authors gratefully acknowledge the financial support of the U.S. Department of Energy through the National Energy Technology Laboratory (Award No. DE-FC26-04NT42114) and the National Renewable Energy Laboratory (Award No. NDC-5-44408-02**)**, the University of Minnesota Initiative for Renewable Energy and the Environment, and the University of Minnesota Supercomputing Institute. Any opinions, findings, conclusions, or recommendations expressed herein, are those of the author (s) and do not necessarily reflect the views of the DOE.

Nomenclature

A	area, m^2
F	view factor
F(L / S)	function, equation (21b)
g	gravitational acceleration, m/s^2
h_{gap}	heat transfer coefficient in the gap, W/m^2K
h_{top}	top heat transfer coefficient, W/m^2K
G	incident solar radiation, W/m^2
k	thermal conductivity, W / mK
L	channel length, m
Nu^*	global channel Nusselt number, $q_1''S/k(\overline{T_1}-T_o)$
$\overline{Nu}$	average channel Nusselt number, $q_1''S/k(\overline{T_1}-T_o)$
$\overline{Nu^*}$	global average channel Nusselt number, $q_1''S/k(\overline{T_1}-T_o)$
Nu_{gap}	gap Nusselt number, $h_{gap}\delta/k$
p	pressure, kg/ms^2
P	modified pressure, $p-p_e+\rho_o g\sin\phi(x-L)$, kg/ms^2
P*	dimensionless pressure
Pr	Prandtl number, ν/α
q"	heat flux, W/m^2
R	radiation number, $\sigma q_1''^3 S^4/k^4$
Ra	gap Rayleigh number, $g\beta(\overline{T_{PV}}-T_{glass})\delta^3/\nu\alpha$
Ra"	modified channel Rayleigh number, $g\beta q_1'' S^5/\nu\alpha kL$
S	channel spacing, m
T	temperature, ºC
T_{glass}	glass temperature, ºC
T_{sky}	sky temperature, ºC
u	streamwise velocity, m / s
u_o	characteristic fluid velocity, m / s
u_m	mean fluid velocity, m / s
v	transversal velocity, m / s
x	coordinate, m
x*	dimensionless coordinate, x / L
y	coordinate, m
y*	dimensionless coordinate, y / S

Greek Symbols

α thermal diffusivity, m^2/s
β thermal expansion coefficient, K^{-1}
β_{PV} PV cell temperature coefficient, $1/^oC$
γ PV cell solar irradiance coefficient
δ distance between the PV module and glass sheet, m
ε emissivity
Θ dimensionless temperature, $Tk/q_1^{"}S$
θ temperature difference ($T-T_o$), ^oC
θ^* dimensionless temperature difference, $\theta k/q_1^{"}S$
ν kinematic viscosity, m^2/s
ρ density, kg/m^3
σ Stefan-Boltzmann constant
$(\tau\alpha)_{eff}$ transmittance-absorptance product
ϕ inclination angle, deg

Subscripts

1 heated (top) wall
2 bottom wall
b bulk
be bulk exit
c cross section
e channel exit
i channel inlet
o reference
PV photovoltaic
s surface
top top wall of the channel

References

Aung W., 1972. Fully developed laminar free convection between vertical plates heated asymmetrically. International Journal of Heat and Mass Transfer. 15, 1577-1580.

Aung W., 1972. Developing laminar free convection between vertical plates with asymmetric heating. International Journal of Heat and Mass Transfer. 15, 2293-2308.

Azevedo L.F.A., Sparrow E.M., 1985. Natural convection in open-ended inclined channels. Journal of Heat Transfer. 107, 893-901.

Bar-Cohen A., Rosenhow W. M., 1984. Thermally optimum spacing of vertical, natural convection cooled, parallel plate. Journal of Heat Transfer. 106, 116-123.

Bianco N., Morrone, B., Nardini S., Naso V., 2000. Experiments on natural convection in inclined channels, Heat and Technology. 18(2), 23-45.

Bianco N., Langellotto L., Manca O., Nardini S., Naso V., 2006. Numerical analysis of radiative effects on natural convection in vertical convergent and symmetrically heated channels. Numerical Heat Transfer. Part A, 49, 369-391.

Brinkworth B.J., Cross, B. M., Marshall, R.H., Hongxing Y., 1997. Thermal regulation of photovoltaic cladding. Solar Energy. 61, 169-178.

Brinkworth B.J., 2000. A procedure for the routine calculation of laminar free and mixed convection in inclined ducts. International Journal of Heat and Fluid Flow. 61, 456-462.

Brinkworth B.J., Marshall, R.H., Ibrahim Z., 2000. A validated model of naturally ventilated PV cladding. Solar Energy. 69, 67-81.

Brinkworth B.J., 2002. Coupling of convective and radiative heat transfer in PV cooling ducts. Journal of Solar Energy Engineering. 124, 250-255.

Brinkworth B.J., Sandberg M., 2005. A validated procedure for determining the buoyancy-induced flow in ducts. Building Services Engineering and Technology. 26 (1), 35-48.

Brinkworth B.J., Sandberg M., 2006. Design procedure for cooling ducts to minimize efficiency loss due to temperature rise in PV arrays. Solar Energy. 80, 89-103.

Gordon, J., 2001. Solar Energy, the State of the Art: ISES Position Papers. James & James (Science Publishers) Ltd, London, pp. 145-221.

Manca O., Nardini S., Naso V., 1992. Experiments on natural convection in inclined channels, General Papers in Heat Transfer and Heat transfer in Hazardous Waste Processing. 212, 41-46.

Mattei M., Notton G., Cristofari C., Muselli M., Poggi P., 2006. Calculation of the polycrystalline PV module temperature using a simple method of energy balance, Renewable Energy. 31, 553-567.

Moshfegh B., Sandberg M., 1996. The investigation of fluid flow and heat transfer in vertical channel heated from one side by PV elements. Part I – numerical study. In Proceedings of the Fourth Renewable Energy Congress, Denver, USA, pp. 248-253.

Moutsogolu A., Wong Y.H., 1989. Convection-radiation interaction in buoyancy-induced channel flow. Journal of Thermophysics. 3(2), 175-181.

Patankar, Suhas V. V., 1980. Numerical Heat Transfer and Fluid Flow. Hemisphere Publishing Corporation, pp. 113-154.

Qin Lin., Harrison S.F., 2003. Experimental study of natural convection in an asymmetrical heated inclined channel with radiation exchange. In Proceedings of HT2003 ASME Summer Heat Transfer Conference, Las Vegas, Nevada, USA, pp. 1-5.

Tonui J.K., Tripanagnostopoulos Y., 2008. Performance improvement of PV/T solar collectors with natural air flow operation. Solar Energy. 82, 1-12.

Webb B.W., Hill D. P., 1989. High Rayleigh number laminar natural convection in an asymmetrically heated vertical channel. Journal of Heat Transfer. 111, 649-656.

Table 1. Model input parameters

Parameter	**Value**
Roof slope	30 degrees
Ambient temperature, T_o	300K
Sky temperature, T_{sky} [1]	300K
Wind velocity, V	1 m/s
PV surface and glass emissivity, ε_{PV}, ε_{glass}	0.9
PV surface absorptivity, α_{PV}	0.9
Glass absorptivity, α_{glass}	0.1
transmittance-absorptance product of the PV surface, $(\tau\alpha)_{eff}$	0.85
PV cell efficiency at standard temperature, η_o	0.15
PV cell temperature coefficient, β_{PV} [2]	-0.1 %/K
PV cell solar irradiance coefficient, γ	0.025

[1] The sky temperature is assumed to be identical to the ambient (typical for hazy days). This is a conservative assumption. Higher radiative heat exchange between the panel top surface and channel walls and the environment is expected on clear days, when the sky temperature can be far below the ambient value.

[2] For crystalline and polycrystalline silicon modules (c-Si and p-Si) β_{PV} is between -0.05 %/°C and -0.1 %/K (Mattei et al., 2006). The temperature coefficient of amorphous silicon modules (a-Si) is lower, 0.0125 %/K. In the current analysis, a conservative value of -0.1%/K is used.

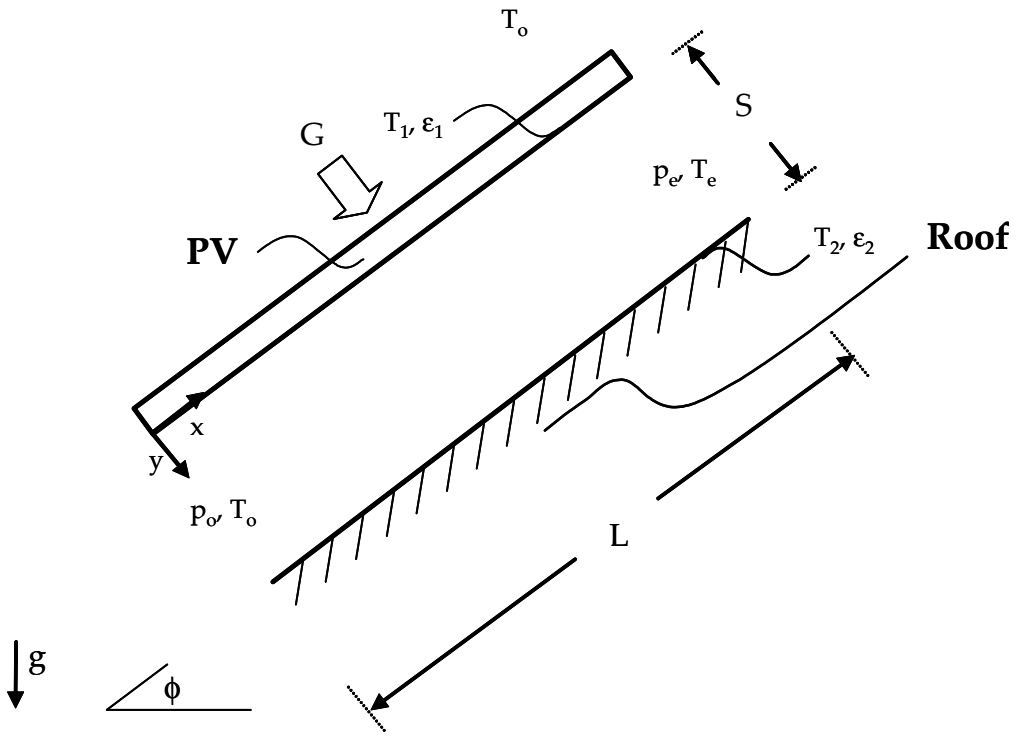

Figure 1. Rooftop integrated PV, with an air cooling channel below the PV panel.

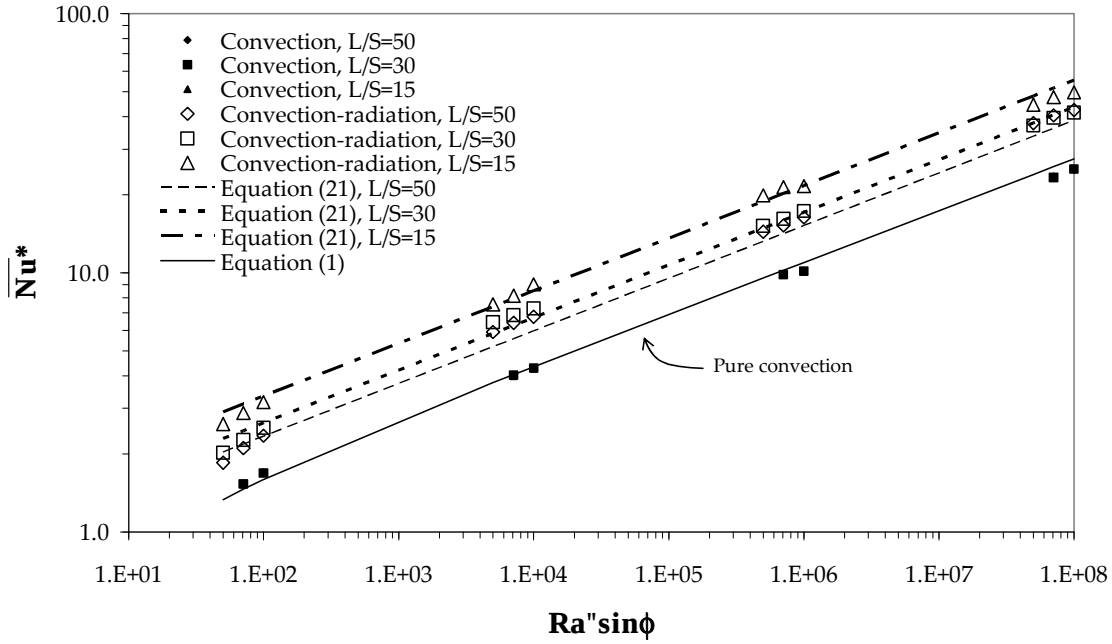

Figure 2. Average Nusselt number vs. Rayleigh number for channel aspect ratios of 15, 30 and 50 and $2.4\times10^{-11}\leq R\leq1.2\times10^{4}$. Data for pure convection ($\varepsilon=0$) and convection-radiation cooling modes ($\varepsilon=0.9$) are shown.

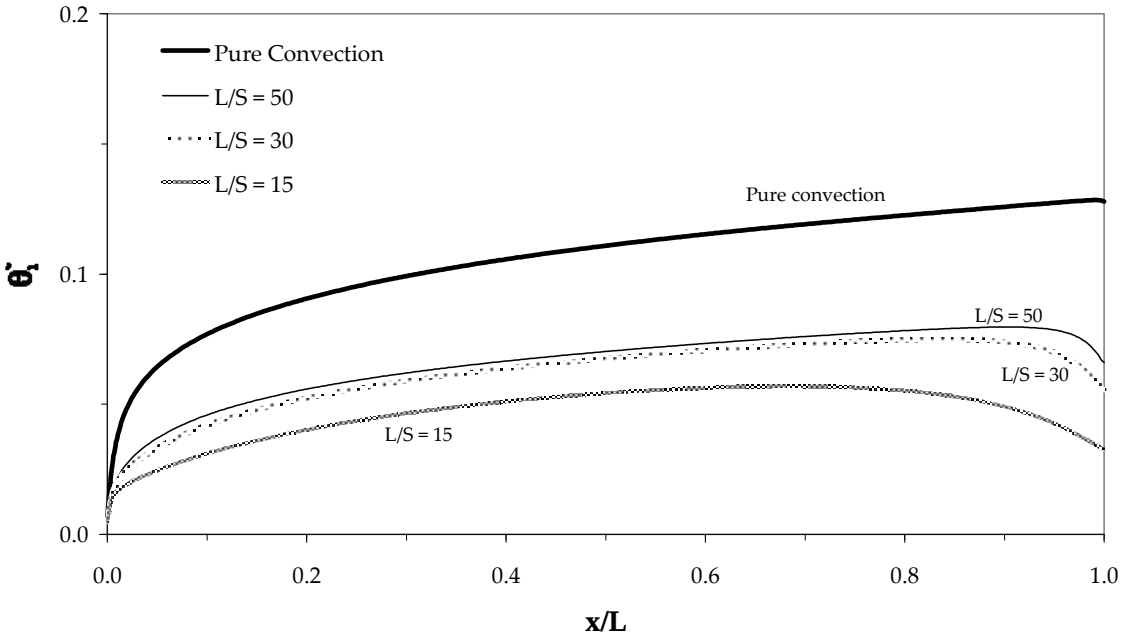

Figure 3. Dimensionless temperature distribution along the heated (top) wall. Combined convection and radiation. Ra" = 10^{6} and ϕ=45 degrees.

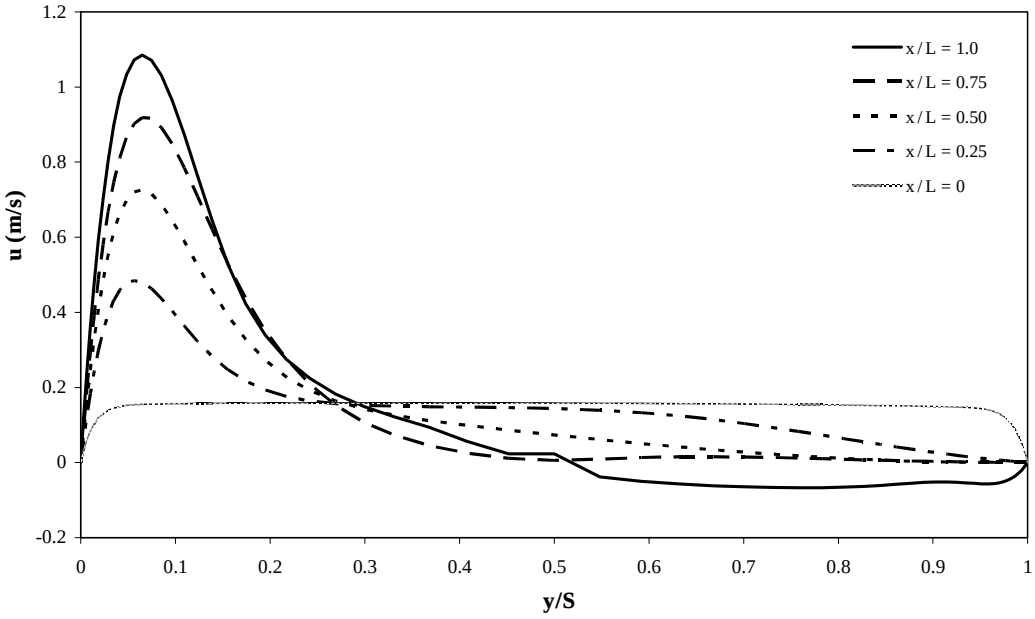

(a)

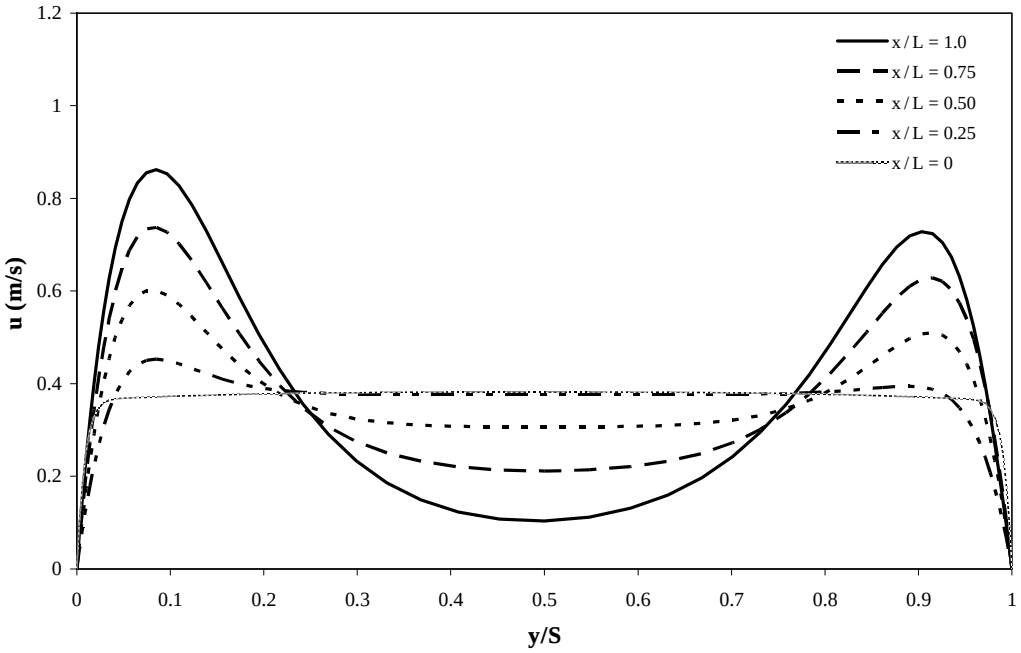

(b)

Figure 4. Velocity profiles at five axial positions along the length of a 0.8m wide channel. The heated wall is at $y/S=0$. The channel length is 2.4m, $q_1^{"}=210 W/m^2$ and $\phi=45$ degrees. $Ra"=10^6$ (a) Pure convection. (b) Combined convection / radiation.

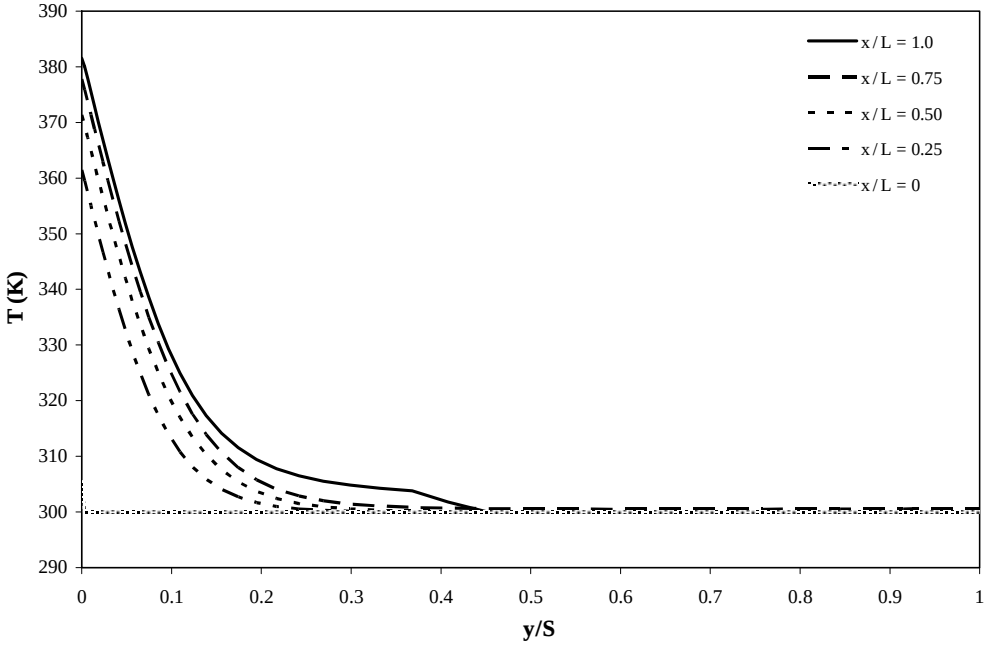

(a)

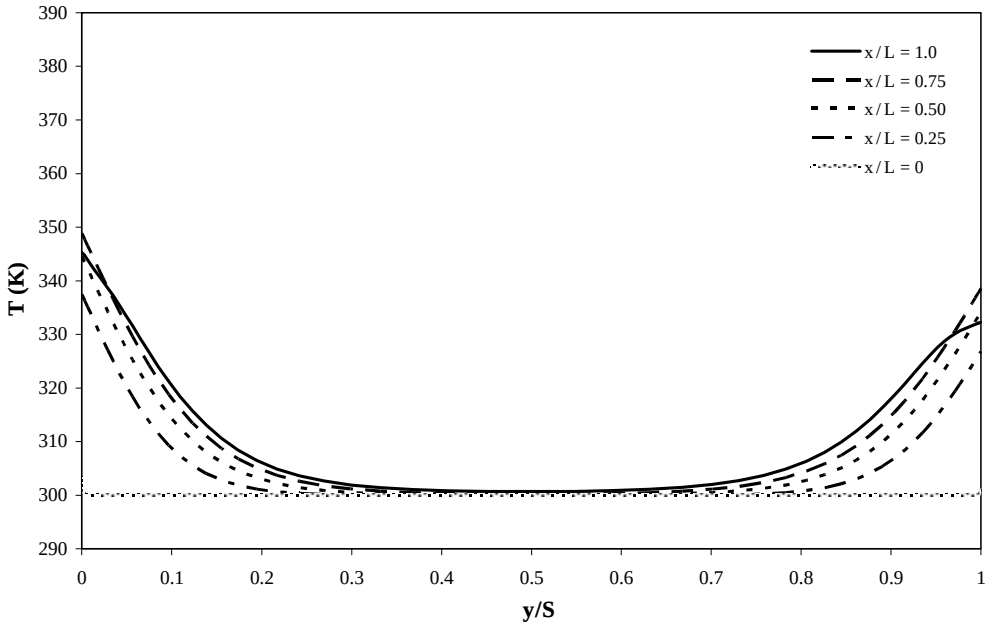

(b)

Figure 5. Temperature profiles at five axial positions along the length of a 0.8m wide channel. The heated wall is at $y/S=0$. The channel length is 2.4m, $q_1''=210 W/m^2$ and $\phi=45$ degrees. $Ra''=10^6$ (a) Pure convection. (b) Combined convection/radiation.

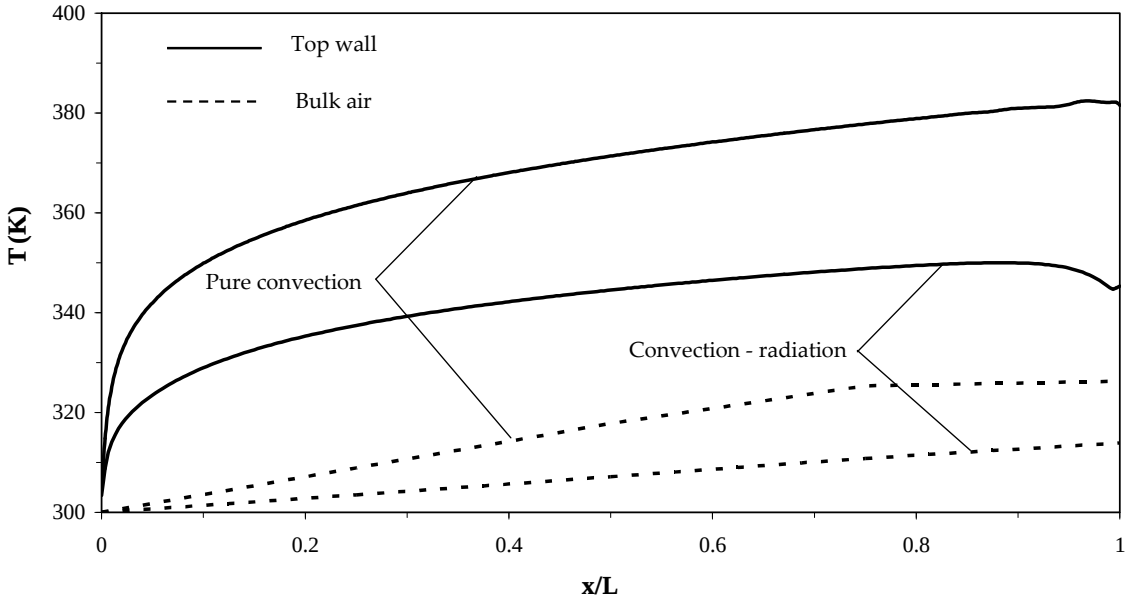

Figure 6. Local bulk (mean) air and top wall temperatures in the channel. Ra" = 10^6, L / S = 30, $\phi = 45^{\circ}$.

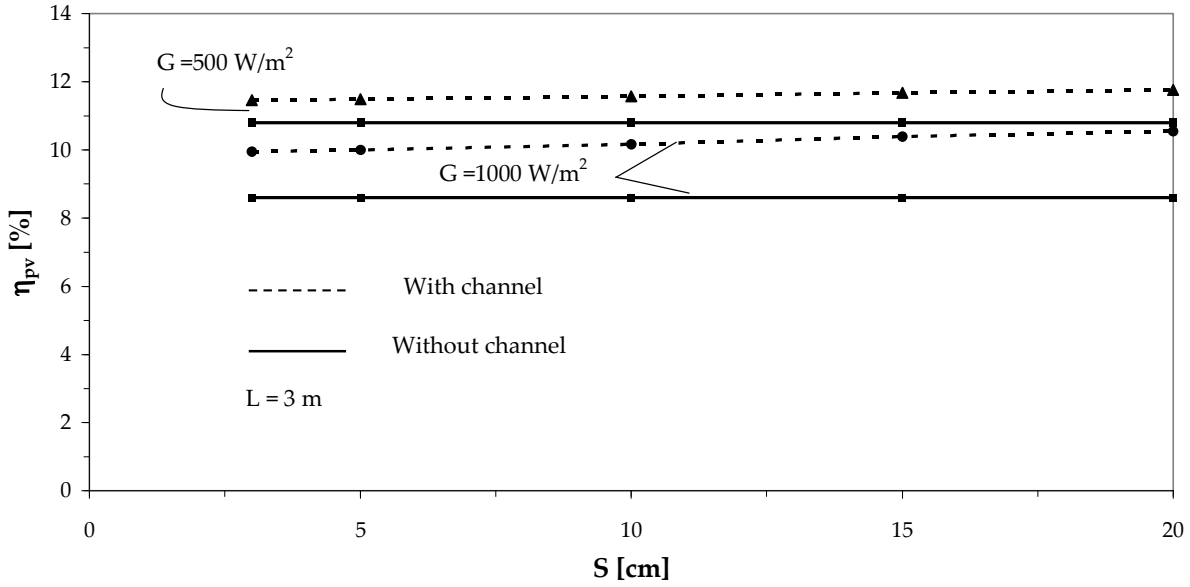

Figure 7. The effect of the channel spacing on the PV conversion efficiency at different solar radiation levels. The channel length is 3m, ϕ=30°.

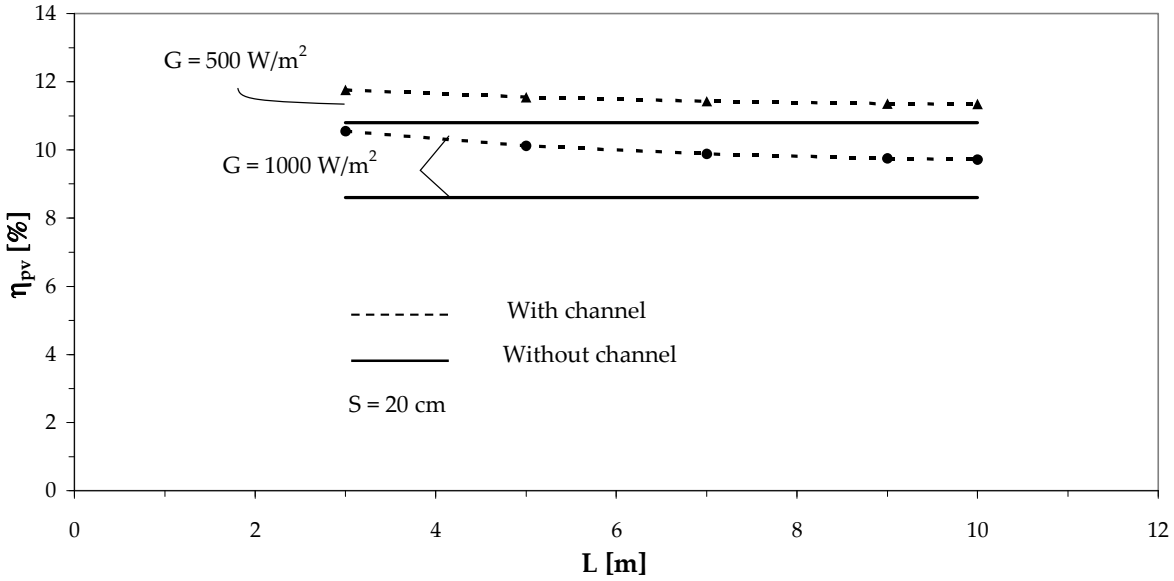

Figure 8. The effect of the channel length on the PV conversion efficiency at different solar radiation levels. The channel spacing is 20 cm, ϕ=30°.

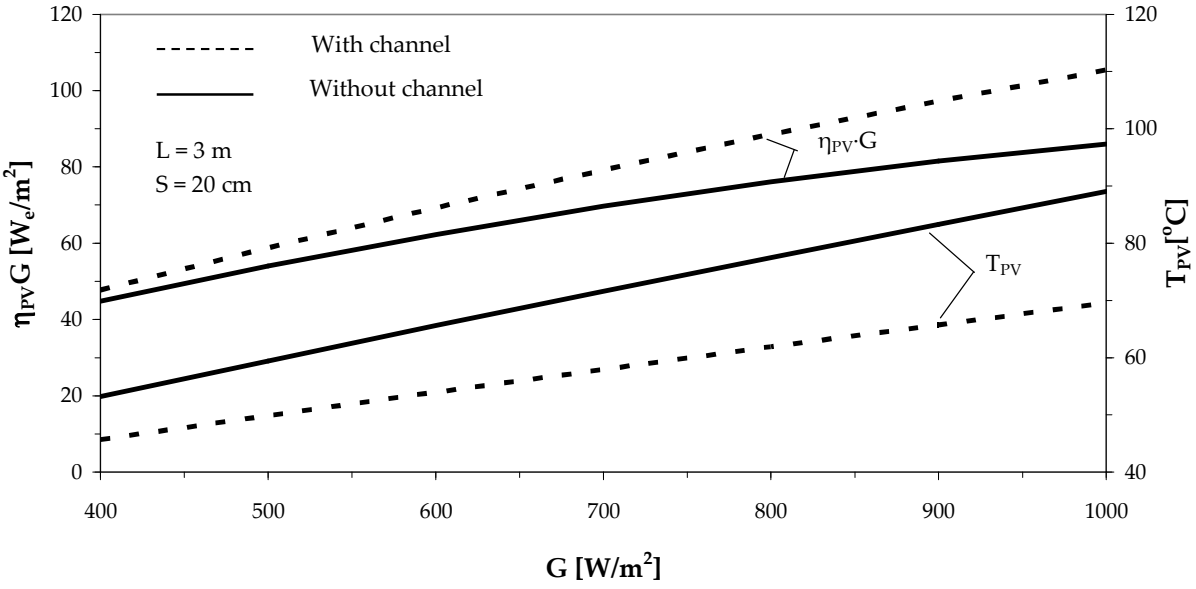

Figure 9. The effect of the solar radiation on the PV production rate. The channel length is 3m, S=20 cm, ϕ=30°.